The Organometallic Chemistry of the Ru(001) Surface

Thesis by
John Ethan Parmeter

In Partial Fulfillment of the Requirements
for the Degree of
Doctor of Philosophy

California Institute of Technology
Pasadena, California

1988

(Submitted 18 December 1987)

To my parents.

Acknowledgments

I owe a great deal of thanks to my advisor, Henry Weinberg. During my stay at Caltech, he helped to create a working atmosphere that was both enjoyable and productive, and gave me a great deal of latitude to pursue those scientific problems in which I was particularly interested. He was a constant source of advice and knowledge, and I have great respect for him both as a scientist and a person.

Many thanks are also due to other members of the Weinberg research group with whom I have had the privilege of working. Brad Anton showed much kindness and patience in teaching me how to utilize and care for the EELS system, and left me with an experimental apparatus in excellent working condition. Malina Hills and Udo Schwalke were good friends and valued coworkers during much of my stay here, both of whom taught me a lot about surface science. Youqi Wang showed a great deal of good humor in assisting with the ammonia experiments (although it might be more accurate to say that I assisted him). Yongkui Sun and Dale Johnson have provided many useful scientific discussions, and I have enjoyed a number of nonscientific diversions with them. Most of all I would like to thank Charles Buddie Mullins for his friendship and support over the last four years. It has been a pleasure to know and interact with several other members of the Weinberg group: Paul Beeken, Chun-yu Chan, Jim Engstrom, Lynn Forrester, Greg Gajda, Steve George, Eric Hood, Chuan Kang, Art Lee, Phil Szuromi, Brian Toby, Wilman Tsai, John Vajo, Jenna Zinck, and anyone else I've forgotten.

I am grateful to AT&T Bell Laboratories for supporting me with a graduate fellowship over the past few years.

I am indebted to numerous members of the Caltech staff in the various machine, electronics and glass shops. I particularly thank Kathy Lewis for her kind and careful typing (and retyping, and retyping) of this thesis and all other manuscripts I have given her over the years.

Among my many friends both in and out of Caltech, I especially want to thank Jim and Ellen Strauss and Brian and Eileen Keelan for the fun times we shared.

Finally, and most importantly, I want to thank my family, especially my parents, for all the love and support they have given me not only during my stay at Caltech but throughout my life. Their

encouragement in good times and bad has made all this possible.

Abstract

The organometallic chemistry of the hexagonally close-packed Ru(001) surface has been studied using electron energy loss spectroscopy and thermal desorption mass spectrometry. The molecules that have been studied are acetylene, formamide and ammonia. The chemistry of acetylene and formamide has also been investigated in the presence of coadsorbed hydrogen and oxygen adatoms.

Acetylene is adsorbed molecularly on Ru(001) below approximately 230 K, with rehybridization of the molecule to nearly sp^3 occurring. The principal decomposition products at higher temperatures are ethylidyne (CCH_3) and acetylide (CCH) between 230 and 350 K, and methylidyne (CH) and surface carbon at higher temperatures. Some methylidyne is stable to approximately 700 K. The preadsorption of hydrogen does not alter the decomposition products of acetylene, but reduces the saturation coverage and also leads to the formation of a small amount of ethylene (via an η^2-$CHCH_2$ species) which desorbs molecularly near 175 K. Preadsorbed oxygen also reduces the saturation coverage of acetylene but has virtually no effect on the nature of the molecularly chemisorbed acetylene. It does, however, lead to the formation of an sp^2-hybridized vinylidene (CCH_2) species in the decomposition of acetylene, in addition to the decomposition products that are formed on the clean surface. There is no molecular desorption of chemisorbed acetylene from clean Ru(001), hydrogen-presaturated Ru(001), or oxygen-presaturated Ru(001).

The adsorption and decomposition of formamide has been studied on clean Ru(001), hydrogen-presaturated Ru(001), and Ru(001)-p(1x2)-O (oxygen adatom coverage = 0.5). On clean Ru(001), the adsorption of low coverages of formamide at 80 K results in CH bond cleavage and rehybridization of the carbonyl double bond to produce an η^2(C,O)-NH_2CO species. This species is stable to approximately 250 K at which point it decomposes to yield a mixture of coadsorbed carbon monoxide, ammonia, an NH species and hydrogen adatoms. The decomposition of NH to hydrogen and nitrogen adatoms occurs between 350 and 400 K, and the thermal desorption products are NH_3 (~315 K), H_2 (~420 K), CO (~480 K) and N_2 (~770 K). At higher formamide coverages, some formamide is adsorbed molecularly at 80 K, leading both to molecular desorption and to the formation of a new surface intermediate between 300 and 375 K that is identified tentatively as η^1(N)-NCHO. On Ru(001)-

p(1x2)-O and hydrogen-presaturated Ru(001), formamide adsorbs molecularly at 80 K in an η^1(O)-NH_2CHO configuration. On the oxygen-precovered surface, the molecularly adsorbed formamide undergoes competing desorption and decomposition, resulting in the formation of an η^2(N,O)-NHCHO species (analogous to a bidentate formate) at approximately 265 K. This species decomposes near 420 K with the evolution of CO and H_2 into the gas phase. On the hydrogen precovered surface, the η^1(O)-NH_2CHO converts below 200 K to η^2(C,O)-NH_2CHO and η^2(C,O)-NH_2CO, with some molecular desorption occurring also at high coverage. The η^2(C,O)-bonded species decompose in a manner similar to the decomposition of η^2(C,O)-NH_2CO on the clean surface, although the formation of ammonia is not detected.

Ammonia adsorbs reversibly on Ru(001) at 80 K, with negligible dissociation occurring as the surface is annealed. The EEL spectra of ammonia on Ru(001) are very similar to those of ammonia on other metal surfaces. Off-specular EEL spectra of chemisorbed ammonia allow the ν(Ru-NH_3) and $\rho(NH_3)$ vibrational loss features to be resolved near 340 and 625 cm^{-1}, respectively. The intense $\delta_s(NH_3)$ loss feature shifts downward in frequency with increasing ammonia coverage, from approximately 1160 cm^{-1} in the low coverage limit to 1070 cm^{-1} at saturation. In coordination compounds of ammonia, the frequency of this mode shifts downward with decreasing charge on the metal atom, and its downshift on Ru(001) can be correlated with the large work function decrease that the surface has previously been shown to undergo when ammonia is adsorbed. The EELS data are consistent with ammonia adsorption in on-top sites. Second-layer and multilayer ammonia on Ru(001) have also been characterized vibrationally, and the results are similar to those obtained for other metal surfaces.

Table of Contents

CHAPTER I

Introduction

The field of organometallic surface chemistry has been developing rapidly over the past few years. The application of surface-sensitive techniques to study the chemistry of atoms and diatomic molecules on well-defined, single crystalline transition metal surfaces under ultrahigh vacuum conditions has been pursued extensively, and the chemistry of ethylene and acetylene has also received considerable attention. The primary motivation for most of this work was, and to some degree remains, the hope of gaining insight into the mechanisms of various surface catalytic reactions that are of industrial importance, such as the Fischer-Tropsch and ammonia syntheses. More recently, however, there has also been increased interest in the comparison between surface chemistry and the chemistry of organometallic compounds. Such aspects of surface and cluster chemistry as ligand bonding, ligand reactivity, and the effects of electron withdrawing or donating ligands or adsorbates on the chemical properties of the surface or cluster are of particular importance. It is this comparison between surface chemistry and organometallic cluster chemistry that provides the principal motivation for the research presented in this thesis.

The comparison between surface and cluster chemistry, particularly with regard to the identification of stable ligands, is complicated by the fact that the principal experimental techniques employed are not analogous. X-ray diffraction is by far the most important technique for analyzing the structure and bonding of ligands in organometallic compounds, but since this technique is not surface sensitive it cannot be used to identify ligands adsorbed on metal surfaces. Consequently, the most important techniques utilized to identify stable intermediates on metal surfaces have been vibrational spectroscopies. Among these, electron energy loss spectroscopy (EELS) has proven to be the most powerful and versatile (1), and more than any other experimental technique allows rather complex surface species to be identified unambiguously. This technique thus provides a solid basis for comparisons between surface and organometallic chemistry, and when infrared (IR) vibrational data are available for organometallic ligands that are closely related to those identified on a metal surface particularly incisive comparisons can be made. The research discussed herein has utilized EELS as the primary experimental technique, along with thermal desorption mass spectrometry (TDMS). The latter technique allows the identification of the ultimate gas phase decomposition products of a given molecule on a metal sur-

face.

This thesis discusses the chemistry of acetylene, formamide and ammonia on clean and chemically-modified Ru(001) surfaces. The hexagonally close-packed Ru(001) surface has been the subject of numerous previous surface science investigations, both because of the importance of ruthenium in surface catalytic processes (2) and because, due to its location in the center of the periodic table, it is reactive enough that interesting chemical reactions occur with a wide variety of molecules but not so reactive that stable intermediate species cannot be isolated and identified under the proper conditions. The preadsorption of electron withdrawing oxygen adatoms can alter the chemistry of this surface towards various molecules (3), just as electron withdrawing ligands in organometallic compounds effect the ligand bonding and reactivity that these compounds exhibit. Consequently, the effect of preadsorbed oxygen on the chemistry exhibited by acetylene and formamide on Ru(001) has been studied. The effects of preadsorbed atomic hydrogen have also been investigated, since hydrogen adatoms are a decomposition product of both of these molecules on Ru(001), and could thus influence the decomposition pathways of these molecules on this surface and lead to different intermediates than are formed on the clean surface.

The chemistry of acetylene has been studied on a number of single crystalline transition metal surfaces (4). Below approximately 200-250 K it is generally molecularly adsorbed, with substantial rehybridization of the carbon-carbon double bond to between sp^2 and sp^3 occurring. Strong similarities have been noted previously between the EEL spectra of acetylene on some metal surfaces and the IR spectra of coordinated acetylene in certain organometallic compounds (5), which has led to some tentative conclusions regarding the binding site of acetylene on these surfaces. Annealing metal surfaces with adsorbed acetylene usually leads to molecular dissociation rather than desorption, and a variety of decomposition products have been identified including ethylidyne (CCH_3), vinylidene (CCH_2), acetylide (CCH) and methylidyne (CH). These species ultimately decompose upon further annealing to yield hydrogen gas and some form of surface carbon. The studies of acetylene on Ru(001) were undertaken in order to attempt both to gain information concerning the nature of molecularly chemisorbed acetylene on this surface and to elucidate the decomposition mechanism. The coadsorption of hydrogen

and acetylene offers the possibility of forming ethylene and other more highly hydrogenated intermediates. Coadsorption experiments with atomic oxygen were undertaken primarily because oxygen has been found to alter strongly the nature of chemisorbed ethylene on several metal surfaces (6-9), from an sp^3-hybridized di-σ-bonded species to a π-bonded sp^2-hybridized species. Th coadsorption of oxygen and acetylene has received virtually no attention previously (10).

The adsorption of formamide has not been studied previously on any single crystalline metal surface. However, a large number of formamide-derived ligands are known in organometallic cluster chemistry, and in some cases IR data are available (11). Since several closely-related molecules such as formic acid (12), acetone (3), formaldehyde (13) and methylamine (14) have been studied on Ru(001), we have chosen to study the chemistry of this molecule on clean Ru(001), oxygen precovered Ru(001) and hydrogen precovered Ru(001). An issue of particular importance is to what degree the surface chemistry of formamide is dominated by either the carbonyl group or the NH_2 group. This will determine whether the surface chemistry of this molecule on Ru(001) resembles more closely that of formaldehyde or that of methylamine, or, if both the carbonyl and NH_2 groups are important, that of formic acid.

The adsorption of ammonia on Ru(001) has been the subject of several previous investigations (15-17). In contrast to acetylene and formamide, the "chemistry" of this molecule on Ru(001) is simple and was previously well understood; following adsorption at 80-100 K, the molecule simply desorbs reversibly between 150 and 350 K, with negligible dissociation occurring as the surface is heated. The purpose of this study was therefore not the identification of stable decomposition intermediates, but a thorough vibrational characterization of the molecularly adsorbed ammonia under various conditions of coverage and temperature. Since only molecular ammonia was present on the surface under all conditions studied, close attention could be paid to such physical phenomena as frequency shifts of certain vibrational modes as a function of coverage. Detailed comparisons can be made between the surface and organometallic chemistry of ammonia, since there is a large amount of IR data available for ammonia ligands in metal compounds (18).

References

1. Ibach, H. and Mills, D. L., "Electron Energy Loss Spectroscopy and Surface Vibrations", Academic Press, New York, 1982.

2. For example, see Aika, K.-I., Angew. Chem. Int. Ed. Engl. 1986, 25, 558.

3. For example, see Anton, A.B.; Avery, N.R.; Toby, B.H.; Weinberg, W.H., J. Am. Chem. Soc. 1986 108 684.

4. See Chaps. II and II, and references therein.

5. Bandy, B. J.; Chesters, M. A.; Pemble, M. E.; McDougall, G. S.; Sheppard, N., Surface Sci. 1984, 139, 87.

6. Stuve, E.M.; Madix, R.J.; Brundle, C.R., Surface Sci. 1985 152/153 532.

7. Seip, U.; Tsai, M.-C.; Küppers, J.; Ertl, G., Surface Sci. 1984, 147, 65.

8. Steininger, H.; Ibach, H.; Lehwald, S., Surface Sci. 1982, 117, 685.

9. Barteau, M. A.; Broughton, J. Q.; Menzel, D., Appl. Surface Sci. 1984, 19, 92.

10. The only previous EELS study of coadsorbed oxygen and acetylene is on a silver surface, where the acetylene is π-bonded and thus maintains its sp hybridization. Stuve, E. M.; Madix, R. J.; Sexton, B. A., Surface Sci. 1982, 123, 491.

11. See Chaps. V and VII, and references therein.

12. Toby, B. H.; Avery, N. R.; Anton, A. B.; Weinberg, W. H., J. Elec. Spec. Rel. Phen. 1983, 29, 317.

13. Anton, A.B.; Parmeter, J.E.; Weinberg, W.H., J. Am. Chem. Soc. 1986 108 1823.

14. Hills, M. M., PhD Thesis, California Institute of Technology, 1986.

15. Danielson, L.R.; Dresser, M.J.; Donaldson, E.E.; Dickinson, J.T., Surface Sci. 71,599 (1978).

16. Danielson, L.R.; Dresser, M.J.; Donaldson, E.E.; Sandstrom, D.R., Surface Sci. 1978, 71, 615.

17. Benndorf, C.; Madey, T.E., Surface Sci. 1983, 135, 164.

18. Nakamoto, K., in "Infrared and Raman Spectra of Inorganic and Coordination Compounds", Third Edition, Wiley & Sons, New York, 1978, 197-202.

CHAPTER II

The Interaction of Acetylene with the Ru(001) Surface

[This chapter was published as a paper by J. E. Parmeter, M. M. Hills and W. H. Weinberg, in *The Journal of the American Chemical Society* 1986, 108, 3563.]

Reprinted from the Journal of the American Chemical Society, 1986, *108*, 3563.

Interaction of Acetylene with the Ru(001) Surface

J. E. Parmeter,† M. M. Hills, and W. H. Weinberg*

Contribution from the Division of Chemistry and Chemical Engineering, California Institute of Technology, Pasadena, California 91125. *Received October 8, 1985*

Abstract: The adsorption and decomposition of acetylene on the hexagonally close-packed Ru(001) surface has been studied by using high-resolution electron energy loss spectroscopy and thermal desorption mass spectrometry. Below 230 K, acetylene is molecularly adsorbed on this surface with rehybridization of the acetylenic carbon atoms to nearly sp^3 occurring. Between 230 and 250 K, the acetylene undergoes both dehydrogenation and hydrogenation reactions, resulting in the formation of two stable surface intermediates, ethylidyne (CCH_3) and acetylide (CCH). Both the ethylidyne and the acetylide decompose near 350 K, accompanied by hydrogen desorption and leaving only methylidyne (CH) and carbon adatoms on the surface. The methylidyne decomposes with hydrogen evolution into the gas phase between approximately 480 and 700 K.

I. Introduction

The interaction of unsaturated hydrocarbon molecules with a variety of low Miller index single-crystalline transition-metal surfaces has been the focus of much research in surface science recently.[1] These studies are of obvious importance both in quantifying the relationships between the bonding of hydrocarbon ligands to multinuclear homogeneous complexes and their bonding to surfaces and in view of the role that such hydrocarbons play in industrial, heterogeneous catalytic processes. The application of modern, sophisticated experimental techniques to the study of hydrocarbon adsorption and decomposition on metals has led to the identification of a number of surface species which may act as intermediates in these catalytic surface reactions and which have been observed in organometallic cluster compounds. Perhaps the most useful technique in understanding the structure and bonding of adsorbates on metal surfaces has been vibrationally inelastic electron scattering which is usually termed high-resolution electron energy loss spectroscopy (EELS), especially when employed in combination with thermal desorption mass spectrometry (TDMS). Recently, the results of two different EELS and TDMS studies of ethylene adsorption on the hexagonally close-packed Ru(001) surface have been reported.[2,3] As a natural extension of this work, we report here a similar investigation of the adsorption and decomposition of acetylene on Ru(001).

Acetylene adsorption has been studied previously with EELS on a wide variety of metal surfaces, including Cu(111),[4] Cu(100),[5] Cu(110),[5] Ag(110),[6] Ni(111),[7] Ni(110),[8] Pd(111),[8,9] Pd(100),[9,10] Pd(110),[4] Pt(111),[11] Rh(111),[12] Fe(110),[13] Fe(111),[14] W(110),[15] W(111),[16] and W(100).[17] With the exception of the Ag(110) surface, on which the adsorption is weak and reversible below 160 K, acetylene is adsorbed molecularly, but with the molecule *strongly* distorted from its gas-phase structure, in all the cases where adsorption below 200 K has been reported. Typically, the molecularly adsorbed acetylene is stable at temperatures below approximately 250–350 K. The single most important spectroscopic indication of the degree of rehybridization of molecular acetylene upon adsorption is the carbon–carbon stretching frequency, which is 1974 cm^{-1} in gas-phase acetylene.[18] However, a large number of metal surfaces, including Cu(111), Cu(100), Cu(110), Pd(111), Pd(110), Ni(110), and Pt(111), on which acetylene is adsorbed molecularly, exhibit carbon–carbon stretching frequencies in the 1300–1400-cm^{-1} range, indicative of a rehybridization of the carbon atoms to between sp^2 and sp^3 and an approximate carbon–carbon bond order of 1.5. On other surfaces, even more extensive rehybridization of the acetylene molecule occurs, resulting in still lower carbon–carbon stretching frequencies. These surfaces include Fe(110) (ν_{CC} = 1240 cm^{-1}), Ni(111) (ν_{CC} = 1220 cm^{-1}), Pd(100) (ν_{CC} = 1210 cm^{-1}), and Fe(111) (ν_{CC} = 1145 cm^{-1}). Further insight into the degree of distortion that the molecule experiences upon adsorption is given by the reduction of the carbon–hydrogen stretching frequencies in going from the gas phase to the chemisorbed phase. Finally, the relative intensities of the carbon–hydrogen bending and carbon–carbon stretching modes may serve to delimit the geometry and the binding site of the adsorbed species.[4] It is both to investigate these issues and to quantify the connection with ethylene adsorption that we have undertaken this study of acetylene adsorption on Ru(001).

The mechanism by which molecularly adsorbed acetylene decomposes on metal surfaces is also of great interest. The initial dissociation step may be either carbon–carbon bond cleavage to produce methylidyne (CH) or carbon–hydrogen bond cleavage and formation which may result in a number of different adsorbed hydrocarbon intermediates. Initial cleavage of the carbon–carbon bond has been reported on Ni(111) at 400 K[7] and on Fe(110) at approximately 320 K[13] to form surface methylidyne. Initial cleavage of carbon–hydrogen bonds occurs on the Pt(111), Pd(100), and Pd(111) surfaces. On Pt(111), formation of a CCH_2 species via hydrogen transfer has been proposed as the initial step in acetylene decomposition.[11] On Pd(100), a hydrogen atom is abstracted from the molecularly adsorbed species by the surface between 300 and 450 K, resulting in the formation of an acetylide (CCH).[9] The Pd(111) surface exhibits interesting and complex behavior, with the formation of both acetylide and ethylidyne (CCH_3) above 300 K.[9] These species dehydrogenate thermally at higher temperatures, possibly via methylidyne intermediates. In view of the recent identification of both ethylidyne and methylidyne as decomposition products of ethylene on Ru(001),[2,3] a similar study of the decomposition of acetylene on this surface is of obvious importance.

In this paper, we first discuss thermal desorption measurements

† AT&T Bell Laboratories predoctoral fellow.

(1) For example, see: Muetterties, E. L.; Rhodin, T. N.; Band, E.; Brucker, G. F.; Pretzer, W. R. *Chem. Rev.* **1979**, *79*, 91.
(2) Bartess, M. A.; Broughton, J. Q.; Menzel, D. *Appl. Surf. Sci.* **1984**, *19*, 92.
(3) Hills, M. M.; Parmeter, J. E.; Mullins, C. B.; Weinberg, W. H. *J. Am. Chem. Soc.*, preceding paper in this issue.
(4) Bandy, B. J.; Chesters, M. A.; Pemble, M. E.; McDougall, G. S.; Sheppard, N. *Surf. Sci.* **1984**, *139*, 87.
(5) Avery, N. R., unpublished results.
(6) Stuve, E. M.; Madix, R. J.; Sexton, B. A. *Surf. Sci.* **1982**, *123*, 491.
(7) (a) Lehwald, S.; Ibach, H. *Surf. Sci.* **1979**, *89*, 425. (b) Ibach, H.; Lehwald, S. *J. Vacuum Sci. Technol.* **1981**, *18*, 625.
(8) Gates, J. A.; Kesmodel, L. L. *J. Chem. Phys.* **1982**, *76*, 4281.
(9) Kesmodel, L. L.; Waddill, G. D.; Gates, J. A. *Surf. Sci.* **1984**, *138*, 464.
(10) Kesmodel, L. L. *J. Chem. Phys.* **1983**, *79*, 4646.
(11) Ibach, H.; Lehwald, S. *J. Vacuum Sci. Technol.* **1978**, *15*, 407.
(12) Dubois, L. H.; Castner, D. J.; Somorjai, G. A. *J. Chem. Phys.* **1980**, *72*, 5234.
(13) Erley, W.; Baro, A. M.; Ibach, H. *Surf. Sci.* **1982**, *120*, 273.
(14) Sesp, U.; Tsai, M.-C.; Küppers, J.; Ertl, G. *Surf. Sci.* **1984**, *147*, 65.
(15) Backx, C.; Willis, R. F.; Feuerbacher, B.; Fitton, B. *Surf. Sci.* **1977**, *68*, 516.
(16) Backx, C.; Feuerbacher, B.; Fitton, B.; Willis, R. F. *Surf. Sci.* **1977**, *63*, 193.
(17) Hamilton, J. C.; Swanson, N.; Waclawski, B. J.; Celotta, R. J. *J. Chem. Phys.* **1981**, *74*, 4156.
(18) Herzberg, G. *Infrared and Raman Spectra of Polyatomic Molecules*; Van Nostrand: New York, 1945.

0002-7863/86/1508-3563$01.50/0

after acetylene adsorption on Ru(001) and then EEL spectra of both multilayer and chemisorbed molecular acetylene on this surface. The EEL spectra provide evidence for a highly distorted, nearly sp^3-hybridized, molecularly adsorbed acetylene in the chemisorbed overlayer at temperatures below approximately 230 K. We then turn to a discussion of the thermal decomposition of acetylene, which leads to the formation of both acetylide and ethylidyne between approximately 230 and 350 K. These species decompose below 400 K to yield methylidyne and surface carbon.

II. Experimental Procedures

The EEL spectrometer used in these studies, as well as the ultra-high-vacuum (UHV) chamber in which it is contained, has been described in detail elsewhere.[19] Briefly, the stainless steel UHV chamber is pumped by a 220 L/s Varian ion pump and a titanium sublimation pump, and base pressures below 5×10^{-11} torr are obtained routinely. The home-built EEL spectrometer is of the Kuyatt-Simpson type, with 180° hemispherical deflectors serving as the energy dispersing elements in both the monochromator and the analyzer. The monochromator is spatially fixed, but the analyzer is rotatable to allow off-specular spectra to be measured. All spectra presented and referred to in this paper were collected in the specular direction unless otherwise noted. The impact energy of the incident electron beam was approximately 4 eV in all cases, and the beam was incident on the Ru(001) crystal at an angle of 60° with respect to the surface normal. The instrumental energy resolution in these studies, defined as the full-width at half-maximum of the elastically scattered beam, varied from 60 to 80 cm^{-1}, while count rates in the elastic peak varied from 1.5×10^4 to 3×10^5 cps.

The Ru(001) crystal was cooled by using liquid nitrogen, and temperatures as low as 80 K were obtained routinely. Crystal cleaning was achieved by using the well-established techniques of argon ion sputtering and heating the crystal in a background of oxygen.[20] The cleanliness of the surface was verified with EELS. Some of the EEL spectra presented in section III show a small amount of CO contamination (below 1–2% of a monolayer) due to adsorption from the background. Not surprisingly, it was found that these varying and low concentrations of coadsorbed CO did not affect the EEL spectra of acetylene and its decomposition products.

Thermal desorption mass spectrometry was performed in a separate UHV chamber also containing a Ru(001) crystal and equipped with a quadrupole mass spectrometer (UTI 100C) with a skimmer to discriminate between desorption from the crystal surface and desorption from the crystal edges and support leads, as well as an Auger electron spectrometer for verifying surface cleanliness. Heating rates between 5 and 20 K/s were used in the TDMS experiments. Crystal cooling and cleaning were accomplished as in the EELS chamber.

The C_2H_2 used in these studies was obtained from an industrial acetylene tank (95% purity) and was purified as it was introduced into a glass flask by passage through a dry ice/methanol slurry. The main purpose of this procedure was to remove acetone, which is always added to prevent explosions when acetylene is stored under high pressures. The C_2D_2 (99 atom % deuterated) was obtained from MSD Isotopes. The stainless steel leak lines through which the acetylene was introduced into the UHV chamber were flushed several times with C_2H_2 or C_2D_2, in order to passivate them toward acetylene decomposition, before any acetylene was introduced into the UHV chamber. Mass spectra of the C_2D_2 and C_2H_2 which were admitted into the UHV chamber showed no traces of any impurities. Multilayer EEL spectra also showed no detectable impurities.

III. Results and Discussion

A. Thermal Desorption Mass Spectrometry. Thermal desorption measurements after acetylene adsorption on Ru(001) at 80 K were performed for acetylene exposures in the range of 0.2–10 langmuir (1 langmuir = 10^{-6} torr s). The only desorption products detected in the temperature range between 80 and 800 K were molecular acetylene and hydrogen. Benzene, ethylene, ethane, and methane were specifically looked for and were not detected under any circumstances.

Molecular acetylene desorbs only in a sharp peak at 95 K. Since this peak appears only for acetylene exposures greater than 5 langmuir and does not saturate for increasing exposures above 5 langmuir, it may be assigned unambiguously as the desorption of a multilayer state. *No* molecular acetylene desorbs from the chemisorbed monolayer state of acetylene on the Ru(001) surface.

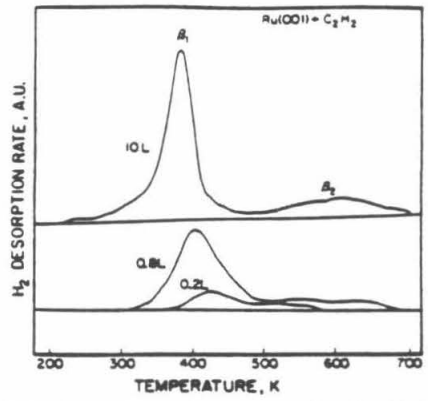

Figure 1. H_2 thermal desorption spectra resulting after the Ru(001) surface at 80 K is exposed to 0.2, 0.8, and 10 langmuir of C_2H_2. The heating rate used in recording these spectra is approximately 20 K s^{-1}.

The hydrogen thermal desorption spectra that result after 0.2-, 0.8-, and 10-langmuir acetylene exposures on Ru(001) at 80 K are shown in Figure 1. The 0.2- and 0.8-langmuir exposures correspond, respectively, to approximately 20% and 70% of saturation acetylene coverage, and the 10-langmuir exposure, as the results discussed above suggest, is more than sufficient to saturate the monolayer. Indeed, hydrogen thermal desorption spectra are identical for all acetylene exposures greater than 5 langmuir, confirming that a 5-langmuir exposure corresponds to saturation coverage of chemisorbed acetylene on Ru(001) and that the hydrogen thermal desorption features shown in Figure 1 correspond to the decomposition of these chemisorbed species. The spectra in Figure 1 reveal two main desorption features, a low-temperature (β_1) peak and a broad, high-temperature (β_2) peak. The β_1 peak is centered at 425 K for a 0.2-langmuir acetylene exposure and shifts downward to 380 K for saturation acetylene exposures. This behavior is characteristic of second-order desorption kinetics. The β_2 peak is quite broad, extending from about 480 to 580 K for 0.2-langmuir acetylene exposures and from 480 to 700 K for saturation exposures.

As will be shown from the EELS results, the only hydrocarbon species resulting from acetylene decomposition on Ru(001) above 400 K is methylidyne. Thus, the high-temperature β_2 desorption peak of hydrogen results from methylidyne decomposition to yield carbon adatoms and H_2(g). The β_1 desorption peak of hydrogen results from surface hydrogen that is formed from the dehydrogenation of ethylidyne (and to a lesser degree from acetylene decomposition to acetylide), as will be discussed later. For initial acetylene exposures of 0.4 langmuir or more, the ratio of the β_1-to-β_2 peak areas is 3:1 within experimental error, indicating that one-fourth of the hydrogen initially present in the chemisorbed acetylene is eventually present in methylidyne. For 0.2-langmuir acetylene exposures, the ratio of the β_1-to-β_2 peak areas is more difficult to determine due to peak overlap, but it is approximately 2:1, indicating that one-third of the hydrogen atoms initially present in the acetylene are eventually present in methylidyne. Thus, relatively more methylidyne is formed for low initial acetylene exposures.

Since neither monolayer acetylene nor other hydrocarbons desorb molecularly from Ru(001), all of the chemisorbed acetylene decomposes on the surface to yield eventually H_2(g) and carbon adatoms. Thus, there is a one-to-one correspondence between the amount of acetylene adsorbed in the monolayer and the total amount of hydrogen desorbing in the β_1 and β_2 thermal desorption peaks. Consequently, the total amount of hydrogen desorbing following an acetylene exposure may be compared to the amount of hydrogen desorbing from the clean Ru(001) surface following a saturation exposure to H_2,[21] and this may be used to calculate

(19) Thomas, G. E.; Weinberg, W. H. *Rev. Sci. Instrum.* **1979**, *50*, 497.
(20) Thomas, G. E.; Weinberg, W. H. *J. Chem. Phys.* **1979**, *70*, 954.

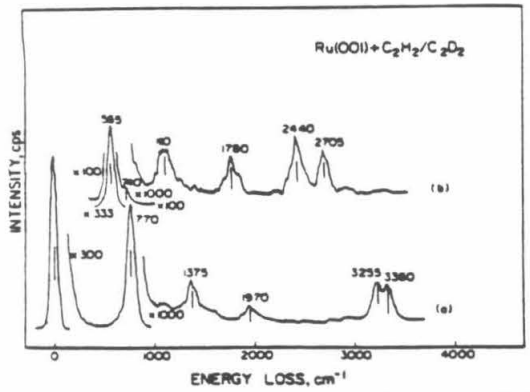

Figure 2. EEL spectra that result from 10-langmuir exposures of (a) C_2H_2 and (b) C_2D_2 to the Ru(001) suface at 80 K. These spectra are characteristic of condensed acetylene multilayers.

Table I. Vibrational Frequencies (cm^{-1}) for C_2H_2 and C_2D_2 in Gas and Crystalline Phases and for C_2H_2 and C_2D_2 Multilayers on Ru(001) at 80 K

mode	gas[18]	crystalline IR[22a]	multilayers on Ru(001)
	C_2H_2		
CH s bend (ν_4)	612		605[b]
CH a bend (ν_5)	729	761, 769	770
CC stretch (ν_2)	1974		1970
CH a stretch (ν_3)	3287	3226	3255
CH s stretch (ν_1)	3374		3360
	C_2D_2		
CD s bend (ν_4)	505		545[b]
CD a bend (ν_5)	539	562, 568	565
CC stretch (ν_2)	1762		1780
CD a stretch (ν_3)	2439	2393	2440
CD s stretch (ν_1)	2701		2705

[a] Crystalline IR data at 63 K. [b] Estimated from frequency of $\nu_4 + \nu_5$ combination band. s = symmetric, a = asymmetric.

the acetylene coverage. This yields a saturation fractional coverage of approximately 0.27 for acetylene adsorption on Ru(001).

B. Electron Energy Loss Spectroscopy. 1. Multilayer State. As indicated above, exposing the Ru(001) surface at 80 K to approximately 5 langmuir or more of C_2H_2 or C_2D_2 results in the condensation of molecular multilayers of acetylene on the surface. The EEL spectra of C_2H_2 and C_2D_2 multilayers on the Ru(001) surface are shown in Figure 2, and the observed vibrational frequencies are listed in Table I, together with data for both gas-phase and crystalline acetylene. These multilayer spectra are useful as a supplement to TDMS data, both in verifying the purity of the acetylene used in these experiments and in determining when saturation coverage of chemisorbed acetylene is obtained. For both C_2H_2 and C_2D_2, all fundamental modes are clearly resolved except ν_4, the Raman-active carbon–hydrogen symmetric bending mode, which is obscured by the intense, IR-active asymmetric bending mode, ν_5. As in the case of gas-phase IR spectra of acetylene,[18] the frequency of the ν_4 mode may be estimated from the observed $\nu_5 + \nu_4$ combination band, which occurs at 1375 cm^{-1} for C_2H_2 multilayers and 1110 cm^{-1} for C_2D_2 multilayers. Not surprisingly, the IR-active modes of the acetylene multilayers are close in frequency to both those of crystalline acetylene[22] and those of gas-phase acetylene.[18] The feature near 740 cm^{-1} in Figure 2b is probably due to a small amount of C_2H_2 in the deuterated acetylene. This impurity is on the order of 1% or less.

2. Molecularly Chemisorbed Acetylene. Annealing the Ru(001) surface on which acetylene multilayers are present to above 95 K, or exposing the Ru(001) surface to less than 5 langmuir of acetylene at 80 K, results in the formation of a surface species which is stable to approximately 230 K. This chemisorbed species is identified easily as molecularly adsorbed acetylene which has undergone extensive rehybridization upon adsorption. The observed vibrational modes for C_2H_2 and C_2D_2 are listed together with their assignments in Table II, and the relevant EEL spectra are presented in Figure 3. For comparison, the vibrational data for acetylene in two organometallic cobalt compounds are listed also in Table II. These data will be discussed below in relation to possible bonding geometries for acetylene on Ru(001).

Table II. Vibrational Modes of Molecularly Adsorbed Acetylene on Ru(001) in the Temperature Range 80–230 K, with Corresponding Frequencies from the Cobalt Compounds $Co_2(CO)_6(C_2H_2)$[24] and $Co_4(CO)_{10}(C_2H_2)$[25] Presented for Comparison. All Frequencies Are Reported in cm^{-1}

	Ru(001)				
mode[a]	C_2H_2	C_2D_2	$\nu(C_2H_2)/\nu(C_2D_2)$	$Co_2(CO)_6$-(C_2H_2)	$Co_4(CO)_{10}$-(C_2H_2)
CH a stretch				3116	3020
	2940	2210	1.33		
CH s stretch				3086	2993
CC stretch	1135	1085	1.05	1403	1199
CH bend	980	715	1.37	894	983, 1120
CH bend	765	585	1.35	768	837, 922
MC a stretch	520	obscured		605	619
MC s stretch	375	350	1.07	551	?

[a] s = symmetric, a = asymmetric.

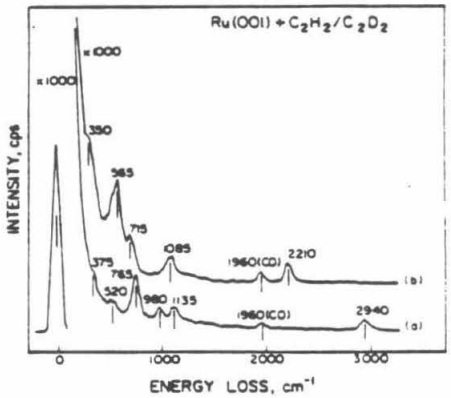

Figure 3. EEL spectra that result when the Ru(001) surface at 80 K is exposed to 5 langmuir of (a) C_2H_2 and (b) C_2D_2 and heated to 150 K. The spectra were recorded at 80 K. These spectra are characteristic of chemisorbed acetylene.

The mode assignments follow in a straightforward fashion from a comparison of the spectra of hydrogenated and deuterated acetylene. The loss feature at 2940 (2210) cm^{-1} for C_2H_2 (C_2D_2) is clearly due to a carbon–hydrogen (carbon–deuterium) stretching vibration. In both cases, the symmetric and asymmetric stretching modes are not resolved. The intense mode at 765 cm^{-1}, which shifts down to 565 cm^{-1} upon deuteration, is assigned to a carbon–hydrogen bending mode, as is the less intense mode which shifts from 980 to 715 cm^{-1} upon deuteration. The feature which appears at 1135 cm^{-1} in the C_2H_2 spectrum and at 1085 cm^{-1} in the C_2D_2 spectrum clearly does not shift sufficiently to be a hydrogenic mode and is thus assigned as the carbon–carbon stretching vibration. Modes at 520 and 375 cm^{-1} in the C_2H_2 spectrum are assigned, respectively, to the asymmetric and symmetric metal–carbon stretching modes of adsorbed acetylene. The latter mode occurs at 350 cm^{-1} for C_2D_2, while the asymmetric metal–carbon stretch in the deuterated species is obscured by the carbon–deuterium bending mode that is centered at 565 cm^{-1}. There is no other set of mode assignments that consistently ac-

(21) Shimizu, H.; Christmann, K.; Ertl, G. *J. Catal.* **1980**, *61*, 412.
(22) Glocker, G.; Morrell, C. E. *J. Chem. Phys.* **1936**, *4*, 15.

counts for the observed spectra.

Off-specular EEL spectra indicate that the carbon–carbon stretching vibration at 1135 cm^{-1} in C_2H_2 and the carbon–hydrogen bending vibration at 765 cm^{-1} are principally dipolar excited modes, while the carbon–hydrogen stretching vibration at 2940 cm^{-1} and the carbon–hydrogen bend at 980 cm^{-1} are excited primarily by nondipolar mechanisms.[23] These data suggest that the carbon–hydrogen bend at 765 cm^{-1} involves motion of the hydrogen atoms largely perpendicular to the surface, while the carbon–hydrogen bend at 980 cm^{-1} involves motion of the hydrogen atoms largely parallel to the surface. However, without detailed knowledge of the surface binding site of chemisorbed acetylene, assignment of these bending modes as "in-plane" or "out-of-plane" is not possible. No additional vibrational modes are observed in off-specular spectra.

The observed carbon–carbon stretching frequency of 1135 cm^{-1} for chemisorbed C_2H_2 corresponds to a carbon–carbon bond order nearly equal to one, with the carbon atoms being nearly sp^3 hybridized. This may be seen by comparison to the gas-phase carbon–carbon stretching frequencies of ethane (ν_{CC} = 995 cm^{-1}) and ethylene (ν_{CC} = 1623 cm^{-1}).[18] Although this is the lowest carbon–carbon stretching frequency which has heretofore been observed for chemisorbed acetylene on any transition-metal surface, it is quite close to the value of 1145 cm^{-1} which has been observed for C_2H_2 on Fe(111).[14] The carbon–hydrogen stretching frequency of 2940 cm^{-1} is also consistent with carbon atoms that are nearly sp^3 hybridized; typical values for ν_{CH} are 2800–3000 cm^{-1} for sp^3-hybridized carbon atoms and 2950–3100 cm^{-1} for sp^2 hybridized carbon atoms.[18]

A comparison of the carbon–carbon stretching frequency of 1135 cm^{-1} for acetylene chemisorbed on Ru(001) to the carbon–carbon stretching frequencies of the acetylene ligands in the cobalt compounds listed in Table II suggests that such a low value of ν_{CC} is not at all unreasonable for acetylene adsorbed on a metal surface. The decrease in frequency of 204 cm^{-1}, from ν_{CC} = 1403 to 1199 cm^{-1}, in going from a two-cobalt atom cluster to a four-cobalt atom cluster suggests that a further decrease in ν_{CC} might be expected as the metal "cluster" becomes infinitely large (i.e., a metal surface). This should be especially true of the surfaces of the relatively more reactive iron group metals, as opposed to surfaces of the nickel–palladium–platinum triad on which acetylene adsorption has been studied more extensively.

Based on the EELS data alone, any conclusions regarding the nature of the adsorption site for acetylene on Ru(001) must be somewhat speculative. It has been suggested[4] that adsorbed C_2H_2 species exhibiting strong carbon–hydrogen bending modes in the 670–770-cm^{-1} region, together with relatively weak carbon–carbon stretching modes, are the result of a "di-σ + π"-bonding structure in which the plane of a cis M—CH=CH—M complex is tilted significantly with respect to the surface normal through the interaction of the C=C bond with a third metal atom. Such a model accounts successfully for the dipolar enhancement of the intense carbon–hydrogen bending mode in these surface complexes, assigned as the γ_{CH} out-of-plane bend. Such species occur when acetylene is adsorbed on Ni(110), Pd(111), Pd(110), Rh(111), and Pt(111). However, on all of these surfaces, the adsorbed acetylene is characterized by a carbon–carbon stretching frequency between 1300 and 1400 cm^{-1}. Consequently, it is not clear that the same structure should apply to C_2H_2 on Ru(001). Indeed, the low carbon–carbon stretching frequency of 1135 cm^{-1} argues against any model which invokes π-bonding between the carbon–carbon bond and the surface. Possible alternative bonding geometries are suggested by the organometallic compounds listed in Table II. In the compound $Co_2(CO)_6(C_2H_2)$,[24] the plane containing the C_2H_2 group bisects the cobalt–cobalt vector and is perpendicular to it. A similar bonding configuration could be obtained for acetylene on Ru(001) if the carbon atoms of acetylene occupy adjacent, inequivalent threefold hollow sites on the surface (Figure 4a). Since these adjacent adsites are separated by 1.56 Å on this surface,[25] slightly farther apart than the length of a carbon–carbon single bond in a hydrocarbon molecule (1.54 Å), it is probable that the carbon atoms would not be centered directly above the threefold sites if such a bonding geometry were to occur. In the compound $Co_4(CO)_{10}(C_2H_2)$,[26] the carbon–carbon bond of the acetylene ligand lies parallel to a cobalt–cobalt bond, with each carbon atom being σ-bonded to one of these two cobalt atoms and with a four-centered, μ-type bond between the carbon atoms and the remaining two cobalt atoms. An analogous bonding situation on Ru(001) would be achieved if the two carbon atoms of the acetylene are σ-bonded to nearest-neighbor ruthenium atoms and with a four-centered bond between the carbon atoms and the two ruthenium atoms on either side of this carbon–carbon bond (Figure 4b). It should be emphasized that the observation of a dipolar-enhanced carbon–carbon stretching mode in specular EEL spectra does not rule out such bonding models in which the carbon–carbon bond lies very nearly parallel to the surface, since charge coupling between the adsorbed acetylene and the metal may result in a substantial dynamic dipole being associated with the ν_{CC} vibration.[27]

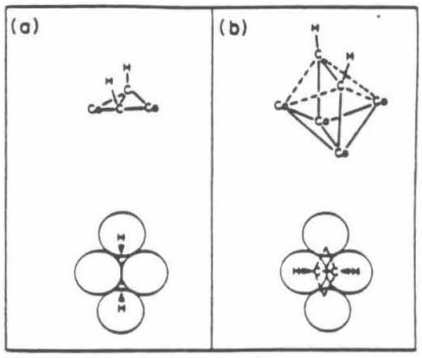

Figure 4. (a) Metal–acetylene structure of the organometallic compound $Co_2(CO)_6(C_2H_2)$,[24] and an analogous bonding configuration for acetylene on the Ru(001) surface. (b) Metal–acetylene structure of the organometallic compound $Co_4(CO)_{10}(C_2H_2)$,[26a] and an analogous bonding configuration for acetylene on the Ru(001) surface.

In summary, molecularly adsorbed acetylene on Ru(001) exhibits vibrational frequencies characteristic of essentially a carbon–carbon single bond and sp^3-hybridized carbon atoms. Although we have discussed two *possible* bonding configurations based on a comparison with organometallic cobalt complexes, we stress that this is speculative and feel that additional studies of the vibrational spectra of acetylene in cluster compounds and additional measurements with other surface-sensitive techniques are necessary before firm conclusions concerning the nature of the binding site on Ru(001) may be drawn.

3. Thermal Decomposition of Chemisorbed Acetylene. When the Ru(001) surface is heated with molecularly chemisorbed acetylene to temperatures in the range of 250–350 K, marked changes occur in the EEL spectra. Figure 5a shows the EEL spectrum that results when the surface represented in Figure 3a of adsorbed C_2H_2 is annealed to 300 K. The most obvious changes are the disappearance of the carbon–hydrogen bending mode of molecularly adsorbed acetylene at 980 cm^{-1} and the appearance of a new mode at 1360 cm^{-1}, which is comparable in intensity to the mode at 1140 cm^{-1}. In addition, the strong carbon–hydrogen bending mode which occurs at 765 cm^{-1} for molecularly adsorbed

(23) For a discussion of EELS scattering mechanisms, see: Ibach, H.; Mills, D. L. *Electron Energy Loss Spectroscopy and Surface Vibrations*; Academic: New York, 1982.

(24) Iwashita, Y.; Tamura, F.; Nakamura, A. *Inorg. Chem.* **1969**, *8*, 1179.

(25) This distance is calculated easily from the nearest-neighbor separation of 2.71 Å in bulk ruthenium; see: Kittel, C. *Introduction to Solid State Physics*; 5th ed.; Wiley: New York, 1976.

(26) Gervasio, G.; Rossetti, R.; Stanghellini, P. L. *Organometallics* **1985**, *4*, 1612.

(27) Reference 23, pp 171–172.

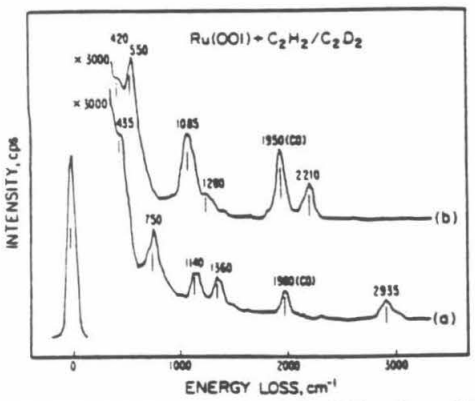

Figure 5. EEL spectra that result when the Ru(001) surface at 80 K is exposed to 5 langmuir of (a) C_2H_2 and (b) C_2D_2 and heated to 300 K. These spectra were recorded at 80 K and show the characteristic features of acetylide and ethylidyne.

acetylene shifts down slightly (~15 cm^{-1}) in frequency. Finally, the metal–carbon stretching modes of adsorbed acetylene at 375 and 520 cm^{-1} are no longer present but are replaced by a new mode at 435 cm^{-1}.

Spectra of deuterated acetylene on Ru(001) which has been annealed to 300 K (Figure 5b) show similar changes. The intense carbon–deuterium bend of molecularly adsorbed C_2D_2 shifts downward slightly from 565 to 550 cm^{-1}, the carbon–deuterium bend at 715 cm^{-1} is greatly reduced in intensity or completely absent, and a new mode appears at 420 cm^{-1}. In addition, a relatively broad feature appears between 1080 and 1120 cm^{-1}, and a weaker feature appears at 1260 cm^{-1}.

These observed changes that occur in the EEL spectra when the surface is annealed to temperatures above 250 K might be accounted for in two different ways. One possibility is that acetylene remains molecularly chemisorbed on the surface under these conditions but has undergone a change in molecular orientation or adsorption site such that the observed spectral changes result. The second possibility is that a surface reaction has taken place, resulting in the formation of one or more new surface species. The first of these two possibilities is most unlikely in view of the previously discussed thermal desorption spectra. The fact that the low temperature tail of the β_1 hydrogen thermal desorption peak extends to below 250 K for saturation acetylene coverages indicates that some carbon–hydrogen bond cleavage has occurred by this temperature. Furthermore, attempting to rationalize the EEL spectra observed after heating to 300 K in terms of molecularly adsorbed acetylene would require assigning the 1360-cm^{-1} peak in the C_2H_2 spectra to a carbon–hydrogen bending mode, which is inconsistent with all existing vibrational data for acetylene adsorbed on surfaces or as a ligand in organometallic compounds.[28] In addition, the bands at 1140 and 1360 cm^{-1} in Figure 5a disappear at a slightly lower temperature than the band at 750 cm^{-1}. Hence, these two modes cannot be assigned as belonging to the same surface species that gives rise to the 750-cm^{-1} mode. *The possibility that the EEL spectra in Figure 5 correspond to some altered form of molecularly chemisorbed acetylene may therefore be ruled out unambiguously.*

Consequently, it must be concluded that the EEL spectra shown in Figure 5 are characteristic of at least two different reaction products that result from the thermally activated decomposition of acetylene on Ru(001). Indeed, the observed vibrational modes may be explained easily in terms of two species, namely acetylide and ethylidyne. Mode assignments for both species are listed in Table III. Ethylidyne has previously been isolated and identified as a product of ethylene decomposition on Ru(001),[2,3] and modes of approximately equal intensity at 1140 cm^{-1} (carbon–carbon stretch) and 1360 cm^{-1} [$\delta_s(CH_3)$] are characteristic of this species. To confirm further the identity of this species, off-specular EEL spectra were measured which showed additional vibrational modes at 990 cm^{-1} [$\rho(CH_3)$] and 1440 cm^{-1} [$\delta_s(CH_3)$], as is the case for ethylidyne formed by ethylene decomposition. The remaining vibrational modes in Figure 5 may be assigned to the acetylide species. The 750-cm^{-1} mode is a carbon–hydrogen bend, and the 435-cm^{-1} mode is a metal–carbon stretch. The latter is far too intense to be attributed solely to the metal–carbon stretch of coadsorbed CO, and since a mode of this intensity was not observed in the case of ethylidyne formed from ethylene on Ru(001), we attribute it mainly to the acetylide species. It is possible, however, that the symmetric metal–carbon stretch of ethylidyne, which occurs at 480 cm^{-1} for ethylidyne formed from ethylene decomposition,[3] also contributes to the intensity of this mode. As may be seen in Table III, deuterated spectra are consistent with these assignments. The feature at 1085 cm^{-1} in the C_2D_2 spectrum is due to the overlap of the carbon–carbon stretch and the $\delta_s(CD_3)$ mode of deuterated ethylidyne. In addition, the weak mode which appears at 1260 cm^{-1} in the deuterated spectra may be assigned to the carbon–carbon stretch of the acetylide. This frequency is too high to be due to any sort of carbon–deuterium vibration, since no modes (except the carbon–hydrogen stretch) appear above 1360 cm^{-1} in the specular spectra of acetylide and ethylidyne. The corresponding mode for acetylide is expected to be upshifted slightly (it appears at 1290 cm^{-1} for acetylide formed from ethylene decomposition) and is thus obscured by the $\delta_s(CH_3)$ mode of ethylidyne. Finally, it should be noted that the carbon–hydrogen (carbon–deuterium) stretching frequencies of the acetylide and the ethylidyne are not well resolved and therefore must be at approximately the same frequency.

Since ethylidyne has a larger hydrogen-to-carbon atom ratio than acetylene, it is obvious that not all of the molecularly adsorbed acetylene on Ru(001) may be converted to ethylidyne when the surface is heated. This is consistent with the observation that ethylidyne is formed only when acetylide is formed simultaneously. Thus, the *overall* chemical conversion which results in ethylidyne formation may be written as the self-hydrogenation reaction

$$2C_2H_2(a) \rightarrow CCH(a) + CCH_3(a)$$

This is not meant to imply, however, that acetylide and ethylidyne

Table III. Vibrational Modes Observed for Ethylidyne and Acetylide Present on the Ru(001) Surface in the Temperature Range 250–350 K due to Acetylene Decomposition. All Frequencies Are Given in cm^{-1}

CCH_3 (ethylidyne)			
mode	C_2H_3	C_2D_3	$\nu(C_2H_3)/\nu(C_2D_3)$
CC stretch	1140	~1150[a]	0.98
$\delta_s(CH_3)$	1360	~1030[a]	1.30
CH stretch[b]	~2935	~2210	1.33
$\delta_s(CH_3)$[c]	1440		
$\rho(CH_3)$[c]	990	800	1.24
CCH (acetylide)			
mode	C_2H	C_2D	$\nu(C_2H)/\nu(C_2D)$
CH bend	750	550	1.36
CC stretch	obscured	1260	
CH stretch[b]	~2935	~2210	1.33
RuC stretch	435	420	1.04

[a] These two modes overlap in the deuterated spectra, and the frequencies given are best estimates based on several different spectra. [b] The CH and CD stretching modes of the acetylide and ethylidyne species are not well resolved. [c] These modes are observed mainly in off-specular spectra; they are very weak or absent in specular EEL spectra.

(28) To our knowledge, no CH bending mode above 1000 cm^{-1} has been identified previously for acetylene in an organometallic complex. The only CH bending frequency identified previously for chemisorbed acetylene which lies above 1150 cm^{-1} is one of 1415 cm^{-1} on Fe(110), a surface species for which all four possible acetylene CH bending modes were observed in specular EEL spectra.[3]

Table IV. Vibrational Frequencies (cm^{-1}) of the Carbon–Hydrogen Bending and Stretching Modes of Methylidyne in Two Organometallic Compounds and on Several Metal Surfaces

	$Co_3(\mu_3\text{-}CH)(CO)_9$[34]	$Ru_3(CO)_9H_3(\mu_3\text{-}CH)$[35]	Fe(111)[14]	Ni(111)[30]	Pd(111)[31]	Pt(111)[32]	Rh(111)[33]	Ru(001) (this work)
CH bend	850	894	795	790	762	850	770	800
CH stretch	3041	2988	3015	2980	3002	3100	3025	3010

are formed in a ratio of 1:1, since it is obvious that acetylide formation may occur without ethylidyne formation. As written, this reaction says nothing concerning the mechanism of acetylide and ethylidyne formation from acetylene, an issue of obvious fundamental importance. We have not been able to isolate spectroscopically a CCH_2 species or any other intermediate in the formation of ethylidyne under these conditions. Coadsorption experiments with acetylene and hydrogen on Ru(001) are currently in progress, which may shed light on the mechanism of acetylide and ethylidyne formation.[29]

The ethylidyne that is formed on Ru(001) has been discussed in detail in previous studies of ethylene adsorption[2,3] and, consequently, will not be considered further here. However, since we have not previously described the acetylide species in detail, a discussion of this species is in order. Very few acetylide species have been identified previously on metal surfaces. On Ag(110) with preadsorbed oxygen, an acetylide has been identified as the result of acetylene decomposition.[6] However, since the carbon atoms in this species retain an sp hybridization, as evidenced by a carbon–hydrogen stretching frequency of 3250 cm^{-1}, this species is clearly not closely related to the acetylide that is formed on Ru(001). Acetylene decomposition on Pd(100) and Pd(111),[9] however, leads to the formation of an acetylide which is very similar to the one that is observed on Ru(001), the former being characterized by an intense carbon–hydrogen bend at 750 cm^{-1}, a weak carbon–carbon stretch at 1340 cm^{-1}, and a rather weak carbon–hydrogen stretch at 3000 cm^{-1}. From these data it was suggested that the acetylide on the palladium surfaces has both carbon atoms bonded to the surface, with the carbon–carbon bond axis either parallel or slightly skewed relative to the surface plane. This is consistent with a weak carbon–carbon stretching vibration and an intense carbon–hydrogen bending vibration, in accordance with the surface dipole selection rule for EELS.[23] The same conclusions very likely apply to the acetylide on Ru(001), and the somewhat lower carbon–carbon (1260 cm^{-1} for CCD) and carbon–hydrogen (~2935 cm^{-1}) stretching frequencies on the ruthenium surface suggest a slightly lower carbon–carbon bond order than occurs in the acetylide on palladium, although in both cases the bond order is clearly between one and two. This slightly lower carbon–carbon bond order may be related to the lower decomposition temperature of acetylide on Ru(001). On this surface the acetylide has decomposed entirely by 400 K, while on Pd(100) at least some acetylide remains on the surface to 650 K. Finally, we note that it is quite reasonable that the carbon–carbon stretching frequency of adsorbed acetylide is somewhat higher than that of chemisorbed acetylene on Ru(001), since the former may have some double bond character due to the additional electron no longer involved in a carbon–hydrogen bond.

Annealing the Ru(001) surface to temperatures of 400 K or higher causes the decomposition of both the acetylide and the ethylidyne, and a new surface species appears which is characterized by vibrational modes at 440 (415), 800 (615), and 3010 (2255) cm^{-1} in the case of C_2H_2 (C_2D_2). The vibrational spectra for the hydrogenated and deuterated forms of this species are shown in Figure 6. Based on the previous studies of ethylene decomposition on Ru(001), and comparison to vibrational data for a number of previously identified surface species[14,30-33] and analogous organometallic compounds,[34,35] the vibrational modes

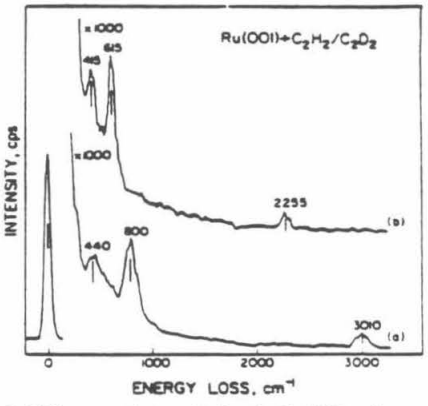

Figure 6. EEL spectra that result after the Ru(001) surface at 80 K is exposed to 5 langmuir of (a) C_2H_2 and (b) C_2D_2, annealed to 400 K, and recooled to 80 K. These spectra are characteristic of a methylidyne species.

of this new species are identified easily, respectively, as the metal–carbon stretch, the carbon–hydrogen (carbon–deuterium) bend, and the carbon–hydrogen (carbon–deuterium) stretch of a surface methylidyne. The carbon–hydrogen modes are listed in Table IV and compared to those for other methylidyne species on surfaces and in the organometallic compounds $Ru_3(CO)_9H_3(\mu_3\text{-}CH)$ and $Co_3(\mu_3\text{-}CH)(CO)_9$. A significant feature of the methylidyne spectra is the complete lack of any vibrational features between 1000 and 2000 cm^{-1} which might have been associated with a carbon–carbon stretching vibration. Note that the frequency of the carbon–hydrogen bend of methylidyne is approximately 50 cm^{-1} higher than, and thus quite distinct from, the carbon–hydrogen bend of the acetylide which exists at lower temperatures and that the carbon–hydrogen stretch is also upshifted by about 70 cm^{-1}. It should be pointed out that, in addition to methylidyne, there must be a rather large concentration (approximately 0.4 monolayer) of carbon adatoms on the Ru(001) surface at 400 K, since the thermal desorption spectra indicate that a large fraction of the hydrogen initially present in the acetylene has desorbed from the surface by this temperature. Heating the surface to slightly over 700 K desorbs the remaining hydrogen, and EEL spectra measured at 800 K verify that all spectral features due to methylidyne have disappeared. All that remains is a weak loss feature near 600 cm^{-1}, which may be attributed to the presence of carbon adatoms.

Both chemical intuition and the structures of the organometallic complexes listed in Table IV suggest that the most likely coordination site for methylidyne on Ru(001) is one in which the carbon atom occupies a threefold hollow site. Indeed, the observed carbon–hydrogen bending and stretching modes of methylidyne on Ru(001) resemble most closely those of methylidyne on the hexagonally close-packed Ni(111) surface, on which a structure has been proposed in which the carbon atom occupies a threefold hollow site, and the carbon–hydrogen bond axis is tilted slightly with respect to the surface normal. The latter allows the carbon–hydrogen bending mode to become dipolar active and could

(29) Parmeter, J. E.; Hills, M. M.; Weinberg, W. H., unpublished results.
(30) Demuth, J. E.; Ibach, H. *Surf. Sci.* **1978**, *78*, L747.
(31) Gates, J. A.; Kesmodel, L. L. *Surf. Sci.* **1983**, *124*, 68.
(32) Reference 23, Chapter 6.
(33) Dubois, L. H.; Somorjai, G. A. *Am. Chem. Soc., Symp. Ser.* **1980**, *32*, 1.
(34) Howard, M. W.; Kettle, S. F.; Orton, I. A.; Powell, D. B.; Sheppard, N.; Skinner, P. *J. Chem. Soc., Faraday Trans. 2*, **1981**, *77*, 397.
(35) Eady, C. R.; Johnson, B. F. G.; Lewis, J. *J. Chem. Soc., Dalton Trans.* **1977**, 477.

account for its relatively high intensity in the methylidyne spectra on Ru(001). Spectra taken 10° off-specular do indeed indicate a marked reduction in the intensity of the carbon–hydrogen bending mode on Ru(001), which suggests that this mode is dipolar enhanced in specular EEL spectra and that the carbon–hydrogen bond axis may be tilted slightly with respect to the surface normal. These conclusions are in agreement with those of Barteau et al.[2] for methylidyne formed from ethylene decomposition on Ru(001).

Two closely related issues remain to be addressed regarding acetylene decomposition on Ru(001). The first is the relative concentrations of acetylide and ethylidyne formed upon decomposition of molecularly chemisorbed acetylene between 230 and 250 K. Unfortunately, neither the EELS nor the TDMS results discussed here can provide an unambiguous answer to this question. Clearly, stoichiometry requires that unless some acetylene is dehydrogenated completely to C_2 dimers below 250 K, a possibility which seems unlikely and for which there is no spectroscopic evidence, no more than half of the chemisorbed acetylene may be converted to ethylidyne, while the rest decomposes to acetylide. Taking into account the saturation acetylene coverage of 0.27 monolayer, this places an upper limit of approximately 0.14 monolayer on the total concentration of the ethylidyne produced. A suitable lower limit is not so easily derived. Since the desorption of hydrogen begins slightly below 250 K for a saturation exposure of acetylene, it is obvious that not all of the hydrogen that results from acetylide formation contributes to ethylidyne formation. Rather, an overall reaction such as

$$C_2H_2(a) \rightarrow CCH(a) + \tfrac{1}{2}H_2(g)$$

also occurs to some extent. Consequently, the surface concentration of acetylide is greater than that of ethylidyne, although the exact ratio is not known.

The second remaining question involves the mechanism of methylidyne formation; i.e., is the methylidyne formed via carbon–carbon bond cleavage of acetylide, via decomposition of ethylidyne, or via a combination of both of these mechanisms? Since acetylide and ethylidyne decompose in very similar temperature ranges, the former between approximately 350 and 380 K and the latter between approximately 330 and 360 K (as judged both from this acetylene study and our previous ethylene study[3]), EEL spectra are of little use in answering this question. However, some information may be gleaned from the fact that the ratio of the areas of the β_1-to-β_2 hydrogen thermal desorption peaks is less for low initial acetylene exposures compared to higher exposures. This implies that relatively more methylidyne is formed from acetylene decomposition at low initial coverages of the latter. In our study of ethylene decomposition on Ru(001),[3] it was found that the ratio of acetylide to ethylidyne formed upon ethylene decomposition was larger at lower initial ethylene coverages relative to higher initial coverages, and it would be expected that this is true in the case of acetylene as well. This is in accord with the fact that ethylidyne occupies only one site on the surface, while an acetylide and two hydrogen adatoms occupy at least three sites. Consequently, the former should be favored at higher initial coverages of acetylene. Therefore, a relatively greater amount of acetylide formation leads to a relatively greater amount of methylidyne formation, and it follows that acetylide must have a greater tendency to decompose to yield methylidyne than does ethylidyne. Thus, the dominant mechanism of acetylide decomposition appears to be carbon–carbon bond cleavage to give C(a) and CH(a), while the dominant mechanism of ethylidyne decomposition is to two C(a) and three H(a). This is in agreement with the more conclusive EELS results for ethylene decomposition on Ru(001),[3] which show more clearly the decomposition of ethylidyne prior to the decomposition of acetylide and with little or no methylidyne formation accompanying the ethylidyne decomposition.

Further evidence that methylidyne is formed largely from acetylide decomposition was provided by adsorbing acetylene at 350 K. A subsequent hydrogen thermal desorption spectrum showed that the area of the β_2 desorption peak (from methylidyne) is enhanced by approximately a factor of 2 compared with that observed after a saturation exposure of acetylene at 80 K. Since the desorption of surface hydrogen is rapid at 350 K, the probability of ethylidyne formation under these conditions is negligible. On the other hand, acetylide is stable at 350 K, and its surface concentration was found to be enhanced relative to adsorption at 80 K, followed by annealing. This enhancement in the surface concentration of acetylide correlated with the enhancement in the surface concentration of methylidyne that was observed strongly implicating acetylide as the major source of methylidyne. However, the possibility that a small amount of ethylidyne decomposes to give methylidyne or that a small amount of acetylide decomposes to 2C(a) + H(a) rather than to C(a) and methylidyne cannot be ruled out completely.

In summary, the overall mechanism of acetylene decomposition on Ru(001) may be written as

$$C_2H_2(g) \xrightarrow{<230\ K} C_2H_2(a)$$

$$C_2H_2(a) \xrightarrow{230\text{–}250\ K} CCH(a) + CCH_3(a)$$

$$CCH(a) \xrightarrow{350\text{–}380\ K} C(a) + CH(a)$$

$$CCH_3(a) \xrightarrow{330\text{–}360\ K} 2C(a) + 3H(a)$$

$$2H(a) \xrightarrow{\sim 380\ K} H_2(g)$$

$$CH(a) \xrightarrow{480\text{–}700\ K} C(a) + {}^1/_2H_2(g)$$

IV. Conclusions

The principal conclusions of this work may be summarized as follows:

1. Molecularly adsorbed acetylene on Ru(001) is stable below 230 K and is characterized by a carbon–carbon stretching frequency of 1135 cm^{-1}, corresponding to carbon atoms that are very nearly sp^3 hybridized. This is the lowest carbon–carbon stretching frequency yet observed for molecularly adsorbed acetylene on a transition-metal surface. The saturation coverage of molecularly adsorbed acetylene on Ru(001) is approximately 0.27 monolayer.

2. Molecularly adsorbed acetylene does not desorb intact from Ru(001) but rather is an intermediate to dehydrogenation and hydrogenation which occurs between 230 and 250 K, yielding acetylide and ethylidyne.

3. The acetylide and ethylidyne decompose near 350 K, leaving methylidyne as the only hydrocarbon species on the surface by 400 K, along with carbon adatoms. The decomposition of ethylidyne (and perhaps to some degree the decomposition of acetylide) produces surface hydrogen, which recombines and desorbs as $H_2(g)$. This desorption occurs at 425 K for very low initial coverages of acetylene and at 380 K for a saturation coverage of chemisorbed acetylene.

4. The methylidyne decomposes between 480 and 700 K, yielding $H_2(g)$ and leaving only carbon on the surface.

Acknowledgment. This work was supported by the National Science Foundation under Grant CHE-8516615. Acknowledgment is also made to the Donors of the Petroleum Research Fund, administered by the American Chemical Society, for the partial support of this research.

Registry No. C_2H_2, 74-86-2; Ru, 7440-18-8; CCH_3, 67624-57-1; CCH, 29075-95-4; CH, 3315-37-5.

CHAPTER III

The Coadsorption of Hydrogen and Acetylene on the Ru(001) Surface

[This chapter was published as a paper by J. E. Parmeter, M. M. Hills and W. H. Weinberg, in *The Journal of the American Chemical Society* 1987, 109, 72.]

Reprinted from the Journal of the American Chemical Society, 1987, *109*, 72.

The Coadsorption of Hydrogen and Acetylene on the Ru(001) Surface

J. E. Parmeter,† M. M. Hills, and W. H. Weinberg*

Contribution from the Division of Chemistry and Chemical Engineering, California Institute of Technology, Pasadena, California 91125. *Received June 23, 1986*

Abstract: The adsorption of acetylene on Ru(001) surfaces with various coverages of preadsorbed hydrogen has been investigated by using high-resolution electron energy loss spectroscopy and thermal desorption mass spectrometry. The presence of a saturation coverage of dissociatively adsorbed hydrogen ($\theta_H \simeq 0.85$) inhibits the subsequent adsorption of acetylene, reducing the fractional saturation coverage of chemisorbed acetylene at 80 K from approximately 0.25 to 0.11. Partial hydrogenation of the chemisorbed acetylene occurs as the surface is heated above 150 K, resulting in the formation of an η^2-$CHCH_2$ species. Further hydrogenation of η^2-$CHCH_2$ to ethylene occurs also, with 0.01 monolayer of ethylene desorbing at 175 K. The remainder of the chemisorbed acetylene is not hydrogenated to ethylene but undergoes carbon–hydrogen bond cleavage and formation to yield acetylide (CCH) and ethylidyne (CCH_3) above 230 K, as on clean Ru(001). The ratio of ethylidyne to acetylide is greater, however, on the hydrogen presaturated surface.

I. Introduction

The adsorption of acetylene has been studied on a number of single-crystalline transition-metal surfaces under ultrahigh vacuum (UHV) conditions,[1-15] both to gain insight into the interaction of alkynes with such surfaces and to isolate stable surface intermediates in order to make a connection with the bonding of similar ligands in organometallic complexes. In nearly all cases, acetylene adsorbs molecularly at low temperatures ($T \leq 250$ K) but with substantial rehybridization of the carbon–carbon triple bond occurring. We have recently reported the results of a study of acetylene adsorption and reaction on the hexagonally close-packed Ru(001) surface by using high-resolution electron energy loss spectroscopy (EELS) and thermal desorption mass spectrometry (TDMS).[16] It was found that acetylene chemisorbs molecularly on this surface below 230 K with rehybridization of

† AT and T Bell Laboratories Predoctoral Fellow.

(1) Bandy, B. J.; Chesters, M. A.; Pemble, M. E.; McDougall, G. S.; Sheppard, N. *Surf. Sci.* **1984**, *139*, 87.
(2) Avery, N. R. *J. Am. Chem. Soc.* **1985**, *107*, 6711.
(3) Stuve, E. M.; Madix, R. J.; Sexton, B. A. *Surf. Sci.* **1982**, *123*, 491.
(4) Lehwald, S.; Ibach, H. *J. Surf. Sci.* **1979**, *89*, 425.
(5) Ibach, H.; Lehwald, S. *J. Vacuum Sci. Technol.* **1981**, *18*, 625.
(6) Gates, J. A.; Kesmodel, L. L. *J. Chem. Phys.* **1982**, *76*, 4281.
(7) Kesmodel, L. L.; Waddill, G. D.; Gates, J. A. *Surf. Sci.* **1984**, *138*, 464.
(8) Kesmodel, L. L. *J. Chem. Phys.* **1983**, *79*, 4646.
(9) Ibach, H.; Lehwald, S. *J. Vacuum Sci. Technol.* **1978**, *15*, 407.
(10) Dubois, L. H.; Castner, D. J.; Somorjai, G. A. *J. Chem. Phys.* **1980**, *72*, 5234.
(11) Erley, W.; Baro, A. M.; Ibach, H. *Surf. Sci.* **1982**, *120*, 273.
(12) Seip, U.; Tsai, M.-C.; Küppers, J.; Ertl, G. *Surf. Sci.* **1984**, *147*, 65.

0002-7863/87/1509-0072$01.50/0

the carbon atoms to nearly sp^3, as judged by a carbon–carbon stretching frequency of 1135 cm^{-1}.[17] The chemisorbed acetylene undergoes both carbon–hydrogen bond cleavage and bond formation when the surface is heated above 230 K, yielding two stable intermediates on the surface, namely acetylide (CCH) and ethylidyne (CCH_3). The acetylide and ethylidyne decompose below 400 K, leaving methylidyne (CH) and surface carbon, with desorption of H_2 centered at 375 K. The methylidyne decomposes below 800 K with further H_2 desorption between 480 and 800 K, leaving only carbon on the surface. The desorption of neither molecular acetylene nor any other hydrocarbons occurs.

An issue of fundamental importance in understanding alkyne hydrogenation reactions on transition-metal surfaces is the interaction of chemisorbed acetylene with coadsorbed hydrogen. The reactions of coadsorbed hydrogen and acetylene have been studied previously on the hexagonally close-packed Pt(111),[9] Pd(111),[6,7] Rh(111),[10] and Ni(111)[4] surfaces and also on the stepped Ni-[5(111) × (110)] surface.[4] Since the reactions of ethylene,[18,19] hydrogen,[20-22] and coadsorbed ethylene and hydrogen[23] on Ru(001) have all been studied previously with EELS and TDMS, this is an obviously desirable surface on which to conduct hydrogen and acetylene coadsorption experiments. We report here the results of such an investigation, also employing both EELS and TDMS, of acetylene coadsorption and reaction with preadsorbed hydrogen on Ru(001). These results provide unambiguous evidence for the hydrogenation of acetylene to ethylene under UHV conditions, and they yield additional information that permits important comparisons to acetylene and ethylene decomposition on clean Ru(001).

II. Experimental Procedures

The EEL spectrometer and the UHV chamber which houses it have been described in detail elsewhere.[24] The resolution of the spectrometer varied between 60 and 80 cm^{-1} (full-width at half-maximum), while maintaining a count rate of 2×10^3 counts per s in the elastically scattered beam with an incident electron beam energy of approximately 4 eV. All EEL spectra presented and discussed here were measured in the specular direction, which was 60° from the surface normal. The angle of acceptance of the electron energy analyzer was approximately 2°.

Thermal desorption mass spectrometric measurements were performed both in the EELS chamber and in a separate UHV chamber that has been described elsewhere.[25] This UHV chamber was equipped with a skimmer on the mass spectrometer in order to minimize the effects of desorption from the crystal edge (the area of which is approximately 8% of the oriented surface area) and the support leads. While most TDM spectra collected in the EEL chamber (including those in Figures 1 and 3) employed a temperature base, the TDM spectra in this second chamber were time base spectra with a computer algorithm for baseline subtraction, and this provided more accurate coverage determinations. All coverages reported in this paper are based on this more accurate method. The desorption peak temperatures reported here are accurate to within approximately ±5 K, and the heating rate was approximately 8 $K \cdot s^{-1}$ in all cases.

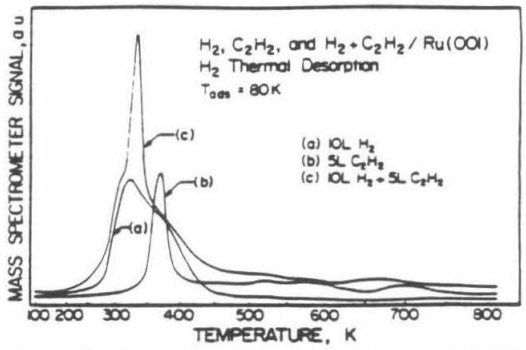

Figure 1. The H_2 thermal desorption spectra resulting after the Ru(001) surface at 80 K is exposed to (a) 10 L H_2, (b) 5 L C_2H_2, and (c) 10 L H_2 followed by 5 L C_2H_2. Note that the base line is not identical for the three cases and that the abscissa is nonlinear. The abbreviation a.u. denotes arbitrary units.

The Ru(001) crystals in both UHV chambers were cleaned by using standard techniques of Ar^+ sputtering and annealing in oxygen.[26] Surface cleanliness was monitored via EELS and TDMS in the EELS chamber and via Auger electron spectroscopy and TDMS in the second UHV chamber.

The H_2 and D_2 used in this study were obtained from Matheson with reported purities of 99.9995 and 99.5%, respectively. These gases were used without further purification, and their mass spectra gave no indication of any impurities. Previous studies of H_2 adsorption on Ru(001)[20-22] have shown that the adsorption is dissociative at all temperatures examined ($T \geq 75$ K), with the hydrogen adatoms giving rise to very weak EELS loss features near 800 and 1150 cm^{-1}. In addition to the appearance of these loss features, hydrogen adsorption on clean Ru(001) resulted in an increase in the intensity of the elastically scattered peak (surface reflectivity) by about a factor of two, an effect which has been noted previously.[27]

The C_2D_2 (99 atom % deuteriated) was obtained from MSD Isotopes and used without further purification. The C_2H_2 was obtained from an industrial acetylene tank (95% purity) and was purified as described elsewhere.[16] Both the C_2H_2 and C_2D_2 showed mass spectral cracking patterns that were virtually identical with those reported in the literature,[28] and no impurities could be detected in either case. Thermal desorption measurements were performed with C_2D_4 in order to make a comparison with the observed desorption of ethylene following acetylene and hydrogen coadsorption on Ru(001). The C_2D_4 (99 atom % deuteriated) was also obtained from MSD Isotopes, and its purity was verified via mass spectrometry.

Gas exposures were effected by backfilling the UHV chambers through leak valves. The stainless steel vacuum lines leading to the leak valves were flushed several times with the relevant gas prior to the introduction of the gas into the UHV chamber. All reported exposures were measured with a Bayard–Alpert ionization gauge, uncorrected for relative ionization probabilities. Exposures are reported in units of Langmuirs, where 1 Langmuir = 1 L = 10^{-6} torr-s.

III. Results

A. Thermal Desorption Mass Spectrometry. Thermal desorption mass spectra were measured for acetylene adsorbed at 80 K on the Ru(001) surface with varying coverages of preadsorbed hydrogen. Similar to acetylene adsorption on the clean Ru(001) surface,[16] where hydrogen is the only thermal desorption product from chemisorbed acetylene, hydrogen is the principal thermal desorption product resulting from chemisorbed acetylene on the hydrogen precovered surface. There is no desorption, for example, of methane, ethane, benzene, or acetylene (other than the desorption of condensed acetylene multilayers at 95 K). However, in contrast to acetylene adsorption on clean Ru(001), small amounts (≤0.01 monolayer) of ethylene are observed to

(13) Backx, C.; Willis, R. F.; Feuerbacher, B.; Fitton, B. *Surf. Sci.* **1977**, *68*, 516.
(14) Backx, C.; Feuerbacher, B.; Fitton, B.; Willis, R. F. *Surf. Sci.* **1977**, *63*, 193.
(15) Hamilton, J. C.; Swanson, N.; Waclawski, B. J.; Celotta, R. J. *J. Chem. Phys.* **1981**, *74*, 4156.
(16) Parmeter, J. E.; Hills, M. M.; Weinberg, W. H. *J. Am. Chem. Soc.* **1986**, *108*, 3563.
(17) For comparison, the carbon–carbon stretching frequencies of acetylene, ethylene, and ethane in the gas phase are 1974, 1623, and 995 cm^{-1}, respectively. See, for example, Herzberg, G. *Infrared and Raman Spectra of Polyatomic Molecules*; Van Nostrand, New York, 1945.
(18) Barteau, M. A.; Broughton, J. Q.; Menzel, D. *Appl. Surf. Sci.* **1984**, *19*, 92.
(19) Hills, M. M.; Parmeter, J. E.; Mullins, C. B.; Weinberg, W. H. *J. Am. Chem. Soc.* **1986**, *108*, 3554.
(20) Shimizu, H.; Christmann, K.; Ertl, G. *J. Catal.* **1980**, *61*, 412.
(21) Barteau, M. A.; Broughton, J. Q.; Menzel, D. *Surf. Sci.* **1983**, *88*, 384.
(22) Conrad, H.; Scala, R.; Stenzel, W.; Unwin, R. *J. Chem. Phys.* **1984**, *81*, 6371.
(23) Hills, M. M.; Parmeter, J. E.; Weinberg, W. H. *J. Am. Chem. Soc.*, in press.
(24) Thomas, G. E.; Weinberg, W. H. *Rev. Sci. Instrum.* **1979**, *50*, 497.
(25) Williams, E. D.; Sobrero, A. C.; Weinberg, W. H. *J. Chem. Phys.* **1982**, *76*, 1150.
(26) Thomas, G. E.; Weinberg, W. H. *J. Chem. Phys.* **1979**, *70*, 954.
(27) Thiel, P. A.; Weinberg, W. H. *J. Chem. Phys.* **1980**, *73*, 4081.
(28) Cornu, A.; Massot, G. *Compilation of Mass Spectral Data*; Hayden and Son Ltd.: London, 1975.

desorb following acetylene adsorption on the Ru(001) surface with a sufficient concentration of preadsorbed hydrogen. This indicates clearly that chemisorbed acetylene and hydrogen adatoms can react on Ru(001) under these conditions.

1. Hydrogen Thermal Desorption. Figure 1 shows H_2 thermal desorption spectra for saturation exposures of both H_2 (a) and C_2H_2 (b) on Ru(001) and for a saturation exposure of C_2H_2 on a Ru(001) surface which had been presaturated with hydrogen (c). A saturation hydrogen exposure on Ru(001) gives rise to a broad thermal desorption peak centered at 325 K with a shoulder near 380 K, as shown in Figure 1a, and corresponds to a hydrogen adatom fractional surface coverage of 0.85,[20] i.e., 1.39×10^{15} atoms-cm^{-2}. The hydrogen adatoms occupy exclusively threefold hollow sites, and the peak splitting is due to adatom–adatom interactions.[22] As may be seen in Figure 1b, a saturation exposure of acetylene on Ru(001) gives rise to a sharp hydrogen desorption peak centered near 375 K, with a less intense and very broad feature between approximately 480 and 800 K which displays three weak maxima. The saturation fractional coverage of acetylene adsorbed on clean Ru(001) is 0.25 ± 0.03, as judged by the H_2 thermal desorption spectra. (Recall that only H_2 is observed to desorb from the Ru(001) surface on which acetylene is adsorbed.)

Comparison of spectra b and c of Figure 1 shows that the principal H_2 desorption peak is somewhat sharpened and downshifted by approximately 35 K, from 375 to 340 K, when the Ru(001) surface is presaturated with hydrogen. This peak corresponds to ethylidyne decomposition, which on the hydrogen precovered surface occurs at a slightly lower temperature than on the clean surface (see section III.B). On the clean surface, the peak at 375 K also involves a small contribution from hydrogen adatoms that are formed when acetylene decomposes to acetylide and that do not react further to form ethylidyne. On the hydrogen precovered surface, the peak at 340 K also involves substantial amounts of preadsorbed hydrogen adatoms. Clearly visible on both sides of the 340-K peak in Figure 1c are shoulders which are characteristic of hydrogen desorption from the clean surface and which result from the recombinative desorption of hydrogen adatoms that are not influenced significantly by the presence of coadsorbed hydrocarbon species. The leading edge of Figure 1c is downshifted slightly relative to that of Figure 1a due to the increased hydrogen adatom *density* in the former case.

Between 480 and 800 K, the H_2 thermal desorption spectra for both acetylene and acetylene with preadsorbed hydrogen show very broad peaks of low intensity. Since the desorption of hydrogen from the clean Ru(001) surface is complete below 500 K, these features clearly result from reaction-limited hydrogen desorption due to the decomposition of a surface hydrocarbon species. Our previous EELS results for acetylene decomposition on Ru(001) have shown that methylidyne is the only hydrocarbon species present on the surface above 400 K.[16] Consequently, hydrogen desorption above 480 K is necessarily due to methylidyne decomposition for acetylene adsorption on Ru(001). The fact that three desorption maxima are observed above 480 K for saturation acetylene coverages (only one maximum is observed for low coverages) and the broad temperature range for methylidyne decomposition results from variations in the local coverage of carbon and methylidyne. Similarly, EEL spectra for coadsorbed hydrogen and acetylene on Ru(001) demonstrate that methylidyne is the only hydrocarbon species on the surface above 400 K. Therefore, in this case also, hydrogen desorption above 480 K is due to methylidyne decomposition. The amounts of hydrogen that desorb between 480 and 800 K indicate that approximately 0.13 monolayer of methylidyne is formed for a saturation exposure of acetylene on clean Ru(001), while only about 0.04 monolayer of methylidyne is formed following a saturation exposure of acetylene on the hydrogen presaturated Ru(001) surface. The hydrogen thermal desorption peaks from the decomposition of methylidyne occur at somewhat lower temperatures for acetylene coadsorbed with hydrogen, similar to the case of lower acetylene coverages on the clean surface.[16] The higher desorption temperatures on the initially clean surface are probably due to a stabilization of methylidyne by the higher concentration of coadsorbed carbon

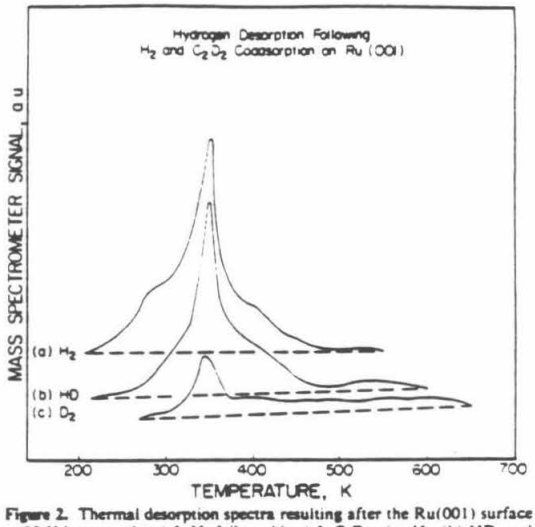

Figure 2. Thermal desorption spectra resulting after the Ru(001) surface at 80 K is exposed to 1 L H_2 followed by 1 L C_2D_2: (a) H_2, (b) HD, and (c) D_2. Dashed lines are approximate baselines for the three spectra.

adatoms, which block surface sites that are necessary for carbon–hydrogen bond cleavage and also hinder hydrogen–hydrogen recombination. The lower concentration of carbon adatoms in the case of coadsorbed acetylene and hydrogen is a consequence of the fact that preadsorbed hydrogen partially inhibits the adsorption of acetylene on Ru(001).

By comparison to the amount of hydrogen that desorbs following a saturation exposure of H_2 on Ru(001), the amount of acetylene which adsorbs and decomposes to yield (eventually) H_2(g) and surface carbon on the hydrogen presaturated Ru(001) surface is estimated to be approximately 0.10 monolayer. To obtain this estimate, time integrated TDM spectra corresponding to Figure 1a are subtracted from similarly time integrated TDM spectra corresponding to Figure 1c, with no peak deconvolution required. Since the only other desorption product resulting from acetylene adsorption on hydrogen presaturated Ru(001) is 0.01 monolayer of ethylene (see section III.A.2), this indicates that approximately 0.11 monolayer of acetylene is chemisorbed on this surface. Thus, the presence of 0.85 monolayer of hydrogen adatoms on the Ru(001) surface inhibits acetylene chemisorption substantially, reducing the saturation acetylene coverage by approximately 60%.

Figure 2 shows H_2, HD, and D_2 thermal desorption spectra from a Ru(001) surface which has been exposed to 1 L of H_2 followed by a subsaturation exposure of 1 L of C_2D_2 at 80 K. A 1-L hydrogen exposure corresponds to 0.57 ± 0.05 monolayer of hydrogen adatoms, and the amount of C_2D_2 that adsorbs is approximately 0.11 monolayer. The equivalent coverages of the various hydrogen isotopes that desorb are approximately 0.22 monolayer of H_2, 0.12 monolayer of HD, and 0.05 monolayer of D_2. Thus the isotopic mixing of hydrogen and deuterium is not complete; a purely statistical distribution would be 0.21 monolayer of H_2, 0.16 monolayer of HD, and 0.03 monolayer of D_2. Several aspects of these thermal desorption spectra are noteworthy. The first is that no D_2 and only a trivial amount of HD desorb below 230 K, the temperature at which acetylene decomposition begins on both the clean and the hydrogen precovered Ru(001) surfaces. This indicates that virtually no H/D exchange occurs between the coadsorbed hydrogen adatoms and chemisorbed acetylene. Thus the reaction

$$DCCD(a) + H(a) \rightarrow HCCD(a) + D(a)$$

is not facile on this surface. Second, small amounts of both H_2 and HD are desorbed between 480 and 600 K, indicating the decomposition of a CH methylidyne species. Thus, a small amount

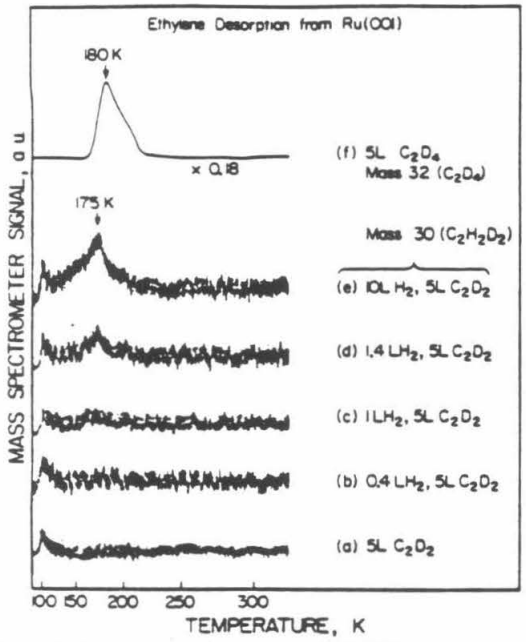

Figure 3. Thermal desorption spectra of CHDCHD (m = 30 amu) recorded after the Ru(001) surface at 80 K is exposed to (a) 5 L C_2H_2, (b) 0.4 L H_2 followed by 5 L C_2D_2, (c) 1 L H_2 followed by 5 L C_2D_2, (d) 1.4 L H_2 followed by 5 L C_2D_2, and (e) 10 L H_2 followed by 5 L C_2D_2. In spectra b–e the initial absolute hydrogen adatom coverages are approximately 0.35, 0.6, 0.75, and 0.85, respectively. Spectrum f shows the CD_2CD_2 (m = 32 amu) desorption that results following a 5 L C_2D_4 exposure at 80 K. The apparent peak just above 100 K in spectra a–e is a spectrometer effect and should be ignored. Note that the abscissa is nonlinear.

(~0.01–0.02 monolayer) of the preadsorbed hydrogen adatoms have reacted with a hydrocarbon species below 480 K to become incorporated into the hydrocarbon adlayer and form eventually CH. It is also worth noting that methylidyne decomposition is complete below 700 K, consistent with the initial acetylene coverage of 0.11 monolayer.

2. Ethylene Thermal Desorption. Ethylene desorption following the coadsorption of hydrogen and acetylene on Ru(001) at 80 K was studied by using four combinations of hydrogen and acetylene isotopes, namely $H_2 + C_2H_2$, $H_2 + C_2D_2$, $D_2 + C_2H_2$, and $D_2 + C_2D_2$. Of these various combinations, $H_2 + C_2D_2$ and $D_2 + C_2H_2$ are the most useful since the presence of different hydrogen isotopes, in principle, allows different isotopes of ethylene to be desorbed. Consequently, the isotopes of ethylene that are observed to desorb provide mechanistic insight into the surface reaction (provided that desorption occurs at a temperature below which H/D exchange between adsorbed hydrogen and the adsorbed hydrocarbons is not important). The coadsorption of H_2 and C_2H_2 is the least useful for monitoring ethylene desorption, since any desorbed ethylene occurs at 28 amu (C_2H_4), and the presence of carbon monoxide (also at 28 amu) in the chamber background leads to a large, sloping background in the mass 28 thermal desorption spectra. This makes the detection of small amounts of C_2H_4 difficult.

Thermal desorption spectra of ethylene-d_2 ($C_2H_2D_2$) following the coadsorption of H_2 and C_2D_2 on Ru(001) at 80 K are shown in Figure 3a–e. The surface was exposed to various fluxes of hydrogen, as indicated, and then saturated with C_2D_2. The initial hydrogen coverages were calculated by comparing the amount of hydrogen desorbed following a given exposure on the clean Ru(001) surface to the amount desorbed following a saturation exposure on Ru(001). The C_2D_4 thermal desorption spectrum resulting from a saturation exposure of perdeuterioethylene on Ru(001) is shown in Figure 3f. Ethylene-d_2 is desorbed following H_2 and C_2D_2 coadsorption only for $\theta_H \geq 0.6$. The peak desorption temperature of 175 ± 5 K is in excellent agreement with thermal desorption data for ethylene adsorbed on Ru(001) [cf. Figure 3f and ref 19], and the observations that the desorption peak temperature does not shift with increasing hydrogen adatom coverage and occurs at nearly the same temperature as ethylene desorption following ethylene adsorption on Ru(001)[19] suggest that this is a desorption-limited reaction with first-order desorption kinetics. Assuming a constant preexponential factor of the desorption rate coefficient of 10^{13} s^{-1}, an activation energy of desorption of approximately 10–11 kcal/mol is estimated.[29]

Comparison to the thermal desorption spectrum for a saturation exposure of chemisorbed C_2D_4 on Ru(001), where approximately 0.06 monolayer of ethylene desorbs molecularly at 180 K, allows the coverages of ethylene-d_2 that are desorbed to be estimated for various hydrogen precoverages (to within approximately a factor of two). For fractional hydrogen precoverages of 0.6, 0.75, and 0.85, approximately 0.002, 0.005, and 0.01 monolayer of $C_2H_2D_2$ are desorbed, respectively. Since approximately 0.10 monolayer of acetylene adsorbs and decomposes on Ru(001) which is presaturated with hydrogen, this indicates that approximately 9% of the chemisorbed acetylene is hydrogenated on this surface *and* desorbs as ethylene.

Ethylene-d_2 (at 30 amu) is the only isotope of ethylene which desorbs from Ru(001) following the coadsorption of H_2 and C_2D_2. No detectable desorption (i.e., <0.001 monolayer) is observed at 31 amu (C_2HD_3) or at 32 amu (C_2D_4), and only a very weak features is observed at 29 amu which is due to the C_2HD_2 cracking fragment of ethylene-d_2, rather than ethylene-d_1 (C_2H_3D). Thermal desorption spectra of coadsorbed D_2 and C_2H_2 on Ru(001) yield similar results: only ethylene-d_2 is observed as a desorption product. Thus, it is clear that the ethylene desorption at 175 K results from the reaction of chemisorbed molecular acetylene with two preadsorbed hydrogen adatoms and that the sequential addition of the two hydrogen atoms is irreversible.

B. Electron Energy Loss Spectroscopy. As noted in section I, hydrogen adsorption on Ru(001) has been investigated previously with EELS.[21,22] The observed loss features near 800 and 1150 cm^{-1}, due to the presence of hydrogen adatoms in threefold hollow sites, are extremely weak and are obscured by various hydrocarbon modes when either coadsorbed ethylene or acetylene is present.[16,19] The molecular chemisorption of acetylene on clean Ru(001) below 230 K produces a very nearly sp^3 hybridized species which is characterized by the following loss features in the case of C_2H_2 (C_2D_2): ruthenium–carbon stretching modes at 375 (350) and 520 cm^{-1} (not resolved for C_2D_2); CH (CD) bending modes at 765 (565) and 980 (715) cm^{-1}; a carbon–carbon stretching mode at 1135 (1085) cm^{-1}; and a CH (CD) stretching mode at 2940 (2210) cm^{-1}.[16] The EEL spectra for saturation exposures of C_2H_2 and C_2D_2 on Ru(001), corresponding to approximately 0.25 monolayer of chemisorbed acetylene, are shown in Figure 4a and b. The spectra in Figure 4 also show loss features due to small amounts (<0.01 monolayer) of CO adsorbed from the chamber background. It has been found previously that these small and varying amounts of CO do not affect the EEL spectra of chemisorbed acetylene or its decomposition products.[16]

Also shown in Figure 4 are EEL spectra of C_2H_2 adsorbed on a hydrogen presaturated Ru(001) surface (c) and of C_2D_2 adsorbed on a deuterium presaturated Ru(001) surface (d). The major difference between these spectra and those of Figure 4a and b is the appearance of a new vibrational mode, which occurs at 1440 cm^{-1} for coadsorbed H_2 and C_2H_2 and at 1175 cm^{-1} for coadsorbed D_2 and C_2D_2. The frequency of this mode is in the range characteristic of a CH_2 (CD_2) scissoring vibration, and the observed frequency shift upon deuterium substitution [$\delta(CH_2)/\delta(CD_2) = 1.23$] confirms this assignment. This indicates that a new surface species has been formed containing a CH_2 group.

(29) Redhead, P. A. *Vacuum* **1962**, 203.

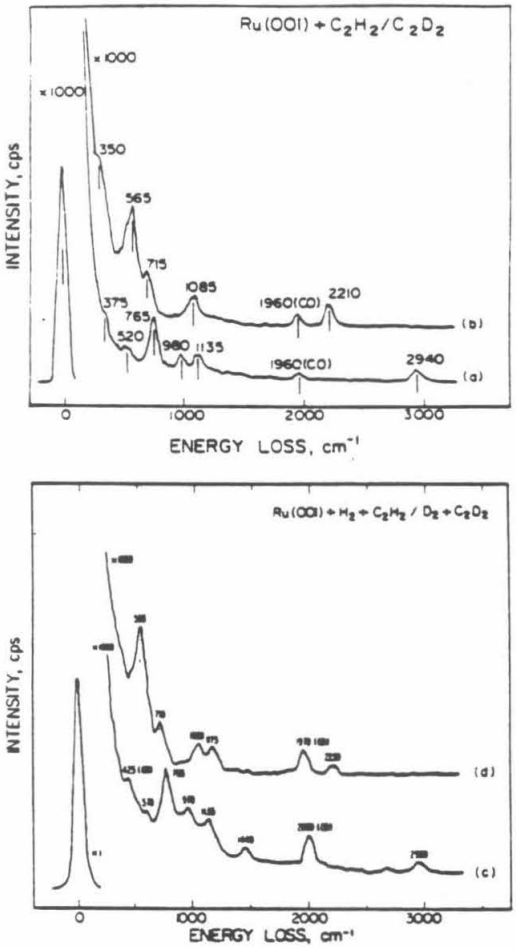

Figure 4. The EEL spectra that result when the Ru(001) surface at 80 K is exposed to (a) 5 L C_2H_2, (b) 5 L C_2D_2, (c) 10 L H_2 followed by 5 L C_2H_2, and (d) 10 L D_2 followed by 5 L C_2D_2 and then annealed to 150 K and recooled to 80 K prior to spectral collection. Spectra a and b are characteristic of molecularly chemisorbed acetylene, while spectra c and d show features characteristic both of chemisorbed acetylene and $CHCH_2$ ($CDCD_2$). In spectra c and d, the low-frequency metal–carbon modes are not resolved due to the somewhat poorer cutoff of the elastic peak. The apparent shift of the high-frequency metal–carbon mode in spectrum c compared to spectrum a is not very reproducible and may also be due to the poorer elastic peak cutoff.

which is in agreement with our TDMS results showing ethylene desorption at 175 K. However, the EEL spectra of Figure 4c and d are not due to chemisorbed ethylene (or a combination of chemisorbed ethylene and acetylene), as judged by a comparison with previous studies of ethylene adsorption on Ru(001).[18,19] The CH_2 scissoring mode is thus assigned to an η^2-$CHCH_2$ species, the logical intermediate in the hydrogenation of acetylene to ethylene. (The η^2 designation indicates that both carbon atoms of the $CHCH_2$ species are bonded directly to the surface but does *not* imply nearly equal metal–carbon bond lengths or anything else regarding the structure of $CHCH_2$.) An η^1-$CHCH_2$ species containing a carbon–carbon double bond (vinyl) is ruled out due to the lack of a carbon–carbon stretching mode above 1500 cm^{-1}. Other CH_2-containing species such as η^2-CCH_2 or CH_2 (methylene), that require the breaking of carbon–hydrogen or carbon–carbon bonds of acetylene in order to be formed, are excluded in view of the observed lack of H/D exchange below 230 K, the fact that CH bonds of chemisorbed acetylene are not broken below 230 K on clean Ru(001), and the observed lack of carbon–carbon bond cleavage below 340 K.

Since the modes characteristic of chemisorbed acetylene are still present in Figure 4c and d, the surface contains a mixture of chemisorbed acetylene and η^2-$CHCH_2$ after annealing to 150 K. This observation is in agreement with previous results for hydrogen and acetylene coadsorption on the stepped Ni{5(111) × ([10)] surface, where the appearance of a δ (CH_2) mode at 150 K was taken as evidence for the formation of a mixed overlayer of $CHCH_2$ and chemisorbed acetylene.[4] The η^2-$CHCH_2$ should also give rise to CH_2 wagging, twisting, and rocking modes, which would be expected, respectively, near 1150, 900, and 775 cm^{-1}, based on a comparison to chemisorbed ethylene on Ru(001).[19] These modes are not resolved due to overlap with various modes of chemisorbed acetylene (or, in some cases, perhaps because they are intrinsically weak). However, spectra c and d of Figure 4 do exhibit slight changes in the frequencies and relative intensities of some modes compared to spectra a and b, and these differences are no doubt due at least partially to the presence of additional modes of η^2-$CHCH_2$ that are not well-resolved. This may very well also be the reason for the relatively poorer resolution in the 750–1150 cm^{-1} region of spectrum c, compared to spectrum a.

Further hydrogenation of η^2-$CHCH_2$ and desorption of ethylene occurs between 150 and 250 K, as indicated by the thermal desorption results of Figure 3. EEL spectra show that a small amount of η^2-$CHCH_2$ is present on the surface at 200 K, but that it is completely gone by 250 K. Molecularly chemisorbed acetylene decomposes near 230 K, as on the clean surface, and the surface species present from 250 to 340 K are acetylide (which is stable to nearly 400 K) and ethylidyne, as in the case of acetylene adsorbed on clean Ru(001).[16] The acetylide is characterized primarily by a strong CH bending mode at 750 cm^{-1}, while ethylidyne is characterized by modes of nearly equal intensity at 1140 [ν(CC)] and 1360 [δ_s (CH_3)] cm^{-1}. The decomposition of acetylene on the hydrogen presaturated Ru(001) surface differs, however, from the decomposition of acetylene on clean Ru(001) in that the ratio of ethylidyne to acetylide is increased on the hydrogen presaturated surface. On the clean surface, there is slightly more acetylide than ethylidyne (as judged from both EELS and TDMS); while on the hydrogen precovered surface, the ratio of ethylidyne to acetylide is approximately 3:2, as estimated from EEL spectra which are virtually identical with those resulting from ethylene decomposition for saturation ethylene coverages on clean Ru(001).[19] In addition, the ethylidyne decomposes at a slightly lower temperature on the hydrogen precovered surface, where EELS features due to this species have disappeared by 350 K. On the other hand, some ethylidyne is stable to at least 360 K when acetylene decomposes on the clean Ru(001) surface.

When C_2H_2 (C_2D_2) is adsorbed on Ru(001) and the surface is annealed between 400 and 700 K, a methylidyne species is formed that is characterized by the following vibrational modes: a ruthenium–carbon stretch at 440 (415), a CH(CD) bend at 800 (615), and a CH(CD) stretch at 3010 (2255) cm^{-1}. When C_2H_2 is adsorbed on a hydrogen presaturated Ru(001) surface and the surface is annealed to these same temperatures, the same CH species is formed in smaller concentrations, as discussed in section III.A.1. The coadsorption of H_2 and C_2D_2 or D_2 and C_2H_2, followed by annealing to over 400 K, leads to the production of both hydrogenated (CH) and deuteriated (CD) methylidyne on Ru(001), although CD predominates in the former case and CH in the latter. This mixing of hydrogen isotopes in the methylidyne is in agreement with our thermal desorption results, and provides unequivocal evidence for the incorporation of preadsorbed hydrogen into the hydrocarbon adlayer. The mechanisms of the incorporation of preadsorbed hydrogen into various hydrocarbon species will be discussed in a subsequent publication.[30]

(30) Parmeter, J. E.; Hills, M. M.; Weinberg, W. H., manuscript in preparation.

IV. Discussion

All the TDMS and EELS results reported here are consistent with the partial hydrogenation of acetylene on a hydrogen presaturated Ru(001) surface to produce low concentrations of a $CHCH_2$ species and ethylene. The $CHCH_2$ is a stable intermediate in the synthesis of ethylene, and the ethylene formed desorbs near 175–180 K, as does ethylene that desorbs following ethylene adsorption. Furthermore, the data prove that the formation of both $CHCH_2$ and ethylene results from the reaction of preadsorbed hydrogen with chemisorbed acetylene and not from a disproportionation reaction involving hydrogen adatoms that originate from acetylene decomposition. (This is not surprising since neither $CHCH_2$ nor ethylene is observed via EELS or TDMS in the absence of preadsorbed hydrogen, and because chemisorbed acetylene is stable on the clean surface to 230 K.) Acetylene that is not hydrogenated to ethylene decomposes to acetylide and ethylidyne near 230 K as on the clean Ru(001) surface, although the ratio of ethylidyne to acetylide is increased. The data also indicate that H/D exchange does not occur to an appreciable extent between chemisorbed acetylene and preadsorbed hydrogen on this surface, but that such exchange does occur for at least one of the decomposition products of acetylene. The formation of detectable amounts of ethylene that desorb below 200 K after hydrogen and acetylene coadsorption on Ru(001) under UHV conditions is significant in view of the lack of precedent for this reaction on other metal surfaces.

Coadsorbed hydrogen and acetylene react near room temperature to form ethylidyne on the Pt(111),[9] Pd(111),[6,7] and Rh(111)[10] surfaces. Ethylidyne is also produced, along with acetylide, as a decomposition product of acetylene on both Pd(111)[7] and Ru(001).[16] The reactions of coadsorbed acetylene and hydrogen below 200–250 K, however, have received somewhat less attention. On Ni(111), coadsorbed hydrogen and acetylene do not react below 250 K.[4] Experiments performed on Pt(111) are somewhat inconclusive. A recent TDMS study has reported ethylene desorption at 250 K following H_2 and C_2H_2 coadsorption on this surface,[31] whereas a previous EELS study reported that coadsorbed hydrogen and acetylene do not react on Pt(111) below 280 K, at which temperature ethylidyne is formed.[9]

Hydrogenation of acetylene to $CHCH_2$ has been observed with EELS, however, for coadsorbed hydrogen and acetylene at 150 K on the stepped Ni[5(111) × ($\bar{1}$10)] surface.[4] Adsorption of acetylene on this hydrogen presaturated surface produces a mixture of chemisorbed molecular acetylene and a $CHCH_2$ species similar to the case of Ru(001), as discussed in section III.B. The ruthenium and nickel surfaces differ markedly, however, in the extent of H/D exchange observed between the adsorbed hydrocarbon species and the preadsorbed hydrogen at low-surface temperatures. While little exchange occurs on Ru(001) below 230 K, exchange is facile on Ni[5(111) × ($\bar{1}$10)] at 150 K. This difference may be correlated with the ability of the two surfaces to dehydrogenate acetylene. On the clean nickel surface, acetylene has been found to dehydrogenate partially even at 150 K,[4] while chemisorbed acetylene is stable to 230 K on Ru(001). Unfortunately, no thermal desorption data are available for the nickel surface, so it is not known whether any ethylene is formed and desorbed from this surface. Given the dehydrogenation ability of this nickel surface, however, ethylene desorption would seem to be unlikely.

Although it is apparent that the ethylene formed from acetylene hydrogenation on Ru(001) is produced via a $CHCH_2$ intermediate, the bonding and hybridization of this intermediate are less obvious. Since only the δ (CH_2) mode of the $CHCH_2$ is distinguished clearly from the modes of coadsorbed molecular acetylene in the EEL spectra, conclusions concerning the hybridization of the carbon atoms in $CHCH_2$ are not easily drawn. The $CHCH_2$ species formed in Ni[5(111) × ($\bar{1}$10)] was assigned, on the basis of a CH_2 stretching mode at 3050 cm^{-1}, as being sp^2 hybridized, although no ν(CC) mode was identified.[4] A $CHCH_2$ ligand has been identified in the organometallic complex $Os_3(CHCH_2)(H)(CO)_{10}$ which is σ-bonded to one osmium atom with a π-bond to a second osmium atom.[32] The carbon atoms of the $CHCH_2$ ligand are intermediate between sp^3 and sp^2 hybridization with strongly coupled ν (CC) and δ (CH_2) modes at 1310 and 1476 cm^{-1}. Although these precedents might suggest a $CHCH_2$ species with at least some double bond character, we believe that the $CHCH_2$ species formed on Ru(001) is more nearly sp^3 hybridized. The lack of any carbon–hydrogen stretching mode above 3000 cm^{-1} or any carbon–carbon stretching mode above 1200 cm^{-1} is suggestive of sp^3 hybridization, although this is not conclusive because these modes could be too weak to be detected. More significantly, both chemisorbed acetylene and ethylene on Ru(001) are essentially sp^3 hybridized, and since $CHCH_2$ is an intermediate in the conversion of acetylene to ethylene, it would be expected to have a similar structure. Such an π^2-$CHCH_2$ species would have both carbon atoms bonded directly to the surface, with the carbon–carbon bond either parallel or (more likely) slightly skewed with respect to the surface plane.

As stated previously, the decomposition products of chemisorbed acetylene are the same on the hydrogen presaturated Ru(001) surface as on the clean surface, namely ethylidyne and acetylide. As would be expected, the presence of surface hydrogen shifts the ratio of these two decomposition products toward more ethylidyne, the product that contains more hydrogen atoms. This is evident both in EEL spectra measured after annealing to 250–300 K and in the TDM spectra which show a smaller amount of methylidyne [which forms primarily (or exclusively) from acetylide, rather than ethylidyne, decomposition[16,19]] decomposing on the hydrogen precovered surface. Another difference between the clean and hydrogen presaturated surfaces is the slightly higher decomposition temperature of ethylidyne on the clean surface, which is evident in both EEL and TDM spectra. This is due to the lower concentration of hydrocarbon species on the hydrogen presaturated surface.

V. Conclusions

The adsorption of acetylene on Ru(001) with preadsorbed hydrogen has been studied by using high-resolution electron energy loss spectroscopy and thermal desorption mass spectrometry. The principal conclusions of this work may be summarized as follows.

1. The dissociative adsorption of hydrogen on Ru(001) inhibits the subsequent adsorption of acetylene. The reduction in the saturation coverage of acetylene is approximately 60% if the surface is saturated with hydrogen (from 0.25 monolayer on the initially clean surface to 0.11 monolayer on the hydrogen presaturated surface with $\theta_H = 0.85$).

2. Hydrogen thermal desorption spectra following the adsorption of acetylene on the hydrogen presaturated Ru(001) surface show features that are characteristic of hydrogen and acetylene adsorbed separately, although the major H_2 desorption peak resulting from acetylene decomposition is downshifted by 35 K from 375 to 340 K. This is the result of a slightly lower decomposition temperature for ethylidyne (one of the two major decomposition products of acetylene) on the hydrogen presaturated surface.

3. Thermal desorption spectra of H_2, HD, and D_2 from coadsorbed H_2 and C_2D_2 on Ru(001) indicate that some of the preadsorbed hydrogen is incorporated into surface hydrocarbon species, since both H_2 and HD are observed to desorb well above the temperature at which they desorb following adsorption on either the clean Ru(001) surface or the Ru(001) surface with various coverages of carbon adatoms. Electron energy loss spectra show that the stable hydrocarbon species leading to H_2 and HD desorption above 480 K is methylidyne. No D_2 and only a trivial amount of HD desorb from the surface below 230 K where acetylene decomposition begins, indicating that H/D exchange between chemisorbed acetylene and preadsorbed hydrogen is not facile. Thus hydrogen is incorporated into surface hydrocarbon species by H/D exchange between preadsorbed hydrogen and one or more of the decomposition products of acetylene.

4. Following saturation acetylene exposures on hydrogen presaturated Ru(001), approximately 0.01 monolayer of ethylene

(31) Megiris, C. E.; Berlowitz, P.; Butt, J. B.; Kung, H. H. *Surf. Sci.* **1985**, *159*, 184.

(32) Andrews, J. R.; Kettle, S. F. A.; Powell, D. B.; Sheppard, N. *Inorg. Chem.* **1982**, *21*, 2874.

desorbs from the surface at 175 K. Thus, ethylene desorption accounts for approximately 9% of the chemisorbed acetylene under these conditions. Furthermore, the coadsorption of H_2 and C_2D_2 shows that the desorbed ethylene consists entirely of mass 30, i.e., CHDCHD, implying that ethylene formation results from the reaction of two preadsorbed hydrogen adatoms with molecularly chemisorbed acetylene. Ethylene formation and desorption is observed only if the initial coverage of hydrogen adatoms exceeds approximately 70% of saturation (about 0.6 monolayer). No other hydrocarbons desorb from Ru(001) following hydrogen and acetylene coadsorption at 80 K (except for condensed multilayers of acetylene).

5. Electron energy loss spectra show that at 150 K the hydrocarbon adphase is a mixture of molecularly chemisorbed acetylene and a CH_2-containing species that is inferred to be $CHCH_2$ (for H_2 and C_2H_2 coadsorption). In addition to the ethylene desorption at 175 K, annealing the surface to 230 K causes the decomposition of chemisorbed acetylene. The two decomposition products, ethylidyne and acetylide, are the same as in the case of acetylene decomposition on the initially clean surface, although the ratio of ethylidyne to acetylide is increased.

Acknowledgment. This research was supported by the National Science Foundation (Grant No. CHE-8516615).

CHAPTER IV

The Chemistry of Acetylene on the Ru(001)-p(2x2)-O and Ru(001)-p(1x2)-O Surfaces

Abstract

The chemisorption and decomposition of acetylene on Ru(001) surfaces with ordered p(2x2) and p(1x2) overlayers of oxygen adatoms has been studied using high-resolution electron energy loss spectroscopy and thermal desorption mass spectrometry. The chemisorbed acetylene species formed on these oxygen precovered surfaces are not significantly different from molecularly chemisorbed acetylene on clean Ru(001), although one of the two types of chemisorbed acetylene formed on the clean surface is not formed on Ru(001)–p(1x2)–O. The preadsorption of oxygen reduces the saturation coverages of chemisorbed acetylene, which is approximately 0.39 on clean Ru(001), 0.31 on Ru(001)–p(2x2)–O and 0.09 on Ru(001)–p(1x2)–O. As on clean Ru(001), the chemisorbed acetylene on the oxygen-precovered surfaces does not desorb upon annealing but rather decomposes between 200 and 350 K to produce a number of stable intermediates These intermediates include ethylidyne (CCH_3), acetylide (CCH), methylidyne (CH), and an sp^2-hybridized vinylidene (CCH_2) species. The vinylidene is formed in particularly large amounts on Ru(001)–p(2x2)–O after annealing to 350 K, and appears to be stabilized strongly by the presence of coadsorbed oxygen because it is formed not at all or in trivial amounts on clean Ru(001). The stability, formation and decomposition of the various intermediates is discussed. The decomposition of all of these intermediates leads eventually to hydrogen desorption, which is complete on both oxygen-precovered surfaces by approximately 700 K.

I. Introduction

The chemistry of acetylene on clean, single crystalline transition metal surfaces has received a great deal of attention during the past decade (**1-4**). We have previously used high-resolution electron energy loss spectroscopy (EELS) and thermal desorption mass spectrometry (TDMS) to study the adsorption and decomposition of acetylene on clean Ru(001) (**2**), concluding that molecularly chemisorbed acetylene is very nearly sp^3-hybridized on this surface and that it decomposes near 250 K to produce a mixture of acetylide (CCH) and ethylidyne (CCH_3), both of which decompose between 350 and 400 K to yield methylidyne and surface carbon. The methylidyne decomposes between 500 and 700 K, and hydrogen desorbs from the surface between approximately 250 and 700 K. We have also studied the coadsorption of hydrogen and acetylene on Ru(001) (**3**), showing that small amounts of acetylene can be hydrogenated to ethylene via an intermediate inferred to be an sp^3-hybridized vinyl ($CHCH_2$) species.

More recently, Jakob et al. (**4**) have also studied acetylene adsorption on clean Ru(001), and have shown that the molecularly chemisorbed phase below 200 K consists of two species, designated Type I and Type II acetylene. The former exhibits a rather strong ν(CC) EELS loss feature near 1130 cm^{-1}, while the latter gives rise to strong CH bending loss features near 760 and 980 cm^{-1}. They also obtained a higher saturation acetylene coverage (0.43 monolayer vs. our 0.27 monolayer) and reported a number of similarities and minor differences in the interpretation of acetyelene decomposition.

The preadsorption of oxygen induces dramatic changes in the bonding of molecularly chemisorbed ethylene on several metal surfaces. On clean Pd(100) (**5**), Fe(111) (**6**), Pt(111) (**7**) and Ru(001) (**8-10**), ethylene is di-σ-bonded with rehybridization to sp^3. However, in the presence of a sufficient concentration of preadsorbed oxygen adatoms, it bonds to all of these surfaces in a π-bonded configuration, retaining its sp^2 hybridization. It is thus of interest to study the coadsorption of oxygen and acetylene on Ru(001), in order to determine whether the electron-withdrawing oxygen adatoms induce similar changes in the bonding of acetylene. The coadsorption of oxygen and acetylene has received surprisingly little attention in the past (**11**). The large data base now available concerning the adsorption of ethylene (**8-10,12-13**) and acetylene (**2-4**) on clean and chemically modified Ru(001) sur-

faces makes this surface an ideal one on which to investigate this issue. Accordingly, we report here an EELS and TDMS study of acetylene adsorption and decomposition on two different oxygen-precovered Ru(001) surfaces. Oxygen adsorbs dissociatively on Ru(001) at 80 K, and the oxygen adatoms occupy threefold hollow sites exclusively (**14**).

The two oxygen-precovered surfaces we have chosen to investigate are the well-characterized and reproducible Ru(001)–p(2x2)–O and Ru(001)–p(1x2)–O surfaces. Figure 1 shows the structures and EEL spectra of these surfaces. The p(2x2) oxygen adatom overlayer corresponds to an oxygen adatom coverage of 0.25 relative to the surface concentration of ruthenium atoms, which is 1.58 x 10^{15} cm^{-2} (**15**). The p(1x2) oxygen adatom overlayer corresponds to an oxygen adatom coverage of 0.5, which is the saturation coverage of oxygen adatoms that can be obtained by exposing the Ru(001) surface to oxygen gas under ultrahigh vacuum (UHV) conditions. The electron-withdrawing effect of the oxygen adatoms increases the work function by 0.2 eV in the case of the p(2x2) overlayer and 1.06 eV in the case of the p(1x2) overlayer (**14**). While clean Ru(001) is characterized by a featureless EEL spectrum, the ordered oxygen overlayers give rise to distinctive vibrational loss features (**16**). On Ru(001)–p(2x2)–O, an intense loss feature occurs at 535 cm^{-1} due to the vibration of the oxygen adatoms perpendicular to the surface, ν_s(RuO). A loss feature is also present at 250 cm^{-1} due to the coupling of the oxygen adatom vibrations to a ruthenium surface phonon. The corresponding loss features on Ru(001)–p(1x2)–O occur at 585 and 240 cm^{-1}, and an additional loss feature due to the asymmetric ruthenium-oxygen stretching vibration, ν_a(RuO), occurs at 430 cm^{-1}. The latter mode involves motion of the oxygen atoms largely parallel to the surface, but not entirely so due to the coupling of this mode to ν_s(RuO). It should be pointed out that the real (i.e. non-ideal) p(1x2)-O overlayer actually consists of three types of independent and otherwise identical domains that are rotated 120° with respect to one another. Where these domains meet there will be small areas that are relatively oxygen-deficient, and which may exhibit chemistry more typical of the p(2x2)-O overlayer.

II. Experimental Procedures

Most of the pertinent details concerning the EEL spectrometer used in these studies and the UHV chamber housing it have been described elsewhere (**17**). In our previous study of the chemistry of

acetylene on clean Ru(001) (**2**), the thermal desorption measurements were performed in a separate UHV chamber (**18**) which also contains a Ru(001) crystal but which was more specifically designed to perform thermal desorption measurements. In this chamber, the crystal-to-mass spectrometer distance was much less than in the EELS chamber, and the mass spectrometer was interfaced to a computer which allowed the simultaneous monitoring of up to six different masses in thermal desorption spectra. The mass spectrometer in this chamber also had an attached skimmer to better distinguish desorption from the crystal face from desorption from crystal edges, support leads, etc. Since a more recent study of acetylene on Ru(001) (**4**) has reported qualitatively similar but quantitatively different thermal desorption results than those we obtained in our previous study, we have performed numerous additional thermal desorption measurements with acetylene in both of our UHV chambers. This has led to the conclusion that faulty computer software did indeed lead, in our previous study (**2**), to a calculated saturation coverage of acetylene that was too low by approximately 30%. Therefore, all of the thermal desorption measurements in the present study were performed in the same UHV chamber that houses the EEL spectrometer.

The acetylene and oxygen used in these studies, and their handling, have been discussed elsewhere, as have the cleaning and cooling of the Ru(001) crystal (**2,10**).

III. Results

A. Thermal Desorption Mass Spectrometry

Following large acetylene exposures on Ru(001)–p(2x2)–O and Ru(001)–p(1x2)–O at 80 K, only H_2, CO and multilayer acetylene are observed to desorb when the surface is annealed from 80 K to above 900 K. Multilayer acetylene desorbs near 95 K. The acetylene multilayers were discussed in detail previously (**2**) and will not be considered further here.

Figure 2 shows the hydrogen (m/e = 2 amu) thermal desorption spectra that result following 5 L C_2H_2 exposures to (a) clean Ru(001), (b) Ru(001)–p(2x2)–O and (c) Ru(001)–p(1x2)–O at 80 K. On all three surfaces, hydrogen desorption is complete near 700 K, and the onset of desorption is near 250 K on clean Ru(001), near 215 K on Ru(001)–p(2x2)–O, and near 300 K on Ru(001)–p(1x2)–O. Each

spectrum shows a relative minimum in the rate of H_2 evolution near 450-480 K, and the percentage of H_2 desorbing below this minimum is estimated to be approximately 55-60% on clean Ru(001), 45-50% on Ru(001)–p(2x2)–O, and 20-40% on Ru(001)–p(1x2)–O. Note that the value for clean Ru(001) is lower than our previously published value of 75% (2).

The saturation coverage of acetylene on each surface following adsorption at 80 K was estimated by comparing the integrated intensities of the thermal desorption spectra of Fig. 2 with the integrated intensities of H_2 thermal desorption spectra measured following saturation (10 L) hydrogen exposures to clean Ru(001) (the latter of which were obtained immediately prior to the oxygen and acetylene exposures). For clean Ru(001), a saturation hydrogen adatom coverage of 0.85 was assumed in accordance with the previously published value of Shimizu et al. (19). The resulting saturation acetylene coverages, which are accurate to approximately ±0.05 monolayer, are 0.39 monolayer on clean Ru(001), 0.31 monolayer on Ru(001)–p(2x2)–O, and 0.09 monolayer on Ru(001)–p(1x2)–O. Note that the value of 0.39 on clean Ru(001) is higher than our previously published value of 0.27 (2), which we now believe to be in error. Note also that our coverages must be multiplied by 1/0.85 = 1.18 in order to be compared directly to the clean surface coverage in Ref. 4, since a saturation hydrogen adatom coverage of unity was assumed in that study.

Following exposures of acetylene on Ru(001)–p(2x2)–O and Ru(001)–p(1x2)–O, the desorption of carbon monoxide was also observed due to the recombination of carbon (formed from acetylene decomposition and oxygen adatoms. This desorption occurred between approximately 450 and 780 K on both surfaces, with a peak desorption temperature of approximately 620 K. Since the relative uncertainty in our determination of the saturation acetylene coverage on Ru(001)–p(1x2)–O using hydrogen thermal desorption is quite large (0.09 ± 0.05), we attempted to measure the amount of CO desorbed from this surface following a saturation acetylene exposure. Since a sloping background is always present in mass 28 thermal desorption spectra obtained in our chamber due to the presence of CO in the chamber background, and since the recombinatively desorbed CO desorbs over a broad temperature range, this estimate is rather crude. However, a reasonable baseline could be obtained by performing a mass 28 thermal desorption spectrum after exposing the *clean* Ru(001) surface to a saturation acetylene

exposure at 80 K (where no recombinative CO desorption occurs), and subtracting this baseline from the mass 28 thermal desorption spectrum for C_2H_2 on Ru(001)–p(1x2)–O. The remaining integrated intensity was compared to that obtained for a mass 28 thermal desorption spectrum following a saturation CO exposure on clean Ru(001) at room temperature, where the carbon monoxide coverage is known to be approximately 0.68 (20). The result obtained is that approximately 0.17 monolayer of CO desorbs recombinatively, corresponding to an acetylene coverage of approximately 0.08, in very good agreement with the H_2 thermal desorption result.

B. Electron Energy Loss Spectroscopy

i. Molecularly Chemisorbed Acetylene on Ru(001)-p(2x2)-O

Figure 3 shows the EEL spectra that result when the Ru(001)–p(2x2)–O surface at 80 K is exposed to (a) 0.2 L C_2H_2, (b) 2 L C_2H_2 and (c) 2 L C_2D_2. The spectrum of Fig. 3(a) is dominated by Type I acetylene and is similar to previous results obtained for low coverages of chemisorbed acetylene on clean Ru(001) (4), with the dominant loss features being ν(CC) (1110 cm^{-1}) and ν(CH) (2990 cm^{-1}). The frequencies of these modes are very similar to their clean surface values, with ν(CH) being slightly (approximately 40 cm^{-1}) upshifted. The weak shoulder that is present at 730 cm^{-1} indicates the presence of a very small amount of Type II acetylene as well. At a near saturation exposure [cf. Fig. 3(b)], much more Type II acetylene is clearly present, as evidenced by the CH bending loss features at 740 and 960 cm^{-1}. The EEL spectrum of Fig. 3(b) is very similar to that obtained for a saturation acetylene exposure on Ru(001) at 80 K followed by annealing to 150 K (2). The shoulders near 420 and 470 cm^{-1} in Fig. 3(a) and (b) probably derive intensity mainly from the RuC stretching modes of the chemisorbed acetylene, although contributions from ν_s(RuO) due to p(1x2)-like defects in the p(2x2)-O overlayer cannot be excluded in (b) (16). The EEL spectrum of Fig. 3(c) is due to a near saturation coverage of deuterated acetylene on Ru(001)–p(2x2)–O, and again clearly shows a mixture of Type I [ν(CC) = 1100 cm^{-1}) and Type II (CD bend as a shoulder at 680 cm^{-1}, downshifted from 960 cm^{-1} in C_2H_2) acetylene. The strong CD bend of the Type II acetylene is downshifted from 740 cm^{-1} in C_2H_2 to approximately 565 cm^{-1} (2,4), overlapping with the ν_s(RuO) and ν(RuC) loss features, and forming a broad feature centered at 525 cm^{-1}. As with C_2H_2, the frequencies of the observed loss features for

both types of C_2D_2 are shifted very slightly, or not at all, compared to the clean surface.

It should be noted that the relative amounts of Type I and Type II acetylene formed on Ru(001)–p(2x2)–O following a saturation C_2H_2 exposure at 80 K were found to be somewhat variable. The intensity of the Type I acetylene ν(CC) loss feature at 1130 cm^{-1} varied from being approximately as intense as the Type II CH bending mode at 960 cm^{-1} [as in Fig. 3(b)] to only about a third as intense in some other spectra. The latter probably correspond to surfaces with oxygen adatom coverages slightly greater than 0.25, so that small areas of the surface have a p(1x2)-O rather than a p(2x2)-O structure. The formation of a complete p(1x2)-O overlayer blocks the formation of Type I acetylene completely (cf. Sec. III.B.ii).

The chemisorbed acetylene on Ru(001)–p(2x2)–O is stable below 200 K, beginning to decompose in the temperature range between 200 and 250 K. Thus, the chemisorbed acetylene is not stabilized compared to the clean surface, where decomposition begins near 230 K (**2**).

ii. Molecularly Chemisorbed Acetylene on Ru(001)-p(1x2)-O

Electron energy loss spectra of acetylene adsorbed on Ru(001)–p(1x2)–O are shown in Fig. 4. The most prominent result, evident in Fig. 4(a), is that even for very low coverages, only Type II acetylene is formed, as evidenced by the lack of the characteristic ν(CC) loss feature near 1130 cm^{-1} of Type I acetylene (**4**). Occasionally, a very weak peak was observed near 1130 cm^{-1} (approximately one-tenth as intense as the 960 cm^{-1} loss feature of Type II acetylene), due, presumably, to an oxygen adatom coverage of slightly less than the ideal p(1x2) coverage of 0.5, or to the formation of Type I acetylene at p(1x2)-O domain boundaries.

The spectrum of Fig. 4(b) corresponds to a saturation coverage of C_2H_2 on Ru(001)–p(1x2)–O. The surface was annealed briefly to 120 K following acetylene adsorption at 80 K in order to desorb small amounts of multilayer acetylene. Again, only Type II acetylene is present, displaying the characteristic CH bending modes at 755 and 970 cm^{-1} and ν(CH) at 3000 cm^{-1}. The carbon-carbon stretch is also resolved as a weak loss feature at 1220 cm^{-1}. We were not able to resolve this loss feature on clean Ru(001) or Ru(001)–p(2x2)–O, most likely due to overlap with the ν(CC) loss feature of Type I acetylene, but the frequency observed here is quite close to the frequency of 1260 cm^{-1} reported by

Jakob et al. for clean Ru(001) (4). Finally, there is a very intense loss feature at 530 cm^{-1} which is assigned as a ruthenium-carbon stretching mode of the adsorbed acetylene. Similar frequencies have been observed for this mode on clean Ru(001) (2,4), although this loss feature was not nearly so intense in those cases.

Figure 4(c) shows the EEL spectrum that results when the Ru(001)–p(1x2)–O surface is exposed to 2 L of C_2D_2 at 80 K, followed by annealing to 120 K to remove any multilayer acetylene. The only loss features of the chemisorbed acetylene that are resolved clearly are ν(CD) at 2230 cm^{-1} and ν(CC) at 1190 cm^{-1}, which are due to Type II acetylene. The downshifted CD bending modes, the RuC stretching modes and the ν_s(RuO) mode all overlap, froming a broad loss feature centered at 565 cm^{-1}.

Both EELS and TDMS results indicate that chemisorbed acetylene begins to decompose near 300 K on Ru(001)–p(1x2)–O. It is thus stabilized significantly compared to the clean Ru(001) surface.

iii. Decomposition of Chemisorbed Acetylene on Ru(001)-p(2x2)-O

A series of EEL spectra obtained following the adsorption of 2L of C_2H_2 on Ru(001)–p(2x2)–O at 80 K followed by annealing to various temperatures is shown in Fig. 5. In the discussion that follows, it is useful to refer to Table I, which summarizes the vibrational spectra of species identified previously in the decomposition of acetylene and ethylene on various Ru(001) surfaces (2-4,8-13). As noted previously, decomposition begins between 200 and 250 K, and annealing from 80 to 250 K causes several changes in the EEL spectrum. The loss features due to Type II acetylene decrease in intensity, the loss feature near 1135 cm^{-1} increases in intensity, and new loss features appear at 1345 and 1415 cm^{-1}. The loss feature at 1345 cm^{-1} and the increase in intensity of the 1135 cm^{-1} loss feature are attributed to $\delta_s(CH_3)$ and ν(CC) of ethylidyne. Since ethylidyne (CCH_3) contains more hydrogen atoms than acetylene, a dehydrogenation product must also be present. Indeed, acetylide (CCH) is present but cannot be unambigously resolved in Fig. 5(b) because its characteristic CH bending loss feature occurs at nearly the same frequency (approximately 750 cm^{-1}) as the intense CH bend of Type II acetylene. Finally, the loss feature at 1415 cm^{-1} is due in part to $\delta_s(CH_3)$ of ethylidyne, although its intensity suggests the presence of a $\delta(CH_2)$ mode due either to a vinyl ($CHCH_2$) or, more likely, to a vinylidene (CCH_2) species. Note that little, if any, Type I acetylene has decomposed by

250 K. Annealing to 300 K results in the formation of additional ethylidyne and a strong decrease in the intensity of the Type II acetylene CH bending mode near 955 cm^{-1}, which indicates clearly that the 765 cm^{-1} loss feature of Fig. 5(c) is due primarily to acetylide rather than Type II acetylene.

Much more pronounced changes occur when the surface is annealed from 300 to 350 K. Strong loss features appear at 1435, 885 and 435 cm^{-1} which are due to the formation of an sp^2-hybridized vinylidene species which we have identified previously as a decomposition product of ethylene on Ru(001)–p(2x2)–O (**9,10**). The mode assignments are ν(CC) and $\delta(CH_2)$ (uncoupled), 1435 cm^{-1}; $\omega(CH_2)$, 885 cm^{-1}; and ν(Ru-CCH_2), 435 cm^{-1}. Some ethylidyne is also present as evidenced by the loss features at 1125 and 1320 cm^{-1}, and, in fact, the amount of ethylidyne seems to be reduced only slightly compared to the 300 K spectrum, as evidenced by the intensity of the latter mode. The loss feature at 775 cm^{-1} is due to δ(CH) of acetylide. The 995 cm^{-1} loss feature is more problematic; both vinylidene [$\rho(CH_2)$] and the ethylidyne [$\rho(CH_3)$] have loss features that occur near this frequency, but both of these modes are usually quite weak. It appears that virtually all of the chemisorbed acetylene has decomposed by 350 K. The 955 cm^{-1} loss feature of Type II acetylene has disappeared completely, and the decomposition of Type I acetylene is indicated by the large decrease in the intensity of the loss feature near 1140 cm^{-1} upon annealing from 300 to 350 K. It is interesting to note that the decomposition of the Type I acetylene correlates with the appearance of the strong modes due to sp^2-hybridized vinylidene.

Annealing to 380 K results in the decomposition of much of the vinylidene, an upshift in the center of the peak near 3000 cm^{-1} due to CH stretching modes, and the development of a broad loss feature centered at 810 cm^{-1}. The last feature grows in intensity upon annealing to 450 K, while all of the loss features due to vinylidene disappear, and loss features remain at 980, 1150 and 1370 cm^{-1}. While these last three modes are due primarily to ethylidyne, they are quite broad, and contributions from the carbon-carbon stretching vibrations of C_2 dimers or other forms of surface carbon cannot be excluded (**4,12**). In fact, a corresponding EEL spectrum for C_2D_2 on Ru(001)–p(2x2)–O annealed to 450 K shows a broad, weak loss feature at 1315 cm^{-1} due to some type of carbon-carbon stretching mode(s). Annealing to 600 K leaves only the ν_s(RuO) loss feature at 530 cm^{-1}, the loss feature at 805

cm^{-1} (*now rather sharp*), and a CH stretching loss feature at 3050 cm^{-1}. The loss features at 805 and 3050 cm^{-1} have been assigned previously to the δ(CH) and ν(CH) modes, respectively, of an inclined methylidyne (CH) species (**2,8,12**).

Finally, annealing to 800 K causes all of the methylidyne to decompose and the oxygen to be titrated away [as CO(g)] by surface carbon, leaving very weak loss features near 445 and 595 cm^{-1} which are due to surface carbon. These EELS results are in good qualitative agreement with the thermal desorption results, of which the latter show the desorption of H_2 to be complete near 700 K.

iv. Decomposition of Chemisorbed Acetylene on Ru(001)-p(1x2)-O

The decomposition of acetylene on Ru(001)–p(1x2)–O was also investigated, and a series of EEL spectra obtained following a 4 L exposure at 80 K with annealing to various temperatures is shown in Fig. 6. It is clear from inspection of Fig. 6 that many of the same decomposition products occur that are formed on Ru(001)–p(2x2)–O, and we note here only some of the more interesting differences.

Probably the most striking difference is that much less sp^2-hybridized vinylidne is formed than on Ru(001)–p(2x2)–O. In the 350 K EEL spectrum [Fig. 6(d)], loss features are present at 1420, 910 and 450 cm^{-1} which can be attributed entirely or in part to this species, but in comparison to the remaining loss features in the spectrum these are much less intense than the corresponding ones in Fig. 5(d). The fact that virtually no Type I acetylene is formed on Ru(001)–p(1x2)–O [although a trivial amount is present in Fig. 6(a) as evidenced by ν(CC) at 1115 cm^{-1}] tends to support the observation that on Ru(001)–p(2x2)–O most of the sp^2-hybridized vinylidene is formed via decomposition of Type I acetylene rather than Type II acetylene.

Apart from this obvious difference, the spectra are similar to those of Fig. 5 in many respects, although on Ru(001)–p(1x2)–O no decomposition products appear at 250 K, again suggesting that the chemisorbed acetylene is stabilized slightly on this surface. Ethylidyne is clearly formed on both surfaces and in each case at least some appears to be stable to 450 K. The spectra obtained following annealing to 450 and 600 K on both oxygen-precovered surfaces are very similar indeed, the only notable difference being the presence of a broad loss feature near 1315 cm^{-1} in Fig. 6(h) that is not apparent in Fig. 5(g). This feature is attributed to carbon-carbon stretching modes of some form of

surface carbon (4,12).

IV. Discussion

A. Molecularly Chemisorbed Acetylene

Table II lists the frequencies of various vibrational loss features of chemisorbed Type I and Type II acetylene on clean Ru(001), Ru(001)–p(2x2)–O and Ru(001)–p(1x2)–O. It is immediately apparent that ordered oxygen overlayers do not significantly affect the vibrational spectra of either type of acetylene on Ru(001). The only frequency shift that is large enough to have any significance and which appears to be reproducible is the upshift of the ν(CH) freuqency of Type II acetylene to 3000 cm^{-1} on Ru(001)–p(1x2)–O, which is approximately 60 cm^{-1} higher than its clean surface value. However, this does not seem to indicate a rehybridization of the Type II acetylene towards sp^2, since the ν(CC) frequency we measure is slightly *lower* thank that reported by Jakob et al. on clean Ru(001) (4). It can be concluded that the structure and bonding of acetylene on the oxygen-precovered surfaces is virtually identical to the sturcture and bonding on the clean surface, and that the electron-withdrawing effect of the oxygen has a negligible influence on these properties.

It was found that the preadsorption of oxygen inhibits the adsorption of acetylene on Ru(001), with the p(2x2)-O overlayer reducing the saturation coverage by approximately 20% and the p(1x2)-O overlayer reducing it by approximately 75% compared to the clean surface. This coverage reduction could be due both to stearic and to electronic effects of the preadsorbed oxygen. The fact that the vibrational spectra of chemisorbed acetylene are not changed significantly in the presence of oxygen suggests that stearic (i.e. site-blocking) effects are of primary importance, and in fact the lack of formation of Type I acetylene on Ru(001)–p(1x2)–O can be explained in terms of a site-blocking argument based on the previously proposed adsorption sites of Type I and Type II acetylene (4). The Type I acetylene is believed to occupy μ-sites and the Type II acetylene Δ-sites, as shown in Fig. 7. It can be seen that in the μ-type bonding the two carbon atoms of acetylene occupy adjacent threefold hollow sites, which on Ru(001) are located 1.56 Å apart (15). If it is assumed that a preadsorbed oxygen adatom blocks the adsorption of acetylene into the three adjacent threefold hollow sites, then the formation of Type I acetylene is possible on Ru(001)–p(2x2)–O up to a maximum coverage of θ (Type I) =

0.25. However, on Ru(001)–p(1x2)–O there do not exist two adjacent threefold hollow sites neither of which is directly adjacent to a threefold hollow site already occupied by an oxygen adatom, and thus *Type I bonding is not possible*. On the other hand, Δ-type bonding involves essentially bonding of the entire acetylene molecule over a single threefold hollow site, and is thus possible on both Ru(001)–p(2x2)–O and Ru(001)–p(1x2)–O. We therefore believe that the EELS evidence concerning the lack of Type I acetylene formation on Ru(001)–p(1x2)–O provides support for the previously proposed bonding geometries of Type I and Type II acetylene. It must also be pointed out, however, that site-blocking arguments alone cannot explain the low saturation coverage of acetylene on Ru(001)–p(1x2)–O, since enough threefold hollow sites not adjacent to oxygen atoms are still present on this surface to form up to a quarter monolayer of Type II acetylene. (There are actually a half monolayer of such threefold sites, but it is stearically possible only to put an acetylene molecule at half of these.) The saturation acetylene coverage of 0.09 monolayer must therefore be influenced by some electronic effect, e.g. by a reduction in the local density of states at the Fermi level due to the electrons "tied-up" in ruthenium-oxygen bonding, making less electron density available for ruthenium-acetylene bonding.

Another possible explanation for the low saturation acetylene coverage on Ru(001)–p(1x2)–O is that acetylene adsorption could be limited to p(1x2) domain boundaries that are relatively oxygen-deficient and thus are similar to small areas of p(2x2)-O structure on the surface. This would suggest that no acetylene adsorption and decomposition would be observed on a hypothetical, perfect Ru(001)–p(1x2)–O surface, for either stearic or electronic reasons. If this is the case, the lack of Type I acetylene on the Ru(001)–p(1x2)–O surface is still qualitatively understandable, since it would be unlikely to have two of the adjacent, available threefold hollow sites in the small regions defining the domain boundaries.

It is interesting to compare the bonding of molecularly chemisorbed ethylene and acetylene on clean and oxygen-precovered Ru(001) surfaces. On clean Ru(001), ethylene is rehybridized to sp^3 in a di-σ-bonded configuration (**8,12**), while on Ru(001)–p(2x2)–O (**9,10**) and Ru(001)–p(1x2)–O (**8-10**) it forms an sp^2-hybridized, π-bonded species. Acetylene, on the other hand, forms the same two species

on clean Ru(001) and Ru(001)–p(2x2)–O, and while one of these (Type I acetylene) is not formed on Ru(001)–p(1x2)–O due to geometric effects, the bonding of Type II acetylene (and its vibrational spectrum) is virtually identical to its bonding (and vibrational spectrum) on the other two surfaces. The fact that ethylene is approximately sp^2-hybridized on the oxygen-precovered surfaces, while acetylene is nearly sp^3-hybridized, is a consequence of the differing energies of the π^* orbitals of ethylene and acetylene. The Fermi levels of the Ru(001), Ru(001)–p(2x2)–O and Ru(001)–p(1x2)–O surfaces lie approximately 5.5, 5.7 and 6.6 eV below the vacuum level, respectively (21,14). The unoccupied π^* orbitals of gas phase ethylene ($1b_{2g}$) and acetylene (π_g) lie at -2.85 and -6.1 eV with respect to the vacuum level, respectively (22,13). Upon adsorption, these orbital energies will downshift and broaden (24), but the π^* orbital of ethylene should still lie substantially above the Fermi levels of the three ruthenium surfaces, making electron backdonation from the metal 5d band difficult, especially on the oxygen-precovered surfaces, and resulting in only minor rehybridization of the ethylene on these two surfaces. On the other hand, the π^* orbitals of chemisorbed acetylene will lie near or below the Fermi levels of all three ruthenium surfaces, so that strong rehybridization occurs even on Ru(001)–p(1x2)–O.

B. Decomposition of Molecularly Chemisorbed Acetylene

The decomposition of molecularly chemisorbed acetylene has now been studied on clean Ru(001) (2,4), Ru(001)–p(2x2)–O and Ru(001)–p(1x2)–O. The discussion presented here will consider separately the different intermediates that are observed, and will address related issues for all three surfaces.

i. Acetylide (CCH)

Since studies of acetylene decomposition on the three ruthenium surfaces cited above have been made primarily for saturation coverages and under UHV conditions where adsorption of residual hydrogen should be negligible, and since in any case hydrogen does not chemisorb on the two oxygen-precovered surfaces at the temperatures where acetylene decomposition begins, the hydrogen atoms that are needed to produce ethylidyne from acetylene must be provided by the decomposition of other acetylene molecules. On clean Ru(001), the source of this hydrogen appears to be almost entirely carbon-hydrogen bond cleavage to produce acetylide, i.e.

$$C_2H_2(a) \longrightarrow CCH(a) + H(a) .$$

The acetylide has also been identified in the case of ethylene decomposition on Ru(001) (**12**), and is characterized principally by a strong bending mode, δ(CH), at approximately 750 cm^{-1}. Its remaining vibrational loss features, ν(CC) at 1290 cm^{-1} and ν(CH) at 2960 cm^{-1}, are often obscured by the presence of loss features due to other surface species.

On all ruthenium surfaces studied, the temperature at which acetylide begins to form would appear to be identical to that where acetylene decomposition begins, namely between 200 and 250 K on clean Ru(001) and Ru(001)–p(2x2)–O, and near 300 K on Ru(001)–p(1x2)–O. The decomposition of acetylide formed from acetylene decomposition on clean Ru(001) has been reported to be complete by 380 K (**2**) or 450 K (**4**), although this discrepancy is due to differing interpretations of the upshift in the prominent δ(CH) mode that occurs near 400 K [cf. Sec. IV.B.iv]. Since acetylide appears to be more stable than ethylidyne and vinylidene on clean Ru(001), we do not believe that it is likely to be an intermediate in the formation of those species.

ii. Vinylidene (CCH_2)

We have shown that annealing an acetylene-saturated Ru(001)–p(2x2)–O surface to 350 K leads to the formation of substantial amounts of an sp^2-hybridized vinylidene species, characterized primarily by intense loss features at 1435 [ν(CC) + $\delta(CH_2)$], 885 [$\omega(CH_2)$] and 435 [$\nu(Ru–CCH_2)$] cm^{-1}. The same species is formed on Ru(001)–p(2x2)–O as the result of ethylene decomposition (**9,10**). It has begun to decompose by 380 K and appears to be gone entirely by 450 K, and its disappearance correlates with the formation of an intense δ(CH) mode near 800 cm^{-1}. Its appearance correlates with the decomposition of Type I acetylene, but the mechanism of the (probably not elementary) reaction

$$C_2H_2 \text{ (Type I)} \longrightarrow sp^2–CCH_2$$

is not known. We regard a direct 1,2-hydrogen transfer reaction as unlikely, since the geometry of the [C···H···C] transition state would probably result in a large activation barrier, although this is certainly a possibility.

Small concentrations of a species that gives rise to a $\delta(CH_2)$ mode appear to be present following acetylene adsorption on Ru(001)–p(2x2)–O and annealing to 250 K and on Ru(001)–p(1x2)–O at least

in the temperature range of 300-400 K. The species involved is probably also vinylidene, although the presence of a vinyl ($CHCH_2$) species cannot be ruled out. We stress once again that the presence of relatively little vinylidene in the decomposition of acetylene on Ru(001)–p(1x2)–O, as judged from the relatively low intensity of the 1410-1435 cm^{-1} loss feature compared to the other loss features, is strong supporting evidence for the proposition that it is primarily Type I acetylene that gives rise to vinylidene formation on Ru(001)–p(2x2)–O.

On clean Ru(001) there has been some disagreement concerning the formation of vinylidene in acetylene decomposition. Ethylidyne (cf. Sec. IV.B.iii) formed from acetylene on clean Ru(001) gives rise to loss features near 1140, 1360 and 1440 cm^{-1}, and based on slight changes in the relative intensities of these loss features between 300 and 350 K Jakob et al. (4) concluded that another surface species was present and contributing to the intensity of the 1140 and 1440 cm^{-1} loss features. This species was identified as vinylidene, with $\delta(CH_2)$ at 1440 cm^{-1} and $\omega(CH_2)$ at 1140 cm^{-1}. On the other hand, we do not believe that our own data for annealing temperatures between 230 and 350 K justify the conclusion that any species other than acetylide and ethylidyne is present. We cannot rule out, however, the presence of very small amounts of vinylidene on clean Ru(001). We believe that spectrum 5(d) of this paper indicates clearly that the amount of vinylidene present due to acetylene decomposition on clean Ru(001) is indeed very small, since on the clean surface the 1440 cm^{-1} loss feature never has much greater intensity than the 1360 cm^{-1} loss feature. We also believe that *any* vinylidene formed on clean Ru(001) would more likely be sp^3-hybridized than sp^2-hybridized, just as ethylene is sp^3-hybridized on clean Ru(001) but sp^2-hybridized on the oxygen-precovered ruthenium surfaces. An sp^3-hybridized vinylidene species on clean Ru(001) would indeed be expected to have a CH_2 wagging frequency near 1200 cm^{-1}, rather than near 900 cm^{-1} as in the case of sp^2-hybridized vinylidene (25).

In summary, the p(2x2) oxygen adatom overlayer enhances substantially the stability of sp^2-hybridized vinylidene on Ru(001), whether formed from ethylene or acetylene decomposition.

iii. Ethylidyne (CCH_3)

Ethylidyne is formed as a decomposition product of acetylene on clean Ru(001) (2,4), Ru(001)–p(2x2)–O and Ru(001)–p(1x2)–O. It is characterized primarily by two loss features of

approximately equal intensity, $\delta_s(CH_3)$ at approximately 1360 cm^{-1} and $\nu(CC)$ at approximately 1140 cm^{-1}. On Ru(001)–p(2x2)–O it appears at an annealing temperature of approximately 250 K, reaches its maximum concentration by about 300 K, and has completely decomposed by about 500 K. The corresponding temperatures on Ru(001)–p(1x2)–O are approximately 300, 350 and 500 K, although the latter is difficult to judge due to the presence of carbon-carbon stretching loss features in the 1000-1400 cm^{-1} regime at elevated temperatures. Ethylidyne is thus stabilized on the oxygen precovered surfaces compared to clean Ru(001), where it has decomposed completely by about 360-370 K (**2,4,8,10**).

Our previous results (**2**) and those of Jakob et al. (**4**) are slightly different regarding the temperature of ethylidyne formation from acetylene decomposition on clean Ru(001). We found that adsorption of a saturation coverage of acetylene at 80 K followed by annealing produced ethylidyne by 250 K, with little change in the concentration of this species between 250 and 350 K. They found that following adsorption of a saturation coverage of acetylene at 130 K, ethylidyne was formed only after annealing to 300 K. This difference may be due to the fact that our saturated monolayer after adsorbing at 80 K and annealing to 150 K consisted of a strong mixture of Type I and Type II acetylene, while their saturated monolayer at 130 K consisted almost entirely of Type II acetylene. It is quite possible that these two types of acetylene would undergo slightly different chemistry on clean Ru(001), given that they apparently do so in the presence of a p(2x2) oxygen adatom overlayer.

The mechanism of ethylidyne formation from acetylene on metal surfaces is of considerable importance but has received relatively little attention. We proposed no mechanism in our previous study of acetylene adsorption on clean Ru(001) (**2**). Jakob et al. (**4**) recently proposed as a tentative mechanism

$$\mathrm{CHCH(Type\ II)(a)} \xrightarrow[1]{} \mathrm{CCH_2(a)} \xrightarrow[2]{+H} \mathrm{CCH_3(a)}\ ,$$

for the decomposition of Type II acetylene on clean Ru(001), where the hydrogen atoms in the second step are provided by the decomposition of additional acetylene molecules to acetylide. At about the same time, Hills (**26**) independently proposed the similar but slightly more complex mechanism

$$CHCH(a) \xrightarrow[1]{+H} CHCH_2(a) \xrightarrow[2]{-H} CCH_2(a) \xrightarrow[3]{+H} CCH_3(a)$$
$$CCH_2(a) \xrightarrow[4]{-H} CCH(a)$$

In this scheme, the $CHCH_2$ and CCH_2 are viewed as rather unstable reaction intermediates which react quickly to produce one of the two principal products of acetylene decomposition below approximately 350 K, namely ethylidyne and acetylide. The hydrogen atoms in the first step are again produced by the direct decomposition of some acetylene to acetylide. The vinyl ($CHCH_2$) intermediate was invoked primarily for two reasons. First, it avoids the formation of vinylidene via the stable acetylide species (as does the mechanism of Jakob et al.) and also via direct 1,2-hydrogen atom transfer in acetylene, which is likely to have a high activation barrier (27). Second, the formation of vinyl from acetylene is very plausible in view of the fact that small amounts of acetylene on Ru(001) can be hydrogenated to ethylene near 175 K in the presence of preadsorbed hydrogen (3). The experiments with coadsorbed oxygen and acetylene can unfortunately shed little light on to what extent either or both of these mechanisms is operating. The best way to attempt to distinguish between the two is to coadsorb D_2 and C_2H_2 or H_2 and C_2D_2. In the former case, the mechanism of Jakob et al. would produce ethylidyne primarily of the CCH_2D type, while the mechanism of Hills would produce primarily ethylidyne of the $CCHD_2$ type. Our results for C_2H_2 adsorbed on a deuterium presaturated surface and annealed to 300 K (26) show primarily the formation of CCD_2H [$\delta_s(CD_2H)$ = 1150 cm^{-1}] and CCD_3 [$\delta_s(CD_3)$ = 1050 cm^{-1}], with a smaller amount of $CCDH_2$ [$\delta_s(CDH_2)$ = 1260 cm^{-1}] and no CCH_3. While the predominance of CCD_2H is more consistent with the mechanism of Hills, our data base is not extensive and the mixture of ethylidyne products suggests that more than one mechanism and/or exchange reactions may be occurring. Future investigations along these lines would be of obvious interest.

The products of ethylidyne decomposition on Ru(001) are also controversial, and no fewer than three decomposition reactions have been proposed for ethylidyne decomposition on the clean surface. These are the following:

$$CCH_3(a) \longrightarrow C(a) + CH(a) + 2H(a) \quad (8)\,,$$
$$CCH_3(a) \longrightarrow 2C(a) + 3H(a) \quad (2,12)\,, \text{ and}$$
$$CCH_3(a) \longrightarrow CCH(a) + 2H(a) \quad (4)\,.$$

We are currently of the opinion that all of these reactions may occur to some extent, depending on the local concentrations of various surface species. However, on Ru(001)–p(2x2)–O it is primarily the decomposition of vinylidene (and possibly also acetylide) that correlates with the appearance of the intense δ(CH) mode of methylidyne near 800 cm^{-1}, and not the decomposition of ethylidyne. The same appears to be true on Ru(001)–p(1x2)–O.

iv. Methylidyne (CH)

When acetylene is adsorbed on Ru(001) (**2,4**), Ru(001)–p(2x2)–O or Ru(001)–p(1x2)–O, and the surface is annealed to temperatures in the range of approximately 400-700 K, at least one intermediate is formed that is characterized by a strong δ(CH) loss feature near 800 cm^{-1} and a ν(CH) loss feature in the range of 3000-3050 cm^{-1}. The same is true of ethylene adsorption on Ru(001) (**8,12**) and Ru(001)–p(2x2)–O (**9,10**). Broad, weak loss features are sometimes present as well between 1000 and 1500 cm^{-1} (**4,12**). The hydrogen-containing species was originally assigned by Barteau et al. as a bent methylidyne (CH) (**8**). We subsequently endorsed this assignment (**3,12**), and attributed the loss features between 1000 and 1500 cm^{-1} to ν(CC) loss features of carbon dimers (**12**). More recently, Jakob et al. have suggested that a number of carbonaceous fragments are present on Ru(001) between 400 and 700 K, possibly incuding methylidyne, acetylide and larger species (**4**).

While the coexistence of several hydrogen-containing surface species in this temperature range cannot be ruled out (especially since some may be present in very low concentrations), we still favor methylidyne as being the principal hydrogen-containing species present. We have not found the intensity of the δ(CH) mode near 800 cm^{-1} to show much correlation with the weak loss features between 1000 and 1500 cm^{-1}, and occasionally the δ(CH) and ν(CH) loss features are isolated quite cleanly in the absence of these modes [cf. Fig. 5(g)]. We thus prefer to identify these weak features with some (possibly several) forms of surface carbon. We do not believe that the presence of three weak H_2 thermal decomposition maxima between 500 and 700 K (**3,4**) is inconsistent with the presence of only methylidyne and surface carbon, given the possible effects of variations in the local concentrations of these species on the surface and the averaging effects that occur in thermal desorption spectra. Ace-

tylide has a substantially lower frequency CH bending mode (approximately 750 cm^{-1}) than methylidyne and does not appear to be present on either the clean or oxygen-precovered surfaces above 400-450 K.

Methylidyne seems to be formed via the decomposition of several surface species, including acetylide, vinylidene and (directly or indirectly) ethylidyne on both oxygen-precovered Ru(001) surfaces. Its decomposition is complete near 700 K on both of these surfaces and on clean Ru(001).

V. Summary

Electron energy loss spectroscopy and thermal desorption mass spectrometry have been used to investigate the adsorption and decomposition of acetylene on Ru(001)–p(2x2)–O and Ru(001)–p(1x2)–O, and the results have been compared to those of previous studies of acetylene on clean Ru(001). The principal conclusions of this study are the following:

(1) The saturation coverages of acetylene adsorbed on clean Ru(001), Ru(001)–p(2x2)–O and Ru(001)–p(1x2)–O at 80 K are approximately 0.39, 0.31 and 0.09, respectively. These coverages are based on the assumption that the saturation coverage of hydrogen adatoms on Ru(001) following exposure to H_2 at 80 K is 0.85 monolayer.

(2) On Ru(001)–p(2x2)–O, as on clean Ru(001) (**4**), two types of acetylene are formed: Type I at low coverages and Type II at high coverages. On Ru(001)–p(1x2)–O only Type II acetylene is formed. This supports the previous suggestion that Type I acetylene adsorbs in μ-sites, since such adsorption sites are available on Ru(001) and Ru(001)–p(2x2)–O but not on Ru(001)–p(1x2)–O (assuming that preadsorbed oxygen atoms block adjacent threefold hollow sites towards the adsorption of acetylene carbon atoms).

(3) The molecularly chemisorbed acetylene species formed on Ru(001)–p(2x2)–O and Ru(001)–p(1x2)–O are very similar to the corresponding species formed on clean Ru(001), as judged by their EEL spectra. This is in marked contrast to the adsorption of ethylene, which is di-σ-bonded on clean Ru(001) and π-bonded on Ru(001)–p(2x2)–O and Ru(001)–p(1x2)–O. This difference is due to the lower energy of the acetylene π^* orbitals compared to the

ethylene π^* orbital. The lower π^* orbital energies in the case of acetylene lead to a nearly sp^3 hybridization of this molecule on all three surfaces.

(4) As on clean Ru(001), chemisorbed actylene on Ru(001)–p(2x2)–O and Ru(001)–p(1x2)–O does not desorb molecularly but decomposes completely to yield $H_2(g)$ as the only hydrogen-containing thermal desorption product. Decomposition begins just above 200 K on Ru(001)–p(2x2)–O and near 300 K on Ru(001)–p(1x2)–O.

(5) As on clean Ru(001), the decomposition of acetylene on the oxygen-precovered surfaces is complex and involves a number of stable intermediates. The reactions may be summarized as follows (these clearly are not intended to represent elementary steps):

Ru(001)-p(2x2)-O

$$\text{CHCH (Type II)} \xrightarrow{\sim 200\text{–}300\text{K}} \text{CCH} + \text{CCH}_3 + \text{H}$$

(small amounts of CCH_2 and/or $CHCH_2$ are probably also formed)

$$\text{CHCH (Type I)} \xrightarrow{\sim 300\text{–}350\text{K}} \text{CCH}_2\ (sp^2)$$

$$\text{CCH,CCH}_2\text{,CCH}_3 \xrightarrow{\sim 350\text{–}450\text{K}} \text{CH} + \text{surface carbon} + \text{H}$$

$$\text{CH} \xrightarrow{\sim 500\text{–}700\text{K}} \text{surface carbon} + \text{H}$$

$$2\text{H} \xrightarrow{\sim 215\text{–}700\text{K}} \text{H}_2\text{(g)}$$

Ru(001)-p(1x2)-O

$$\text{CHCH (Type II)} \xrightarrow{\sim 300\text{–}350\text{K}} \text{CCH} + \text{CCH}_2 + \text{CCH}_3 + \text{H}$$

$$\text{CCH,CCH}_2\text{,CCH}_3 \xrightarrow{\sim 400\text{–}450\text{K}} \text{CH} + \text{surface carbon} + \text{H}$$

$$\text{CH} \xrightarrow{\sim 500\text{–}700\text{K}} \text{CH surface carbon} + \text{H}$$

$$2\text{H} \xrightarrow{\sim 300\text{–}700\text{K}} \text{H}_2\text{(g)}$$

(6) An sp^2-hybridized vinylidene species is formed in especially large amounts on Ru(001)–p(2x2)–O from the decomposition of Type I acetylene. Little if any of this vinylidene is formed either on Ru(001)–p(1x2)–O (where no Type I acetylene forms) or on clean Ru(001) (where there is no stabilization by coadsorbed oxygen).

Acknowledgments: The authors gratefully acknowledge the assistance of Dale Johnson in obtaining some of the thermal desorption spectra. This work was supported by the National Science Foundation via Grant No. CHE-8617826.

References

1. H. Ibach and D. L. Mills, *Electron Energy Loss Spectroscopy and Surface Vibrations*, Academic Press, N.Y., 1982, p. 294.

2. J. E. Parmeter, M. M. Hills and W. H. Weinberg, J. Am. Chem. Soc. **108**, 3563 (1986).

3. J. E. Parmeter, M. M. Hills and W. H. Weinberg, J. Am. Chem. Soc. **109**, 72 (1987).

4. P. Jakob, A. Cassuto and D. Menzel, Surface Sci., to be published.

5. E. M. Stuve, R. J. Madix and C. R. Brundle, Surface Sci. **152/153**, 532 (1985).

6. U. Seip, M.-C. Tsai, J. Küppers and G. Ertl, Surface Sci. **147**, 65 (1984).

7. H. Steininger, H. Ibach and S. Lehwald, Surface Sci. **117**, 685 (1982).

8. M. A. Barteau, J. Q. Broughton and D. Menzel, Appl. Surface Sci. **19**, 92 (1984).

9. M. M. Hills, J. E. Parmeter and W. H. Weinberg, J. Am. Chem. Soc. **109**, 597 (1987).

10. M. M. Hills, J. E. Parmeter and W. H. Weinberg, J. Am. Chem. Soc. **109**, 4224 (1987).

11. E. M. Stuve, R. J. Madix and B. A. Sexton, Surface Sci. **123**, 491 (1982).

12. M. M. Hills, J. E. Parmeter, C. B. Mullins and W. H. Weinberg, J. Am. Chem. Soc. **108**, 3554 (1986).

13. M. M. Hills, J. E. Parmeter and W. H. Weinberg, J. Am. Chem. Soc. **108**, 7215 (1986).

14. T. E. Madey, H. A. Engelhardt and D. Menzel, Surface Sci. **48**, 304 (1975).

15. This surface density of ruthenium atoms as well as the 1.56 Å distance between adjacent threefold hollow sites is calculated easily from the 2.71 Å nearest-neighbor distance on this surface. C. Kittel, in "Introduction to Solid State Physics", 5th ed., Wiley & Sons, N.Y., 1976, p. 31.

16. T. S. Rahman, A. B. Anton, N. R. Avery and W. H. Weinberg, Phys. Rev. Letters **51**, 1979 (1983).

17. G. E. Thomas and W. H. Weinberg, Rev. Sci. Instr. **50**, 497 (1979);

18. E. D. Williams and W. H. Weinberg, Surface Sci. **82**, 93 (1979).

19. H. Shimizu, K. Christmann and G. Ertl, J. Catal. **61**, 412 (1980).

20. H. Pfnür, D. Menzel, F. M. Hoffmann, A. Ortega and A. M. Bradshaw, Surface Sci. **93**, 431 (1980).

21. K. Wandelt, J. Hulse and J. Küppers, Surface Sci. **104** 212 (1981).

22. R. S. Mulliken, J. Chem. Phys. **71** 556 (1979).

23. D. F. Dance and I. C. Walker, Chem. Phys. Lett. **18** 601 (1973).

24. J. E. Demuth and D. E. Eastman, Phys. Rev. B **13**, 1523 (1976).

25. Reference 1, p. 195.

26. M. M. Hills, Ph.D. Thesis, California Institute of Technology, **1987**, pp. 154-163.

Table I: *Vibrational* frequencies (in cm^{-1}) of various hydrocarbon intermediates identified previously in the decomposition of acetylene and ethylene on clean and/or chemically modified Ru(001) surfaces. This is a summary of data from Refs. 2-4 and 8-13.

Species	Mode	Frequency
(1) Ethylidyne (CCH_3)	$\nu_a(CH_3)$	3000-3045 vw
	$\nu_s(CH_3)$	2910-2970 s
	$\delta_a(CH_3)$	1440-1450 w
	$\delta_s(CH_3)$	1340-1370 s
	$\nu(CC)$	1120-1140 s
	$\rho(CH_3)$	970-1000 w
	T_z	450-480 w
(2) Vinylidene (CCH_2)	$\nu_a(CH_2)$	3050 w
	$\nu_s(CH_2)$	2985 m
	$\nu(CC) + \delta(CH_2)$	1435 vs
	$\rho(CH_2)$	965 w
	$\omega(CH_2)$	895 s
	T_z	455 s
(3) Acetylide (CCH)	$\nu(CH)$	2935-2960 w
	$\nu(CC)$	1290 w
	$\delta(CH)$	750-770 s
	T_z	435 m
(4) Methylidyne (CH)	$\nu(CH)$	3010-3030 w
	$\delta(CH)$	800-840 s
	T_z	440-550 m

s = strong, m = medium, w = weak, v = very.

Table II. Vibrational frequencies (in cm^{-1}) of molecularly chemisorbed acetylene on Ru(001), Ru(001)–p(2x2)–O and Ru(001)–p(1x2)–O.

Acetylene Loss Features		Clean Ru(001) (2)	(4)	Ru(001)–p(2x2)–O (this work)	Ru(001)–p(1x2)–O (this work)
Type I	ν(CH)	n.o.	2950	2990	present not at all or in trivial amounts*
	ν(CC)	1135	1110	1110-1130	
Type II	ν(CH)	2940	2950	2955	3000
	ν(CC)	n.o.	1260	n.o.	1220
	CH bends	980	975	960	960
		765	740	740	750
	ν(RuC)	520	540	n.o.	530
		375	370	n.o.	n.o.

n.o. = not observed.

*When very small amounts are present, ν(CC) = 1115.

Figure Captions

Figure 1: The structures and unit cells of (a) Ru(001)–p(2x2)–O and (b) Ru(001)–p(1x2)–O. Also shown are the EEL spectra corresponding to (c) the p(2x2) and (d) the p(1x2) oxygen adatom overlayers.

Figure 2: The H_2 (m/e = 2 amu) thermal desorption spectra that result following a 5 L C_2H_2 exposure to (a) clean Ru(001), (b) Ru(001)–p(2x2)–O and (c) Ru(001)–p(1x2)–O at 80 K. The heating rate was approximately 10 K-s^{-1} in all cases. The three spectra are only approximately to scale with respect to one another; each one was calibrated separately against a saturation H_2 exposure.

Figure 3: The EEL spectra obtained following the exposure of acetylene to Ru(001)–p(2x2)–O at 80 K. The exposures are (a) 0.2 L C_2H_2, (b) 2 L C_2H_2 and (c) 2 L C_2D_2.

Figure 4: The EEL spectra obtained following the adsorption of acetylene on Ru(001)–p(1x2)–O at 80 K. The exposures are (a) 0.2 L C_2H_2, (b) 2 L C_2H_2 and (c) 2 L C_2D_2. In (b) and (c) the surface was annealed briefly to 120 K following acetylene adsorption in order to remove small amounts of multilayer acetylene.

Figure 5: Electron energy loss spectra showing the thermal decomposition of acetylene (C_2H_2) on Ru(001)–p(2x2)–O. The annealing temperatures are (a) 80 K, (b) 250 K, (c) 300 K, (d) 350 K, (e) 380 K, (f) 450 K, (g) 600 K and (h) 800 K. The exposure was of 2 L C_2H_2 at 80 K.

Figure 6: Electron energy loss spectra showing the thermal decomposition of acetylene (C_2H_2) on Ru(001)–p(1x2)–O. The annealing temperatures are (a) 200 K, (b) 250 K, (c) 300 K, (d) 350 K, (e) 400 K,(f) 450 K, (g) 500 K, (h) 600 K and (i) 700 K. The exposure was of 4 L C_2H_2 at 80 K.

Figure 7: (a) Illustration of the previously proposed bonding sites (4) for Type I (μ-site) and Type II (Δ-site) acetylene on Ru(001). (b) The structures of Ru(001)–p(1x2)–O and Ru(001)–p(2x2)–O. Assuming that the acetylene carbon atoms cannot occupy threefold

sites directly adjacent to those occupied by oxygen adatoms, μ-site bonding is possible on Ru(001)–p(2x2)–O but not on Ru(001)–p(1x2)–O.

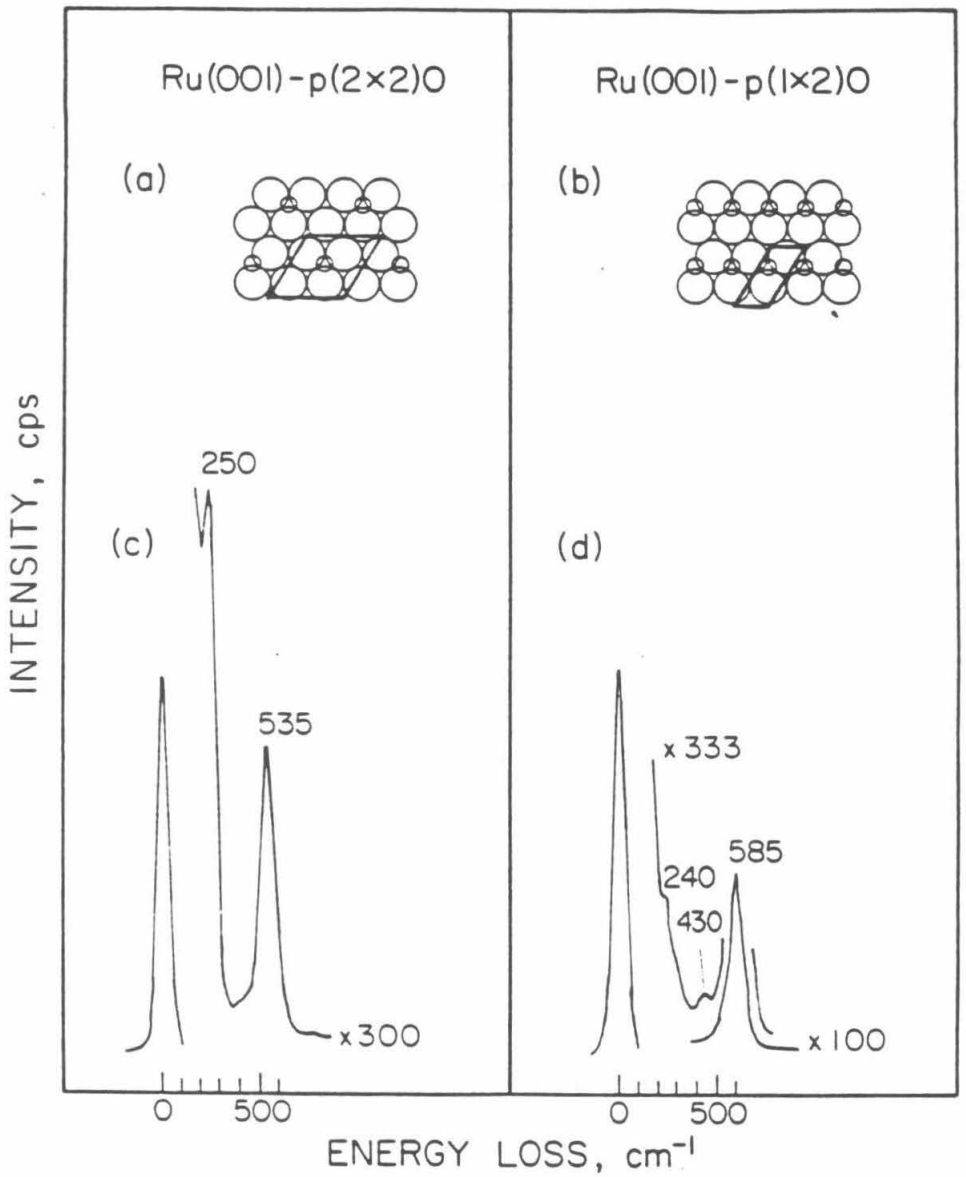
Ru(001)-p(2×2)O
Ru(001)-p(1×2)O
(a)
(b)
(c)
(d)
250
535
x300
x333
585
240
430
x100
INTENSITY, cps
0
500
0
500
ENERGY LOSS, cm⁻¹

Figure 1

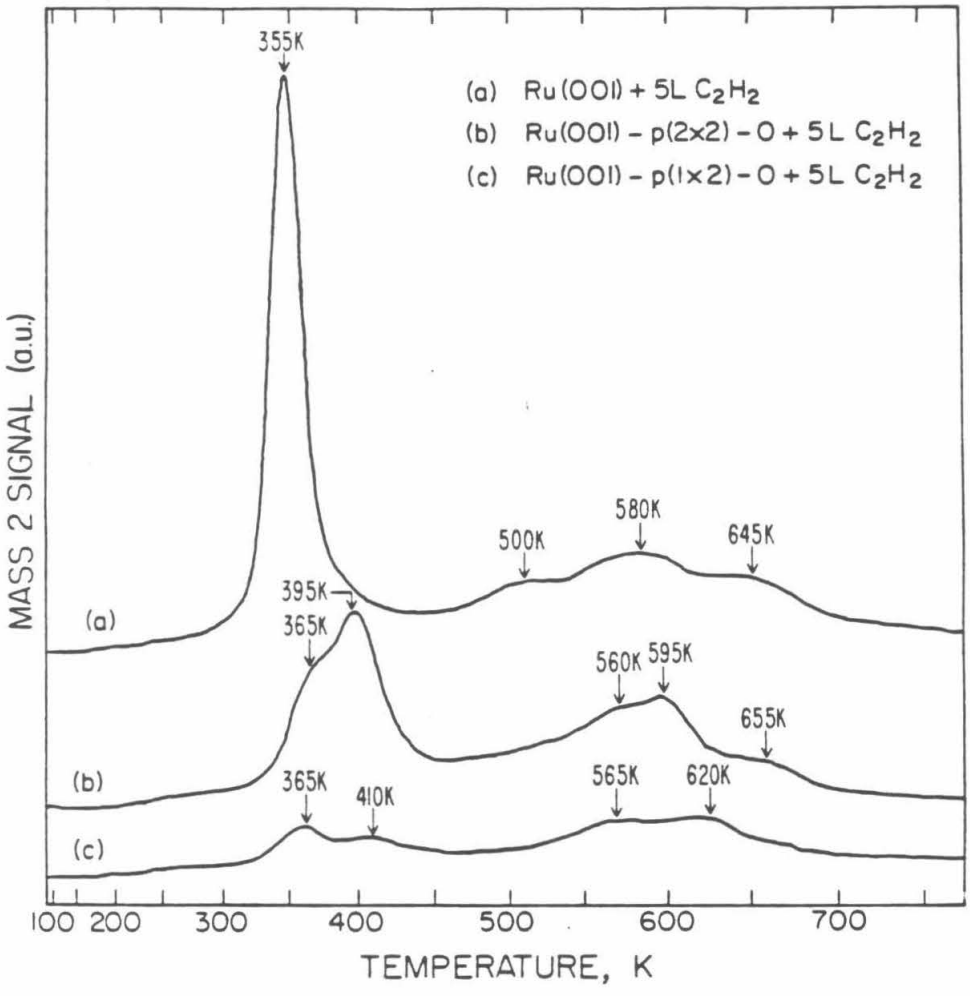
355K
(a) Ru(001) + 5L C_2H_2
(b) Ru(001) – p(2×2) – O + 5L C_2H_2
(c) Ru(001) – p(1×2) – O + 5L C_2H_2
MASS 2 SIGNAL (a.u.)
500K
580K
645K
395K
365K
(a)
560K
595K
655K
(b)
365K
410K
565K
620K
(c)
100 200 300 400 500 600 700
TEMPERATURE, K

Figure 2

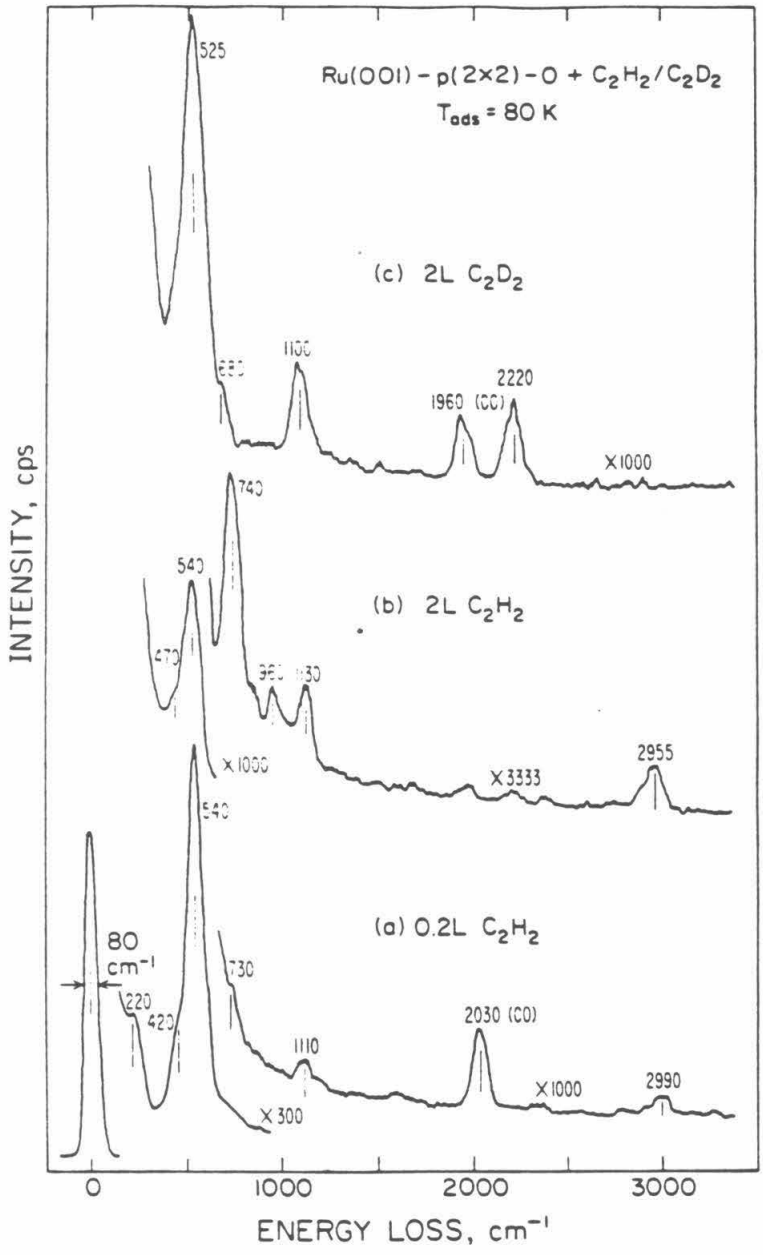
Ru(001) - p(2×2) - O + C_2H_2/C_2D_2
T_{ads} = 80 K
(c) 2L C_2D_2
525
1100
2220
1960 (CO)
X1000
(b) 2L C_2H_2
740
540
470
X1000
X3333
2955
(a) 0.2L C_2H_2
540
80 cm⁻¹
220
420
730
1110
2030 (CO)
X1000
2990
X300
INTENSITY, cps
0
1000
2000
3000
ENERGY LOSS, cm⁻¹

Figure 3

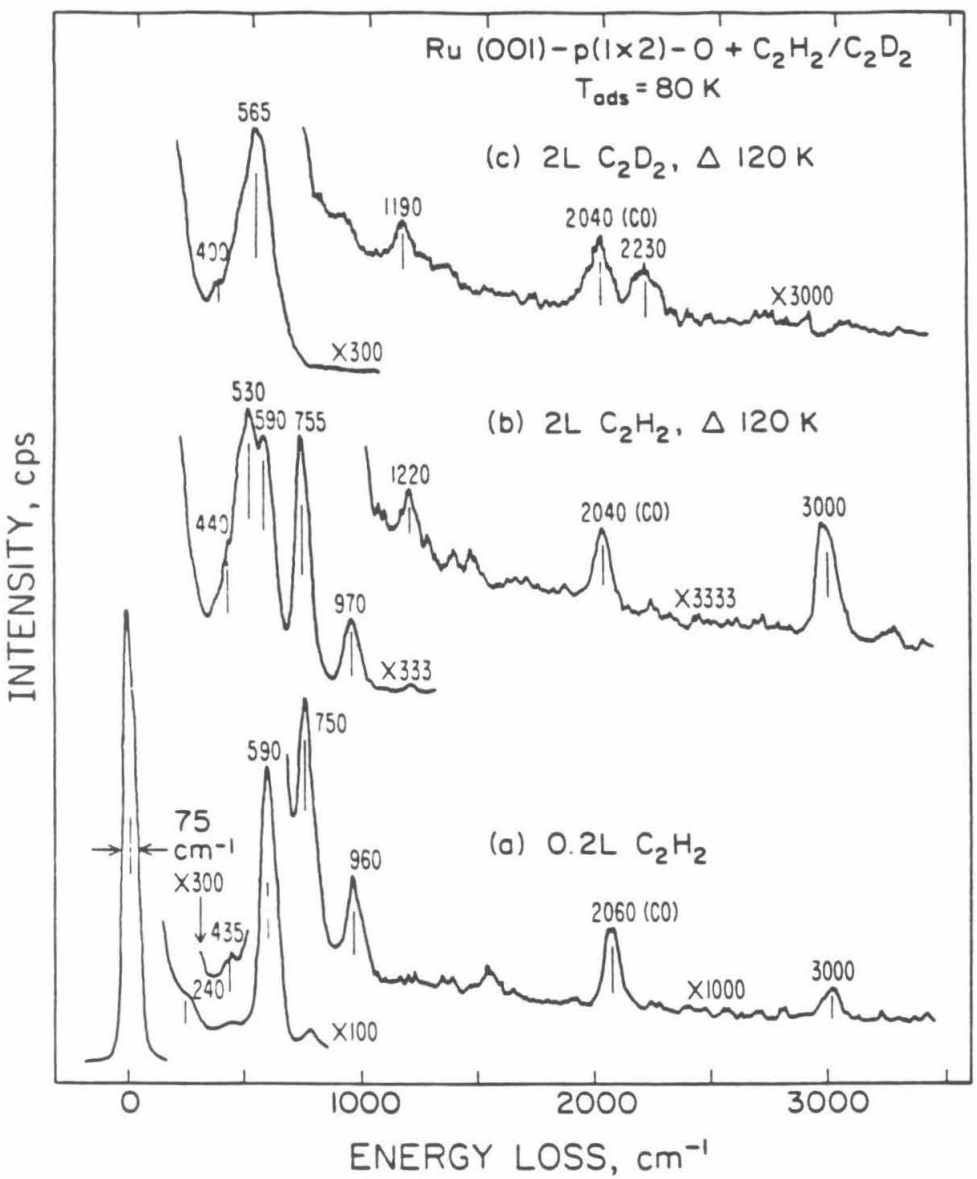
Ru (001)-p(1×2)-O + C_2H_2/C_2D_2
T_{ads} = 80 K
(c) 2L C_2D_2, Δ 120 K
565
400
1190
2040 (CO)
2230
X3000
X300
(b) 2L C_2H_2, Δ 120 K
530
590
755
440
1220
2040 (CO)
3000
X3333
970
X333
(a) 0.2L C_2H_2
750
590
75 cm⁻¹
960
X300
435
2060 (CO)
240
X1000
3000
X100
INTENSITY, cps
0
1000
2000
3000
ENERGY LOSS, cm⁻¹

Figure 4

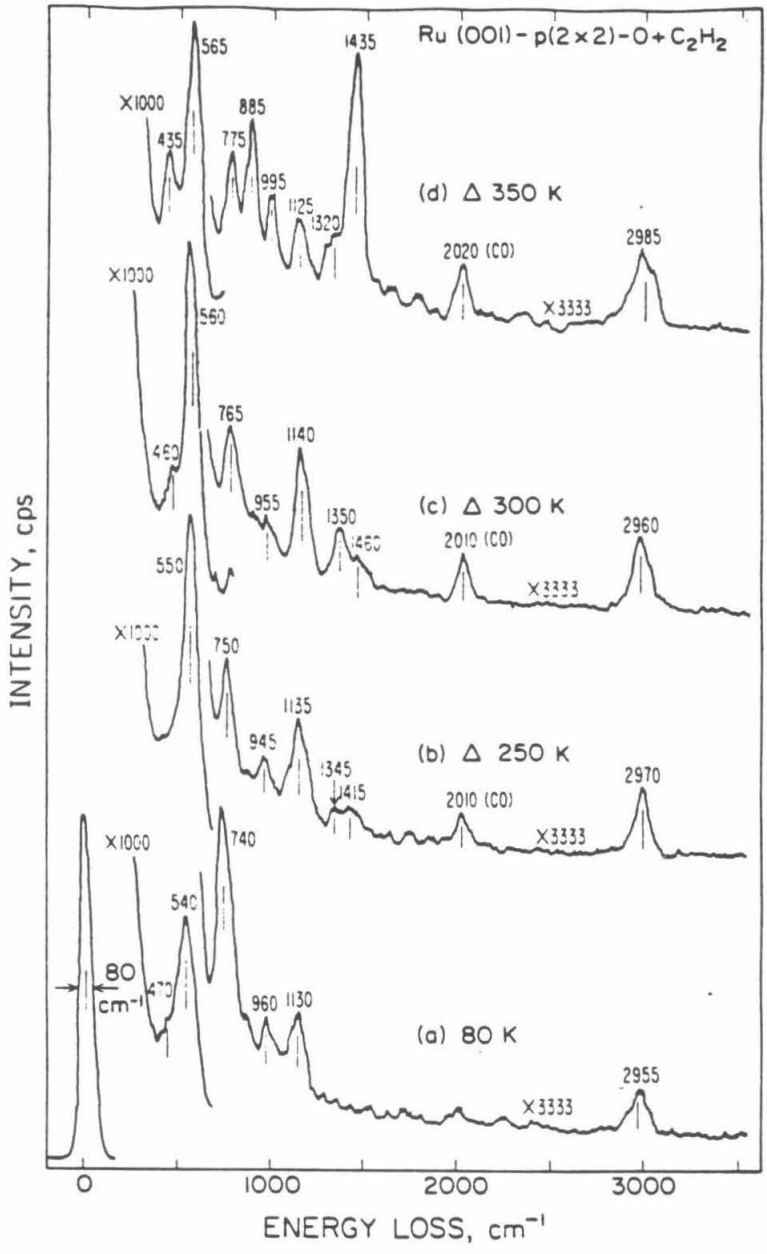
Ru (001) - p(2×2)-O+C2H2
(d) Δ 350 K
(c) Δ 300 K
(b) Δ 250 K
(a) 80 K
X1000
X3333
565
435
775
885
995
1125
1320
1435
2020 (CO)
2985
560
460
765
955
1140
1350
1460
2010 (CO)
2960
550
750
945
1135
1345
1415
2010 (CO)
2970
540
740
80
cm-1
960
1130
2955
INTENSITY, cps
0
1000
2000
3000
ENERGY LOSS, cm-1

Figure 5

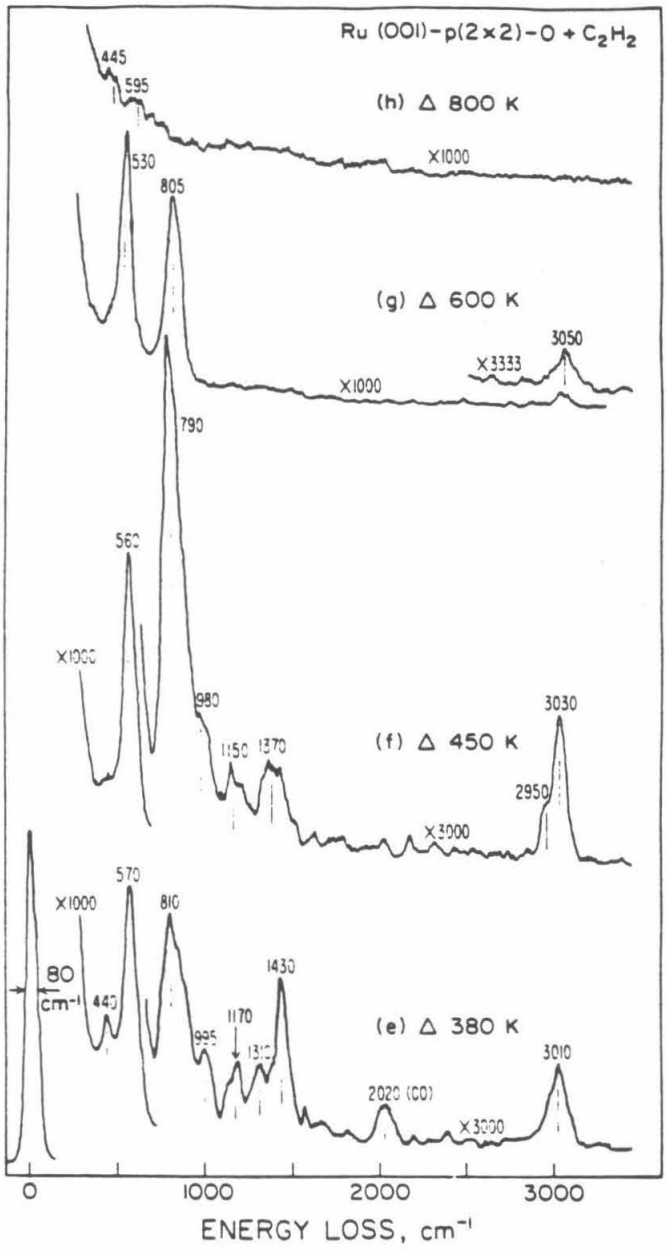
Ru (001)-p(2×2)-O + C_2H_2
(h) Δ 800 K
445
595
530
805
×1000
(g) Δ 600 K
3050
×3333
×1000
790
560
×1000
980
1150
1370
(f) Δ 450 K
3030
2950
×3000
570
×1000
810
80 cm⁻¹
440
1430
1170
995
1310
(e) Δ 380 K
3010
2020 (CO)
×3000
0
1000
2000
3000
ENERGY LOSS, cm⁻¹

Figure 5

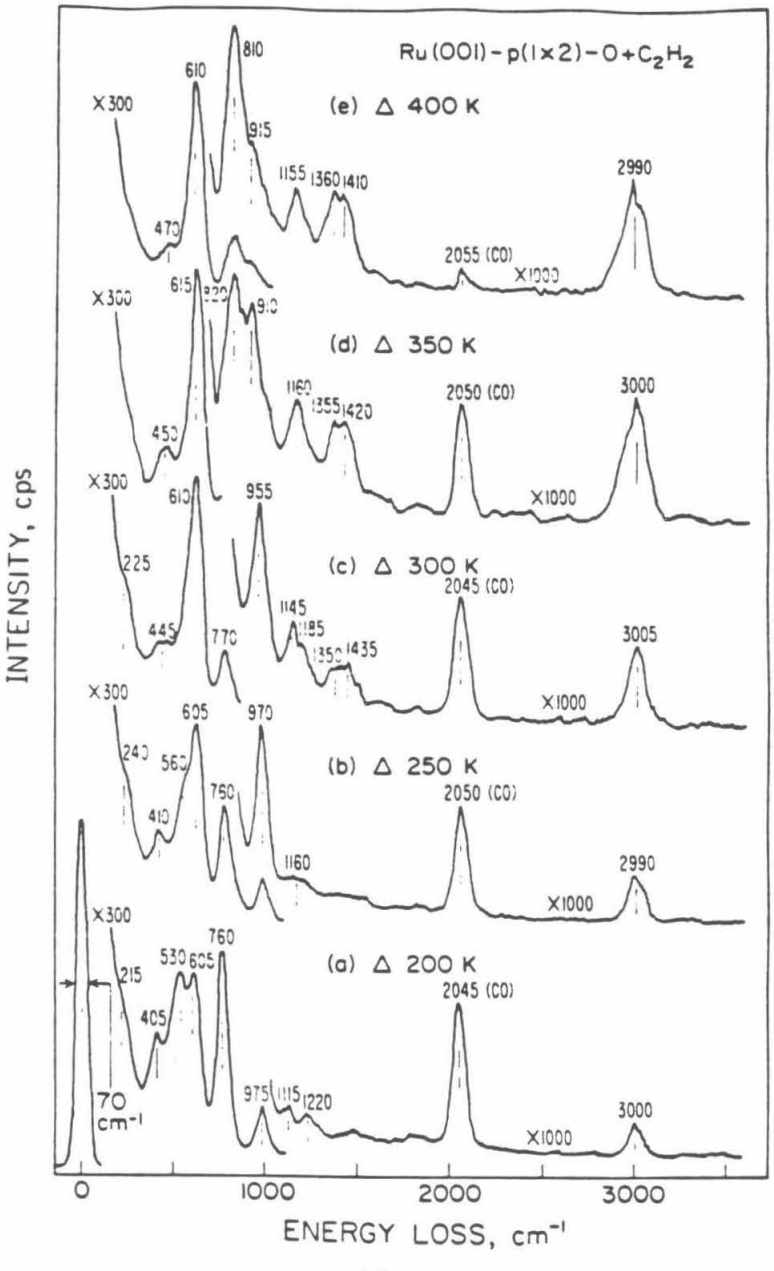
Ru(001)-p(1×2)-O+C2H2
(e) Δ 400 K
(d) Δ 350 K
(c) Δ 300 K
(b) Δ 250 K
(a) Δ 200 K
X300
X1000
610
810
915
1155
1360
1410
2990
470
2055 (CO)
615
910
1160
1420
2050 (CO)
3000
450
955
225
445
770
1145
1435
2045 (CO)
3005
605
970
240
560
410
750
1160
2990
760
530
605
215
405
975
1115
1220
2045 (CO)
3000
70 cm-1
INTENSITY, cps
0
1000
2000
3000
ENERGY LOSS, cm-1

Figure 6

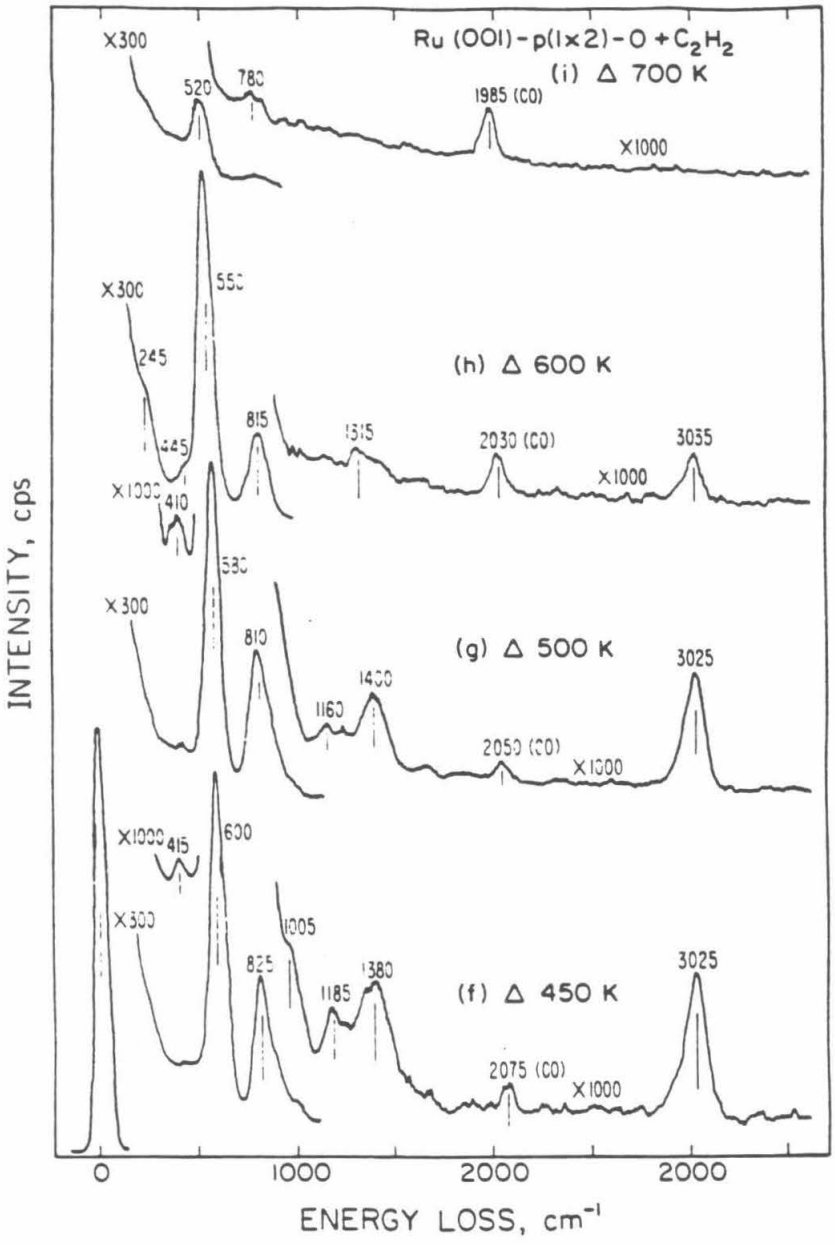
Ru (001) - p(1×2) - O + C_2H_2
(i) Δ 700 K
(h) Δ 600 K
(g) Δ 500 K
(f) Δ 450 K
X300
X1000
520
780
1985 (CO)
550
245
445
410
815
1315
2030 (CO)
3035
530
810
1160
1400
2050 (CO)
3025
415
600
1005
825
1185
1380
2075 (CO)
INTENSITY, cps
0
1000
2000
2000
ENERGY LOSS, cm^{-1}

Figure 6

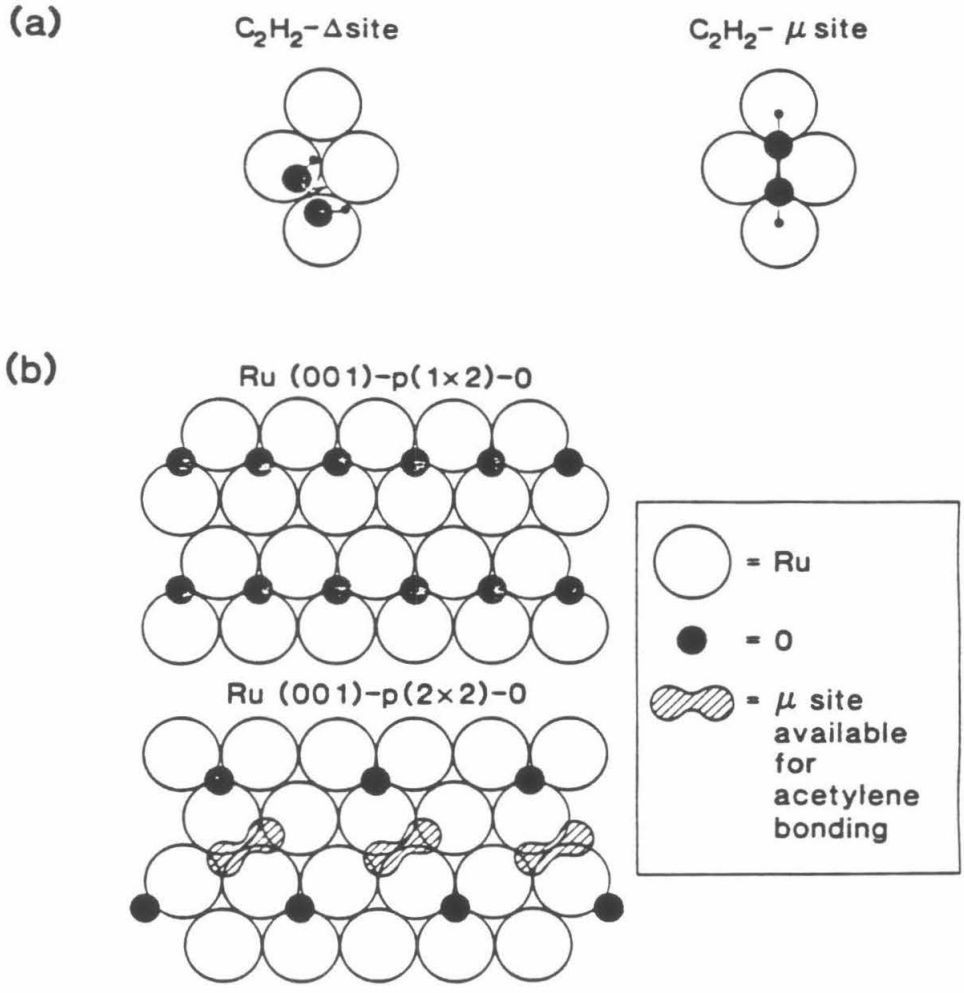
(a)
C_2H_2-Δsite
C_2H_2-μ site
(b)
Ru (001)-p(1×2)-O
Ru (001)-p(2×2)-O
= Ru
= O
= μ site available for acetylene bonding

Figure 7

CHAPTER V

The Interaction of Formamide with the Ru(001) Surface

[This chapter has been accepted for publication as a paper by J. E. Parmeter, U. Schwalke and W. H. Weinberg, in *The Journal of the American Chemical Society*.]

Abstract

The adsorption and decomposition of formamide (NH_2CHO) on the hexagonally close-packed Ru(001) surface have been studied using high-resolution electron energy loss spectroscopy and thermal desorption mass spectrometry. At 80 K, the initial adsorption of formamide results in CH bond cleavage and the formation of an η^2(C,O)-NH_2CO species. This species decomposes upon annealing to 250 K, leaving a mixture of CO, NH_3, NH and hydrogen adatoms on the surface. The NH_3 and CO desorb near 315 and 480 K, respectively, whereas the NH decomposes below 400 K to nitrogen and hydrogen adatoms. Recombinative desorption of H_2 occurs at 420 K, while recombinative desorption of N_2 occurs near 770 K. For higher initial formamide coverages (where the fractional coverage of formamide that decomposes exceeds approximately 0.05 monolayer), molecular adsorption in an η^1(O)-NH_2CHO configuration is observed also at 80 K. This species undergoes competing desorption and decomposition at 225 K to an intermediate believed to be N-bonded NHCHO, which in turn converts to a species tentatively identified as η^1(N)-NCHO at 300 K. The latter species decomposes to chemisorbed CO, N and H near 375 K. Following a saturation formamide exposure on Ru(001) at 80 K, approximately 0.15 monolayer of formamide decomposes upon subsequent annealing, with approximately two-thirds of the total decomposing via the η^2(C,O)-NH_2CO intermediate and the remainder reacting via the η^1(O)-NH_2CHO.

I. Introduction

High-resolution electron energy loss spectroscopy (EELS) has emerged as one of the most important experimental techniques for studying the reactions of molecules on well-characterized metal surfaces (1), especially in delimiting reaction mechanisms via the isolation of reaction intermediates. Such studies are of interest not only because of the obvious importance of understanding molecule-metal surface interactions in heterogeneous catalytic processes, but also because they allow comparisons to be made between the bonding and reactivity of various ligands in multinuclear homogeneous metal clusters and that on metal surfaces. Recently, we have reported the results of an EELS and thermal desorption mass spectrometric (TDMS) study of the interaction of formamide (NH_2CHO) with the Ru(001)-p(1x2)-O surface, i.e. the hexagonally close-packed ruthenium surface on which an ordered p(1x2) overlayer of oxygen adatoms (fractional coverage of one-half) is present (2). We report here the results of an EELS and TDMS study of the adsorption and decomposition of formamide on the clean (reduced) Ru(001) surface.

From the point of view of chemisorption, formamide is a rather complex molecule, containing two heteroatoms and a carbonyl double bond. Thus, there are several ways that formamide might adsorb molecularly on a metal surface: via the electron lone pairs on the oxygen and/or nitrogen atoms (although in gas phase formamide there is no electron lone pair isolated strictly on the nitrogen atom), or in an η^2(C,O) configuration with rehybridization of the carbonyl double bond. A number of decomposition intermediates are also possible, as may be appreciated by considering the variety of formamide-derived ligands that have been identified in organometallic compounds. These include η^1(C)-CONHR (3), η^1(N)-NHCOR (4), η^2(C,O)-NR_2CO (5), η^2(N,O)-NRCHO (both chelating and bridging) (6), and the tautomers η^2(C,N)-HOCNR and η^2(C,N)-OCNHR (R=H, alkyl or aryl) (7). These species are depicted schematically in Fig. 1 with R=H, the case relevant to formamide decomposition on a metal surface.

In our study of formamide chemisorption on the Ru(001)-p(1x2)-O surface (2), it was found that below 225 K formamide bonds to the surface via a lone pair of electrons on the oxygen atom, i.e. the formamide adsorbs molecularly below 225 K in an η^1(O)-NH_2CHO configuration. At 225 K, the

η^1(O)–NH_2CHO converts to η^2(N,O)–NH_2CHO that is bonded to the surface via electron lone pairs on both the oxygen and nitrogen atoms. The η^2(N,O)–NH_2CHO converts near 260 K to η^2(N,O)–NHCHO, the nitrogen-containing analogue of the η^2-formate that has been identified previously on Ru(001) as an intermediate in the decomposition of formic acid (**8**). For sufficiently high initial formamide coverages, both of these conversions are accompanied by some molecular desorption of formamide. The η^2(N,O)–NHCHO is stable on the Ru(001)-p(1x2)-O surface to 420 K, at which temperature it decomposes, evolving gaseous CO and H_2 and leaving nitrogen adatoms on the surface. The nitrogen adatoms recombine and desorb as N_2 near 570 K, leaving the p(1x2)-O overlayer intact. For a saturation formamide exposure, approximately 0.05 monolayer of η^2(N,O)–NHCHO is formed and decomposes on this surface. (A monolayer is defined as 1.58×10^{15} cm^{-2}, the density of ruthenium atoms on the Ru(001) surface.)

Electronegative adsorbates such as oxygen adatoms can alter the chemical reactivity of metal surfaces, just as electron withdrawing ligands modify the properties and reactivity of organometallic compounds. Comparing the reactions of formamide on the Ru(001)-p(1x2)-O surface and on clean Ru(001) is of particular interest in view of the fact that ordered oxygen overlayers are known to alter the chemistry of both acetone (**9**) and formaldehyde (**10**) on Ru(001). On clean Ru(001), both acetone and formaldehyde adsorb at 80 K principally via rehybridization of the CO double bond in an η^2(C,O) configuration. In the case of formaldehyde, some decomposition to CO, η^2(C,O)-HCO, and hydrogen adatoms occurs as well. On the Ru(001)-p(2x2)-O surface, adsorption at 80 K of both molecules occurs primarily in an η^1(O) configuration, with bonding to the surface occurring via an electron lone pair on the oxygen atom. Thus, in the case of the adsorption of formamide on clean Ru(001) at 80 K, we might expect the formation of η^2(C,O)–NH_2CHO or η^2(C,O)–NH_2CO, rather than the formation of η^1(O)–NH_2CHO, which occurs on the Ru(001)-p(1x2)-O surface. Such species could also lead to different decomposition products compared to those from η^1(O)–NH_2CHO.

II. Experimental Details

The EEL spectrometer and the ultrahigh vacuum (UHV) chamber housing it have been described elsewhere (**11**), as have the methods of cleaning the Ru(001) crystal (**12**) and handling the formamide

(2). Typical parameters for the EEL spectra shown and discussed in this paper are the following: resolution (full-width at half-maximum of the elastically scattered electron beam), 70-80 cm^{-1}; count rate (elastically scattered peak), 2 x 10^5 cps; impact energy of the incident electron beam, 4 eV; and (fixed) angle of incidence of the electron beam, 60° with respect to the surface normal. All EEL spectra were measured in the specular direction, except when it is stated explicitly otherwise. The UHV chamber also contained a quadrupole mass spectrometer for performing TDMS measurements and for an analysis of background gases. The heating rate in all thermal desorption spectra was approximately 8 $K\text{-}s^{-1}$. The base pressure in the UHV chamber was less than 10^{-10} Torr. Liquid nitrogen cooling allowed crystal temperatures as low as 80 K to be attained. The crystal was heated resistively and cleaned by annealing in a background of oxygen or, occasionally, by argon ion sputtering.

The NH_2CHO used in this study was obtained from Aldrich with a reported purity of 99%, and was purified further as discussed elsewhere (2). Its purity was verified in situ using mass spectrometry. Both EELS and TDMS experiments were also performed with N-deuterated formamide, ND_2CHO (MSD Isotopes, 98 at % D). Although H/D exchange into the ND_2 group resulted in the presence of small amounts of NHDCHO and/or NH_2CHO in the ND_2CHO (13), these experiments were nevertheless useful in helping to assign various EELS loss features, and they also yielded qualitative information concerning H_2 thermal desorption.

III. Results

A. Thermal Desorption Mass Spectrometry

Following a saturation exposure of formamide on the clean Ru(001) surface at 80 K, five different species are observed to desorb between approximately 200 and 800 K, namely, molecular formamide, carbon monoxide, hydrogen, nitrogen and ammonia (14). Species specifically looked for and not observed to desorb include H_2O, HCN, NO, H_2CO and HNCO. The five molecular species detected with TDMS are discussed separately below.

1. Molecular Formamide

Figure 2 shows a series of thermal desorption spectra of NH_2CHO (m/e = 45 amu) following vari-

ous exposures of formamide to the clean Ru(001) surface at 80 K. For exposures less than approximately 4 L (1 L ≡ 1 Langmuir ≡ 10^{-6} Torr-s), no molecular desorption occurs, indicating that at low coverages all of the adsorbed formamide decomposes. For exposures greater than approximately 4 L, a molecular desorption peak appears at 225 K. The peak temperature does not shift with increasing exposures (i.e. coverage), indicative of a first-order desorption reaction. Assuming a preexponential factor of the desorption rate coefficient of 10^{13} s^{-1}, an activation energy of desorption (equal to the heat of adsorption since adsorption is not activated) of approximately 13 kcal-mol^{-1} is calculated for this desorption state (15). This desorption feature is most likely due to monolayer rather than second layer formamide (2), especially since the amount of formamide that decomposes (approximately 0.15 monolayer, cf. Sec. III.A.2) seems very low to correspond to monolayer saturation. For exposures greater than approximately 8 L, a second thermal desorption peak appears at 210 K. This peak does not saturate with increasing exposure and is due to the desorption of condensed formamide multilayers, in agreement with previous results for formamide desorption from the Ru(001)-p(1x2)-O surface (2).

2. Carbon Monoxide

Thermal desorption spectra of CO (m/e = 28 amu, with a cracking fragment at m/e = 12 amu distinguishing it from N_2) following various exposures of NH_2CHO to Ru(001) at 80 K are shown in Fig. 3. There is a single CO thermal desorption peak which occurs at 480 K for the lowest exposures studied (fractional surface coverage of CO desorbed of approximately 0.01 monolayer) and shifts downward to 410 K at saturation. Despite this downshift in peak temperature with increasing coverage, this is a first-order, desorption-limited reaction, since low coverages of chemisorbed CO on clean Ru(001) also desorb near 480 K (16), the recombinative desorption of CO formed from carbon and oxygen adatoms occurs only above 500 K on this surface (17), and EEL spectra show clearly that molecularly adsorbed CO is present from 250 to above 400 K [cf. Sect. III.B]. The most reasonable cause of the downshift in the CO desorption temperature with increasing formamide exposures is the increasing coverage of nitrogen adatoms between 400 and 500 K, which are also present due to formamide decomposition [cf. Sect. III.B]. The ruthenium-carbon bond of adsorbed CO is formed by electron donation from the 5σ (carbon lone pair) orbital of CO to the surface, accompanied by electron

backdonation from the metal sd-band to the $2\pi^*$ antibonding orbital of CO (**18**). The (relatively) electronegative nitrogen adatoms withdraw electron density from the surface ruthenium atoms, presumably reducing the extent of the backbonding and leading to a lowered CO desorption temperature. A similar effect has been observed for CO that is coadsorbed with ordered overlayers of oxygen adatoms on Ru(001) (**19**).

The saturation coverage of CO on Ru(001) is known to be approximately 0.68 monolayer (**20**). Since all of the formamide that decomposes on the Ru(001) surface gives rise to CO as a reaction product, there is a one-to-one correspondence between the amount of CO that desorbs for a given formamide coverage and the amount of formamide that decomposes. Thus, by comparing the time-integrated intensities of the CO thermal desorption peaks for saturation exposures of both CO and NH_2CHO, the amount of NH_2CHO that decomposes for a saturation formamide exposure may be calculated. This comparison yields an estimate of 0.15 monolayer of irreversibly adsorbed NH_2CHO following a saturation formamide exposure on Ru(001) at 80 K, or approximately 2.3×10^{14} molecules-cm^{-2}.

3. Hydrogen

Figure 4 shows a series of H_2 (m/e = 2 amu) thermal desorption spectra that were measured following various NH_2CHO exposures to Ru(001) at 80 K, as well as the H_2 thermal desorption spectrum that results following a saturation exposure of H_2 on Ru(001). For an exposure of 0.5 L of formamide there is a single desorption peak at 420 K, which shifts downward with increasing exposures. This is a second-order desorption peak resulting from the recombinative desorption of hydrogen adatoms, since the H_2 thermal desorption spectra that result from 0.5-1 L formamide exposures are identical to those that result from low H_2 exposures on Ru(001), where the adsorption is dissociative and the desorption is second-order (**21**). For a 2 L NH_2CHO exposure, the single H_2 desorption peak has downshifted to 395 K. Following a 4 L exposure, three peaks appear at 325, 380 and 405 K. Finally, a 10 L exposure (slightly greater than saturation) gives rise to a rather complex desorption spectrum, with the three previously mentioned peaks now at 300, 375 and 410 K, and a fourth peak at 280 K.

Thermal desorption spectra of H_2, HD and D_2 following saturation exposures of ND_2CHO on Ru(001) (not shown) were also measured in order to determine the origin of the hydrogen desorbing in

the four peaks of Fig. 4(e). The 410 K peak consisted almost entirely of D_2 with a small amount of HD, indicating that the hydrogen desorbing in this peak originates primarily, if not entirely, from the NH_2 group of the formamide. (It should be recalled that a small amount of NHDCHO and/or NH_2CHO was present in the ND_2CHO sample.) The peak at 375 K was very rich in HD and contained no D_2. Sample contamination precluded a quantitative analysis of the relative amounts of H_2, HD and D_2 desorbing in each peak.

Since the saturation coverage of hydrogen adatoms on Ru(001) is known to be approximately 0.85 (21), and the amount of NH_2CHO that decomposes following a saturation exposure on Ru(001) is known to be approximately 0.15 from the CO data discussed above, the H_2 thermal desorption spectra may be used to estimate very approximately the amount of NH_3 that is formed and desorbed following a saturation formamide exposure. The hydrogen thermal desorption spectra indicate that approximately 0.39 monolayer of hydrogen adatoms are desorbed as H_2, corresponding to the decomposition of 0.13 monolayer of NH_2CHO. The amount of ammonia that is desorbed is thus approximately 0.15-0.13 = 0.02 monolayer. Although the absolute accuracy of this estimate is poor (probably no better than a factor of two), it is clear that the amounts of H_2 and CO that desorb are in a ratio of nearly 3:2, so that most of the formamide that decomposes must produce only CO, H_2 and N_2 as desorption products. The amount of NH_3 that is desorbed is quite small, and the formation of NH_3 represents a minor reaction pathway.

4. Nitrogen

Figure 5 shows the m/e = 14 amu (N cracking fragment of N_2, which distinguishes it from CO) thermal desorption spectrum that results following a saturation exposure of NH_2CHO on Ru(001) at 80 K. Nitrogen is desorbed between approximately 555 and 810 K, with a maximum desorption rate near 685 K. For a 0.5 L NH_2CHO exposure, the nitrogen desorbs with a peak temperature of approximately 770 K. The fact that molecularly adsorbed N_2 on Ru(001) desorbs below 150 K (22) and the clear evidence for the presence of nitrogen adatoms in EEL spectra measured following NH_2CHO adsorption and annealing to above 400 K (cf. Sect. III.B) prove unambiguously that this desorption of N_2 results from the recombinative desorption of nitrogen adatoms that are formed from the decomposition of for-

mamide.

5. Ammonia

Thermal desorption spectra for m/e = 17 amu following various exposures of formamide to the Ru(001) surface at 80 K are shown in Fig. 6. Thermal desorption spectra of mass 18 were also measured and the lack of water desorption verifies that the desorption peaks in Fig. 6 do not correspond to an OH cracking fragment of desorbed H_2O. However, the 235 K thermal desorption peak appears at the same temperature and coverage as a molecular formamide thermal desorption peak and appears to be due entirely to a formamide cracking fragment. Thus, only the desorption peak at 285-315 K is due to ammonia desorption. Ammonia desorption is observed for all formamide exposures, which ranged from 0.3 L to saturation. At low coverage, the peak temperature is 315 K, and it shifts down in temperature to 285 K when this peak is saturated. For relatively low initial coverages of formamide ($\leq$2 L, the ammonia that is produced is identified clearly with EELS (cf., Fig. 8) and is hence desorption-limited. Following saturation formamide exposures, very little ammonia is identified with EELS, and then 285 K desorption peak appears to be mainly reaction-limited. The initial desorption temperature of 315 K is in agreement with the results of a previous, detailed study of ammonia adsorption on clean Ru(001), in which it was shown that ammonia desorbed in a single peak centered at 315 K for initial ammonia coverages less than approximately 15% of saturation (**14**). The total amount of ammonia that desorbs following a saturation formamide exposure is estimated to be $\leq$0.02 monolayer, based on the previously discussed CO and H_2 thermal desorption measurements. Essentially all of the ammonia that is formed desorbs rather than decomposes (**14**).

B. Electron Energy Loss Spectroscopy

In discussing the EEL spectra of NH_2CHO on Ru(001), it is convenient to consider separately two distinct coverage regimes. For low initial coverages (exposures <2 L, where the amount of NH_2CHO that decomposes is less than approximately 0.05 monolayer), only a single surface species is detected by EELS following adsorption at 80 K. For higher coverages (exposures >2 L, where the amount of formamide decomposing is greater than approximately 0.05 monolayer), an additional surface species is present at 80 K due to the passivation of the surface by the products of the initial adsorption reaction.

The low and high coverage regimes are thus treated separately below.

1. Low Coverage

The EEL spectra that result following 0.5 L exposures of NH_2CHO and ND_2CHO to the clean Ru(001) surface at 80 K are shown in Fig. 7. In both spectra there is a weak loss feature near 2000 cm^{-1} due to ν(CO) of a very small amount (<0.005 monolayer) of coadsorbed CO. This CO is adsorbed from the chamber background and is not due to formamide decomposition. In addition, the ND_2CHO spectrum shows a weak ν(NH) loss feature at 3380 cm^{-1} due to a small amount of NHDCHO and/or NH_2CHO contamination. The other loss features in both spectra disappear concomitantly upon annealing to approximately 250 K, and may therefore be assigned to a single surface species that is formed upon the adsorption of formamide at 80 K.

For a number of reasons, the species present on the surface at 80 K may be identified as NH_2CO. First, both spectra of Fig. 7 show no evidence of a carbon-hydrogen stretching mode in the 2800-3100 cm^{-1} region, and corresponding spectra measured off-specular also show no evidence of a ν(CH) mode. The latter measurement is of importance because ν(CH) modes are often detected most easily in off-specular EEL spectra (1). Since the ν(CH) mode is clearly detected in several formamide-derived species (including the parent molecule) on the Ru(001)-p(1x2)-O surface (2), it is concluded that carbon-hydrogen bond cleavage has occurred upon the adsorption of formamide at 80 K. Second, since there are no vibrational modes in either spectrum due to oxygen adatoms (23), nitrogen adatoms [see Fig. 9(c)], or CO (other than a trivial amount of CO adsorbed from the chamber background), it is apparent that the carbon-nitrogen and carbon-oxygen bonds of formamide remain intact. This conclusion is justified since our previous studies of formamide decomposition on Ru(001)-p(1x2)-O show that loss features due to carbon monoxide and atomic oxygen are easily detected in the presence of coadsorbed formamide and its decomposition products (2). Third, the clear presence of two nitrogen-deuterium stretching modes in the ND_2CHO spectrum, the NH_2 wagging mode at 820 cm^{-1} which shifts down to approximately 600 cm^{-1} upon N-deuteration, and the mode at 1580 cm^{-1} in the NH_2CHO spectrum which shifts down markedly upon N-deuteration [indicating that this mode has substantial $\delta(NH_2)$ character] all indicate that the NH_2 bonds are not broken. Taken together, these arguments serve to

identify the species that is present on the surface as NH_2CO. Such a species may be either η^1(C)-bonded (**3**), η^2(C,O)-bonded (**5**), or η^2(C,N)-bonded (**7**) (cf. Fig. 1, illustrations 1, 3 and 5b). However, η^2(C,N)-$OCNH_2$ species in organometallic compounds exhibit strong ν(CO) modes near 1775 cm^{-1} (**7**), and all organometallic analogues of η^1(C)–$CONH_2$ exhibit strong ν(CO) stretching modes between 1500 and 1650 cm^{-1} (**3**). Since these modes are clearly lacking in Fig. 7(b), the surface species is identified as η^2(C,O)-NH_2CO. Since the carbon-oxygen bond of the η^2(C,O)-NH_2CO has undergone substantial rehybridization, its bond order is significantly less than two. The precise carbon-oxygen and carbon-nitrogen bond orders are somewhat indeterminate, however, since several resonance structures may be drawn for this surface species (cf. Sect. IV). It might be noted in passing that the observation of two metal-ligand stretching frequencies (see below) is another argument that the surface species present is not η^1(C)-$CONH_2$ (**24**). It should be pointed out that hydrogen adatoms are also present on the surface together with the η^2(C,O)-NH_2CO, but are not detected by EELS due to their very weak loss features.

Due to substantial coupling among several vibrational modes of η^2(C,O)-NH_2CO and η^2(C,O)-ND_2CO, a complete mode assignment is not possible without the benefit of a normal mode analysis. However, several of the observed loss features may be assigned unambiguously. The peaks at 270(270) and 360(370) cm^{-1} in the case of η^2(C,O)-NH_2CO [η^2(C,O)-ND_2CO] are both assigned to ruthenium-NH_2CO stretching modes. The peak at 820 cm^{-1} in Fig. 7(a) shifts down to approximately 600 cm^{-1} upon N-deuteration, so that it overlaps with the peak at 655 cm^{-1}, forming a single broad feature centered at 615 cm^{-1}. As stated above, the 820 cm^{-1} peak is thus identified as the NH_2 wagging mode, $\omega(NH_2)$, and the peak at 655 cm^{-1} is identified as the NCO bending mode, δ(NCO). The peak at 3370 cm^{-1} in Fig. 7(a) is due to the unresolved $\nu_s(NH_2)$ and $\nu_a(NH_2)$ modes, while in the case of η^2(C,O)-ND_2CO, $\nu_s(ND_2)$ and $\nu_a(ND_2)$ occur at 2455 and 2560 cm^{-1}, respectively. Four additional peaks appear in each spectrum, at 1015, 1300, 1370 and 1580 cm^{-1} for η^2(C,O)-NH_2CO; and at 980, 1085, 1285 and 1440 cm^{-1} for η^2(C,O)-ND_2CO. In the case of η^2(C,O)-NH_2CO, four modes are expected between 1000 and 1600 cm^{-1}, as observed: the symmetric and asymmetric NCO stretching modes, and the NH_2 scissoring and rocking modes. However, coupling among these four modes is evidently significant and renders the mode descriptions ν_s(NCO), ν_a(NCO), $\delta(NH_2)$ and $\rho(NH_2)$ rather meaningless. We note

again, however, that the 1580 cm^{-1} mode in Fig. 7(a) must have substantial $\delta(NH_2)$ character, since the highest of these four "middle frequency modes" of $\eta^2(C,O)$-ND_2CO occurs at a frequency 140 cm^{-1} lower than this. The observed vibrational frequencies and partial mode assignments for $\eta^2(C,O)$-NH_2CO and $\eta^2(C,O)$-ND_2CO are summarized in Table I. For comparison, Table II provides vibrational frequencies and mode assignments for liquid and gas-phase formamide.

The EEL spectra of low coverages of formamide adsorbed on clean Ru(001) at 80 K show that $\eta^2(C,O)$-NH_2CO remains on the surface when the surface is annealed briefly to temperatures below approximately 230 K, at which point decomposition of the $\eta^2(C,O)$-NH_2CO begins. The only change in the EEL spectra for annealing temperatures below 230 K is that following annealing to 200 K the $\omega(NH_2)$ mode [$\omega(ND_2)$ in the case of $\eta^2(C,O)$-ND_2CO] increases in intensity by approximately a factor of two, while the intensities of the other vibrational modes of $\eta^2(C,O)$-NH_2CO remain essentially constant. This suggests a reorientation of the NH_2 group as the surface is heated. The intensity of the $\omega(NH_2)$ mode is expected to be greatest when it involves motion of the NH_2 hydrogen atoms that is largely perpendicular to the surface (**25**).

Annealing the Ru(001) surface on which $\eta^2(C,O)$-NH_2CO is present to 250 K causes the vibrational features due to $\eta^2(C,O)$-NH_2CO to disappear completely, leaving the EEL spectrum shown in Fig. 8(a). This EEL spectrum is characterized by intense peaks at 460, 1160 and 1985 cm^{-1}, and by weak peaks at approximately 690, 1350, 1590 and 3315 cm^{-1}. The intense peaks at 460 and 1985 cm^{-1} are identified easily as ν(RuC) and ν(CO) of carbon monoxide adsorbed in on-top sites (**20,26**). Based on a comparison to an EEL spectrum of ammonia adsorbed on the Ru(001) surface at 80 K and annealed briefly to 300 K (θ_{NH_3} ~ 0.02-0.03 monolayer) [Fig. 8(b)], the peaks at 1160, 1590 and (in part) 3315 cm^{-1} are identified as being due to adsorbed ammonia. Previous EELS studies of NH_3 adsorbed on Pt(111) (**27**), Ag(110) (**28**), Ni(111) (**29**), Ni(110) (**29**), and Fe (110) (**30**) have yielded very similar EEL spectra, and these modes are assigned as $\delta_s(NH_3)$, $\delta_a(NH_3)$ and $\nu_s(NH_3)$, respectively. Finally, the modes at 690 and 1350 cm^{-1}, and part of the intensity of the 3315 cm^{-1} mode, are due to a third surface species which is identified as adsorbed NH. The mode assignments for this species are the following: ν(NH), 3315 cm^{-1}; δ(NH), 1350 cm^{-1}; and ν(Ru-NH), 690 cm^{-1} (see below). Thus the

three spectroscopically isolated decomposition products of η^2(C,O)-NH_2CO on Ru(001) are CO, NH_3 and NH (**31**). The mode assignments of the EEL spectrum of Fig. 8(a) are summarized in Table III.

When the Ru(001) surface on which η^2(C,O)-ND_2CO is adsorbed is annealed to 250 K, the CO modes are again observed at 460 and 1985 cm^{-1}. Rather than a single sharp and intense peak at 1160 cm^{-1}, however, four overlapping peaks are observed between 900 and 1160 cm^{-1} due to the symmetric deformation mode of four different ammonia isotopes: ND_3, ND_2H, NDH_2 and NH_3. The observed frequencies are 900 cm^{-1} (ND_3), 990 cm^{-1} (ND_2H), 1090 cm^{-1} (NDH_2), and 1160 cm^{-1} (NH_3). The major species formed is ND_2H, and substantial amounts of ND_3 are also formed. (A crude estimate based on the intensities of the symmetric deformation modes is that the ratio of ND_2H to ND_3 is approximately 3:2.) A ν(ND) loss feature is present at 2450 cm^{-1}, and a very weak ν(NH) loss feature is present at 3295 cm^{-1}. The δ_s modes of the various ammonia isotopes, as well as the δ(ND) mode of coadsorbed ND, are not well resolved. However, a weak loss feature near 680 cm^{-1} is due to ν(Ru-ND), and the ND species undoubtedly contributes to the intensity of the ν(ND) loss feature.

Annealing the surface represented by Fig. 8(a) to 350 K causes the adsorbed ammonia to desorb molecularly, leaving only CO and NH in subsequent EEL spectra (**31**) and allowing a more definitive characterization of the NH species. Figure 9(a) shows the specular EEL spectrum of the surface following annealing to 350 K, while Fig. 9(b) shows the EEL spectrum of the same surface, but measured 10° off-specular toward the surface normal. The importance of the off-specular spectrum is that it allows the weak ν(Ru-NH) mode of adsorbed NH at 690 cm^{-1} to be resolved much more clearly from the tail of the elastic peak that is attenuated more rapidly than the loss peaks in off-specular measurements. Note that annealing from 250 K [Fig. 8(a)] to 350 K [Fig. 9(a)] causes the integrated intensity of the ν(NH) mode at 3315 cm^{-1} to decrease by only approximately 40%, indicating that the NH does indeed contribute significantly to the intensity of this mode in Fig. 8(a). Table IV lists the vibrational modes of adsorbed NH and compares them to those of the adsorbed NH species identified previously as a product of hydrazine decomposition on Ni(111) (**32**). The observed δ(NH) frequency of 1350 cm^{-1} is well within the range of 1200-1420 cm^{-1} observed for δ(NH) in organic imides (**33**). Table IV also lists the vibrational frequencies of the various modes of ND formed from ND_2CHO decomposition on

Ru(001), which are the following: ν(ND), 2460 cm^{-1}; δ(ND), 1050 cm^{-1}; and ν(Ru-ND), 680 cm^{-1}. The corresponding vibrational frequencies of ND on Ni(111) are listed as well.

Annealing the Ru(001) surface to just over 400 K results in the decomposition of NH, leaving only CO, nitrogen adatoms, and a small amount of hydrogen adatoms on the surface. The nitrogen adatoms are identified by a loss feature at 580 cm^{-1} due to the vibration of these atoms perpendicular to the surface, i.e. ν_s(RuN). This mode appears as a shoulder on the ν_s(RuC) mode of coadsorbed carbon monoxide, when the latter is present. Annealing to 500 K desorbs the CO (and all remaining hydrogen), leaving only nitrogen adatoms on the surface [Fig. 9(c)]. The ν_s(RuN) mode of the nitrogen adatoms remains present (and of constant intensity) in EEL spectra after the surface is annealed to 700 K, then attenuates and disappears as the surface is annealed to just over 800 K, in agreement with the N_2 thermal desorption results for low coverages of formamide.

2. High Coverage

For initial formamide exposures at 80 K that are greater than approximately 2 L (but below the exposures necessary to condense formamide multilayers), both η^2(C,O)-NH_2CO and molecular formamide are observed as adsorption products using EELS. The molecular formamide is η^1(O)-NH_2CHO, the same species that is formed following formamide adsorption at 80 K on the Ru(001)-p(1x2)-O surface (**2**). Although many of the loss features due to η^1(O)-NH_2CHO overlap to some degree the loss features due to η^2(C,O)-NH_2CO, the ν(CO) loss peak of the former species is quite strong and is resolved clearly at 1670 cm^{-1}, and the ν(CH) loss peak is also observed at 2880 cm^{-1}. The frequency of ν(CO) indicates that the CO double bond is maintained in the molecularly adsorbed formamide.

The decomposition of η^1(O)-NH_2CHO (**34**) is difficult to monitor with EELS, since η^2(C,O)-NH_2CO and/or its decomposition products are always present as well, depending on the annealing temperature. Indeed, for a saturation formamide exposure, the η^2(C,O)-NH_2CO is stabilized by the higher surface coverage, and a small amount is present to 290 K. As on Ru(001)-p(1x2)-O (**2**), the η^1(O)-NH_2CHO that is formed undergoes competing desorption and conversion to another surface species at 225 K for a sufficiently high initial exposure (4 L or greater). For formide exposures between 2 and 4 L, only decomposition of η^1(O)-NH_2CHO is observed. This new surface species is stable to

approximately 300 K, but is not easily identifiable due to the presence of several other species on the surface in this temperature range. However, this intermediate does exhibit vibrational loss features at 1675 cm^{-1} [ν(CO)] and 2920 cm^{-1} [ν(CH)], and lacks the strong $\omega(NH_2)$ loss feature at 970 cm^{-1} which characterizes η^2(N,O)-NH_2CHO on the Ru(001)-p(1x2)-O surface (**2**). These vibrational features probably cannot be attributed to η^1(O)-NH_2CHO, which, if it does not convert to another species, desorbs well below 300 K. The possible nature of this intermediate, which is identified tentatively as η^1(N)-NHCHO, will be discussed in Sect. IV.

Annealing the formamide saturated Ru(001) surface to temperatures in the range of 300 to 350 K causes all of the η^2(C,O)-NH_2CO to decompose and all of the ammonia that is formed to desorb, leaving a much simpler EEL spectrum. Identical EEL spectra are obtained if formamide is adsorbed on Ru(001) at room temperature and annealed to 350 K to desorb residual ammonia (cf. Fig. 10). The species detected in such EEL spectra include CO, NH and a small amount of nitrogen adatoms (**31**). More significantly, a new surface species is detected which must arise from the decomposition of η^1(O)-NH_2CHO via the unidentified intermediate discussed in the previous paragraph. This new species maintains the carbon-hydrogen bond as indicated by a ν(CH) loss feature at 2940 cm^{-1}, and shows an intense loss feature at 1770 cm^{-1} that is characteristic of a carbonyl double bond in which the oxygen atom is not coordinated to the metal atom via an electron lone pair donor bond. The new species is thus identified as containing a formyl (HCO) group. Three such species must be considered in determining the identity of this intermediate: η^1(C)-HCO (η^1-formyl, which could be formed from carbon-nitrogen bond cleavage of formamide), η^1(N)-NHCHO, and η^1(N)-NCHO. The possibility of η^1-formyl formation can be ruled out since all η^1-formyl ligands identified in organometallic compounds have a ν(CO) frequency between 1540 and 1614 cm^{-1} (**35**), more than 150 cm^{-1} lower than the frequency of 1770 cm^{-1} observed in the present case. In addition, η^1-formyl is not observed as a decomposition product of formaldehyde on Ru(001) (**10**), so its formation from formamide is not expected, especially above 300 K. On the other hand, η^1(N)-NHCRO ligands identified in organometallic compounds have ν(CO) frequencies between 1708 and 1758 cm^{-1} (**4**), in good agreement with the present data, and an η^1(N)-NCHO species would be expected to have a similar ν(CO) frequency. A definite distinction

between η^1(N)-NHCHO and η^1(N)-NCHO is not possible because the presence of significant amounts of coadsorbed NH in the EEL spectrum of Fig. 10 makes it impossible to determine whether or not the intermediate gives rise to a nitrogen-hydrogen stretching vibration. We tentatively prefer η^1(N)-NCHO over η^1(N)-NHCHO, because we believe that the latter species is present below 300 K and would probably undergo NH bond cleavage below 375 K. The identification of this intermediate as η^1(N)-NCHO would allow all the loss features in Fig. 10 to be identified as follows. The intense loss features at 430 and 2000 cm^{-1} are due to carbon monoxide, while the features at 3280 and (in part) 1380 cm^{-1} are due to NH. The weak feature at 565 cm^{-1} indicates that a small amount of NH has decomposed, leaving nitrogen adatoms on the surface. The remaining loss features can be attributed to vibrational modes of η^1(N)-NCHO: ν(CH), 2940 cm^{-1}; ν(CO), 1770 cm^{-1}; π(CH), 1150 cm^{-1}; δ(NCO), 760 cm^{-1}; and ν_s(RuN), 340 cm^{-1}. The peak at 1380 cm^{-1} is quite broad and probably derives intensity from δ(CH) and ν(CN) of η^1(N)-NCHO as well as from δ(NH) of coadsorbed NH, since this peak is more intense [relative to the ν(NH) peak] than would be expected if only NH were present. As the surface is annealed to progressively higher temperatures, the loss features at 2940, 1770, 1150, 760 and 340 cm^{-1} attenuate and disappear in unison, verifying that they are due to a single surface species. The EEL spectrum of Fig. 10 is thus fully consistent with the presence of an η^1(N)-NCHO species.

Further annealing of the formamide saturated Ru(001) surface to 375 K causes the η^1(N)-NCHO to dissociate to carbon monoxide, nitrogen adatoms and (by inference) hydrogen adatoms, so that only these species and NH remain on the surface. In contrast to the low coverage data, EEL spectra show that some NH is still present on the surface at 400 K, but that it decomposes completely by 430 K. The desorption of CO (and all remaining hydrogen) is complete below 500 K, leaving only nitrogen adatoms on the surface which are manifest in EEL spectra by ν_s(RuN) at 580 cm^{-1}. The recombinative desorption of N_2 is complete by 810 K, leaving the clean Ru(001) surface following annealing to this temperature.

An additional issue of importance is the branching ratio for the two observed decomposition mechanisms of formamide on Ru(001), i.e. of the approximately 0.15 monolayer of formamide that decomposes following a saturation exposure, how much decomposes via η^2(C,O)-NH_2CO and how

much via η^1(O)-NH_2CHO and η^1(N)-NCHO? This branching ratio may be estimated using the intensity of the 2000 cm^{-1} carbon monoxide loss peak following annealing to 300 K, since by this temperature all the η^2(C,O)-NH_2CO has decomposed to CO and either NH or NH_3, while little if any of the η^1(N)-NCHO has yet decomposed. This estimate makes use of the known coverage versus intensity relationship for this CO loss feature **(20)**. The resulting estimate is that approximately 0.10 monolayer of formamide decomposes via the η^2(C,O)-NH_2CO intermediate, while the remaining approximately 0.05 monolayer decomposes via η^1(N)-NCHO.

Finally, as discussed in Sect. III.A.1, exposing the clean Ru(001) surface at 80 K to approximately 8 L or more of NH_2CHO results in the condensation of molecular multilayers of formamide, which desorb when the surface is annealed to 210 K. As expected, these multilayers are identical to those formed on the Ru(001)-p(1x2)-O surface **(2b)**.

IV. Discussion

It has been shown that the adsorption of low coverages of formamide on clean Ru(001) (i.e. where the amount of formamide that decomposes is less than 0.05 monolayer) at 80 K results in CH bond cleavage and rehybridization of the carbonyl double bond to produce an η^2(C,O)-NH_2CO species and a hydrogen adatom. No other surface species is identified by EELS below 230 K. The only thermal desorption products detected for these low formamide exposures ($\leq$2 L) are CO near 480 K, H_2 near 420 K, N_2 near 770 K and NH_3 near 315 K. The CO and NH_3 result from molecular desorption, while the H_2 and N_2 result from the recombinative desorption of hydrogen and nitrogen adatoms.

The structure and bonding of the η^2(C,O)-NH_2CO is of considerable interest since such a species has not been identified previously on a metal surface. Unfortunately, the lack of a definitive mode assignment due to the presence of significant mode coupling places limits on the conclusions that can be drawn. Several organometallic analogues have been synthesized and characterized, but vibrational data are scarce. In most of these η^2(C,O)-NR_2CO ligands, the CO and CN bond orders are less than two and greater than one, so that substantial mode coupling occurs between ν(CO) and ν(CN), making the mode descriptions ν_s(NCO) and ν_a(NCO) more meaningful. A series of mononuclear uranium and thorium compounds have been synthesized with the metal-formide group represented by the resonance

structures shown below (5a).

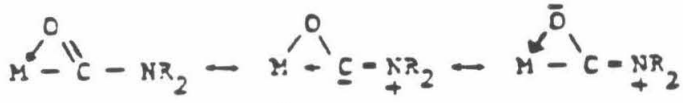

(M = U or Th, R = alkyl, additional ligands not shown.)

These compounds have ν_s(NCO) frequencies between 1491 and 1559 cm^{-1}, and ν_s(NCO) frequencies between 1298 and 1346 cm^{-1}. Also relevant to η^2(C,O)-NH_2CO on Ru(001) are the η^2(C,O)-NR_2CO ligands in several trinuclear ruthenium (5c,e) and osmium (5b,d) complexes, the structures of which have been represented as follows:

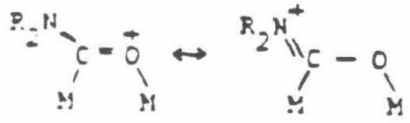

(M = Ru or Os, R = alkyl, additional ligands not shown.)

Although IR data with mode assignments are not available for these compounds, X-ray structures show clearly that both the CO and CN bonds of the OCN group have bond lengths intermediate between those expected for single and double bonds. For example, the $OCN(CH_3)_2$ ligand in $HRu_3(OCN(CH_3)_2)(CO)_{10}$ has CO and CN bond lengths of 1.287 and 1.340 Å (5c), respectively, while "typical" C=O, C-O, C=N and C-N bond lengths are approximately 1.22, 1.43, 1.27 and 1.47 Å, respectively (36). We expect that the structure of η^2(C,O)-NH_2CO on Ru(001) is similar to the structures observed for the η^2(C,O)-NR_2CO ligands in these trinuclear ruthenium and osmium complexes, and indeed the rehybridization of the CO bond may occur to an even greater extent on the extended ruthenium surface due to the following additional resonance structure:

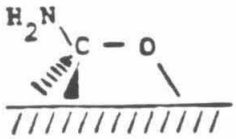

The species most closely related to η^2(C,O)-NH_2CO that has been identified previously on Ru(001) is η^2(C,O)-HCO (η^2-formyl), which is formed (along with chemisorbed CO and hydrogen adatoms) following relatively low exposures of formaldehyde to this surface at 80 K (**10**). The η^2-formyl has a ν(CO) frequency of 1180 cm^{-1}, indicative of a CO bond order of approximately 1.3. In this case, the assignment of ν(CO) is straightforward and meaningful, because coupling to the CH bending modes is insignificant. [The mode identified as ν(CO) shifts down only slightly to 1160 cm^{-1} upon deuteration of the formyl.] The decomposition of η^2(C,O)-NH_2CO is similar to that of η^2-formyl on Ru(001) in that carbon monoxide is the only oxygen- or carbon-containing decomposition product. The η^2(C,O)-NH_2CO is considerably more stable than η^2-formyl, however, since the latter decomposes to carbon monoxide and hydrogen adatoms upon annealing to only 120 K. The fact that formamide can undergo CH bond cleavage at 80 K on Ru(001) is not surprising in view of the fact that formaldehyde does. The CH bond energies of these two molecules are similarly low: 87 kcal in formaldehyde (**37**) and 89 kcal in formamide (**38**).

The spectroscopically observed decomposition products of η^2(C,O)-NH_2CO, appearing in the temperature range 230-250 K, are CO, NH_3 and NH. Additional hydrogen adatoms also result from the decomposition of this species, since very little ammonia ($\leq$0.02 monolayer) is produced. The rate-limiting step in this decomposition is almost certainly CN bond cleavage to produce NH_2 and CO, because if NH bond cleavage preceded CN bond cleavage, NH_3 would probably not be formed (**39**). Since NH_2 is not observed spectroscopically, it is concluded that this species is unstable on Ru(001) at 250 K (on the time scale of seconds at these surface coverages) and rapidly dehydrogenates to NH or is hydrogenated by a hydrogen adatom to NH_3. The ammonia that is produced desorbs molecularly at 315 K, in agreement with previous studies of ammonia adsorption on Ru(001) (**14a**).

The NH species observed on Ru(001) from formamide decomposition is only the second NH species that has been identified spectroscopically on a metal surface. The first was NH formed from hydrazine decomposition on Ni(111) (**32**), and Table IV shows that the vibrational frequencies of the two species are quite similar. Since the only examples known to us of NH ligands in organometallic complexes are in complexes containing at least three metal atoms with the nitrogen atom in a threefold

hollow site among three metal atoms (40), it is very likely that NH on Ru(001) occupies threefold hollow sites as well. This is undoubtedly also true of the NH on Ni(111), a surface that has the same hexagonally close-packed structure as Ru(001).

The decomposition of ND_2CHO on Ru(001) leads to the formation of chemisorbed ammonia, with ND_2H and ND_3 being formed in an approximate ratio of 3:2. We suspect that the minor amounts of NDH_2 and NH_3 that are formed result from sample contamination by NHDCHO and NH_2CHO. The adsorption at 80 K of pure ND_2CHO would produce η^2(C,O)-ND_2CO and hydrogen adatoms. Decomposition of η^2(C,O)-ND_2CO would then produce (presumably) a short-lived ND_2 species, which would either dehydrogenate to ND with the production of a deuterium adatom or be hydrogenated to ammonia by a hydrogen adatom or, in some cases, by a deuterium adatom formed from ND_2 decomposition to ND. Since there will be more hydrogen adatoms present on the surface than deuterium adatoms, the ammonia that is formed would be mainly ND_2H with a smaller amount of ND_3. The formation of some NDH_2 could conceivably result from H/D exchange into ND_2H, but preliminary results suggest that this reaction should not occur under these conditions (39). As expected, the "NH" formed from ND_2CHO decomposition is almost entirely ND, and the small amount of NH formed may result from sample contamination or from H exchange into ND.

For sufficiently high formamide exposures (≥2 L) to the Ru(001) surface at 80 K, molecularly adsorbed η^1(O)-NH_2CHO is observed in EELS in addition to η^2(C,O)-NH_2CO. This indicates that the initial products of adsorption, η^2(C,O)-NH_2CO and hydrogen adatoms, passivate the surface with respect to subsequent CH bond cleavage and CO bond rehybridization so that at higher coverages the molecularly adsorbed η^1(O)-NH_2CHO species is formed as on the Ru(001)-p(1x2)-O surface (2). A similar but more complex situation occurs in the case of formaldehyde adsorption on Ru(001), where the following adsorption products appear sequentially with increasing exposure at 80 K: CO + 2H, η^2(C,O)-HCO + H, η^2(C,O)-H_2CO and η^1(O)-H_2CO (10). In the case of formamide adsorption on Ru(001) at 80 K, no η^2(C,O)-NH_2CHO species is detected unambiguously for intermediate formamide exposures, which might have been expected from the formaldehyde results. It is possible, however, that such a species is formed in small amounts, but that its loss features cannot be resolved from those of the other surface

species that are present.

The η^1(O)-NH_2CHO decomposes completely upon annealing for formamide exposures less than 4 L (amount of formamide decomposing less than approximately 0.10 monolayer), whereas for exposures greater than 4 L it undergoes competing desorption and decomposition at 225 K. While we have no quantitative estimate of the amount of η^1(O)-NH_2CHO that desorbs molecularly, the amount that decomposes following a a saturation formamide exposure is approximately 0.05 monolayer. Two stable decomposition intermediates are observed in the decomposition of η^1(O)-NH_2CHO, one that is present from approximately 225 to 300 K and the second from 300 to 375 K. The species that is stable from approximately 300 to 375 K is probably η^1(N)-NCHO, analogous to the NH species formed from η^2(C,O)-NH_2CO decomposition, but with the hydrogen atom replaced by a formyl group. This species decomposes to CO, nitrogen adatoms, and hydrogen adatoms upon annealing the surface to 375 K. The first intermediate, present from 225 to 300 K, contains a carbon-oxygen double bond [ν(CO) = 1675 cm^{-1}] and a carbon-hydrogen bond [ν(CH) = 2920 cm^{-1}], but lacks the intense $\omega(NH_2)$ loss feature at 970 cm^{-1} that characterizes η^2(N,O)–NH_2CHO on Ru(001)-p(1x2)-O (**2**), a species that is formed on that surface by conversion of η^1(O)-NH_2CHO at 225 K and which is bonded to the surface via electron lone pairs on both the oxygen and nitrogen atoms. While the identification of this intermediate is uncertain, it seems likely that the coordination of the nitrogen atom to the surface must occur at 225 K in order to lead to the eventual formation of η^1(N)-NCHO. We suggest that on Ru(001) this occurs via nitrogen-hydrogen bond cleavage to produce an N-bonded NHCHO species that maintains the carbonyl double bond and the donor bond between the oxygen atom and the metal surface, as shown below:

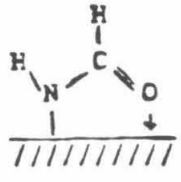

This species could convert to η^1(N)-NCHO at 300 K by simultaneously undergoing cleavage of the remaining nitrogen-hydrogen bond and the oxygen-ruthenium donor bond. It is not clear in detail, however, why such an N-bonded NHCHO species would not convert to the formate-like species η^2(N,O)–NHCHO [cf. Fig. 1, species (4)], which is formed upon nitrogen-hydrogen bond cleavage of

η^2(N,O)–NH_2CHO at 265 K on Ru(001)-p(1x2)-O (2). In general, the answer undoubtedly lies largely in the differing electronic properties of the Ru(001) and Ru(001)-p(1x2)-O surfaces.

A final issue to be addressed is the complex nature of the hydrogen thermal desorption spectra. For a saturation formamide exposure, the following reactions produce hydrogen adatoms as the surface is heated [assuming the presence of both N-bonded NHCHO and NCHO intermediates in η^1(O)-NH_2CHO decomposition]:

(i) $NH_2CHO(g) \overset{80K}{\rightarrow} \eta^2(C,O)\text{–}NH_2CO + H + \eta^1(O)\text{–}NH_2CHO,$

(ii) $\eta^1(O)\text{–}NH_2CHO \overset{225K}{\rightarrow} NHCHO + H,$

(iii) $\eta^2(C,O)\text{–}NH_2CO \overset{230\text{–}290K}{\rightarrow} CO + NH + H \text{ (or } CO + NH_3),$

(iv) $NHCHO \overset{300K}{\rightarrow} \eta^1(N)\text{–}NCHO + H,$

(v) $\eta^1(N)\text{–}NCHO \overset{375K}{\rightarrow} CO + N + H,$

(vi) $NH \overset{375\text{–}430K}{\rightarrow} N + H.$

Here (g) denotes a gas phase species, and all other species are adsorbed. If we consider a saturation exposure of ND_2CHO, and neglect contamination by NHDCHO or NH_2CHO, reactions (i) and (v) will produce hydrogen adatoms, while reactions (ii), (iii), (iv) and (vi) will produce deuterium adatoms (41). Although the four hydrogen desorption peaks at 280, 300, 375 and 410 K (cf. Fig. 4) cannot be assigned exclusively to surface hydrogen produced by any single reaction listed above, several conclusions can be drawn. First, since NH decomposes above 375 K, the hydrogen produced by NH decomposition must desorb in the 410 K peak (with perhaps a small amount desorbing in the 375 K peak). Indeed, the desorption of hydrogen at 300 K is a minor piece of evidence supporting the decomposition of η^1(N)-NHCHO to η^1(N)-NCHO at this temperature. This scheme is also in agreement with thermal desorption results for ND_2CHO that show the 410 K peak to contain mainly D_2, a result that shows the

hydrogen in this peak is derived largely from the ND_2 group of the initially adsorbed formamide. Some HD also desorbs at 410 K since not all of the hydrogen adatoms formed by reaction (v) desorb immediately in the 375 K peak. Thus, while not all hydrogen in the 410 K peak results from NH decomposition, it is NH decomposition near 410 K that increases the surface hydrogen (H or D) adatom concentration and serves to trigger this intense desorption peak. Similarly, the desorption of hydrogen at 280, 300 and 375 K is probably triggered by reactions (iii), (iv) and (v), respectively (42). Indeed, the desorption of hydrogen at 300 K is a minor piece of evidence supporting the decomposition of η^1(N)-NHCHO to η^1(N)-NCHO at this temperature. This scheme is also consistent with large amounts of HD in the 375 K peak (cf. Sect. III.A.3), since reaction (v) produces hydrogen adatoms which will recombine with adatoms on the surface, and the latter will be primarily deuterium rather than hydrogen. We emphasize once again that the problem of sample contamination (and, to a lesser degree, the difficulty of peak deconvolution) makes a more quantitative analysis of the amounts of H_2, HD and D_2 desorbed in each peak impossible.

V. Conclusions

Following a saturation formamide exposure on the clean Ru(001) surface at 80 K, approximately 0.15 monolayer of formamide decomposes. This decomposition occurs via two distinct mechanisms. The major one, accounting for 0.10 monolayer of formamide that decomposes at saturation, is the only decomposition mechanism that occurs at low coverage and may be written as follows (the temperatures given are for the low coverage limit):

$$NH_2CHO(g) \xrightarrow{80K} \eta^2(C,O)\text{–}NH_2CO + H$$

$$\eta^2(C,O)\text{–}NH_2CO \xrightarrow{230\text{–}250K} CO + NH + H + NH_3$$

$$NH_3 \xrightarrow{315K} NH_3(g)$$

$$CO \xrightarrow{480K} CO(g)$$

$$NH \xrightarrow{400\text{–}430K} N + H$$

$$2H \xrightarrow{420K} H_2(g)$$

$$2N \xrightarrow{770K} N_2(g)$$

At saturation, approximately 0.08 monolayer of NH and 0.02 monolayer of NH_3 is produced.

For exposures greater than 2 L, where the amount of formamide that decomposes is greater than approxmately 0.05 monolayer, a second decomposition mechanism occurs. In this mechanism, η^1(O)-bonded molecular formamide, formed from formamide adsorption at 80 K, converts near 225 K to an intermediate believed to be an N-bonded NHCHO species. At 300 K, this intermediate converts to an intermediate tentatively identified as η^1(N)-NCHO, a species analogous to NH but with the hydrogen atom replaced by a formyl group. This intermediate decomposes near 375 K to coadsorbed carbon monoxide, and nitrogen and hydrogen adatoms. For exposures greater than 4 L, where the amount of formamide that decomposes is greater than approximately 0.09 monolayer, some molecular desorption of η^1(O)-NH_2CHO occurs also at 225 K.

The reactions and surface intermediates observed in formamide decomposition on clean Ru(001) and on Ru(001)-p(1x2)-O are quite different. However, η^1(O)-NH_2CHO is formed on both surfaces under certain conditions of coverage and temperature. The amount of formamide that decomposes following a saturation exposure increases by a factor of three, from 0.05 to 0.15 monolayer, in going from the oxygen covered to the clean surface.

Acknowledgment: The authors are grateful to Dr. Malina Hills for assistance in obtaining the ammonia thermal desorption spectra. This research was supported by the National Science Foundation (Grant No. CHE-8516615), and the Petroleum Research Fund (Grant No. 15454-ACS).

References

1. Ibach, H. and Mills, D. L., "Electron Energy Loss Spectroscopy and Surface Vibrations" **1982**, Academic Press, New York.

2. (a) Parmeter, J.E.; Schwalke, U.; Weinberg, W.H., J. Am. Chem. Soc., in press. (b) Parmeter, J.E.; Schwalke, U.; Weinberg, W.H., J. Am. Chem. Soc., submitted.

3. (a) Kruse, A. E.; Angelici, R. J., J. Organomet. Chem. **1970**, 24, 231. (b) Behrens, H.; Jungbauer, A., Z. Naturforsch. **1979**, 34b, 1477. (c) Sacco, A.; Giannoccaro, P.; Vasapollo, G., Inorganica Chimica Acta **1984**, 83, 125. (d) Lindsay, A. J.; Kim, S; Jacobson, R. A.; Angelici, R. J., Organomet. **1984**, 3, 1523.

4. Burgess, K.; Johnson, B. F. G.; Lewis, J., J. Chem. Soc. Dalton Trans. **1983**, 1179.

5. (a) Fagan, P.J.; Manriquez, J.M.; Vollmer, S.H.; Day, C.S.; Day, V.W.; Marks, T.J., J. Am. Chem. Soc. **1981**, 103, 2206. (b) Azam, K.A.; Yin, C.C.; Deeming, A.J., J. Chem. Soc. Dalton Trans. **1978**, 1201. (c) Szostak, R.; Strouse, C.E.; Kaesz, H.D., J. Oranomet. Chem. **1980**, 191, 243. (d) Mayr, A.; Lin, Y-C.; Boag, N.M.; Kaesz, H.D., Inorg. Chem. **1982**, 21, 1704. (e) Kampe, C.E.; Boag, N.M.; Kaesz, H.D., J. Molecular Cat. **1983**, 21, 297.

6. (a) Rossi, R.; Duatti, A.; Magon, L.; Casellato, U.; Graziani, R.; Toniolo, L., Inorganica Chimica Acta **1983**, 74, 77. (b) Sahajpal, A.; Robinson, R.D., Inorg. Chem. **1979**, 18, 3572. (c) Schwering, H.-U.; Weidlein, J., Chimia **1973**, 27, 535. (d) Jennings, J.R.; Wade, K.; Wyatt, B.K., J. Chem. Soc. (A) **1968**, 2535. (e) Adams, R.D.; Golembeski, N.M., J. Organomet. Chem. **1979**, 171, C21. (f) Adams, R.D.; Golembeski, N.M., Selegue, J.P., Inorg. Chem. **1981**, 20, 1242.

7. (a) Lin, Y.C.; Knobler, C.B.; Kaesz, H.D., J. Am. Chem. Soc. **1981**, 103, 1216. (b) Kaesz, H.D.; Knobler, C.B.; Andrews, M.A.; van Buskirk, G.; Szostak, R.; Strousse, C.E.; Lin, Y.C.; Mayr, A., Pure & Appl. Chem. **1982**, 54, 131.

8. (a) Avery, N. R.; Toby, B. H.; Anton, A. B.; Weinberg, W. H., Surface Sci. **1982**, 122, L574. (b) Toby, B. H.; Avery, N. R.; Anton, A. B.; Weinberg, W. H., J. Electron Spectros. Related Ph. **1983**, 29, 317.

9. (a) Avery, N. R.; Anton, A. B.; Toby, B. H.; Weinberg, W.H., J. Electron Spectros. Related Ph. 1983, 29, 233. (b) Avery, N. R.; Weinberg, W. H.; Anton, A. B.; Toby, B. H., Phys. Rev. Lett. 1983, 51, 682. (c) Anton, A. B.; Parmeter, J.E.; Weinberg, W. H., J. Am. Chem. Soc. 1986, 108, 684.

10. (a) Anton, A. B.; Parmeter, J. E.; Weinberg, W. H., J. Am. Chem. Soc. 1985, 107, 5558. (b) Anton, A. B.; Parmeter, J. E.; Weinberg, W. H., J. Am. Chem. Soc. 1985, 108, 1823.

11. Thomas, G. E.; Weinberg, W. H., Rev. Sci. Instrum. 1979, 50, 497.

12. Thomas, G. E.; Weinberg, W. H., J. Chem. Phys. 1979, 70, 954.

13. The exchange of hydrogen into the ND_2 group of ND_2CHO may occur in the metal line through which formamide is passed before entering the UHV chamber or on the walls of the UHV chamber.

14. Since the amount of ammonia desorbed is very small, it was difficult to detect via TDMS in the EELS chamber, and these TDMS experiments were carried out in a companion UHV chamber in which the mass specrometer is closer to the crystal. The production of ammonia was also demonstrated unambiguously by EELS. For previous TDMS results concerning ammonia on Ru(001), see (a) Benndorf, C.; Madey, T.E., Surface Sci. 1983, 135, 164; and (b) Danielson, L.; Dresser, M.J.; Donaldson, E.E.; Dickinson, J.T., Surface Sci. 1978, 71, 599. In (a), the saturation (monolayer) coverage of ammonia on Ru(001) was estimated to be 0.25 monolayer.

15. Redhead, P. A., Vacuum 1962, 203.

16. (a) Madey, T. E.; Menzel, D., J. Appl. Phys. 1974, Suppl. 2, Pt. 2, 229. (b) Pfnür, H.; Feulner, P.; Engelhardt, H.A.; Menzel, D., Chem. Phys. Lett. 1978, 59, 481. (c) Pfnür, H.; Feulner, P.; Menzel, D., J. Chem. Phys. 1983, 79, 4613.

17. Hills, M. M.; Parmeter, J. E.; Weinberg, W. H., J. Am. Chem. Soc., submitted.

18. (a) Blyholder, G., J. Phys. Chem. 1964, 68, 2772. (b) Blyholder, G., J. Phys. Chem. 1975, 79, 756.

19. Anton, A.B.; Avery, N.R.; Madey, T.E.; Weinberg, W.H., J. Chem. Phys. 1986, 85, 507.

20. Pfnür, H.; Menzel, D.; Hoffmann, F.M.; Ortega, A.; Bradshaw, A.M., Surface Sci. **1980**, 93, 431.

21. (a) Shimizu, H.; Christmann, K.; Ertl, G., J. Catal. **1980**, 61, 412. (b) Schwarz, J.A., Surface Sci. **1979**, 87, 525. (c) Barteau, M. A.; Broughton, J. Q.; Menzel, D., Surface Sci. **1983**, 88, 384. (d) Conrad, H.; Scala, R.; Stenzel, W.; Unwin, R., J. Chem. Phys. **1984**, 81, 6371.

22. See Ref. 19 above, as well as Anton, A.B.; Avery, N.R.; Toby, B.H.; Weinberg, W.H., J. Electron Spectros. Related Ph. **1983**, 29, 181.

23. Thomas, G.E.; Weinberg, W.H., J. Chem. Phys. **1978**, 69, 3611.

24. An additional argument against η^1(C)–NH_2CO is the fact that this ligand is known in organometallic chemistry only in compounds containing a single metal atom. When more than one metal atom is present, the observed bonding configuration is η^2(C,O)–NH_2CO or, more rarely, η^2(C,N)–$OCNH_2$. See Refs. 3, 5 and 7.

25. This is a consequence of the so-called surface dipole selection rule. See Chs. 1 and 3 of Ref. 1.

26. (a) Thomas, G. E.; Weinberg, W. H., J. Chem. Phys. **1979**, 70, 1437. (b) Refs. 12 and 20.

27. Sexton, B.A.; Mitchell, G.E., Surface Sci. **1980**, 99, 523.

28. Gland, J.L.; Sexton, B.A.; Mitchell, G.E., Surface Sci. **1982**, 115, 623.

29. Fisher, G.B.; Mitchell, G.E., J. Electron Spectros. Related Ph. **1983**, 29, 253.

30. Erley, W.; Ibach, H., Surface Sci. **1982**, 119, L357.

31. Hydrogen adatoms are also present on the surface but are not detected by EELS due to their small cross section for inelastic scattering (**21d**).

32. Gland, J.L.; Fisher, G.B.; Mitchell, G.E., Chem. Phys. Lett. **1985**, 119, 89.

33. (a) Bigotto, A.; Galasso, V., Spectrochim. Acta **1979**, 35A, 725. (b) Woldbaek, T.; Klaeboe, P.; Christensen, D.H., Acta Chem. Scand. **1976**, A30, 531.

34. An unknown amount of η^1(O)–NH_2CHO also desorbs at 225 K, so that this species undergoes competing desorption and decomposition following exposures $\gtrsim$4 L.

35. (a) Gladysz, J.A.; Tam, W., J. Am. Chem. Soc. **1978**, 100, 2545. (b) Tam, W.; Wong, W.; Gla-

dysz, J.A., J. Am. Chem. Soc. **1979**, 101, 1589. (c) Winter, S.R.; Cornett, G.W.; Thompson, E.A., J. Organomet. Chem. **1977**, 133, 339. (d) Gladysz, J.A.; Williams, G.M.; Tam, W.; Johnson, D.L., J. Organomet. Chem. **1977**, 140, C1. (e) Gladysz, J.A.; Selover, J.C., Tetrahedron Lett. **1978**, 319. (f) Collins, T.J.; Roper, W.R., J.C.S. Chem. Comm. **1976**, 1044.

36. The "typical" bond lengths are estimated from covalent radii. See Jolly, W.L., "The Principles of Inorganic Chemistry" **1976**, McGraw-Hill, N.Y., p. 36.

37. Golden, D.M.; Benson, S.W., Chem. Rev. **1969**, 69, 125.

38. Kahumoto, T.; Saito, K.; Imamura, A., J. Phys. Chem. **1985**, 89, 2286.

39. Preliminary experiments with coadsorbed NH and hydrogen and coadsorbed ammonia and hydrogen suggest that NH cannot be hydrogenated to ammonia on Ru(001) under UHV conditions, and also that deuterium adatoms do not exchange into adsorbed ammonia. Parmeter, J.E., unpublished results.

40. (a) Fjare, D.E.; Gladfelter, W.L., J. Am. Chem. Soc. **1981**, 103, 1572. (b) Fjare, D.E.; Gladfelter, W.L., Inorg. Chem. **1981**, 20, 3533.

41. This analysis also assumes that no H/D exchange occurs among the various adsorbed surface species.

42. The fact that an H_2 thermal desorption peak occurs at 300 K following saturation exposures supports the idea of a dehydrogenation reaction occurring at this temperature and thus, indirectly, supports the presence of an N-bonded NHCHO species which converts to an N-bonded NCHO species.

43. Suzuki, I., Bull. Chem. Soc. Jpn. **1960**, 33, 1359.

44. (a) Evans, J.C., J. Chem. Phys. **1954**, 22, 1228. (b) King, S.T., J. Phys. Chem. **1971**, 75, 405.

Table I. Frequencies in cm^{-1} of the observed vibrational modes of η^2(C,O)-NH_2CO and η^2(C,O)-ND_2CO on Ru(001).

Mode	η^2(C,O)-NH_2CO	η^2(C,O)-ND_2CO	Frequency Shift
$\nu_a(NH_2)$		2560	−1.32
	3370[a]		
$\nu_s(NH_2)$		2455	−1.37
See text*	1580,1370	1440,1285	-
	1300,1015	1085,980	
$\omega(NH_2)$	820	~600[b]	−1.37
δ(NCO)	655	~650[b]	−1.01
ν(Ru–NH_2CO)	360	370	0.97
	270	270	1.00

*Coupling among these four modes precludes specific mode assignments. The (uncoupled) modes involved are ν_s(NCO), ν_a(NCO), $\delta(NH_2)$ and $\rho(NH_2)$.

[a] This feature is broad, and the $\nu_a(NH_2)$ and $\nu_s(NH_2)$ modes are not resolved clearly.

[b] These two modes overlap in the case of η^2(C,O)–ND_2CO.

Table II. Frequencies in cm^{-1} and mode assignments for liquid NH_2CHO, liquid ND_2CHO and gas phase NH_2CHO.

Mode	$NH_2CHO(l)$ (43)	$ND_2CHO(l)$ (43)	$NH_2CHO(g)$ (44)
$\nu_a(NH_2)$	3330	2556	3545
$\nu_s(NH_2)$	3190	2385	3451
ν(CH)	2882	2887	2852
ν(CO)	1690	1667	1734
$\delta(NH_2)$	1608	1118	1572
δ(CH)	1391	1398	1378
ν(CN)	1309	1338	1255
π(CH)	1056	1056	1030
$\rho(NH_2)$	1090	912	1059
$\omega(NH_2)$	750	450	602
$\tau(NH_2)$	200	-	289
δ(NCO)	608	570	565

a = asymmetric, s = symmetric

Table III. Summary of vibrational frequencies in cm^{-1} and mode assignments for the decomposition products of η^2(C,O)-NH_2CO on Ru(001) after annealing to 250 K.

Species	Mode	Frequency
CO	ν(CO)	1985
	ν(Ru-CO)	460
NH_3	$\nu(NH_3)$[a]	3315
	$\delta_a(NH_3)$	1590
	$\delta_s(NH_3)$	1160
NH	ν(NH)	3315
	δ(NH)	1350
	ν(Ru-NH)	690

[a] The $\nu_s(NH_3)$ and $\nu_a(NH_3)$ modes of adsorbed NH_3 are not resolved from the ν(NH) mode of coadsorbed NH.

Table IV. Vibrational frequencies in cm^{-1} and mode assignments for NH and ND on Ru(001) (this work) and Ni(111) (32).

	Ru(001)			Ni(111)		
Mode	NH	ND	Shift	NH	ND	Shift
ν(NH)	3315	2460	1.35	3340	2480	1.35
δ(NH)	1350	1050	1.29	1270	950	1.34
ν(M-NH)	690	680	1.01	620	580	1.07

Figure Captions

Figure 1: Several possible decomposition products of formamide on a metal surface. All of these species have known organometallic analogues (in some of which one or both hydrogens are replaced by an alkyl or aryl group).

Figure 2: The molecular formamide (m = 45 amu) thermal desorption spectra that result following various exposures of NH_2CHO to the clean Ru(001) surface at 80 K. The approximate formamide exposures are (a) 2 L, (b) 4 L, (c) 6 L, (d) 8 L and (e) 12 L.

Figure 3: Thermal desorption spectra of CO (m = 28 amu) that result following various exposures of NH_2CHO to the clean Ru(001) surface at 80 K. The approximate formamide exposures are (a) 0.3 L, (b) 1 L, (c) 5 L and (d) 10 L.

Figure 4: Thermal desorption spectra of H_2 (m = 2 amu) that result following various exposures of NH_2CHO to the clean Ru(001) surface at 80 K. The inset compares H_2 thermal desorption spectra that result following saturation exposures of H_2 and NH_2CHO on this surface. The approximate formamide exposures are (a) 0.5 L, (b) 1 L, (c) 2 L, (d) 4 L and (e) 10 L.

Figure 5: The m = 14 amu (N cracking fragment of N_2) thermal desorption spectrum that results following a saturation exposure of NH_2CHO to the clean Ru(001) surface at 80 K.

Figure 6: Thermal desorption spectra for m/e = 17 amu that result when the Ru(001) surface at 80 K is exposed to approximately (a) 0.4 L, (b) 2 L, (c) 5 L and (d) 8 L of formamide. Only the high-temperature feature corresponds to ammonia desorption; the peak at 235 K is due to a molecular formamide cracking fragment.

Figure 7: The EEL spectra that result following 0.5 L exposures of (a) NH_2CHO and (b) ND_2CHO to the clean Ru(001) surface at 80 K. These spectra are characteristic of η^2(C,O)-NH_2CO and η^2(C,O)-ND_2CO.

Figure 8: (a) The EEL spectrum that results when the Ru(001) surface represented in Fig. 7(a) is annealed briefly to 250 K. (b) The EEL spectrum that results when the clean Ru(001) surface at 80 K is exposed to approximately 1 L NH_3 and annealed to 300 K.

Figure 9: (a) The EEL spectrum that results when the Ru(001) surface represented in Fig. 7(a) is annealed briefly to 350 K. (b) An EEL spectrum of the same surface measured 10° off-specular. (c) The EEL spectrum that results when the surface represented in Fig. 7(a) is annealed briefly to 500 K.

Figure 10: The EEL spectrum that results when the clean Ru(001) surface at 300 K is exposed to 2 L of NH_2CHO and annealed briefly to 350 K.

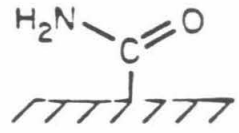

(1) $\eta^1(C)-CONH_2$

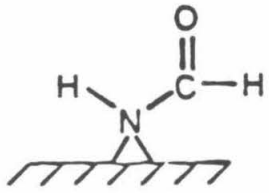

(2) $\eta^1(N)-NHCHO$

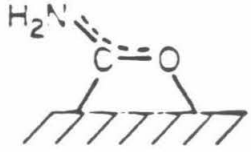

(3) $\eta^2(C,O)-NH_2CO$

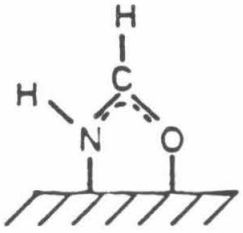

(4) $\eta^2(N,O)-NHCHO$

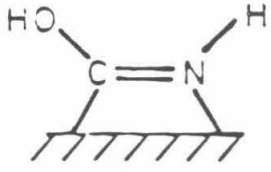

(5a) $\eta^2(C,N)-HOCNH$

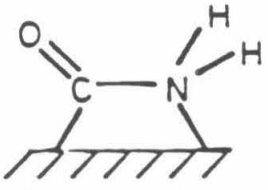

(5b) $\eta^2(C,N)-OCNH_2$

Figure 1

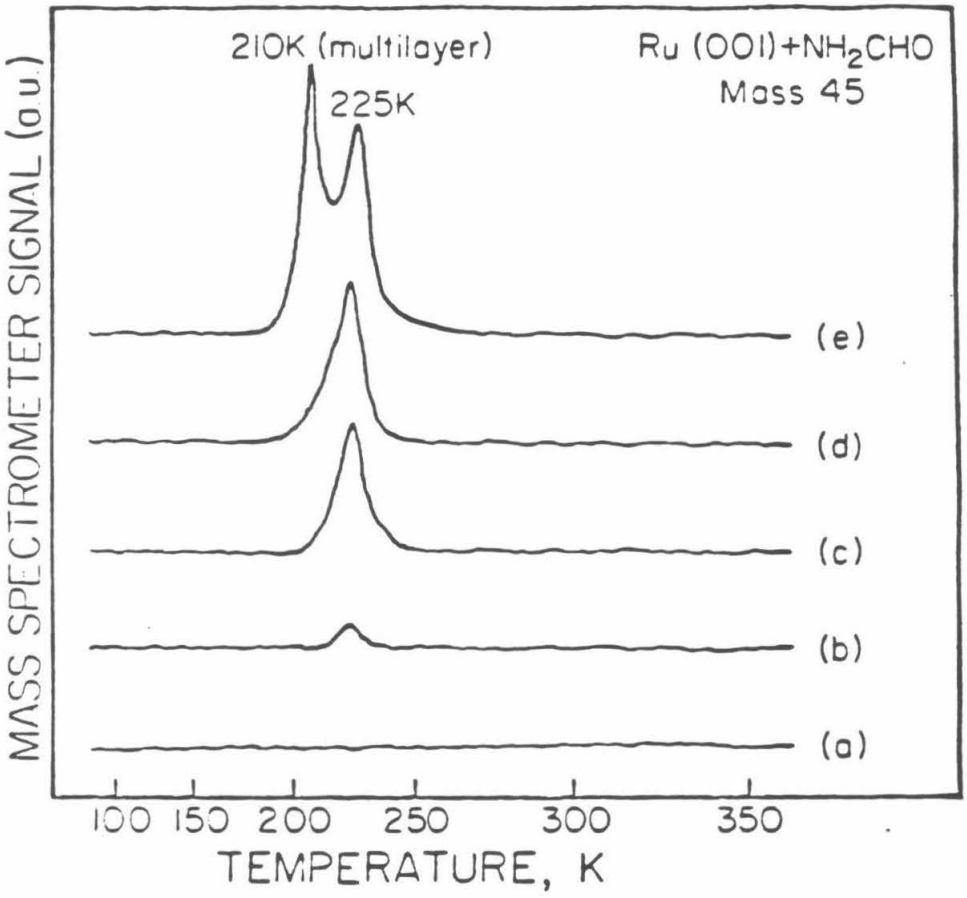
210K (multilayer)
225K
Ru (001)+NH2CHO
Mass 45
(e)
(d)
(c)
(b)
(a)
MASS SPECTROMETER SIGNAL (a.u.)
100 150 200 250 300 350
TEMPERATURE, K

Figure 2

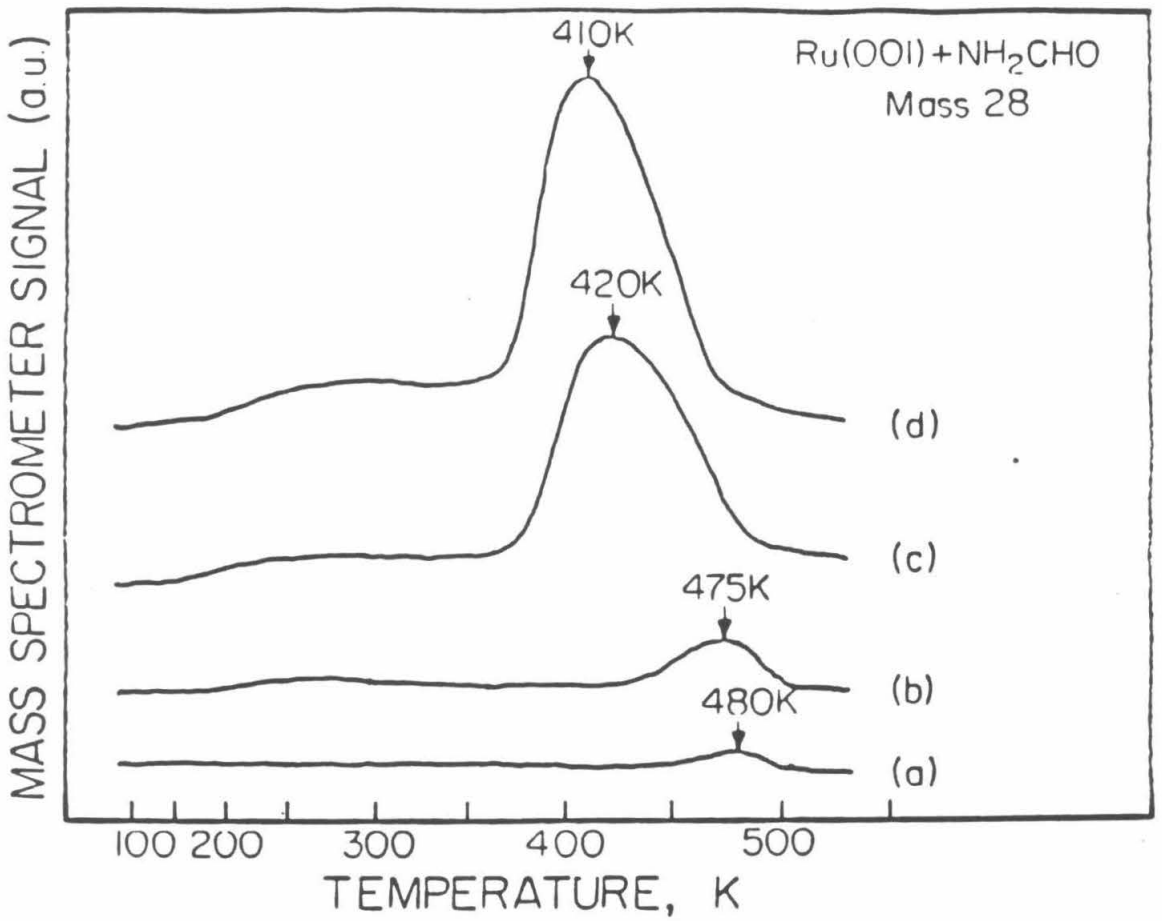
410K
Ru(001)+NH2CHO
Mass 28
420K
(d)
(c)
475K
(b)
480K
(a)
MASS SPECTROMETER SIGNAL (a.u.)
100 200 300 400 500
TEMPERATURE, K

Figure 3

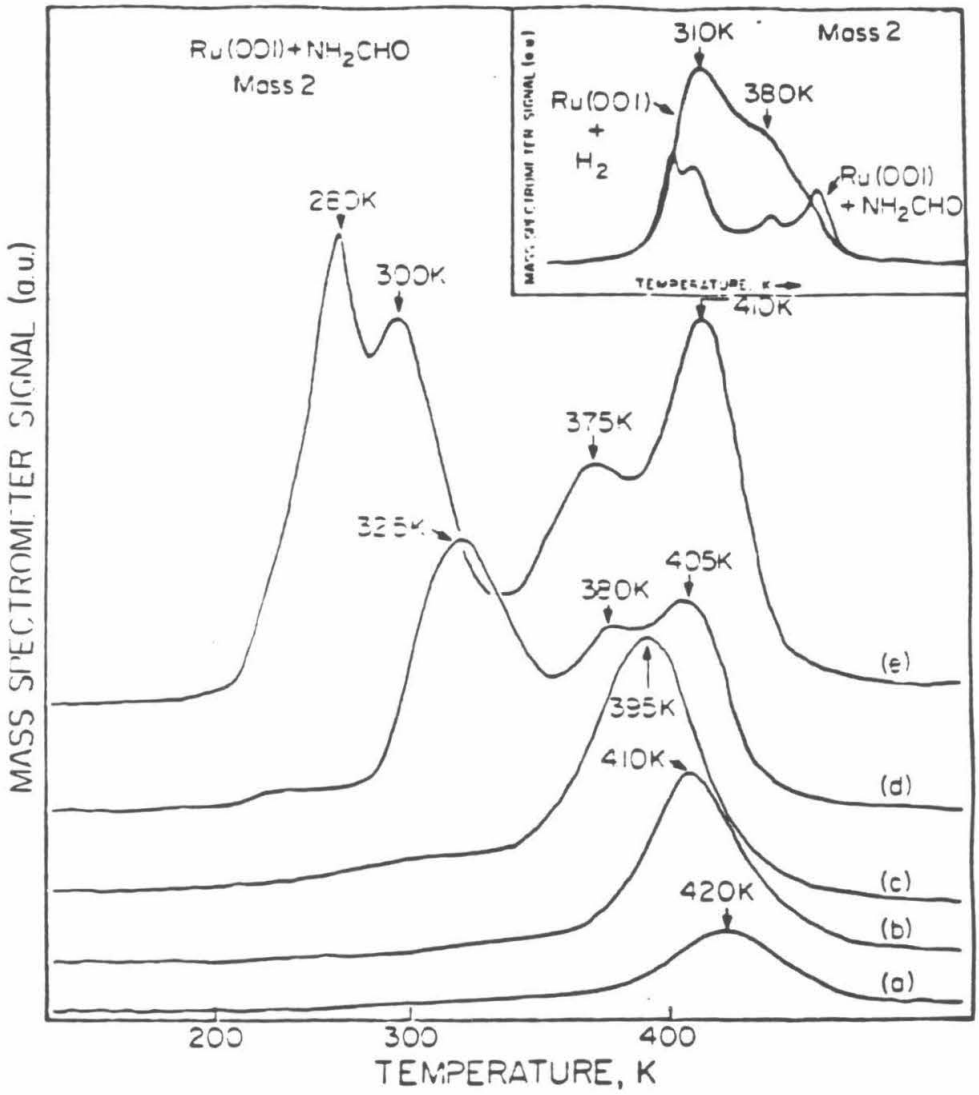
Ru(001)+NH2CHO
Mass 2
MASS SPECTROMETER SIGNAL (a.u.)
280K
300K
325K
375K
380K
395K
405K
410K
420K
(e)
(d)
(c)
(b)
(a)
200
300
400
TEMPERATURE, K
310K
Mass 2
Ru(001)
+
H2
380K
Ru(001)
+NH2CHO
410K

Figure 4

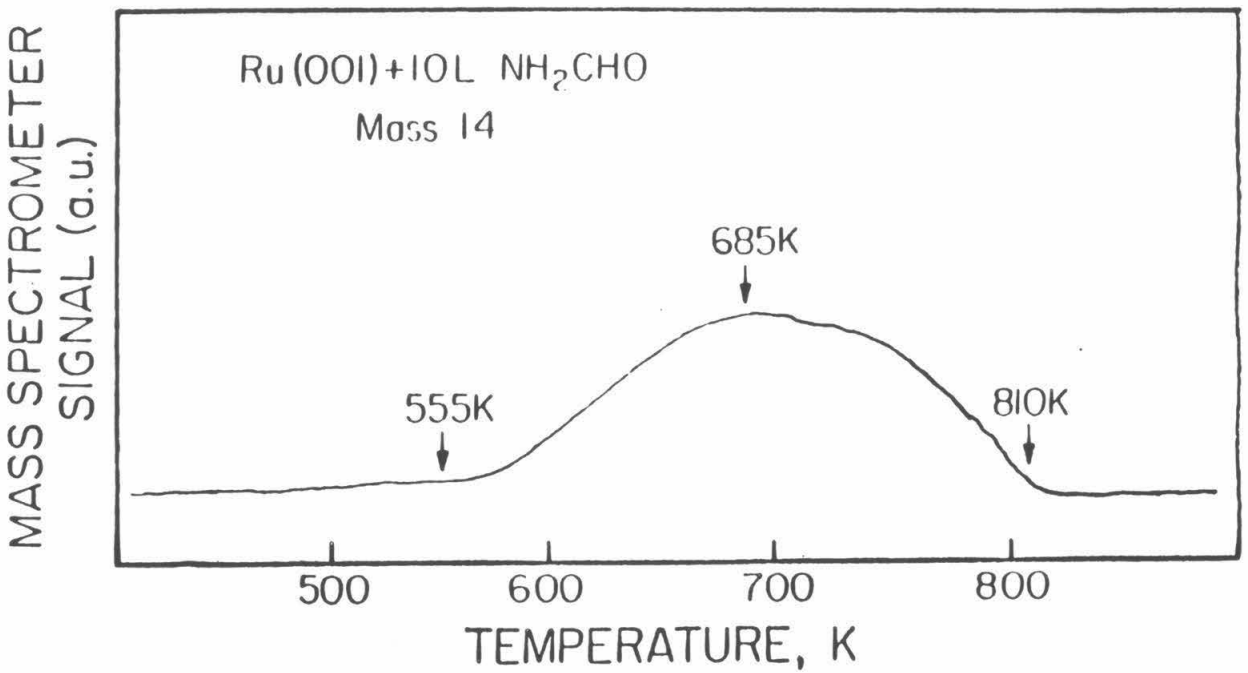
Ru(001)+10L NH2CHO
Mass 14
685K
555K
810K
MASS SPECTROMETER SIGNAL (a.u.)
500
600
700
800
TEMPERATURE, K

Figure 5

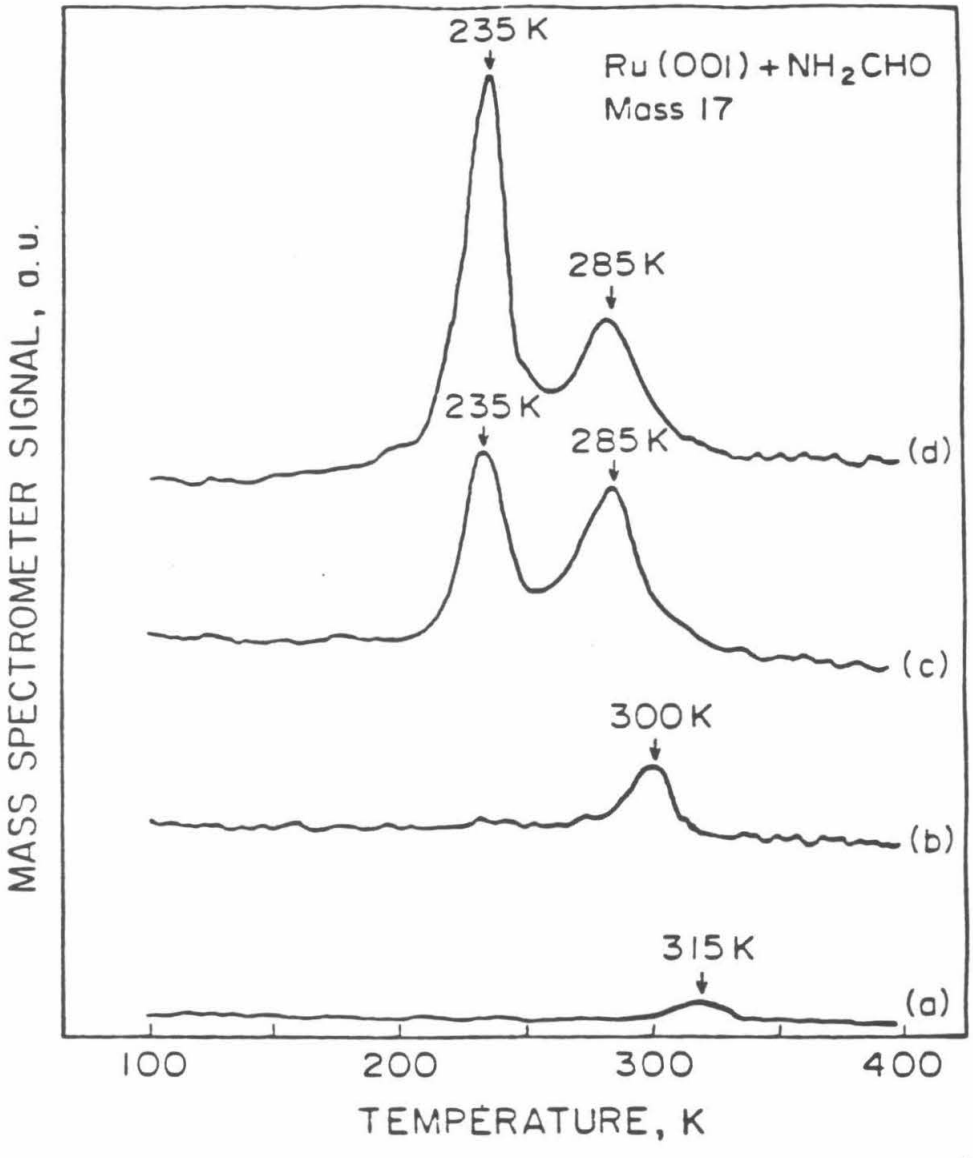
235 K
Ru (001) + NH2CHO
Mass 17
285 K
235 K
285 K
(d)
(c)
300 K
(b)
315 K
(a)
MASS SPECTROMETER SIGNAL, a.u.
100
200
300
400
TEMPERATURE, K

Figure 6

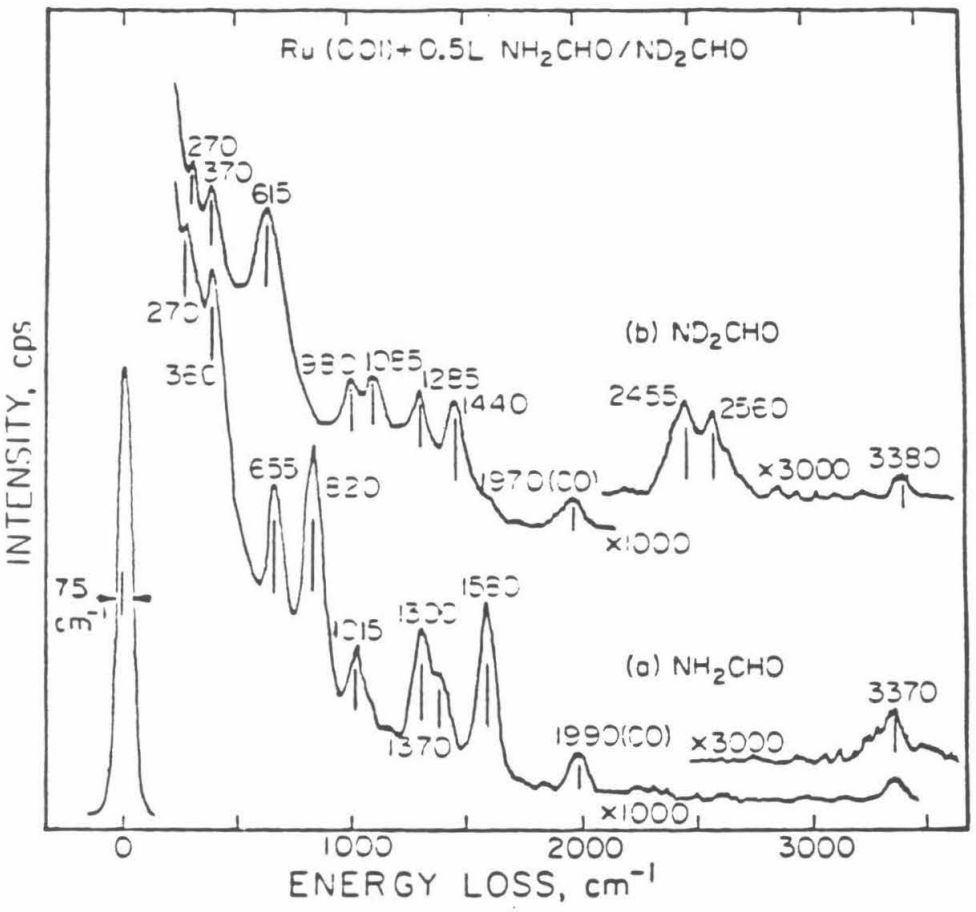
Ru (001)+0.5L NH2CHO/ND2CHO
270
370
615
270
380
980
1085
1285
1440
655
820
1015
1300
1580
1370
1990(CO)
x1000
(a) NH2CHO
3370
x3000
75 cm-1
(b) ND2CHO
2455
2560
x3000
3380
1970(CO)
x1000
INTENSITY, cps
0
1000
2000
3000
ENERGY LOSS, cm-1

Figure 7

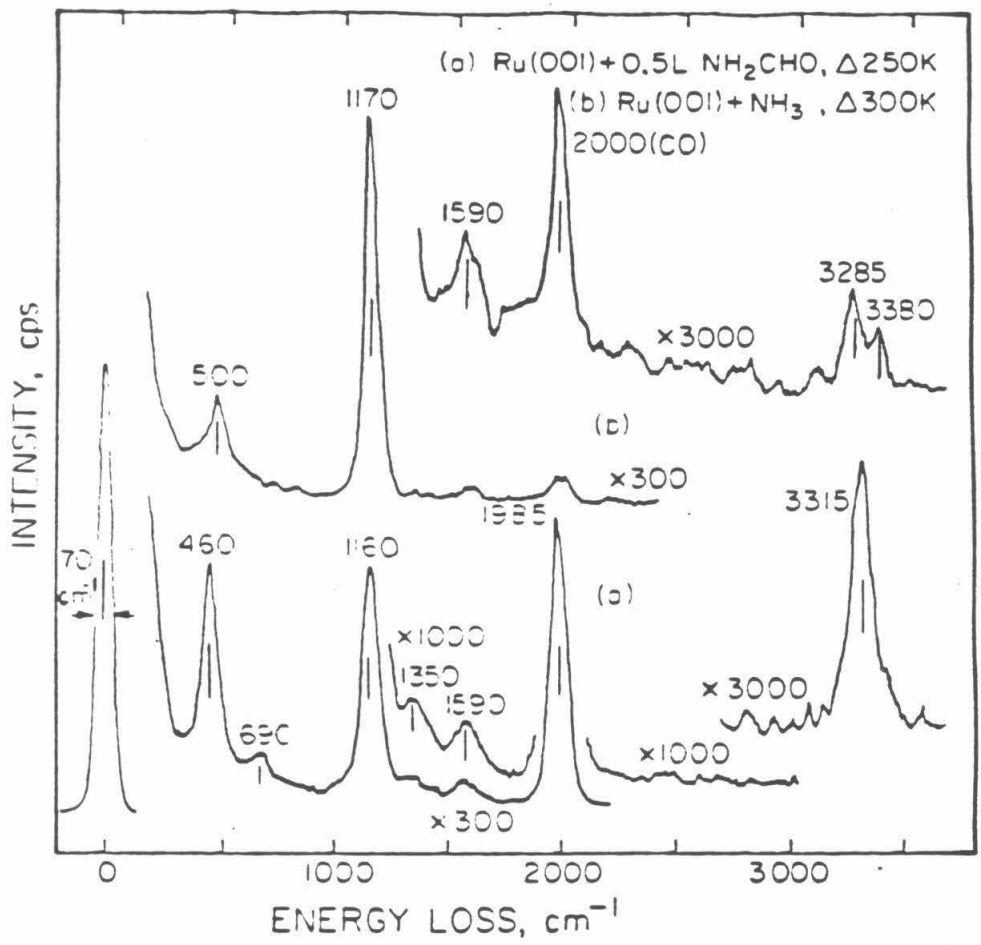
(a) Ru(001)+0.5L NH2CHO, Δ250K
(b) Ru(001)+NH3 , Δ300K
2000(CO)
1170
1590
3285
3380
×3000
500
(b)
×300
1935
3315
460
1160
(a)
70
×1000
1350
1590
×3000
690
×1000
×300
INTENSITY, cps
0
1000
2000
3000
ENERGY LOSS, cm-1

Figure 8

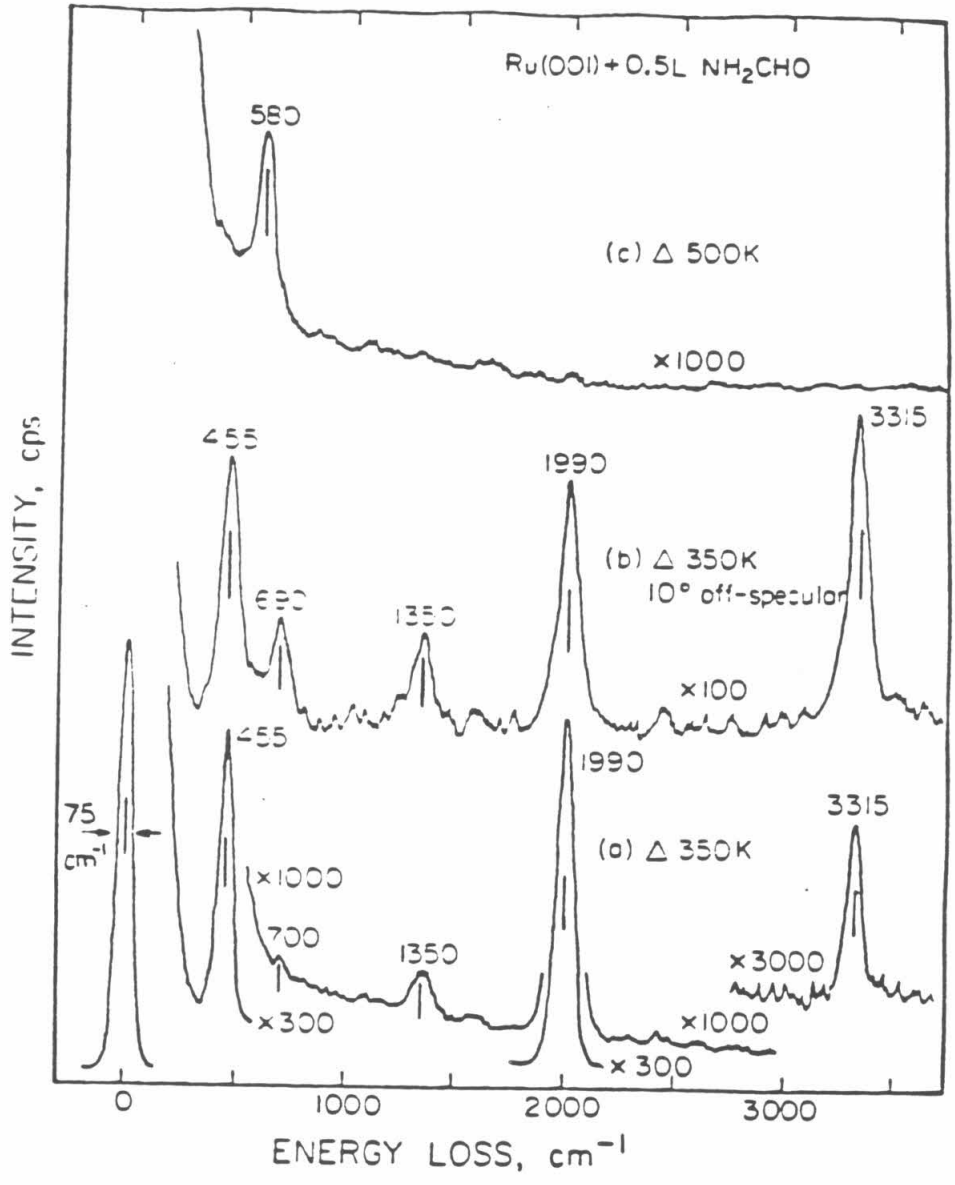
Ru(001)+0.5L NH2CHO
580
(c) Δ 500K
×1000
455
1990
3315
(b) Δ 350K
10° off-specular
690
1350
×100
455
1990
3315
75
cm-1
(a) Δ 350K
×1000
700
1350
×3000
×300
×1000
×300
INTENSITY, cps
0
1000
2000
3000
ENERGY LOSS, cm-1

Figure 9

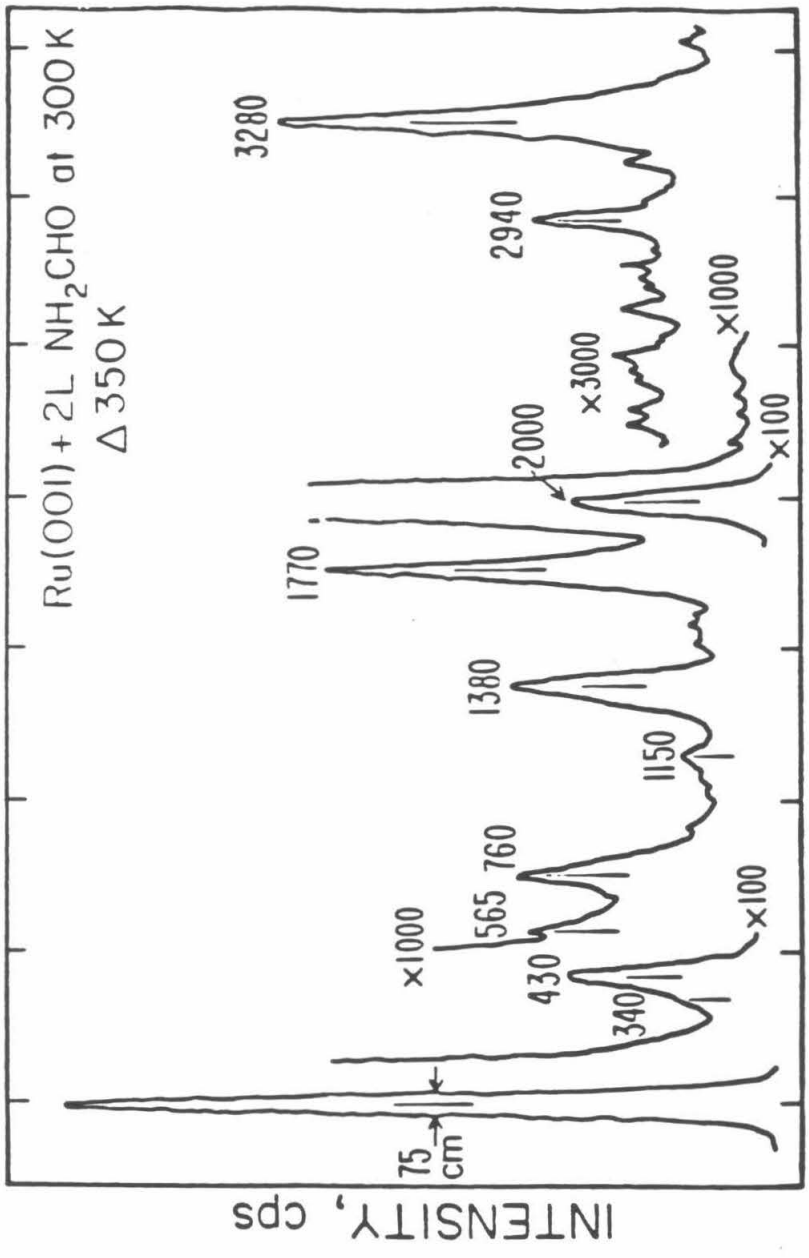
Ru(001) + 2L NH_2CHO at 300 K
Δ 350 K
INTENSITY, cps
ENERGY LOSS, cm
0
1000
2000
3000
75 cm
340
430
×1000
565
760
1150
1380
×100
1770
2000
×3000
2940
×1000
×100
3280

Figure 10

CHAPTER VI

The Adsorption of Formamide on the Ru(001)-p(1x2)-O Surface: The Spectroscopic Identification of η^2(N,O)-NHCHO

[This chapter was published as a Communication by J. E. Parmeter, U. Schwalke and W. H. Weinberg, in *The Journal of the American Chemical Society* **1987**, 109, 1876.]

Abstract

The adsorption and decomposition of formamide on a Ru(001) surface with an ordered p(1x2) overlayer of oxygen adatoms have been studied using high-resolution electron energy loss spectroscopy and thermal desorption mass spectrometry. Below approximately 260 K, formamide is chemisorbed molecularly on this surface in a manner such that the carbonyl double bond is maintained [ν(CO) = 1660 cm^{-1}]. The formamide undergoes NH bond cleavage near 260 K to form an η^2(N,O)-NHCHO species, which is the nitrogen-containing analogue of a bidentate formate. This species is stable to approximately 420 K, at which point it decomposes, evolving CO and H_2 and leaving nitrogen adatoms on the surface. These desorb as N_2 near 570 K, leaving the p(1x2)-O overlayer intact on the surface.

Reprinted from the Journal of the American Chemical Society, 1987, *109*, 1876.

Adsorption of Formamide on the Ru(001)–p(1×2)-O Surface: The Spectroscopic Identification of η^2(N,O)-NHCHO

J. E. Parmeter,† U. Schwalke,‡ and W. H. Weinberg*

Division of Chemistry and Chemical Engineering
California Institute of Technology
Pasadena, California 91125
Received August 11, 1986

Despite their importance as prototypes for studying amino acid chemistry, the interaction of amides with well-characterized single-crystalline metal surfaces has not been studied previously. A variety of transition-metal–formamido compounds have been synthesized and characterized, however, and a number of formamide-derived ligands have been observed, including η^1(C)-$CONR_2$ (R = H, alkyl or aryl),[1] η^2(N,O)-NRCRO,[2] η^1(N)-NHC(R)O,[3] η^2(C,O)-NR_2CO,[4] η^2(C,N)-OCNHR,[5] and η^2(C,N)-HOCNH.[6] In this paper, we present preliminary results of an electron energy loss spectroscopic (EELS) and thermal desorption mass spectrometric (TDMS) study of formamide adsorption on the Ru(001) surface on which an ordered p(1×2) overlayer of oxygen adatoms is present. This study provides evidence for the formation of an η^2(N,O)-NHCHO species, analogous to the η^2-formate formed from formic acid decomposition on the initially clean Ru(001) surface.[7,8]

The ultrahigh vacuum chamber in which the EELS and TDMS experiments were performed has been described previously,[9] as have the properties and method of preparation of the Ru(001)–p(1×2)-O surface.[10-12] The p(1×2)-O overlayer corre-

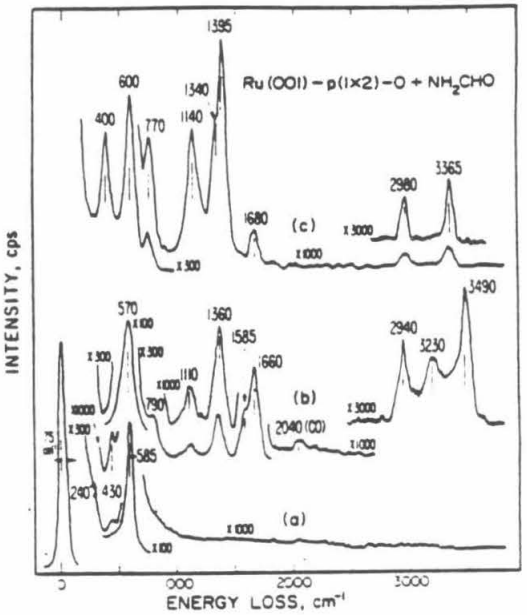

Figure 1. (a) EEL spectrum of the Ru(001)–p(1×2)-O surface. (b) The EEL spectrum that results following a 5×10^{-7} torrs exposure of NH_2-CHO to the Ru(001)–p(1×2)-O surface at 80 K, showing the characteristic features of molecular chemisorbed formamide. (c) The EEL spectrum that results when the surface of (b) is annealed briefly to 400 K and recooled to 80 K, showing the characteristic features of η^2(N,-O)-NHCHO.

Table I. Vibrational Frequencies in cm^{-1} and Mode Assignments of Molecularly Chemisorbed Formamide on the Ru(001)–p(1×2)-O Surface at 80 K and of Gas-Phase and Liquid Formamide

mode	NH_2CHO/ Ru(001)–p(1×2)-O	NH_2CHO (gas)[13,14]	NH_2CHO (liquid)[13,15]
$\nu_a(NH_2)$	3490	3545	3388
$\nu_s(NH_2)$	3230	3451	3207
ν(CH)	2940	2852	2881
ν(CO)	1660	1734	1681
$\delta(NH_2)$	1585	1572	1611
ν(CN)	1360	1255	1309
δ(CH)	n.o.	1378	1391
π(CH)	n.o.	1030	1050
NH_2 deformations[a]	1110, 790	1059, 602, 289	1090, 750, 200
δ(NCO)	~525[b]	565	595
ν(Ru–NH_2CHO)	310[c]		

[a] The assignment of the NH_2 rocking, wagging, and twisting modes for the molecular formamide is somewhat controversial. thus, we have not attempted to assign these modes. [b] Overlaps with ν_s(RuO) of oxygen adatoms. [c] Not well resolved in Figure 1b; sharpens with annealing. n.o. = not observed, a = asymmetric, s = symmetric.

† AT&T Bell Laboratories Predoctoral Fellow.
‡ Feodor-Lynen Research Fellow of the Alexander von Humboldt Foundation.

(1) (a) Lindsay, A. J.; Kim, S.; Jacobson, R. A.; Angelici, R. J. *Organometallics* **1984**, *3*, 1523. (b) Kruse, A. E.; Angelici, R. J. *J. Organomet. Chem.* **1970**, *24*, 231. (c) Sacco, A.; Giannoccaro, P.; Vasapollo, G. *Inorg. Chim. Acta* **1984**, *83*, 125. (d) Behrens, H.; Yungbauer, A. Z. *Naturforsch., B* **1979**, *34B*, 1477.

(2) (a) Schwering, H.-U.; Weidlein, J. *Chimia* **1973**, *27*, 535. (b) Rossi, R.; Duatti, A.; Magon, L.; Casellato, U.; Graziani, R.; Toniolo, L. *Inorg. Chim. Acta* **1983**, *74*, 77. (c) Jennings, J. R.; Wade, K.; Wyatt, B. K. *J. Chem. Soc. A* **1968**, 2535. (d) Adams, R. D.; Golembeski, N. M. *J. Organomet. Chem.* **1979**, *171*, C21.

(3) Burgess, K.; Johnson, B. F. G.; Lewis, J. *J. Chem. Soc., Dalton Trans.* **1983**, 1179.

(4) (a) Fagan, P. J.; Manriquez, J. M.; Vollmer, S. H.; Day, C. S., Day, V. W.; Marks, T. J. *J. Am. Chem. Soc.* **1981**, *103*, 2206. (b) Szostak, R.; Strouse, C. E.; Kaesz, H. D. *J. Organomet. Chem.* **1980**, *191*, 243. (c) Mayr, A.; Lin, Y.-C.; Boag, N. M.; Kaesz, H. D. *Inorg. Chem.* **1982**, *21*, 1704. (d) Kampe, C. E.; Boag, N. M.; Kaesz, H. D. *J. Mol. Catal.* **1983**, *21*, 297. (e) Azam, K. A.; Yin, C. C.; Deeming, A. J. *J. Chem. Soc., Dalton Trans.* **1981**, 91.

(5) (a) Kaesz, H. D.; Knobler, C. B.; Andrews, M. A.; van Buskirk, G.; Szostak, R.; Strouse, C. E.; Lin, Y. C.; Mayr, A. *Pure Appl. Chem.* **1982**, *54*, 131. (b) Lin, Y.-C.; Knobler, C. B.; Kaesz, H. D. *J. Am. Chem. Soc.* **1981**, *103*, 1216.

(6) See ref 5a,b. This ligand and the preceding one coexist as a tautomeric mixture.

(7) Toby, B. H.; Avery, N. R.; Anton, A. B.; Weinberg, W. H. *J. Electron Spectrosc. Relat. Phenom.* **1983**, *29*, 317.

(8) Avery, N. R.; Toby, B. H.; Anton, A. B.; Weinberg, W. H. *Surf. Sci.* **1982**, *122*, L574.

(9) Thomas, G. E.; Weinberg, W. H. *Rev. Sci. Instrum.* **1979**, *50*, 497.

(10) Madey, T. E.; Engelhardt, H. A.; Menzel, D. *Surf. Sci.* **1975**, *48*, 304.

(11) Parrott, S. L.; Praline, G.; Koel, B. E.; White, J. M.; Taylor, T N. *J. Chem. Phys.* **1979**, *71*, 3352.

(12) Rahman, T. S.; Anton, A. B.; Avery, N. R.; Weinberg, W. H. *Phys. Rev. Lett.* **1983**, *51*, 1979.

0002-7863/87/1509-1876$01.50/0

Table II. Vibrational Frequencies in cm^{-1} and Mode Assignments of η^2(N,O)-NHCHO and η^2(N,O)-NDCHO on Ru(001)–p(1×2)-O[a]

mode	η^2-NHCHO (η^2-NDCHO)	η^2-OCHO[c]	$[R_2MN(CH_3)C(CH_3)O]_2$[2a]
ν(NH)	3365 (2480) w		
ν(CH)	2980 (2960) w	2920 w	
ν_s(NCO)[b]	n.o.	n.o.	1571–1585 st
ν_a(NCO)[b]	1395 (1360) st	1360 st	1392–1400 st
CH bend[c]	1340 (unresolved) sh	n.o.	
NH bend[c]	1140 (920) m		
δ(NCO)[b]	770 (760) m	805 m	n.r.
ν(Ru–NHCHO)[b]	400 (400) st	380 st	355–492 m

[a] s = symmetric, a = asymmetric, st = strong, m = medium, w = weak, sh = shoulder, n.o. = not observed, n.r. = not reported. [b] In the case of η^2-OCHO (formate), the closely related modes are, of course, ν_s(OCO), ν_a(OCO), δ(OCO), and ν(Ru-OCHO), respectively. [c] Since data for CH and NH bending modes in analogous organometallic compounds are lacking, we do not attempt to assign these bending modes as in-plane (δ) or out-of-plane (π).

sponds to a fractional coverage of 0.5, and the oxygen adatoms occupy threefold hollow sites on the hexagonally close-packed Ru(001) surface.[11,12] The most notable feature of the EEL spectrum of Figure 1a is the strong mode at 585 cm^{-1} which is due to the symmetric stretching vibration of the oxygen adatoms normal to the surface. The asymmetric ruthenium–oxygen stretch and a ruthenium surface phonon give rise to weaker modes at 430 and 240 cm^{-1}, respectively.[12]

Adsorption of submonolayer concentrations of formamide on the Ru(001)–p(1×2)-O surface at 80 K leads to molecularly chemisorbed formamide, as may be seen from the EEL spectrum of Figure 1b and the mode assignments that are listed in Table I. The fact that the ν(CO), ν(CN), $\delta(NH_2)$, and ν(CH) modes are all present, together with the lack of any modes not due to molecular formamide, indicates that little, if any, dissociation has occurred. The frequencies of the ν(CO) (1660 cm^{-1}) and ν(CN) (1360 cm^{-1}) modes are evidence that no significant rehybridization of these bonds occurs upon adsorption. The slightly lowered frequency of the ν(CO) mode, relative to its gas-phase value of 1734 cm^{-1},[13,14] suggests coordination to the surface via a lone pair of electrons on the oxygen atom, as has been observed for acetone[16] and formaldehyde[17] on Ru(001) surfaces on which ordered overlayers of oxygen are present. The loss feature at 570 cm^{-1} in Figure 1b is broadened because it results from the overlap of two modes: the ν_s(RuO) mode of the oxygen adatoms and the intense δ(NCO) mode of the molecularly adsorbed formamide.[18] The loss feature at 1360 cm^{-1} may involve the in-plane CH bending mode as well as the ν(CN) mode.

Annealing the Ru(001)–p(1×2)-O surface to 260 K causes the molecularly adsorbed formamide to decompose (which is accompanied by the desorption of H_2[20]), resulting in the formation of a new surface species that is stable to 420 K. This new species is identified by its EEL spectrum (Figure 1c) as η^2(N,O)-NHCHO, the nitrogen-containing analogue of the η^2-formate formed on Ru(001) as the result of formic acid decomposition:[7]

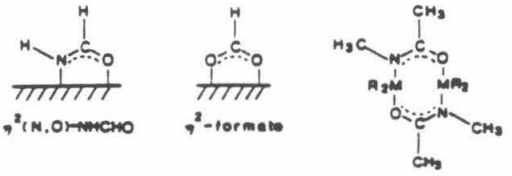

The η^2(N,O)-NHCHO is also related closely to the $N(CH_3)C(CH_3)O$ ligands in compounds of the type shown at the right, above.[2a] Vibrational data for all of these species are summarized in Table II, and data for η^2(N,O)-NDCHO formed from ND_2-CHO decomposition on Ru(001)–p(1×2)-O are presented also. Since η^2(N,O)-NHCHO differs from η^2-formate only in that an oxygen atom has been replaced by an NH group, the skeletal and metal–ligand stretching modes of these two species should occur at very similar frequencies, and it can be seen that this is indeed true for the NCO (OCO) symmetric stretch, the NCO (OCO) scissoring mode, and the metal–ligand stretch.[21] The increase in frequency of δ(NCO) compared with that of the gas-phase formamide (565–770 cm^{-1}) is very similar to the observed increase in δ(OCO) in going from gas-phase formic acid to η_2-formate on Ru(001) (625 to 805 cm^{-1}) and is indicative of delocalized π-bonding within the NCO group. The agreement among the ν_s(NCO) frequencies of η^2(N,O)-NHCHO and the series of (four) $[R_2MN(CH_3)C(CH_3)O]_2$ compounds is clearly excellent. Single CH and NH stretching modes are identified, and no NH_2 scissoring mode is observed at 1500–1600 cm^{-1}. These facts, together with the H_2 desorption near 260 K mentioned above, indicate that one NH bond of the formamide NH_2 group has been cleaved. The EEL spectrum of Figure 1c is thus fully consistent with the presence of an η^2(N,O)-NHCHO species and in excellent agreement with EEL and IR data for closely related surface and organometallic species. Other formamide-derived ligands that have been identified in organometallic compounds[1-4] are inconsistent with the EEL spectrum of Figure 1c for at least one of several reasons: they have no hydrogen atom bonded to the formamide carbon atom; they contain NH_2 groups; they contain CN or CO double bonds (which should give rise to intense stretching modes in the 1500–1800-cm^{-1} region); their δ(NCO) modes should occur at substantially lower frequency. We note finally that we observe no EELS (e.g., ν(OH) or $\delta(OH_2)$ modes) or TDMS (e.g., H_2O desorption) evidence for the formation of OH bonds in this work.

The η^2-NHCHO decomposes when the surface is annealed to 420 K, with reaction-limited CO and H_2 desorbing at this temperature. Nitrogen adatoms remain on the surface to approximately 600 K, at which temperature recombinative desorption of N_2 occurs, leaving the p(1×2)-O overlayer intact. At a saturation coverage of molecularly chemisorbed formamide on the Ru(001)–p(1×2)-O surface, approximately 0.05 monolayer of η^2-NHCHO forms and decomposes.

In summary, formamide chemisorbs molecularly on the Ru(001)–p(1×2)-O surface beow 260 K, in a manner such that the double-bond character of the CO bond is maintained. Annealing the surface to 260 K results in the formation of η^2(N,O)-NHCHO, which decomposes at 420 K. A more detailed account of this work will be presented elsewhere.[19]

Acknowledgment. Principal support of this work was provided by the National Science Foundation under Grant CHE-8516615. Acknowledgment is made also to the donors of the Petroleum Research Fund, administered by the American Chemical Society, for partial support.

(13) Evans, J. C. *J. Chem. Phys.* **1954**, *22*, 1228.
(14) King, S. T. *J. Phys. Chem.* **1971**, *75*, 405.
(15) Suzuki, I. *Bull. Chem. Soc. Jpn.* **1960**, *33*, 1359.
(16) Avery, N. R.; Weinberg, W. H.; Anton, A. B.; Toby, B. H. *Phys. Rev. Lett.* **1983**, *51*, 682.
(17) Anton, A. B.; Parmeter, J. E.; Weinberg, W. H. *J. Am. Chem. Soc.* **1986**, *108*, 1823.
(18) The δ(NCO) mode has been identified unambiguously from EEL spectra of formamide adsorbed on a hydrogen-presaturated Ru(001) surface at 80 K.[19] The same molecularly chemisorbed species is formed, and there is no ν(RuO) mode at 585 cm^{-1} that overlaps with the δ(NCO) mode.
(19) Parmeter, J. E.; Schwaiko, U.; Weinberg, W. H., unpublished results.
(20) The amount of H_2 desorbed at 260 K is approximately one-third of the total amount of H_2 that is desorbed as a consequence of the decomposition of formamide on the surface. Any desorption of H_2 from Ru(001)–p(1×2)-O must be reaction-limited because this surface does not chemisorb H_2 under UHV conditions.[17] For sufficiently high initial formamide coverages, some molecular desorption occurs as well.
(21) The ν_s(NCO) mode involves motion of atoms largely parallel to the surface and is apparently very weak and cannot be identified positively. It may contribute to the inensity of the feature at 1680 cm^{-1}. This feature persists to some degree when the surface is annealed to 450 K and the modes due to η^2(N,O)-NHCHO have disappeared. It is due largely or entirely to a very small amount of molecular formamide readsorbed from the chamber background.

CHAPTER VII

The Interaction of Formamide with the Ru(001)-p(1x2)-O Surface

[This chapter was published as a paper by J. E. Parmeter, U. Schwalke and W. H. Weinberg, in *The Journal of the American Chemical Society* 1987, 109, 5083.]

Abstract

The adsorption and decomposition of formamide on a Ru(001) surface on which is present an ordered p(1x2) overlayer of oxygen adatoms have been studied using electron energy loss spectroscopy and thermal desorption mass spectrometry. Below 260 K, formamide is chemisorbed molecularly on this surface, with two different forms existing above and below 225 K, independent of coverage. The form present below 225 K bonds to the surface via an electron lone pair of the formamide oxygen atom, while the form present above 225 K bonds to the surface via electron lone pairs on both the oxygen and nitrogen atoms. Annealing to 260 K results in the partial decomposition of the chemisorbed formamide to an η^2(N,O)-NHCHO species, analogous to η^2-formates that have been identified on transition metal surfaces and in organometallic compounds. For sufficiently high initial formamide coverages, the chemical conversions occurring at both 225 and 260 K are accompanied by some desorption of molecular formamide. The η^2(N,O)-NHCHO decomposes near 420 K, evolving H_2 and CO, and leaving nitrogen adatoms on the surface. The nitrogen adatoms recombine and desorb near 570 K, leaving the p(1x2)-O overlayer intact on the surface. For a saturation formamide exposure, approximately 0.05 monolayer of η^2(N,O)-NHCHO forms and decomposes on this surface.

I. Introduction

At a sufficiently low surface temperature, most if not all molecular adsorbates can chemisorb without dissociation on metal surfaces. The two most common ways for this to occur are by bonding through an electron lone pair localized on one atom of the adsorbed molecule, or through the rehybridization of a molecular π-bond so that the molecule is bound to the surface in a di-σ bonded configuration. The former type of bonding occurs commonly for simple oxygen- and nitrogen-containing adsorbates such as H_2O (1) and NH_3 (2), while ethylene is a prototypical example of a molecule that on most clean metal surfaces bonds to the surface through extensive rehybridization of a molecular π-bond (3). Molecules containing both heteroatoms with electron lone pairs and one or more π-bonds are thus of interest in studying metal surface-adsorbate interactions, since it is clear that several different surface bonding configurations are possible. Previous surface studies with a number of such molecules, including formic acid (4), acetone (5), formaldehyde (6) and various heterocyclic aromatic compounds (7), have been conducted, and in all cases have shown that the relative amounts of bonding via electron lone pairs and π-bond rehybridization are dependent upon surface temperature, surface coverage, and the nature of the surface.

The interaction of amides with well-characterized, single crystalline metal surfaces has received virtually no attention. The only study known to us of any amide on any metal surface is a very brief account of the decomposition of N,N-dimethylformamide (DMF) on Pt(111) (8), in which it was reported that the decomposition of DMF on this surface proceeds primarily via the evolution of HCN into the gas phase. However, the nature of molecularly adsorbed DMF and any intermediates leading to HCN evolution were not addressed. A determination of the structure and bonding of molecularly adsorbed amides on metal surfaces is of obvious interest in view of the above discussion, since bonding to the surface could be via the electron lone pair on the nitrogen atom, via an electron lone pair on the oxygen atom, through lone pairs on both heteroatoms, or through rehybridization of the CO double bond. These four possible bonding configurations of molecularly adsorbed formamide are shown schematically in Fig. 1.

Considering the variety of amide-derived ligands characterized structurally in organometallic com-

pounds, it is also clear that amide decomposition on metal surfaces may give rise to a number of different surface intermediates. These ligands include η^1(C)-CONHR (R = H, alkyl or aryl) (**9**), η^1(N)-NHCOH (**10**), η^2(C,O)-NR_2CO (**11**), η^2(N,O)-NRCRO (both chelating and bidentate bridging) (**12**), and the tautomers η^2(C,N)-HOCNR and η^2(C,N)-OCNHR (**13**). The structures of these ligands are shown schematically in Fig. 2 with R = H, the case that is relevant to formamide decomposition on metal surfaces. The identification of such ligands on a metal surface is of obvious importance in establishing a relationship between the chemistry of formamide on metal surfaces and in organometallic compounds. An additional issue of fundamental importance is the degree to which the stable intermediates formed by amide decomposition on metal surfaces are related to the intermediates formed by the decomposition of related molecules such as aldehydes (**6**), carboxylic acids (**4**) and amines (**14**).

One of the most powerful techniques for studying the structures and reactions of molecular adsorbates on single crystalline metal surfaces of low area is high-resolution electron energy loss spectroscopy (EELS) (**15**), especially when supplemented by thermal desorption mass spectrometry (TDMS). In this paper we present the results of an EELS and TDMS study of the interaction of the simplest amide, formamide, with a Ru(001) surface that has been modified chemically by an ordered p(1x2) overlayer of oxygen adatoms. A detailed study of the adsorption and decomposition of formamide on the clean Ru(001) surface will be presented elsewhere (**16**).

The properties of the p(1x2)-O overlayer on the hexagonally close-packed Ru(001) surface have been discussed in detail previously (**17**). Figure 3 shows an EEL spectrum of the Ru(001)-p(1x2)-O surface, as well as the structure and unit cell of this surface. The fractional coverage of oxygen adatoms is 0.5, and they occupy threefold hollow sites exclusively. The EEL spectra of this surface show a strong peak at 585 cm^{-1} due to the ruthenium-oxygen symmetric stretching mode, with the ruthenium-oxygen asymmetric stretching mode, and a ruthenium surface phonon giving rise to weaker peaks at 430 and 240 cm^{-1}, respectively. Formamide adsorption has been studied on the Ru(001)-p(1x2)-O surface as well as on the clean Ru(001) surface because the presence of the electronegative oxygen adatoms alters the electronic properties of this surface and might thus be expected to cause changes in the surface chemistry of formamide, as has been observed previously for acetone (**5a**) and

formaldehyde (**6b**) adsorbed on clean and oxygen-modified Ru(001) surfaces. In addition to changing the electronic properties of the surface, the oxygen could also alter the surface chemistry of formamide by reacting directly with it to form species that cannot be formed following formamide adsorption on clean Ru(001).

II. Experimental Procedures

The EEL spectrometer and the UHV chamber housing it have been described in detail elsewhere (**18**). The home-built EEL spectrometer employs 180° hemispheres as the electron energy dispersing elements both in the monochromator and the analyzer. The spectra shown in this paper were collected in the specular direction, which was 60° with respect to the surface normal, with an electron impact energy of approximately 4 eV. The resolution, defined as the full-width at half-maximum of the elastically scattered beam, varied between 70 and 90 cm^{-1}, while maintaining an elastic peak count rate of approximately 2 x 10^5 cps.

The UHV chamber containing the EEL spectrometer and the Ru(001) crystal was pumped by a 220 $l\text{-}s^{-1}$ Varian noble vacion pump and a titanium sublimation pump, and had a working base pressure below 10^{-10} Torr. This chamber also contained a UTI-100C quadrupole mass spectrometer for thermal desorption measurements and analysis of background gases.

Liquid nitrogen cooling was employed to achieve crystal temperatures as low as 80 K. The Ru(001) crystal was cleaned using the well-established techniques of Ar^+ sputtering and annealing in a background of approximately 5 x 10^{-8} Torr O_2 (**19**). Surface cleanliness was verified by both EELS and H_2 TDMS. The p(1x2)-O overlayer was prepared by exposing the clean Ru(001) surface at 80 K to 2 L O_2 (1 L ≡ 1 Langmuir = 10^{-6} Torr-s) and annealing to 400 K. The presence of a well-ordered and complete p(1x2)-O overlayer was always verified by EELS prior to exposure of the surface to formamide at 80 K. Subsequent EEL spectra were measured after annealing to an indicated temperature and recooling to 80 K.

Formamide (99% reported purity) was obtained in the liquid state from Aldrich. It was introduced into the UHV chamber by backfilling through an UHV leak valve. The liquid formamide sample

was contained in a small cell with a glass-to-metal connector, which was mounted by a miniconflat flange directly below the leak valve so that the sample-to-leak valve distance was approximately seven inches. A valve just below the miniconflat flange led via a stainless steel line to a mechanical pump so that the sample container could be evacuated after the sample was mounted. The metal tubing between the glass-to-metal seal and the leak valve was baked thoroughly and evacuated by the mechanical pump prior to all formamide exposures. Because of the high boiling point of formamide (210°C) (**20**), the sample had to be heated while an exposure was being made. This was accomplished by passing current through a wire coil wrapped around the glass sample container. During formamide exposures, the purity of the formamide was verified *in situ* via mass spectrometry. The principal impurity during formamide exposures was water, and, in general, the sample had to be heated several times and the metal between the sample and the leak valve had to be baked and evacuated several times before sufficiently pure formamide exposures could be achieved.

Experiments were also performed with N-deuterated formamide, ND_2CHO, obtained from MSD Isotopes (98 atom % - D). Although the ND_2CHO was always at least slightly contaminated with NDHCHO or NH_2CHO due to H/D exchange into the ND_2 group, as evidenced by NH stretching modes in the EEL spectra of ND_2CHO and its decomposition products, the EEL spectra resulting from ND_2CHO exposures were nevertheless useful in helping to assign various vibrational modes. The fact that NH stretching modes appeared in multilayer EEL spectra of the ND_2CHO indicates that these modes cannot be attributed entirely to H/D exchange occurring on the Ru(001)-p(1x2)-O surface.

III. Results

A. Thermal Desorption Mass Spectrometry

Following exposure of the Ru(001)-p(1x2)-O surface to formamide at 80 K, four thermal desorption products were observed to desorb between approximately 200 and 700 K: molecular formamide (NH_2CHO), CO, H_2 and N_2. There was no detectable desorption, for example, of NH_3, H_2O, HCN, NO, H_2CO, HNCO or CO_2. The desorption of molecular formamide and its decomposition products will be discussed separately.

1. Molecular Formamide Desorption

Figure 4 shows a series of thermal desorption spectra for molecular formamide (m/e = 45 amu) following various exposures of formamide to the Ru(001)-p(1x2)-O surface. For formamide exposures of less than approximately 1.5 L, no molecular desorption was observed, indicating that for low initial coverages all of the adsorbed formamide decomposes irreversibly on this surface. As the exposure is increased, three molecular desorption peaks appear sequentially at 255, 225 and 210 K. The lowest temperature desorption peak is quite sharp and does not saturate with increasing exposure. It may therefore be assigned unambiguously as resulting from the desorption of condensed formamide multilayers. The remaining two peaks are assigned to monolayer thermal desorption features, although the possibility that the 225 K thermal desorption feature corresponds to the desorption of second-layer formamide cannot be ruled out completely.

As may be seen in Fig. 4, the desorption peak at 255 K appears at lower exposures than the peak at 225 K, and neither peak displays any detectable shift in temperature as a function of coverage. This latter fact, coupled with the EELS results (cf. Sect. III.B) showing only molecular formamide on the surface below 260 K, indicates that both peaks result from the first-order desorption of molecular formamide, rather than from a recombinative desorption process. Using the method of Redhead (21) and assuming a "normal" first-order preexponential factor for the rate coefficient of desorption of 10^{13} s^{-1}, the molecular adsorption states desorbing at 225 and 255 K may be assigned activation energies of desorption (heats of adsorption) of approximately 13 and 15 kcal mol^{-1}, respectively. When both states are saturated, the ratio of the amount of formamide desorbing in the 225 K peak to the amount desorbing in the 255 K peak is approximately 2:1, although there is a rather large uncertainty in this ratio due to the overlap of the two peaks. Unfortunately, there is no simple method of determining the absolute coverages of formamide desorbing in each peak. Further discussion of the nature of these two desorption states is deferred to Sect. IV.

2. Thermal Desorption of the Products of Formamide Decomposition: CO, H_2, and N_2

As stated above, formamide decomposition on the Ru(001)-p(1x2)-O surface results in the desorption of CO, H_2 and N_2, when the surface is annealed to 700 K. Figure 5 shows the CO (m/e = 28 amu,

with a C cracking fragment at m/e = 12 amu) thermal desorption spectrum that results following a saturation formamide exposure at 80 K. A sloping background is present between 100 and 300 K due to desorption of background CO or formamide decomposition on heating wires, support leads, etc. There is a single, rather sharp desorption peak at 420 K with a small shoulder at 385 K. This shoulder is due to desorption from the surface of very small amounts (≤0.01 monolayer) of CO that is adsorbed from the chamber background, as will be discussed in Sect. III.B.1. The peak at 420 K is the only feature resulting from formamide decomposition on the Ru(001)-p(1x2)-O surface, and since it desorbs at a higher temperature than low coverages of CO adsorbed on Ru(001)-p(1x2)-O **(19)**, this is a reaction-limited desorption peak resulting from the decomposition of a surface intermediate. By comparison with thermal desorption results for CO adsorbed on clean Ru(001), where the saturation coverage is approximately 0.68 **(22)**, this peak is estimated to correspond to approximately 0.05 monolayer of CO. Since the only observed decomposition reaction of formamide on the Ru(001)-p(1x2)-O surface is to CO, H_2 and nitrogen adatoms, this corresponds to the fractional coverage of formamide that decomposes on this surface following a saturation exposure.

Figure 5 shows the H_2 (m/e = 2 amu) thermal desorption spectrum that results following a saturation formamide exposure on the Ru(001)-p(1x2)-O surface at 80 K. Again, a peak is observed at 420 K. The fact that this peak is coincident with the CO desorption peak at 420 K suggests strongly that both peaks result from the decomposition of the same surface species. There is also a weak maximum near 265 K, which is reproducibly above background. Better resolution of this desorption state, which contains only approximately 0.05 monolayer of hydrogen adatoms, was not possible with our experimental apparatus. However, H_2 desorption is expected at this temperature, since EEL spectra provide clear evidence for NH bond cleavage at 260 K and hydrogen has been observed not to chemisorb on Ru(001)-p(1x2)-O **(6b)**.

Desorption of molecular nitrogen (m/e = 28 amu, with an N cracking fragment at m/e = 14 amu) occurs between approximately 520 and 630 K, with a maximum desorption rate at approximately 570 K. A mass 14 thermal desorption spectrum is shown in the inset of Fig. 5. The desorption of N_2 in this temperature range results from the recombinative desorption of nitrogen adatoms, because molecu-

larly chemisorbed N_2 on both clean and oxygen precovered Ru(001) surfaces desorbs well below 200 K (23). The fact that no desorption of NO occurs as a result of the combination of nitrogen and oxygen adatoms is in agreement with previous studies of NO (24) and NO_2 (25) adsorption and decomposition on Ru(001).

B. Electron Energy Loss Spectroscopy

In discussing the EELS results for formamide adsorbed on the Ru(001)-p(1x2)-O surface, it is convenient to consider three different regimes of coverage and temperature. First, submonolayer coverages below 260 K give rise to molecularly chemisorbed formamide. Second, annealing to over 260 K results in the decomposition of molecularly chemisorbed formamide to a stable surface intermediate, which decomposes at a higher temperature. Note that this reaction coincides very nearly with the observed desorption of H_2 at 265 K and the desorption of molecular formamide at 255 K. Third, large formamide exposures below 210 K result in the condensation of formamide multilayers. These three cases will be discussed separately below. It is important to note that for all submonolayer coverages, EEL spectra collected after annealing to a given temperature are identical for formamide on Ru(001)-p(1x2)-O. Thus, the same surface species are formed independent of coverage, although, as the thermal desorption results indicate, the fraction of monolayer formamide that desorbs molecularly *is* a function of coverage. Therefore, only EEL spectra for a low initial formamide exposure (0.5 L) are discussed explicitly without loss of generality.

1. Molecularly Chemisorbed Formamide

Molecularly chemisorbed formamide exists on the Ru(001)-p(1x2)-O surface below 260 K, and there is no evidence for any decomposition of formamide below this temperature. Two different forms of molecularly chemisorbed formamide are observed, a low-temperature form that predominates below approximately 225 K, and a high-temperature form that predominates above 225 K. The conversion between these two forms is a function of temperature only. Note that the conversion temperature coincides with the 225 K formamide thermal desorption peak, suggesting that at high coverage the low-temperature form undergoes competing desorption and conversion to the high-temperature form.

Figure 6(a) shows the EEL spectrum that results when the Ru(001)-p(1x2)-O surface at 80 K is exposed to 0.5 L of formamide (NH_2CHO). This EEL spectrum is characteristic of the low-temperature form of molecularly chemisorbed formamide. The mode assignments are reasonably straightforward and are listed in Table I, along with data for liquid (**26**) and gas phase (**27**) formamide. The vibrational modes identified most easily and unambiguously are $\nu_a(NH_2)$, $\nu_s(NH_2)$, ν(CH), ν(CO) and $\delta(NH_2)$, which occur at 3490, 3230, 2940, 1660 and 1585 cm^{-1}, respectively. The mode at 1360 cm^{-1} is assigned to the overlapping ν(CN) and δ(CH) modes. The modes at 1110 and 790 cm^{-1} are assigned, in accordance with the data for liquid formamide, as being due to the $\rho(NH_2)$ and $\omega(NH_2)$ modes, respectively. The $\tau(NH_2)$ and π(CH) modes are not resolved, although a shoulder on the low energy side of the $\rho(NH_2)$ mode might be due to π(CH). The intense broad peak (FWHM $\approx$ 125 cm^{-1}) at 570 cm^{-1} is due to the overlap of the δ(NCO) mode of chemisorbed formamide at approximately 525 cm^{-1} (**28**) and ν_s(RuO) of the p(1x2)-O overlayer at 585 cm^{-1}. Comparison of this mode to the ν_s(RuO) modes of Figs. 3, 6(b) and 7 (FWHM = 75 cm^{-1} for these features) shows that it is indeed much broader than it would be if only ν_s(RuO) were involved. In some spectra measured after adsorption at 80 K, and in all spectra measured following annealing to 200 K, the weak ν_s(Ru–NH_2CHO) mode is resolved near 300 cm^{-1}, although it is not resolved in spectrum 6(a) due to the relatively poor elastic peak cutoff. Finally, the weak feature at 2040 cm^{-1} is due to a very small amount (<0.01 monolayer) of coadsorbed CO. This CO is adsorbed from the chamber background and is *not* the result of formamide decomposition. This mode disappears from the EEL spectra following annealing to 400 K, indicating that the desorption of this CO corresponds to the 385 K shoulder in the CO thermal desorption spectrum of Fig. 5(a).

Figure 6(b) shows the EEL spectrum which results following a 0.5 L exposure of ND_2CHO to the Ru(001)-p(1x2)-O surface at 80 K. Although some NDHCHO contamination is present in this spectrum (as evidenced by a loss feature at 3380 cm^{-1}), the modes of ND_2CHO are assigned easily. These are listed in parentheses in Table I together with the NH_2CHO/ND_2CHO frequency ratios and the corresponding data for liquid formamide. The observed frequency shifts upon N-deuteration are in excellent agreement with those reported for liquid formamide and confirm the mode assignments given

in Table I and discussed in the preceding paragraph. The frequency shift of the δ(NCO) mode upon N-deuteration is slightly greater than expected, which suggests that this mode may be coupled to one of the ND_2 deformation modes.

Annealing the surface to temperatures between approximately 225 and 260 K results in the formation of the second form of molecularly chemisorbed formamide, the EEL spectrum of which is shown in Fig. 6(c) (for the case of NH_2CHO). The most striking difference between this form of formamide and the low-temperature form is the presence of a rather intense loss feature at 970 cm^{-1}, the appearance of which correlates with the disappearance of the mode at 790 cm^{-1} in Fig. 6(a). This 970 cm^{-1} loss feature shifts down to 770 cm^{-1} in the case of ND_2CHO (not shown), and the large frequency shift upon N-deuteration indicates that it must be due to an NH_2 deformation mode. This is assigned to the NH_2 wagging mode of chemisorbed formamide, which is almost certainly adsorbed such that this mode involves motion of the NH_2 hydrogen atoms largely perpendicular to the surface. Figure 6(c) also shows a rather intense and well-resolved ν(Ru-NH_2CHO) peak at 315 cm^{-1}, in contrast to Fig. 6(a). The other differences between the EEL spectra of the low- and high-temperature forms of molecularly chemisorbed formamide are minor.

The ν(CO) frequencies of the two forms of molecularly chemisorbed formamide indicate clearly that the CO double bond is maintained in each case. Hence, for both forms, bonding to the surface is via lone pair donor bonds with the oxygen and/or nitrogen atoms rather than by rehybridization of the CO bond. Since the distinction among η^1(O)-NH_2CHO, η^1(N)-NH_2CHO, and η^2(N,O)-NH_2CHO is difficult, further discussion of the nature of the two forms of molecularly chemisorbed formamide is deferred to Sects. III.B.2 and IV.

2. Decomposition of Chemisorbed Formamide

Chemisorbed formamide of the type characterized by the EEL spectrum of Fig. 6(c) remains on the Ru(001)-p(1x2)-O surface to approximately 260 K, at which temperature conversion to another species occurs. This conversion coincides both with the highest temperature (255 K) molecular formamide thermal desorption peak and with the low temperature H_2 thermal desorption peak. Consequently, this form of molecularly chemisorbed formamide undergoes competing desorption and

decomposition, just as the form present at lower temperatures undergoes competing desorption and conversion to the high-temperature form. The surface species formed at 260 K is stable to 420 K, and its decomposition, as monitored by EELS, coincides with the CO and H_2 thermal desorption peaks shown in Fig. 5. Based on the EEL spectrum of Fig. 7(a), this new species is identified as η^2(N,O)-NHCHO [cf. Fig. 2, structure (4)]. This species is analogous to the η^2(O,O)-OCHO (η^2-formate) formed from formic acid decomposition on both Ru(001) and a number of other metal surfaces (**4**). The vibrational modes of η^2–NHCHO are assigned and compared with those of related organometallic compounds (**12c**) and to those of η^2-formate on Ru(001) (**4a,b**) in Table II. Figure 7(b) shows the EEL spectrum of η^2(N,O)-NDCHO formed from ND_2CHO decomposition, and the vibrational frequencies of this species are listed in parentheses in Table II.

The identification of the species represented by the EEL spectrum of 7(a) as η^2–NHCHO follows from the presence of single ν(NH) and ν(CH) modes, the lack of a $\delta(NH_2)$ mode near 1580 cm^{-1}, the lack of a strong carbonyl ν(CO) mode in the range of 1500-1800 cm^{-1}, and the similarity of its skeletal modes to those of both η^2-formate on Ru(001) (**4a,b**) and the related organometallic compounds of the type shown below (**12c**):

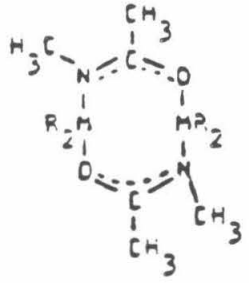

M = Ga or In, and R = CH_3 or C_2H_5

Note especially the close agreement between the ν_s(NCO) modes of η^2–NHCHO and the η^2-$N(CH_3)C(CH_3)O$ complexes, and between the δ(NCO) [δ(OCO)] and ν(Ru-NHCHO) [ν(Ru-OCHO)] modes of η^2–NHCHO and η^2-formate. The increase in the frequency of δ(NCO) in going from gas phase formamide to η^2(N,O)-NHCHO (565 to 770 cm^{-1}) is similar to the frequency increase of δ(OCO) in going from gas phase formic acid to η^2-formate on Ru(001) (625 to 805 cm^{-1}), and is indicative of delocalized π-bonding within the NCO group. The EEL spectrum of η^2-NDCHO also helps to confirm

the assignment of the modes observed at 1395, 770 and 400 cm^{-1} in the EEL spectrum of η^2–NHCHO, since none of these modes shifts significantly upon N-deuteration. A weak peak which occurs between 1630 and 1680 cm^{-1} may or may not be due partially to the ν_s(NCO) mode of η^2–NHCHO. Since this peak also appears in EEL spectra after annealing to over 420 K which has caused the stronger modes of η^2–NHCHO to disappear, it must be attributed primarily to a small amount of molecularly chemisorbed formamide that has readsorbed from the chamber background. The frequency of this mode is somewhat higher than the frequencies of the ν_s(NCO) modes in the related gallium and indium complexes, although the ν_s(NCO) modes of a similar series of aluminum complexes are somewhat closer, ranging from 1580 to 1621 cm^{-1} (**12b**). Thus, the ν_s(NCO) mode may be partially responsible for the loss feature appearing at 1670 cm^{-1}, or it may be simply too weak to be observed. Note that this mode should not be strictly dipolar-forbidden in the case of η^2-NHCHO, unlike ν_s(OCO) in η^2-formate.

The assignment of the CH and NH in-plane (δ) and out-of-plane (π) bending modes is less straightforward than the assignment of the skeletal, frustrated translational, CH stretching, and NH stretching modes. The shoulder at 1340 cm^{-1} in Fig. 7(a) is quite reproducible and is assigned as δ(CH), in good agreement with the δ(CH) frequency of 1377 cm^{-1} in sodium formate (**29**). This mode is not resolved in the case of η^2-NDCHO due to the slight downshift of the ν_s(NCO) mode to 1360 cm^{-1}. The mode at 1140 cm^{-1} in η^2–NHCHO is downshifted to 920 cm^{-1} in η^2-NDCHO, and is thus assigned as an NH bending mode, although without vibrational data for η^2–NHCHO complexes it is not obvious whether this is the π(NH) or δ(NH) mode. The frequency of 1140 cm^{-1} seems more reasonable for the π(NH) mode, whereas the relatively strong intensity of the peak corresponding to this mode in Fig. 7(a) would seem suggestive of the δ(NH) mode (see Sect. IV.B). The weak feature at 1140 cm^{-1} in Fig. 7(b) is probably due to the presence of η^2–NHCHO as an impurity in η^2-NDCHO; note also the ν(NH) loss peak at 3330 cm^{-1} in this spectrum. The peak at 1230 cm^{-1} in Fig. 7(b) is probably due to δ(ND) which is upshifted and not resolved from ν_s(NCO) in the case of η^2-NHCHO [which suggests further that the NH bend at 1140 cm^{-1} is indeed π(NH)]. This would require an anomalously small frequency shift of the δ(NH) mode upon deuteration ($\lesssim$1.18), a condition which could be satisfied if this mode couples to the ν_s(NCO) mode (**30**). No mode is observed that can be clearly attributed to π(CH),

although this mode could contribute to the intensity of the 1140 cm^{-1} feature in either spectrum of Fig. 7. The preferred mode assignments for the CH and NH bending modes are listed in Table II. Despite some uncertainty in the detailed assignment of the CH and NH bending modes, the identification of η^2-(N,O)-NHCHO can be made unambiguously on the basis of the other observed vibrational modes. Other formamide-derived ligands that have been identified in organometallic chemistry can be eliminated easily based on the observed EEL spectra [cf. Sect. IV.B].

Upon annealing to 420 K, the modes due to η^2–NHCHO disappear, leaving only the characteristic features of the p(1x2)-O overlayer (and a weak mode near 1650 cm^{-1} due to readsorbed formamide) in subsequent EEL spectra. Since the TDMS results indicate that CO and H_2 are evolved from the surface at 420 K, it can be concluded that both of these desorption products result from η^2–NHCHO decomposition, and that only nitrogen adatoms remain on the Ru(001)-p(1x2)-O surface above 420 K. Nitrogen adatoms are not detected by EELS because the ν_s(RuN) mode is obscured by the ν_s(RuO) mode of the p(1x2)-O overlayer (note that $\theta_O \sim 10\theta_N$). However, the presence of nitrogen adatoms above 420 K is confirmed by the recombinative desorption of N_2 that is observed near 570 K. Thus the decomposition products of η^2–NHCHO on Ru(001)-p(1x2)-O are N(a), H_2(g) and CO(g).

3. Formamide Multilayers

Molecular multilayers of formamide condense on the Ru(001)-p(1x2)-O surface when this surface at 80 K is exposed to approximately 7 L or more of formamide. The multilayers desorb at 210 K, and EEL spectra measured after annealing to temperatures in the range of 80-200 K are identical. Multilayer EEL spectra are shown in Fig. 8 both for NH_2CHO and ND_2CHO, and the observed vibrational modes are listed in Table III. It may be seen by comparison of Tables I and III that, in general, the vibrational modes of the formamide multilayers are even closer to those of liquid formamide than are those of the low-temperature form of chemisorbed formamide. Two extremely intense loss features are characteristic of the $NH_2CHO(ND_2CHO)$ multilayers: a lattice mode at 220(160) cm^{-1} (that may couple to the NH_2 twisting mode which occurs at 200 cm^{-1} in liquid NH_2CHO) and the NH_2 wagging mode at 710(565) cm^{-1}. This latter mode and the NH_2 stretching modes are quite broad, indicative of considerable hydrogen bonding within the multilayers. The NH_2 (ND_2) asymmetric stretch is downshifted by

approximately 120 cm^{-1} compared with that of the chemisorbed formamide at 80 K. For NH_2CHO multilayers, the peak at 1380 cm^{-1} is assigned to the overlapping δ(CH) and ν(CN) modes, while the peak at 1075 cm^{-1} is assigned to the overlapping π(CH) and $\rho(NH_2)$ (rocking deformation) modes. In both cases, the frequencies observed are intermediate between those of the two constituent bands in liquid NH_2CHO. For ND_2CHO multilayers, the ν(CN) and δ(CH) modes are resolved and occur at 1355 and 1415 cm^{-1}, respectively, and the broad feature centered at 1030 cm^{-1} is due to the overlapping $\delta(ND_2)$, π(CH) and $\rho(ND_2)$ modes [and perhaps some intensity is derived also from the overtone of the $\omega(ND_2)$ mode]. Note that the loss feature centered at 3305 cm^{-1} indicates that once again some NDHCHO or NH_2CHO impurity is present in the ND_2CHO.

IV. Discussion

A. Molecularly Chemisorbed Formamide

The EEL spectra of Fig. 6(a) and (c) indicate clearly the presence of two slightly different forms of chemisorbed formamide on the Ru(001)-p(1x2)-O surface below 260 K. Since the observed CO stretching frequencies show that extensive rehybridization of the CO bond does not occur in either case (i.e. the CO double bond is maintained), bonding to the surface must occur via an electron lone pair on either the oxygen or nitrogen atom, or possibly via electron lone pairs on both of these atoms. Thus, there are three distinct, possible bonding configurations, corresponding to structures (I), (II) and (III) of Fig. 1. In all three of these configurations, the bonding may be thought of in simple Lewis acid-base terms, with the formamide molecule acting as the Lewis base and the surface as the Lewis acid.

The distinction among these three forms of molecularly chemisorbed formamide is not trivial. It is conceivable that two of these three forms could coexist on the surface below 225 K, with desorption of the more weakly bound form occurring at this temperature. However, the sudden appearance of the rather intense 970 cm^{-1} mode when the surface is annealed to 225 K, coupled with the lack of any evidence for two different formamide species in Fig. 6(a), indicates that a conversion from one formamide species to another is occurring at 225 K. The most likely scenario is one in which chemisorbed formamide of type (I) or (II) is converted to the more strongly bound, bidentate species (III). This model is especially appealing intuitively since η^2(N,O)-NH_2CHO is the logical intermediate to the η^2(N,O)-

NHCHO formed at 260 K. In addition, it is quite possible that the conversion of (I) or (II) to (III) would require some desorption of (I) or (II) at high coverages, as is observed, for electronic reasons. This effect of competing desorption and conversion to a more highly coordinated species has been observed previously for other metal-adsorbate systems (**31**).

It is likely for several reasons that the low-temperature form of molecularly chemisorbed formamide is η^1(O)-NH_2CHO. First, it is well known that the oxygen atom of formamide is much more basic than the nitrogen atom in homogeneous organic chemistry (**32**). It thus seems reasonable to expect that the oxygen atom would be more basic (in the Lewis sense) with respect to bonding to a metal surface. Second, data from a study of the N-bonded and O-bonded isomers of $(NH_3)_5Co(NH_2CHO)^{3+}$ suggest that O-bonded amides are more stable in organometallic compounds than N-bonded amides (**33**). It was found that the N-bonded form of $[(NH_3)_5Co(NH_2CHO)](ClO_4)_3$ isomerizes to the O-bonded form in the solid state. It was also found that heating $[(NH_3)_5Co(H_2O)](ClO_4)_3$ in N,N-dimethylformamide produced only the O-bonded isomer of $(NH_3)_5Co(NMe_2CHO)^{3+}$. Third, the ν(CO) frequency of 1660 cm^{-1} for the low-temperature form of molecularly chemisorbed formamide is somewhat reduced from the gas phase value of 1734 cm^{-1}, and similar decreases in ν(CO) have been observed previously for η^1(O)-acetone (**5a**) and η^1(O)-formaldehyde (**6b**) on oxygen-precovered Ru(001) surfaces. On the other hand, infrared data for η^1(N)-NHCRO complexes [cf. Fig. 2, structure 2] show that in all cases the frequency of ν(CO) is greater than 1700 cm^{-1} (**10**), and we would expect ν(CO) to be similarly high for an η^1(N)-formamide in which the formamide oxygen atom does not interact directly with the surface. Finally, an η^1(O)-NH_2CHO would be expected to maintain a nearly planar structure (gas phase formamide has a planar structure), and the NH_2 wagging vibration would involve motion of the NH_2 hydrogen atoms out of this plane and largely parallel to the surface. Hence, the $\omega(NH_2)$ mode would be expected to be rather weak in specular EEL spectra, as observed in Fig. 6(a). On the other hand, η^1(N)-NH_2CHO should result in a more intense NH_2 wagging mode, since the NH_2 group will no longer be in (or nearly in) a plane perpendicular to the surface; and this mode will involve motion of the NH_2 hydrogen atoms largely perpendicular to the surface. Taken together, these arguments provide a strong case for the low-temperature from of molecularly chemisorbed formamide being η^1(O)-NH_2CHO.

For the reasons discussed above, and because of the appearance of an intense $NH_2(ND_2)$ wagging mode at 970(770) cm^{-1}, it is very likely that the high-temperature form of molecularly chemisorbed formamide is η^2(N,O)-NH_2CHO. Indeed, the large upshift in the frequency of $\omega(NH_2)$ from 790 to 970 cm^{-1} in going from the low- to the high-temperature form is in itself suggestive of N-coordination to the surface. The other observed NH_2 modes of molecularly chemisorbed formamide are not shifted greatly upon N-coordination because they do not involve motion of the NH_2 hydrogen atoms directly towards the surface, which in the case of $\omega(NH_2)$ increases the restoring force associated with this vibration and results in the large frequency increase. A similar phenomenon occurs with the $\delta_s(NH_3)$ mode of ammonia when this molecule adsorbs on metal surfaces (2), and the frequency of this mode shifts from 950 cm^{-1} in the gas phase to approximately 1150 cm^{-1}. The fact that the conversion of η^1(O)-NH_2CHO to η^2(N,O)-NH_2CHO occurs only when the surface is annealed to 225 K indicates that an activation energy of approximately 13 kcal mol^{-1} is associated with this conversion. This activation barrier is probably associated with the partial rotation of the NH_2 group about the CN bond, and the distortion of the NH_2 group which the formamide molecule must undergo in order for the nitrogen atom to coordinate to the surface. As stated previously, the η^1(O)-NH_2CHO probably maintains the planar structure of gas phase formamide, for which the activation barrier to rotation of the NH_2 group about the CN bond has been measured to be 18 kcal-mol^{-1} (34). In η^2(N,O)-NH_2CHO, however, the nitrogen is expected to obtain an approximately tetrahedral bonding geometry, with the hydrogen atoms of the NH_2 group disposed symmetrically about, but no longer in, the OCN plane [cf. Fig. 1, structure (III)]. Thus, the plane containing the NH_2 group must rotate approximately 90° about the CN bond and the NH bonds must tilt away from the surface in order for the nitrogen atom to approach the surface in the proper orientation.

While the molecular formamide thermal desorption peak at 255 K is undoubtedly due to desorption from the monolayer, the desorption peak at 225 K could be attributed either to monolayer or second-layer desorption. The fact that this lower temperature desorption peak occurs at the same temperature as the conversion of the low-temperature form of chemisorbed formamide to the high-temperature form suggests that this is a monolayer desorption state, while the proximity of the 225 K

desorption peak to the multilayer desorption peak at 210 K might suggest that it results from second-layer desorption. [The low-temperature form of chemisorbed formamide identified by EELS is clearly not second-layer formamide, since it is present even following very low initial exposures.] While there is precedent for resolving second-layer thermal desorption features in thermal desorption spectra, such features were not resolved in the case of η^1(O)-bonded formaldehyde (**6**) or acetone (**5**) adsorption on oxygen-precovered Ru(001) surfaces. We thus favor (slightly) the assignment of the 225 K thermal desorption feature as a monolayer desorption state.

B. Formamide Decomposition

It has been shown that the high-temperature form of molecularly chemisorbed formamide decomposes near 260 K with H_2 evolution to produce η^2(N,O)-NHCHO with some molecular desorption occurring for sufficiently high coverages. The η^2–NHCHO would be of C_s symmetry if all five of its atoms were located in a plane perpendicular to the Ru(001)-p(1x2)O surface, and of C_1 symmetry if this is not the case. According to the surface dipole selection rule, eight vibrational modes should be observed in specular EEL spectra for C_s symmetry (**35**): ν(NH), ν(CH), ν_a(NCO), ν_s(NCO), δ(CH), δ(NH), δ(NCO) and ν(Ru-NH_2CHO). (Note, however, that this does *not* imply that all of these modes are dipolar in nature.) For C_1 symmetry, all of these modes should be dipole-allowed in specular EEL spectra, and, in addition, the π(CH) and π(NH) modes should also be dipole-allowed. However, it is possible that not all dipole-allowed modes will be observed in specular EEL spectra because some modes may be intrinsically weak and/or accidentally degenerate with stronger modes; and for C_s symmetry it is possible that the dipole-forbidden π(NH) and π(CH) modes could be observed (but probably very weakly) in specular EEL spectra due to scattering via nondipolar (i.e. impact) mechanisms. As an example of the former possibility, note that no ν_a(NCO) mode is identified conclusively for η^2–NHCHO even though this mode is technically dipole-allowed for either C_s or C_1 symmetry. Since the identification of η^2–NHCHO as having either C_s or C_1 symmetry hinges on the dipole activity of the π(NH) and π(CH) modes, and since neither of these modes can be assigned with complete confidence, the symmetry of η^2–NHCHO must be regarded as uncertain. If the mode at 1140(920) cm^{-1} in the case of η^2–NHCHO (η^2-NDCHO) is indeed π(NH), then this would be strong evidence for C_s sym-

metry, since off-specular EEL spectra indicate that this mode is largely dipolar in nature. This is contrary to our expectation, however, that η^2–NHCHO should be planar, just as η^2-formate is planar.

Another important question regarding the structure of η^2–NHCHO on the Ru(001)-p(1x2)-O surface is whether this species is chelating or bridging, i.e. is it bonded to only one ruthenium atom or to at least two ruthenium atoms?

Chelating Bridging

Organometallic analogues are known for both the chelating and bridging structures shown above (12). Analogous organometallic compounds are also known for chelating and bridging η^2-formates, and these may be distinguished from one another by the frequency difference between the ν_a(OCO) and ν_s(OCO) modes (29). However, since the ν_a(NCO) mode is not identified positively for η^2–NHCHO on Ru(001)-p(1x2)-O, this criterion cannot be used to establish whether the η^2–NHCHO is bridging or chelating. Nevertheless, it is extremely likely that the η^2–NHCHO is bridge-bonded for three reasons. First, the strong ν_s(NCO) mode of η^2–NHCHO on Ru(001)-p(1x2)-O, occurring at 1395 cm^{-1}, is in perfect agreement with the ν_s(NCO) modes observed for bridging $N(CH_3)C(CH_3)O$ species in the gallium and indium compounds referenced in Table II, while a series of chelating η^2-NArCHO (Ar = aryl) species in rhenium, ruthenium and osmium compounds have ν_s(NCO) modes that are more than 100 cm^{-1} lower in frequency, ranging from 1250 to 1290 cm^{-1} (12a,b). Second, η^2(N,O)-NRCHO ligands that have been identified in organometallic compounds are chelating only in mononuclear metal compounds and bridging in polynuclear metal compounds (12), and the behavior of the surface with respect to ligand bonding should be more similar to the polynuclear metal compounds. Third, all η^2-formates identified previously on metal surfaces which have been assigned structures have been identified as bridging rather than chelating (4).

Although it has been shown that the EEL spectra of Fig. 7 are fully consistent with an η^2(N,O)-NHCHO species, it is instructive to consider briefly other plausible species which might be formed from formamide decomposition on the Ru(001)-p(1x2)-O surface, and to eliminate them on the basis of these EEL spectra. Although all of the species depicted in Fig. 2 have analogues in organometallic chemistry, it can be shown easily that all but η^2(N,O)-NHCHO are inconsistent with the EEL spectra of Fig. 7. Species (1), (3), (5a) and (5b) lack CH bonds, a fact which in itself is sufficient to eliminate them from consideration. (The rather sharp peak at 2980 cm^{-1} in the EEL spectrum of Fig. 7(a) is much too narrow to be due to a hydrogen-bonded NH or OH stretching mode, and the frequency of this mode does not shift significantly upon N-deuteration.) Species (1), (2), (5a) and (5b) contain CO or CN double bonds which, based on the organometallic studies cited in Sec. I, should give rise to intense stretching modes near 1500-1650, 1700-1750, 1600 and 1775 cm^{-1}, respectively. Species (1), (3) and (5b) contain NH_2 groups, which is inconsistent with the lack of a $\delta(NH_2)$ mode, the presence of only a single ν(NH) peak in Fig. 7(a), and the observed desorption of H_2 at 265 K. Species (1), (2), (5a) and (5b) contain well-defined single and double skeletal bonds and should thus have δ(NCO) frequencies similar to those of gas phase formamide or formic acid (565 and 625 cm^{-1}), rather than near 800 cm^{-1} as for the case of η^2-formate on Ru(001). Species (5a) contains an OH group, and there is no spectroscopic evidence for the formation of either free [ν(OH) >3500 cm^{-1}] or hydrogen-bonded [ν(OH) lowered and broadened] OH bonds in Fig. 7(a). Thus all the species depicted in Fig. 2 except η^2(N,O)-NHCHO are inconsistent with the EEL spectra of Fig. 7. On the other hand, the η^2(N,O)-NHCHO is completely consistent with both the EEL spectra and the TDMS results.

It is interesting to compare the products observed in η^2–NHCHO decomposition to those observed in η^2-formate decomposition on Ru(001). The η^2-formate decomposes via two competing mechanisms near 350 K, one of which produces adsorbed CO and atomic oxygen and the other evolving gaseous CO_2 (**4a,b**):

$$\eta^2\text{–HCOO(a)} \rightleftharpoons \begin{matrix} \text{H(a) + O(a) + CO(a)} \\ \text{H(a) + } CO_2\text{(g)} \end{matrix}$$

The decomposition of η^2–NHCHO to H_2(g), N(a) and CO(g) is analogous to the first of these reactions, although in this case the H_2 and CO that are evolved are reaction-limited desorption products since

neither carbon monoxide nor hydrogen is adsorbed on the Ru(001)-p(1x2)-O surface at the temperature of η^2–NHCHO decomposition. The decomposition of η^2–NHCHO to HNCO(g) and ½ H_2(g) would be analogous to the second formate decomposition reaction, but it is not observed.

Finally, it should be emphasized that there is no evidence for any direct interaction or chemical reaction between the oxygen adatoms of the p(1x2)-O overlayer and formamide or its decomposition products.There is no desorption of H_2O, NO or high-temperature (recombinative) CO (36) following formamide adsorption. There is no evidence in any EEL spectra for the formation of OH or NO bonds, and EEL spectra measured after annealing to 700 K show all of the characteristic features of the p(1x2)-O overlayer, which are completely unaffected by the adsorption and decomposition of formamide.

V. Conclusions

Below 260 K, formamide adsorbs molecularly on the Ru(001)-p(1x2)-O surface. Two different forms of molecularly chemisorbed formamide are observed: a low-temperature form below 225 K and a high-temperature form between 225 and 260 K. The low-temperature form bonds to the surface via an oxygen electron lone pair only, while the high-temperature form bonds to the surface through lone pairs on both the oxygen and the nitrogen atoms. For sufficiently high coverages, the conversion at 225 K is accompanied by some desorption of molecular formamide. Molecular multilayers of formamide may be condensed on the Ru(001)-p(1x2)-O surface at temperatures below 210 K.

At 260 K, the high-temperature form of molecularly chemisorbed formamide undergoes NH bond cleavage and converts to a bridging η^2(N,O)-NHCHO species. This conversion is accompanied by molecular formamide desorption if a sufficiently high coverage is involved. The η^2–NHCHO decomposes at 420 K yielding adsorbed nitrogen adatoms and evolving H_2 and CO. The nitrogen adatoms recombine and desorb near 600 K, leaving the p(1x2)-O overlayer intact. For a saturation formamide coverage, approximately 0.05 monolayer of η^2–NHCHO forms and decomposes.

Acknowledgment:

Principal support of this work was provided by the National Science Foundation under Grant No. CHE-8516615. Acknowledgment is made also to the donors of the Petroleum Research Fund, administered by the American Chemical Society, for partial support.

References

1. (a) Stuve, E. M.; Madix, R. J.; Sexton, B. A., Surface Sci. **1981**, 111, 11. (b) Stuve, E. M.; Madix, R. J.; Sexton, B. A., J. Vac. Sci. Technol. **1982**, 20, 590. (c) Sexton, B.A., J. Vac. Sci. Technol. **1979**, 16, 1033. (d) Baro, A.M.; Erley, W., J. Vac. Sci. Technol. **1982**, 20, 580. (e) Andersson, S.; Davenport, J.W., Solid State Commun. **1978**, 28, 677. (f) Ibach, H.; Lehwald, S., Surface Sci. **1980**, 91, 187. (g) Fisher, G.B.; Sexton, B.A., Phys. Rev. Lett. **1980**, 44, 683. (h) Sexton, B.A., J. Vac. Sci. Technol. **1980**, 94, 435. (i) Thiel, P. A.; Hoffmann, F.M.; Weinberg, W.H., J. Chem. Phys. **1981**, 75, 5556. (j) Thiel, P. A.; Hoffmann, F.M.; Weinberg, W.H., Phys. Rev. Lett. **1982**, 49, 501.

2. (a) Gland, J.L.; Sexton, B.A.; Mitchell, G.E., Surface Sci. **1982**, 115, 623. (b) Erley, W.; Ibach, H., Surface Sci. **1982**, 119, L357. (c) Sexton, B.A.; Mitchell, G.E., Surface Sci. **1980**, 99, 539. (d) Sexton, B.A.; Mitchell, G.E., Surface Sci. **1980**, 99, 523. (e) Gland, J.L.; Sexton, B.A., J. Catal. **1981**, 68, 286. (f) Fisher, G.B.; Mitchell, G.E., J. Electron Spectros. Related Ph. **1983**, 29, 253.

3. (a) Backx, C.; de Groot, C.P.M.; Biloen, P., Appl. Surface Sci. **1980**, 6, 256. (b) Backx, C.; de Groot, C.P.M., Surface Sci. **1982**, 115, 382. (c) Nyberg, C.; Tengstal, C.G.; Andersson, S.; Holmes, M.W., Chem. Phys. Lett. **1982**, 87, 87. (d) Lehwald, S.; Ibach, H.; Steininger, H., Surface Sci. **1982**, 117, 342. (e) Demuth, J.E.; Ibach, H.; Lehwald, S., Phys. Rev. Lett. **1978**, 40, 1044. (f) Bertolini, J.C.; Rousseau, J., Surface Sci. **1979**, 83, 531. (g) Lehwald, S.; Ibach, H., Surface Sci. **1979**, 89, 425. (h) Ibach, H.; Hopster, H.; Sexton, B. A., Appl. Surface. Sci. **1977**, 1,1. (i) Ibach, H.; Lehwald, S., J. Vac. Sci. Technol. **1978**, 15, 407. (j) Baro, A.M., Ibach, H., J. Chem. Phys. **1981**, 74, 4194. (k) Steininger, H.; Ibach, H.; Lehwald, S., Surface Sci. **1982**, 117, 342. (l) Dubois, L. H.; Castner, D. J.; Somorjai, G. A., J. Chem. Phys. **1980**, 72, 5234. (m) Barteau, M. A.; Broughton, J. Q.; Menzel, D., Appl. Surface Sci. **1984**, 19, 92. (n) Hills, M. M.; Parmeter, J. E.; Mullins, C. B.; Weinberg, W. H., J. Am. Chem. Soc. **1986**, 108, 3554.

4. (a) Avery, N. R.; Toby, B. H.; Anton, A. B.; Weinberg, W. H., Surface Sci. **1982**, 122, L574. (b)

Toby, B. H.; Avery, N. R.; Anton, A. B.; Weinberg, W. H., J. Elec. Spec. Rel. Phen. **1983**, 29, 317. (c) Sexton, B.A.; Madix, R.J., Surface Sci. **1981**, 105, 177. (d) Sexton, B.A., Surface Sci. **1979**, 88, 319. (e) Sexton, B.A., J. Vac. Sci. Technol. **1980**, 17, 141. (f) Avery, N.R., Surface Sci. **1982**, 11/12, 774.

5. (a) Avery, N. R.; Weinberg, W. H.; Anton, A. B.; Toby, B. H., Phys. Rev. Lett. **1983**, 51, 682. (b) Avery, N. R.; Anton, A. B.; Toby, B. H.; Weinberg, W.H., J. Electron Spectros. Related Ph. **1983**, 29, 233. (c) Avery, N. R., Surface Sci. **1983**, 125, 771.

6. (a) Anton, A. B.; Parmeter, J. E.; Weinberg, W. H., J. Am. Chem. Soc. **1985**, 107, 5558. (b) Anton, A. B.; Parmeter, J. E.; Weinberg, W. H., J. Am. Chem. Soc. **1985**, 108, 1823. (c) Richter, L.J.; Ho, W., J. Chem. Phys. **1985**, 83, 2165. (d) Stuve, E. M.; Madix, R. J.; Sexton, B. A., Surface Sci. **1982**, 119, 279. (e) Wachs, I.E.; Madix, R. J., Surface Sci. **1979**, 84, 375.

7. (a) DiNardo, N.J.; Avouris, P.; Demuth, J.E., J. Chem. Phys. **1984**, 81, 2169. (b) Sexton, B.A., Surface Sci. **1985**, 163, 99. (c) Demuth, J.E.; Christmann, K.; Sanda, P.N., Chem. Phys. Lett. **1980**, 76, 201. (d) Demuth, J.E.; Sanda, P.N., Phys. Rev. Lett. **1981**, 47, 61. (e) Avouris, P.; Demuth, J.E., J. Chem. Phys. **1981**, 75, 4783. (f) Avouris, P.; Demuth, J.E., J. Chem. Phys. **1981**, 75, 5953. (g) Demuth, J.E.; Avouris, P.; Sanda, P.N., J. Vac. Sci. Technol. **1982**, 20, 588. (h) Demuth, J.E.; Avouris, P., Phys. Rev. Lett. **1981**, 47, 61.

8. Garwood, G.A.; Hubbard, A.T.; Surface Sci. **1982**, 118, 223.

9. (a) Sacco, A.; Giannoccaro, P.; Vasapoloo, G., Inorganica Chimica Acta **1984**, 83, 125. (b) Kruse, A. E.; Angelici, R. J., J. Organomet. Chem. **1970**, 24, 231. (c) Behrens, H.; Jungbauer, A., Z. Naturforsch. **1979**, 34b, 1477. (d) Lindsay, A. J.; Kim, S; Jacobson, R. A.; Angelici, R. J., Organomet. **1984**, 3, 1523.

10. Burgess, K.; Johnson, B. F. G.; Lewis, J., J. Chem. Soc. Dalton Trans. **1983**, 1179.

11. (a) Szostak, R.; Strouse, C.E.; Kaesz, H.D., J. Oranomet: Chem. **1980**, 191, 243. (b) Mayr, A.; Lin, Y-C.; Boag, N.M.; Kaesz, H.D., Inorg. Chem. **1982**, 21, 1704. (c) Kampe, C.E.; Boag, N.M.; Kaesz, H.D., J. Molecular Cat. **1983**, 21, 297. (d) Fagan, P.J.; Manriquez, J.M.; Vollmer,

S.H.; Day, C.S.; Day, V.W.; Marks, T.J., J. Am. Chem. Soc. **1981**, 103, 2206. (e) Yasuda, H.; Araki, T.; Tani, H., J. Organomet. Chem. **1973**, 49, 103. (f) Azam, K.A., Yin, C.C.; Deeming, A.J., J. Chem. Soc. Dalton Trans. **1978**, 1201.

12. (a) Rossi, R.; Duatti, A.; Magon, L.; Casellato, U.; Graziani, R.; Toniolo, L., Inorganica Chimica Acta **1983**, 74, 77. (b) Sahajpal, A.; Robinson, R.D., Inorg. Chem. **1979**, 18, 3572. (c) Schwering, H.-U.; Weidlein, J., Chimia **1973**, 27, 535. (d) Jennings, J.R.; Wade, K.; Wyatt, B.K., J. Chem. Soc. (A) **1968**, 2535. (e) Adams, R.D.; Golembeski, N.M., J. Organomet. Chem. **1979**, 171, C21. (f) Adams, R.D.; Golembeski, N.M., Selegue, J.P., Inorg. Chem. **1981**, 20, 1242.

13. (a) Lin, Y.C.; Knobler, C.B.; Kaesz, H.D., J. Am. Chem. Soc. **1981**, 103, 1216. (b) Kaesz, H.D.; Knobler, C.B.; Andrews, M.A.; van Buskirk, G.; Szostak, R.; Strousse, C.E.; Lin, Y.C.; Mayr, A., Pure & Appl. Chem. **1982**, 54, 131. The η^2(C,N)-HONCR and η^2(C,N)-OCNHR coexist as an equilibrium mixture.

14. Baca, A.G.; Schulz, M.A.; Shirley, D.A., J. Chem. Phys. **1985**, 83, 6001.

15. (a) Ibach, H. and Mills, D. L., "Electron Energy Loss Spectroscopy and Surface Vibrations" **1982**, Academic Press, New York. (b) Weinberg, W.H., Methods of Explerimental Physics **1985**, 22, 23.

16. Parmeter, J.E.; Schwalke, U.; Weinberg, W.H., to be published.

17. (a) Madey, T. E.; Engelhardt, H. A.; Menzel, D., Surface Sci. **1975**, 48, 304. (b) Parrott, S. L.; Praline, G.; Koel, B. E.; White, J. M.; Taylor, T. N., J. Chem. Phys. **1979**, 71, 3352. (c) Rahman, T. S.; Anton, A. B.; Avery, N. R.; Weinberg, W. H., Phys. Rev. Letters **1983**, 51, 1979.

18. Thomas, G. E.; Weinberg, W. H., Rev. Sci. Instrum. **1979**, 50, 497.

19. Thomas, G. E.; Weinberg, W. H., J. Chem. Phys. **1979**, 70, 954.

20. Aldrich Catalog, Aldrich Chemical Co. **1984-85**, 563.

21. Redhead, P. A., Vacuum **1962**, 203.

22. Pfnür, H.; Menzel, D.; Hoffmann, F.M.; Ortega, A.; Bradshaw, A.M., Surface Sci. **1980**, 93, 431.

23. (a) Anton, A.B.; Avery, N.R.; Toby, B.H.; Weinberg, W.H., J. Electron Spectros. Related Ph. **1983**, 29, 181. (b) Anton, A.B.; Avery, N.R.; Madey, T.E.; Weinberg, W.H., J. Chem. Phys. **1986**, 85, 507.

24. (a) Thomas, G.E.; Weinberg, W.H., Phys. Rev. Lett. **1978**, 41, 958. (b) Thiel, P. A.; Weinberg, W.H.; Yates, Jr., J.T., J. Chem. Phys. **1979**, 71, 1643. (c) Thiel, P. A.; Weinberg, W.H.; Yates, Jr., J.T., Chem. Phys. Lett. **1979**, 67, 403. (d) Thiel, P. A.; Weinberg, W.H., J. Chem. Phys. **1980**, 73, 4081. (e) Schwalke, U.; Weinberg, W.H., in preparation.

25. (a) Schwalke, U.; Parmeter, J.E.; Weinberg, W.H., J. Chem. Phys. **1986**, 84, 4036. (b) Schwalke, U.; Parmeter, J.E.; Weinberg, W.H., Surface Sci., in press.

26. Suzuki, I., Bull. Chem. Soc. Jap., **1960**, 33, 1359.

27. (a) Evans, J.C., J. Chem. Phys. **1954**, 22, 1228. (b) King, S.T., J. Phys. Chem. **1971**, 75, 405.

28. The frequency of 525 cm^{-1} for δ(NCO) is obtained from EEL spectra of NH_2CHO adsorbed on hydrogen presaturated Ru(001) at 80 K, where the same molecular formamide species is formed but there is no overlapping ν_s(RuO) mode.

29. Nakamoto, K., "Infrared and Raman Spectra of Inorganic and Coordination Compounds", Third Edition **1978**, Wiley & Sons, New York, 231-233.

30. Coupling between ν_s(NCO) and δ(NH) is possible for η^2–NHCHO since both of these modes are of the same symmetry and are expected to occur in the same frequency range. Such coupling could lead to very different intensities for δ(NH) in η^2–NHCHO and δ(ND) in η^2-NDCHO, as well as an anomalously small frequency shift for this mode upon N-deuteration.

31. See for example, Avery, N.R., Surface Sci. **1984**, 137, L109, as well as Refs. (6b) and (7a) above.

32. Streitwieser, Jr., A.; Heathcock, C.H., "Introduction to Organic Chemistry" **1976**, Macmillan, New York, 466-467.

33. Balahura, R.J.; Jordan, R.B., J. Am. Chem. Soc. **1970**, 92, 1533.

34. Ref. 32, p. 452.

35. See Chaps. 1 and 3 of Ref. 15.

36. Carbon monoxide formed from the recombinative desorption of carbon and oxygen adatoms on Ru(001) desorbs in the temperature range of 550-700 K. Hills, M.M.; Parmeter, J.E.; Weinberg, W.H., J. Am. Chem. Soc., submitted.

Table I. Vibrational modes and assignments for the low-temperature form of molecularly chemisorbed NH_2CHO (ND_2CHO) on Ru(001)-p(1x2)-O. The frequency ratios $\nu(NH_2CHO)/\nu(ND_2CHO)$ are also listed in parentheses following the ND_2CHO frequencies. Data for liquid phase NH_2CHO and ND_2CHO, and for gas phase NH_2CHO are given for comparison. All frequencies are in cm^{-1}.

	Ru(001)-p(1x2)-O		NH_2CHO(l) (26)	
Mode	NH_2CHO	(ND_2CHO, ratio)	[ND_2CHO(l), ratio]	NH_2CHO(g) (27)
$\nu_a(NH_2)$	3490	(2630,1.33)	3330 (2556,1.30)	3545
$\nu_s(NH_2)$	3230	(2380,1.36)	3190 (2385,1.34)	3451
ν(CH)	2940	(2930,1.00)	2882 (2887,1.00)	2852
ν(CO)	1660	(1650,1.01)	1690 (1667,1.01)	1734
$\delta(NH_2)$	1585	(1140,1.39)	1608 (1118,1.44)	1572
δ(CH)	1360	(1380,0.99)	1391 (1398,0.99)	1378
ν(CN)			1309 (1338,0.98)	1255
π(CH)	n.o.	n.o.	1056 (1056,1.00)	1030
$\rho(NH_2)$	1110	(920,1.21)	1090 (912,1.20)	1059
$\omega(NH_2)$	790	n.o.	750 (450,1.67)	289
$\tau(NH_2)$	n.o.	n.o.	200	602
δ(NCO)	−525[a]	(460,1.14)	608 (570,1.07)	565
ν(Ru–NH_2CHO)	300[b]	(280,1.07)[b]		

[a] Overlaps with ν_s(RuO) of oxygen adatoms in the case of NH_2CHO.

[b] Not resolved in the spectrum shown; sharpens with annealing to 200 K.

n.o. = not observed, a = asymmetric, s = symmetric.

Table II. Vibrational modes and assignments for η^2(N,O)-NHCHO on the Ru(001)-p(1x2)-O surface. Vibrational modes for η^2-NDCHO and the corresponding η^2–NHCHO/η^2-NDCHO frequency ratios are listed in parentheses. Data for η^2(O,O)-OCHO (η^2-formate) and for the compounds $[R_2MN(CH_3)C(CH_3)O]_2$ (M = Ga or In, R = CH_3 or CH_2CH_3) are given for comparison. All frequencies are in cm^{-1}.

Mode	η^2(N,O)-NHCHO [η^2(N,O)-NDCHO, ratio], Ru(001)-p(1x2)-O	η^2-formate, Ru(001) (4a,b)[a]	$[R_2MN(CH_3)C(CH_3)O]_2$ (12c)
ν(NH)	3365(2480,1.36) w	-	-
ν(CH)	2980(2960,1.01) w	2920 w	-
ν_a(NCO)[a]	n.o.(n.o.)	n.o.	1571-1585 st
ν_s(NCO)[a]	1395(1360,1.03) st	1360 st	1392-1400 st
δ(NH)	n.o.(1230) m	-	-
π(NH)	1140(920,1.24) m	-	-
δ(CH)	1340(n.o.) sh	n.o.	-
π(CH)	n.o.(n.o.)	n.o.	-
δ(NCO)[a]	770(760,1.01) m	805 m	n.o.
ν(M-ligand)	400(400,1.00) st	380 st	363-492 st

[a] In the case of η^2-formate, these skeletal modes are obviously OCO modes rather than NCO modes.

s = symmetric, a = asymmetric, st = strong, m = medium, w = weak, sh = shoulder, n.o. = not observed.

Table III. Vibrational frequencies and mode assignments for multilayer NH_2CHO and ND_2CHO on the Ru(001)-p(1x2)-O surface. All frequencies are in cm^{-1}. For corresponding frequencies of liquid formamide, see Table I.

Mode	NH_2CHO	ND_2CHO
$\nu_a(NH_2)$	3370	2505
$\nu_s(NH_2)$	3230	2395
ν(CH)	2910	2885
ν(CO)	1710	1675
δ(CH)	1380	1415
ν(CN)		1355
$\delta(NH_2)$	1625	
$\rho(NH_2)$	1075	1030
π(CH)		
$\omega(NH_2)$	710	565
δ(NCO)	n.o.	n.o.
lattice[a]	220	160

s = symmetric, a = asymmetric, n.o. = not observed.

[a] Probably coupled to $\tau(NH_2)$.

Figure Captions

Figure 1: Schematic representation of four possible bonding configurations for formamide that is molecularly adsorbed on a metal surface. Structures (I), (II) and (III) involve bonding via heteroatom electron lone pairs, while structure (IV) involves bonding through rehybridization of the CO double bond. The arrows indicate lone pair donor bonds.

Figure 2: Several possible decomposition products of formamide on a metal surface. All of these species have known organometallic analogues (in some of which one or both hydrogens are replaced by an alkyl or aryl group).

Figure 3: The EEL spectrum of the Ru(001)-p(1x2)-O surface. The inset shows the surface structure (large circle = ruthenium atom; small circle = oxygen atom) and the unit cell (dashed line). The fractional coverage of oxygen adatoms is 0.5. The loss feature at 585 cm^{-1} is magnified by a factor of 300 compared to the elastic peak, and the remainder of the EEL spectrum is magnified by a factor of 1000.

Figure 4: The molecular formamide (m = 45 amu) thermal desorption spectra that result following various exposures of NH_2CHO to the Ru(001)-p(1x2)-O surface at 80 K. The heating rate is approximately 8 $K\text{-}s^{-1}$ in all cases.

Figure 5: Thermal desorption spectra of (a) CO (m = 28 amu), (b) H_2 (m = 2 amu) and (c) *(inset)* N_2 (m = 14 amu, N cracking fragment) following a saturation NH_2CHO exposure of approximately 8 L on the Ru(001)-p(1x2)-O surface at 80 K. The heating rate is approximately 8 $K\text{-}s^{-1}$ in all cases. The shoulder at 385 K in the CO spectrum is due to desorption of CO adsorbed from the chamber background. Dashed lines are approximate baselines. Note the different temperature scale in (c).

Figure 6: The EEL spectra that result when the Ru(001) surface at 80 K is exposed to (a) 0.5 L NH_2CHO at 80 K, (b) 0.5 L ND_2CHO at 80 K, and (c) 0.5 L NH_2CHO at 80 K followed by momentary annealing to 225 K. Corresponding EEL spectra for any given exposure are virtually identical, provided the exposure is not large enough to condense formamide mul-

tilayers.

Figure 7: The EEL spectra that result when the Ru(001)-p(1x2)-O surface at 80 K is exposed to (a) 0.5 L NH_2CHO at 80 K and (b) 0.5 L ND_2CHO at 80 K, and annealed momentarily to 400 K. These spectra are characteristic of η^2(N,O)-NHCHO and η^2(N,O)-NDCHO.

Figure 8: The EEL spectra that result when the Ru(001)-p(1x2)-O surface at 80 K is exposed to (a) 10 L NH_2CHO and (b) 10 L ND_2CHO, showing the characteristic features of formamide multilayers.

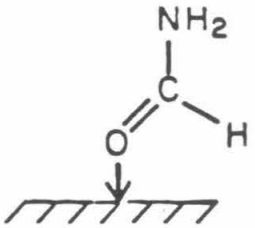

(I) $\eta^1(O)-NH_2CHO$

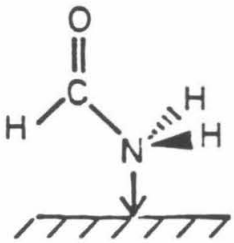

(II) $\eta^1(N)-NH_2CHO$

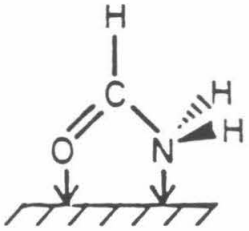

(III) $\eta^2(N,O)-NH_2CHO$

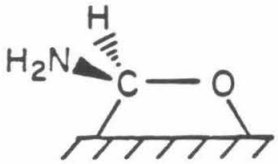

(IV) $\eta^2(C,O)-NH_2CHO$

Figure 1

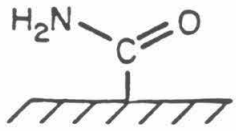

(1) $\eta^1(C)-CONH_2$

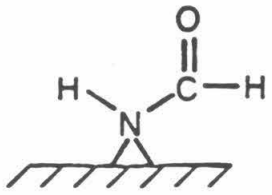

(2) $\eta^1(N)-NHCHO$

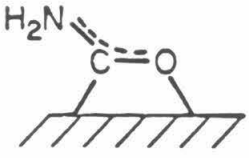

(3) $\eta^2(C,O)-NH_2CO$

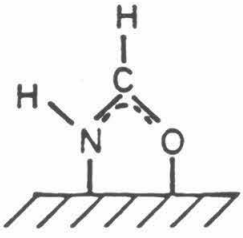

(4) $\eta^2(N,O)-NHCHO$

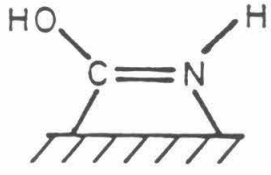

(5a) $\eta^2(C,N)-HOCNH$

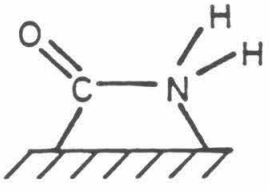

(5b) $\eta^2(C,N)-OCNH_2$

Figure 2

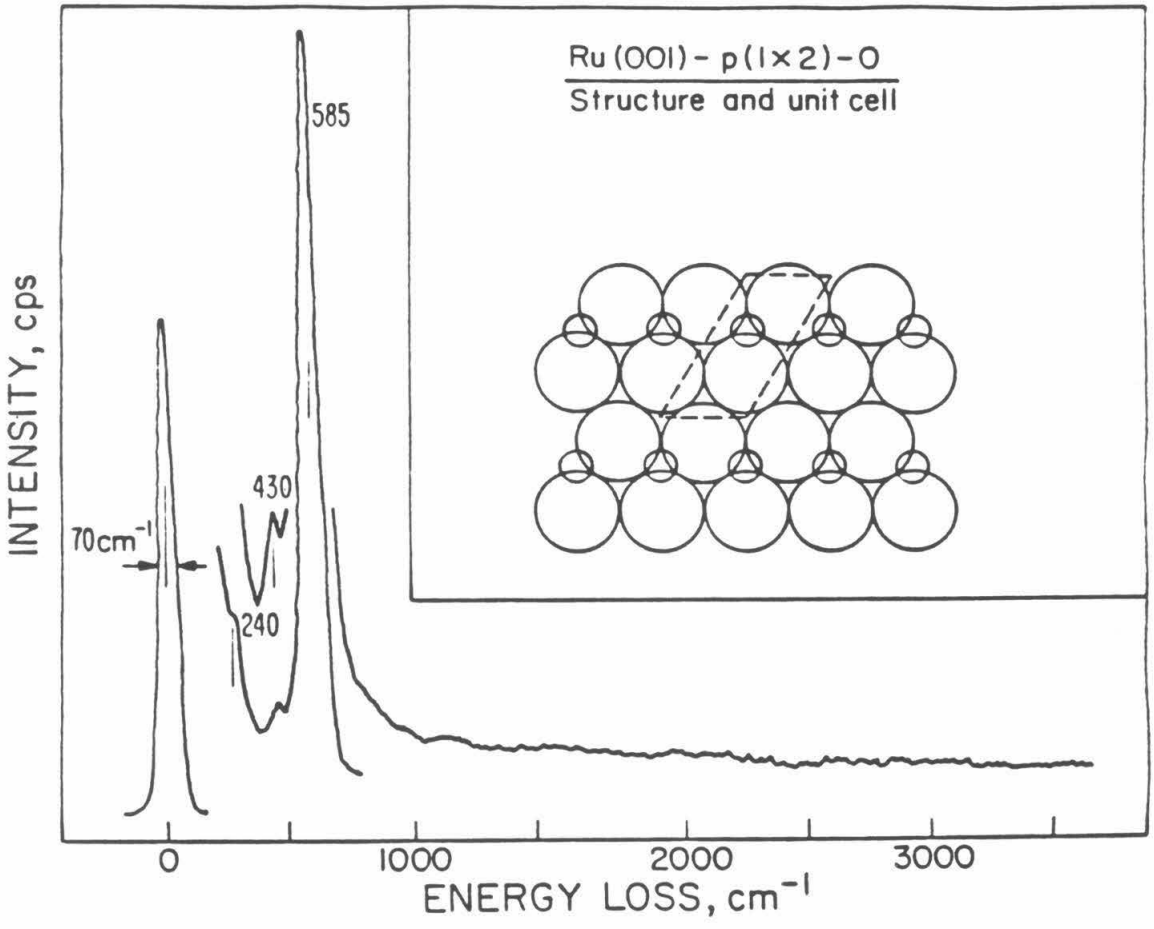
Ru(001) - p(1×2)-O
Structure and unit cell
585
430
240
70cm⁻¹
INTENSITY, cps
0
1000
2000
3000
ENERGY LOSS, cm⁻¹

Figure 3.

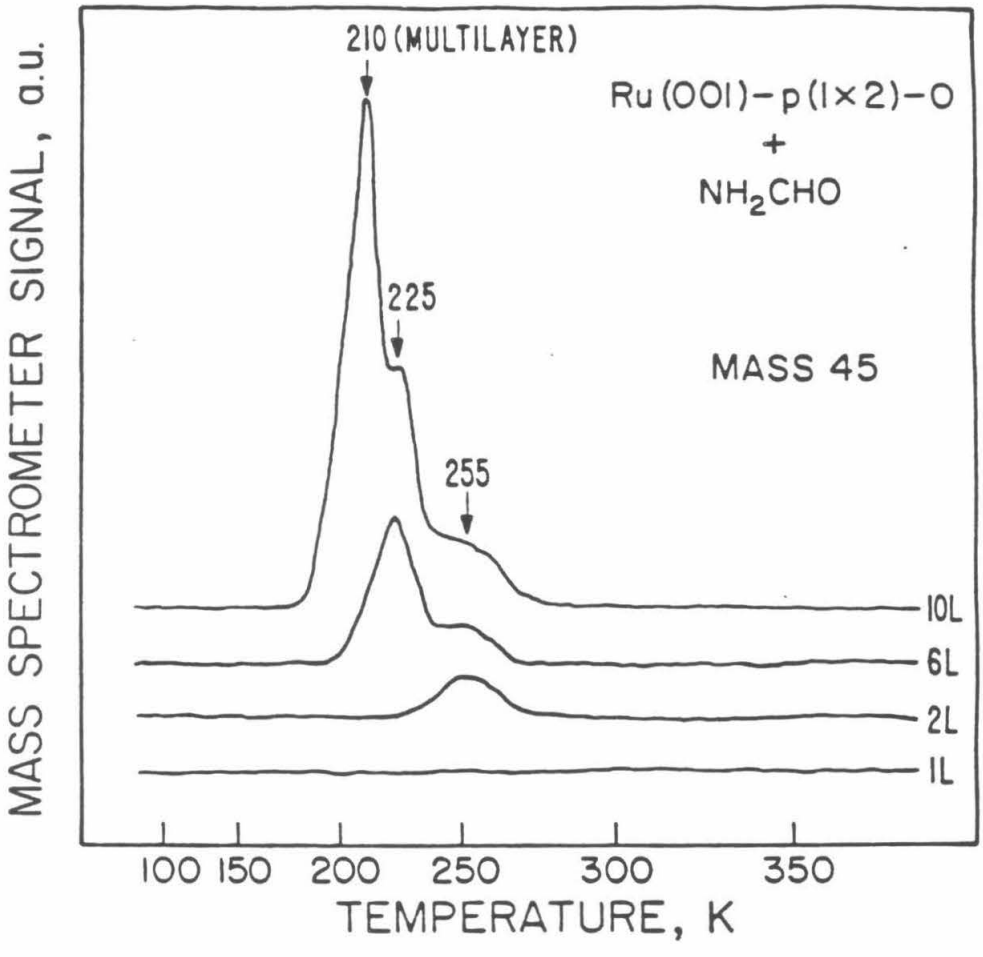
210 (MULTILAYER)
Ru(001)-p(1×2)-O
+
NH2CHO
225
MASS 45
255
10L
6L
2L
1L
MASS SPECTROMETER SIGNAL, a.u.
100 150 200 250 300 350
TEMPERATURE, K

Figure 4

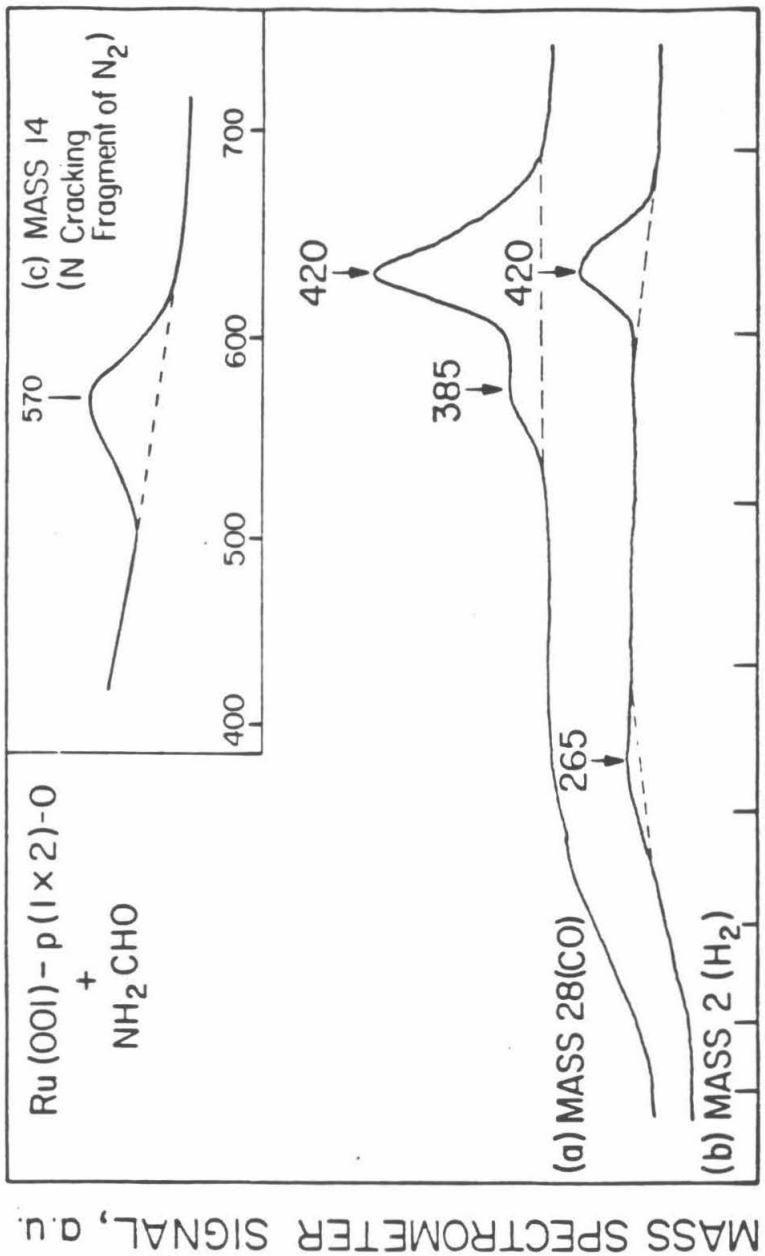
Ru (001) - p (1 x 2) - O
+
NH_2CHO
(c) MASS 14
(N Cracking
Fragment of N_2)
570
400
500
600
700
420
385
420
265
(a) MASS 28(CO)
(b) MASS 2 (H_2)
100 150 200 250 300 350 400 450
TEMPERATURE, K
MASS SPECTROMETER SIGNAL, a.u.

Figure 5

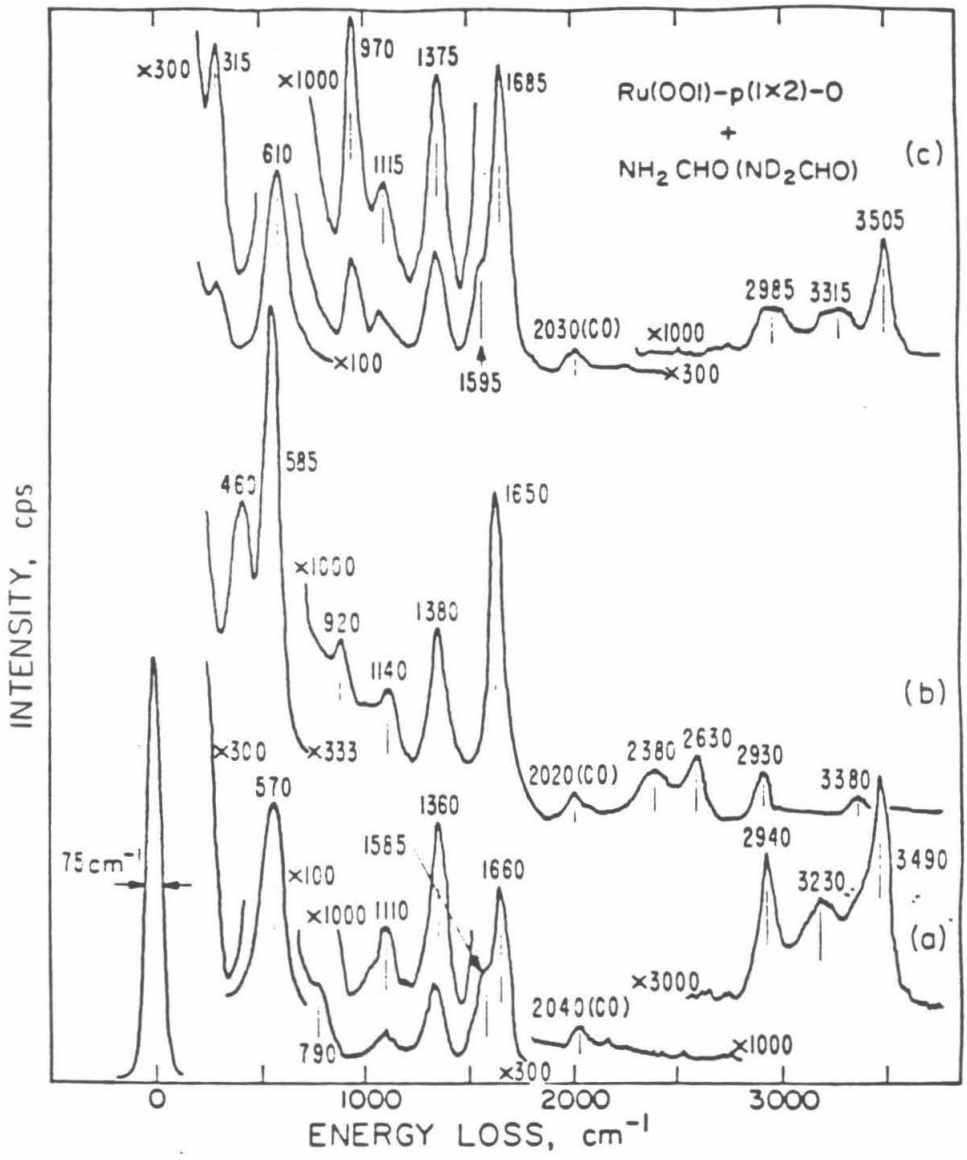
Ru(001)-p(1×2)-O
+
NH2 CHO (ND2CHO)
(c)
(b)
(a)
×300
315
×1000
970
1375
1685
610
1115
×100
1595
2030(CO)
×1000
×300
2985
3315
3505
460
585
1650
×1000
920
1380
1140
×300
×333
2020(CO)
2380
2630
2930
3380
570
1360
1585
2940
3230
3490
75 cm⁻¹
×100
×1000
1110
1660
790
×3000
2040(CO)
×1000
×300
INTENSITY, cps
0
1000
2000
3000
ENERGY LOSS, cm⁻¹

Figure 6

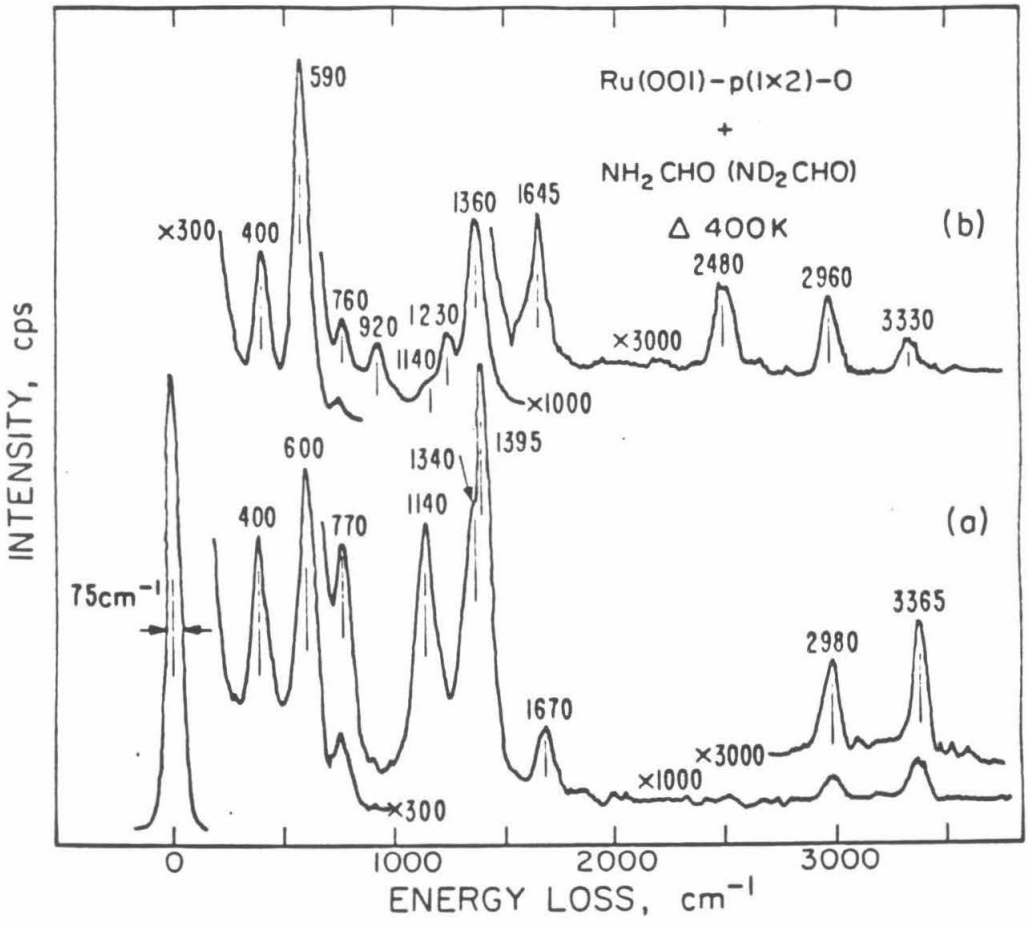
Ru(001)-p(1×2)-O
+
NH2CHO (ND2CHO)
Δ 400K
(b)
(a)
590
400
760
920
1230
1140
1360
1645
×300
×3000
×1000
2480
2960
3330
600
400
770
1340
1140
1395
75cm⁻¹
1670
2980
3365
×300
×1000
×3000
INTENSITY, cps
0
1000
2000
3000
ENERGY LOSS, cm⁻¹

Figure 7

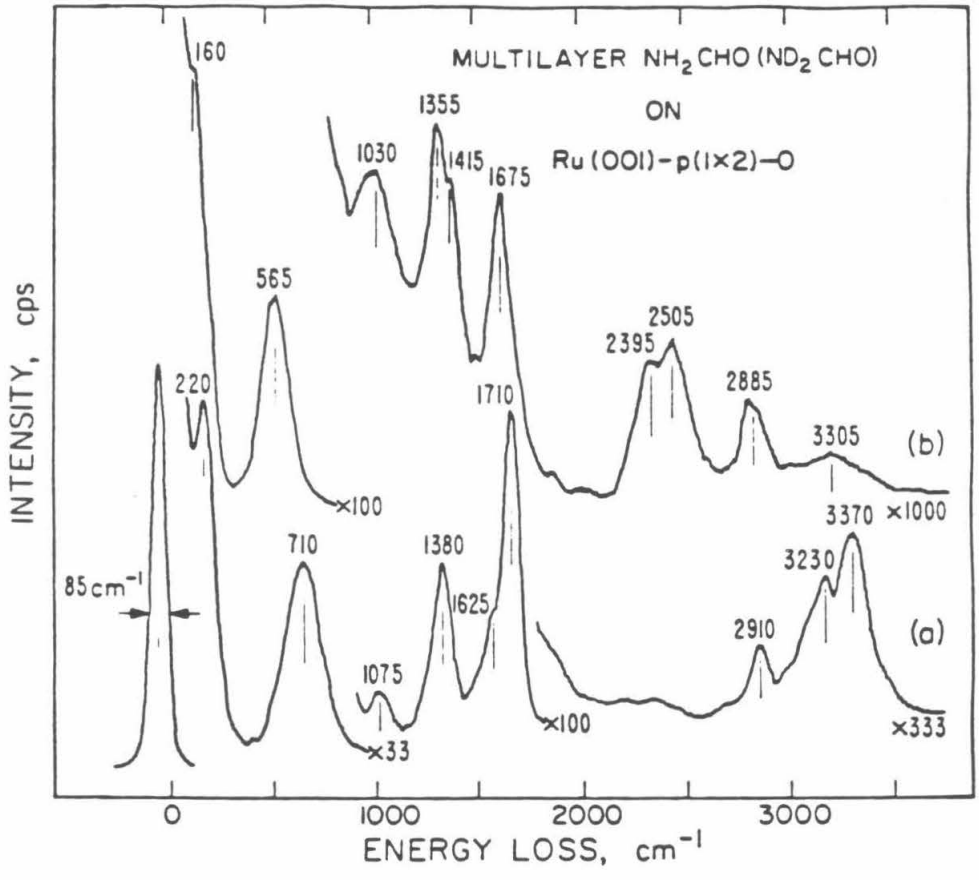
MULTILAYER NH2CHO (ND2 CHO)
ON
Ru (001) - p(1×2)—O
160
1355
1030
1415
1675
565
2505
2395
220
2885
1710
3305
(b)
×100
×1000
3370
710
1380
3230
85 cm-1
1625
2910
(a)
1075
×33
×100
×333
0
1000
2000
3000
ENERGY LOSS, cm-1
INTENSITY, cps

Figure 8

CHAPTER VIII

The Interaction of Formamide with Hydrogen-Presaturated Ru(001): The Conversion of η^1(O)-NH_2CHO to η^2(C,O)-Bonded Species

[This chapter will be submitted as a paper by J. E. Parmeter and W. H. Weinberg, to *The Journal of the American Chemical Society*.]

Abstract

Both the adsorption and the decomposition of formamide (NH_2CHO) have been studied on a hydrogen-presaturated (θ_H – 0.85) Ru(001) surface using high-resolution electron energy loss spectroscopy and thermal desorption mass spectrometry. At a surface temperature of 80 K, the formamide chemisorbs molecularly via an electron lone pair on the oxygen atom in an η^1(O)–NH_2CHO configuration. The η^1(O)–NH_2CHO undergoes competing desorption and conversion to η^2(C,O)–NH_2CHO below 225 K, with only conversion to η^2(C,O)–NH_2CHO occurring for sufficiently low formamide coverages. Further annealing of the surface to 250 K causes the η^2(C,O)–NH_2CHO to undergo carbon-hydrogen bond cleavage to produce η^2(C,O)–NH_2CO, and this species decomposes below 300 K to produce CO, additional hydrogen adatoms and NH. The NH decomposes near 400 K to nitrogen and hydrogen adatoms, and the desorption of the following reaction products (approximate peak desorption temperatures) is observed: CO (450 K), H_2 (305, 360 and 405 K) and N_2 (770 K). Following a saturation formamide exposure, approximately 0.05 monolayer of formamide decomposes on the hydrogen-presaturated surface.

I. Introduction

The interactions of organic molecules containing more than one double bond and/or a heteroatom with well-defined transition metal surfaces under ultrahigh vacuum (UHV) conditions has been the subject of much study recently (1). These molecules are of particular interest because several bonding configurations are possible for the adsorbed molecule, such as π- or di-σ-bonding via the molecular double bond or σ-donor bonding via a heteroatom electron lone pair. The electronic structure of the substrate (i.e. the metal surface) is manifest in the nature of (molecular) ligand bonding and in the reactions that the ligand undergoes, just as the electronic properties of a catalyst surface are manifest in the rates and mechanisms of its catalytic reactions. Studies of the adsorption of such molecules can possibly identify surface intermediates which may be involved in high-pressure heterogeneously catalyzed surface reactions, but which cannot be identified directly under reaction conditions due to their low steady-state concentrations. In addition, the intermediates identified on transition metal surfaces and their stability can be compared with those in organometallic compounds, thus rendering more systematic the connection between surface chemistry and organometallic chemistry. We have reported recently the results of studies of formamide adsorption and decomposition both on the clean Ru(001) surface (2) and on the Ru(001) surface that is modified chemically by an ordered p(1x2) overlayer of oxygen adatoms (θ_o = 0.5, where θ = 1 corresponds to a surface concentration of 1.58 x 10^{15} cm^{-2}) (3,4). We report here the results of a study of the adsorption and decomposition of formamide on a Ru(001) surface with a saturation precoverage of hydrogen adatoms. Hydrogen adatoms are a product of the decomposition of formamide on clean Ru(001), and could alter both the products of formamide decomposition and their stability.

Our previous studies of formamide on the Ru(001) and Ru(001)-p(1x2)-O surfaces showed that the presence of the p(1x2) oxygen adatom overlayer alters profoundly the chemistry of this molecule on this hexagonally close-packed ruthenium surface. On the oxygen-precovered surface at 80 K, adsorption occurs molecularly via an electron lone pair on the oxygen atom of the formamide to form an η^1(O)–NH_2CHO species. Upon annealing to 225 K, the η^1(O)–NH_2CHO converts to a slightly different molecularly chemisorbed species believed to be η^2(N,O)–NH_2CHO, and upon annealing to 265 K, the

latter species undergoes NH bond cleavage to produce a formate-like η^2(N,O)-NHCHO species. For sufficiently high initial formamide coverages, molecular desorption of formamide also occurs near 260 and 225 K. The η^2(N,O)–NHCHO is stable to 420 K, the temperature at which it decomposes, evolving CO and H_2 and leaving nitrogen adatoms on the surface. The nitrogen adatoms desorb as N_2 near 570 K, leaving the p(1x2) oxygen adatom overlayer intact. Annealing a saturated overlayer of chemisorbed formamide results in the formation and decomposition of approximately 0.05 monolayer of η^2(N,O)–NHCHO. A summary of the reactions of formamide on the Ru(001)-p(1x2)-O surface is delineated in Fig. 1(a).

In dramatic contrast, formamide adsorption on the clean Ru(001) surface at 80 K results initially in carbon-hydrogen bond cleavage and rehybridization of the CO bond to produce an η^2(C,O)–NH_2CO species. This species decomposes near 250 K, leaving a mixture of CO, NH_3, NH and hydrogen adatoms on the surface. The small amount of NH_3 that is formed (~0.02 monolayer) desorbs molecularly near 300 K, while the NH decomposes to nitrogen and hydrogen adatoms between 350 and 400 K. Hydrogen adatom recombination results in H_2 desorption below 420 K, while the carbon monoxide desorbs molecularly between 350 and 500 K. Finally, the nitrogen adatoms combine and desorb as N_2 between approximately 700 and 810 K, regenerating the clean surface. In addition, for higher initial formamide coverages at 80 K, molecular adsorption occurs in an η^1(O)-bonded configuration, as on the oxygen-precovered suface. The η^1(O)–NH_2CHO either desorbs molecularly upon annealing to 225 K, or decomposes ($\leq$0.05 monolayer) to form an η^1(N)–NCHO species (5) near 300 K. This species decomposes below 375 K to adsorbed carbon monoxide, hydrogen and nitrogen. Annealing a saturated overlayer of formamide chemisorbed on Ru(001) at 80 K gives rise to the decomposition of approximately 0.15 monolayer of formamide. The principal decomposition mechanism of formamide on clean Ru(001) is depicted in Fig. 1(b).

In view of these results, the adsorption of formamide on a Ru(001) surface that has been presaturated with hydrogen is of obvious interest. The initial product of adsorption at 80 K could conceivably be η^1(O)–NH_2CHO as on Ru(001)-p(1x2)-O, η^2(C,O)–NH_2CO as on clean Ru(001), or η^2(C,O)–NH_2CHO. The formation of η^1(O)–NH_2CHO at 80 K rather than η^2(C,O)-bonded species

would suggest that hydrogen adatoms are effective in inhibiting the conversion of η^1(O)–NH_2CHO to η^2(C,O)-bonded species, through electronic and/or steric effects. If η^2(C,O)-bonded species are formed, the first η^2(C,O)-bonded adsorption product observed could be η^2(C,O)–NH_2CHO, rather than η^2(C,O)–NH_2CO as on clean Ru(001), if the preadsorbed hydrogen adatoms are effective in preventing CH bond cleavage of adsorbed formamide at 80 K. This might be expected not only because the fraction of vacant sites for hydrogen adatoms is much lower than on the clean surface, but also because the ruthenium-hydrogen binding energy is lower by approximately 4 kcal-mole^{-1} at high hydrogen coverages. The temperatures at which any conversions among these three species or any other observed reaction products occur, and the stability of the η^2(C,O)–NH_2CO species compared with the clean surface can be studied also in order to estimate changes in apparent kinetic barriers. Finally, it is possible that additional, hydrogenated intermediates (for example, a species containing a hydroxyl group) will be observed that are not formed on either clean Ru(001) or Ru(001)-p(1x2)-O.

In order to understand fully the reactions of formamide on a hydrogen-presaturated Ru(001) surface, it is necessary to understand the properties of hydrogen alone on Ru(001). A number of studies have dealt with this subject (**6-12**). At all temperatures investigated to date ($T \geq 80$ K), hydrogen adsorbs dissociatively on Ru(001). The hydrogen adatoms occupy threefold hollow sites exclusively, and no ordered overlayers are known to form at any coverage. The saturation coverage of hydrogen adatoms has been estimated to be 0.85 ± 0.15 monolayer (**6**). When the hydrogen-saturated Ru(001) surface is annealed, recombinative desorption of H_2 occurs between approximately 275 and 425 K, with a maximum desorption rate near 320 K and a shoulder near 380 K (**6,9**). This peak splitting is due to repulsive adatom-adatom interactions and/or a weakening of the ruthenium-hydrogen bond at high coverages. At saturation coverage, hydrogen adatoms give rise to two very weak EELS features near 840 and 1135 cm^{-1}, which are due, respectively, to the asymmetric and symmetric ruthenium-hydrogen stretching modes (**8,10**). Both of these loss features are sufficiently weak that they often cannot be observed when other surface species are present that give rise to loss features in the same frequency range.

The organometallic chemistry of formamide and related ligands containing an NCO group has

received considerable attention recently (13-33). The ligands η^1(O)–NH_2CHO, η^2(C,O)–NH_2CHO and η^2(C,O)-NH_2CO are of particular relevance to the present study. Compounds containing η^1(O)-bonded amide ligands have been synthesized and characterized in which the metal atom is Pt (II) (13) and Co (III) (14). The latter complex, $(NH_3)_5Co(NH_2CHO)^{3+}$, has a carbon-oxygen stretching frequency of 1675 cm^{-1}, in good agreement with that of 1660 cm^{-1} of η^1(O)–NH_2CHO on Ru(001)-p(1x2)-O (3,4). A number of compounds of rutheniuim- and osmium-containing η^2(C,O)–NR_2CO (R=H or alkyl) ligands have been synthesized (19-24), and while some infrared data are available, mode assignments have not, to our knowledge, been given. We know of no organometallic analogues of η^2(C,O)–NH_2CHO, although analogous η^2(C,O)-bonded formaldehyde (34) and acetone (35) ligands have been identified in organometallic compounds, and η^2(C,O)–H_2CO (36) and η^2(C,O)–$(CH_3)_2CO$ (37) have been identified previously on Ru(001). Both on the Ru(001) surface and in the organometallic compounds, these ligands have carbon-oxygen stretching frequencies between 1000 and 1300 cm^{-1}.

II. Experimental Details

The experimental techniques employed in this study were high-resolution electron energy loss spectroscopy (EELS) and thermal desorption mass spectrometry (TDMS). The EELS and TDMS experiments were performed in an UHV chamber that has been described in detail elsewhere (38). The home-built EEL spectrometer is of the Kuyatt-Simpson type, with electrostatic hemispheres serving as the energy dispersing elements in both the monochromator and analyzer. Typical experimental parameters for the EELS measurements were the following: impact energy, approximately 4 eV; resolution (full-width at half-maximum of the elastically scattered beam), 75 cm^{-1}; count rate, 2 x 10^5 cps in the elastically scattered beam; and (fixed) angle of incidence of the incident electron beam, 60° with respect to the surface normal. All EEL spectra were measured with electron collection in the specular direction, except as noted. The EEL spectra were measured after annealing the crystal at a rate of approximately 10 K-s^{-1} to an indicated temperature with immediate recooling of the surface to 80 K.

The UHV chamber was pumped by a 220 l-s^{-1} Varian noble vacion pump and a titanium sublimation pump. The background pressure was below 2 x 10^{-10} Torr during all EELS measurements, and the base pressure was below 5 x 10^{-11} Torr. Liquid nitrogen cooling allowed crystal temperatures as low as

80 K to be obtained routinely. The Ru(001) crystal was cleaned by annealing cycles between 1100 and 1500 K in a background of 5 x 10^{-8} Torr O_2, followed by annealing to 1650 K in vacuum. Occasionally, argon ion sputtering was also employed (1 keV, 1-2 μA current at the crystal for 2-3 hours). The Ru(001) surface was judged to be clean when it exhibited both a featureless EEL spectrum and H_2 thermal desorption spectra that are characteristic of the clean surface **(6,9)**.

The UHV chamber also contained a quadrupole mass spectrometer for performing thermal desorption measurements and for monitoring the purity of the gases introduced into the UHV chamber. All thermal desorption spectra were obtained with a heating rate of 6-10 K-s^{-1}. Exposures were effected by backfilling the UHV chamber through leak valves. The formamide used in this study was obtained from Aldrich (reported minimum purity of 99%), and the hydrogen was obtained from Matheson (reported minimum purity of 99.9995%). The detailed procedure of admitting formamide into the UHV chamber has been discussed elsewhere **(4)**.

III. Results

A. Thermal Desorption Mass Spectrometry

The clean Ru(001) surface at 80 K can be nearly saturated with hydrogen adatoms [$\theta_H \approx 0.85$ **(6)**] by exposure to 5L (1L ≡ 1 Langmuir ≡ 10^{-6} Torr-s) or more of H_2. When the hydrogen-presaturated surface is exposed to various fluxes of NH_2CHO at 80 K, the following species are detected in subsequent TDM spectra: NH_2CHO, CO, H_2 and N_2. The exposures quoted below were measured with an ionization gauge, and are uncorrected for the relative ionization probabilities of the various gases.

Figure 2 shows molecular NH_2CHO thermal desorption spectra (m/e = 45 amu) following various exposures of NH_2CHO to the hydrogen-presaturated Ru(001) surface at 80 K. For a 0.5 L exposure, no molecular desorption occurs, indicating that all of the adsorbed formamide decomposes upon heating. For exposures greater than 1 L, a desorption peak appears at 225 K; and for exposures greater than approximately 2.5 L, a second desorption peak appears at 210 K, the latter of which does not saturate with increasing exposures. In agreement with the results of our previous studies of formamide adsorption on clean Ru(001) and Ru(001)-p(1x2)-O **(2,4)**, the 210 K peak is attributed to the desorption of

condensed formamide multilayers, while the 225 K peak is due to the desorption of monolayer formamide. The temperatures of these two desorption peaks and the amount of formamide that desorbs in the 225 K peak are nearly identical within experimental error for both the clean and the hydrogen-presaturated surface. Both peaks appear at a lower exposure, however, on the hydrogen-presaturated surface.

Thermal desorption spectra of CO (m/e = 28 amu) are shown in Fig. 3 for saturation NH_2CHO exposures on both clean and hydrogen-presaturated Ru(001). A single CO thermal desorption peak is observed in each case, at 410 K on the clean surface, (a), and at 450 K on the hydrogen-covered surface, (b). On the clean surface, the CO thermal desorption peak occurs at 480 K following a 0.5 L NH_2CHO exposure and shifts downward continuously to 410 K at saturation (2). The downshift is much less pronounced on the hydrogen-precovered surface (from 470 to 450 K) consistent with the lower formamide coverages that are involved. Both EEL spectra [cf. Sec. III.B] and previous thermal desorption measurements following CO adsorption on Ru(001) (39) show clearly that the thermal desorption spectra of Fig. 3 result from molecularly adsorbed CO, rather than from the recombination and desorption of carbon and oxygen adatoms (40). The amount of CO that is desorbed following a saturation NH_2CHO exposure on hydrogen-presaturated Ru(001) allows the fractional surface coverage of formamide that decomposes to be estimated as approximately 0.05 monolayer, compared with 0.15 monolayer on the initially clean surface and 0.05 monolayer on Ru(001)-p(1x2)-O. The coverage of 0.05 monolayer corresponds to approximately 8×10^{13} formamide molecules-cm^{-2} (41).

Figure 4 shows hydrogen thermal desorption spectra (m/e = 2 amu) for a hydrogen-saturated Ru(001) surface, (a), and for a hydrogen-saturated Ru(001) surface that has been exposed to 6 L NH_2CHO, (b). As noted previously, thermal desorption spectra of H_2 from hydrogen-saturated Ru(001) show a peak at 320 K with a shoulder near 380 K. Thermal desorption spectra of H_2 from the hydrogen-presaturated surface with coadsorbed NH_2CHO show a desorption maximum at 305 K, a pronounced shoulder at 360 K and a weak shoulder at 405 K. As in the case of the decomposition of formamide on clean Ru(001) (2), the recombinative desorption of molecular nitrogen (m/e = 28 amu, with a cracking fragment at m/e = 14 amu) is observed. The range of desorption temperatures (approxi-

mately 740-810 K) and the peak temperature (approximately 770-790 K) are similar for similar coverages of irreversibly adsorbed formamide in the two cases.

B. Electron Energy Loss Spectroscopy

As noted previously, the adsorption of hydrogen on Ru(001) leads to the appearance of two very weak loss features near 840 and 1125 cm^{-1}. These are due to the asymmetric and symmetric ruthenium-hydrogen stretching modes, respectively, of hydrogen adatoms adsorbed in threefold hollow sites. The EEL spectrum of Fig. 5(a) is observed when the hydrogen-presaturated surface is exposed to 0.5 L NH_2CHO at 80 K. This exposure results in approximately 0.03 monolayer of molecularly adsorbed formamide. For comparison, Fig. 5(b) shows the EEL spectrum that results when the Ru(001) surface with an ordered p(1x2) overlayer of oxygen adatoms ($\theta_0 = 0.5$) is exposed to 0.5 L NH_2CHO at 80 K (**3,4**). Although there are slight differences in the frequencies and relative intensities of some loss features, it is clear that the same surface species is formed in both cases. This species has been identified previously as $\eta^1(O)$–NH_2CHO, molecularly chemisorbed formamide that is bonded to the surface via a lone pair of electrons on the oxygen atom of the formamide (**3,4**). The mode assignments for this species are given in Table I, and the frequencies compare well to those of liquid (**43**) and gas phase (**44**) formamide. The carbonyl stretching frequency of 1670 cm^{-1} is characteristic of a carbon-oxygen double bond and indicates clearly that no significant rehybridization of this bond has occurred. The assignment of the various NH_2 modes has been confirmed for $\eta^1(O)$–NH_2CHO on the Ru(001)-p(1x2)-O surface by measuring EEL spectra of adsorbed ND_2CHO (**4**). The identity of the weak loss feature at 670 cm^{-1} in Fig. 5(a) is uncertain, but it is possibly due to $\tau(NH_2)$. The loss features at 795 and 1115 cm^{-1} are too intense to be attributed solely to the ruthenium-hydrogen stretching modes of the coadsorbed hydrogen adatoms. The broad feature at 570 cm^{-1} in Fig. 5(b) is due to two overlapping loss features: δ(NCO) of $\eta^1(O)$–NH_2CHO at 525 cm^{-1}, and ν_s(RuO) of the coadsorbed oxygen adatoms at 585 cm^{-1}. Neither spectrum in Fig. 5 shows evidence for any formamide decomposition after adsorption at 80 K. The very weak loss feature near 2000 cm^{-1} in both spectra is due to less than 0.005 monolayer of carbon monoxide adsorbed from the chamber background (**42**).

The EEL spectra of Fig. 5(c) and (d) result when the hydrogen-presaturated Ru(001) surface at 80

K is exposed to 2 L and 4 L of formamide, respectively. Note by comparison to Fig. 2 that while Fig. 5(a) corresponds to a coverage where no formamide desorbs molecularly, Fig. 5(c) corresponds to a coverage where some formamide desorbs molecularly in the 225 K desorption peak, and Fig. 5(d) corresponds to a coverage where multilayer formamide is present. The EEL spectrum of Fig. 5(c) is also characteristic of η^1(O)-bonded formamide, but due to the increased coverage it shows some pronounced differences compared with Fig. 5(a). The most noticeable difference is the very intense, broadened and downshifted $\omega(NH_2)$ loss feature at 710 cm^{-1}, and the NH_2 stretching region shows a broad, multipeaked structure. These changes are attributable to hydrogen-bonding among the adsorbed formamide molecules (**43**). In addition, the 1115 cm^{-1} loss feature has been replaced by a sharper feature at 1050 cm^{-1}. The EEL spectrum of Fig. 5(d) shows similar changes, as well as an intense loss at 215 cm^{-1} due to a lattice mode of the formamide multilayers. A loss feature at 2400 cm^{-1} is also resolved, which is due to a combination band of the loss features at 710 and 1695 cm^{-1}. Similar changes in the EEL spectra of formamide on Ru(001)-p(1x2)-O at 80 K were also observed as the exposure was increased (**4**).

Annealing the Ru(001) surface represented by Fig. 5(a) briefly to 150 K (**45**) causes the partial conversion of η^1(O)–NH_2CHO to one or more different surface species, and by 200 K this conversion is complete. The same conversion occurs if the surface represented by Fig. 5(c) or (d) is annealed, but at slightly higher temperatures; the conversion is complete by 215 K following a 2 L formamide exposure and by 230 K following a 4L exposure. The EEL spectrum measured after annealing the surface of Fig. 5(a) to 200 K is shown in Fig. 6(a), and it is obviously very similar (but not identical) to the EEL spectrum of η^2(C,O)–NH_2CO on clean Ru(001) that is shown in Fig. 6(b). The intense ν(CO) loss feature of η^1(O)–NH_2CHO at 1660 cm^{-1} has disappeared completely, while a loss feature remains at 1585 cm^{-1} that is considerably stronger than the $\delta(NH_2)$ loss feature of η^1(O)–NH_2CHO. The intense δ(NCO) mode of η^1(O)–NH_2CHO has disappeared also, leaving a broad peak near 445 cm^{-1}, a weak peak at 300 cm^{-1}, and two rather intense peaks at 655 and 825 cm^{-1}. Loss features due to nitrogen-hydrogen and carbon-hydrogen stretching vibrations are present near 3335 and 2885 cm^{-1}, respectively, while a weak peak at 1975 cm^{-1} indicates the continuing presence of less than 0.005 monolayer of

coadsorbed carbon monoxide. Additional loss features are present at 1395, 1300, 1135 and 1015 cm^{-1}, with the last peak being very weak. The intensity of the 1135 cm^{-1} peak is due partially to ν_s(RuH) of hydrogen adatoms.

While the EEL spectrum of Fig. 6(a) is clearly similar to that of η^2(C,O)–NH_2CO on clean Ru(001), a significant difference is the presence of the ν(CH) loss feature at 2885 cm^{-1}, indicating that a species containing a carbon-hydrogen bond is present on the surface. Since this mode is not observed in the case of η^2(C,O)–NH_2CO on clean Ru(001) and because it loses little intensity in spectra measured 10° off-specular (**46**), it cannot be assigned as a combination band of the modes with loss features at 1300 and 1585 cm^{-1}, and the lack of the intense ν(CO) loss feature at 1660 cm^{-1} indicates that it cannot be due either to the presence of η^1(O)–NH_2CHO or to any other formamide species that maintains the carbonyl double bond. It is therefore attributed to η^2(C,O)–NH_2CHO, which is stabilized by the presence of coadsorbed hydrogen. A small amount of η^2(C,O)–NH_2CO might also be present on the surface represented by Fig. 6(a). Since these two species are expected to have rather similar EEL spectra, a clear distinction between the two cannot be made. The mode assignments for η^2(C,O)–NH_2CO on clean Ru(001) are listed in Table I along with those for η^2(C,O)–NH_2CHO from Fig. 6(a), and the EEL spectrum of Fig. 6(a) is discussed further in Sec. IV.

Annealing the surface to 250 K [cf. Fig. 6(c)] results in the disappearance of the ν(CH) loss feature, indicating that the conversion of η^2(C,O)–NH_2CHO to η^2(C,O)–NH_2CO has gone to completion. The intensity of the carbon monoxide loss feature at 1975 cm^{-1} has increased significantly, suggesting that approximately 0.01 monolayer of η^2(C,O)–NH_2CO has decomposed to carbon monoxide, NH and hydrogen adatoms (vide infra). In addition, the loss features at 825 and 1135 cm^{-1} have decreased somewhat in intensity relative to the other loss features in the spectrum. After annealing the surface to 300 K, all loss features due to η^2(C,O)–NH_2CO have disappeared completely. This is true for all formamide coverages.

Figure 7(a), (b) and (c) show the EEL spectra obtained after annealing the same surface to 300, 350 and 500 K, respectively. Figure 7(c) shows only a single loss feature at 575 cm^{-1} due to ν_s(RuN) of nitrogen adatoms, consistent with the thermal desorption results which indicate that only nitrogen

desorbs from the surface above 500 K. Since this loss feature disappears upon annealing to 850 K, its identification with nitrogen adatoms is unambiguous. The spectra of Fig. 7 measured after annealing the surface to 300 and 350 K show intense loss features at 445 and 1990 cm^{-1}, which are due to ν(Ru-CO) and ν(CO) of approximately 0.03 monolayer of carbon monoxide (**47**). In addition, Fig. 7(a) shows losses at 800, 1140, 1395, 1660 and 3315 cm^{-1}, and Fig. 7(b) shows losses at 1375 and 3310 cm^{-1}. The loss features near 3310 and 1375 cm^{-1} disappear concomitantly near 400 K, and are assigned to ν(NH) and δ(NH), respectively, of an NH species, in accordance with our previous results for formamide decomposition on clean Ru(001) (**2**). The disappearance of these loss features upon annealing to 400 K correlates with the appearance of the 575 cm^{-1} loss feature, indicating that the NH decomposes to nitrogen and hydrogen adatoms as on clean Ru(001) (**2**). The loss features at 800 and 1140 cm^{-1} are attenuated greatly upon annealing from 300 to 350 K, and are due primarily to the presence of hydrogen adatoms. The 1660 cm^{-1} loss feature is assigned to ν(CO) of a small amount of η^1(O)–NH_2CHO that is readsorbed from the chamber background, in agreement with our previous results for formamide adsorption on Ru(001)-p(1x2)-O (**4**). Note that such a small amount of η^1(O)–NH_2CHO could be present in any of the EEL spectra of Fig. 6 and would be barely detectable due to overlap with the loss feature near 1590 cm^{-1}. In summary, our EELS results indicate that the stable decomposition products of η^2(C,O)–NH_2CO on hydrogen-presaturated Ru(001) are CO, NH and hydrogen adatoms. As on clean Ru(001) (**2**), there is no evidence for the formation of a stable NH_2 species, although the possibility that very small amounts of NH_2 might be present cannot be ruled out completely based on the EELS data alone.

IV. Discussion

On hydrogen-presaturated Ru(001) at 80 K, formamide adsorbs molecularly through a lone pair of electrons on the oxygen atom in an η^1(O)-bonded configuration. The bonding of η^1(O)–NH_2CHO to the surface may be thought of as a Lewis acid-Lewis base interaction, with the surface acting as a Lewis acid and the formamide as a Lewis base. This η^1(O)–NH_2CHO is the same molecular species that is formed on Ru(001)-p(1x2)-O at 80 K (**3,4**), and is quite different from the η^2(C,O)–NH_2CO which is formed following low exposures of formamide on clean Ru(001) at 80 K [although

η^1(O)–NH_2CHO is formed following high formamide exposures on clean Ru(001)] (**2**). Thus, the preadsorption of hydrogen makes a quantitative difference in the bonding of formamide on Ru(001) at 80 K, just as the preadsorption of oxygen does.

It is of interest that both a saturation hydrogen coverage (θ_H ~ 0.85) and an ordered p(1x2) overlayer of oxygen adatoms (θ_O = 0.5) cause the same alteration of the bonding of formamide to Ru(001) at 80 K (compared with the clean surface). The fact that η^1(O)–NH_2CHO is formed on hydrogen-presaturated Ru(001) rather than η^2(C,O)-bonded species indicates that the hydrogen adatoms increase the activation barrier for the formation of η^2(C,O)-bonded species. This increased activation barrier could result from either steric or electronic effects, or a combination of both. Due to the very similar electronegativities of ruthenium (2.2) and hydrogen (2.1) (**47**), the adsorption of hydrogen has only a small effect on the work function of the Ru(001) surface; a saturation hydrogen coverage at 95 K causes the work function to decrease by only 10 meV (**9**). This is in contrast to the formation of a p(1x2) oxygen adatom overlayer on Ru(001), which causes the work function of this surface to increase by 1.06 eV (**48**) and thus favors strongly lone pair donor bonding [e.g. η^1(O)-bonding] over η^2(C,O)-bonding, the latter of which involves significant electron backdonation from the surface metal atoms to the π^* orbital(s) of the ligand. Nevertheless, the formation of (nearly) a complete monolayer of ruthenium-hydrogen bonds with a bond strength of approximately 60 kcal-mol^{-1} must have a significant effect on the nature of the ruthenium-formamide interaction at 80 K. While the Fermi level of the Ru(001) surface is raised slightly by a saturation hydrogen coverage (as evidenced by the small work function decrease), the local density of states at the Fermi level will be *decreased* due to the "tying up" of electrons involved in covalent bonding to the hydrogen. This effect could make backdonation less facile than on the clean surface and thus increase the activation barrier for the η^1(O)–NH_2CHO to η^2(C,O)–NH_2CHO conversion.

It should be noted that while the same η^1(O)–NH_2CHO species is formed on hydrogen-presaturated Ru(001) and Ru(001)-p(1x2)-O at 80 K, different decomposition products of this species are observed in each case which can be correlated with the different perturbations of the ruthenium by the hydrogen and the oxygen. On the hydrogen-presaturated surface, where the separation between the

Fermi level and the formamide π^* orbital is 1.07 eV less than on the oxygen-precovered surface, the η^1(O)–NH_2CHO converts to η^2(C,O)–NH_2CHO, which undergoes significant carbon-oxygen bond rehybridization that results in part from electron backdonation from the metal to the formamide π^* orbital. On the other hand, η^1(O)–NH_2CHO on Ru(001)-p(1x2)-O converts to η^2(N,O)–NH_2CHO, which bonds to the surface via lone pair donor bonds on both the oxygen and nitrogen atoms. Thus, on hydrogen-presaturated Ru(001), the η^1(O)–NH_2CHO converts to the molecularly adsorbed species with the greatest metal-to-formamide charge transfer, while on Ru(001)-p(1x2)-O it converts to the molecularly adsorbed species with the greatest formamide-to-metal charge transfer.

The conversion of the initially adsorbed η^1-formamide species to η^2(C,O)-bonded species is in agreement with our previous assignment of the former as being η^1(O)-bonded rather than η^1(N)-bonded, since the conversion of an η^1(N)-bonded to an η^2(C,O)-bonded species is unlikely. The η^1(O)-bonding configuration is expected to be favored over η^1(N)-bonding for molecular formamide, because in the gas phase molecule there is no electron lone pair strictly localized on the nitrogen atom due to the partial double bond character of the carbon-nitrogen bond (which results in a planar structure for the gas phase molecule). It has been noted previously (**4**) that the observed ν(CO) frequency of the η^1-bonded formamide of approximately 1670 cm^{-1}, which is substantially reduced from the gas phase value of 1734 cm^{-1} (**44**), provides additional support for η^1(O)-bonding. This is in agreement with IR data for the organometallic compounds trans-$PtCl_2(C_2H_4)(NH_2CONH_2)$ and trans-$PtCl_2(C_2H_4)[(CH_3)_2NCHO]$, where a decrease in the frequency of ν(CO) upon coordination was observed for both urea and dimethylformamide, and was taken as evidence that the urea and dimethylformamide ligands are O-bonded rather than N-bonded (**14**). In contrast, the N-bonded urea ligands in trans-$PtCl_2(urea)_2$ exhibit ν(CO) at 1725 cm^{-1}, 46 cm^{-1} higher than ν(CO) in free urea (**14**).

The EEL spectra that were measured following annealing of the hydrogen-saturated Ru(001) surface with a few hundreths of a monolayer of adsorbed η^1(O)–NH_2CHO to 200 K [cf. Fig. 6(a)] are quite similar to those of η^2(C,O)–NH_2CO on clean Ru(001) (**2**), but a significant difference is the presence of the loss feature at 2885 cm^{-1} due to a carbon-hydrogen stretching mode. This indicates that a species containing a carbon-hydrogen bond is present, and since the ν(CH) loss feature is as strong as

that in Fig. 5(a) while the strong modes at 1660 and 525 cm^{-1} have disappeared completely, it cannot be attributed to residual η^1(O)–NH_2CHO. Possible decomposition products of formamide that contain carbon-hydrogen bonds also cannot account for this loss feature. For example, the observed frequency of 2885 cm^{-1} is approximately 100 cm^{-1} lower than the ν(CH) frequencies of methylidyne (**49,50**) and η^2(C,O)-NHCHO [and the remainder of the EEL spectrum of Fig. 6(a) is not consistent with the latter] (**3,4**). No strong loss feature is observed between approximately 1700 and 1800 cm^{-1}, as would be expected for either η^1(N)–NCHO or η^1(N)-NHCHO (**33**). A formyl (CHO) species is not expected to be stable on Ru(001) at 200 K, since η^1(C)-HCO was not observed in the decomposition of formaldehyde on Ru(001) at 80 K (**36**), and η^2(C,O)-HCO is not stable above 120 K on this surface (**36**). In addtion, there is no evidence for the production of NH_3 or NH at or below 200 K. Thus, this loss feature is interpreted as being due to the presence of η^2(C,O)–NH_2CHO, which is stabilized with respect to carbon-hydrogen bond cleavage by the large concentration of hydrogen adatoms on the surface.

The EEL spectrum of η^2(C,O)–NH_2CHO is expected to be similar to that of η^2(C,O)–NH_2CO, though not identical. Only a single resonance structure can be written for di-σ-bonded η^2(C,O)–NH_2CHO, and the carbon-nitrogen and carbon-oxygen bonds are expected to be pure single bonds:

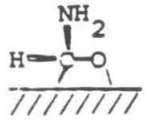

A π-bonded structure containing a carbon-oxygen double bond is also possible for η^2(C,O)–NH_2CHO, but is not expected to contribute significantly to the actual structure of this ligand on the ruthenium surface. On the other hand, three different resonance structures can contribute to the structure of η^2(C,O)–NH_2CO:

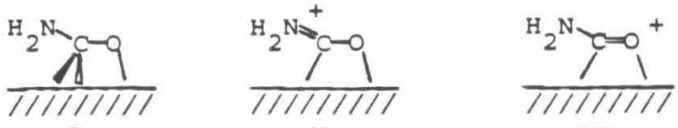

(i) (ii) (iii)

Thus η^2(C,O)–NH_2CHO is expected to have lower ν(CN) and ν(CO) frequencies than η^2(C,O)–NH_2CO, and probably also differing amounts of coupling of these modes to the various NH_2 deformation modes [e.g., less coupling to $\delta(NH_2)$ near 1585 cm^{-1} and more to $\omega(NH_2)$ near 820 cm^{-1}]. Since the EEL spectrum of Fig. 6(a) is so similar to that of η^2(C,O)–NH_2CO on clean Ru(001) [Fig. 6(b)], one possible interpretation of this spectrum is that it is due to a mixture of η^2(C,O)–NH_2CO and η^2(C,O)–NH_2CHO. A more likely possibility, however, is that resonance structure (i) is by far the most important in the actual structure of η^2(C,O)–NH_2CO, so that the carbon-oxygen and carbon-nitrogen bonds are essentially single bonds in both surface species. The marked changes in the frequencies and intensities of the ruthenium-ligand stretching modes below 500 cm^{-1} on the hydrogen-presaturated surface compared with the clean surface no doubt result from both the different bonding geometry of η^2(C,O)–NH_2CHO compared with η^2(C,O)–NH_2CO and a perturbation of the bonding of both species on the hydrogen-presaturated surface caused by the coadsorbed hydrogen adatoms.

Further annealing of the surface, which has been exposed to 0.5 L of formamide, to 250 K reduces the ν(CH) loss feature to the level of noise, consistent with the complete conversion of the η^2(C,O)–NH_2CHO to η^2(C,O)–NH_2CO. The increase in the intensity of the loss feature due to ν(CO) of carbon monoxide indicates that some of the η^2(C,O)–NH_2CO (approximately 0.01 monolayer) has decomposed to CO, NH and hydrogen adatoms. The decrease in the intensity of the 1135 cm^{-1} loss feature upon annealing from 200 to 250 K suggests that at 200 K this mode derives most of its intensity from a carbon-hydrogen bending mode of η^2(C,O)–NH_2CHO rather than from ν_s(RuH) of hydrogen adatoms, since very little surface hydrogen desorbs below 250 K. The decomposition of η^2(C,O)–NH_2CO to CO, NH and hydrogen adatoms is complete after annealing to 300 K. Low coverages ($\theta < 0.05$) of η^2(C,O)–NH_2CO on Ru(001) are thus stabilized slightly by the presence of hydrogen adatoms, since the decomposition of a similar coverage of η^2(C,O)–NH_2CO on clean Ru(001) is complete by 250 K (2). However, for a saturation coverage of formamide on clean Ru(001), a small amount of η^2(C,O)–NH_2CO is stable to 280 K, as on the hydrogen-presaturated surface.

A surprising aspect of the decomposition of η^2(C,O)–NH_2CO on the hydrogen-presaturated surface is that we did not detect the formation of ammonia either by EELS or TDMS. On clean Ru(001),

the decomposition of η^2(C,O)–NH_2CO led to the formation of both NH and ammonia, although the former was the principal NH_x decomposition product (2). The ammonia was detected in EEL spectra by the observation of the very intense $\delta_s(NH_3)$ mode at 1160 cm^{-1} and also by the weak $\delta_a(NH_3)$ mode at 1590 cm^{-1}, while mass 17 thermal desorption spectra showed clearly a desorption peak near 300 K that correlated with the disappearance of these two loss features. The production of both NH and ammonia on the clean surface is believed to result from the dehydrogenation and hydrogenation of a short-lived NH_2 species that is not spectroscopically isolated, i.e.

$$\eta^2(C,O)\text{–}NH_2CO \longrightarrow CO + [NH_2]$$

$$[NH_2] \xrightarrow{} NH + H$$

$$[NH_2] \xrightarrow{+H} NH_3$$

From this point of view, the ratio of NH_3 to NH that are formed would be expected to increase as the concentration of hydrogen adatoms on the surface is increased. It is possible that a small amount of ammonia could be formed on the hydrogen-presaturated surface without being detected spectroscopically, especially if its desorption is reaction-limited in the presence of surface hydrogen at 250-300 K. Another possibility is that the η^2(C,O)–NH_2CO undergoes NH bond cleavage prior to CN bond cleavage on the hydrogen-precovered surface, due to repulsive interactions between coadsorbed carbon monoxide and hydrogen (51). Once a single NH bond has been cleaved (to produce presumably a short-lived NHCO species), it is unlikely that any ammonia will be formed, since adsorbed NH does not appear to react with coadsorbed hydrogen adatoms to form ammonia under these conditions on this surface (2).

The amount of formamide that decomposes (i.e., the amount that adsorbs irreversibly) following a saturation formamide exposure on hydrogen-presaturated Ru(001) is approximately 0.05 monolayer, compared with 0.15 monolayer on clean Ru(001). The fact that preadsorbed hydrogen inhibits the chemisorption and decomposition of formamide on Ru(001) is not surprising. Similar coverages of hydrogen have been found previously to inhibit significantly the irreversible adsorption of ethylene (52) and acetylene (53) on Ru(001). In addition, a saturation hydrogen coverage was found to block completely the adsorption of oxygen on this surface at 80 K (12).

In addition to decomposing, some of the $\eta^1(O)$–NH_2CHO desorbs molecularly following formamide exposures of approximately 1 L or more on hydrogen-presaturated Ru(001), as evidenced by the 225 K molecular formamide thermal desorption peak. Note that this desorption temperature is not inconsistent with the EEL spectrum of Fig. 7(a), which corresponds to a 0.5 L exposure. As pointed out previously, the $\eta^1(O)$- to $\eta^2(C,O)$-bonding conversion occurs at slightly higher temperatures for higher coverages. Using Fig. 2 to estimate the formamide exposure corresponding to monolayer saturation as approximately 2.5 L and the exposure where molecular desorption begins as 0.8 L, and assuming a constant probability of adsorption of unity at 80 K (which is justified because multilayer condensation is observed), the amount of reversibly adsorbed formamide in the 225 K desorption peak is estimated to be very approximately 0.10 monolayer, compared with the approximately 0.05 monolayer that adsorbs irreversibly. We favor the assignment of the 225 K NH_2CHO desorption feature as being due to $\eta^1(O)$-NH_2CHO rather than second-layer formamide because it is unlikely that all of the $\eta^1(O)$-NH_2CHO would convert to $\eta^2(C,O)$–NH_2CHO and none would desorb at a temperature below that of H_2 desorption with a hydrogen adatom coverage of approximately 0.85 monolayer.

Hence, our results are consistent with the following overall decomposition mechanism for formamide on hydrogen-presaturated Ru(001) [(g) denotes a gas phase species; all other species are adsorbed]:

(1) $NH_2CHO(g) \rightarrow \eta^1(O)$–$NH_2CHO$

(2) $\eta^1(O)$–$NH_2CHO \rightarrow \eta^2(C,O)$–$NH_2CHO$

(3) $\eta^2(C,O)$–$NH_2CHO \rightarrow \eta^2(C,O)$–$NH_2CO + H$

(4) $\eta^2(C,O)$–$NH_2CO \rightarrow CO + NH + H$

(5) $NH \rightarrow N + H$

(6) $CO \rightarrow CO(g)$

(7) $2H \rightarrow H_2(g)$

(8) $2N \rightarrow N_2(g)$,

where reaction (4) is clearly not an elementary reaction. The intermediates of this decomposition reaction are analogous to those observed in the decomposition of formaldehyde on Ru(001), namely

η^1(O)–H_2CO, η^2(C,O)-H_2CO and η^2(C,O)-HCO (**36**).

V. Conclusions

The principal conclusions of this work can be summarized as follows:

1. Formamide adsorbs on hydrogen-presaturated Ru(001) (θ_H ~ 0.85) at 80 K via an electron lone pair on the oxygen atom in an η^1(O)–NH_2CHO configuration. This is the same bonding configuration as is observed for formamide adsorbed on Ru(001)-p(1x2)-O at 80 K, and is in contrast to the η^2(C,O)–NH_2CO species formed when low coverages of formamide are adsorbed on clean Ru(001) at 80 K [although some η^1(O)–NH_2CHO is formed on clean Ru(001) following high formamide exposures at 80 K]. Thus, the preadsorption of hydrogen influences the initial bonding configuration of formamide on this surface.

2. The saturation monolayer coverage of formamide on hydrogen-presaturated Ru(001) at 80 K is approximately 0.15 monolayer, of which 0.05 monolayer decomposes and 0.10 monolayer desorbs near 225 K. The preadsorbed hydrogen therefore passivates the surface with respect to formamide adsorption and decomposition, since on clean Ru(001) approximately 0.25 monolayer of formamide adsorbs in the monolayer at 80 K, of which 0.15 monolayer decomposes.

3. The η^1(O)–NH_2CHO formed on hydrogen-presaturated Ru(001) converts to η^2(C,O)–NH_2CHO below 200 K, and this species subsequently undergoes carbon-hydrogen bond cleavage below 250 K to form η^2(C,O)–NH_2CO. This is in marked contrast to the chemistry of η^1(O)–NH_2CHO on Ru(001)-p(1x2)-O, which converts to η^2(N,O)–NH_2CHO near 225 K and then undergoes nitrogen-hydrogen bond cleavage near 265 K to produce a formate-like η^2(N,O)-NHCHO species. Thus, the same surface species undergoes different reactions on Ru(001) surfaces that have been modified chemically by the presence of different adspecies (due to the different electronic and stearic effects that these adspecies produce).

4. The η^2(C,O)–NH_2CO formed on hydrogen-presaturated Ru(001) decomposes to yield CO, hydrogen adatoms and NH. The NH decomposes to nitrogen and hydrogen adatoms near 400 K; and CO, H_2 and N_2 desorb, regenerating the clean Ru(001) surface following annealing above 800 K.

Acknowledgments

This research was supported by the National Science Foundation (Grant # CHE-8617826).

References

1. See, for example, Refs. 36 and 37 below, and references therein, as well as a number of additional references in Ref. 4.
2. J. E. Parmeter, U. Schwalke and W. H. Weinberg, J. Am. Chem. Soc., in press.
3. J. E. Parmeter, U. Schwalke and W. H. Weinberg, J. Am. Chem. Soc. **109**, 1876 (1987).
4. J. E. Parmeter, U. Schwalke and W. H. Weinberg, J. Am. Chem. Soc. **109**, 5083 (1987).
5. The species formed near 300 K could also be assigned as η^1(N)-NHCHO. See Ref. 2 for details.
6. H. Shimizu, K. Christmann and G. Ertl, J. Catal. **61**, 412 (1980).
7. M. A. Barteau, J. Q. Broughton and D. Menzel, Surface Sci. **133**, 443 (1983).
8. H. Conrad, R. Scala, W. Stenzel and R. Unwin, J. Chem. Phys. **81**(12), 6371 (1984).
9. P. Feulner and D. Menzel, Surface Sci. **154**, 465 (1985).
10. P. J. Feibelman and D. R. Hamann, Surface Sci. **149**, 48 (1985).
11. J. Hrbek, J. Catal. **100**, 523 (1986).
12. J. Hrbek, J. Phys. Chem. **90**, 6217 (1986).
13. M. A. M. Meester, D. J. Stufkens and K. Vrieze, Inorg. Chim. Acta **16**, 191 (1976).
14. R. J. Balahura and R. B. Jordan, J. Am. Chem. Soc. **92**, 1533 (1970).
15. A. Sacco, P. Giannoccaro and G. Vasapoloo, Inorganica Chimica Acta **83**, 125 (1984).
16. A. E. Kruse and R. J. Angelici, J. Organomet. Chem. **24**, 231 (1970).
17. H. Behrens and A. Jungbauer, Z. Naturforsch. **34b**, 1477 (1979).
18. A. J. Lindsay, S. Kim, R. A. Jacobson and R. J. Angelici, Organomet. **3**, 1523 (1984).
19. R. Szostak, C. E. Strouse and H. D. Kaesz, J. Oranomet. Chem. **191**, 243 (1980).
20. A. Mayr, Y.-C. Lin, N. M. Boag and H. D. Kaesz, Inorg. Chem. **21**, 1704 (1982).
21. C. E. Kampe, N. M. Boag and H. D. Kaesz, J. Molecular Cat. **21**, 297 (1983).
22. P. J. Fagan, J. M. Manriquez, S. H. Vollmer, C. S. Day, V. W. Day and T. J. Marks, J. Am. Chem.

Soc. **103**, 2206 (1981).

23. H. Yasuda, T. Araki and H. Tani, J. Organomet. Chem. **49**, 103 (1973).

24. K. A. Azam, C. C. Yin and A. J. Deeming, J. Chem. Soc. Dalton Trans. 1201 (1978).

25. R. Rossi, A. Duatti, L. Magon, U. Casellato, R. Graziani and L. Toniolo, Inorganica Chimica Acta **74**, 77 (1983).

26. A. Sahajpal and R. D. Robinson, Inorg. Chem. **18**, 3572 (1979).

27. H.-U. Schwering and J. Weidlein, J., Chimia **27**, 535 (1973).

28. J. R. Jennings, K. Wade and B. K. Wyatt, J. Chem. Soc. (A), 2535 (1968).

29. R. D. Adams and N. M. Golembeski, J. Organomet. Chem. **171**, C21 (1979).

30. R. D. Adams, N. M. Golembeski and J. P. Selegue, Inorg. Chem. **20**, 1242 (1981).

31. Y. C. Lin, C. B. Knobler and H. D. Kaesz, J. Am. Chem. Soc. **103**, 1216 (1981).

32. H. D. Kaesz, C. B. Knobler, M. A. Andrews, G. van Buskhirk, R. Szostak, C. E. Strousse, Y. C. Lin and A. Mayr, Pure Appl. Chem. **54**, 131 (1982).

33. K. Burgess, B. F. G. Johnson and J. Lewis, J. Chem. Soc. Dalton Trans., 1179 (1983).

34. (a) K. L. Brown, G. R. Clark, C. E. L. Headford, K. Marsden and W. R. Roper, J. Am. Chem. Soc. **101**, 503 (1979). (b) S. Gambarotta, C. Floriani, A. Chiesi-Villa and C. Guastini, J. Am. Chem. Soc. **104**, 2019 (1982). (c) W. E. Buhro, A. T. Patton, C. E. Strouse, J. A. Gladysz, F. B. McCormick and M. C. Etter, J. Am. Chem. Soc. **105**, 1056 (1983).

35. (a) R. Countryman and B. R. Penfold, J. Cryst. Mol. Struct. **2**, 281 (1972). (b) T. T. Tsou, J. C. Huffman and J. K. Kochi, Inorg. Chem. **18**, 2311 (1979). (c) Additional references in Ref. 37(a).

36. A. B. Anton, J. E. Parmeter and W. H. Weinberg, J. Am. Chem. Soc. **107**, 5558 (1985); **108**, 1823 (1986).

37. (a) N. R. Avery, A. B. Anton, B. H. Toby and W. H. Weinberg, J. Elect. Spect. **29**, 233 (1983). (b) N. R. Avery, W. H. Weinberg, A. B. Anton and B. H. Toby, Phys. Rev. Letters **51**, 682 (1983). (c) A. B. Anton, N. R. Avery, B. H. Toby and W. H. Weinberg, J. Am. Chem. Soc. **108**, 684 (1986).

38. G. E. Thomas and W. H. Weinberg, Rev. Sci. Instr. **50**, 497 (1979);

39. (a) T. E. Madey and D. Menzel, J. Appl. Phys., Suppl. 2, Pt. 2, 229 (1974). (b) H. Pfnür, P. Feulner, H. A. Engelhardt and D. Menzel, Chem. Phys. Lett. **59**, 481 (1978). (c) H. Pfnür, P. Feulner and D. Menzel, J. Chem. Phys. **79**, 4613 (1983).

40. The recombinative desorption of carbon and oxygen adatoms, evolving CO, occurs with a maximum rate near 650 K on this surface. M. M. Hills, J. E. Parmeter and W. H. Weinberg, J. Am. Chem. Soc. **109**, 4224 (1987).

41. The density of surface ruthenium atoms is 1.58×10^{15} cm^{-2}.

42. (a) G. E. Thomas and W. H. Weinberg, J. Chem. Phys. **69**, 3611 (1978). (b) H. Pfnür, D. Menzel, F. M. Hoffmann, A. Ortega and A. M. Bradshaw, Surface Sci. **93**, 431 (1980).

43. I. Suzuki, Bull. Chem. Soc. Jap. **33**, 1359 (1960).

44. (a) J. C. Evans, J. Chem. Phys. **22**, 1228 (1954). (b) S. T. King, J. Phys. Chem. **75**, 405 (1971).

45. For suficiently high initial formamide coverages, some molecular desorption is observed also.

46. Vibrational modes that are primarily impact excited, including virtually all hydrogenic stretching modes, are approximately as strong in off-specular EEL spectra as in specular EEL spectra. This is in contrast to modes that are primarily dipole excited (and combination bands of such modes), which are much stronger on-specular. See H. Ibach and D. L. Mills, in "Electron Energy Loss Spectroscopy and Surface Vibrations" (Academic, New York, 1982), Chs. 1 and 3.

47. W. L. Jolly, in "The Principles of Inorganic Chemistry", McGraw-Hill, New York, 1976, p. 43.

48. T. E. Madey, H. A. Engelhardt and D. Menzel, Surface Sci. **48**, 304 (1975).

49. M. M. Hills, J. E. Parmeter, C. B. Mullins and W. H. Weinberg, J. Am. Chem. Soc. **108**, 3554 (1986).

50. J. E. Parmeter, M. M. Hills and W. H. Weinberg, J. Am. Chem. Soc. **108**, 3563 (1986).

51. E. D. Williams, P. A. Thiel, J. T. Yates, Jr. and W. H. Weinberg, J. Chem. Phys. **72**, 3496 (1980). While this paper deals with coadsorbed hydrogen and carbon monoxide on Rh(111), similar results are expected on Ru(001).

52. M. M. Hills, J. E. Parmeter and W. H. Weinberg, J. Am. Chem. Soc. **108**, 7215 (1986).

53. J. E. Parmeter, M. M. Hills and W. H. Weinberg, J. Am. Chem. Soc. **109**, 72 (1987).

Table I: Vibrational frequencies (in cm^{-1}) and mode assignments for various formamide-derived species on Ru(001)-p(1x2)-O, hydrogen-presaturated Ru(001) (θ_H = 0.85), and clean Ru(001). Data for gas phase and liquid formamide are given for comparison.

	NH_2CHO		$\eta^1(O)$–NH_2CHO		$\eta^2(C,O)$–NH_2CHO	$\eta^2(C,O)$–NH_2CO
Mode	Gas (44)	Liquid (43)	Ru(001)-p(1x2)-O θ_O = 0.5 (4)[a]	Ru(001)+H (this work)[a]	Ru(001)+H (this work)[b]	Ru(001) (2)
$\nu_a(NH_2)$	3545	3330	3490	3500	3335	3510[c]
$\nu_s(NH_2)$	3451	3190	3230	3220		3380[c]
ν(CH)	2852	2882	2940	2945	2890	-
ν(CO)	1734	1690	1660	1670	[d]	[d]
$\delta(NH_2)$	1572	1608	1585	1585	[d]	[d]
ν(CN)	1255	1309	⊤ 1360	⊤ 1355	[d]	[d]
δ(CH)	1378	1391	⊥	⊥	n.o	-
π(CH)	1030	1056	n.o.	n.o.	1135	-
$\rho(NH_2)$	1059	1090	1110	1115	[d]	[d]
$\omega(NH_2)$	289(?)	750	790	795	825	820
$\tau(NH_2)$	602	200	n.o.	670(?)	n.o.	n.o.
δ(NCO)	565	608	525	525	655	655
ν(Ru-ligand)	-	-	300	n.o.	300,445	270,360

a = asymmetric, s = symmetric, n.o. = not observed.

[a] These frequencies are based on 0.5 L formamide exposures. At higher coverages, some frequency shifts are observed due to hydrogen-bonding among the adsorbed molecules.

[b] These vibrational frequencies are based on the EEL spectrum of Fig. 6(a), in which some $\eta^2(C,O)$–NH_2CO may also be present.

[c] These modes are well-resolved only in off-specular spectra.

[d] In the case of $\eta^2(C,O)$–NH_2CHO, modes occur with frequencies of 1585, 1395, 1300 and 1015 cm^{-1}, which are due to $\delta(NH_2)$, $\rho(NH_2)$, ν_s(NCO) and ν_a(NCO). Since coupling among these modes is significant, specific assignments cannot be given. The situation is similar for $\eta^2(C,O)$–NH_2CO, which on clean Ru(001) exhibits loss features at 1580, 1370, 1300 and 1015 cm^{-1}.

Figure Captions

Figure 1. The principal decomposition mechanisms of formamide (a) on the Ru(001) surface with an ordered p(1x2) overlayer of oxygen adatoms (θ_0 = 0.5) and (b) on clean Ru(001). The NH and NH_3 that are formed from η^2(C,O)–NH_2CO decomposition on clean Ru(001) are probably formed via the dehydrogenation and hydrogenation of a short-lived NH_2 species which results upon carbon-nitrogen bond cleavage of η^2(C,O)–NH_2CO, but the NH_2 is not spectroscopically identified.

Figure 2. Thermal desorption spectra of molecular formamide (m/e = 45 amu) following various exposures of formamide to a hydrogen-presaturated Ru(001) surface at 80 K.

Figure 3. Thermal desorption spectra of CO (m/e = 28 amu) following saturation (8 L) formamide exposures on (a) clean Ru(001) at 80 K, and (b) a hydrogen-presaturated [10 L H_2 exposure] Ru(001) surface at 80 K.

Figure 4. Thermal desorption spectra of H_2 (m/e = 2 amu) from a Ru(001) surface that has been exposed to (a) 10 L H_2 (saturation) at 80 K, and (b) 10 L of H_2 followed by 8 L of NH_2CHO at 80 K.

Figure 5. The EEL spectra that result following (a) a 0.5 L NH_2CHO exposure on hydrogen-presaturated Ru(001), (b) a 0.5 L NH_2CHO exposure to Ru(001)-p(1x2)-O, (c) a 2 L NH_2CHO exposure to hydrogen-presaturated Ru(001), and (d) a 4 L NH_2CHO exposure to hydrogen presaturated Ru(001). All exposures were made, and all EEL spectra measured, with the surface held at a temperature of 80 K.

Figure 6. The EEL spectra that result from the following treatments of a Ru(001) surface: (a) 10 L H_2 followed by 0.5 L NH_2CHO and annealed to 200 K; (b) 0.5 L NH_2CHO; and (c) 10 L H_2 followed by 0.5 L NH_2CHO and annealed to 250 K. All exposures were made, and all EEL spectra measured, with the surface held at a temperature of 80 K.

Figure 7. The EEL spectra that result when a hydrogen-presaturated Ru(001) surface is exposed to 0.5 L NH_2CHO at 80 K and then annealed to (a) 300 K, (b) 350 K, and (c) 500 K.

$NH_2CHO/Ru(001)-p(1\times2)-O$

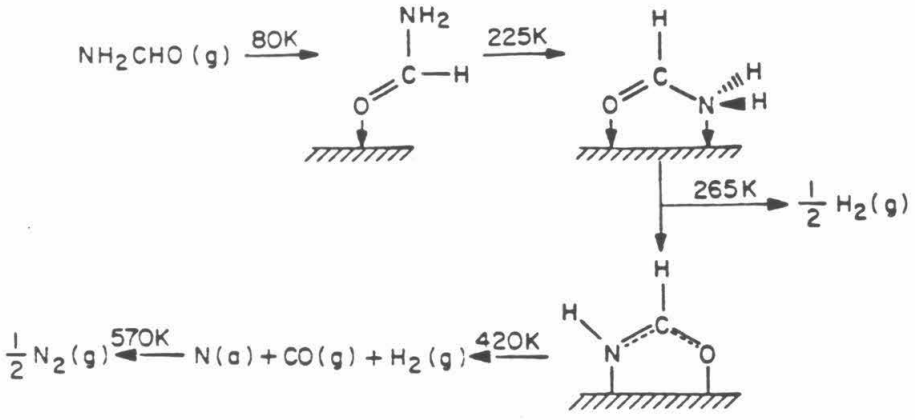

$NH_2CHO/Ru(001)$

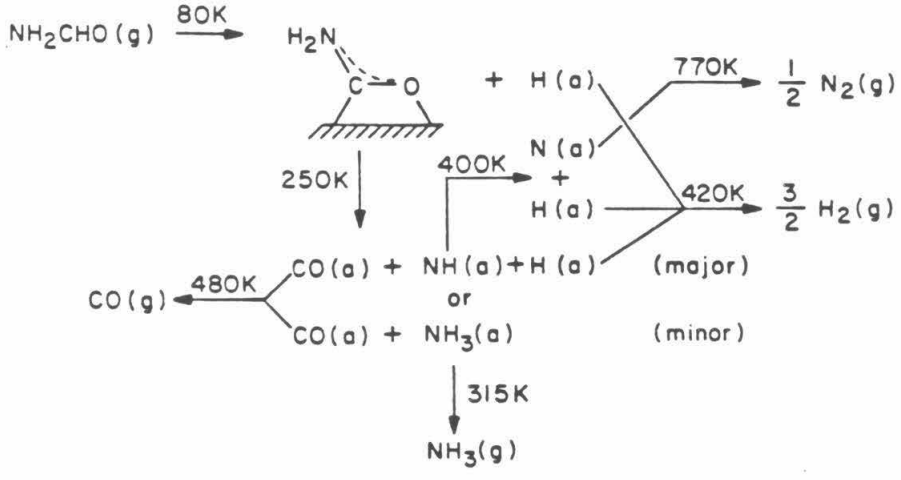

Figure 1

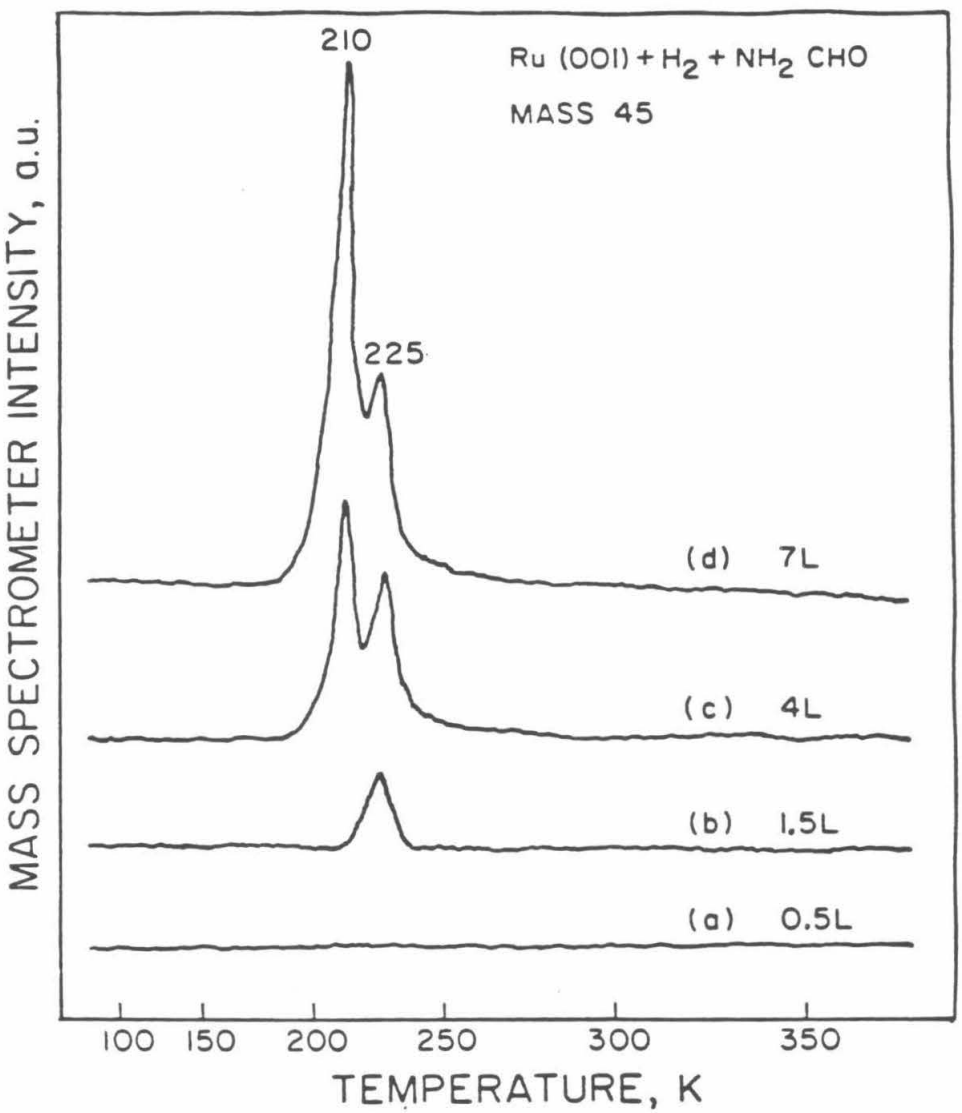
210
225
Ru (001) + H_2 + NH_2 CHO
MASS 45
(d) 7L
(c) 4L
(b) 1.5L
(a) 0.5L
MASS SPECTROMETER INTENSITY, a.u.
100 150 200 250 300 350
TEMPERATURE, K

Figure 2

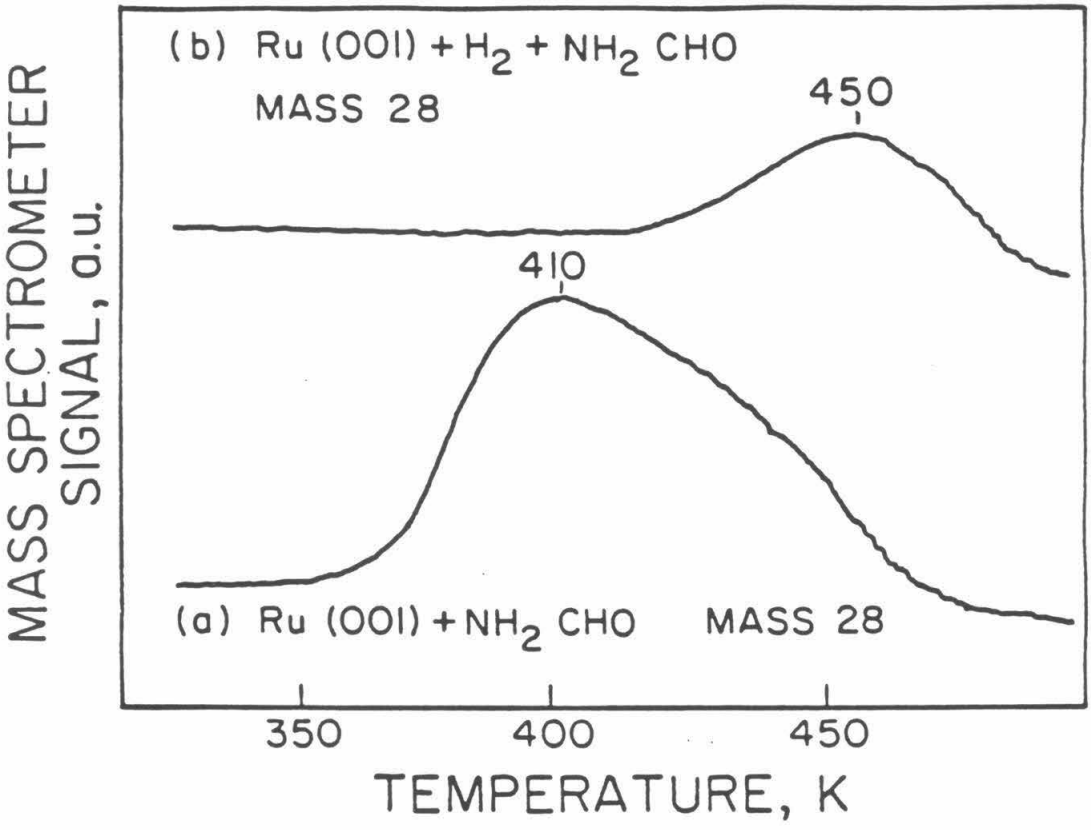
(b) Ru (001) + H_2 + NH_2 CHO
MASS 28
450
410
(a) Ru (001) + NH_2 CHO MASS 28
MASS SPECTROMETER SIGNAL, a.u.
350
400
450
TEMPERATURE, K

Figure 3

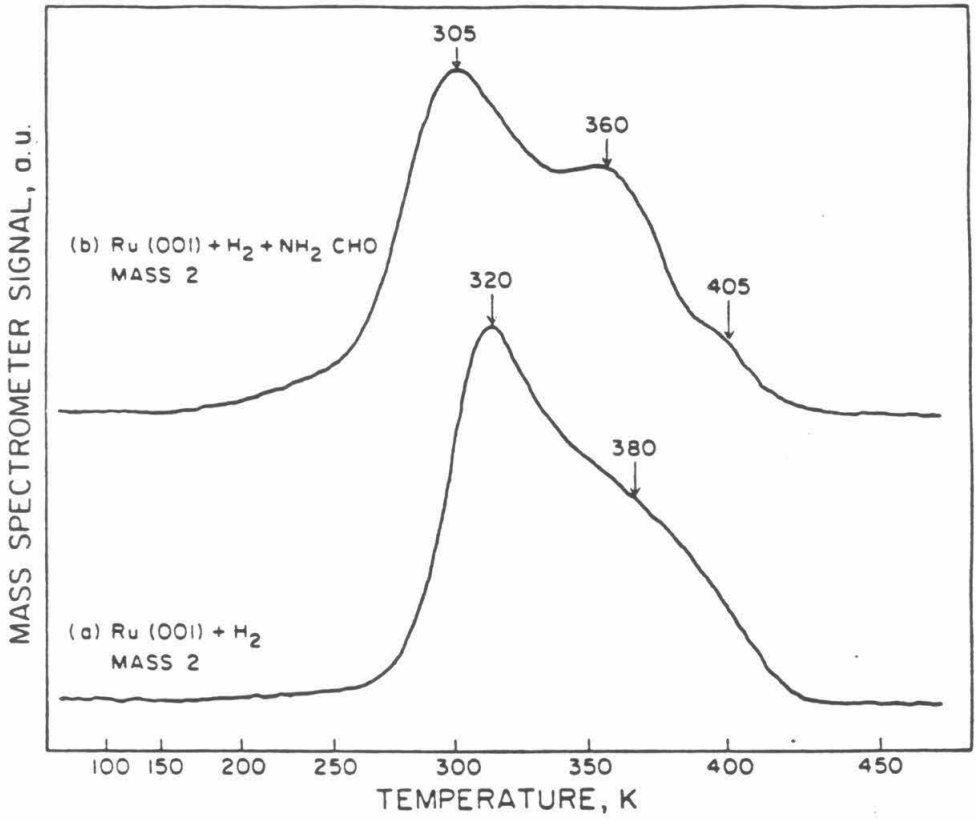
305
360
320
405
380
(b) Ru (001) + H_2 + NH_2 CHO
MASS 2
(a) Ru (001) + H_2
MASS 2
MASS SPECTROMETER SIGNAL, a.u.
100 150 200 250 300 350 400 450
TEMPERATURE, K

Figure 4

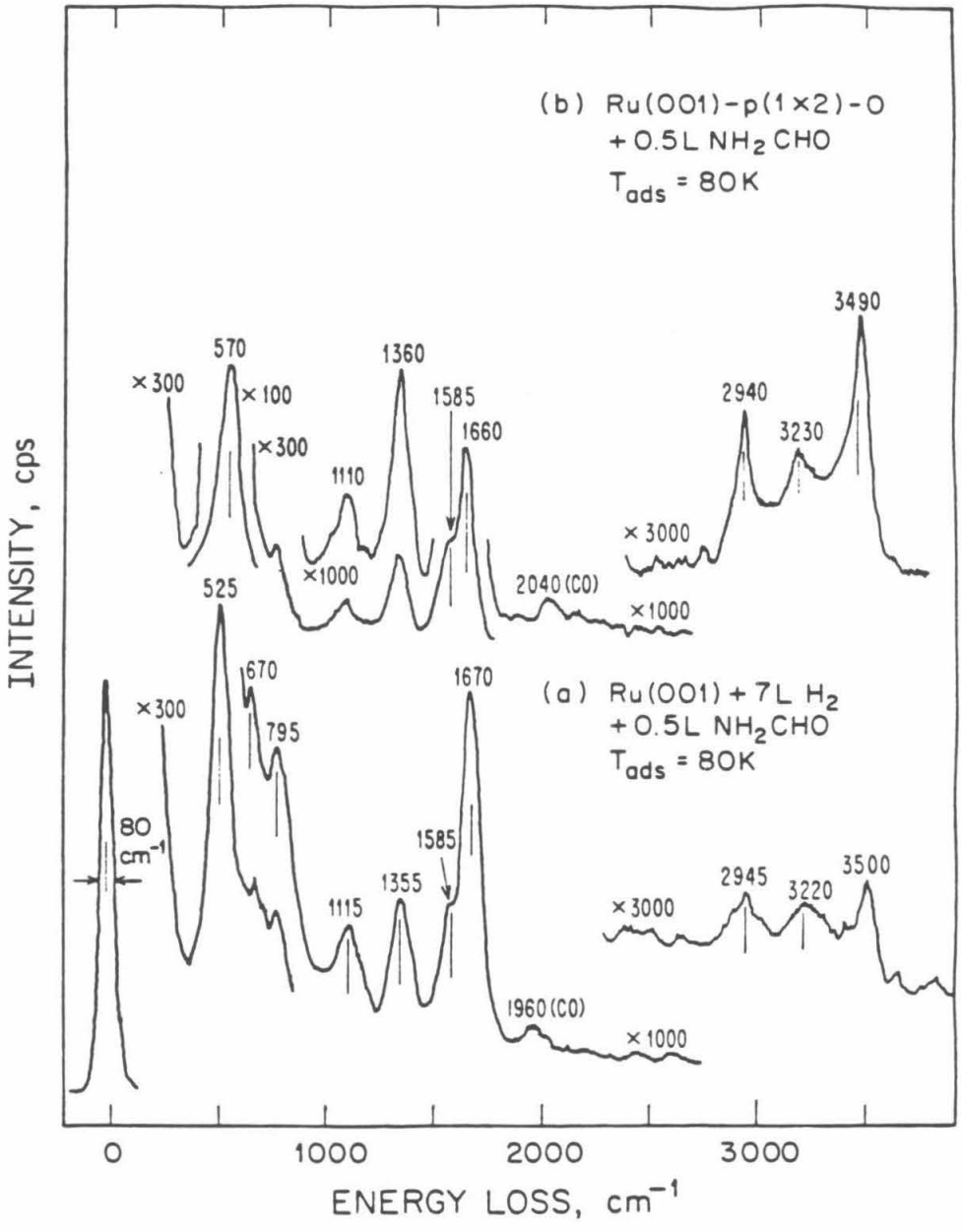
(b) Ru(001)-p(1×2)-O
+ 0.5L NH2CHO
Tads = 80K
×300
570
×100
×300
1360
1585
1660
1110
×1000
2040(CO)
×1000
×3000
2940
3230
3490
(a) Ru(001) + 7L H2
+ 0.5L NH2CHO
Tads = 80K
×300
525
670
795
80 cm-1
1115
1355
1585
1670
1960(CO)
×1000
×3000
2945
3220
3500
INTENSITY, cps
0
1000
2000
3000
ENERGY LOSS, cm-1

Figure 5

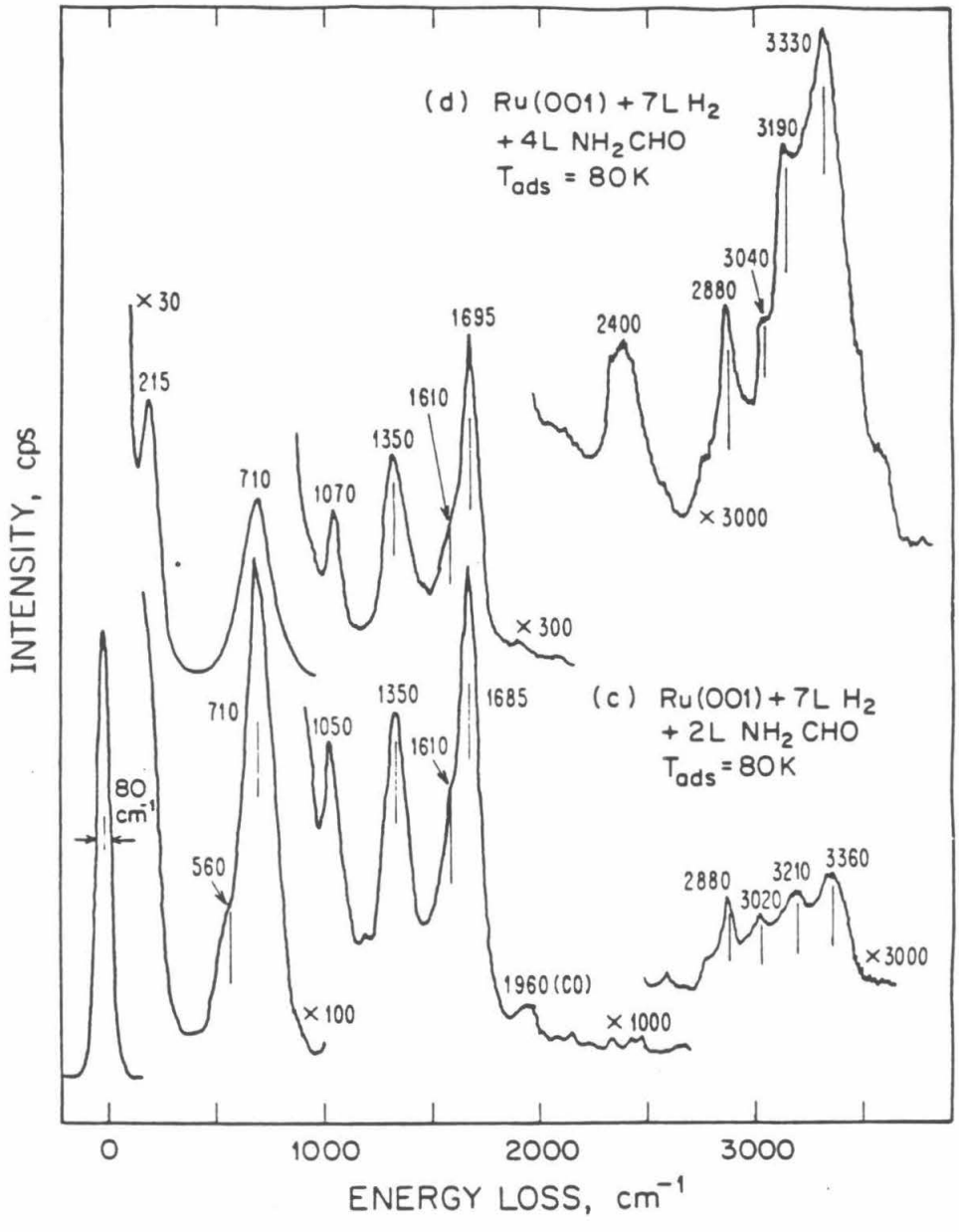
(d) Ru(001) + 7L H2
+ 4L NH2CHO
Tads = 80K
3330
3190
3040
2880
2400
1695
1610
1350
1070
710
215
×30
×3000
×300
(c) Ru(001) + 7L H2
+ 2L NH2 CHO
Tads = 80K
1685
1610
1350
1050
710
560
80 cm-1
2880
3020
3210
3360
×3000
1960 (CO)
×1000
×100
INTENSITY, cps
0
1000
2000
3000
ENERGY LOSS, cm-1

Figure 5

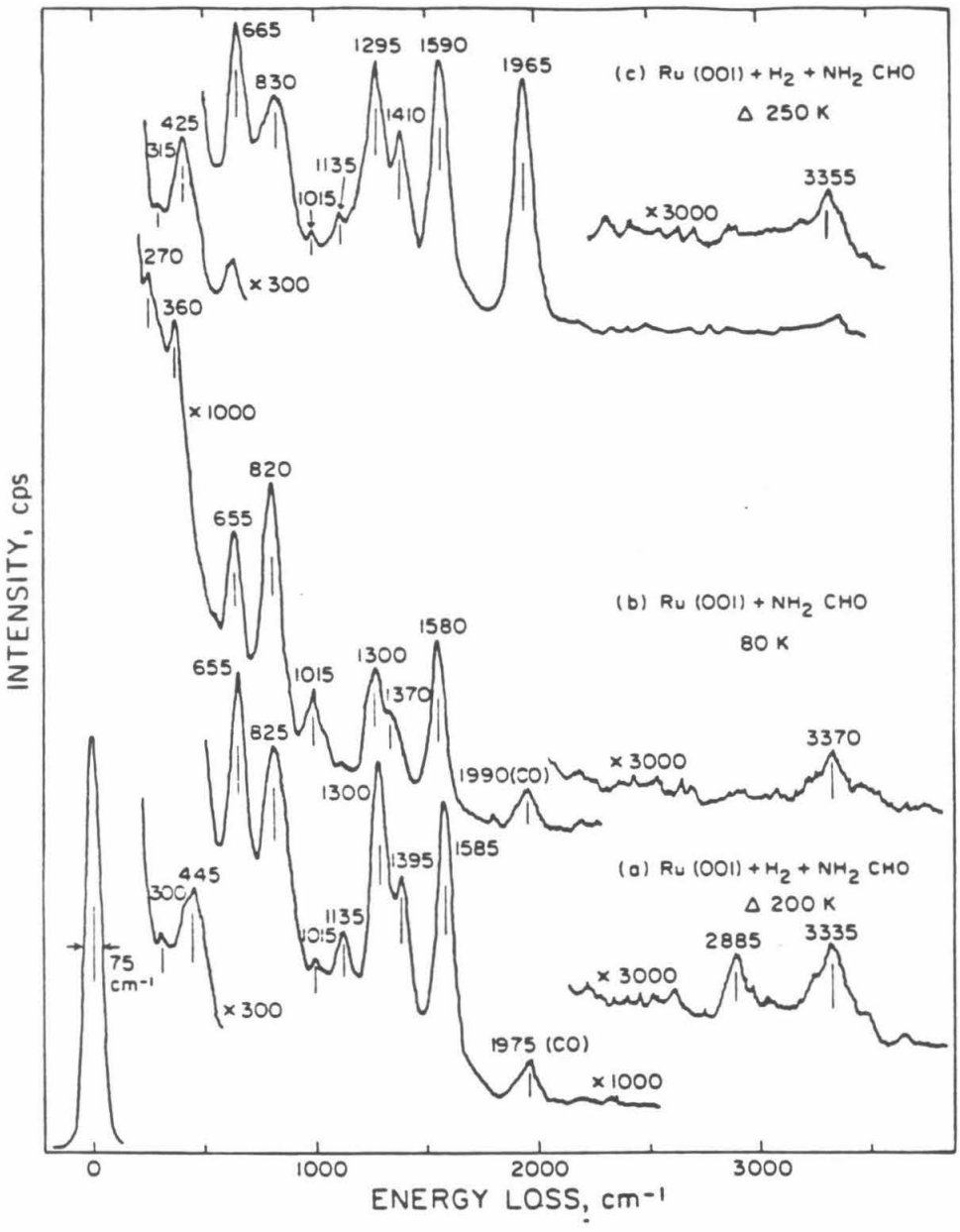
(c) Ru (001) + H_2 + NH_2 CHO
Δ 250 K
665
830
425
315
1135
1015
1295
1590
1410
1965
3355
×3000
270
×300
360
×1000
820
655
(b) Ru (001) + NH_2 CHO
80 K
655
1015
1300
1580
1370
825
1300
1990(CO)
×3000
3370
(a) Ru (001) + H_2 + NH_2 CHO
Δ 200 K
445
300
1135
1015
1395
1585
75 cm⁻¹
×300
2885
3335
×3000
1975 (CO)
×1000
INTENSITY, cps
0
1000
2000
3000
ENERGY LOSS, cm⁻¹

Figure 6

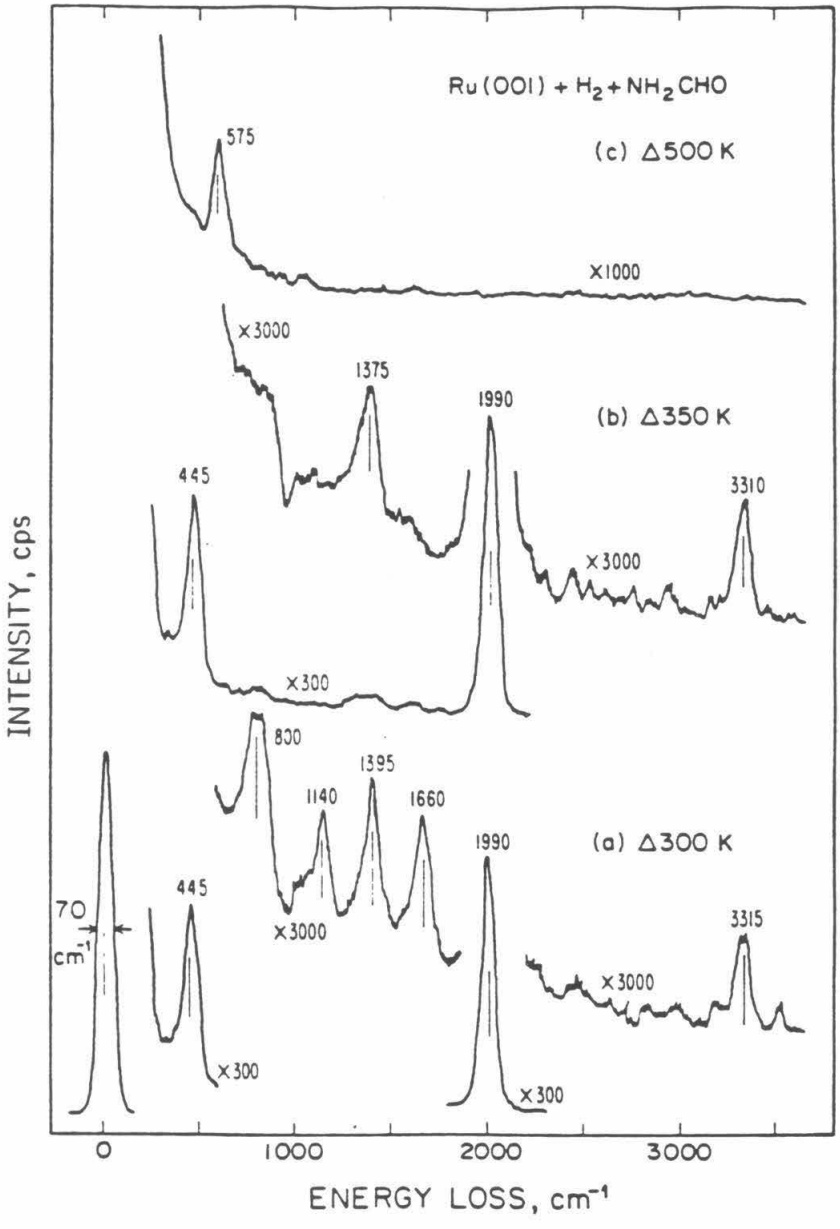
Ru(001) + H2 + NH2CHO
(c) Δ500 K
575
×1000
×3000
1375
1990
(b) Δ350 K
445
3310
×3000
×300
800
1395
1140
1660
1990
(a) Δ300 K
70 cm-1
445
3315
×3000
×3000
×300
×300
INTENSITY, cps
0
1000
2000
3000
ENERGY LOSS, cm-1

Figure 7

CHAPTER IX

Electron Energy Loss Spectroscopy of Ammonia on Ru(001)

[This chapter has been submitted as a paper by J. E. Parmeter, Y. Wang, C. B. Mullins and W. H. Weinberg, to *The Journal of Chemical Physics*.]

Abstract

The adsorption of ammonia on Ru(001) has been studied using high-resolution electron energy loss spectroscopy. Multilayer, second-layer and monolayer ammonia have been characterized vibrationally. These three states desorb near 115, 130 and between approximately 150 and 350 K, respectively. The symmetric deformation mode of chemisorbed ammonia shifts down in frequency continuously with increasing coverage from approximately 1160 cm^{-1} in the low-coverage limit to approximately 1070 cm^{-1} at (monolayer) saturation. The frequency of this mode in coordination compounds of ammonia is sensitive to the charge on the metal atom (increasing with increasing positive charge), and the frequency shift of this mode on the Ru(001) surface can be correlated with the work function decrease that this surface undergoes as the ammonia coverage increases. Off-specular EEL spectra allow the weak NH_3 rocking mode and the frustrated translation of the ammonia perpendicular to the surface (i.e. the metal-nitrogen stretch) of chemisorbed ammonia to be resolved near 625 and 340 cm^{-1}, respectively. These modes have not been identified in previous EELS studies of chemisorbed ammonia on hexagonally close-packed metal surfaces. Second-layer and multilayer ammonia yield EEL spectra similar to those observed on other metal surfaces. In agreement with previous results, the adsorption of ammonia on Ru(001) at 80 K, followed by annealing, leads only to reversible desorption.

I. Introduction

The adsorption of ammonia on well-defined single-crystalline metal surfaces under ultrahigh vacuum (UHV) conditions has received considerable attention in recent years (1-31). This subject is of interest both because it relates to industrial catalytic processes such as ammonia synthesis (32), and because ammonia is a prototypical example of a weak donor ligand that bonds to metal atoms both in organometallic compounds (33-42) and on surfaces via the electron lone pair on the nitrogen atom. As part of a continuing study of the chemistry of nitrogen-containing molecules on the hexagonally close-packed Ru(001) surface (43-48), we report here the results of a high-resolution electron energy loss spectroscopic (EELS) investigation of ammonia adsorption on this surface.

The interaction of ammonia with Ru(001) has been the focus of several previous studies (18-23). Danielson et al. (18) employed thermal desorption mass spectrometry (TDMS), Auger electron spectroscopy, and low-energy electron diffraction (LEED) to study this system, and concluded that for adsorption temperatures below 300 K the chemisorbed ammonia desorbed completely reversibly, with negligible dissociation occurring upon annealing. Dissociation could be induced only by electron beam bombardment of the adsorbed ammonia, or by exposing the surface to large fluences of ammonia with the surface temperature maintained above 300 K. Benndorf and Madey (21) used LEED, TDMS, electron stimulated desorption ion angular distribution (ESDIAD) measurements, and work function change ($\Delta\phi$) measurements to study ammonia adsorption on Ru(001), and also concluded that for low adsorption temperatures (approximately 80 K) ammonia adsorption is completely reversible. They showed that large ammonia exposures at 80 K lead to ammonia desorption over a broad temperature range, with monolayer desorption between approximately 150 and 350 K (and displaying weak maxima near 180 and 270 K), desorption of second-layer ammonia at 140 K, and multilayer desorption in a sharp peak at 115 K. Both ESDIAD and $\Delta\phi$ measurements supported the expected model of bonding for monolayer ammonia, namely via the lone pair of electrons on the nitrogen atom. The saturation monolayer coverage of chemisorbed ammonia was estimated to be approximately 0.25 monolayer (or 3.9×10^{14} molecules-cm^{-2}) based primarily on LEED data and in analogy to previous studies of ammonia adsorption on Pt(111) (5) and Ni(110) (11). It was also suggested that ammonia adsorbs in threefold hollow

sites on this surface.

Electron energy loss spectroscopy has been used previously to study ammonia adsorption on Pt(111) (3), Ni(111) (9), Ni(110) (9), Ag(110) (1), Ag(311) (2) and Fe (110) (28). In all cases, ammonia adsorbs molecularly at low temperatures (approximately 80-120 K) and only on Fe(110) (28) and Ni(110) (11) does significant dissociation occur as the surface is annealed. The EEL spectra of ammonia adsorbed in the monolayer are dominated in most cases by a strong loss feature occurring between approximately 1050 and 1170 cm^{-1}, which is due to the NH_3 symmetric deformation mode. Considerably weaker loss features occur in the frequency ranges of 1580-1650, 3200-3320 and 3340-3400 cm^{-1}, which are due, respectively, to the NH_3 asymmetric (degenerate) deformation, symmetric stretch and asymmetric (degenerate) stretch. The characteristic frequency ranges for the NH_3 rocking mode and the frustrated translation of the ammonia perpendicular to the surface (i.e. the metal-nitrogen stretch, $\nu(M-NH_3) \equiv T_z$) are much less certain, however. The NH_3 rocking mode has not been identified previously for chemisorbed ammonia on any metal surface, although a frequency of 720 cm^{-1} has been reported for second-layer ammonia on Pt(111) (3). The $\nu(M-NH_3)$ mode has been identified on only three of the metal surfaces studied, and there is a large variation in the reported values: 340 cm^{-1} on Fe(110) (28), 470 cm^{-1} on Ag(311) (2) and 570 cm^{-1} on Ni(110) (9). It was partly in the hope of identifying these latter two modes clearly that we undertook this study of ammonia on Ru(001). As in several of the previous studies, we have measured EEL spectra of both NH_3 and ND_3 in order to confirm our mode assignments. Several of the earlier studies have also characterized second-layer and multilayer ammonia vibrationally. As might be expected, the formation of a second-layer, molecularly adsorbed state (desorbing between 120 and 160 K) and of a multilayer state (desorbing between 110 and 120 K) appears to be a general feature of ammonia adsorption on these metal surfaces, and both the second-layers and the multilayers show some common EEL features on all surfaces on which they have been studied.

II. Experimental Details

The EEL spectrometer used in this study, and the UHV chamber housing it, have been described in detail elsewhere (49). The spectrometer employs 180° hemispheres as the energy dispersing

elements in both the monochromator and the analyzer. The analyzer is rotatable within the scattering plane to allow off-specular EEL spectra to be measured. Typical parameters used in obtaining the EEL spectra presented here were the following: energy of the electron beam incident on the surface, 4 eV; resolution (full-width at half-maximum of the elastically scattered beam), 50-85 cm^{-1}; count rate in the elastic peak, 1-3 x 10^5 counts per second; and (fixed) angle of incidence of the electron beam, approximately 60° with respect to the surface normal. All EEL spectra were collected in the specular direction, except as noted. All EEL spectra were recorded with the surface at a temperature of 80-100 K, after annealing to indicated temperatures.

The stainless steel UHV chamber was pumped by a 220 l-s^{-1} Varian noble vacion pump and a titanium sublimation pump. Typical working pressures during experiments were in the range of 1-3 x 10^{-10} Torr. The Ru(001) crystal could be cooled to 80 K using liquid nitrogen, and could be heated resistively to temperatures exceeding 1600 K. After each experiment, the surface was heated to 1000 K prior to the next exposure in order to desorb any trace amounts of atomic nitrogen (50) that might be formed as the result of ammonia decomposition at defects or the cracking of ammonia on hot filaments, as well as any residual hydrogen (51) and carbon monoxide (52) adsorbed from the chamber background. Periodic, extensive cleaning of the surface was accomplished both by argon ion sputtering and annealing the crystal in a background of oxygen. Surface cleanliness was verified by EELS, and by H_2 (51) and CO (52) thermal desorption spectra that are characteristic of the clean surface.

The UHV chamber also contains a quadrupole mass spectrometer for performing TDMS experiments, and for the analysis both of background gases and of the purity of the ammonia that was admitted into the chamber. The thermal desorption measurements performed in connection with this work were obtained with a heating rate of approximately 8 K-s^{-1}. The NH_3 used in these studies was obtained from Matheson (99.99% reported purity) and was purified by several freeze-pump-thaw cycles. The NH_3 exposures were performed by backfilling the UHV chamber through a leak valve, and the purity of the NH_3 was verified in situ using mass spectrometry. The ND_3 was obtained from MSD Isotopes (99 atom % D). Due to H/D exchange of the deuterated ammonia either on the walls of the UHV chamber or in the stainless steel leak lines, ND_3 could not be admitted into the chamber cleanly through

a leak valve and was therefore admitted into the chamber via a directional beam doser consisting of a microcapillary array. The purity of the ND_3 adsorbed on the surface was best monitored by comparing the integrated intensities of the ND and NH stretching vibrations measured in subsequent EEL spectra. All exposures were effected at a surface temperature of 80 K, except as noted.

III. Results

A. Thermal Desorption Mass Spectrometry

Since a detailed study of the thermal desorption of ammonia from Ru(001) has already been carried out (21), this subject was investigated only briefly, primarily to determine the appropriate ammonia exposures and annealing temperatures to obtain EEL spectra characteristic of multilayer, second-layer and (various coverages of) monolayer ammonia. In reasonable agreement with the previous results, we detect the desorption of second-layer ammonia at 130 K for exposures in excess of approximately 1 L (1 L ≡ 1 Langmuir ≡ 10^{-6} Torr-s), and the desorption of multilayer ammonia at 115 K for exposures exceeding approximately 2 L. While the two monolayer desorption maxima were not well resolved using our apparatus, our EELS results (cf. Sect. III.B) indicated that monolayer ammonia desorbed between approximately 150 and 350 K. This is also in good agreement with the previous results.

The possibility that some of the ammonia dissociates rather than desorbs as the surface is annealed was investigated briefly using H_2 thermal desorption. The H_2 thermal desorption spectra that were measured following saturation ammonia exposures were compared to those obtained following saturation hydrogen exposures on Ru(001). This allowed the maximum possible amount of ammonia that dissociates to be estimated by using the known saturation coverage of hydrogen adatoms (approximately 0.85 monolayer) on Ru(001) (51). The amount of hydrogen adatoms that desorbed was never greater than 0.03 monolayer, which corresponds at most to 0.01 monolayer of NH_3. This could correspond to the decomposition of a small amount of ammonia at defect sites. However, such a small amount of hydrogen desorption could also result from the adsorption of hydrogen from the residual gas or from a small hydrogen impurity in the ammonia sample. Thus, we are in complete agreement with the previous conclusion (18,21) that ammonia decomposition is negligible on Ru(001) following ammonia adsorption at 80-100 K.

B. Electron Energy Loss Spectroscopy

Electron energy loss spectra for several coverages of ammonia on Ru(001) at 80-90 K are shown in Fig. 1. The exposures involved correspond to submonolayer coverages; no second-layer or multilayer ammonia is present in any of these spectra with the exception of spectrum (d), where a very small amount of second-layer ammonia is probably present. Following a 0.1 L ammonia exposure, only a single loss feature is resolved at 1155 cm^{-1}. For larger ammonia exposures, this loss feature shifts downward in frequency, reaching approximately 1085 cm^{-1} following a 1 L exposure. It is by far the most intense loss feature for all submonolayer coverages, and is identified easily as being due to $\delta_s(NH_3)$, the symmetric deformation mode of molecularly adsorbed ammonia. At all coverages, it is strongly upshifted in frequency from its gas phase value of 950 cm^{-1} (53). Following a 0.5 L exposure, a second loss feature is observed at 3265 cm^{-1} due to the (unresolved) symmetric and asymmetric NH_3 stretching modes. Increasing the exposure to 0.7 L allows these two modes to be resolved at 3270 and 3370 cm^{-1}, respectively, and another loss feature becomes apparent at 1560 cm^{-1} which is assigned as the asymmetic deformation mode of ammonia, $\delta_a(NH_3)$. Following a 1 L exposure all of these loss features are again resolved, and a very weak loss feature appears at 2145 cm^{-1} which is assigned as the overtone of the NH_3 symmetric deformation. Another loss feature appears at 330 cm^{-1}. While this feature may derive some intensity from the very weak frustrated translational mode (normal to the surface) of the chemisorbed ammonia (cf. Fig. 3), it is most likely due primarily to the presence of a very small amount of second-layer ammonia, which exhibits an intense loss feature due to a librational mode at 360 cm^{-1} (cf. Fig. 6 and Table II). The vibrational frequencies of chemisorbed ammonia on Ru(001) are summarized in Table I, and compared to those of gas phase ammonia (53), and of ammonia chemisorbed on several other single crystalline metal surfaces. (Information is also included in this table that is derived from off-specular data, cf. Fig. 3.) It should be noted that while the weak loss features due to $\delta_a(NH_3)$, $\nu_s(NH_3)$ and $\nu_a(NH_3)$ occasionally were found to have frequencies differing by as much as ± 40 cm^{-1} from the average values listed in Table I, they showed no consistent frequency shifts as a function of coverage. Although such shifts would be difficult to detect due to the low intensities of these loss features, all of these features could usually be detected in off-specular spectra following

exposures as low as 0.5 L.

A typical EEL spectrum of a saturated monolayer of ND_3 on Ru(001) is shown in Fig. 2. The surface was prepared by exposing the Ru(001) crystal at 100 K to approximately 30 L ND_3, followed by annealing to 150 K to remove multilayer and second-layer ND_3. The intense $\delta_s(ND_3)$ mode occurs at 835 cm^{-1}. As in the case of $\delta_s(NH_3)$, the frequency of this mode was found to shift up with decreasing coverage, and it occurred near 910 cm^{-1} in the low coverage limit. The $\delta_a(ND_3)$, $\nu_s(ND_3)$ and $\nu_a(ND_3)$ modes occur at frequencies of 1165, 2335 and 2515 cm^{-1}, respectively. The frequencies of these modes are also listed in Table I, and the observed frequency shifts upon deuteration clearly support the assignments. A very weak loss feature is observed at 1455 cm^{-1} in Fig. 2. A similar loss feature was observed in the EEL spectrum of second-layer ND_3 on Pt(111) and was attributed to $\delta_a(ND_2H)$ of a small ND_2H impurity (3). The slight asymmetry on the high energy side of the $\delta_s(ND_3)$ loss feature could also be due to the presence of a small amount of ND_2H. The weak loss feature at 2930 cm^{-1} is most likely due to ν(CH) of a small hydrocarbon impurity (54).

Off-specular EEL spectra of both NH_3 and ND_3 allowed two additional loss features to be resolved clearly in the low-frequency region. Figure 3 shows EEL spectra of nearly saturated monolayers of (a) NH_3 and (b) ND_3 obtained with the analyzer rotated approximately 5° off-specular (towards the surface normal). In addition to the loss features observed in specular EEL spectra, Fig. 3(a) shows features at 625 and 340 cm^{-1}, and Fig. 3(b) shows features at 480 and 350 cm^{-1}. Based on the observed frequency shifts and a comparison to vibrational data for metal-amine compounds (cf. Sect. IV.A), the loss feature at 625(480) cm^{-1} is assigned to the $NH_3(ND_3)$ rocking mode, $\rho(NH_3)$, and the loss feature at 340(350) cm^{-1} is assigned to the frustrated translation of the ammonia perpendicular to the surface, $\nu(Ru–NH_3)$. Both of these modes are absent in gas phase ammonia, where the "rock" corresponds to a free rotation and the "frustrated translation" to a free translation of the molecule. The low intensity of the $\nu(Ru–NH_3)$ mode is consistent with previous results for ammonia adsorption on hexagonally close-packed metal surfaces, in which no metal-nitrogen stretching mode was resolved (3,9). Due to the low intensities of the $\rho(NH_3)$ and $\nu(Ru–NH_3)$ loss features, it is impossible to say whether or not these modes undergo frequency shifts as a function of coverage. Note that in the off-

specular EEL spectra presented here the $\delta_s(NH_3)$ [$\delta_s(ND_3)$] loss feature has decreased greatly in intensity relative to the other loss features of chemisorbed ammonia. This indicates that this mode is strongly dipole-enhanced in specular EEL spectra, while the remaining modes of chemisorbed ammonia are primarily impact excited (55). It should be noted that the $\rho(NH_3)$ mode was occasionally observed as a very weak shoulder in specular EEL spectra, near 650 cm^{-1} for NH_3 and near 500 cm^{-1} for ND_3. Indeed, such shoulders are barely visible in Figs. 1(d) and 2, but the frequency cannot be assigned accurately based on these spectra.

Figure 4 shows the variation in the frequency of the symmetric deformation mode of ammonia adsorbed on Ru(001) at 80 K as a function of the ammonia exposure. The exposure of 1 L corresponds to the coverage where the second-layer thermal desorption feature just begins to appear. However, this coverage does not correspond to monolayer saturation because the second layer begins to form before the monolayer is saturated (21); it is estimated that this exposure corresponds to approximately 80% of monolayer saturation or an absolute coverage of approximately 0.2 (56). Note that the assumption of a constant probability of adsorption, in agreement with the results of Benndorf and Madey (21) and as expected for NH_3 at 80 K given that ammonia multilayers condense at this temperature, means that the coverages are directly proportional to the ammonia exposure. The frequency of the $\delta_s(NH_3)$ mode decreases monotonically with increasing coverage, from approximately 1155 cm^{-1} following a 0.1 L NH_3 exposure to approximately 1085 cm^{-1} following a 1.0 L NH_3 exposure. The frequency decrease is very nearly linear with coverage, although there may be a slight decrease in the absolute value of the slope at high coverages. A linear least-squares fit to the data yields

$$\delta_s(NH_3) = -69.6\epsilon + 1157 , \qquad (1)$$

where $\delta_s(NH_3)$ is the frequency of the NH_3 symmetric deformation mode in cm^{-1}, and ϵ is the exposure in Langmuirs.

Figure 5 shows the variation with annealing temperature of the frequency of the symmetric deformation mode of ammonia adsorbed on Ru(001) for a number of different ammonia exposures at 80 K. Following all exposures, the surface was annealed first to 150 K to be certain that only monolayer ammonia was present. It may be seen by comparison to Fig. 4 that annealing from 80 to 150 K gen-

erally did not change the frequency of $\delta_s(NH_3)$ by more than 10 cm^{-1} for exposures of 1 L or less. Following a 0.1 L ammonia exposure, the frequency of $\delta_s(NH_3)$ is nearly constant at 1150-1160 cm^{-1} regardless of annealing temperature. This is consistent with the fact that the coverage is not changing for annealing temperatures between 80 and 300 K: for such a low exposure (i.e. coverage) the ammonia desorbs only in a single peak near 315 K (21). On the other hand, the exposures of 2.0 and 8.0 L correspond to exposures well in excess of monolayer saturation, and annealing the surface to 150 K in each case produces a saturated monolayer of ammonia. Thus the measured frequencies in these two cases should be the same for annealing temperatures of 150 K and greater, and this is found to be true within experimental error ($\pm$10 cm^{-1}). The measured frequencies increase markedly as the surface is annealed from 150 to 230 and 300 K, because for a saturated monolayer of ammonia, significant molecular desorption occurs in these temperature ranges (21). This results in a decrease in the coverage and thus an increase in the symmetric deformation frequency, as would be expected from an inspection of Fig. 4. For initial exposures of 0.5 and 1.0 L, the measured frequencies for any given annealing temperature fall between those obtained following 0.1 L or saturation exposures, and also increase (though less dramatically than for saturation exposures) with increasing annealing temperature. These results are all consistent with the $\delta_s(NH_3)$ frequency being a function of ammonia coverage only; the annealing temperature appears to have no effect other than to change the coverage. It should be noted that the two data points obtained following annealing to 350 K correspond to trivial amounts ($\leq$0.01 monolayer) of ammonia readsorbed from the chamber background, since the thermal desorption of ammonia from Ru(001) is complete between 300 and 350 K. The $\delta_s(NH_3)$ frequency of 1160 cm^{-1} thus corresponds to the zero-coverage limit for ammonia on Ru(001), in agreement with the data of Fig. 4 and Eq. (1).

Electron energy loss spectra of second-layer NH_3 and ND_3 on Ru(001) are shown in Fig. 6, and the observed frequencies are compared to those of second-layer ammonia on other metal surfaces in Table II. The EEL spectra were obtained after the Ru(001) surface at 85 K was exposed to large fluences of NH_3 and ND_3, followed by annealing to 120 K to remove multilayer ammonia. The loss features due to $\delta_s(NH_3)$, $\delta_a(NH_3)$, $\nu_s(NH_3)$ and $\nu_a(NH_3)$ are assigned easily as for monolayer ammonia.

The $\delta_s(NH_3)$ loss feature of second-layer NH_3 at 1145 cm^{-1} shows a pronounced shoulder at 1070 cm^{-1}, which is due to the partially screened $\delta_s(NH_3)$ loss feature of monolayer NH_3. The corresponding shoulder in the case of ND_3 is not so well resolved because the peak frequencies are closer together (i.e. approximately 50 rather than 75 cm^{-1} splitting). The spectrum of NH_3 (ND_3) contains an intense mode at 360 (280) cm^{-1} assigned to the NH_3 twisting mode $\tau(NH_3)$ (equivalent to the frustrated librational mode R_{xy}). Note that this mode is not observed for monolayer ammonia because in that case it corresponds to a free rotation about the ruthenium-nitrogen bond. Evidence for this free rotation in the monolayer has been obtained from ESDIAD data (21). This rotation is hindered in the second layer due to hydrogen bonding of the second-layer ammonia molecules to the monolayer ammonia. The EEL spectrum of Fig. 6(a) also shows loss features at 545 and 225 cm^{-1} which we tentatively assign, respectively, to the NH_3 rocking mode and frustrated translation (perpendicular to the surface) T_z of the second-layer ammonia. The coresponding loss features are not well resolved in the case of ND_3 due to overlap with the $\tau(ND_3)$ loss feature at 280 cm^{-1}. Both spectra of Fig. 6 show a weak loss feature near 1400 cm^{-1}, the identity of which is uncertain. As stated previously, a similar loss feature has been attributed to $\delta_a(ND_2H)$ of an ND_2H impurity in the case of second-layer ND_3 on Pt(111) (3). In the case of NH_3, the 1415 cm^{-1} loss feature is probably a combination band (i.e. 360 + 1070 and/or 1145) (1,3,28). We can think of no impurity that would give rise to a loss feature in this frequency range; $\delta(H_2O)$ of water occurs at the considerably higher frequency of 1560 cm^{-1} (57).

Figure 7 shows EEL spectra of (a) NH_3 and (b) ND_3 multilayers on Ru(001), and the vibrational frequencies and their assignments are listed in Table III along with data for solid ammonia and for NH_3 multilayers on other metal surfaces. Both of the EEL spectra in Fig. 7 were measured following ammonia exposures of approximately 30 L. The loss features due to the $\nu_s(NH_3)$, $\nu_a(NH_3)$, $\delta_s(NH_3)$ and $\delta_a(NH_3)$ modes are again assigned in a straightforward manner. Both spectra also show a weak loss feature due to the $\delta_s(NH_3)$ overtone/double loss. A strong loss feature at 200 cm^{-1} in both cases corresponds to an ammonia lattice mode (i.e. a frustrated translation of the ammonia molecules within the multilayers). Two strong librational modes are observed, one at 540 (420) cm^{-1} and the other a shoulder at 460 (350) cm^{-1}. These frequencies are somewhat higher than those reported previously for

both ammonia multilayers and solid ammonia (58), although we note that the frequencies were lower if only a few layers of ammonia were present (e.g. approximately 370 and 450 cm^{-1} following an 8 L NH_3 exposure). Both spectra show low intensity tails on the high energy side of the $\nu_s(NH_3)$ loss features, the origins of which are not entirely clear, although they may be due to combination bands of $\nu_s(NH_3)$ [$\nu_s(ND_3)$] and the librational and/or frustrated translational modes. The peak at 3370 cm^{-1} in the ND_3 multilayer spectrum is due primarily to the combination band $\delta_s(ND_3) + \nu_s(ND_3)$, although ν(NH) modes due to contamination of the ND_3 sample may also contribute to its intensity. A loss feature of similar intensity was observed at 4480 cm^{-1} in NH_3 multilayer spectra that were scanned to higher loss energy, and this peak is assigned as $\delta_s(NH_3) + \nu_s(NH_3)$.

IV. Discussion

A. Comparison to Ammonia on Other Metal Surfaces and in Coordination Compounds

The EEL spectra that have been obtained for ammonia adsorbed on Ru(001) show strong similarities to those obtained when ammonia is adsorbed on other hexagonally close-packed metal surfaces [i.e. Pt(111) (3) and Ni(111) (9)], and on the pseudo-close-packed Fe(110) surface (28). On the more highly corrugated surfaces, the EELS data currently available do not provide a consistent picture. On Ag(110) (1), the EEL spectra of adsorbed ammonia are very similar to the spectra obtained for ammonia on the more densely-packed surfaces, with the $\delta_s(NH_3)$ loss feature at 1050 cm^{-1} being by far the most intense feature in the entire spectrum. The EEL spectra of ammonia adsorbed on Ag(311) are also similar, although in this case a mode of moderate intensity was observed at 470 cm^{-1} that was assigned as ν(Ag–NH_3) (2). The EEL spectra of ammonia on Ni(110) are surprisingly different, with $\delta_s(NH_3)$, $\delta_a(NH_3)$ and $\nu_a(NH_3)$ loss features of comparable intensity and an additional strong mode at 570 cm^{-1} that was assigned as ν(Ni–NH_3) (9). However, this mode assignment does not appear to have been verified by obtaining EEL spectra of chemisorbed ND_3 on this surface. Despite the lack of a consistent pattern of mode intensities on the highly-corrugated surfaces, the mode frequencies of $\delta_s(NH_3)$, $\delta_a(NH_3)$, $\nu_s(NH_3)$ and $\nu_a(NH_3)$ are quite similar on all of the metal surfaces where ammonia chemisorption has been studied by EELS. This fact, along with the consistent pattern of mode intensities on Ru(001), Pt(111), Ni(111), Fe(110) and Ag(110), suggests some useful comparisons to infrared data for metal

compounds containing ammonia ligands.

Table IV provides a compilation of vibrational data for ammonia adsorbed on metal surfaces and in four different classes of metal-ammonia compounds. The data for the metal compounds show some interesting trends with regard to the charge (both formal and actual) on the metal atom. Note that the "electron richness" of the metal atoms in these compounds is expected to follow the order

$$M(NH_3)_6^{2+} > M(NH_3)_4^{2+} > M(NH_3)_6^{3+} .$$

The frequency of the $\delta_s(NH_3)$ mode is very charge sensitive and shifts upward with increasing charge on the metal atom, having average values of 1158 cm^{-1} in the $M(NH_3)_6^{2+}$ compounds, 1333 cm^{-1} in the $M(NH_3)_6^{3+}$ compounds and intermediate average values in the case of the $M(NH_3)_4^{2+}$ compounds. The changes observed in the frequency of this mode when the metal atom is changed and the charge held constant are minor compared to those resulting from charge changes (59). The $\rho(NH_3)$ and $\nu(M-NH_3)$ modes are also charge sensitive and show marked upshifts in frequency in going from the $M(NH_3)_6^{2+}$ to the $M(NH_3)_6^{3+}$ metal compounds, although in these cases there is somewhat larger overlap between the frequency ranges for these compounds and the $M(NH_3)_4^{2+}$ compounds. The $\nu_a(NH_3)$ mode is slightly charge sensitive, and shifts upward in frequency with decreasing charge on the metal atom. The $\nu_s(NH_3)$ and $\delta_a(NH_3)$ modes are not sensitive to the oxidation state of the metal atom and show no consistent frequency shifts.

Comparing the EELS data for ammonia on metal surfaces to the data for coordination compounds reveals immediately that the $\delta_s(NH_3)$ frequencies observed on surfaces are very similar to those observed in the $M(NH_3)_6^{2+}$ compounds, although the average frequency of 1119 cm^{-1} and the high and low extremes are all 40-50 cm^{-1} lower for the adsorbed ammonia. It is expected that the $\delta_s(NH_3)$ frequencies would be somewhat lower on metal surfaces, since the formal oxidation state of the surface metal atoms is zero. Thus, the observed frequencies of this mode for ammonia adsorbed on a number of metal surfaces appear to correlate well with the IR data for coordination compounds. The same is true in the case of the $\nu_a(NH_3)$ mode, the average frequency of which is higher on surfaces than in the coordination compounds. However, this is of only minor significance because this mode is only slightly charge sensitive, and due to its low intensity and overlap with the $\nu_s(NH_3)$ loss feature, its frequency on

any given surface cannot be determined as accurately as that of $\delta_s(NH_3)$.

The fact that the $\delta_s(NH_3)$ frequencies of chemisorbed ammonia are similar to those of $M(NH_3)_6^{2+}$ compounds suggests that the frequencies of the other two vibrational modes that are strongly charge sensitive, $\rho(NH_3)$ and $\nu(M–NH_3)$, might also be similar in these two cases. While very few data for these two vibrational modes of chemisorbed ammonia are available, our results provide strong support for this proposition. The measured $\rho(NH_3)$ frequency of 625 cm^{-1} is well within the range of 592-769 cm^{-1} reported for the $M(NH_3)_6^{2+}$ compounds, and is slightly lower than the average value of 656 cm^{-1}, just as our measured average $\delta_s(NH_3)$ frequency of 1115 cm^{-1} is slightly lower than the average value of 1158 cm^{-1} in these compounds. The $\rho(NH_3)$ frequencies of the $M(NH_3)_6^{3+}$ compounds are considerably higher, ranging from 748 to 857 cm^{-1}.

In the case of $\nu(M–NH_3)$, the available data for ammonia on metal surfaces present a more complex picture, but our measured frequency of 340 cm^{-1} is in good agreement with data for the $M(NH_3)_6^{2+}$ compounds and identical to the value reported for ammonia on the pseudo-close-packed Fe(110) surface (**28**). The reported values of $\nu(M–NH_3)$ for Ag(311) (**2**) and Ni(110) (**9**) of 470 and 570 cm^{-1}, respectively, are considerably higher and similar to those observed in the $M(NH_3)_6^{3+}$ compounds (462 to 527 cm^{-1}), even though the observed $\delta_s(NH_3)$ frequencies on both surfaces are very similar to those observed on close-packed and pseudo-close-packed surfaces and in the $M(NH_3)_6^{2+}$ compounds. While this difference is no doubt related in some way to the highly corrugated structures of the Ag(311) and Ni(110) surfaces, its exact explanation is unclear. In general, however, the comparison of the vibrational spectra of chemisorbed and coordinated ammonia appears promising, and also serves to point out the importance of obtaining off-specular spectra when EELS is used to study ammonia chemisorption.

B. Origins of the Frequency Shift of $\delta_s(NH_3)$: Correlation with Work Function Data

The pronounced charge sensitivity of the $\delta_s(NH_3)$ frequency in coordination compounds also provides an explanation for the observed shift in the frequency of this mode as a function of coverage for ammonia chemisorbed on Ru(001). The work function change of Ru(001) as a function of ammonia coverage at 80 K has been studied by Benndorf and Madey (**21**), and the work function was found to decrease monotonically by approximately 1.8 eV as the coverage is increased from zero to 0.25

monolayer. The work function change is saturated only after a total ammonia coverage of approximately 0.6 monolayer, and the work function is then approximately 2.3 eV less than on the clean surface. The decrease in the work function is initially linear with coverage, but it increases slightly less rapidly with coverage above a coverage of approximately 0.15 to 0.20 monolayer, and much less rapidly above 0.25 monolayer. The work function decrease results from a net transfer of electrons from the ammonia to the ruthenium surface atoms, so that the "electron-richness" of these surface atoms is increased as the coverage increases. The decreased "charge" on the metal atoms then leads to a lower $\delta_s(NH_3)$ frequency, just as in the coordination compounds of Table IV.

The magnitude of this "charge", or the number of electrons donated to each surface metal atom by the ammonia adlayer for a given ammonia coverage, can be estimated approximately using the surface-ammonia dipole moment of 1.9 D calculated by Benndorf and Madey (21), and assuming a surface-nitrogen bond distance of 2.15 Å (60). This suggests that approximately 0.18 electron is transferred to the surface per adsorbed ammonia molecule. While the dipole moment of 1.9 D was based on the slope of the work function change vs. ammonia coverage curve in the limit of zero coverage, the curve is only slightly nonlinear below a coverage of 0.25, and a large part of this nonlinearity is probably due to the fact that some adsorption into the second layer occurs before the monolayer is completely saturated (21). Our results showing that the frequency of $\delta_s(NH_3)$ decreases nearly linearly with coverage up to at least a coverage of approximately 80% of monolayer saturation supports this point of view, and it is therefore reasonable to assume this same dipole moment for each adsorbed ammonia molecule up to monolayer saturation. Thus, for a saturation monolayer ammonia coverage of 0.25, an average of approximately 0.045 electron is transferred to each surface ruthenium atom from the ammonia adlayer.

This interpretation of the frequency shift of $\delta_s(NH_3)$ has several important implications regarding ammonia chemisorption on Ru(001) and other metal surfaces. First, it suggests that this downshift should occur as the ammonia coverage is increased on all metal surfaces, and that the magnitude of the shift should scale approximately with the amount of charge transfer characteristic of ammonia adsorption. This hypothesis cannot yet be tested fully due to a lack of experimental data, but it is interesting

to note that on Fe(110) a comparable work function decrease (approximately 2 eV) (26) and frequency shift (from 1170 to 1105 cm^{-1}) (28) have been found. The Pt(111) surface exhibits a work function decrease of approximately 2.7 eV when a monolayer saturation coverage of ammonia is adsorbed (5). While the published EEL spectra for monolayer ammonia on this surface show $\delta_s(NH_3)$ frequencies varying from at least 1170 to 1090 cm^{-1} (3), it is not clear whether there is a monotonic shift as a function of coverage. It must also be pointed out that a series of EEL spectra for various ammonia coverages on Ag(311) show no apparent shift in the frequency of this mode (2). Work function data are not available for this surface. This interpretation suggests also that the $\delta_s(NH_3)$ frequency of ammonia chemisorbed on Ru(001) should be increased by the presence of electronegative adatoms such as oxygen, and decreased by the presence of electropositive adatoms such as alkali metals. In the case of oxygen, however, the effects of hydrogen bonding will complicate the analysis (23).

Finally, we note that frequency shifts as a function of ammonia coverage might also be expected for the $\rho(NH_3)$ and $\nu(Ru–NH_3)$ modes of ammonia chemisorbed on Ru(001), since these modes are also charge-sensitive for ammonia in coordination compounds. We cannot address this question unambiguously because the loss features due to these modes are below our limit of detectability for ammonia coverages less than approximately half of monolayer saturation. In addition, these low frequency modes are likely to be more affected than the $\delta_s(NH_3)$ mode by such effects as tilting of the ammonia at high coverages, a phenomenon which has been proposed to occur based on ESDIAD results (21).

C. Adsorption Site of NH_3 on Ru(001)

The adsorption site(s) of ammonia on metal surfaces has been the subject of some disagreement in the literature. Based on indirect evidence obtained using a variety of experimental techniques, it has been suggested that ammonia adsorbs with the nitrogen atom in threefold hollow sites on Ru(001) (21), Pt(111) (3), Ir(111) (17) and Ni(111) (9), and with the nitrogen atom in the long bridging sites on the pseudo-close-packed Fe(110) surface (26). On the other hand, the on-top site was favored for ammonia adsorption on Al(111) (31), and calculations for ammonia adsorption on Al(111) (61) and Cu(111) (62) support this model, showing the interaction between the nitrogen lone pair and the threefold hollow sites to be repulsive. The great similarities among the EEL spectra of ammonia chemisorbed on

Ru(001), Pt(111) (3), Ni(111) (9), Fe(110) (28) and Ag(110) (1) suggest (but do not prove) that a common adsorption site is occupied on all of these surfaces.

For several reasons, we prefer the on-top site as the bonding site of chemisorbed ammonia on Ru(001). The primary reason is that the vibrational frequencies of adsorbed ammonia agree so well with those of ammonia ligands in hexamine compounds, which are "on-top" by definition. We would expect that the frequencies of $\rho(NH_3)$ and especially $\nu(Ru-NH_3)$ would be substantially different if bonding occurred in threefold hollow or twofold bridge sites. This hypothesis cannot be tested because *there is no example known to us in metal cluster chemistry of an ammonia ligand that occupies a threefold hollow or twofold bridging site, or any site other than an on-top site* (63). The same is true of the closely-related phosphine (PR_3) ligands. In fact, to our knowledge, NH_3, $NH_2(NR_2)$ and NH(NR) ligands occupy only on-top, twofold bridging and threefold hollow sites, respectively, in organometallic compounds (63).

We note also that the Fe(110) surface contains no true threefold hollow sites, although it is possible that the pseudo-threefold sites on this surface might be sufficiently similar to true threefold sites to give rise to virtually identical EEL spectra for an adsorbed species. All of these arguments support the intuitive expectation that a strong σ-electron donor such as ammonia should adsorb on the most electron deficient site on these surfaces, namely, the on-top site (62). While none of these points taken alone is compelling, we believe that together they provide considerable support for on-top bonding. Hopefully, additional data for ammonia adsorption on surfaces and (especially) in metal clusters will clarify this issue.

D. Second-Layer and Multilayer Ammonia

As pointed out in Sect. III.B, the EELS spectra of second-layer ammonia on Ru(001) show strong similarities to those obtained on other metal surfaces. Most notably, the strong $\tau(NH_3)$ loss feature at 350 cm^{-1} is very similar both in frequency and intensity to the corresponding loss features on Pt(111) (3), Ag(110) (1) and Ni(110) (9). Surprisingly, the corresponding loss feature on Ag(311) (2) was observed at the substantially lower frequency of 260 cm^{-1}. Nevertheless, it appears that a strong $\tau(NH_3)$ loss feature near 350 cm^{-1} is characteristic of second-layer ammonia on most surfaces and may

be used as a vibrational fingerprint for the second layer. Note that the librational modes reported to date for multilayer ammonia [cf. Table III] occur at frequencies greater than 400 cm^{-1}. The intensity of the $\tau(NH_3)$ loss feature, and the fact that it is strongly attenuated in off-specular EEL spectra indicate that it is dipole-enhanced and thus belongs to a totally symmetric representation of the surface/second-layer ammonia complex. This suggests that at least some of the second-layer ammonia is adsorbed with the molecular axis tilted significantly with respect to the surface normal. This is in agreement with the ESDIAD results of Benndorf and Madey (21), who observed normal emission of H^+ for second-layer but not monolayer ammonia, and interpreted this in terms of a tilting of the molecules within the second layer.

We note also that our $\rho(NH_3)$ frequency of second-layer ammonia of 545 cm^{-1} is substantially lower in frequency than that of 720 cm^{-1} reported for second-layer ammonia on Pt(111) (3). The corresponding loss feature in the case of second-layer ND_3 on Pt(111) occurred at 570 cm^{-1} (3). In our study, the corresponding mode in the case of ND_3 was not resolved unambiguously, although in some EEL spectra of second-layer ND_3 a shoulder was observed at approximately 450 cm^{-1}. For both of these reasons, and because this mode has not been identified in EEL spectra of second-layer ammonia on other metal surfaces, our assignment should be regarded as tentative.

The vibrational frequencies of multilayer NH_3 and ND_3 on Ru(001) are in reasonably good agreement with those of solid ammonia, although the frustrated translational and librational modes occur at slightly higher frequencies. We emphasize that even though all ammonia layers above the second are indistinguishable in thermal desorption spectra, quite large ammonia exposures were necessary in order to obtain an EEL spectrum of true ammonia multilayers, i.e. a spectrum that showed no changes with increasing exposure of the surface to ammonia at 85 K. The main changes for lower exposures were in the frequencies of the librational modes, which shifted upward with increasing exposure until a total exposure of 15-20 L was reached. This would correspond, very approximately, to 15 "layers" of ammonia. It is possible that some of the previously reported librational frequencies of ammonia multilayers on metal surfaces would have been upshifted further if the exposures had been increased, and the fact that the observed librational frequencies of multilayer ammonia are in all cases higher than

those of the strong librational mode of second-layer ammonia is consistant with our results.

V. Conclusions

High-resolution electron energy loss spectroscopy has been used to study the interaction of ammonia with the Ru(001) surface. The results are generally in agreement with those of previous studies of the ammonia/Ru(001) system utilizing other experimental techniques. In particular, we find no significant decomposition of ammonia following exposures to the Ru(001) surface at 80-100 K, and our EEL spectra support the desorption temperatures for multilayer, second-layer and monolayer ammonia that have been reported previously. The principal new conclusions that may be drawn from the EELS results are the following:

1. Monolayer ammonia on Ru(001) exhibits EEL spectra with $\delta_s(NH_3)$, $\delta_a(NH_3)$, $\nu_s(NH_3)$ and $\nu_a(NH_3)$ frequencies very similar to those of ammonia chemisorbed on other close-packed and pseudo-close-packed metal surfaces. In addition, the NH_3 rocking mode and the frustrated translational mode of the ammonia perpendicular to the surface are observed in off-specular EEL spectra and occur at frequencies of approximately 625 and 340 cm^{-1}, respectively. The $\rho(NH_3)$ mode has not been identified previously for chemisorbed ammonia, and the ν(metal-NH_3) mode has been identified only rarely. These results indicate the importance of obtaining off-specular spectra in EELS studies of chemisorbed ammonia.

2. The vibrational spectra of ammonia chemisorbed on Ru(001) and other metal surfaces of similar geometry are very similar to those of hexamine 2+ compounds, $M(NH_3)_6^{2+}$, and agree much less well with those of $M(NH_3)_6^{3+}$ and $M(NH_3)_4^{2+}$ compounds, regardless of the type of metal atom and counter ions in the complexes. Thus, both on surfaces and in coordination compounds, the real (not formal) "oxidation state" of the metal is of paramount importance in determining the vibrational frequencies of coordinated ammonia.

3. The intense $\delta_s(NH_3)$ mode of chemisorbed NH_3 on Ru(001) shifts down continuously and essentially linearly with increasing coverage, from 1160 cm^{-1} in the low coverage limit to 1070 cm^{-1} at monolayer saturation. This parallels the downshift of the frequency of this

mode in coordination compounds as the charge on the metal atom decreases. This change can be correlated with the large decrease (~1.8 eV) in the work function of the Ru(001) surface that occurs as ammonia is adsorbed (**21**), making the surface atoms, in effect, more "negatively charged".

4. The EELS results, and the organometallic literature concerning NH_3 ligands, are more consistent with chemisorbed NH_3 bonding in on-top sites, rather than in threefold sites.

5. The vibrational characteristics of second-layer and multilayer ammonia on Ru(001) are generally quite similar to those of second-layer and multilayer ammonia on other metal surfaces. The intense $\tau(NH_3)$ loss feature near 350 cm^{-1} appears to be a general feature of second-layer ammonia on most metal surfaces. The fact that this mode is dipolar in nature suggests a tilting of the molecular axis of the second-layer ammonia away from the surface normal, consistent with previous ESDIAD results (**21**). While all layers above the second are indistinguishable in thermal desorption spectra, substantially larger coverages (i.e. approximately 15 "layers") of condensed ammonia are necessary to obtain a multilayer EEL spectrum which does not change when additional exposures are made.

Acknowledgments: We are indebted to Dr. Udo Schwalke for assistance in the early stages of this work. Helpful discussions with Professors J. E. Bercaw and W. A. Goddard are gratefully acknowledged. This work was supported by the National Science Foundation under Grant No. CHE-8617826

References

1. J. L. Gland, B. A. Sexton and G. E. Mitchell, Surface Sci. **115**, 623 (1982)..

2. S. T. Ceyer and J. T. Yates, Jr., Surface Sci. **155**, 584 (1985).

3. B. A. Sexton and G. E. Mitchell, Surface Sci. **99**, 523 (1980).

4. B. A. Sexton and G. E. Mitchell, Surface Sci. **99**, 539 (1980).

5. G. B. Fisher, Chem. Phys. Lett. **44**, 683 (1981).

6. J. L. Gland, Surface Sci. **71**,327 (1978).

7. J. L. Gland and V. N. Korchak, J. Catal. **53**, 9 (1978).

8. J. L. Gland and E. B. Kollin, Surface Sci. **104**, 478 (1981).

9. G. B. Fisher and G. E. Mitchell, J. Electron Spectros. Rel. Phen. **29**, 253 (1983).

10. C. W. Seabury, T. N. Rhodin, R. J. Purtell and R. P. Merrill, Surface Sci. **93**, 117 (1980).

11. M. Grunze, M. Golze, R. K. Driscoll and P. A. Dowber, J. Vac. Sci. Technol. **18**, 611 (1981).

12. K. Jacobi, E. S. Jensen, T. N. Rhodin and R. P. Merrill, Surface Sci. **108**, 397 (1981).

13. T. E. Madey, J. E. Houston, C. W. Seabury and T. N. Rhodin, J. Vac. Sci. Tech. **18**, 476 (1981).

14. F. P. Netzer and T. E. Madey, Phys. Rev. Lett. **47**, 921 (1981).

15. F. P. Netzer and T. E. Madey, Surface Sci. **119**, 422 (1982).

16. M. Grunze, P. A. Dowber and C. R. Brundle, Surface Sci. **128**, 311 (1983).

17. R. J. Purtell, R. P. Merrill, C. W. Seabury and T. N. Rhodin, Phys. Rev. Lett. **44**, 1279 (1980).

18. L. R. Danielson, M. J. Dresser, E. E. Donaldson and J. T. Dickinson, Surface Sci. **71**, 599 (1978).

19. L. R. Danielson, M. J. Dresser, E. E. Donaldson and D. R. Sandstrom, Surface Sci. **71**, 615 (1978).

20. T. E. Madey and J. T. Yates, Jr., in: Proc. 7th Intern. Vacuum Congr. and 3rd Intern. Conf. on Solid Surfaces, Eds. R. Dobrozemsky et al. (Vienna, 1977), 1183.

21. C. Benndorf and T. E. Madey, Surface Sci. **135**, 164 (1983).

22. C. Benndorf and T. E. Madey, Chem. Phys. Lett. **101**, 59 (1983).

23. T. E. Madey, C. Benndorf, D. L. Doering and S. Semancik, in: Proc. 8th Intern. Congr. on Catalysis **4**, 51 (1984).

24. M. Grunze, F. Bozso, G. Ertl and M. Weiss, Appl. Surface Sci. **1**, 241 (1978).

25. M. Drechsler, H. Hoinkes, H. Kaarmann, H. Wilsch, G. Ertl and M. Weiss, Appl. Surface Sci. **3**, 217 (1979).

26. M. Weiss, G. Ertl and F. Nitschke, Appl. Surface Sci. **3**, 614 (1979).

27. M. Grunze and G. Ertl, in Ref. 20, p. 1137.

28. W. Erley and H. Ibach, Surface Sci. **119**, L357 (1982).

29. K. Kishi and M. W. Roberts, Surface Sci. **62**, 252 (1977).

30. I. D. Gay, M. Textor, R. Mason and Y. Iwasawa, Proc. Roy Soc. A **356**, 25 (1977).

31. F. P. Netzer and T. E. Madey, Chem. Phys. Lett. **88**, 315 (1982).

32. See, for example, G. C. Bond, *Catalysis by Metals*, Academic Press, N.Y., 1962.

33. J. R. Hall G. A. Swile, J. Organomet. Chem. **42**, 479 (1972).

34. R. P. Shibaeva, L. P. Rozenberg, R. M. Lobkovskaya, A. E. Shilov and G. B. Shulpin, J. Organomet. Chem. **220**, 271 (1981).

35. L. M. Vallarino and S. W. Sheargold, Inorg. Chim. Acta **36**, 243 (1979).

36. W. Rigby, J. A. McCleverty and P. M. Maitlis, J. Chem. Soc. Dalton Trans. 382 (1979).

37. B. P. Sullivan, J. A. Baumann, T. J. Meyer, D. J. Salmon, H. Lehmann and A. Ludi, J. Am. Chem. Soc. **99**, 7368 (1977).

38. H. Lehmann, K. J. Schenk, G. Chapuis and A. Ludi, J. Am. Chem. Soc. **101**, 6197 (1979).

39. D. Rehder, J. Organomet. Chem. **37**, 303 (1972).

40. J. E. Ellis and K. L. Fjare, Organomet. **1**, 898 (1982).

41. D. Sellmann, A. Brandl and R. Endell, J. Organomet. Chem. **111**, 303 (1976).

42. M. Herberhold, F. Wehrmann, D. Neugebauer and G. Huttner, J. Organomet. Chem. **152**, 329 (1978).

43. A. B. Anton, N. R. Avery, B. H. Toby and W. H. Weinberg, J. Elect. Spect. **29**, 181 (1983).

44. A. B. Anton, N. R. Avery, T. E. Madey and W. H. Weinberg, J. Chem. Phys. **85**, 507 (1986)

45. U. Schwalke, J. E. Parmeter and W. H. Weinberg, J. Chem. Phys. **84**, 4036 (1985).

46. U. Schwalke, J. E. Parmeter and W. H. Weinberg, Surface Sci. **178**, 625 (1986).

47. J. E. Parmeter, U. Schwalke and W. H. Weinberg, J. Am. Chem. Soc. **109**, 1876 (1987).

48. J. E. Parmeter, U. Schwalke and W. H. Weinberg, J. Am. Chem. Soc. **109**, 5083 (1987).

49. G. E. Thomas and W. H. Weinberg, Rev. Sci. Instr. **50**, 497 (1979).

50. The recombinative desorption of nitrogen adatoms from Ru(001) occurs near 800-850 K (**21**).

51. The recombinative desorption of hydrogen adatoms from Ru(001) occurs below 450 K; H. Shimizu, K. Christmann and G. Ertl, J. Catal. **61**, 412 (1980).

52. The desorption of molecularly chemisorbed CO from Ru(001) occurs below 500 K. (a) T. E. Madey and D. Menzel, J. Appl. Phys., Suppl. 2, Pt. 2, 229 (1974); (b) H. Pfnür, P. Feulner, H. A. Engelhardt and D. Menzel, Chem. Phys. Lett. **59**, 481 (1978); (c) H. Pfnür, P. Feulner and D. Menzel, J. Chem. Phys. **79**, 4613(1983).

53. H. Ibach and D. L. Mills, *Electron Energy Loss Spectroscopy and Surface Vibrations*, Academic Press, N.Y., 1982, p. 348.

54. While it is unclear exactly what this impurity might be, this loss feature is quite clear in off-specular spectra, consistent with its assignment as a ν(CH) mode. It seems too low in frequency to be due to a ν(NH) mode.

55. For a discussion of dipole and impact scattering, see Ref. 53, Chs. 1 and 3.

56. The estimate of 80% of monolayer saturation is arrived at from both the thermal desorption spectra of Ref. 21, and by noting in Fig. 5 that the minimum $\delta_s(NH_3)$ frequency for monolayer ammonia on Ru(001) is approximately 1070 cm^{-1}, and assuming the frequency decrease to be linear up to saturation.

57. P. A. Thiel, F. M. Hoffmann and W. H. Weinberg, J. Chem. Phys. **75**, 5556 (1981).

58. O. S. Binbrek and A. Anderson, Chem. Phys. Lett. **15**, 421 (1972), and references therein.

59. For example, consider the $\delta_s(NH_3)$ frequencies (in cm^{-1}) of the following series of $M(NH_3)_6^{2+}$ compounds: Mn, 1146; Fe, 1156; Co, 1163; Ni, 1176; Zn, 1145. On the other hand, there is a large frequency difference between $Co(NH_3)_6^{2+}$ (1163) and $Co(NH_3)_6^{3+}$ (1329).

60. This distance appears to be typical of metal-nitrogen bond distances in organometallic compounds of ammonia. See, for example, Ref. 38.

61. K. Hermann, P. S. Bagus and C. W. Bauschlicher, Phys. Rev. B **31**, 6371 (1985).

62. C. W. Bauschlicher, J. Chem. Phys. **83**, 2619 (1985).

63. These statements are based on a thorough search of the "Dictionary of Organometallic Compounds", Chapman and Hall, London, 1984. While data for ammonia are not very extensive, the data for PR_3 ligands are, and they indicate that only on-top sites are occupied.

64. Nakamoto, K., "Infrared and Raman Spectra of Inorganic and Coordination Compounds", Third Edition **1978**, Wiley & Sons, New York, 197-202.

Table I. Vibrational frequencies (in cm^{-1}) and mode assignments for gas phase ammonia, and for chemisorbed ammonia on several metal surfaces.

Mode	NH_3(g) (53)	ND_3(g) (53)	Ru(001) NH_3 (this work)	Ru(001) ND_3 (this work)	Pt(111) (3)	Ni(111) (9)	Ni(110) (9)	Fe(110) (28)
$\nu_a(NH_3)$	3414	2556	3370	2515	3340	3360	3350	3370
$\nu_s(NH_3)$	3337	2420	3260	2335	3240	3270	3200	3290
$\delta_a(NH_3)$	1628	1191	1580	1165	1600	1580	1580	1640
$\delta_s(NH_3)$	950	747	1070-1160	835-910	1140	1140	1120	1105-1170
$\rho(NH_3)$	-	-	625[a]	480[a]	n.o.	n.o.	n.o.	n.o.
$\nu(M-NH_3)$	-	-	340[a]	350[a]	n.o.	n.o.	570	340
							Ag(110) (1)	Ag(311) (2)
							3390	
								3410
							3320	
							1640	1648
							1050	1100
							n.o.	n.o.
							n.o.	470

s = symmetric, a = asymmetric, n.o. = not observed.

[a] Generally observed only in off-specular EEL spectra.

Table II. Vibrational frequencies (in cm^{-1}) and mode assignments for second-layer NH_3 and ND_3 on Ru(001), and for second-layer NH_3 on several other metal surfaces.

	Ru(001)					
	NH_3	ND_3	Pt(111)	Ag(110)	Ni(110)	Ag(311)
Mode	(this work)		(3)	(1)	(9)	(2)
$\tau(NH_3)$[a]	360	280	350	340	360	260
$\rho(NH_3)$	545	n.o.[b]	720	n.o.	n.o.	n.o.
$\delta_s(NH_3)$	1145	885	1190	1100	1110	1100
$\delta_a(NH_3)$	1625	1190	1630	1630	1630	1650
$\nu_s(NH_3)$	3225	2340	3150	3320	3200	3410
$\nu_a(NH_3)$	3350	2505	3320	3390	3340	
T_z	225	n.o.	n.o.	n.o.	n.o.	n.o.

s = symmetric, a = asymmetric, n.o. = not observed.

[a] This mode is also referred to in the literature as R_{xy} (≡ rotation about an axis normal to the surface), or simply as ν_l (a "frustrated libration"), although the latter designation alone is ambiguous.

[b] In some EEL spectra, a shoulder was present at approximately 450 cm^{-1} that might be assigned to $\rho(ND_3)$.

Table III. Vibrational frequencies (in cm^{-1}) and mode assignments for solid ammonia, and for ammonia multilayers on several metal surfaces.

	Solid Ammonia		Ru(001)		Pt(111)	Ag(110)	Ag(311)
	NH_3	ND_3	NH_3	ND_3	NH_3	NH_3	NH_3
Mode	(58)[a]	(58)[a]	(this work)		(3)	(1)	(2)
ν_t[b]	138-184	132-174	200	200	n.o.	140	n.o.
ν_l[c]	325-386	242-312	460	350	410	400	430
ν_l[c]	412-462	315-406	540	420			
$\delta_s(NH_3)$	1057-1080	815-836	1100	865	1120	1070	1150
$\delta_a(NH_3)$	1630-1679	1183-1217	1640	1220	1640	1630	1570
$\nu_s(NH_3)$	3160-3330	2318-2336	3230	2380	n.o.	3320	n.o.
$\nu_a(NH_3)$	3370-3378	2505-2511	3380	2520	3320	3380	n.o.

s = symmetric, a = asymmetric, n.o. = not observed.

[a] A range of values is given for each frequency of solid NH_3 and ND_3, based on several IR and Raman studies at temperatures ranging from 18 to 151 K. In some studies, more than one frequency was observed due to crystal splitting.

[b] ν_t ≡ frustrated translation or lattice mode.

[c] ν_l ≡ frustrated libration. Since there is some confusion over the assignments of these modes in the literature, we do not attempt to assign them to specific librations.

Table IV. *Vibrational* frequencies (in cm^{-1}) for various modes of ammonia adsorbed on Ru(001) and other metal surfaces (1-3,9,28), and in various types of inorganic compounds (64). The first number given in each case is the average frequency for the specific mode in a certain type of compound, and is followed in parentheses by the number of compounds that was used in calculating the average. Below this, the range (low and high extremes) is listed for the same mode.

Mode	Ru(001) (this work)	Other Metal Surfaces[a]	$M(NH_3)_6^{3+}$ (64)[b]	$M(NH_3)_6^{2+}$ (64)[c]	$M(NH_3)_4^{2+}$ tetrahedral (64)[d]	$M(NH_3)_4^{2+}$ square-planar (64)[e]
$\nu_a(NH_3)$	3370	3363(5) 3340- 3400	3269(3) 3240- 3310	3336(7) 3300- 3353	3316(3) 3233- 3354	3272(3) 3236- 3327
$\nu_s(NH_3)$	3260	3264(5) 3200- 3320	3183(3) 3130- 3250	3200(7) 3160- 3250	3226(3) 3150- 3267	3165(3) 3156- 3170
$\delta_a(NH_3)$	1580	1615(6) 1580- 1648	1616(6) 1587- 1630	1601(8) 1585- 1610	1608(3) 1596- 1617	1612(3) 1563- 1669
$\delta_s(NH_3)$	1115 1070- 1160	1119(6)[f] 1050- 1170	1333(6) 1290- 1368	1158(8) 1091- 1220	1227(3) 1176- 1253	1298(3) 1279- 1325
$\rho(NH_3)$	625	Not observed previously	806(6) 748- 857	656(8) 592- 769	683(3) 670- 693	807(3) 735- 849
$\nu(M-NH_3)$ (A_1)	340	Reported Values of 340,470, 570	488(6) 462- 527	332(6) 298- 370	409(3) 370- 432	481(3) 420- 524

s = symmetric, a = asymmetric, n.o. = not observed.

[a] Data are for Ag(110), Ag(311), Pt(111), Ni(111), Ni(110) and Fe(110).

[b] Data are for M = Cr, Ru, Os, Co, Rh and Ir.

[c] Data are for M = Mg, Mn, Fe, Ru, Co, Ni, Zn and Cd.

[d] Data are for M = Co, Zn and Cd.

[e] Data are for M = Pd, Pt and Cu.

[f] In the case of Fe(110), where $\delta_s(NH_3)$ was reported to shift in frequency as a function of coverage (28), an average value was used as the characteristic frequency of chemisorbed ammonia.

Figure Captions

Figure 1. The EEL spectra that result following several exposures of NH_3 to the Ru(001) surface at 80 K. (In the case of the 0.7 L exposure, the surface temperature was closer to 90 K, and the elastic peak count rate was only 2×10^4).

Figure 2. The EEL spectrum that results after a Ru(001) surface with condensed multilayers of ND_3 is annealed to 150 K. This spectrum is characteristic of monolayer ND_3.

Figure 3. Off-specular EEL spectra of monolayer (a) NH_3 and (b) ND_3 on Ru(001). Prior to spectral collection, the surface was annealed to 150 K to remove any second-layer ammonia.

Figure 4. The frequency of the $\delta_s(NH_3)$ mode of chemisorbed ammonia on Ru(001) as a function of ammonia coverage. The approximate coverages given are relative to the surface concentration of ruthenium atoms, which is 1.57×10^{15} cm^{-2}, and they are based on the assumption that the saturation (monolayer) ammonia coverage is 0.25.

Figure 5. The frequency of the $\delta_s(NH_3)$ mode of chemisorbed ammonia on Ru(001) as a function of annealing temperature for several initial exposures.

Figure 6. The EEL spectra that result when a Ru(001) surface with condensed multilayers of (a) NH_3 and (b) ND_3 is annealed to 120 K. These spectra are characteristic of second-layer ammonia.

Figure 7. The EEL spectra of condensed multilayers of (a) NH_3 and (b) ND_3 on Ru(001). The exposures were approximately 30 L at a surface temperature of 85 K.

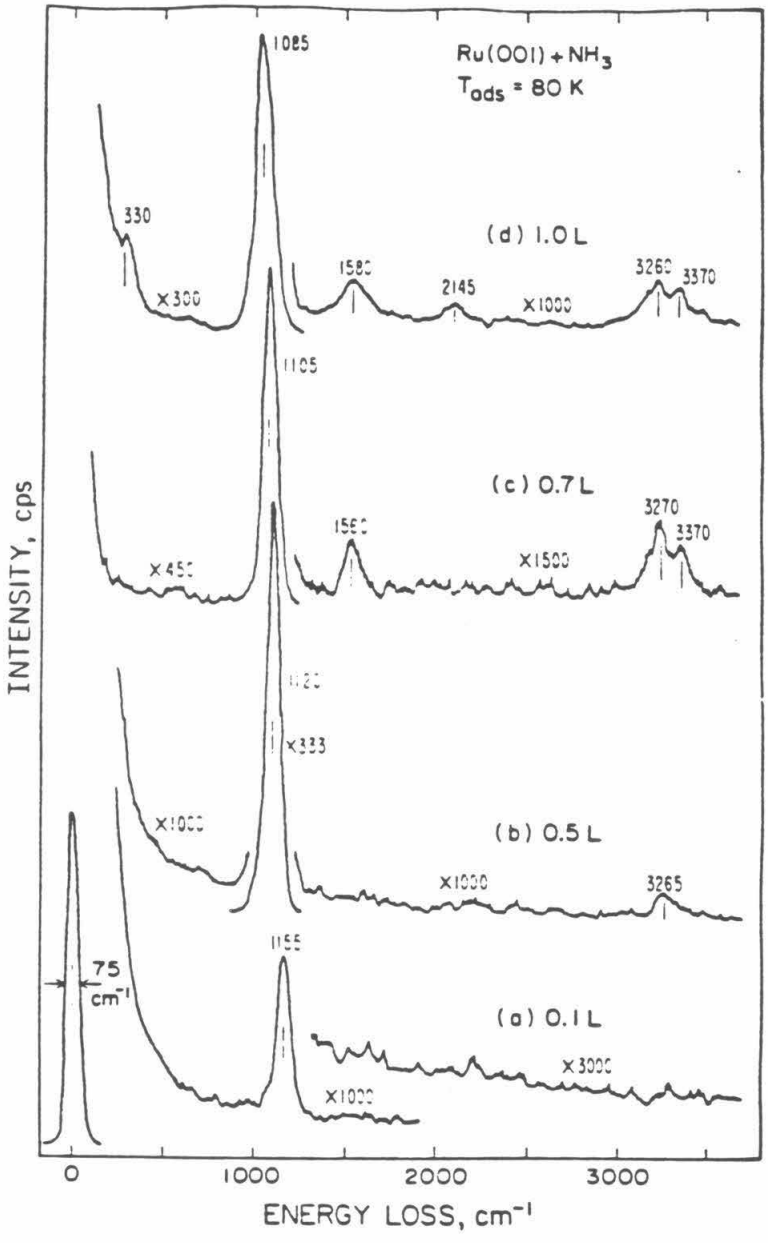
Ru(001) + NH3
Tads = 80 K
(d) 1.0 L
(c) 0.7 L
(b) 0.5 L
(a) 0.1 L
1085
330
1580
2145
3260
3370
1105
3270
3370
1155
3265
75 cm-1
INTENSITY, cps
ENERGY LOSS, cm-1
0
1000
2000
3000

Figure 1

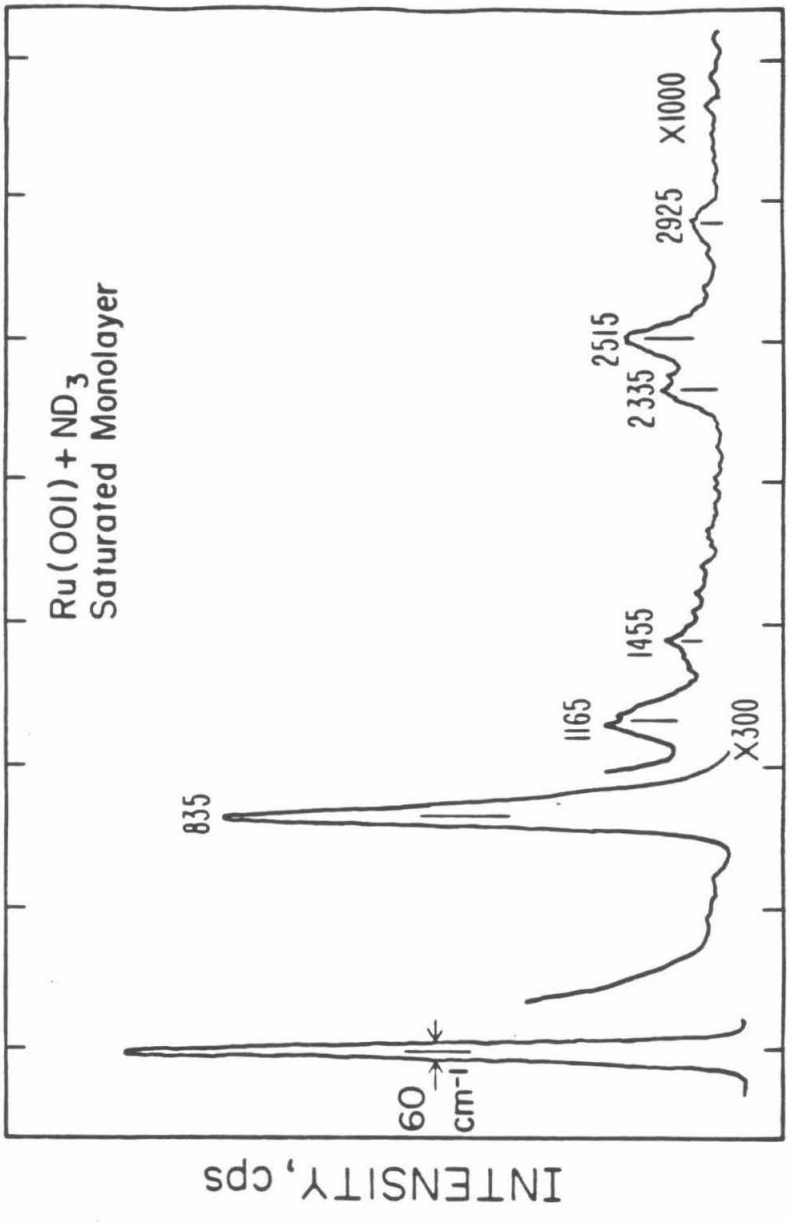
Ru(001) + ND3
Saturated Monolayer
835
60 cm-1
1165
1455
X300
2515
2335
2925
X1000
0
1000
2000
3000
ENERGY LOSS, cm-1
INTENSITY, cps

Figure 2

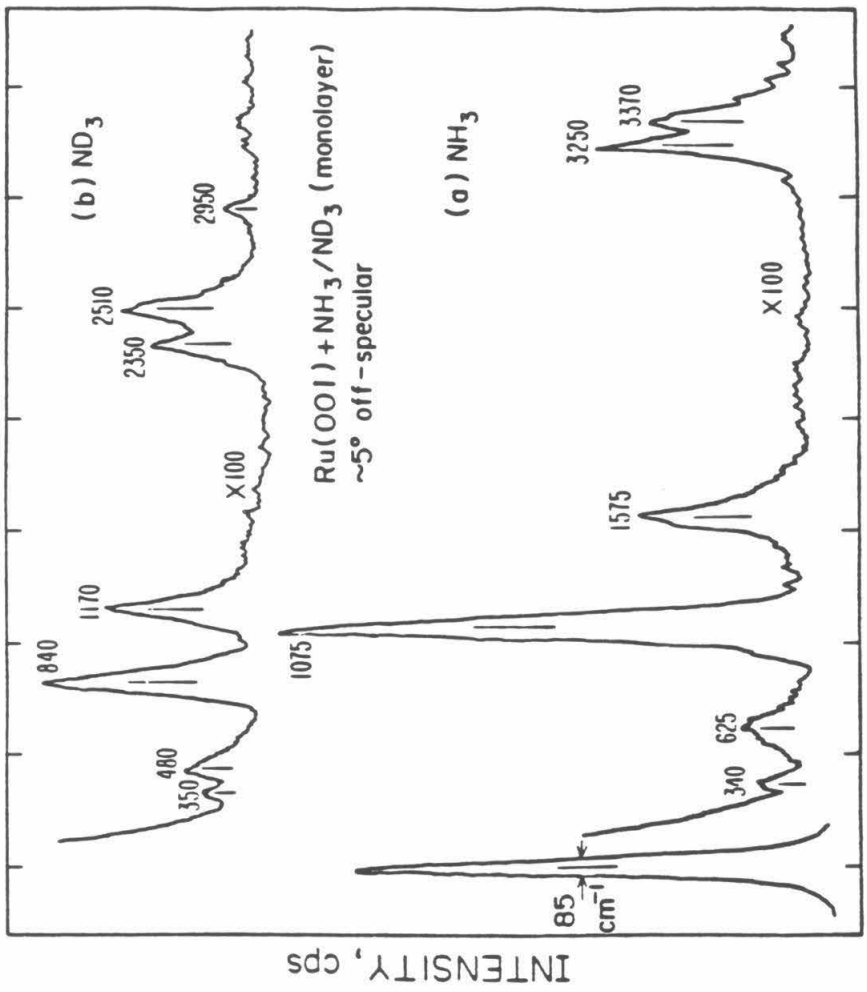
(b) ND_3
(a) NH_3
$Ru(001) + NH_3/ND_3$ (monolayer)
~5° off-specular
480
350
840
1170
X100
1075
2510
2350
2950
1575
3250
3370
X100
625
340
85 cm^{-1}
0
1000
2000
3000
ENERGY LOSS, cm^{-1}
INTENSITY, cps

Figure 3

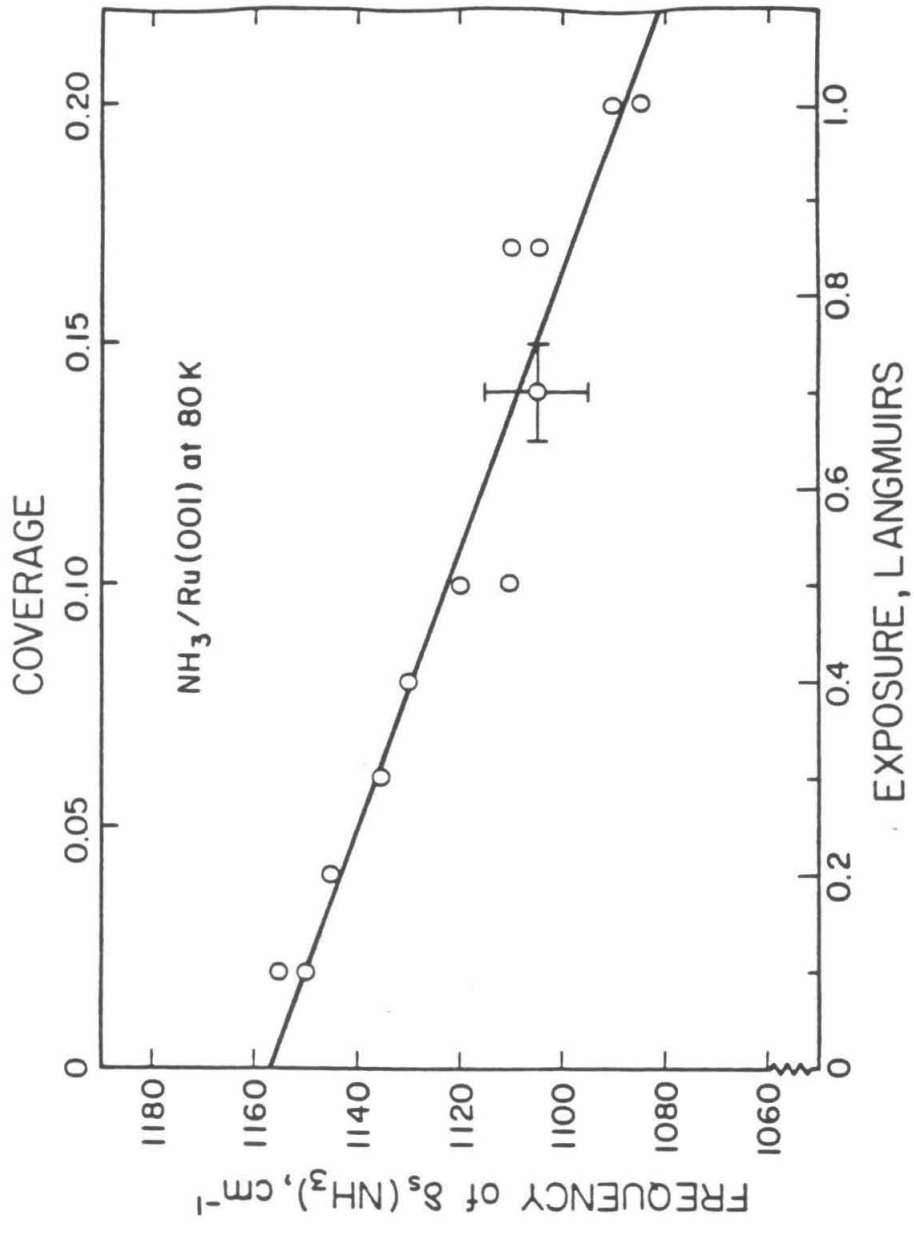
COVERAGE
0
0.05
0.10
0.15
0.20
NH_3/Ru(001) at 80 K
FREQUENCY of $\delta_s(NH_3)$, cm^{-1}
1180
1160
1140
1120
1100
1080
1060
EXPOSURE, LANGMUIRS
0
0.2
0.4
0.6
0.8
1.0

Figure 4

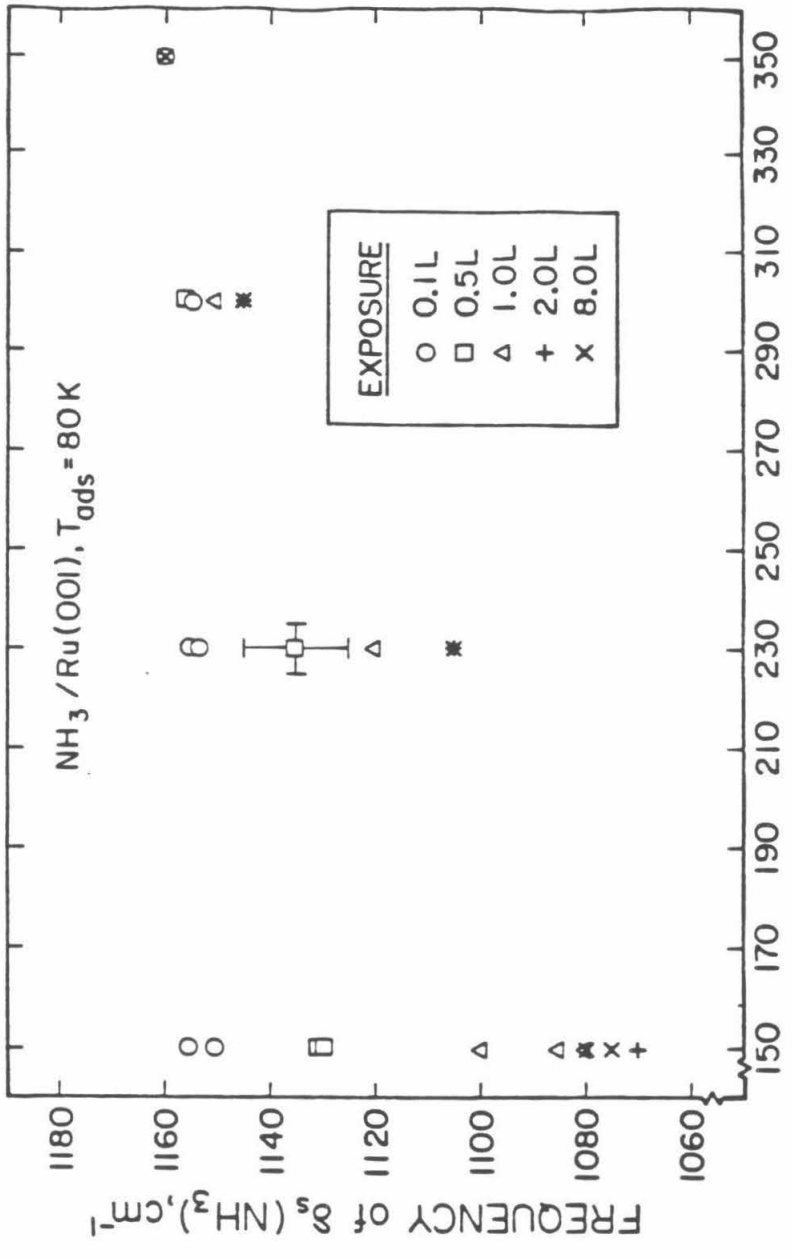
NH_3 /Ru(001), T_{ads} = 80 K
EXPOSURE
○ 0.1L
□ 0.5L
△ 1.0L
+ 2.0L
× 8.0L
FREQUENCY of $\delta_s(NH_3)$, cm^{-1}
1180
1160
1140
1120
1100
1080
1060
150 170 190 210 230 250 270 290 310 330 350
ANNEALING TEMPERATURE, K

Figure 5

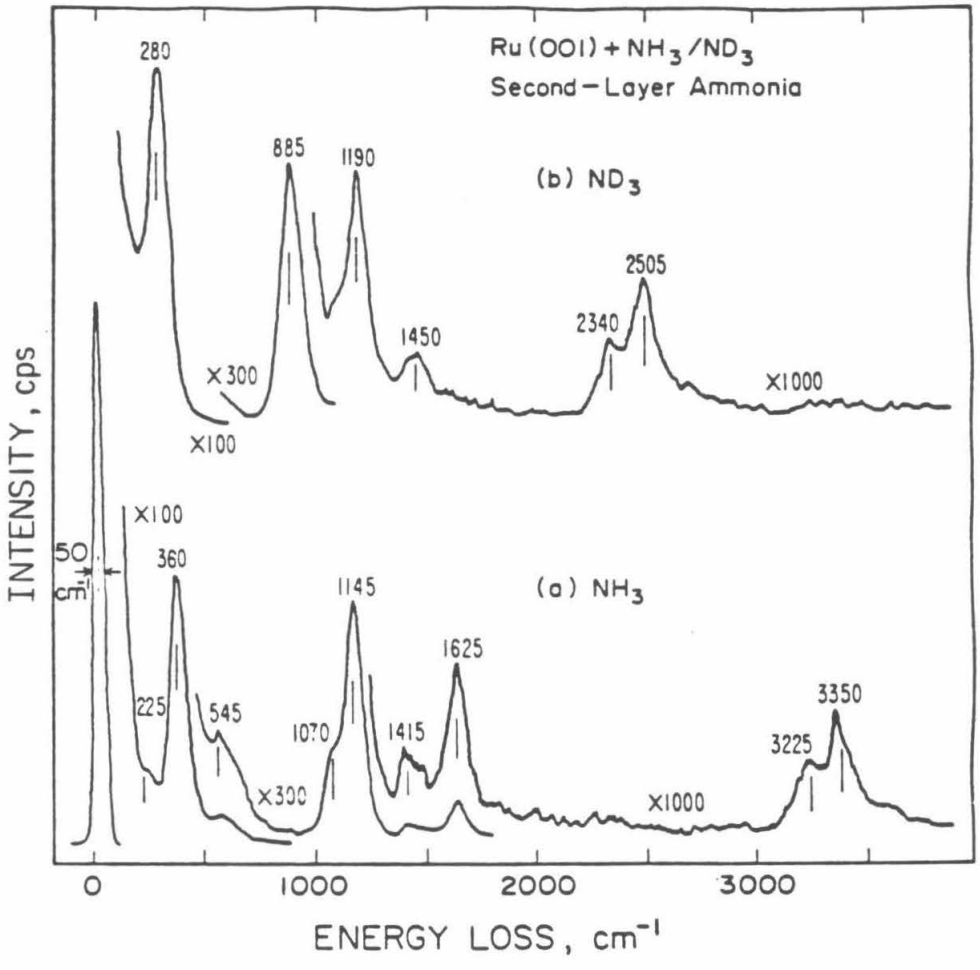
Ru(001) + NH3/ND3
Second-Layer Ammonia
(b) ND3
280
885
1190
2505
2340
1450
X300
X100
X1000
(a) NH3
X100
50 cm-1
360
1145
1625
3350
225
545
1070
1415
3225
X300
X1000
INTENSITY, cps
0
1000
2000
3000
ENERGY LOSS, cm-1

Figure 6

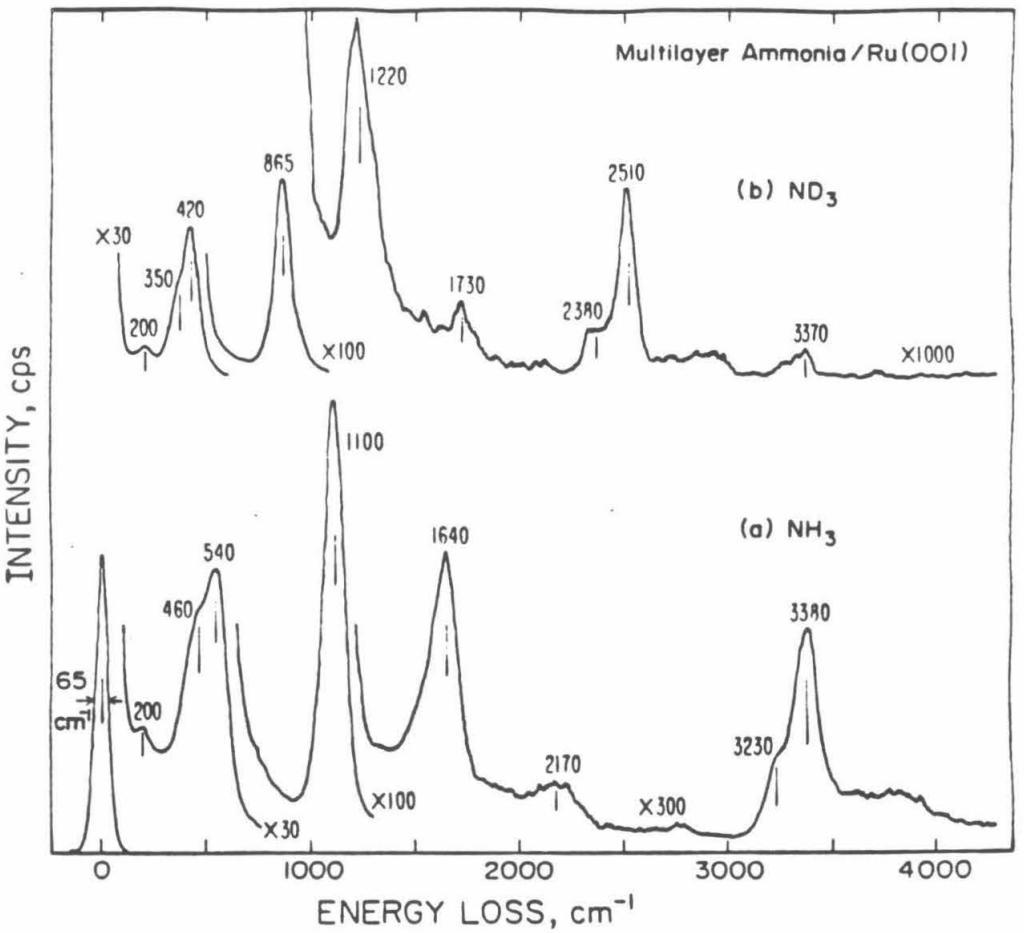
Multilayer Ammonia/Ru(001)
(b) ND_3
(a) NH_3
INTENSITY, cps
ENERGY LOSS, cm^{-1}
0
1000
2000
3000
4000
X30
420
350
200
865
1220
X100
1730
2380
2510
3370
X1000
1100
1640
540
460
65 cm
200
X30
X100
2170
X300
3230
3380

Figure 7

CHAPTER X

Conclusions

The chemistry of acetylene, formamide and ammonia on clean and chemically modified Ru(001) surfaces has been studied using electron energy loss spectroscopy (EELS) and thermal desorption mass spectrometry (TDMS). The decomposition mechanisms of acetylene and formamide have been investigated on clean Ru(001), oxygen-precovered Ru(001) and hydrogen-precovered Ru(001), and whenever possible analogies have been drawn to the organometallic cluster chemistry of these two molecules and to the surface chemistry of closely-related molecules on the Ru(001) surface. Molecularly adsorbed ammonia on Ru(001) has been characterized vibrationally, and a detailed comparison has been made between chemisorbed ammonia on several metal surfaces and ammonia ligands in a number of metal compounds.

The adsorption of acetylene on clean Ru(001) results in strong rehybridization of the molecule from sp to nearly sp^3; the ν(CC) frequency of 1135 cm^{-1} for chemisorbed acetylene on Ru(001) is the lowest that has been identified on any metal surface. The chemisorbed acetylene is stable to approximately 230-250 K, at which point it decomposes to yield ethylidyne (CCH_3) and acetylide (CCH) as stable surface intermediates. Both of these intermediates decompose in the temperature range of 350-400 K, evolving hydrogen gas and leaving methylidyne (CH) and carbon on the surface. The methylidyne decomposes between 500 and 700 K with further hydrogen evolution. There is no molecular desorption of chemisorbed acetylene from Ru(001); the only thermal desorption product is hydrogen. The preadsorption of a saturation coverage of hydrogen adatoms on Ru(001) leads to the formation and desorption of a small amount of ethylene when acetylene is adsorbed, via an intermediate inferred to be an η^2–$CHCH_2$ species.

The chemisorption and decomposition of acetylene on Ru(001)-p(2x2)-O and Ru(001)-p(1x2)-O has been studied also. In contrast to ethylene, which is di-σ-bonded on clean Ru(001) (**1,2**) but π-bonded on Ru(001)-p(2x2)-O and Ru(001)-p(1x2)-O (**3**), the bonding of chemisorbed acetylene on the oxygen-precovered surfaces is not altered significantly compared with its bonding on the clean surface. This difference can be understood in terms of the higher energy of the antibonding π^* orbital of ethylene compared with the π^* orbitals of acetylene. This results, in the case of ethylene, in very little metal-to-π^* electron backdonation on the "electron-poor" oxygen-precovered surfaces, so that rehybridi-

zation to sp^3 does not occur and the π-bonded ethylene species is formed. In the case of acetylene, however, backdonation is facile on all three surfaces and in all cases nearly sp^3-hybridized acetylene species are formed. In addition, it has been shown recently (4) that the chemisorbed acetylene on Ru(001) actually consists of a mixture of two different molecularly adsorbed species, one with a strong ν(CC) loss feature at 1135 cm^{-1} and a second with a very weak ν(CC) loss feature near 1250 cm^{-1}. The preadsorption of oxygen on the surface favors the formation of the latter species relative to the former, which is not formed at all on the oxygen-presaturated surface. Finally, the preadsorption of oxygen inhibits acetylene adsorption significantly. The saturation coverages of chemisorbed acetylene on clean Ru(001), Ru(001)-p(2x2)-O and Ru(001)-p(1x2)-O are approximately 0.39, 0.31 and 0.09, respectively.

The decomposition of acetylene on Ru(001)-p(2x2)-O and Ru(001)-p(1x2)-O involves all of the intermediates that have been identified on clean Ru(001), and on Ru(001)-p(2x2)-O substantial amounts of an sp^2-hybridized vinylidene (CCH_2) species are formed. This species is not formed in the decomposition of acetylene on clean Ru(001), but has been identified previously in the decomposition of ethylene on Ru(001)-p(2x2)-O (3).

The adsorption and decomposition of formamide has been studied on clean Ru(001), Ru(001)-p(1x2)-O and hydrogen-saturated Ru(001). On clean Ru(001) at 80 K, the primary mode of formamide adsorption involves CH bond cleavage and rehybridization of the carbonyl double bond to produce an η^2(C,O)-NH_2CO species. This species decomposes at approximately 230-250 K, producing coadsorbed CO, NH, NH_3 and hydrogen adatoms. Decomposition of the NH species to nitrogen adatoms and additional hydrogen adatoms occurs between 350 and 400 K, and the thermal desorption products are CO (~480 K), NH_3 (~315 K), H_2 (~420 K) and N_2 (~770 K). At high coverages at 80 K, some molecular adsorption of formamide occurs also, and a competing, minority decomposition pathway occurs which involves the formation of an η^1(N)-NCHO or η^1(N)-NHCHO species between approximately 300 and 350 K. For sufficiently high coverages, some molecular desorption occurs near 225 K.

On Ru(001)-p(1x2)-O, formamide is molecularly chemisorbed below approximately 265 K. Two slightly different forms of the molecule exist above and below 225 K. The low-temperature form is

η^1(O)-NH_2CHO, bonded to the surface via an electron lone pair on the formamide oxygen atom. The high-temperature form is believed to be η^2(N,O)-NH_2CHO, bonded to the surface via electron lone pairs on both the oxygen and nitrogen atoms. Annealing the surface to temperatures in the range of approximately 265-400 K results in NH bond cleavage and the formation of a formate-like η^2(N,O)-NHCHO species. This species is stable to approximately 420 K, at which point it decomposes, evolving CO and H_2 and leaving only nitrogen adatoms on the Ru(001)-p(1x2)-O surface. The nitrogen adatoms recombine and desorb as N_2 near 570 K, leaving the p(1x2)-O overlayer intact. For sufficiently high formamide exposures, some molecular desorption occurs near 255 and 225 K. Following a saturation exposure, only 0.05 monolayer of formamide decomposes on Ru(001)-p(1x2)-O, compared to 0.15 monolayer on clean Ru(001).

The adsorption of formamide on hydrogen-presaturated Ru(001) at 80 K leads to the formation of the same molecularly adsorbed species that is formed on Ru(001)-p(1x2)-O at 80 K, namely, η^1(O)-NH_2CHO. However, the subsequent chemistry that this species undergoes is quite different. It converts, between approximately 150 and 200 K, to η^2(C,O)-NH_2CHO, with this latter species converting to η^2(C,O)-NH_2CO by 250 K. The η^2(C,O)-NH_2CO converts below 300 K to CO, NH and hydrogen adatoms, which subsequently react and/or desorb as on clean Ru(001). Approximately 0.05 monolayer of formamide decomposes following a saturation exposure on the hydrogen-presaturated surface.

It has been shown previously that the adsorption of ammonia on Ru(001) at 80 K leads only to reversible desorption, with virtually no molecular dissociation occurring as the surface is heated (**5,6**). The EEL spectra of chemisorbed NH_3 and ND_3 on Ru(001) have been obtained, and while the results are similar to those obtained for ammonia on other hexagonally close-packed metal surfaces (**7,8**), some significant new results have been obtained. First, off-specular EEL spectra have allowed two normal modes of chemisorbed ammonia to be identified which have not been identified previously on close-packed surfaces. These are ν(M–NH_3) at 340 cm^{-1} and $\rho(NH_3)$ at 625 cm^{-1}, with the corresponding modes of ND_3 occurring at approximately 350 and 480 cm^{-1}, respectively. The identification of these modes allows a more detailed comparison between chemisorbed ammonia and ammonia in metal clusters to be made, and shows the importance of obtaining off-specular spectra when EELS is used to

study ammonia chemisorption. Second, it has been shown that the frequency of the $\delta_s(NH_3)$ loss feature of ammonia on Ru(001) undergoes a monotonic and nearly linear downward shift as a function of increasing coverage. The frequency of this mode in mononuclear metal compounds is strongly sensitive to the charge on the metal atom, and the observed frequency shift on Ru(001) can be correlated with the large work function decrease that occurs when ammonia is adsorbed on this surface (**6**). Finally, a detailed comparison has been made between the vibrational spectra of chemisorbed ammonia and ammonia ligands in metal compounds (**9**), and on most metal surfaces the vibrational spectra of chemisorbed ammonia are very similar to the vibrational spectra of ammonia in $M(NH_3)_6^{2+}$ compounds. This has led to a preference for the on-top binding site for ammonia on Ru(001), in contrast to the previous suggestion (**6**) that ammonia occupies threefold hollow sites.

References

1. Barteau, M. A.; Broughton, J. Q.; Menzel, D., Appl. Surface Sci. **1984**, 19, 92.

2. Hills, M. M.; Parmeter, J. E.; Mullins, C. B.; Weinberg, W. H., J. Am. Chem. Soc. **1986**, 108, 3554.

3. Hills, M. M.; Parmeter, J. E.; Weinberg, W. H., J. Am. Chem. Soc. **1987**, 109, 4224.

4. Jakob, P.; Cassuto, A.; Menzel, D., Surface Sci., to be published.

5. Danielson, L.R.; Dresser, M.J.; Donaldson, E.E.; Sandstrom, D.R., Surface Sci. **1978**, 71, 599.

6. Benndorf, C.; Madey, T.E., Surface Sci. **1983**, 135, 164.

7. Sexton, B.A.; Mitchell, G.E., Surface Sci. **1980**, 99, 523.

8. Fisher, G.B.; Mitchell, G.E., J. Electron Spectros. Related Ph. **1983**, 29, 253.

9. Nakamoto, K., in "Infrared and Raman Spectra of Inorganic and Coordination Compounds", Third Edition, Wiley & Sons, New York, **1978**, 197-202.

CHAPTER XI

Appendices

Appendix 1

Adsorption and Decomposition of Formaldehyde on the Ru(001) Surface: The Spectroscopic Identification of η^2-H_2CO and η^2-HCO

[This appendix was published as a Communication by A. B. Anton, J. E. Parmeter and W. H. Weinberg, in *The Journal of the American Chemical Society* **1985**, 107, 5558.]

Abstract

The adsorption and decomposition of formaldehyde on the hexagonally close-packed Ru(001) surface have been studied using high-resolution electron energy loss spectroscopy. Following a saturation exposure of formaldehyde to this surface at 80 K, annealing to 250 K results in the formation of an η^2(C,O)-H_2CO species, i.e. molecular formaldehyde that is adsorbed in a side-on configuration. The carbon-oxygen bond of this species is rehybridized to sp^3, as evidenced by the ν(CO) frequency of approximately 1000 cm^{-1}. At low formaldehyde coverages at 80 K, an η^2(C,O)-HCO species (η^2-formyl) is also identified, with a ν(CO) frequency of 1180 cm^{-1}.

Reprinted from the Journal of the American Chemical Society, 1985, *107*, 5558.

Adsorption and Decomposition of Formaldehyde on the Ru(001) Surface: The Spectroscopic Identification of η^2-H_2CO and η^2-HCO

A. B. Anton, J. E. Parmeter, and W. H. Weinberg*

Division of Chemistry and Chemical Engineering
California Institute of Technology
Pasadena, California 91125

Received May 6, 1985

The interaction of formaldehyde with transition-metal surfaces is of obvious importance in view of the fact that species such as M–CH_2O and M–CHO may play a key role in the catalytic hydrogenation of carbon monoxide.[1-3] Recently, several organometallic complexes have been identified in which both formaldehyde[4-7] and the formyl group[8] function as dihapto (η^2-) ligands. In this paper, we report the results of high-resolution electron energy loss (HREELS) measurements of formaldehyde adsorbed on the hexagonally close-packed Ru(001) surface that demonstrate the existence of both η^2-H_2CO and η^2-HCO. This represents the first spectroscopic identification of either species on any metal surface.

The ultrahigh vacuum (UHV) system in which the experiments were performed has been described previously.[9] HREELS was used to identify surface reaction products after adsorption at 80 K, subsequent annealing up to 600 K, and recooling to 80 K to record the spectra. Gaseous H_2CO and D_2CO were produced by thermal dehydration and depolymerization of their parent polyoxymethylene glycols (paraformaldehyde) and were introduced into the UHV chamber through a leak valve. The H_2CO (D_2CO) produced by this method contains 3–5% H_2O (D_2O) impurity,[10] and, consequently, spectra recorded after heating below 170 K are expected to show vibrational features attributable to small amounts of coadsorbed water.[11]

Exposing the Ru(001) surface at 80 K to 7 langmuirs (1 langmuir = 10^{-6} torr s) or more of H_2CO or D_2CO results in the formation of molecular multilayers of formaldehyde, as evidenced by a comparison of the observed vibrational spectra to the IR spectrum of gaseous formaldehyde.[12] Annealing the surface to 140 K desorbs the multilayer, leaving adsorbed carbon monoxide (θ = 0.20 CO molecules/Ru surface atom),[13] hydrogen adatoms (θ = 0.40),[14] and another surface species (θ = 0.10) which is stable to approximately 250 K. This new species is identified as η^2-formaldehyde. The spectra for H_2CO and D_2CO are shown at the top of Figure 1, and mode assignments are given in Table I. The observed CO stretching frequency of approximately 1000 cm^{-1} is consistent with a reduction in bond order of the CO bond from double to single and is in good agreement with the CO stretching frequency of 1017 cm^{-1} for η^2-H_2CO in the organometallic compound $(PPh_3)_2(CO)_2Os(\eta^2\text{-}H_2CO)$.[4] The observed frequencies and deuteration shifts for the various CH_2 modes agree well with those observed for sp^2-CH_2 groups in various molecules.[15]

Table I. Mode Assignments for η^2-H_2CO (η^2-D_2CO) on Ru(001)

mode	η^2-H_2CO, cm^{-1}	η^2-D_2CO, cm^{-1}	frequency ratio (H_2CO/D_2CO)
ν(CO)	980	1020	0.96
ν_a,ν_s(CH_2)	2940	2225	1.32
δ(CH_2)	1450	1190	1.22
ω(CH_2)	1160	865	1.34
ρ(CH_2)	840	620	1.35

Table II. Mode Assignments for η^2-HCO (η^2-DCO) on Ru(001) with Corresponding Assignments from the Model Compound $HCOOCH_3$ • ($DCOOCH_3$) (See Ref 15)

mode	η^2-HCO, cm^{-1}	$HCOOCH_3$, cm^{-1}	η^2-DCO, cm^{-1}	$DCOOCH_3$, cm^{-1}
ν(CH)	2900	2943	*a*	2216
δ(CH)	1400	1371	980	1048
ν(CO)	1180	1207	1160	1213
π(CH)	1065	1032	825	870
ν(Ru-HCO)	590		550	

a Weak and not resolved from the tail of the strong feature due to adsorbed CO at 1990 cm^{-1}.

(1) Muetterties, E. L., Stein, J. *Chem. Rev.* **1979**, *79*, 479–490.
(2) Eisenberg, R., Hendricksen, D. E. *Adv. Catal.* **1979**, *28*, 79–172.
(3) Dombek, B. D. *Adv. Catal.* **1983**, *32*, 325–416.
(4) Brown, K. L.; Clark, G. R.; Headford, C. E. L.; Marsden, K.; Roper, W. R. *J. Am. Chem. Soc.* **1979**, *101*, 503–505.
(5) Gambarotta, S.; Floriani, C.; Chiesa-Villa, A.; Guastini, C. *J. Am. Chem. Soc.* **1982**, *104*, 2019–2020.
(6) Buhro, W. E., Patton, A. T., Strouse, C. E., Gladysz, J. A., McCormick, F. B., Etter, M. C. *J. Am. Chem. Soc.* **1983**, *105*, 1056–1058.
(7) Kropp, K., Skibbe, V., Erker, G., Kruger, C. *J. Am. Chem. Soc.* **1983**, *105*, 3353–3354
(8) Belmonte, P. A.; Cloke, F. G. N.; Schrock, R. R. *J. Am. Chem. Soc.* **1983**, *105*, 2643–2650.
(9) Thomas, G. E.; Weinberg, W. H. *Rev. Sci. Instrum.* **1979**, *50*, 497–501.
(10) Walker, J. F. "Formaldehyde"; Reinhold: New York, 1964; p 142.
(11) Thiel, F. A.; Hoffmann, F. M.; Weinberg, W. H. *J. Chem. Phys.* **1981**, *75*, 5556–5572.
(12) Herzberg, G. "Infrared and Raman Spectra"; D. Van Nostrand Co.: New York, 1945; p 300.
(13) Thomas, G. E.; Weinberg, W. H. *J. Chem. Phys.* **1979**, *70*, 954–961, 1437–1439. Weinberg, W. H. Methods Exp. Phys. **1985**, *22*, 23–125.
(14) Barteau, M. A., Broughton, J. Q., Menzel, D. *Surf. Sci.* **1983**, *133*, 443–452.
(15) Shimanouchi, T. "Tables of Vibrational Frequencies", Consolidated Vol. I, NSRDS-NBS 39, Vol. II.

0002-7863/85/1507-5558$01.50/0

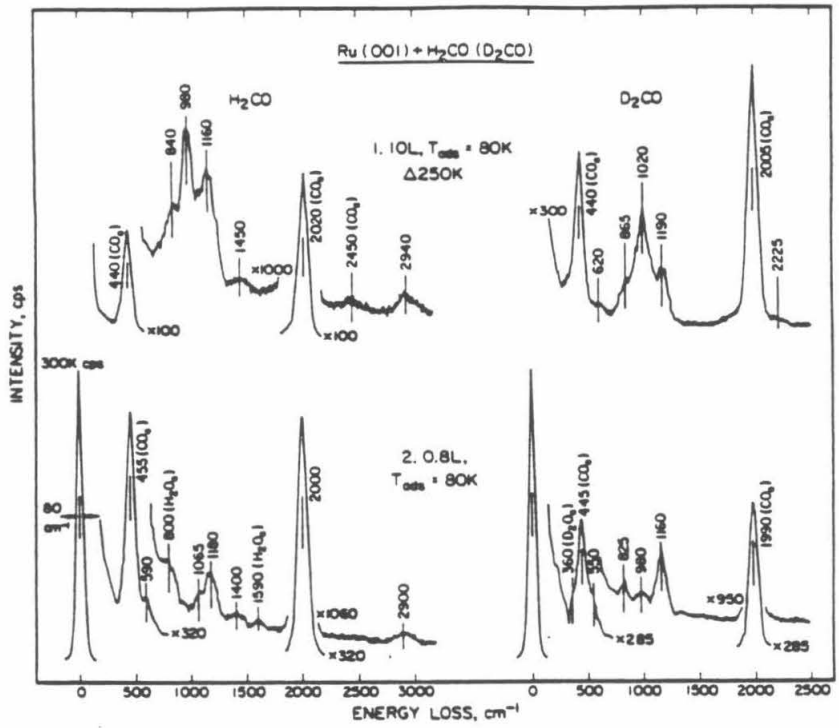

Figure 1. High-resolution electron energy loss spectra of (1) a multilayer exposure (10 langmuirs) of H_2CO (D_2CO) adsorbed on Ru(001) at 80 K and annealed to 250 K and (2) a submonolayer exposure (0.8 langmuir) of H_2CO (D_2CO) on Ru(001) at 80 K. The spectra in (1) are characteristic of η^2-formaldehyde, and those in (2) are characteristic of η^2-formyl. In all these spectra intense modes near 450 and 2000 cm^{-1} are due to adsorbed CO from formaldehyde decomposition, as is the weak combination band occasionally observed near 2450 cm^{-1}.[13] Adsorbed hydrogen adatoms from formaldehyde decomposition are not observed due to their extremely small scattering cross section.[14] Features at 800 and 1590 cm^{-1} in the H_2CO spectrum of (2) and near 360 cm^{-1} in the D_2CO spectrum of (2) are due to H_2O and D_2O,[11] respectively, to which the crystal is exposed unavoidably during the adsorption of H_2CO and D_2CO at 80 K.

Spectra of lower coverages of H_2CO or D_2CO on Ru(001) at 80 K reveal a species that is fundamentally different from the η^2-formaldehyde that results after annealing the formaldehyde multilayer. The spectra obtained after clean Ru(001) is exposed to 0.8 langmuir of H_2CO (or D_2CO) at 80 K are shown at the bottom of Figure 1. Although there is significant decomposition to adsorbed carbon monoxide ($\theta = 0.15$) and hydrogen ($\theta = 0.30$), additional loss features due to another adsorbed species ($\theta = 0.05$) are observed at 2900, 1400, 1180, 1065, and 590 cm^{-1} for H_2CO, and at 1160, 980, 825, and near 550 cm^{-1} for D_2CO. Heating to 100 K causes these features to disappear as this species decomposes to carbon monoxide admolecules and hydrogen adatoms. Weak features at 800 and 1590 cm^{-1} in the H_2CO spectrum and at 360 and 1150 cm^{-1} (obscured by the stronger mode at 1160 cm^{-1} associated with D_2CO adsorption in the spectrum of Figure 1) in the D_2CO spectrum persist to 170 K, the desorption temperature of water from the Ru(001) surface, and can be identified readily with librational and scissoring modes of small amounts of coadsorbed H_2O and D_2O, respectively.[11] The spectra in the bottom panel of Figure 1 can be identified unambiguously as an η^2-HCO (η^2-DCO) adspecies,[8] and the mode assignments are given in Table II. The presence of the η^2-formyl is perhaps not surprising in view of the fact that there is substantial decomposition of the formaldehyde to adsorbed carbon monoxide and hydrogen at low surface coverages, and η^2-formaldehyde exists at saturation monolayer coverage. The formyl ligand, although not heretofore identified on a surface, has been observed as a product of the interaction of formaldehyde with metal centers in organometallic compounds.[1,4,5] As would be expected, there is excellent agreement between the vibrational frequencies of the η^2-HCO (η^2-DCO) bonded to the Ru(001) surface and the corresponding vibrational frequencies of the HCO (DCO) function of the "model compound" $HCOOCH_3$ ($DCOOCH_3$),[15] of which the latter are listed in Table II. The mode at 590 cm^{-1} (550 cm^{-1}) for η^2-HCO (η^2-DCO) is assigned to the frustrated translation of the formyl perpendicular to the surface, its rather high frequency a natural consequence of the relatively low mass of HCO (DCO) and the stiffness of the (one) Ru–O and (two) Ru–C bonds which coordinate it to the surface.

The conditions that lead to the formation of η^2-HCO and η^2-H_2CO provide a consistent picture of the mechanism of H_2CO decomposition on the Ru(001) surface. The η^2-HCO is favored over η^2-H_2CO at low surface coverages because there exist vacant sites at which a hydrogen atom from the decomposing η^2-H_2CO may bind. At higher coverages the absence of such vacant sites inhibits decomposition and favors the formation of η^2-H_2CO. Indeed, precoverage of the Ru(001) surface by a saturation exposure (3 langmuirs) of H_2, followed by exposure to H_2CO at 80 K, results in the formation of η^2-H_2CO at all submonolayer coverages, with essentially no dissociation to adsorbed CO and hydrogen at 80 K.

The spectroscopic identifications put forward in this paper have been confirmed by off-specular HREELS measurements, thermal desorption mass spectrometry results, and complementary experiments concerning H_2CO and D_2CO adsorption on the Ru(001) surface modified by the presence of a p(2×2) ordered overlayer of oxygen adatoms. A complete discussion of all of these results will be presented separately.[16]

(16) Anton, A. B.; Parmeter, J. E.; Weinberg, W. H., unpublished results.

Acknowledgment. This research was supported by the National Science Foundation under Grant CHE-8206487. The assistance of Dr. Neil Avery in the early stages of this work is very much appreciated.

Appendix 2

The Adsorption of Formaldehyde on the Ru(001) and Ru(001)-p(2x2)-O Surfaces

[This appendix was published as a paper by A. B. Anton, J. E. Parmeter and W. H. Weinberg, in *The Journal of the American Chemical Society* 1986, 108, 1823.]

Reprinted from the Journal of the American Chemical Society, 1986, *108*, 1823.

Adsorption of Formaldehyde on the Ru(001) and Ru(001)-p(2×2)O Surfaces

A. B. Anton, J. E. Parmeter, and W. H. Weinberg*

Contribution from the Division of Chemistry and Chemical Engineering, California Institute of Technology, Pasadena, California 91125. *Received September 5, 1985*

Abstract: The adsorption of formaldehyde on the clean Ru(001) surface and a Ru(001) surface on which an ordered p(2×2) overlayer of oxygen adatoms is present has been investigated via high resolution electron energy loss vibrational spectroscopy and thermal desorption mass spectrometry. On the clean Ru(001) surface, the formaldehyde surface bonding interaction at 80 K is primarily via π_{CO} donation and π_{CO}^* backdonation, leading to decomposition to adsorbed hydrogen and CO for low exposures. With subsequent exposure to formaldehyde, a small fractional surface coverage (θ = 0.02–0.03) of η^2-formyl is observed, followed by formation of η^2-formaldehyde (θ = 0.10) and η^1-formaldehyde at saturation (monolayer) coverage. Upon heating, the η^2-formyl decomposes to adsorbed hydrogen and CO by 120 K, and the η^1-formaldehyde desorbs molecularly between 130 and 180 K. Further heating decomposes the remaining η^2-formaldehyde, and thermal desorption measurements indicate that a total of a quarter monolayer of formaldehyde decomposes on the Ru(001) surface under these conditions. The presence of the p(2×2)O overlayer (θ = 0.25) withdraws charge from the surface ruthenium atoms, increasing their Lewis acidity and making σ lone pair donation the dominant formaldehyde surface bonding interaction. Under these conditions, only η^1-formaldehyde is observed for all submonolayer coverages after adsorption at 80 K. After annealing the surface to 300 K to desorb η^1-formaldehyde, small amounts of η^2-formaldehyde (θ = 0.01) and η^2-formate (θ = 0.04) are observed. Compared to the clean surface, more molecular desorption of formaldehyde is observed in the 130–180 K temperature range, and the decomposition activity, as evidenced by the amount of CO and H_2 evolved from the surface, is decreased by a factor of 2 from a quarter to an eighth of a monolayer.

I. Introduction

A number of investigations have sought to elucidate the details of the heterogeneously catalyzed reaction of CO with H_2 to form methanol via studies of methanol adsorption and thermal decomposition on single crystalline metal surfaces. Studies on Ni(111),[1] Cu(100),[2] Pt(111),[3] Pd(100),[4] and Ru(001)[5] which have included results of electron energy loss spectroscopy (EELS) experiments to identify surface intermediates during the annealing of adsorbed overlayers of methanol have demonstrated the formation of an adsorbed methoxy intermediate [(g) denotes gaseous species and (a) adsorbed species], i.e.,

$$CH_3OH(g) \rightarrow CH_3OH(a)$$

and

$$CH_3OH(a) \rightarrow CH_3O(a) + H(a)$$

Heating of the surfaces to temperatures near 300 K resulted in decomposition of the adsorbed methoxy to yield H(a) and CO(a):

$$CH_3O(a) \rightarrow 3H(a) + CO(a)$$

No stable intermediates other than the methoxy could be isolated, indicating that intermediates in the methoxy decomposition, e.g., $H_2CO(a)$ or HCO(a), are less stable and decompose rapidly compared to the methoxy. The study of the chemisorption and thermal decomposition of formaldehyde on these metal surfaces may afford an opportunity to investigate the structures of adsorbed formaldehyde and formyl intermediates, providing a more complete mechanistic picture of methanol decomposition [and by inference, methanol synthesis from H_2 and CO[6]] in terms of elementary surface reactions. Pursuit of this information provides the motivation for the present study of formaldehyde adsorption on the Ru(001) surface.[7]

An early investigation of formaldehyde adsorption on W(100) and W(111) surfaces employing thermal desorption mass spectrometry (TDMS) demonstrated the evolution of H_2 and CO as the principal reaction products, with small amounts of CO_2 and methane produced only at coverages approaching a saturated monolayer.[8] A more recent TDMS study of formaldehyde adsorption on clean and carbided W(100) surfaces showed qualitatively similar results, but also indicated minority evolution of a small amount of methanol from the clean surface and the evolution of methyl formate together with enhanced formation of methanol and methane from the carbided surface.[9] On Ni(110), formaldehyde adsorption yielded H_2, CO, CO_2, H_2O, and methanol as reaction products,[10] and a more recent investigation of the same system,[11] which also included EELS results to identify surface intermediates, qualitatively duplicated the TDMS results of the previous investigation and showed that, in addition to hydrogen and CO from formaldehyde decomposition, methoxy is the primary surface intermediate, and mixed multilayers of solid formaldehyde and polymeric paraformaldehyde are formed at high coverages. Products similar to those observed for the reaction of formaldehyde with tungsten and nickel surfaces were also reported for clean and sulfided Pt(111) surfaces.[12] On an oxygen precovered Ag(110) surface,[13] EEL spectra consistent with an η^2-dioxymethylene species or paraformaldehyde were obtained below 200 K, and decomposition to evolve H_2 and CO_2 through a formate intermediate occurred upon heating the surface to 500 K. Similar results were obtained for formaldehyde adsorption on clean and oxygen precovered Cu(110) surfaces,[14] where EELS identified paraformaldehyde as the only monolayer species on both surfaces at low temperatures. Depolymerization of adsorbed paraformaldehyde released formaldehyde from both surfaces at 225 K. However, EEL spectra for the oxygen precovered surface showed that a reaction of formaldehyde with coadsorbed oxygen also occurred, producing adsorbed formate which decomposed to yield CO_2 and H_2 near 470 K.

More pertinent to the results reported here are studies of the homogeneous chemistry and structures of coordinated formaldehyde and formyl.[15-17] Several stable compounds displaying

(1) Demuth, J. E.; Ibach, H. *Chem. Phys. Lett.* **1979**, *60*, 395.
(2) Sexton, B. A. *Surf. Sci.* **1979**, *88*, 299.
(3) Sexton, B. A., *Surf. Sci.* **1981**, *102*, 271.
(4) Christmann, K.; Demuth, J. *J. Chem. Phys.* **1982**, *76*, 6308.
(5) Hrbek, J.; de Paola, R. A.; Hoffmann, F. M. *J. Chem. Phys.* **1984**, *81*, 2818.
(6) Henrici-Olivé, G.; Olivé, S. *Agnew. Chem., Int. Ed. Engl.* **1976**, *15*, 136.
(7) Anton, A. B.; Parmeter, J. E.; Weinberg, W. H. *J. Am. Chem. Soc.* **1985**, *107*, 5558.
(8) Yates, J. T.; Madey, T. E.; Dresser, M. J. *J. Catal.* **1973**, *30*, 260.
(9) Benziger, J. B.; Ko, E. I.; Madix, R. J. *J. Catal.* **1980**, *64*, 132.
(10) Dickinson, J. T.; Madix, R. J. *Int. J. Chem. Kinet.* **1978**, *10*, 871.
(11) Richter, L. J.; Ho, W. *J. Chem. Phys.* **1985**, *83*, 2165.
(12) Abbas, N. M.; Madix, R. J. *Appl. Surf. Sci.* **1981**, *7*, 241.
(13) Stuve, E. M.; Madix, R. J.; Sexton, B. A. *Surf. Sci.* **1982**, *119*, 279.
(14) Sexton, B. A.; Hughes, A. E., Avery, N. R. *Surf. Sci* **1985**, *155*, 366.

0002-7863/86/1508-1823$01.50/0

η^2(O,C) coordination geometries [bonded to the metal atom(s) through both the oxygen and carbon atoms of the carbonyl, hereafter referred to simply as η^2] for formaldehyde[18-21] and acetaldehyde[22] have been synthesized and characterized structurally. Furthermore, evidence for η^1(O) coordination [bonded end-on to the metal atom through only the oxygen atom, hereafter referred to simply as η^1] has been obtained for a formaldehyde complex of ruthenium.[23] Structures analogous to both of these have been observed for the adsorption of the structurally similar acetone molecule on the Ru(001) surface.[24] Finally, η^1-formyl,[23,25-29] η^2-formyl,[30-32] and similar η^1-acyl complexes[33-37] have also been synthesized and characterized structurally.

This paper presents an EELS and TDMS investigation of the adsorption and reactions of formaldehyde on both the clean Ru(001) surface and a Ru(001) surface modified chemically by the presence of an ordered p(2×2) overlayer of oxygen adatoms. The results of the experiments conducted on the clean Ru(001) surface differ from those described earlier for other single crystalline metal surfaces in that no evidence for associative reactions on the surface is obtained. Instead, only reversible molecular adsorption and decomposition to hydrogen and CO through intermediates similar to those observed in the homogeneous chemistry of model CO hydrogenation reactions are observed. Addition of the p(2×2) oxygen overlayer not only provides an adsorbed reactant which may open surface reaction channels that did not exist on the clean surface, but it also withdraws charge from the surface ruthenium atoms, increasing their Lewis acidity and altering their reactivity toward the reactions identified on the clean surface. The results obtained for formaldehyde adsorption and decomposition provide an interesting and chemically consistent comparison to those obtained previously for the adsorption of acetone on the same clean and oxygen modified surfaces.[24]

II. Experimental Procedures

A description of the EEL spectrometer and the UHV system in which it is contained has been published previously.[38] EEL spectra were recorded at a resolution of 80 cm^{-1} (full-width at half-maximum) with a count rate of 3×10^5 Hz in the specularly reflected, elastically scattered electron beam. Incident electron beam kinetic energies at the sample were 5–6 eV.

The Ru(001) surface was cleaned by using standard techniques of Ar^+ sputtering and annealing in oxygen.[39] Surface cleanliness was monitored via both EELS and TDMS. The ordered p(2×2) overlayer of oxygen adatoms, with an ideal surface coverage of 0.25 monolayer, was prepared by exposing the clean surface to 0.8 L of O_2 (1 L = 10^{-6} torr-s) at 95 K, followed by thermal ordering at a temperature of approximately 350 K.[40,41]

Gaseous H_2CO and D_2CO were produced by thermal dehydration and depolymerization of their parent polyoxymethylene glycols (paraformaldehyde), and the crystal surface was exposed to these gases by backfilling the UHV chamber through leak valves. Exposures quoted in the text were measured with a Bayard–Alpert ionization gauge, uncorrected for relative ionization cross sections.

The formaldehyde used in these experiments was purified by extensive pumping on the solid paraformaldehyde prior to thermal depolymerization. Storage lines which held formaldehyde prior to introduction into the UHV chamber were cleaned and refilled frequently, and the composition of the vapor introduced into the UHV chamber was checked in situ via mass spectrometry. Water is an unavoidable product of the thermal depolymerization reaction[42]

$$H(H_2CO)_nOH \rightarrow nH_2CO(g) + H_2O(g)$$

and high grade paraformaldehydes as were used in this work [H_2CO from Aldrich Chemical Co., and D_2CO from U.S. Services Inc. (98 atom % D)] have an average degree of polymerization near 30. Thus the vapor produced by thermal depolymerization is expected to contain approximately 3 mol % water. Further purification of the vapor, for example, by treatment with standard chemical drying agents, is in general fruitless, since these materials also catalyze the decomposition and polymerization of formaldehyde.[42] Fortunately, the adsorption properties of water on both the clean[43] and oxygen precovered[44] Ru(001) surfaces have been characterized thoroughly by both TDMS and EELS, allowing extraction from the EEL spectra for formaldehyde adsorption those features attributable to the presence of small amounts of coadsorbed water after annealing of the surface to temperatures below 170 K, the low coverage desorption temperature for water on Ru(001). Another impurity in formaldehyde that is produced from depolymerization of paraformaldehyde is methyl formate.[8,42]

Although the formaldehyde used previously[8-14] was prepared by methods nearly identical with those employed here, in most cases little or no mention is made of the presence of water and methyl formate

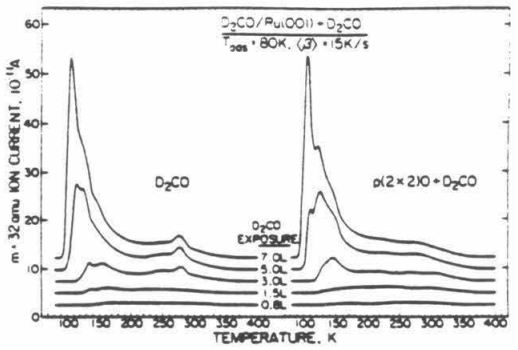

Figure 1. Thermal desorption spectra for increasing exposures of D_2CO on the clean Ru(001) (left) and Ru(001)–p(2×2)O (right) surfaces at 80 K. The average heating rate, (β), for these spectra and the spectra of Figures 2 and 3 was 15 K/s.

(15) Muetterties, E. L.; Stein, J. L. *Chem. Rev.* **1979**, *79*, 479.
(16) Masters, C. *Adv. Organomet. Chem.* **1979**, *17*, 61.
(17) Dombek, B. D. *J. Am. Chem. Soc.* **1980**, *102*, 6855.
(18) Brown, K. L.; Clark, G. R.; Headford, C. E. L.; Marsden, K.; Roper, W. R. *J. Am. Chem. Soc.* **1979**, *101*, 503.
(19) Gambarotta, S.; Floriani, C.; Chiesi-Villa, A.; Guastini, C. *J. Am. Chem. Soc.* **1982**, *104*, 2019; **1985**, *107*, 2985.
(20) Buhro, W. E.; Patton, A. T.; Strouse, C. E.; Gladysz, J. A. *J. Am. Chem. Soc.* **1983**, *105*, 1056.
(21) Kropp, K.; Skibbe, V.; Erker, G.; Krüer, K. *J. Am. Chem. Soc.* **1983**, *105*, 3353.
(22) Adams, H.; Bailey, N. A.; Gauntlett, J. T.; Winter, M. J. *J. Chem. Soc., Chem. Commun.* **1984**, 1360.
(23) Chaudret, B. N.; Cole-Hamilton, D. J.; Nohr, R. S.; Wilkinson, G. *J. Chem. Soc., Dalton Trans.* **1977**, 1546.
(24) Avery, N. R.; Weinberg, W. H.; Anton, A. B.; Toby, B. H. *Phys. Rev. Lett.* **1983**, *51*, 682. Anton, A. B.; Avery, N. R.; Toby, B. H.; Weinberg, W. H. *J. Am. Chem. Soc.*, in press.
(25) Thorn, D. L. *J. Am. Chem. Soc.* **1980**, *102*, 7109; *Organomet.* **1982**, *1*, 197
(26) Wong, W.-K.; Tam, W.; Strouse, C. E.; Gladysz, J. A. *J. Chem. Soc., Chem. Commun.* **1979**, 530.
(27) Casey, C. P.; Neumann, S. M.; Andrews, M. A.; McAlister, D. P. *Pure Appl. Chem.* **1980**, *52*, 625.
(28) Morton, J. R.; Preston, K. F. *Chem. Phys. Lett.* **1984**, *111*, 611.
(29) Casey, C. P.; Meszaros, M. W.; Neumann, S. M.; Cesas, I. G.; Hailer, K. J. *Organomet.* **1985**, *4*, 143.
(30) Moloy, K. G.; Marks, T. J. *J. Am. Chem. Soc.* **1984**, *106*, 7051. Marks, T. J. *Science (Washington, D.C.)* **1982**, *217*, 989.
(31) Belmonte, P. A.; Clarke, F. G. N.; Schrock, R. R. *J. Am. Chem. Soc.* **1983**, *105*, 2643. Churchill, M. R.; Wasserman, H. J. *Inorg. Chem.* **1983**, *21*, 226.
(32) Wolczanski, P. T.; Bercaw, J. E. *Acc. Chem. Res.* **1980**, *13*, 121.
(33) Roper, W. R.; Taylor, G. E.; Waters, J. M.; Wright, L. J. *J. Organomet. Chem.* **1979**, *182*, C46.
(34) Sukel, K.; Schloter, K.; Beck, W.; Ackerman, K.; Schubert, U. *J. Organomet. Chem.* **1983**, *241*, 333.
(35) Merlino, S.; Montagnoli, G.; Braca, G.; Sbrana, G. *Inorg. Chim. Acta* **1978**, *27*, 233.
(36) Longato, B.; Norton, J. R.; Huffmann, J. C.; Marsella, J. A.; Caulton, K. G. *J. Am. Chem. Soc.* **1981**, *103*, 209.
(37) Bristow, G. S.; Hitchcock, P. B.; Lappert, M. F. *J. Chem. Soc., Chem. Commun.* **1982**, 462.
(38) Thomas, G. E.; Weinberg, W. H. *Rev. Sci. Instrum.* **1979**, *50*, 497.
(39) Thomas, G. E.; Weinberg, W. H. *J. Chem. Phys.* **1979**, *70*, 954.
(40) Rahman, T. S.; Anton, A. B.; Avery, N. R.; Weinberg, W. H. *Phys. Rev. Lett.* **1983**, *51*, 1979.
(41) Madey, T. E.; Engelhardt, H. A.; Menzel, D. *Surf. Sci.* **1975**, *48*, 304.
(42) Walker, J. F. "Formaldehyde", 3rd ed.; Reinhold: New York, 1964; pp 44–45, 215.
(43) Thiel, P. A.; Hoffmann, F. M.; Weinberg, W. H. *J. Chem. Phys.* **1981**, *75*, 5556.
(44) Thiel, P. A.; Hoffmann, F. M.; Weinberg, W. H. *Phys. Rev. Lett.* **1982**, *49*, 501.

impurities and their potential importance on the chemistry of the surfaces investigated. For example, small amounts of methane, carbon dioxide, and methyl formate evolution in TDMS after large formaldehyde exposures.[8,9,12] may be due to the adsorption and/or reaction of a methyl formate contaminant. Furthermore, the polymerization of formaldehyde to give adsorbed paraformaldehyde[11,13,14] may not result from the interaction of formaldehyde with the clean metal surface but rather from the interaction of formaldehyde with adsorbed water, which is known to catalyze formaldehyde polymerization rapidly on rather nonreactive surfaces below 100 °C.[42]

Thermal desorption measurements were made in a line-of-sight configuration with a UTI 100C quadrupole mass spectrometer, oriented approximately 40° from the surface normal. Surface coverages of H_2 and CO reported for the reaction product TDMS measurements were obtained by comparing the time integrated ion current of the desorption spectra to those obtained for desorption of known coverages of H_2[45] and CO[46] and are accurate to approximately 10%.

III. Results

A. Thermal Desorption Spectra of Formaldehyde from the Clean Ru(001) and the Ru(001)–p(2×2)O Surfaces. Thermal desorption spectra of D_2CO recorded after the indicated exposures of the clean Ru(001) surface and the Ru(001)–p(2×2)O surface to D_2CO at 80 K are shown at the left and right of Figure 1, respectively. For exposures of 0.8 L or less of D_2CO on both surfaces, no molecular formaldehyde desorption is observed. For exposure of the clean surface to 1.5 L or more of D_2CO, desorption rate maxima associated with monolayer adsorbed states appear near 130 and 155 K. These peaks saturate and shift slightly to lower temperatures for exposures of 5 L or more. Another peak appears near 110 K, the amplitude of which grows without saturation for increasing exposures, indicating that it is associated with multilayers of formaldehyde condensed on the surface. A small sharp peak is also evident near 275 K for exposures of 3 L or more. Activation energies for desorption for the monolayer states desorbing at 130, 155, and 275 K, estimated for first-order desorption kinetics via the method of Redhead with $\nu = 10^{13}$ s^{-1},[47] are 7.3, 8.8, and 16.0 kcal/mol, respectively. Similar results are obtained for desorption from the Ru(001)–p(2×2)O surface, although desorption from the monolayer states near 130 and 155 K is enhanced for equivalent exposures compared to the clean surface, and the state at 275 K is extinguished.

B. Thermal Desorption Spectra of the Decomposition Products, CO and H_2, from Formaldehyde on the Clean Ru(001) and the Ru(001)–p(2×2)O Surfaces. To check for the possible formation of surface reaction products like those identified in earlier studies of formaldehyde adsorption, thermal desorption spectra were recorded at m = 20 amu (D_2O^+, CD_4^+), m = 34 amu (CD_3O^+ the principal cracking fragment of CD_3OD), m = 44 amu (CO_2^+), and m = 64 amu ($DCOOCD_3^+$), in addition to m = 4 amu and m = 28 amu for the principal reaction products, D_2 and CO. No desorption at m = 44 and m = 64 amu was detected for monolayer saturation exposures of both the clean Ru(001) and the Ru(001)–p(2×2)O surfaces to D_2CO at 80 K, and only weak features with intensities lower than those observed for D_2 and CO by factors of 100–1000 were observed at 160–180 K for D_2O and 280–320 K for CD_3OD. Consequently, all D_2O and CD_3OD evolved from both the clean Ru(001) and the Ru(001)–p(2×2)O surfaces are due to impurities in the adsorbed D_2CO. The only desorption products resulting from the interaction of D_2CO with both surfaces are D_2CO, D_2, and CO. Noteworthy in these results is the absence of significant D_2O production from the reaction of deuterium adatoms from D_2CO decomposition with the oxygen adatoms of the p(2×2)O overlayer. This is because the p(2×2)O overlayer destabilizes adsorbed hydrogen into a new binding state with a reduced activation energy for desorption, to be discussed below, decreasing the barrier to hydrogen adatom recombination and desorption.

Thermal desorption spectra of CO recorded after exposure at 80 K of both the clean Ru(001) and the Ru(001)–p(2×2)O surfaces to 0.8, 1.5, and 5.0 L (monolayer saturation) of D_2CO are shown at the top of Figure 2. Also shown for comparison at the bottom of Figure 2 are spectra recorded after the adsorption of CO. In all these spectra, fractional surface coverages are assigned by comparison to spectra recorded for saturation exposures of the clean surface to CO, where θ_{CO} = adsorbed CO molecules per ruthenium surface atom = 49/75 at saturation.[46] Since no other reaction products were observed, the CO coverages indicate directly the amount of D_2CO decomposition. For 0.8 L exposures of both surfaces to D_2CO, comparable amounts of decomposition are observed, 0.08 monolayer on the clean Ru(001) surface and 0.07 monolayer on the Ru(001)–p(2×2)O surface. As the D_2CO exposure is increased, however, decomposition on the clean surface increases relative to that on the oxygen precovered surface, and for 5-L (monolayer saturation) exposures on both surfaces, the decomposition activity of the clean surface [θ_{CO} = 0.26] is twice that of the Ru(001)–p(2×2)O surface [θ_{CO} = 0.13]. The peak shapes and positions are unperturbed compared to those resulting from adsorption of CO on the same surfaces, suggesting that the surfaces are free of other adsorbed species which could affect the CO desorption rate.

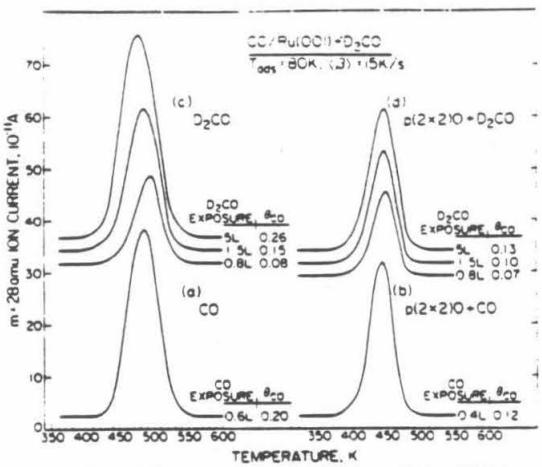

Figure 2. Thermal desorption spectra showing the evolution of CO from Ru(001) following exposure (a) of the clean surface to 0.5 L of CO, (b) of the Ru(001)–p(2×2)O surface to 0.4 L of CO, and (c) of the clean and (d) the Ru(001)–p(2×2)O surfaces to the indicated exposures of D_2CO.

Thermal desorption spectra of D_2 from the decomposition of adsorbed D_2CO, following exposures of both surfaces to D_2CO equal to those used to generate the CO thermal desorption spectra of Figure 2, are shown at the top of Figure 3. For comparison, thermal desorption spectra after D_2 adsorption on both surfaces are shown at the bottom of Figure 3. Coverages for all the spectra are assigned by comparison to the 4.0-L (monolayer saturation) exposure of D_2 on the clean surface where θ_D = 0.85.[45]

Of particular interest are the spectra recorded for the adsorption of D_2 on the Ru(001)–p(2×2)O surface, shown at the bottom of Figure 3. Comparison to the 0.2-L spectrum for D_2 adsorption on the clean surface immediately above shows that the average probability of adsorption up to a coverage of approximately θ_D = 0.15 is increased by a factor of two on the Ru(001)–p(2×2)O surface relative to the clean surface. Desorption of D_2 is complete by 250 K, indicating that the activation energy for desorption is less than 9 kcal/mol [estimated for second-order desorption kinetics via the method of Redhead with $\nu = 10^{-4}$ cm^2 s^{-1},[47]], as compared to 17.0 kcal/mol on the clean surface.[45] The peak near 200 K shifts downward with increasing coverage, indicative of second-order desorption kinetics, and at saturation this state contains 0.23 monolayer of deuterium adatoms. The state at lower temperature, which fills after the state at 200 K and is shown

(45) Shimizu, H.; Christmann, K.; Ertl, G. *J. Catal.* **1980**, *61*, 412.
(46) Williams, E. D.; Weinberg, W. H. *Surf. Sci.* **1979**, *82*, 93.
(47) Redhead, P. A. *Vacuum* **1962**, *12*, 203.

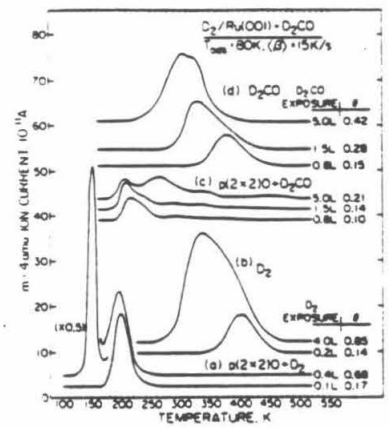

Figure 3. Thermal desorption spectra showing the evolution of D_2 from Ru(001) following the indicated exposures of (a) the Ru(001)–p(2×2)O and (b) the clean Ru(001) surfaces to D_2CO.

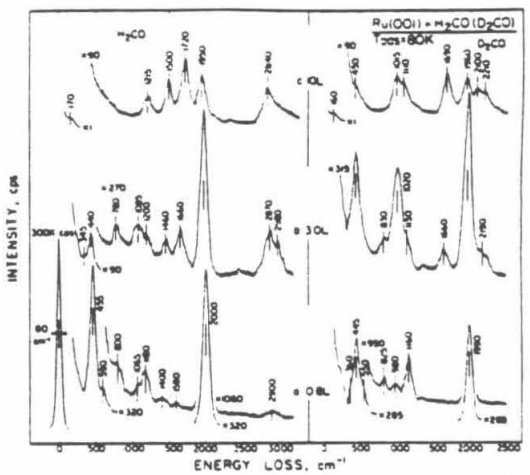

Figure 4. EEL spectra recorded after the indicated exposures of the clean Ru(001) surface to H_2CO (left) and D_2CO (right) at 80 K.

expanded by a factor of 0.5 in Figure 3, contains an additional 0.45 monolayer of deuterium adatoms, and its peak temperature remains constant at 150 K from its initial appearance to the exposure necessary for its saturation (0.4 L). The 2:1 stoichiometry of these two states, plus the near match of their populations to the 0.25 monolayer ideal coverage of the p(2×2)O overlayer, suggests that occupation of the state at 200 K contributes stoichiometrically one deuterium atom per p(2×2)O unit cell, and occupation of the state at 150 K contributes an additional two deuterium atoms per p(2×2)O unit cell. Other experiments[48] have shown that the appearance of both these states is intimately related to the presence of the p(2×2)O overlayer. As the ordered oxygen coverage is increased past 0.25 monolayer, the resulting overlayer is a combination of local regions of both the p(2×2) and the p(1×2) overlayer,[49] which is developed fully at an oxygen coverage of 0.50 monolayer and does not chemisorb hydrogen at these temperatures. For ordered oxygen adatom coverages below 0.25 monolayer, the thermal desorption spectra of adsorbed D_2 are a linear combination of the clean surface and the surface on which the p(2×2)O overlayer is present.

The stoichiometry of the overall decomposition reaction for formaldehyde

$$D_2CO(a) \rightarrow CO(a) + 2D(a)$$

indicates that, in the absence of other surface reactions which consume deuterium, the coverages obtained for the thermal desorption spectra of D_2 at the top of Figure 3 should be twice the coverages obtained for the CO TDMS data of Figure 2. Agreement is obtained within experimental error.

For the thermal desorption spectra obtained after adsorption of D_2CO on the clean Ru(001) surface, all D_2 evolution can be attributed to desorption from the surface after D_2CO decomposition at lower temperature, since the peak shapes and positions match very closely those obtained for the coadsorption of H_2 and CO on Ru(001).[49] On the Ru(001)–p(2×2)O surface, however, features at temperatures above approximately 250 K are clearly due to the decomposition of adsorbed species in this temperature range, as can be deduced by comparison to the spectra for the Ru(001)–p(2×2)O surface shown in Figure 3a and c.

The decreased decomposition activity of the Ru(001)–p(2×2)O surface compared to the clean Ru(001) surface could be attributed reasonably to a decreased amount of formaldehyde adsorption into monolayer states on the oxygen precovered surface, resulting from blocking by the oxygen adatoms of the p(2×2) overlayer of formaldehyde adsorption sites which would otherwise be available on the clean surface. Since the temperature of formaldehyde adsorption, 80 K, is well below the temperature of desorption of condensed multilayers of formaldehyde, 110 K, formaldehyde molecules striking either the clean or the Ru(001)–p(2×2)O surface during exposure at 80 K are expected to adsorb with a probability near unity. Then, the exposures necessary to initiate formation of the multilayer state on each surface in the thermal desorption spectra for formaldehyde give a relative measure of how much formaldehyde is adsorbed into the monolayer states on both surfaces. As may be seen in Figure 1, no desorption from the multilayer state is observed for 3-L exposures of both the clean Ru(001) and the Ru(001)–p(2×2)O surfaces to D_2CO, whereas 5-L exposures produce multilayer desorption from both surfaces. The multilayer state shows greater population for a 5-L exposure of the clean Ru(001) surface to formaldehyde than the Ru(001)–p(2×2)O surface, indicating that more adsorption into monolayer states occurs on the oxygen precovered surface than on the clean Ru(001) surface. Thus, the decreased decomposition activity of the Ru(001)–p(2×2)O surface, compared to the clean Ru(001) surface, must be due to the differences in the reactivity of the adsorbed formaldehyde present on the two surfaces and is not due simply to differences in the amounts of formaldehyde adsorbed.

C. EELS of Formaldehyde on the Clean Ru(001) Surface. EEL spectra recorded after increasing exposures of the clean Ru(001) surface to both H_2CO and D_2CO are shown in Figure 4. For exposures below approximately 0.5 L, total decomposition at 80 K is evidenced by the appearance of only strong vibrational features near 450 and 2000 cm^{-1} due to approximately 0.10 monolayer of adsorbed CO.[39] Features attributable to hydrogen or deuterium adatoms from formaldehyde decomposition are not detected due to their extremely small inelastic scattering cross section on the Ru(001) surface.[50] After a 0.8-L exposure, however, the EEL spectrum of H_2CO shows modes due to other surface species at 590, 800, 1065, 1180, 1400, 1590, and 2900 cm^{-1}. Heating the surface to 120 K causes the modes at 590, 1065, 1180, 1400, and 2900 cm^{-1} to disappear, leaving features at 800 and 1590 cm^{-1} and increasing the intensities of the features due to adsorbed CO by an amount consistent with an increase of the CO coverage of 0.02–0.03 monolayer. Similar results are observed for identical experiments for the adsorption of D_2CO: heating the surface to 120 K removes features near 550 (shoulder), 825,

(48) Anton, A. B.; Weinberg, W. H., unpublished results.
(49) Peebles, D. E.; Schreifels, J. A.; White, J. M. *Surf. Sci.* **1982**, *116*, 117.
(50) Barteau, M. A.; Broughton, J. Q.; Menzel, D. *Surf. Sci.* **1983**, *133*, 443.

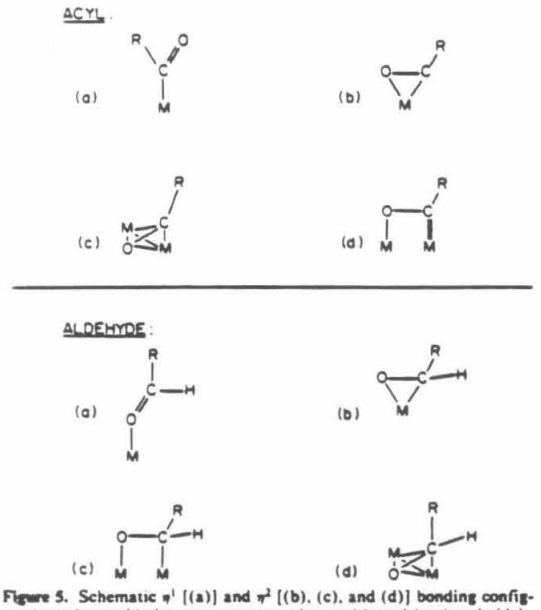

Figure 5. Schematic η^1 [(a)] and η^2 [(b), (c), and (d)] bonding configurations observed in homogeneous complexes with acyl (top) and aldehyde (bottom) ligands.

980, and 1160 cm^{-1}, leaving the shoulder near 360 cm^{-1} and a weak feature at 1150 cm^{-1}. A feature for D_2CO corresponding to that at 2900 cm^{-1} for H_2CO should appear near 2100 cm^{-1}, but would be expected to be quite weak and is not resolved from the tail of the strong feature due to ν(CO) at 1990 cm^{-1}. Spectra which were extended to higher loss energies also showed very weak features at 3500 cm^{-1} for H_2CO and 2500 cm^{-1} for D_2CO which were present both before and after annealing to 120 K. By comparison to EEL spectra obtained for water adsorption on Ru(001),[43] the modes at 800 (360), 1590 (1150), and 3500 (2500) cm^{-1} can be readily assigned to librational modes (frustrated translation), $\delta(H_2O)$ [$\delta(D_2O)$] and ν(OH) [ν(OD)], respectively, of less than 0.01 monolayer of adsorbed H_2O (D_2O) from para-formaldehyde depolymerization. The other features are due to a weakly stable species which is an intermediate in the formaldehyde decomposition to hydrogen adatoms and adsorbed CO.

Due to the prevalance of the formyl ligand in organometallic chemistry, such a species must be considered as a possible intermediate in the decomposition of formaldehyde on the Ru(001) surface. Indeed, the vibrational spectra shown in Figure 4a are consistent with a formyl intermediate bound to the surface in an η^2 configuration (see also Figure 5). A comparison of the spectra in Figure 4a for H_2CO and D_2CO allows immediate identification of the modes at 1180 and 1160 cm^{-1} as being due to the carbon–oxygen stretching vibration. The low frequency indicates that the carbon–oxygen bond order is lowered to nearly one, signifying η^2 coordination to the surface. With this established, the remaining modes for η^2-HCO can be assigned as follows: δ(HCO), the in-plane deformation at 1400 cm^{-1}; π(CH), the out-of-plane deformation at 1065 cm^{-1}; and ν(CH), at 2900 cm^{-1}. The corresponding modes for η^2-DCO are at 980, 825, and near 2100 cm^{-1} (not resolved). Substantial justification for these assignments and the postulated η^2 coordination geometry for formyl on Ru(001) can be obtained by comparison to the normal mode frequencies for the model compounds $HCOOCH_3$ and $DCOOCH_3$,[51] where the HCO and DCO functions of each compound mimic in carbon–oxygen bond order and structural arrangement

(51) Shimanouchi, T. "Tables of Vibrational Frequencies"; Consolidated Vol. 1, NSRDS-NBS 39; Vol. II.

Table I. Assignments of Vibrational Bands (in cm^{-1}) Observed with High Resolution Electron Energy Loss Spectroscopy of η^2-HCO and η^2-DCO on Ru(001)[a]

mode	η^2-HCO	$HCOOCH_3$[51]	η^2-DCO	$DCOOCH_3$[51]
ν(CH)	2900	2943		2216
δ(CH)	1400	1371	980	1048
ν(CO)	1180	1207	1160	1213
π(CH)	1065	1032	825	870
ν(Ru–HCO)	590		550	

[a] Also listed for comparison are the IR bands for the HCO and DCO functions of the model compounds $HCOOCH_3$ and $DCOOCH_3$.

the geometry expected for η^2-formyl on the Ru(001) surface. As may be seen from the results listed in Table I, the correspondence is excellent. The mode at 590 cm^{-1} for η^2-HCO, appearing as a shoulder near 550 cm^{-1} for η^2-DCO, is assigned as the frustrated translation of the formyl perpendicular to the surface.

Exposure of the clean Ru(001) surface to 3.0 L of H_2CO or D_2CO [cf, Figure 4b] adds new features to the EEL spectra which signify the presence of surface species other than η^2-formyl. The appearance of a carbonyl band at 1660 cm^{-1} in both spectra, by analogy to the results obtained for adsorption of the structurally similar acetone molecule on Ru(001),[24] indicates the presence of molecular formaldehyde coordinated to the surface in an η^1 configuration. This bonding configuration, shown schematically in (a) in the bottom panel of Figure 5, results from overlap of a single lobe of the nonbonding lone pair orbital of formaldehyde, localized strongly on the oxygen atom, with a ds hybrid acceptor orbital of the metal, resulting in a net transfer of electron density from the formaldehyde ligand to the metal surface. This σ-donation interaction leaves the skeleton of the formaldehyde molecule unperturbed other than the red-shift of ν(CO) to 1660 cm^{-1} from its value of 1744 cm^{-1} for free H_2CO and 1700 cm^{-1} for free D_2CO.[52] Since the remaining features in both spectra cannot all be attributed to η^1-formaldehyde, another surface species is also present under these conditions. The features at 345 and 780 cm^{-1} in the spectrum for H_2CO are due to the frustrated translational and librational modes of coadsorbed H_2O, respectively,[43] and the corresponding modes in the spectrum of D_2CO are not resolved from the tail of the elastic peak and the strong feature due to adsorbed CO near 450 cm^{-1}. Having identified η^1-formaldehyde by the presence of ν(CO) at 1660 cm^{-1}, the assignments of the remaining features in these spectra and the structural identification of other species present is best left for the discussion of subsequent spectra, where each species is isolated and characterized unambiguously.

The addition of another 7 L of formaldehyde to the clean Ru(001) surface to give a total exposure of 10 L at 80 K produces condensed multilayers of formaldehyde, as was shown in the TDMS results of Figure 1. EEL spectra recorded for H_2CO and D_2CO under these conditions are shown in Figure 4c, and assignments and corresponding frequencies for solid H_2CO and D_2CO[53] are listed in Table II. As was observed for multilayer adsorption of formaldehyde on Ag(110),[12] a strong lattice vibration appears at 170 cm^{-1} for H_2CO (160 cm^{-1} for D_2CO), and the frequencies for all other vibrations correspond more closely to those of solid formaldehyde[53] than to those of gaseous formaldehyde.[52] The intensity of ν(CO) due to adsorbed CO in these spectra indicates that decomposition of approximately 0.15 monolayer of formaldehyde occurs upon adsorption at 80 K.

Shown in Figure 6 are EEL spectra recorded after exposure of the clean Ru(001) surface to 10 L of H_2CO (left) and 10 L of D_2CO (right), followed by annealing to the indicated temperatures. After annealing to 150 K, the mode at 1660 cm^{-1} evident in the 3.0-L spectra of Figure 4b for both H_2CO and D_2CO is absent, indicating that η^1-formaldehyde has desorbed by this temperature and correlating well with the evolution of form-

(52) Herzberg, G. "Infrared and Raman Spectra of Polyatomic Molecules"; Van Nostrand: New York, 1945.

(53) Khoshkoo, H.; Hemple, S. T.; Nixon, E. R. *Spectrochim. Acta, Part A* **1974**, *30A*, 863.

Table II. Assignments of Vibrational Bands (in cm^{-1}) Observed with High Resolution Electron Energy Loss Spectroscopy of H_2CO and D_2CO on Ru(001) and Ru(001)-p(2×2)O[a]

mode and sym. for free formaldehyde	solid[53]		Ru(001) and Ru(001)-p(2×2)O					
			H_2CO			D_2CO		
	H_2CO	D_2CO	multilayer	η^1(80 K)	η^2(250 K)	multilayer	η^1(80 K)	η^2(250 K)
$\nu_a(CH_2)(B_1)$	2843	2214		2970		2210		
			2840		2940		2200–2250	2225
$\nu_s(CH_2)(A_1)$	2831	2095		2850		2100		
$\nu(CO)(A_1)$	1700	1660	1720	1660–1680	980	1690	1640–1660	1020
$\delta(CH_2)(A_1)$	1490	1096	1500	1465	1450	1110	1190	1190
$\rho(CH_2)(B_1)$	1250	990			840			620
			1215	1195–1240		1015	1025	
$\omega(CH_2)(B_2)$	1179	942			1160			865
lattice	161	152	170			160		

[a] Also listed are the IR bands of solid H_2CO and D_2CO.

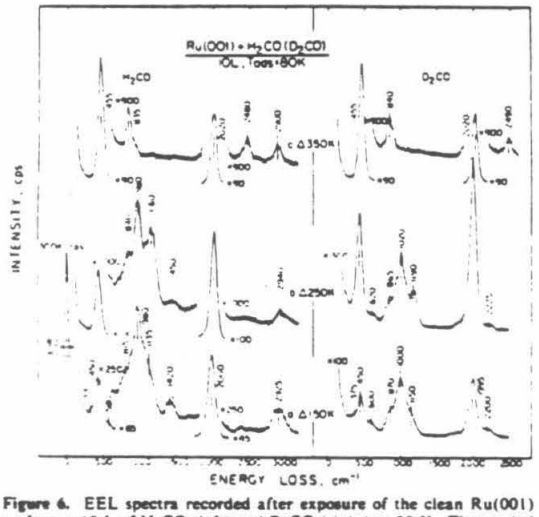

Figure 6. EEL spectra recorded after exposure of the clean Ru(001) surface to 10 L of H_2CO (left) and D_2CO (right) at 80 K. The symbol "Δ" signifies momentary heating of the surface to the indicated temperatures, followed by cooling to 80 K to record the spectra.

aldehyde from the clean surface between 120 and 160 K in the thermal desorption spectra of Figure 1. In the spectrum for H_2CO, Figure 6a's features which may be ascribed to vibrations or the frustrated translation of coadsorbed water are observed as shoulders on both the low and high frequency sides of the mode due to adsorbed CO at 450 cm^{-1}. A broad envelope of poorly resolved bands extends from 750 to 1250 cm^{-1}, a band due to C–H deformation vibrations is evident at 1420 cm^{-1}, and a band due to C–H stretching vibrations is evident at 2925 cm^{-1}. In the corresponding spectrum for D_2CO, a shoulder at 375 cm^{-1} on the low frequency side of the CO vibration at 450 cm^{-1} is observed, which again is due to the frustrated translation of D_2O perpendicular to the surface.[43] Also observed are a weak mode at 600 cm^{-1}, a broad, poorly resolved envelope of bands between 750 and 1250 cm^{-1}, and a weak feature due to C–D stretching modes at 2200 cm^{-1}. The increase in the intensity of ν(CO) at 1995–2000 cm^{-1} in these spectra indicates that an additional 0.07–0.08 monolayer of formaldehyde decomposition has occurred upon annealing to 150 K.

The EEL spectra recorded after annealing to 250 K, Figure 6b, show no change in the intensities of the features due to adsorbed CO, indicating that decomposition has not occurred between 150 and 250 K. The remaining bands sharpen and decrease in intensity, consistent not only with some desorption of the adsorbed species which contribute to these bands but also with ordering of the remaining 0.03 monolayer of adsorbed species which has not decomposed. Results of other experiments for annealing temperatures between 250 and 300 K verify that the features in Figure 6b at 840, 980, 1160, 1450, and 2940 cm^{-1} for H_2CO and at 620, 865, 1020, 1190, and 2225 cm^{-1} for D_2CO maintain their relative intensities and decrease in intensity in unison as the surface is annealed to progressively higher temperatures. As these vibrational features attenuate, those due to adsorbed CO increase in intensity. Consequently, these features are obviously due to a single adsorbed species which decomposes to yield CO in this temperature range.

Comparison of the frequencies observed in Figure 6b to those expected for paraformaldehyde [630, 900–930, 1090–1100, 1235, 1470, and 2900–2980 for paraformaldehyde and 620, 835, 970, 1050–1080, 1130–1160, and 2235 for paradideuterioformaldehyde[54]] confirms that paraformaldehyde is not present on the surface. Similar comparisons allow species such as methoxy[5,11] and η^2-dioxymethylene,[13] which have been observed as adsorbed products of the interaction of formaldehyde with other metal surfaces, to be excluded.

The spectra of Figure 6b are consistent with an η^2 configuration [see also Figure 5, bottom panel] for adsorbed formaldehyde, analogous to that obtained for the adsorption of acetone on the Ru(001) surface.[24] Assignments of each of the observed vibrational modes for both η^2-H_2CO and η^2-D_2CO are listed in Table II. The ν(CO) frequency near 1000 cm^{-1} agrees well with those observed in analogous η^2-formaldehyde complexes.[18,19,21] In addition, the frequencies of the $\nu(CH_2)$, $\omega(CH_2)$, and $\rho(CH_2)$ modes agree well with assignments for methylene groups with sp^3 hybridization in other compounds, as do the frequency shifts upon deuteration [(ν for H_2CO)/(ν for D_2CO) = 1.32 to 1.35].[51,52,55] Noteworthy, however, is the slight increase from 980 to 1020 cm^{-1} of ν(CO) upon deuteration and the less-than-expected[56] decrease from 1450 to 1190 cm^{-1} of $\delta(CH_2)$ upon deuteration [$\delta(CH_2)/\delta(CD_2)$ = 1.22]. The origin of these effects can be explained in terms of a strong interaction between the ν(CO) and $\delta(CD_2)$ modes of η^2-D_2CO. The description of molecular vibrational motion in terms of bending and stretching of isolated units [e.g., $\delta(CH_2)$, ν(CO), $\omega(CH_2)$, etc.] fails when two (or more) vibrational modes involving motion of common atoms and belonging to the same symmetry type have nearly equal frequencies.[52,57] In this circumstance, the resulting normal modes of the molecule are combinations of the two (or more) types of motion, which may produce frequencies substantially different than are expected for vibrations of the isolated units. For η^2-H_2CO, the ν(CO) mode at 980 cm^{-1} and the $\delta(CH_2)$ mode at 1450 cm^{-1}, both of which are of A′ symmetry for η^2-formaldehyde in the expected C_s configuration and derived from A_1 modes of free formaldehyde (see Table II), are largely decoupled due to their disparity in frequency. Thus,

(54) Tadokoro, H.; Kobayashi, M.; Kawaguchi, Y.; *Kobayashi, A.*; Murahashi, S. *J. Chem. Phys.* **1963**, *38*, 703.

(55) Ibach, H., Mills, D. L. "Electron Energy Loss Spectroscopy and Surface Vibrations", Academic Press: New York, 1982.

(56) If hydrogen motion is decoupled from other vibrational motion of a molecule, substitution of deuterium for hydrogen decreases the frequencies of hydrogenic modes by the square root of the H/D mass ratio, and $\nu(H)/\nu(D)$ = 1.41.[52,53]

(57) Colthup, N. B., Daly, L. H., Wiberley, S. E. "Introduction to Infrared and Raman Spectroscopy", Academic Press: New York, 1975.

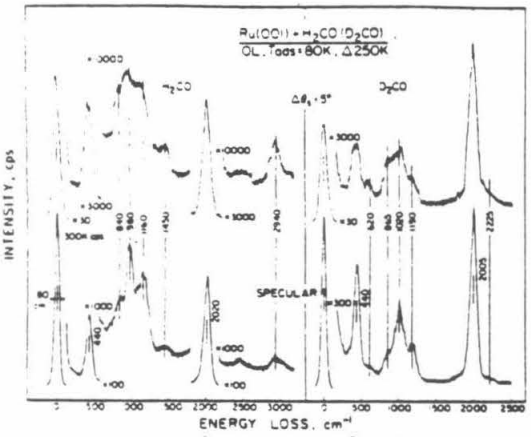

Figure 7. EEL spectra of η^2-H_2CO (left) and η^2-D_2CO (right) recorded in the specular direction (bottom) and 5° out of the specular direction (top).

the $\delta(CH_2)$ vibration involves almost exclusively relative motion of the hydrogen atoms, and the $\nu(CO)$ vibration involves only relative motion of the carbon and oxygen atoms. When deuterium is substituted for hydrogen, however, the frequency of isolated $\delta(CD_2)$ motion shifts to approximately $1450/1.41 = 1030\ cm^{-1}$, where coupling with the $\nu(CO)$ motion is strong. Thus, the resulting normal mode for η^2-D_2CO identified as $\delta(CD_2)$ actually involves substantial $\nu(CO)$ motion, and the mode identified as $\nu(CO)$ contains substantial $\delta(CD_2)$ motion.

In dipolar inelastic scattering, the electrons of the EELS beam incident upon the surface interact with the time-dependent electric field above the surface which results from the oscillation of separated charges in the adsorbed species, exiting the surface in the near specular direction after losing energy to excite a surface vibration.[55] Since the charge separation between the carbon and hydrogen (or deuterium) atoms of the C–H (or C–D) bonds is small with respect to that between carbon and oxygen of the C–O bond, strong dipolar scattering is only expected to occur for those vibrational modes of adsorbed formaldehyde which involve motion of the carbon and oxygen atoms with respect to each other. Since the cross section for dipolar inelastic scattering is strongly peaked in the specular direction, rotation of the electron energy analyzer away from the specular collection geometry where dipolar scattering is dominant attenuates features due to dipolar scattering, i.e., those vibrations which involve C–O motion for adsorbed formaldehyde, with respect to features due primarily to short-range impact scattering, i.e., those vibrations which involve mainly C–H (or C–D) motion for adsorbed formaldehyde.[55] This is clearly illustrated in Figure 7 for both η^2-H_2CO and η^2-D_2CO. Comparison of the top spectrum for η^2-H_2CO, at the left of Figure 7, that was recorded with the electron energy analyzer rotated 5° in the scattering plane away from the specular direction toward the surface normal, to that below it for specular scattering shows that the $\nu(CO)$ mode at $980\ cm^{-1}$ is attenuated sharply with respect to the ρ-, ω-, δ-, and $\nu(CH_2)$ modes of η^2-H_2CO at 840, 1165, 1450, and $2940\ cm^{-1}$, which maintain their relative intensities. In the spectra at the right for η^2-D_2CO, however, both $\nu(CO)$ at $1020\ cm^{-1}$ and $\delta(CD_2)$ at $1190\ cm^{-1}$ are attenuated in unison upon changing from the specular to the off-specular scattering geometry, maintaining their intensities relative to each other but decreasing uniformly with respect to the ρ-, ω-, and $\nu(CD_2)$ modes at 620, 865, and $2225\ cm^{-1}$. The $\delta(CD_2)$ mode of η^2-D_2CO at $1190\ cm^{-1}$ shows much stronger dipolar scattering than the corresponding $\delta(CH_2)$ mode of η^2-H_2CO at $1450\ cm^{-1}$, illustrating the strong coupling of C–O and C–D motion in this vibrational mode of η^2-D_2CO.

Returning to the spectra of Figure 6, the most notable effect of annealing to 350 K [Figure 6c] the Ru(001) surface, upon

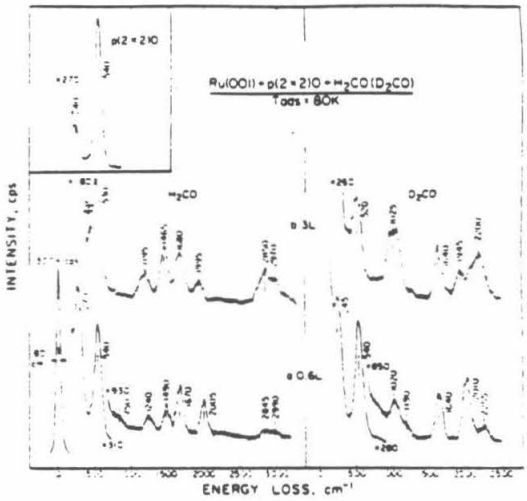

Figure 8. EEL spectra recorded after the indicated exposures of the Ru(001)–p(2×2)O surface to H_2CO (left) and D_2CO (right) at 80 K. Also shown in the inset is the EEL spectrum of the p(2×2) oxygen overlayer.

which η^2-formaldehyde and CO and hydrogen from the decompositon of formaldehyde are adsorbed, is to decompose completely the remaining 0.03 monolayer of η^2-formaldehyde. The CO coverage in spectra (c) of Figure 6 is approximately 0.25 monolayer, and, for coverages of CO above approximately 0.20 monolayer, the vibrational spectrum of adsorbed CO on Ru(001) not only shows modes at 455 and $2020\ cm^{-1}$ due to ν(RuC) and ν(CO), respectively, but also shows weak features at 2450–2490 cm^{-1} due to the combination loss of ν(RuC) + ν(CO) and at 835–840 cm^{-1} due to the overtone of ν(RuC), downshifted from twice the ν(RuC) frequency due to the anharmonicity of the ruthenium–carbon bond.[39] In addition to these features from adsorbed CO, the spectrum for H_2CO shows a weak feature at $2900\ cm^{-1}$ due to a small amount of an unidentifiable hydrocarbon fragment on the surface. Some spectra for both H_2CO and D_2CO recorded after annealing to temperatures between 250 and 350 K showed bands clearly attributable to small amounts (less than 0.01 monolayer) of coadsorbed η^2-formate.[58] These bands are almost certainly due to small concentrations of impurities in the adsorbed formaldehyde and are insignificant.

D. EELS of Formaldehyde on the Ru(001)–p(2×2)O Surface. The EEL spectrum of the p(2×2)O overlayer is shown in the inset of Figure 8. In addition to the feature at 540 cm^{-1} due to motion of the oxygen adatoms in threefold hollow sites perpendicular to the surface, a mode appears at 240 cm^{-1} which results from coupling of the overlayer to a ruthenium surface phonon.[40] The presence of the p(2×2)O overlayer, with an ideal fractional surface coverage of 0.25, changes the work function of the Ru(001) surface by +0.20 eV.[41] Employing a Ru═O bond length of 2.05 Å[40] and ignoring depolarization effects, this change in the work function is equivalent to the transfer of 0.02 electron from the ruthenium surface to each oxygen adatom of the p(2×2)O overlayer,[59] producing a quantifiable increase in the Lewis acidity of the surface ruthenium atoms.

Spectra recorded after adsorption of 0.6 L of H_2CO and D_2CO on the Ru(001)–p(2×2)O surface at 80 K are shown in Figure 8a. The strong mode due to adsorbed oxygen of the p(2×2) overlayer is visible at 540 cm^{-1}, and a broad, weak feature due to librational modes of a small amount of coadsorbed H_2O can

(58) Avery, N. R.; Toby, B. H.; Anton, A. B.; Weinberg, W. H. *Surf. Sci.* **1982**, *122*, L574.
(59) Topping, J. *Proc. R. Soc. London, A* **1927**, *114*, 67.

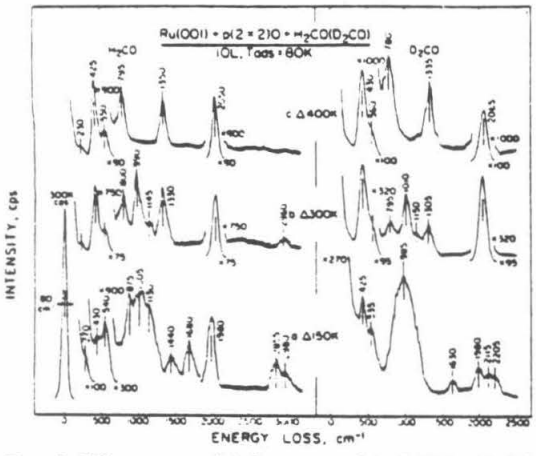

Figure 9. EEL spectra recorded after exposure of the Ru(001)–p(2×2)O surface to 10 L of H_2CO (left) and D_2CO (right) at 80 K, followed by annealing to the indicated temperatures.

be seen at 750 cm^{-1} in the spectrum of H_2CO. Modes due to adsorbed CO from formaldehyde decomposition or background adsorption of CO are present in both spectra with intensities indicative of coverages near 0.01 monolayer. The remaining features in both spectra are due to the presence of η^1-formaldehyde. The band locations and assignments for η^1-H_2CO and η^1-D_2CO are listed in Table II. The strong band at 270 cm^{-1} in the spectrum of H_2CO and the band at 245 cm^{-1} in the spectrum of D_2CO are due to the frustrated translation of the η^1-formaldehyde perpendicular to the surface.

Spectra for 3-L exposures of H_2CO and D_2CO under the same conditions are shown in Figure 8b. Although there are slight changes in the frequencies and relative intensities of some modes, no clear evidence for any species on the Ru(001)–p(2×2)O surface other than η^1-formaldehyde and carbon monoxide is present in the spectra of Figure 8. This conclusion is in agreement with the results of a previous investigation of acetone adsorption on the clean Ru(001) and the Ru(001)–p(2×2)O surfaces,[24] where preadsorption of oxygen stabilized the η^1 form of adsorbed acetone with respect to the η^2 form.

Figure 9 shows spectra recorded after exposure of the Ru(001)–p(2×2)O surface to 10 L of H_2CO and D_2CO, an exposure that is more than sufficient to provide a saturated monolayer of formaldehyde at 80 K, followed by annealing to the indicated temperatures. The decrease in the intensities of the modes due to η^1-formaldehyde in the spectra of Figure 9a, measured after annealing to 150 K, compared to the spectra of Figure 8b, indicates that approximately 80% of the η^1-formaldehyde has desorbed by this temperature. This correlates with the thermal desorption peaks at 130 and 150 K for formaldehyde on the Ru(001)–p(2×2)O surface, shown in Figure 1. The attenuation of the bands due to η^1-formaldehyde is accompanied by the appearance of bands in the frequency range expected for η^2-formaldehyde, at 875, 1005, 1130, and 1440 cm^{-1} in the spectrum for H_2CO and a single, broad band centered at 985 cm^{-1} in the spectrum for D_2CO.

Spectra recorded following annealing to temperatures between 150 and 300 K demonstrate that the broad envelope of bands between 750 and 1250 cm^{-1} in the spectra for both H_2CO and D_2CO changes shape as a surface reaction proceeds which forms the products evident in the spectra of Figure 9b. Significant decomposition of η^2-formaldehyde occurs in this temperature range, as evidenced by the increase in the intensities of the modes due to adsorbed CO. Furthermore, the bands due to η^1-formaldehyde decrease in intensity in this temperature range, and bands near 800 and 1300 cm^{-1} grow concomitantly with the disappearance of the η^1-formaldehyde at annealing temperatures between 200 and 250 K. These bands are due to η^2-formate[58] produced by the reaction of η^1-formaldehyde with the oxygen adatoms of the p(2×2)O overlayer. Slight desorption of η^1-formaldehyde also occurs in this temperature range, producing the very weak desorption rate maxima between approximately 180 and 300 K in the thermal desorption spectra of Figure 1 (right). No η^1-formaldehyde is evident in the EEL spectra for annealing temperatures greater than 250 K. At 300 K [Figure 9b], bands due to 0.04 monolayer of η^2-formate are present at 800 and 1330 cm^{-1} for H_2CO and at 795 and 1305 cm^{-1} for D_2CO. In addition, bands due to 0.01 monolayer of η^2-formaldehyde are evident at 990, 1145, and 2960 cm^{-1} for H_2CO and at 1010 and 1150 cm^{-1} for D_2CO. The high intensity of the ν(CO) mode in these spectra (990 and 1010 cm^{-1}) relative to the other modes of η^2-formaldehyde is probably a result of the perturbation of its bonding interaction with the surface due to the presence of the coadsorbed oxygen of the p(2×2)O overlayer. This perturbation is also evidenced in the increased stability of η^2-formaldehyde on the Ru(001)–p(2×2)O surface; on the clean Ru(001) surface, decomposition of η^2-formaldehyde is complete by 300 K.

Annealing to 400 K decomposes the remaining η^2-formaldehyde, decomposes a fraction of the η^2-formate, and desorbs a fraction of the CO from the surface. The remaining η^2-formate persists to 450 K on the Ru(001)–p(2×2)O surface, and its decomposition produces the broad, weak desorption feature for hydrogen between 400 and 470 K in Figure 3c.[60]

EEL spectra recorded after annealing to temperatures sufficient to desorb all the hydrogen and CO from the surface show the features at 240 and 540 cm^{-1} due to the p(2×2)O overlayer with intensities unchanged from those observed prior to the adsorption of formaldehyde at 80 K. This verifies that little or no consumption of the oxygen adatoms of the p(2×2) overlayer by reaction with formaldehyde or its dissociation products occurs under these experimental conditions.

IV. Discussion

The η^1 and η^2 coordination geometries identified for formaldehyde in the EELS results reported here can be understood qualitatively in terms of the interaction of the valence orbitals of the surface metal atoms with the highest occupied and lowest unoccupied molecular orbitals of free formaldehyde.[24] An η^1 coordination geometry results from overlap of a single lobe of the nonbonding oxygen lone pair orbital of formaldehyde [at 12.0 eV below the vacuum level for free formaldehyde[61]] with a ds hybrid acceptor orbital of the metal, resulting in a net transfer of electron density from the ligand to the metal surface. Presumably due to the low amplitude on the oxygen atom of the π_{CO}^* antibonding orbital of formaldehyde [at 3.1 eV above the vacuum level[61]], little backdonation from the metal to this orbital occurs, as judged by the weak perturbation of the vibrational frequencies for η^1-formaldehyde relative to the frequencies of free formaldehyde (cf. Table II). The role of the metal in this type of interaction is that of a weak Lewis acid, and the resulting metal–formaldehyde bond is correspondingly weak. For example, the thermal desorption spectra of Figure 1 indicate binding energies between 7 and 9 kcal/mol[47] for the desorption features attributable to η^1-formaldehyde at 130 and 155 K.

An η^2 coordination geometry results from overlap of the π_{CO} bonding orbital of formaldehyde [at 14.6 eV below the vacuum level[61]] with a ds hybrid acceptor level of the metal, along with backdonation from the metal into the π_{CO}^* antibonding orbital of the formaldehyde.[62] The strength of this interaction, and, therefore, the probability of its occurrence relative to the η^1 interaction, depends critically on the ability of the ligand–metal bond to facilitate backdonation, since in the absence of backdonation the π donor bond is weaker than the lone pair donor bond which produces η^1 coordination. The importance of backdonation and

(60) Toby, B. H.; Avery, N. R.; Anton, A. B.; Weinberg, W. H., in preparation.
(61) Hess, B.; Bruna, P. J.; Buenker, R. J.; Peyerimhoff, S. D. *Chem. Phys.* **1980**, *18*, 267.
(62) Dewar, M. J. S. *Bull. Soc. Chim. Fr.* **1951**, *18*, C79. Chatt, J.; Duncanson, L. A. *J. Chem. Soc.* **1953**, 2939.

the function of the metal as a Lewis base in this type of interaction is evidenced in the results obtained in structural studies of η^2-aldehyde complexes,[18-22] where in all cases nearly complete rehybridization of the acyl carbon from sp^2 to sp^3 occurs, and the carbon–oxygen bond order for the aldehyde ligands is lowered to nearly one.

The π_{CO}^* antibonding orbital of free formaldehyde is approximately 1.3 eV lower in energy than the corresponding orbital of free acetone [π_{CO}^* at 4.4 eV above the vacuum level for acetone[61]]. This decreases the disparity in energy between this orbital for formaldehyde and the highest occupied levels of the metal with which it interacts in η^2 bonding, facilitating increased backdonation for formaldehyde with respect to acetone. Several aspects of the comparative chemistry of these two ligands can be correlated with this difference. First, the only η^2-acetone complex isolated thus far has the acetone coordinated to an electropositive tantalum center,[63] whereas η^2-formaldehyde complexes have been synthesized with more electronegative osmium[18] and ruthenium[20] centers. Furthermore, η^2-formaldehyde on Ru(001) shows ν(CO) near 1000 cm^{-1}, whereas ν(CO) for η^2-acetone on Ru(001) is near 1300 cm^{-1},[24] indicating more extensive rehybridization of the acyl carbon due to backdonation for η^2-formaldehyde than for η^2-acetone. Finally, the more extensive rehybridization evident for η^2-formaldehyde on Ru(001) results in a lower barrier to its dissociation, explaining the fact that significant decomposition of formaldehyde, presumably through η^2-formaldehyde and η^2-formyl intermediates, occurs on the clean Ru(001) surface at 80 K (cf. Figure 4), whereas decomposition of η^2-acetone on the same surface begins near 200 K.[24]

It is interesting to compare data for the η^2-formaldehyde ligand in organometallic complexes with our results for η^2-formaldehyde on Ru(001). The interaction of formaldehyde with single osmium[18] and vanadium[19] centers as well as the oxidation of coordinated methylene at a rhenium center[20] produces the η^2-formaldehyde configuration shown in (b) in the bottom panel of Figure 5 (R = H). The carbonylation of a zirconium hydride forms a bridging η^2-formaldehyde,[21] as in (c) in the bottom panel of Figure 5. Also of interest is a configuration like that of (d), which has been observed for η^2-acetaldehyde (R = CH_3) in a dimolybdenum complex.[22] All of these compounds have carbon–oxygen bond lengths between 1.35 and 1.59 Å, and those that have been characterized by vibrational spectroscopy have ν(CO) between 1012 and 1160 cm^{-1}, in good agreement with our results for η^2-formaldehyde on Ru(001). The low frequency of ν(CO) for η^2-formaldehyde both on the Ru(001) surface and in these organometallic compounds clearly indicates that the acyl carbon has undergone extensive rehybridization from sp^2 to sp^3. A distinction among these possible bonding configurations for η^2-formaldehyde on Ru(001) is not possible, since the vibrational spectra would differ only in the unresolved, low frequency vibrations which involve motion of the bonds that coordinate the η^2-formaldehyde to the surface.

Although little vibrational data exist for η^2-formyl ligands in homogeneous organometallic compounds, several structures of η^2-formyl have been characterized analogous to those shown in (b),[30] (c),[31] and (d)[32] in the top panel of Figure 5. Those with the structure (b), in which the carbon and oxygen atoms are coordinated to a single metal atom, show ν(CO) frequencies between 1450 and 1600 cm^{-1}, and the low frequency (1180 cm^{-1}) for ν(CO) of η^2-formyl on Ru(001) thus suggests that the η^2-formyl on this surface is coordinated to at least two surface ruthenium atoms. Hence, structures (c) and (d) are regarded as the most likely for η^2-formyl on Ru(001).

It should be noted that a detailed analysis of the point-group symmetry properties of the adsorbate complex, as was carried out successfully for η^1- and η^2-acetone on Ru(001),[24] cannot be done in a straightforward manner for adsorbed formyl or the adsorbed formaldehyde species on Ru(001). Since the dominant contribution to inelastic electron scattering from hydrogenic vibrations is expected to be via an impact rather than a dipolar mechanism at the electron beam energy employed for the EELS measurements reported here, all vibrations involving hydrogenic motion are, in principle, active in both specular and off-specular EELS measurements.[55] For a molecule like formaldehyde in which the skeletal configuration is defined by the orientations of C–H bonds, the polarizations of skeletal vibrations with respect to the symmetry elements of the adsorbate–surface complex cannot be determined by the standard technique of noting the dipolar activity (or inactivity) of signature skeletal modes for specular scattering and applying the "dipolar selection rule"[56] to determine bond orientations. For example, the appearance of the π(CH) vibration in the spectra for η^2-formyl does not rule out the possibility that the η^2-formyl is adsorbed in a configuration with C_s symmetry (with the carbon, hydrogen, and oxygen atoms lying in a mirror symmetry plane perpendicular to the surface), even though the π(CH) mode would be dipolar inactive in this configuration. Indeed, C_s symmetry is expected for both η^2-formaldehyde and η^2-formyl on Ru(001), in analogy to η^2-acetone.

The conditions that lead to the formation of η^2-formyl and η^2-formaldehyde provide a consistent picture of the mechanism of formaldehyde decomposition on the clean Ru(001) surface. For low exposures of formaldehyde to Ru(001) at 80 K, total decomposition to adsorbed CO and hydrogen occurs. This indicates that the activation energy for dissociation of η^2-formaldehyde on Ru(001) at low coverages is less than 4.8 kcal-mol^{-1}.[64] As binding sites for the hydrogen from decomposition are occupied, further decomposition is inhibited sterically, stabilizing both the partial decomposition product η^2-formyl over a small exposure range [Figure 4a] and η^1- and η^2-formaldehyde at coverages approaching a saturated monolayer [Figure 4b]. Annealing to temperatures below the onset of hydrogen desorption renders probable the complete decomposition of η^2-formyl and additional decomposition of η^2-formaldehyde, as η^1-formaldehyde is desorbed and hydrogen adatoms become mobile, exposing the necessary binding sites for the products of η^2-formaldehyde decomposition. For example, the *apparent* activation energy for the decomposition of η^2-formaldehyde at 150 K, 9 kcal-mol^{-1}, represents the steric barrier which η^2-formaldehyde must overcome under these conditions to find binding sites to accommodate the decomposition products, hydrogen and CO, on the surface. These conclusions are supported by the results of EELS measurements for adsorption of formaldehyde at 80 K on the Ru(001) surface precovered with a saturated monolayer of hydrogen adatoms.[48] Only η^1- and η^2-formaldehyde are observed at 80 K for all submonolayer coverages, and very little decomposition is observed until hydrogen desorption commences near 275 K, whereupon decomposition of η^2-formaldehyde proceeds rapidly.

The effect of hydrogen coverage on the rate of dissociation of η^2-formaldehyde has another important consequence for the interpretation of the experimental results reported here. If η^2-formaldehyde has a characteristic activation energy for *molecular desorption* (i.e., heat of adsorption) less than the activation energy for recombination and desorption of hydrogen from the Ru(001) surface, at high surface coverages, where the binding sites for the products of the decomposition of η^2-formaldehyde on the Ru(001) surface are filled and further decomposition is unfavorable, molecular desorption of η^2-formaldehyde would occur. Consequently, the desorption of molecular formaldehyde from the clean surface at 275 K for high surface coverages (cf. Figure 1) is due to the desorption of η^2-formaldehyde. The high binding energy of this adsorbed species on Ru(001) (approximately 115 kcal-mol^{-1}) makes the formation of η^2-formaldehyde far more favorable than the formation of paraformaldehyde on the Ru(001) surface. This estimate of the binding energy is based on the observed rehybridization of the η^2-formaldehyde and should not be confused with the activation energy of desorption of η^2-formaldehyde which

(63) Wood, C. D.; Schrock, R. R. *J. Am. Chem. Soc.* **1979**, *101*, 5421.

(64) The activation energies for these surface reactions are estimated by assuming first-order kinetics, which is appropriate for unimolecular decomposition reactions, and assuming a preexponential factor of the reaction rate coefficient of 10^{13} s^{-1}. The activation energy, E_a, is then obtained by assuming that the characteristic time of the reaction is approximately 1 s, i.e., 10^{-13} $\exp(|E_a|/kT)$.

is approximately 16 kcal-mol^{-1}.

The results of these considerations for the surface chemistry of formaldehyde adsorbed on both the clean and Ru(001)–p(2×2)O surfaces may be illustrated by overall reaction schemes for the monolayer species adsorbed on both surfaces. Initial exposure of the clean Ru(001) surface to formaldehyde at 80 K produces adsorbed CO and hydrogen from decomposition

$$H_2CO(g) \rightarrow CO(a) + 2H(a)$$

Once decomposition has progressed to approximately 0.15 monolayer of formaldehyde, subsequent exposure produces 0.02–0.03 monolayer of η^2-formyl

$$CH_2O(g) \rightarrow \eta^2\text{-}HCO(a) + H(a)$$

Heating the surface upon which η^2-formyl is adsorbed to 120 K decomposes the η^2-formyl. Further exposure to formaldehyde produces both η^1-formaldehyde and 0.10 monolayer of η^2-formaldehyde

$$H_2CO(g) \rightarrow \eta^1\text{-}H_2CO(a)$$

$$H_2CO(g) \rightarrow \eta^2\text{-}H_2CO(a)$$

The η^1-formaldehyde desorbs molecularly between 120 and 160 K

$$\eta^1\text{-}H_2CO(a) \rightarrow H_2CO(g)$$

exposing binding sites for the products of the decomposition of 0.07–0.08 monolayer of η^2-formaldehyde

$$\eta^2\text{-}H_2CO(a) \rightarrow CO(a) + 2H(a)$$

As the surface is heated to 300 K, hydrogen desorption begins, and decomposition of the remaining 0.03 monolayer of η^2-formaldehyde follows rapidly. Hydrogen is evolved from the surface in a desorption rate-limited step between 250 and 350 K, and CO is evolved from the surface in a desorption rate-limited step at 480 K

$$2H(a) \rightarrow H_2(g)$$

$$CO(a) \rightarrow CO(g)$$

Exposure of the Ru(001)–p(2×2)O surface to formaldehyde at 80 K produces η^1-formaldehyde

$$H_2CO(g) \rightarrow \eta^1\text{-}H_2CO(a)$$

Negligible decomposition of formaldehyde is observed under these conditions. Heating the surface to 150 K desorbs approximately 80% of the η^1-formaldehyde

$$\eta^1\text{-}H_2CO(a) \rightarrow H_2CO(g)$$

with conversion also to η^2-formaldehyde. Further heating of the surface to 300 K produces approximately 0.08 monolayer of CO from the decomposition of η^2-formaldehyde and produces approximately 0.04 monolayer of η^2-formate from the reaction of η^1-formaldehyde with the oxygen adatoms of the p(2×2)O overlayer

$$\eta^1\text{-}H_2CO(a) + O(a) \rightarrow \eta^2\text{-}HCOO(a) + H(a)$$

This reaction as well as the decomposition of η^2-formaldehyde produces hydrogen above its characteristic temperature of desorption from the Ru(001)–p(2×2)O surface. Thus hydrogen atom recombination and desorption follow rapidly in the temperature range between 250 and 300 K. Approximately 0.01 monolayer of η^2-formaldehyde remains on the surface at 300 K. Further heating decomposes the remaining η^2-formaldehyde, and decomposition of the η^2-formate occurs between 400 and 450 K

$$\eta^2\text{-}HCOO(a) \rightarrow O(a) + CO(a) + H(a)$$

Again, hydrogen desorption follows rapidly. The CO from decomposition is evolved from the surface in a desorption rate-limited step at 450 K. The p(2×2) oxygen overlayer is left intact on the surface.

The appearance of η^2-formyl as an intermediate to the decomposition of adsorbed formaldehyde on Ru(001) has important implications for the mechanistic understanding of surface catalyzed CO hydrogenation reactions.[15,65] Although the reaction of coordinated CO with hydrogen from borohydride donors has been shown to produce η^1-formyl complexes of rhenium[26,27] and iron[29] under homogeneous conditions, this reaction, represented schematically as [R = alkyl or alkoxide, L = Cp, PPh_3, NO, CO, and/or $P(OC_6H_5)_3$]

$$BR_3H^- + L_xM^N(CO) \rightarrow BR_3 + L_xM(\eta^1\text{-}HCO)^{N-1}$$

involves direct nucleophilic attack by the electron-rich hydrogen atom of the hydride donor at the carbonyl carbon. The resulting compounds are either neutral [$N = +1$[26,27]] or are negatively charged [$N = 0$[29]]. At no point is molecular hydrogen, nor an intermediate *metal* hydride, involved in this elementary reaction. Furthermore, the resulting η^1-formyl is only weakly stable, and the weakened carbon–oxygen bond of η^1-formyl relative to that of the CO which can be formed by its decomposition to the hydrido-carbonyl product drives the equilibrium for the decomposition reaction, represented below, to the right[15,27,30,32]

$$L_xM(\eta^1\text{-}HCO) \rightleftharpoons L + L_{x-1}M(H)(CO)$$

A more realistic model of the elementary CO reduction reaction which must occur under heterogeneous catalytic conditions involves migratory insertion of CO into a metal hydride bond[65]

$$CO + L_xMH \rightarrow L_xM(HCO)$$

Thus far, only one such reaction has been observed under homogeneous conditions, where the reaction of CO with an oxophilic thorium hydride [$(\eta^5\text{-}C_5Me_5)_2Th(H)(OR)$, OR = alkoxide ligand[30]] produces an η^2-formyl like that shown in Figure 5b (upper panel). The ability of the single metal center to coordinate the formyl product in an η^2 configuration was considered crucial to the occurrence of this reaction, since the metal–oxygen bond which is formed increases the stability of the formyl product, shifting the equilibrium for the formyl decomposition reaction toward the desired η^2-formyl product and away from the hydrido–carbonyl product.[30,32,65] Another route to stabilization of the formyl product involves the use of multiple coordination centers for the CO hydrogenation reaction. Two such reactions have been observed under homogeneous conditions, one involving the reaction of CO with a tantalum hydride dimer[31]

$$[(\eta^5\text{-}C_5Me_4Et)Ta(Cl)_2H]_2 + CO \rightarrow (\eta^5\text{-}C_5Me_4Et)_2(Cl)_4Ta_2(H)(\eta^2\text{-}HCO)$$

to produce an η^2-formyl product, the structure of which is like that of Figure 5c (upper panel), and another involving the reaction of a tungsten carbonyl compound with a zirconium hydride[22]

$$(Cp)_2W(CO) + (\eta^5\text{-}C_5Me_5)_2Zr(H)_2 \rightarrow (Cp)_2W{=}CHOZr(H)(\eta^5\text{-}C_5Me_5)_2$$

to produce a "carbene-like" η^2-formyl complex, the structure of which is like that of Figure 5d (upper panel). The η^2 interaction not only stabilizes the η^2-formyl intermediate, increasing the likelihood of its formation, but also increases the likelihood of subsequent attack by hydrogen to form formaldehyde intermediates, leading to oxygenated products, and to carbon–oxygen bond cleavage, leading to hydrocarbon products.[65]

From these results concerning the mechanism of CO activation and reduction under homogeneous conditions, the importance of the η^2-formyl observed in the decomposition of formaldehyde on Ru(001) is clearly evident. This result illustrates the ability of an extended metal surface to provide the proper coordination geometry for this species and supports strongly a surface reaction mechanism for CO hydrogenation which proceeds through an η^2-formyl intermediate. This, coupled with the isolation of stable η^2-formaldehyde on Ru(001), supports also the following reaction mechanism for methanol decomposition on Ru(001)[5] and suggests

(65) Masters, C. *Adv. Organomet. Chem.* **1979**, *17*, 61.

that the reverse reactions may well represent a plausible path for methanol synthesis on Ru(001):

$$CH_3OH(g) \rightarrow CH_3O(a) + H(a)$$

$$CH_3O(a) \rightarrow \eta^2\text{-}H_2CO(a) + H(a)$$

$$\eta^2\text{-}H_2CO(a) \rightarrow \eta^2\text{-}HCO(a) + H(a)$$

$$\eta^2\text{-}HCO(a) \rightarrow CO(a) + H(a)$$

It is interesting to note that a reaction sequence analogous to the reverse of the above set of reactions has been postulated to explain the formation of methanol from CO and hydrogen by $Ru_3(CO)_{12}$ under homogeneous reaction conditions.[17] Our observations should be interpreted as lending support to this proposition.

V. Summary

The important conclusions of this work may be summarized as follows: 1. Initial adsorption of formaldehyde on the clean Ru(001) surface at 80 K is dissociative, producing adsorbed CO and hydrogen. As binding sites for hydrogen adatoms become occupied, the total decomposition is inhibited, leading first to the formation of η^2-formyl and then to molecular adsorption of formaldehyde in both η^1 and η^2 configurations. 2. Heating of the clean surface after a monolayer saturation exposure to formaldehyde at 80 K causes the η^1-formaldehyde to desorb molecularly and the η^2-formaldehyde to decompose (to adsorbed CO and hydrogen). The clean Ru(001) surface is active for the decomposition of approximately a quarter-monolayer of formaldehyde under these conditions. 3. The presence of a p(2×2) oxygen overlayer on the Ru(001) surface increases the Lewis acidity of the surface ruthenium atoms, and adsorption of formaldehyde at 80 K on the Ru(001)–p(2×2)O surface produces vibrational spectra characteristic of η^1-formaldehyde for all submonolayer coverages. 4. Heating of the Ru(001)–p(2×2)O surface after a monolayer saturation exposure to formaldehyde at 80 K causes the η^1-formaldehyde to desorb molecularly, with some conversion to η^2-formaldehyde. In addition to decomposition of the η^2-formaldehyde to CO and hydrogen, reaction of η^1-formaldehyde with the oxygen adatoms of the p(2×2)O overlayer to produce η^2-formate occurs between 150 and 300 K. The Ru(001)–p(2×2)O surface is active for approximately one-half as much formaldehyde decomposition (via both η^2-formaldehyde and η^2-formate intermediates) as the clean surface under these conditions. 5. The appearance of η^2-formyl and η^2-formaldehyde as stable intermediates in the decomposition of formaldehyde on Ru(001) supports a reaction mechanism for CO hydrogenation to methanol under heterogeneous conditions which includes these species as important intermediates.

Acknowledgment. This research was supported by the National Science Foundation under Grant No. CHE-8516615.

Registry No. HCHO, 50-00-0; CO, 630-08-0; Ru, 7440-18-8.

Appendix 3

The Interaction of Ethylene with the Ru(001) Surface

[This chapter was published as a paper by M. M. Hills, J. E. Parmeter, C. B. Mullins and W. H. Weinberg, in *The Journal of the American Chemical Society* 1986, 108, 3554.]

Reprinted from the Journal of the American Chemical Society, 1986, *108*, 3554.

Interaction of Ethylene with the Ru(001) Surface†

M. M. Hills, J. E. Parmeter,‡ C. B. Mullins,§ and W. H. Weinberg*

Contribution from the Division of Chemistry and Chemical Engineering, California Institute of Technology, Pasadena, California 91125. *Received October 8, 1985*

Abstract: The interaction of ethylene with the Ru(001) surface has been investigated via high-resolution electron energy loss spectroscopy and thermal desorption mass spectrometry. Following desorption of an ethylene multilayer at 110 K, di-σ-bonded molecular ethylene is present on the surface. Competing desorption of molecular ethylene and dehydrogenation to form adsorbed ethylidyne (CCH_3) and acetylide (CCH) as well as hydrogen adatoms occur between approximately 150 and 260 K. The ethylidyne is stable to approximately 330 K, whereupon it begins to decompose to carbon and hydrogen adatoms. The desorption of hydrogen occurs in a sharp peak centered at 355 K, resulting from simultaneous ethylidyne decomposition and desorption of surface hydrogen. Further annealing of the overlayer to 380 K causes cleavage of the carbon–carbon bond of the acetylide, creating carbon adatoms and adsorbed methylidyne (CH). The methylidyne decomposes above 500 K with accompanying hydrogen desorption, leaving only carbon adatoms on the surface at 700 K.

I. Introduction

The adsorption and reaction of ethylene on single crystalline surfaces of the groups 8–10 transition metals[1-17] have been the subject of intense study both as a prototype for olefin hydrogenation and dehydrogenation reactions[18-21] and to provide a basis for comparing the bonding of olefins to surfaces with the bonding that has been observed to occur in multinuclear organometallic cluster compounds. Spectroscopic studies of ethylene adsorbed on these surfaces have shown that both the nature of the bonding of molecular ethylene to the substrate as well as the thermal decomposition pathway of the adsorbed ethylene vary widely. For example, ethylene rehybridizes to a di-σ-bonded molecular species when adsorbed on Fe(110), Fe(111), Ni(110), Ni(111), Ni[5(111) × (110)], Pt(111), and Pt(100),[1-7] whereas molecularly adsorbed ethylene on Co(001) at 115 K is π-bonded,[8] as is ethylene adsorbed on Pd(111) at 150 K and on Pd(110) at 110 K.[6,9-13,17] A mixed overlayer of π- and di-σ-bonded ethylene forms on Pd(100) at 150 K.[14,15] Ethylene adsorption on the Ru(001) surface has been

† In this paper the periodic group notation in parentheses is in accord with recent actions by IUPAC and ACS nomenclature committees. A and B notation is eliminated because of wide confusion. Groups IA and IIA become groups 1 and 2. The d-transition elements comprise groups 3 through 12, and the p-block elements comprise groups 13 through 18. (Note that the former Roman number designation is preserved in the last digit of the numbering: e.g., III → 3 and 13.)

‡ AT&T Bell Laboratories predoctoral fellow.

§ Link Foundation predoctoral fellow.

(1) Erley, W.; Baro, A. M.; McBreen, P.; Ibach, H. *Surf. Sci.* **1982**, *120*, 273.
(2) Seip, U.; Tsai, M.-C.; Küppers, J.; Ertl, G. *Surf. Sci.* **1984**, *147*, 65.
(3) Stroscio, J. A.; Bare, S. R.; Ho, W. *Surf. Sci.* **1984**, *148*, 499.
(4) Lehwald, S.; Ibach, H. *Surf. Sci.* **1979**, *89*, 425.
(5) Carr, R. G.; Sham, T. K.; Eberhardt, W. E. *Chem. Phys. Lett.* **1985**, *113*, 63.
(6) Demuth, J. E. *Surf. Sci.* **1979**, *84*, 315.
(7) Steininger, H.; Ibach, H.; Lehwald, S. *Surf. Sci.* **1982**, *117*, 685.
(8) Albert, M. R.; Sneddon, L. G., Plummer, E. W. *Surf. Sci.* **1984**, *147*, 127.
(9) Gates, J. A.; Kesmodel, L. L. *Surf. Sci.* **1982**, *120*, L461.
(10) Gates, J. A.; Kesmodel, L. L. *Surf. Sci.* **1983**, *124*, 68.
(11) Tysoe, W. T., Nyberg, G. L.; Lambert, R. M. *J. Phys. Chem.* **1984**, *88*, 1960.
(12) Ratajczykowa, I.; Szymerska, I. *Chem. Phys. Lett.* **1983**, *96*, 243.
(13) Kesmodel, L. L.; Gates, J. A. *Surf. Sci.* **1981**, *111*, L747.
(14) Stuve, E. M.; Madix, R. *J. J. Phys. Chem.* **1985**, *89*, 105.
(15) Stuve, E. M.; Madix, R. J.; Brundle, C. R. *Surf. Sci.* **1985**, *152/153*, 532.
(16) Dubois, L. H.; Castner, D. G.; Somorjai, G. A. *J. Chem. Phys.* **1980**, *72*, 5234.
(17) Gupta, N. M.; Kamble, V. S.; Iyer, R. M. *J. Catal.* **1984**, *88*, 457.
(18) Chesters, M. A.; McDougall, G. S.; Pemble, M. E.; Sheppard, N. *Appl. Surf. Sci.* **1985**, *22/23*, 369.
(19) Boudart, M.; McDonald, M. A. *J. Phys. Chem.* **1984**, *88*, 2185.
(20) Henrici-Olivé, G.; Olivé, S. *Angew. Chem., Int. Ed. Engl.* **1976**, *15*, 136.

0002-7863/86/1508-3554$01.50/0

studied recently by Barteau and co-workers.[22] A detailed comparison between our more complete study and the preliminary results of Barteau et al.[22] is presented in section IV.

The thermal decomposition of ethylene (ultimately to hydrogen and surface carbon) on the surfaces mentioned above has been investigated by vibrational electron energy loss spectroscopy (EELS), thermal desorption mass spectrometry (TDMS), and UV photoelectron spectroscopy. The thermal decomposition intermediates in ethylene dehydrogenation on Fe(110), Ni(111), Ni[5(111) × (110)], and Ni(110) are acetylene and acetylide (CCH).[1,3,4] Madix and Stuve have postulated the formation of a vinyl group from ethylene adsorbed on Pd(100).[14,15] On Co(001) and Fe(111) no stable surface intermediates were observed; chemisorbed ethylene evidently dehydrogenates completely just below room temperature to carbon and hydrogen.[2,3] On Pt(111), Rh(111), Pd(111), and Pt(100), chemisorbed ethylene dehydrogenates to form ethylidyne below 300 K.[7,9-13,16,23] Thus, ethylene adsorbed on the close-packed surfaces of each of the 4d and 5d groups 8–10 metals studied previously forms ethylidyne.[24] On the other hand, ethylene adsorbed on all of the surfaces of the 3d groups 8–10 metals studied to date, including the close-packed surfaces, dehydrogenates more completely to acetylene, acetylide, or directly to carbon. Hence it is of fundamental interest to determine whether ethylene adsorbed on the Ru(001) surface behaves as it does on the other hexagonal 4d and 5d transition-metal surfaces studied previously [Rh(111), Pd(111), Pt(100), and Pt(111)] or whether it dehydrogenates more completely, as it does on the hexagonal Ni(111) and Co(001) surfaces.

II. Experimental Procedures

The experimental measurements were conducted in two different ultrahigh-vacuum (UHV) chambers, each with base pressures below 1 × 10^{-10} torr. The first UHV chamber is equipped with a quadrupole mass spectrometer, a single pass cylindrical mirror electron energy analyzer with an integral electron gun for Auger electron spectroscopy, and LEED optics. All thermal desorption measurements were carried out in this chamber; data were collected by using an LSI-11 DEC laboratory computer, and linear heating rates of 5–15 K/s were employed. A glass enclosure is placed around the ionizer of the mass spectrometer, and a small aperture in the front of the glass envelope permits sampling of gas that is desorbed only from the well-oriented front of the single crystal. Thus the effects of desorption from the edge of the crystal, the support leads, and the manipulator are excluded from the thermal desorption spectra.[26]

The second UHV chamber contains both a quadrupole mass spectrometer and a home-built EELS spectrometer of the Kuyatt-Simpson type.[27,28] The energy dispersing elements in the EELS monochromator and rotatable analyzer are 180° hemispherical deflectors. The "off-specular" EEL spectra were measured with the analyzer rotated 7–10° from the specular direction, toward the surface normal. All EEL spectra were measured using a beam energy of 4 eV and with the incident beam approximately 60° from the surface normal. The instrumental resolution (full-width at half-maximum of the elastically scattered peak) varied between 60 and 80 cm^{-1}, while maintaining a count rate of approximately 3 × 10^5 cps in the elastic peak. A more extensive description of these UHV chambers as well as the procedures followed for cutting, polishing, mounting, and cleaning the Ru(001) crystals has been discussed in detail previously.[27-30] The cleanliness of the surfaces was monitored with Auger spectroscopy in the first chamber and with EELS in the second.

Research purity hydrogen (99.9995%) and C.P. grade deuterium and ethylene (99.5%) were purchased from Matheson. Research purity tetradeuterated ethylene (99.99%) was obtained from Merck. The H_2, D_2, and C_2D_4 were used without further purification, whereas the C_2H_4 was subjected to freeze–thaw–pump cycles prior to use. The purity of all gases was verified in situ with mass spectrometry.

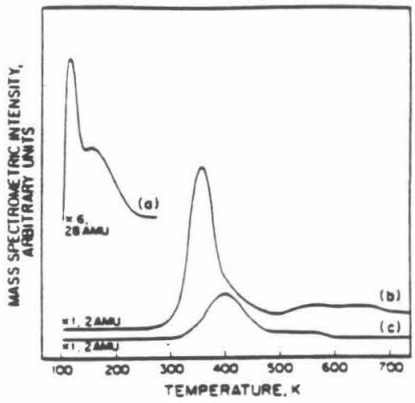

Figure 1. Thermal desorption spectra after C_2H_4 adsorption on Ru(001) at 90 K: (a) C_2H_4 and (b) H_2 desorption following a 1-langmuir exposure and (c) H_2 desorption following a 0.2-langmuir exposure.

III. Results

Typical thermal desorption spectra following exposure of the Ru(001) surface to 1 langmuir (1 langmuir = 1 × 10^{-6} torr s) or more of C_2H_4 at 90 K are shown in Figure 1a and 1b.[31] Only hydrogen and ethylene are observed to desorb from the surface. In particular, no ethane, methane, or acetylene is detected as judged by the absence of 30 and 16 amu peaks and by comparison of the 28, 27, and 26 amu peaks to the cracking pattern of ethylene.

Figure 1b establishes that most of the hydrogen, after an ethylene exposure exceeding 0.6 langmuir, desorbs in a sharp peak centered at 355 K (independent of coverage), with a small high-temperature shoulder above 400 K and a broad tail extending from 500 to 700 K of which the latter represents 10–15% of the desorbing hydrogen. It will be shown below that the major peak corresponds to the desorption of hydrogen enhanced by the decomposition of ethylidyne (one of the decomposition products of ethylene), the shoulder corresponds to desorption-limited hydrogen from the surface, and the high-temperature tail corresponds to the dehydrogenation of surface methylidyne (another decomposition product). The thermal desorption spectrum of molecular ethylene (cf. Figure 1a) shows that ethylene desorbs in a sharp peak centered near 110 K, followed by a broad peak of which the tail extends to approximately 250 K. As discussed below, EEL spectra of the surface on which ethylene is adsorbed and which is annealed to various temperatures show that the higher-temperature peak corresponds to the desorption of di-σ-bonded ethylene, while multilayer ethylene desorbs in the lower-temperature peak. The "multilayer" peak shown in Figure 1a actually corresponds to only desorption from a second layer. This multilayer peak does not saturate with increasing ethylene exposure, however, and is sufficiently intense following a 15-langmuir exposure of ethylene that it obscures the desorption peak due to chemisorbed ethylene.

For lower exposures of ethylene, below 0.6 langmuir, the hydrogen thermal desorption spectra are quite different. The thermal desorption spectrum of H_2 after an ethylene exposure of 0.2 langmuir, shown in Figure 1c, contains a high-temperature tail terminating below 600 K that is due to methylidyne decomposition and a rather broad peak centered at 420 K that shifts to lower temperature as the initial surface coverage of chemisorbed ethylene increases. The latter is essentially identical with that which is observed after adsorption of hydrogen on the clean Ru(001) surface.[32] The maximum rate of H_2 desorption shifts from 420

(21) Dixit, R. S.; Tavlarides, L. L. *Ind. Eng. Chem. Process Des. Dev.* **1983**, *22*, 1.
(22) Barteau, M. A.; Broughton, J. Q.; Menzel, D. *Appl. Surf. Sci.* **1984**, *19*, 92.
(23) Ibach, H. Presented at the Proceedings of the International Conference on Vibrations in Adsorbed Layers, Julich, 1978; paper 64.
(24) The Pt(100) surface reconstructs to a slightly buckled, close-packed (5 × 20) superstructure.[25]
(25) Heilmann, P.; Heinz, K.; Müller, K. *Surf. Sci.* **1979**, *83*, 487.
(26) Feulner, P.; Menzel, D. *J. Vac. Sci. Technol.* **1980**, *17*, 662.
(27) Thomas, G. E.; Weinberg, W. H. *Phys. Rev. Lett.* **1978**, *418* 1181.
(28) Thomas, G. E.; Weinberg, W. H. *Rev. Sci. Instrum.* **1979**, *50*, 497.
(29) Williams, E. D.; Weinberg, W. H. *Surf. Sci.* **1979**, *82*, 93.
(30) Williams, E. D.; Weinberg, W. H. *J. Vac. Sci. Technol.* **1982**, *20*, 534.

(31) All exposures reported are uncorrected for the sensitivity of the ion gauge to the various gases.
(32) Shimizu, H.; Christmann, K.; Ertl, G. *J. Catal.* **1980**, *61*, 412.

Table I. Comparison of Vibration Frequencies of Multilayer C_2H_4 Adsorbed on Ru(001) at 80 K with C_2H_4(g), C_2H_4(l), and C_2H_4(s)[a]

		C_2H_4(g)[33]		C_2H_4(l)[34]		C_2H_4(s)[34]	multilayer C_2H_4
no./repr.	mode	Raman	IR	Raman	IR	IR	on Ru(001)
ν_1 A_g	$\nu_s(CH_2)$	3026	f	3019	3016		3000
ν_{11} B_{2u}		f	2989		2983	2973	
ν_5 B_{1g}	$\nu_a(CH_2)$	3103	f	3075			3095
ν_9 B_{2u}		f	3105		3085	3075	
ν_2 A_g	ν(CC)	1623	f	1621	1620	1616	1630
ν_3 A_g	CH_2 scis.	1342	f	1340	1339	1336	1350
ν_{12} B_{3u}		f	1444		1437	1438	1460
ν_4 A_u	CH_2 twist	f	f		~1010		n.r.
ν_6 B_{1g}	CH_2 rock		f	1236	1239		
ν_{10} B_{2u}		f	810		828	827	860
ν_7 B_{1u}	CH_2 wag	f	949		960	970	970
ν_8 B_{3g}		950	f	943			
	ν_s(RuC)						440

no./repr.	mode	C_2D_4(g)[33]	multilayer C_2D_4 on Ru(001)
ν_1 A_g	$\nu_s(CD_2)$	2251	2310
ν_{11} B_{2u}		2200	
ν_5 B_{1g}	$\nu_a(CD_2)$	2304	n.r.
ν_9 B_{2u}		2345	
ν_2 A_g	ν(CC)	1515	1550
ν_3 A_g	CD_2 scis.	981	1015
ν_{12} B_{3u}		1078	1175
ν_4 A_u	CD_2 twist	728	n.r.
ν_6 B_{1g}	CD_2 rock	1009	n.r.
ν_{10} B_{2u}		586	
ν_7 B_{1u}	CD_2 wag	720	735
ν_8 B_{3g}		780	
	ν_s(RuC)		425

[a] n.r. = not resolved. f = forbidden.

K for an ethylene exposure of 0.2 langmuir to 395 K for a 0.4-langmuir exposure and then drops to 355 K for all ethylene exposures exceeding 0.6 langmuir. The decrease in peak temperature for exposures of ethylene below 0.6 langmuir is indicative of second-order desorption kinetics of surface hydrogen. For these lower exposures of ethylene, below 0.6 langmuir, no desorption of molecular ethylene is observed.

Figure 2a and 2b shows the EEL spectra of 4 langmuir of C_2H_4 and 3 langmuir of C_2D_4, respectively, adsorbed at 80 K on the Ru(001) surface. Consistent with the thermal desorption spectra, a comparison of the observed energy loss features to IR and Raman spectra of gaseous, liquid, and solid ethylene (cf. Table I[33,34]) demonstrates that the overlayers of Figure 2 correspond to molecular multilayers. Note the intense CH_2 wagging mode at 970 cm^{-1}, which is the best fingerprint of molecular ethylene multilayers, and also the carbon–hydrogen stretching mode at 3000 cm^{-1}. The frequencies of both these modes are characteristic of an sp^3-hybridized carbon atom. Table I also shows that the isotopic shifts for multilayer C_2D_4 on Ru(001) are in good agreement with those of C_2D_4(g).

Annealing these overlayers to 110 K desorbs the multilayer, as shown in the thermal desorption spectra (cf. Figure 1a), leaving di-σ-bonded ethylene which is stable to 150 K. The EEL spectra of this chemisorbed species are exhibited in Figure 3a for C_2H_4 and Figure 3b for C_2D_4. The rehybridization of the carbon atoms to nearly sp^3 is reflected in the shifts of the CH_2 wagging mode and the carbon–hydrogen stretching mode to 1145 and 2985 cm^{-1}, respectively. The shoulder at 1040 cm^{-1} is probably due to the carbon–carbon stretching mode, but it is poorly resolved from the CH_2 twisting mode in C_2H_4 and the CD_2 wagging mode in C_2D_4 both of which are at 900 cm^{-1}. A carbon–carbon stretching frequency of 1040 cm^{-1} is consistent with the rehybridization of the carbon atoms of ethylene to sp^3. Other modes of di-σ-bonded

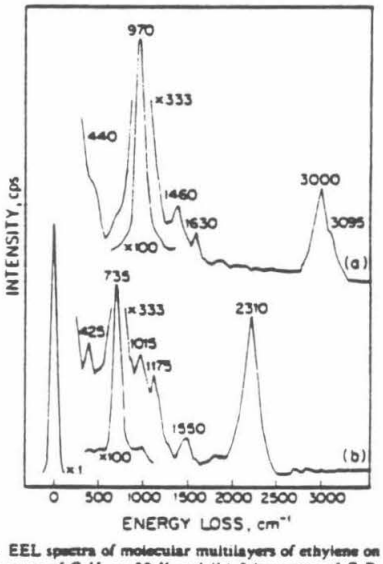

Figure 2. EEL spectra of molecular multilayers of ethylene on Ru(001): (a) 4 langmuir of C_2H_4 at 80 K and (b) 3 langmuir of C_2D_4 at 80 K.

ethylene are the symmetric ruthenium–carbon stretching mode at 460 cm^{-1} (420 cm^{-1} for C_2D_4), the CH_2 rocking mode at 775 cm^{-1}, the CH_2 twisting mode at 900 cm^{-1} (700 cm^{-1} for C_2D_4), and the CH_2 scissoring mode at 1450 cm^{-1} (1210 cm^{-1} for C_2D_4). The CD_2 rocking mode of di-σ-bonded C_2D_4 was not resolved in Figure 3b due to the poorer cutoff in the elastic peak. The symmetric ruthenium–carbon stretching mode of di-σ-bonded

(33) Shimanouchi, T. *NSRDS-NBS* **1972**, *39*, 74.
(34) Brecher, C., Halford, R. S. *J. Chem. Phys.* **1961**, *35*, 1109.

Table II. Comparison of Vibrational Frequencies of Di-σ-bonded C_2H_4 on Ru(001) at 130 K with Other Chemisorbed Ethylene Species, Gaseous Ethylene Compounds, Organometallic Ethylene Compounds, and a Surface Methylene Species[a]

	di-σ-C_2H_4 on										
	Ru(001)	Ni(110)[3]	Ni(111)[4]	Fe(110)[1]	Fe(111)[2]	Pt(111)[7]	C_2H_4(g)[33]	gauche $C_2H_4Br_2$(g)[33]	$K[PtCl_3$-$(C_2H_4)]H_2O$[35]	Ni_3-$(C_2H_4)_4$[36]	CH_2 on Ru(001)[30]
mode C_2H_4 (or CH_2)											
ν_s(CM)	460	420	450	480	580	470				376	n.r.
ν_a(CM)	n.r.	n.r.	610	410	450	560					n.r.
CH_2 rock	775	715	720	720	n.r.	660	826	848	841	910	785
CH_2 twist	900	850	880	915	870	790	f	1104			
CH_2 wag	1145	1145	1110	1105	n.r.	980	949	1278	975	1180	1155
CH_2 scissors	1450	1435	1430	1410	1385	1430	1444	1420	1515	1208	
$\nu_s(CH_2)$	2940	2970	2930	2960	2980	2980	2989	2953	3013	2880	2965
$\nu_a(CH_2)$	3050	n.r.	n.r.	n.r.	n.r.	3000	3096	3005	3075	2908	n.r.
ν(CC)	1040	n.r.	1200	1250	1115	1060	1623	1019	1243	1488	
mode C_2D_4											
ν_s(CM)	420	390	420	440		450					
ν_a(CM)	n.r.	n.r.	590	n.r.		n.r.					
CD_2 rock	n.r.	615	650	635/540		n.r.	586	712			
CD_2 twist	700	725	740	700		600	f	791			
CD_2 wag	900	925	870	850		740	720	947			
CD_2 scissors	1210	1235	1200	1040		1150	1078	1141			
$\nu_s(CD_2)$	2210	2170	2170	2175		2150	2251	2174			
$\nu_a(CD_2)$	2295	2290	2270	n.r.		2250	2304	2271			
ν(CC)	n.r.	n.r.	n.r.	1160		900	1515	1014			

[a] f = forbidden. n.r. = not resolved.

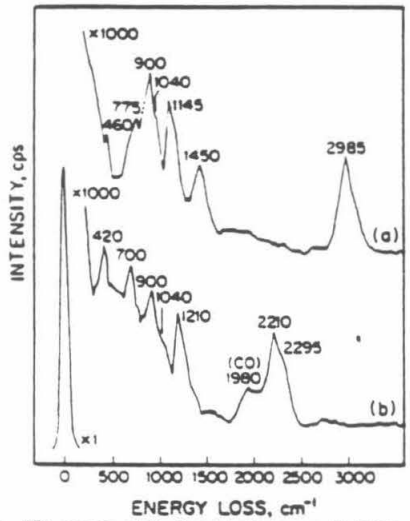

Figure 3. EEL spectra of di-σ-bonded ethylene on Ru(001): (a) 4 langmuir of C_2H_4 annealed to 139 K and (b) 3 langmuir of C_2D_4 annealed to 123 K.

C_2D_4 also contains a small contribution from ν(Ru–CO). The symmetric and asymmetric carbon–hydrogen stretching modes of C_2H_4 at 2940 and 3050 cm^{-1} were resolved in spectra similar to Figure 3a.

Peak assignments for di-σ-bonded ethylene (both C_2H_4 and C_2D_4) on Ru(001) are compared in Table II with those of other chemisorbed ethylene species as well as IR data for $C_2H_4Br_2$(g), C_2H_4(g), Zeise's salt, and a low-valent nickel complex $[Ni(C_2H_4)_4]$.[1-4,7,33,35,36] A comparison of the frequencies of the modes of di-σ-bonded C_2H_4 on Ru(001) to these data shows that ethylene undergoes rehybridization on the Ru(001) surfaces as on Ni(110), Ni(111), and Fe(110).[1,3-5] The existence of a π-bonded ethylene admolecule can be excluded by a comparison to the IR data for Zeise's salt and Ozin's nickel complexes, which have, among other differences, higher frequency CH_2 rocking modes and carbon–carbon stretching modes.

A comparison of EEL spectra of di-σ-bonded ethylene with spectra of diazomethane led to an original assignment of the spectrum of Figure 3a as a bridging methylene species.[37] However, a subsequent review of these and other spectra has shown that the reaction of CH_2N_2 to form C_2H_4 and N_2 may occur in the gas dosing lines prior to introduction into the UHV chamber. An assignment of EEL spectra of uncontaminated diazomethane, which produces μ_2-CH_2 groups on Ru(001), is listed in the last column in Table II. Additional vibrational data concerning bridging methylene may be found elsewhere.[39-43] The adsorption of C_2H_4 on Ru(001) with annealing to 110 K produces di-σ-bonded molecular ethylene, which can be distinguished from μ_2-CH_2 by the intense CH_2 twisting mode at 900 cm^{-1}. In agreement with this conclusion, the thermal desorption spectra of ethylene on Ru(001) show desorption of molecular ethylene up to 250 K.

In an effort to describe further the character of the di-σ-bonded ethylene on Ru(001), isotopic exchange, thermal desorption experiments of coadsorbed C_2H_4 and C_2D_4 were carried out. In all cases, only C_2H_4 and C_2D_4 desorbed from the multilayer. However, all five isotopically labeled species (C_2H_4, C_2H_3D, $C_2H_2D_2$, C_2HD_3, and C_2D_4) appeared in the di-σ-bonded ethylene that desorbs molecularly. Figure 4 shows the relative ratios of these five species that desorb molecularly above 150 K. These ratios were obtained by correcting the areas under the thermal desorption peaks of the 26–32-amu spectra, both for the cracking patterns of the five species and for the relative sensitivity of the mass spectrometer to each species. (These ratios *exclude* multilayer C_2H_4 and C_2D_4.) Figure 4 shows that isotopic exchange is limited, and no mixed species (C_2H_3D, $C_2H_2D_2$, or C_2HD_3) is favored over the other two. On the other hand, the corresponding H_2/HD/D_2 thermal desorption spectra exhibited complete isotopic exchange. The above results suggest that the isotopic mixing observed for

(35) Hiraishi, J. *Spectrochim. Acta, Part A* **1969**, *25A*, 749.
(36) Ozin, G. A. *J. Am. Chem. Soc.* **1978**, *100*, 4750.
(37) George, P. M.; Avery, N. R.; Weinberg, W. H.; Tebbe, F. N. *J. Am. Chem. Soc.* **1983**, *105*, 1393.
(38) EEL spectra of 2.5 langmuir of H_2CN_2 dosed at 80 K, annealed to 192–316 K, and cooled to 80 K prior to measurement.
(39) Fox, D. J.; Schaefer, H. F. *J. Chem. Phys.* **1983**, *78*, 328.
(40) Theopold, K. H.; Bergman, R. G. *J. Am. Chem. Soc.* **1981**, *103*, 2489.
(41) Oxton, I. A.; Powell, D. B.; Sheppard, N.; Burgess, K.; Johnson, B. F. G.; Lewis, J. *Chem. Soc., Chem. Commun.* **1982**, 719.
(42) McBreen, P. H.; Erley, W.; Ibach, H. *Surf. Sci.* **1984**, *148*, 292.
(43) Chang, S.-C.; Kafafi, Z. H.; Hauge, R. H.; Billups, W. E.; Margave, J. L. *J. Am. Chem. Soc.* **1985**, *107*, 1447.

Table III. Comparison of Vibrational Frequencies of Ethylidyne

mode	CCH_3 on Ru(001) at 280 K	CCH_3 on Pd(111) at 300 K[a]	CCH_3 on Pt(111) at 300 K[7]	CCH_3 on Rh(111) at 300 K[16]	$(CO)_9Co_3(\mu_3\text{-}CCH_3)$[45]
ν_s(CM) A_1	480[b]	409	435 vs	450	401
ν_a(CM) E	n.r.[c]	n.r.	600 w	n.r.	555
ρ(CH_3) E	1000	n.r.	980 sh	n.r.	1004
ν(CC) A_1	1140	1080 s	1130 vs	1130	1163
δ_s(CH_3) A_1	1370	1334 vs	1355 vs	1350	1356
δ_a(CH_3) E	1450	1400	1420 sh	n.r.	1420
ν_s(CH_3) A_1	2945	2900 m	2920	2900	2888
ν_a(CH_3) E	3045	n.r.	3050	3000	2930
			Deuterated Species		
ν_s(CM) A_1	480	n.r.	410		393
ν_a(CM) E	n.r.	n.r.	~600		536
ρ(CD_3) E	800	n.r.	790		828
ν(CC) A_1	1150	1120	1160		1182
δ_s(CD_3) A_1	1000	n.r.	990		1002
δ_a(CD_3) E	n.r.	n.r.	1030		1031
ν_s(CD_3) A_1	2190	2181	2080		n.r.
ν_a(CD_3) E	2280	n.r.	2220		2192

[a] n.r. = not resolved. [b] Identified from spectra similar to that of Figure 5a but without CO contamination.

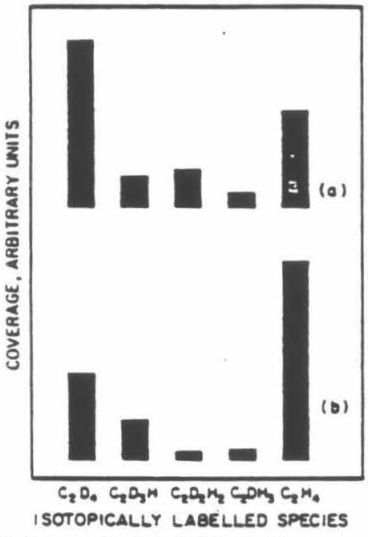

Figure 4. Coadsorption of C_2H_4 and C_2D_4. Relative coverages of C_2H_4, C_2H_3D, $C_2H_2D_2$, C_2HD_3, and C_2D_4 from thermal desorption spectra: (a) 0.6-langmuir exposure of C_2H_4 followed by 3 langmuir of C_2D_4 at 110 K and (b) 1-langmuir exposure of C_2H_4 followed by 3 langmuir of C_2D_4 at 110 K.

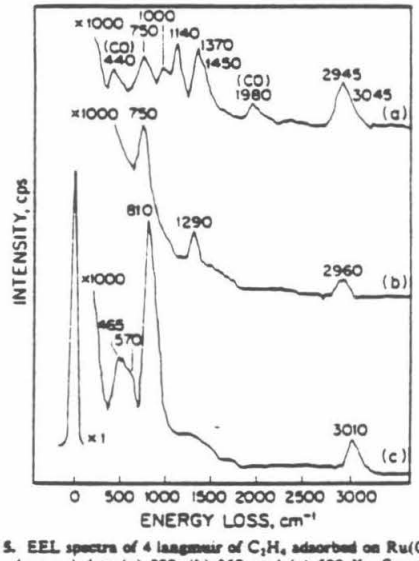

Figure 5. EEL spectra of 4 langmuir of C_2H_4 adsorbed on Ru(001) at 80 K and annealed to (a) 250, (b) 360, and (c) 500 K. Spectrum a exhibits the modes of both ethylidyne and acetylide. Spectrum b is characteristic of acetylide. Spectrum c corresponds to methylidyne.

chemisorbed ethylene that desorbs molecularly results from exchange between an ethylene admolecule and a hydrogen (or deuterium) adatom, since the onset of desorption of the mixed molecular ethylene species ($C_2H_xD_{4-x}$, $1 \leq x \leq 3$) coincides with the initial decomposition of ethylene to ethylidyne, acetylide, and surface hydrogen via carbon–hydrogen bond cleavage.

Annealing di-σ-bonded ethylene to 250 K produces two new carbon-containing surface species as well as hydrogen adatoms. The modes due to surface hydrogen were not resolved in the corresponding EEL spectrum shown in Figure 5a. The weak losses of hydrogen adatoms, which occur at 845 and 1115 cm^{-1},[44] were obscured by various carbon–hydrogen and carbon–carbon modes. However, the presence of hydrogen adatoms was confirmed by stoichiometric considerations and hydrogen postadsorption experiments which will be discussed later. The two hydrocarbon fragments present on the surface have been identified as ethylidyne and acetylide from the EEL spectrum of Figure 5a, the corresponding EEL spectrum of the deuterated species, off-specular EELS measurements, and EEL spectra measured following annealing to various temperatures.

Peak assignments for CCH_3 and CCD_3 are compared in Table III to IR data for a tricobalt ethylidyne complex as well as EELS results for ethylidyne adsorbed on various close-packed groups 8–10 metal surfaces.[4,7,16,45] A triruthenium ethylidyne complex has also been synthesized, but no relevant IR data have been published.[46] For all of the ethylidyne adspecies listed in Table III, the carbon–carbon stretching mode produces a strong, dipolar enhanced peak. By analogy to the structure of the triruthenium and tricobalt organometallic compounds, and considering the relative intensities of the (dipolar-enhanced) carbon–carbon stretching modes, the carbon–carbon bond axis of each of the

(44) Barteau, M. A.; Broughton, J. Q.; Menzel, D. *Surf. Sci.* **1983**, *133*, 443.

(45) Skinner, P.; Howard, M. W.; Oxton, I. A.; Kettle, S. F. A.; Powell, D. B.; Sheppard, N. *J. Chem. Soc., Faraday Trans 2* **1981**, *77*, 1203.

(46) Sheidrick, G. M.; Yesinowski, J. P. *J. Chem. Soc., Dalton Trans* **1975**, 873.

Table IV. Comparison of Vibrational Frequencies of Acetylide[a]

mode	CCH on Ru(001) at 360 K	CCH on Pd(100) at 400 K[48,49]
ν_s(CM)	435	n.r.
ν_a(CM)	n.r.	n.r.
δ(CH)	750	750
ν(CH)	2960	3000
ν(CC)	1290	1340
mode	**CCD**	**CCD**
ν_s(CM)	n.r.	n.r.
ν_a(CM)	n.r.	n.r.
δ(CD)	550	540
ν(CD)	2210	2220
ν(CC)	1260	1340

[a] n.r. = not resolved.

ethylidyne adspecies is nearly perpendicular to the surface plane. A comparison of the EELS losses for CCH_3 and CCD_3 on Ru(001) with IR data for $(CO)_9Co_3(\mu_3\text{-}CCH_3)$ and $(CO)_9Co_3(\mu_3\text{-}CCD_3)$ (cf. Table III) shows that the structure and bonding of the ethylidynes in the two cases are quite similar.

The acetylide species is characterized by a carbon–hydrogen bending mode at 750 cm^{-1}, a carbon–hydrogen stretching mode at 2960 cm^{-1}, and a carbon–carbon stretching mode at 1290 cm^{-1}. The vibrational modes of acetylide are partially obscured by the ethylidyne modes because the ratio of ethylidyne to acetylide present in Figure 4a is approximately 3:2, on the basis of hydrogen thermal desorption measurements. Annealing this overlayer to 360 K decomposes the ethylidyne, leaving acetylide, carbon, and a small concentration of hydrogen adatoms on the surface. Thus the modes of the acetylide are completely resolved in spectra measured after annealing the overlayer to 360 K (cf. Figure 5b). This acetylide also forms from the thermal decomposition of acetylene and is discussed in greater detail in the following paper.[47] We merely note here that these assignments agree quite well with those of Kesmodel et al. for acetylide on Pd(100) for which δ(CH) is 750 cm^{-1}, ν(CC) is 1340 cm^{-1}, and ν(CH) is 3000 cm^{-1}.[48,49]

The EEL spectra of the deuterated acetylide show that the carbon–deuterium bending mode of CCD downshifts to 550 cm^{-1} from 750 cm^{-1} for CCH (cf. Table IV), which compares well with the value of δ(CD) of 540 cm^{-1} for CCD on Pd(100).[48,49] We also observe a slight shift in ν(CC) from 1290 cm^{-1} in CCH to 1260 cm^{-1} in CCD and the expected shift in ν(CD) from 2960 cm^{-1} in CCH to approximately 2210 cm^{-1} in CCD. These losses persist up to 380 K where cleavage of the carbon–carbon bond of the acetylide occurs, forming surface carbon and methylidyne.

The adsorbed methylidyne is identified from the EEL spectrum of Figure 5c with ν(RuC) at 465 cm^{-1}, δ(RuCH) at 810 cm^{-1}, and ν(CH) at 3010 cm^{-1} of which the latter two are significantly higher than the corresponding modes of the acetylide. The disappearance of the 1290-cm^{-1} carbon–carbon stretching mode of acetylide upon annealing to 500 K also assists us in distinguishing acetylide and methylidyne. The mode at 570 cm^{-1} in Figure 5c is the carbon–metal stretching mode of carbon adatoms and/or carbon dimers. The broad feature at 1100–1600 cm^{-1} may be attributed to the carbon–carbon stretching mode of these dimers. The vibrational modes of the methylidyne are compared in Table V to those of high-temperature ($T > 400$ K) methylidynes on various transition-metal surfaces, as well as tricobalt and triruthenium μ_3-CH complexes.[1,2,4,9,10,50-53] Our assignments agree quite well with those of methylidyne adsorbed on the Fe(111), Ni(111), and Pd(111) surfaces and are consistent with those of the organometallic complexes. The isotopic shifts of the vibrational modes of methylidyne adsorbed on Ru(001) are also in agreement with those of $(CO)_4Co_3(\mu_3\text{-}CD)$.

All of the methylidyne modes are eliminated by annealing the Ru(001) surface above 700 K. After this annealation, weak modes near 600 and 1100–1600 cm^{-1} are observed which are attributed to ν(RuC) of carbon adatoms and dimers and ν(CC) of carbon dimers. These modes are present in the EEL spectra of both C_2H_4 and C_2D_4. No other features are present in the high-temperature EEL spectra, supporting the thermal desorption results which show complete desorption of hydrogen (and ethylene) below 700 K.

Bearing in mind what we have learned from EELS concerning the decomposition of ethylene on Ru(001), we now return to a more detailed analysis of the thermal desorption spectra. In the case of ethylene adsorbed on the Ru(001) surface, three reactions generate surface hydrogen below 400 K, namely, (1) C_2H_4 dehydrogenation to CCH(a) and 3H(a), beginning at 150 K; (2) C_2H_4 dehydrogenation to CCH_3(a) and H(a), also beginning at 150 K; and (3) CCH_3 decomposition to 2C(a) or C_2(a) and 3H(a), beginning at 330 K. As shown in Figure 1b, a large ethylene exposure produces a sharp peak at 355 K with a shoulder near 400 K in the hydrogen thermal desorption spectrum, followed by a long, high-temperature tail. Since the high-temperature tail corresponds exclusively to methylidyne decomposition and represents a small fraction of the total hydrogen that is desorbed (approximately 10%), a hydrogen mass balance requires that the desorption which occurs below 500 K corresponds to surface hydrogen from acetylide and ethylidyne formation as well as from ethylidyne decomposition.

For rather low exposures of ethylene, below 0.6 langmuir, the hydrogen thermal desorption spectra are quite different, although the EEL spectra of all coverages of ethylene adsorbed on Ru(001) are qualitatively the same. The thermal desorption spectrum of hydrogen following a low ethylene exposure contains a prominent peak (which shifts as a function of coverage) and also a high-temperature tail (cf. Figure 1c). As shown by the EELS results, the tail corresponds to hydrogen desorption that is limited by methylidyne decomposition. The hydrogen desorbing in the major peak is due to surface hydrogen from ethylene decomposition to ethylidyne and acetylide and ethylidyne decomposition to surface carbon, as is the hydrogen desorbing in the 355 K peak following higher ethylene exposures. The shift in this peak as a function of ethylene coverage indicates that the desorption of this hydrogen is desorption-limited. This is confirmed by experiments conducted on the carbonaceous residue that remains after annealing to 700 K the ruthenium surface which had been exposed to 0.4 langmuir of C_2H_4 at 100 K. Hydrogen was adsorbed on this carbonaceous residue at 90 K, and then a thermal desorption measurement was carried out. The thermal desorption spectra showed that the major hydrogen thermal desorption peak was repopulated, confirming that this peak is due to desorption of surface hydrogen.

The sharp peak at 355 K in the thermal desorption spectra of hydrogen following an exposure of ethylene *exceeding* 0.6 langmuir consists of surface hydrogen formed from ethylene decomposition at lower temperatures (150–280 K) and driven by the presence of that hydrogen from ethylidyne decomposition. The maximum rate of the latter occurs at 355 K. The high-temperature shoulder on this peak (near 400 K) corresponds to desorption of residual surface hydrogen. That the sharp peak at 355 K and its high-temperature shoulder are derived from surface hydrogen has been confirmed by hydrogen postadsorption experiments. First, the Ru(001) surface was exposed to 5 langmuir of C_2H_4 at 90 K, annealed to 800 K, cooled to 90 K, and exposed to 30 langmuir of hydrogen. A subsequent thermal desorption spectrum (Figure 6b) shows a peak at 355 K with a high-temperature shoulder.[54] A comparison with the hydrogen thermal desorption spectrum after an exposure to 5 langmuir of C_2H_4 (Figure 6a) shows that less hydrogen is present in the 355 K peak of Figure 6b and that the leading edge of the peak in this spectrum is not so sharp. These differences are due solely to the presence of ethylidyne decom-

(47) Parmeter, J. E.; Hills, M. M.; Weinberg, W. H. *J. Am. Chem. Soc.*, following paper in this issue.
(48) Kesmodel, L. L. *Vac. Sci. Technol., A* **1984**, *2*, 1083.
(49) Kesmodel, L. L.; Wedill, G. D.; Gates, J. A. *Surf. Sci.* **1984**, *138*, 464.
(50) Demuth, J. E.; Ibach, H. *Surf. Sci.* **1978**, *78*, L238.
(51) Erley, W.; McBreen, P. H.; Ibach, H. *J. Catal.* **1983**, *84*, 229.
(52) Oxton, I. A. *Spectrochim. Acta, Part A* **1982**, *38*, 181.
(53) Howard, M. W.; Kettle, S. F.; Oxton, I. A.; Powell, D. B.; Sheppard, N.; Skinner, P. *J. Chem. Soc., Faraday Trans 2* **1981**, *77*, 397.

(54) EEL spectra of this adlayer support the presence of only carbon and hydrogen adatoms; in particular, no modes of methylidyne are observed.

Table V. Comparison of Vibrational Frequencies of Surface Methylidyne Species to Those of $(CO)_4Co_3(\mu_3\text{-}CH)$ and $(CO)_9H_3Ru_3(\mu_3\text{-}CH)$

mode	CH on Ru(001)	CH on Fe(111)[2]	CH on Fe(110)[1,30]	CH on Ni(111)[4,31]	CH on Pd(111)[9,10]	$(CO)_9H_3Ru_3$-$(\mu_3\text{-}CH)$[32]	$(CO)_4Co_3$-$(\mu_3\text{-}CH)$[33]
ν(CH)	3010	3015	3050	2980	3002	2988	3041
δ(MCH) (e)	810	795	880	790	762	894	850
ν_s(MC) (a_1)	465					670	715
ν_a(MC) (e)	n.r.					424	417
ν(CD)	2250						2268
δ(MCD) (e)	615						680
ν_s(MC) (a_1)	415						696
ν_a(MC) (e)	n.r.						410

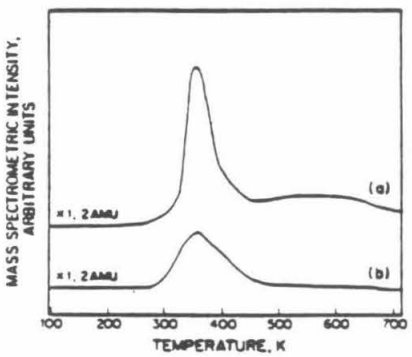

Figure 6. Hydrogen thermal desorption following (a) exposure of 5 langmuir of C_2H_4 and (b) exposure of 5 langmuir of C_2H_4 followed by annealing to 800 K, cooling to 90 K, and exposure to 30 langmuir of H_2.

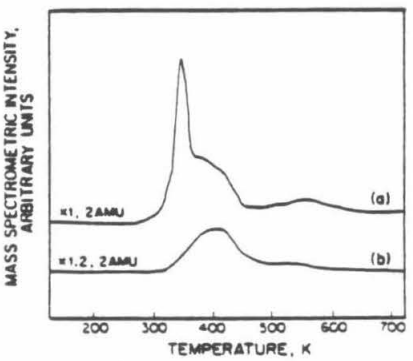

Figure 7. Hydrogen thermal desorption following exposures of (a) 0.4 langmuir of C_2H_4 followed by 2 langmuir of H_2 and (b) 0.4 langmuir of C_2H_4 at 100 K.

position in Figure 6a and its absence in Figure 6b.

In a second experiment, the ruthenium surface was exposed to 0.4 langmuir of C_2H_4, followed by 1 langmuir of H_2 at 90 K. A subsequently measured hydrogen thermal desorption spectrum (Figure 7a) was unlike that following an exposure of 0.4 langmuir of C_2H_4 (Figure 7b). Rather, it appears qualitatively similar to that observed after an exposure of 1 langmiur of C_2H_4 (cf. Figure 1b) in that both spectra contain sharp peaks at 355 K. The major difference between the two spectra of Figure 7 is that more hydrogen adatoms are present in spectrum a, and this is reflected in the much more prominent high-temperature shoulder. Furthermore, more ethylidyne is formed relative to acetylide following the postadsorption of hydrogen, suggesting that this branching ratio is a function of hydrogen coverage. This will be discussed in greater detail in section IV.

To summarize, at all coverages ethylene adsorbes in a di-σ-bonded configuration that decomposes to ethylidyne, acetylide, and surface hydrogen above 150 K. The ethylidyne dehydrogenates above 330 K, generating additional surface hydrogen. The surface hydrogen desorbs at a temperature which decreases with increasing coverage following ethylene exposures below 0.6 langmuir and at 355 K following higher exposures of ethylene. The acetylide decomposes to carbon adatoms and methylidyne near 380 K. Finally, methylidyne decomposes, evolving hydrogen, after annealing above 500 K. For exposures of ethylene below 0.6 langmuir, complete decomposition of methylidyne occurs below 600 K. For higher ethylene exposures, the carbon adatoms (which are present in a higher concentration on the surface) stabilize the methylidyne, such that methylidyne decomposition extends up to 700 K. A plot of ethylene coverage as a function of ethylene exposure as well as a plot of the fractional coverage of ethylene which desorbs molecularly as a function of ethylene exposure is presented in Figure 8.

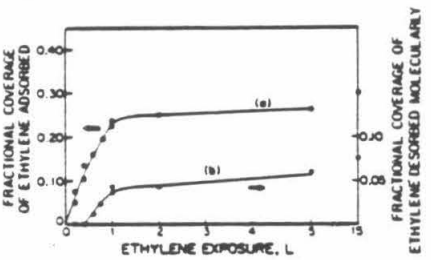

Figure 8. (a) Fractional coverage of chemisorbed C_2H_4 as a function of exposure and (b) fractional coverage of chemisorbed C_2H_4 that desorbs molecularly as a function of exposure. The temperature of adsorption is 80 K.

IV. Discussion

As described in section III, ethylene chemisorbs on the Ru(001) surface in a di-σ-bonded configuration (at a surface temperature below 150 K) and at 80 K condenses into a molecular multilayer that resembles the free ethylene molecule (cf. Table I). As may be seen in Figure 2, all five IR-active modes of ethylene appear in the EEL spectra of the molecular multilayer. In addition, the carbon–carbon stretching mode, the CH_2 rocking mode, and the asymmetric CH_2 scissoring mode were resolved in some spectra. These modes are excited via an impact scattering mechanism.

Chemisorbed ethylene, which is stable below 150 K, is di-σ-bonded to the Ru(001) surface, and assignments of the observed vibrational modes are listed in Table II. This molecularly chemisorbed ethylene on the Ru(001) surface appears to undergo a somewhat greater degree of rehybridization than it does on the

Ni(110), Ni(111), and Fe(110) surfaces.[1,3-5] The differences in frequency between the CH_2 twisting and scissoring modes of C_2H_4 on Ru(001) and on Fe(111) are not unexpected since ethylene on Fe(111) is severely tilted with respect to the surface plane such that two hydrogens are subject to multicenter interactions, which are manifested by a softened ν(CH) mode at 2725 cm^{-1}.[2] This distorted geometry downshifts both the CH_2 wagging and scissoring modes.

Rather little can be said conclusively concerning the symmetry of the di-σ-bonded ethylene on Ru(001). Application of the dipolar selection rule would imply that the symmetry of the adsorbate–substrate complex is C_1, since both the CH_2 rocking and twisting modes appear in figure 3a. However, EEL spectra measured off-specular show that these modes are largely impact excited, and therefore, the dipolar selection rule does not apply. Hence, the symmetry of di-σ-bonded ethylene on Ru(001) remains indeterminant. A near-edge X-ray absorption fine structure (NEXAFS) study of ethylene adsorbed on Pt(111) at 90 K by Horsley and co-workers[55] has shown that ethylene is symmetrically di-σ-bonded to two platinum atoms with the carbon–carbon bond axis parallel to the surface and a carbon–carbon bond length of 1.49 ± 0.03 Å. We expect that di-σ-bonded ethylene would be adsorbed similarly on the Ru(001) surface.

Barteau et al.[22] have reported a di-σ-bonded ethylene species on Ru(001) with a carbon–carbon stretching mode at 1330 cm^{-1}. Our results indicate that their assignments are incorrect, however, for the following reasons. First, they adsorbed ethylene at 170 K, a temperature at which we have shown that di-σ-bonded C_2H_4 has begun to decompose forming a mixed overlayer of C_2H_4(a), CCH_3(a), CCH(a), and H(a). Thus the modes they identify as resulting from di-σ-bonded C_2H_4 are in fact a combination of di-σ-bonded C_2H_4, CCH_3, and CCH modes. The 1330-cm^{-1} loss which they assign to ν(CC) is actually the $\delta_s(CH_3)$ mode of ethylidyne. This feature becomes more intense with further annealing which decomposes the C_2H_4(a) and produces more ethylidyne. Second, our EEL spectra of C_2D_4 on Ru(001) annealed at 170 K show clearly that the previous assignment[22] is incorrect, because the 1330-cm^{-1} loss downshifts to 1000 cm^{-1} in the deuterated spectra, and there are no modes of comparable intensity to the 1300-cm^{-1} mode between 1150 and 2190 cm^{-1} in the deuterated spectra. Barteau and co-workers[22] did not measure any EEL spectra of deuterated ethylene and thus could not distinguish carbon–carbon vibrational modes from hydrogen modes. A comparison of the EEL spectra of C_2H_4 and C_2D_4 is essential to the correct identification of these vibrational modes. As shown in Tables II–IV, EEL spectra of C_2D_4 on Ru(001) annealed between 110 and 400 K confirm our mode assignments for the three adspecies, di-σ-bonded ethylene, ethylidyne, and acetylide. Finally, we note that a carbon–carbon stretching frequency of 1040 cm^{-1} is more reasonable than one of 1330 cm^{-1} for an sp^3-hybridized hydrocarbon species, and it is consistent with the carbon–carbon stretching mode observed at 1135 cm^{-1} for acetylene chemisorbed on Ru(001).[47] It would be expected that ν(CC) of chemisorbed ethylene on Ru(001) would be lower than this value, ruling out the assignment of the 1145-cm^{-1} mode to ν(CC) of C_2H_4. Furthermore, the 1145-cm^{-1} mode shifts considerably (to 900 cm^{-1}) in the spectra of C_2D_4 and certainly cannot be due to ν(CC).

No LEED patterns other than the (1 × 1) of the substrate were observed for the ethylene overlayer between 90 and 300 K. Hence LEED measurements cannot aid in a determination of the ethylene surface structure or absolute coverages. However, thermal desorption results for C_2H_4 and H_2 have been used to estimate the ethylene coverage using the known saturation fractional coverage of hydrogen (0.85).[32] The ethylene coverage (excluding the multilayer) is presented as a function of ethylene exposure in Figure 8a. From this figure, we see that the saturation (fractional) coverage of chemisorbed ethylene is approximately 0.30. Figure 8a was used also to obtain the initial probability of adsorption of ethylene at 100 K, which was found to be unity within the limits of experimental uncertainty. The activation energy of desorption (equal to the heat of adsorption) of di-σ-bonded C_2H_4 was estimated from the thermal desorption measurements. When the method of Redhead[56] is used and a preexponential factor of 10^{13}–10^{14} s^{-1} is assumed, a value of approximately 11.6 ± 1 kcal/mol is obtained. Considering the changes in bond strengths due to rehybridization of the carbon atoms, we have also estimated that the binding energy of di-σ-bonded ethylene is between 105 and 135 kcal/mol. *Thus the observation of a low heat of adsorption for chemisorbed ethylene on Ru(001) does not imply that the ruthenium–carbon bond is weak.*

When the saturated overlayer of chemisorbed ethylene is annealed to 250 K, approximately 20% of the ethylene desorbs, while the remainder dehydrogenates to ethylidyne, acetylide, and surface hydrogen. The stoichiometry of the ethylidyne formed by ethylene decomposition on Pt(111) was confirmed by hydrogen thermal desorption spectra in which approximately 25% of the total hydrogen desorbed from the surface at 300 K, the same temperature at which ethylidyne was shown to form via EELS.[57] Unfortunately, the hydrogen from ethylidyne formation remains adsorbed on the Ru(001) surface, ultimately desorbing with hydrogen from ethylidyne decomposition. Hence we are unable to confirm *directly* the stoichiometry of the ethylene decomposition products from hydrogen thermal desorption spectra. The ethylidyne on Ru(001) begins to decompose at approximately 330 K, whereas the ethylidyne formed on Pt(111) is stable to 400 K.[7] The reduced stability of ethylidyne on Ru(001) is undoubtedly due to the stronger metal–hydrogen and metal–carbon bonds formed on the ruthenium surface, which makes the decomposition of ethylidyne via metal–hydrogen and metal–carbon bond formation more favorable both thermodynamically and kinetically.

The identification of ethylidyne and acetylide as the decomposition products of di-σ-bonded ethylene on Ru(001) can be contrasted to the results of Barteau et al.[22] who only identified ethylidyne. We also note that Barteau assigned the $\rho(CH_3)$ mode of ethylidyne to a loss at 870 cm^{-1}. We observed no such mode in our EEL spectra and cannot account for this discrepancy but merely mention that our assignment of the 1000-cm^{-1} loss to $\rho(CH_3)$ and the observed isotopic shift to 800 cm^{-1} for $\rho(CD_3)$ are in agreement with the frequencies observed for other ethylidyne species.

Our EEL spectra of the thermal evolution of ethylidyne and acetylide on Ru(001) and complementary thermal desorption spectra show that virtually all of the ethylidyne dehydrogenates to surface carbon below 360 K, leaving only CCH(a) and H(a) on the surface. Thus an EEL spectrum measured after annealing to 360 K (Figure 5b) contains only the loss features of acetylide, permitting unambiguous identification of this intermediate. The observation of the carbon–hydrogen bending mode of acetylide at 280 K, prior to the onset of ethylidyne dehydrogenation, implies that acetylide is not a decomposition product of ethylidyne. Further proof of this assertion comes from CO and C_2H_4 coadsorption experiments.[58]

By analogy to all relevant organometallic ethylidyne complexes synthesized to date, it is almost certain that the carbon–carbon bond axis of ethylidyne on Ru(001) is very nearly perpendicular to the surface. This configuration is also supported by the strong intensity of the ν(CC) mode of ethylidyne at 1140 cm^{-1} in the EEL spectrum of Figure 5a and its predominantly dipolar character. Furthermore it is very probable that ethylidyne is bonded to the Ru(001) surface in a threefold hollow site both by analogy to the trimetal μ_3-CCH_3 complexes[45,46] and because ethylidyne has been observed only on hexagonal surfaces.[4,7,16] A further indication of this bonding of ethylidyne on Ru(001) is provided by NEXAFS results of ethylidyne on Pt(111),[55] which showed that the ethylidyne is symmetrically bonded to three

(55) Horsley, J. A.; Stöhr, J.; Koestner, R. J. *J. Chem. Phys.* **1985**, *83*, 3146.

(56) Redhead, P. A. *Vacuum* **1962**, 203.

(57) Ibach, H.; Mills, D. L. *Electron Energy Loss Spectroscopy and Surface Vibrations*; Academic: New York, 1982.

(58) Hills, M. M.; Parmeter, J. E.; Weinberg, W. H., unpublished results.

platinum atoms with the carbon–carbon bond axis essentially perpendicular to the surface.

Next, we consider the effects of simultaneous ethylidyne decomposition and hydrogen desorption on the observed shape of the hydrogen thermal desorption peak. When the Ru(001) surface on which ethylene is adsorbed (exposures above 0.6 langmuir) is annealed to 300 K, hydrogen desorption is observed. In these measurements, hydrogen desorbs at this low temperature due to its higher surface coverage. As the overlayer is annealed to 330 K, additional hydrogen desorbs, and ethylidyne begins to dehydrogenate, replenishing the supply of surface hydrogen. Thus adjacent to the decomposing ethylidyne, an area of high local density of hydrogen adatoms is formed, which accelerates the rate of desorption of hydrogen and gives the hydrogen thermal desorption peak a sharp leading edge. Comparing Figure 6a and 6b, it is clear that the high-temperature shoulder on the 355 K hydrogen thermal desorption peak results from residual surface hydrogen.

For these higher exposures of ethylene, the temperature of the hydrogen thermal desorption peak remains at 355 K independent of coverage. Ethylidyne decomposition dictates this hydrogen desorption since the desorption of hydrogen occurs at a lower temperature in a broader peak at higher hydrogen adatom coverages (from the adsorption of hydrogen). The adsorption and decomposition of ethylene at high coverages is otherwise identical with that for lower coverages with three exceptions. First, a multilayer of ethylene forms which desorbs at 110 K. Second, some of the di-σ-bonded ethylene desorbs (cf. Figure 8b). Finally, the ratio of ethylidyne to acetylide that is formed is increased. Recall that annealing to 400 K the Ru(001) surface on which ethylene is adsorbed not only decomposes the ethylidyne but also causes cleavage of the carbon–carbon bond of the acetylide, leaving methylidyne and carbon adatoms. The high-temperature tail of the hydrogen thermal desorption peak after ethylene adsorption corresponds to dehydrogenation of methylidyne. Consequently, the ratio of ethylidyne to acetylide that is formed from ethylene can be obtained from the relative areas of the 355 K peak and the tail. The acetylide coverage is equal to the coverage of the hydrogen desorbing in the high-temperature tail. The ethylidyne coverage is obtained by subtracting 3 times the acetylide coverage from the coverage of hydrogen desorbing in the 355 K hydrogen thermal desorption peak and its high-temperature shoulder and dividing this number by four. We find that a saturation exposure of ethylene decomposes to ethylidyne and acetylide in the approximate ratio of 60:40, whereas a lower exposure, 0.4 langmuir of C_2H_4, yields a ratio of 50:50. Consequently ethylidyne formation is favored at higher surface coverages. This result may be interpreted in terms of the number of hydrogen adatoms generated by ethylene decomposition to ethylidyne (one per C_2H_4) vs. acetylide (three per C_2H_4). At higher surface coverages, more threefold sites, required for hydrogen adatoms, will be either occupied or blocked. Also, the coverage of hydrogen will be greater as ethylene dehydrogenation proceeds. Thus, the decomposition product that requires fewer vacant surface sites for formation and is composed of more hydrogen atoms, ethylidyne, is favored. The dependence of the ratio of ethylidyne to acetylide formed upon the hydrogen coverage has also been confirmed by hydrogen thermal desorption experiments measured following a saturation ethylene exposure at 350 K. At this temperature, the hydrogen adatom concentration on the surface is reduced. This lower hydrogen coverage caused the acetylide coverage to increase by approximately 50% compared to the coverage of acetylide formed following a saturation ethylene exposure at 80 K, and annealing to 350 K, as judged by the relative intensities of the high-temperature tails in the hydrogen thermal desorption spectra.

Finally, we discuss briefly the mechanism of dehydrogenation of ethylidyne. The EEL spectra measured immediately following the decomposition of ethylidyne show no enhancement of the carbon–hydrogen bending mode of acetylide and provide no evidence for methylidyne formation. Thus, we can rule out both acetylide and methylidyne formation from ethylidyne decomposition and conclude that ethylidyne must dehydrogenate completely to either carbon–carbon dimers [with ν(CC) at 1100–1600 cm^{-1} in the EEL spectra of Figure 5b and 5c] and hydrogen or carbon adatoms and hydrogen. The observed complete dehydrogenation of ethylidyne at a temperature at which acetylide is stable on the surface is quite important. It implies that the reaction coordinate that results in the loss of the first hydrogen atom from ethylidyne is not the one which would lead to the stable surface acetylide. A plausible but most certainly speculative scenario for the dehydrogenation of ethylidyne would involve interaction with an adjacent threefold hollow site, whereas the stable acetylide (almost certainly not oriented parallel to the surface plane) has a structure that is rotated 60° with respect to this reaction coordinate.

V. Conclusions

Ethylene chemisorbs on Ru(001) in a di-σ-bonded configuration at temperatures below approximately 150 K. When heated, competing molecular desorption, dehydrogenation to acetylide, and dehydrogenation to ethylidyne occur. The resulting thermal decomposition scheme for a saturation coverage of chemisorbed ethylene (θ = 0.30) may be depicted as

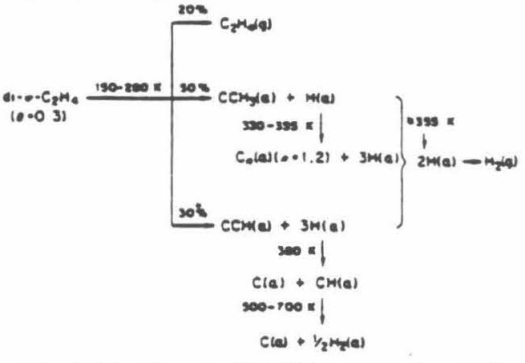

The ethylidyne formed on Ru(001) is less stable than on other groups 8–10 metal surfaces; e.g., it begins to decompose to carbon and hydrogen adatoms near 330 K compared to the decomposition temperature of approximately 400 K observed on Pt(111) and Rh(111). Carbon–carbon bond cleavage of the acetylide occurs at 380 K, producing surface carbon and methylidyne of which the latter dehydrogenates between 500 and 700 K. Following ethylene exposures exceeding 0.6 langmuir, desorption of hydrogen occurs in a sharp peak with a maximum rate of desorption at 355 K, which is limited by ethylidyne decomposition, in a shoulder at approximately 400 K on this peak due to desorption-limited hydrogen and also in a high-temperature tail due to methylidyne decomposition. Hydrogen desorption following lower ethylene exposures becomes desorption-limited, except for the hydrogen that is evolved from the decomposition of methylidyne.

To summarize, ethylene adsorbed on Ru(001) produces both ethylidyne and the more extensively dehydrogenated acetylide. Thus, the behavior of ethylene adsorbed on Ru(001) appears to be intermediate between the more complete dehydrogenation observed on Ni(111) and Co(001) and the exclusive formation of the less dehydrogenated stable ethylidyne species found on the hexagonal surfaces of rhodium, palladium, and platinum.

Acknowledgment. This work was supported by the National Science Foundation under Grant CHE-8516615. Acknowledgment is also made to the donors of the Petroleum Research Fund, administered by the American Chemical Society, for the partial support of this research.

Registry No. C_2H_4, 74-85-1; Ru, 7440-18-8; CCH_3, 67624-57-1; CCH, 29075-95-4; CH, 3315-37-5.

Appendix 4

The Coadsorption of Hydrogen and Ethylene, and of Carbon Monoxide and Ethylene on the Ru(001) Surface

[This appendix was published as a paper by M. M. Hills, J. E. Parmeter and W. H. Weinberg, in *The Journal of the American Chemical Society* 1986, 108, 7215.]

Reprinted from the Journal of the American Chemical Society, 1986, *108*, 7215.

Coadsorption of Hydrogen and Ethylene, and Carbon Monoxide and Ethylene on the Ru(001) Surface

M. M. Hills, J. E. Parmeter,† and W. H. Weinberg*

Contribution from the Division of Chemistry and Chemical Engineering, California Institute of Technology, Pasadena, California 91125. *Received June 25, 1986*

Abstract: A detailed investigation of the coadsorption of ethylene with both preadsorbed hydrogen and preadsorbed carbon monoxide on the Ru(001) surface is reported here. Both preadsorbed hydrogen and carbon monoxide reduce the saturation coverage of subsequently chemisorbed ethylene. The coadsorption of hydrogen with ethylene results in detectable hydrogenation of ethylene to ethane below 250 K, whereas no self-hydrogenation of ethylene to ethane is observed. High-resolution electron energy loss spectra show that ethylene coadsorbed with either hydrogen or carbon monoxide decomposes to ethylidyne (CCH_3) and acetylide (CCH), as it does on the clean surface. Carbon monoxide preadsorption enhances the stability of the ethylidyne such that it decomposes at approximately 420 K, rather than 355 K as on the initially clean Ru(001) surface. Preadsorbed carbon monoxide also reduces the ratio of ethylidyne to acetylide that is formed from ethylene, compared to the ratio observed from an equivalent coverage of ethylene on the clean surface; hydrogen preadsorption, on the other hand, increases this ratio.

I. Introduction

Surprisingly little spectroscopic information is available concerning the interaction of either hydrogen or carbon monoxide with ethylene on well-characterized, single crystalline transition metal surfaces, although much insight regarding the hydrogenation and dehydrogenation of ethylene can be obtained from these measurements. Ratajczykowa and Szymerska[1] have employed mass spectrometry under ultrahigh vacuum (UHV) conditions to investigate the coadsorption of ethylene, hydrogen, and carbon monoxide on Pd(111) between 300 and 330 K, temperatures at which molecularly adsorbed ethylene and ethylidyne (CCH_3) coexist on the clean surface.[2] The relative rates of ethylene hydrogenation and dehydrogenation were compared as functions of hydrogen and carbon monoxide coverage. It was found that the coverage of carbon monoxide controlled the hydrogen coverage, which governed the rate of ethylene hydrogenation relative to ethylene dehydrogenation.

Self-hydrogenation of ethylene to ethane on the Pt(111) surface has been reported by Godbey et al.[3] The maximum rate of ethane formation occurs at 300 K, and this is reduced to 250 K in the presence of preadsorbed hydrogen. Coadsorption of deuterium with ethylene led to the evolution of all isotopically labeled ethane molecules ($C_2H_xD_{6-x}$; $x = 0, 1, \ldots, 6$).

Isotopic exchange between deuterium adatoms and the ethylidyne that is formed from the thermal decomposition of ethylene has been studied on the Pt(111) and Rh(111) surfaces.[4,5] Using static secondary ion mass spectrometry and thermal desorption mass spectrometry, Ogle and White have estimated that this exchange reaction on Pt(111) has an activation barrier of approximately 7 kcal/mol.[4] Using electron energy loss spectroscopy (EELS), Koel et al.[5] found that deuterium incorporation into ethylidyne on Rh(111) at 350 K was slow in the sense that significant isotopic exchange was observed only after a few minutes following exposure of ethylidyne to 1 atm of deuterium, and they postulated the existence of an ethylidene ($CDCH_3$) intermediate in the exchange reaction. In neither investigation was ethylidyne directly observed to be hydrogenated to either ethylidene, ethylene, or ethane.

The coadsorption of hydrogen and ethylene on ruthenium is of particular interest because of the high reactivity of this metal for ethylene hydrogenation and its selectivity in the hydrogenation of monosubstituted olefins.[6] Only rhodium is a more active catalyst than ruthenium for ethylene hydrogenation. Knowledge of the interactions of ethylene and hydrogen on the Ru(001) surface will not only clarify the nature of the hydrogenation reaction of ethylene, but it will also allow important comparisons to the interactions of ethylene and hydrogen on Pt(111) and Rh(111) surfaces, each of which has hexagonal symmetry. The interaction between carbon monoxide and ethylene on ruthenium provides information concerning the effects of a nonreactive coadsorbate on the adsorption, desorption, and dehydrogenation of ethylene. This investigation will also complement previous results for ethylene, acetylene, and acetylene plus hydrogen on the Ru(001) surface.[7-10]

To understand the interactions of hydrogen and carbon monoxide with ethylene on the Ru(001) surface, it is necessary first to understand the interaction of hydrogen, carbon monoxide, and ethylene separately with the clean surface. Hydrogen adsorbs dissociatively in threefold hollow sites on the Ru(001) surface producing weak electron energy loss peaks at 845 and 1115 cm^{-1} at saturation coverage.[11] Thermal desorption spectra of hydrogen exhibit two peaks at high surface coverages, which result from interactions among the adatoms rather than the occupation of geometrically inequivalent surface sites.[12] The high-temperature peak appears first at low coverages with a maximum rate of desorption which downshifts from 450 to 380 K with increasing coverage. The low-temperature peak appears at fractional surface coverages exceeding 0.35, with a maximum rate of desorption occurring near 325 K. The saturation fractional coverage is estimated to be 0.85 ± 0.15.[12]

Carbon monoxide adsorbs molecularly on Ru(001) with a single carbon–oxygen stretching frequency which shifts from 1980 to 2060 cm^{-1} as the coverage increases.[13,14] Under no circumstances has CO been observed to dissociate on the clean surface under UHV conditions. A $(\sqrt{3} \times \sqrt{3})R30°$-CO low-energy electron diffraction (LEED) pattern is formed with an optimal fractional surface coverage of 1/3. For this and lower coverages, the magnitude of the carbon–oxygen stretching frequency suggests

† AT&T Bell Laboratories predoctoral fellow.

(1) Ratajczykowa, I.; Szymerska, I. *Chem. Phys. Lett.* **1983**, *96*, 243.
(2) Gates, J. A.; Kesmodel, L. L. *Surf. Sci.* **1986**, *120*, L461.
(3) Godbey, D.; Zaera, F.; Yeates, R.; Somorjai, G. A. *Surf. Sci.* **1986**, *167*, 150.
(4) Ogle, K. M.; White, J. M. *Surf. Sci.* **1986**, *165*, 234.
(5) Koel, B. E.; Bent, B. E.; Somorjai, G. A. *Surf. Sci.* **1984**, *146*, 211.
(6) Boudart, M.; McDonald, M. A. *J. Phys. Chem.* **1984**, *88*, 2185. Henrici-Olive, G.; Olive, S. *Angew. Chem., Int. Ed. Engl.* **1976**, *15*, 136. Dixit, R. S.; Tavlarides, L. L. *Ind. Eng. Chem., Process Des. Dev.* **1983**, *22*, 1.
(7) Hills, M. M.; Parmeter, J. E.; Mullins, C. B.; Weinberg, W. H. *J. Am. Chem. Soc.*, **1986**, *108*, 3554.
(8) Parmeter, J. E.; Hills, M. M.; Weinberg, W. H. *J. Am. Chem. Soc.* **1986**, *108*, 3563.
(9) Parmeter, J. E.; Hills, M. M.; Weinberg, W. H. *J. Am. Chem. Soc.* **1986**, *108*, 3563.
(10) Barteau, M. A.; Broughton, J. Q.; Menzel, D. *Appl. Surf. Sci.* **1984**, *19*, 92.
(11) Barteau, M. A.; Broughton, J. Q.; Menzel, D. *Surf. Sci.* **1983**, *133*, 443.
(12) Shimizu, H.; Christmann, K.; Ertl, G. *J. Catal.* **1980**, *61*, 412.
(13) Thomas, G. E.; Weinberg, W. H. *J. Chem. Phys.* **1979**, *70*, 1437.
(14) Pfnür, H.; Menzel, D.; Hoffmann, F. M.; Ortega, A.; Bradshaw, A. M. *Surf. Sci.* **1980**, *93*, 431.

0002-7863/86/1508-7215$01.50/0

that the CO is adsorbed in on-top sites. The observation of bridging CO on this surface has not been reported previously. Michalk and co-workers[15] have confirmed the on-top site symmetry of the $(\sqrt{3} \times \sqrt{3})R30°$ overlayer with dynamical LEED calculations. They found also that the CO is adsorbed essentially perpendicularly to the Ru(001) surface with a ruthenium–carbon bond length of 2.0 ± 0.1 Å and a carbon–oxygen bond length of 1.10 ± 0.1 Å. The fractional CO coverage at saturation is 0.65, where a $(5\sqrt{3} \times 5\sqrt{3})R30°$ coincidence LEED pattern, presumably due to a compressed CO overlayer, is observed.[13] Two peaks are observed in the thermal desorption spectra of CO.[16] The high-temperature peak has a maximum desorption rate at approximately 480 K, while the low-temperature peak, which is present at fractional coverages exceeding 1/3, has a maximum rate of desorption near 410 K.

The interaction of ethylene with the clean Ru(001) surface has been discussed in detail recently.[7] To summarize, below 150 K ethylene is chemisorbed molecularly in a di-σ-bonded configuration. Competing molecular desorption and dehydrogenation of the di-σ-bonded ethylene to ethylidyne, acetylide (CCH), and hydrogen adatoms occur between 150 and 250 K. As shown by near-edge X-ray absorption fine structure and LEED calculations, the ethylidyne on Pt(111) is adsorbed in threefold hollow sites.[17,18] This suggests that the ethylidyne adsorbed on Ru(001) also adsorbs in these sites. The ethylidyne on Ru(001) dehydrogenates completely to hydrogen adatoms and either carbon dimers or carbon adatoms with no spectroscopically observable, partially dehydrogenated intermediates.[7] The hydrogen desorbs in a sharp peak at 355 K with a shoulder near 420 K for a saturation coverage of chemisorbed ethylene. Cleavage of the carbon–carbon bond of the acetylide, which yields methylidyne (CH) and surface carbon, is observed at 380 K. Reaction-limited hydrogen desorption occurs between 500 and 700 K as the methylidyne dehydrogenates.

Peebles et al.[19] have shown that preadsorption of carbon monoxide suppresses the high-temperature thermal desorption peak of postadsorbed hydrogen on the Ru(001) surface. The lower temperature thermal desorption peak of hydrogen both decreases in intensity and shifts to lower temperature (from approximately 325 to 305 K) with increasing carbon monoxide coverage.[20] Although it is not known whether these observations are the result of lateral H–CO repulsive interactions giving rise to the formation of high-density islands of hydrogen adatoms in the presence of carbon monoxide or a weakening of the Ru–H bond due to the presence of the coadsorbed carbon monoxide, the former explanation was shown to be correct by a LEED investigation of the coadsorption of hydrogen and CO on Rh(111), where nearly complete segregation of the two species was observed on the surface.[21]

These observations raise several questions. First, how do preadsorbed hydrogen and carbon monoxide affect the subsequent adsorption of ethylene? Second, is the thermal decomposition of ethylene altered by the presence of hydrogen or carbon monoxide, and, if so, how? For example, are ethylidyne and acetylide formed, and, if so, in the same relative concentrations? Finally, can ethylene hydrogenation to ethane be observed under UHV conditions when hydrogen and ethylene are coadsorbed?

II. Experimental Procedures

Thermal desorption mass spectrometry experiments were conducted in a UHV apparatus which has been described in detail previously.[22,23]

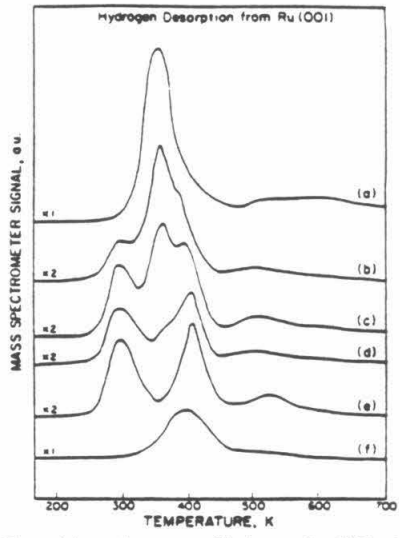

Figure 1. Thermal desorption spectra of hydrogen after C_2H_4 adsorption on the clean and CO precovered Ru(001) surface at 130 K: (a) 1 langmuir of C_2H_4; (b) 0.4 langmuir of CO followed by 1 langmuir of C_2H_4; (c) 0.6 langmuir of CO followed by 1 langmuir of of C_2H_4; (d) 0.8 langmuir of CO followed by 1 langmuir of of C_2H_4; (e) 1.0 langmuir of CO followed by 1 langmuir of of C_2H_4; (f) 0.4 langmuir of C_2H_4.

Briefly, the chamber is pumped by both a 220-L/s noble ion pump and a titanium sublimation pump, which reduce the base pressure below 10^{-10} torr. The crystal is cooled to below 100 K using liquid nitrogen. Linear heating rates of 5–20 K/s are achieved via resistive heating, controlled by a power supply interfaced to an LSI-11 DEC laboratory computer. This UHV chamber contains a UTI-100C quadrupole mass spectrometer enclosed in a glass envelope for selective sampling of gases that desorb from only the well-oriented front surface of the single crystal.[24] Low-energy electron diffraction optics and a rotatable Faraday cup are available for the display of LEED patterns and the measurement of LEED beam profiles. A single-pass cylindrical mirror electron energy analyzer with an integral electron gun is available for Auger electron spectroscopy.

A second UHV chamber was used to conduct high-resolution electron energy loss spectroscopic experiments. This chamber also has a base pressure below 10^{-10} torr using similar pumping techniques: liquid nitrogen cooling and resistive heating of the crystal were similarly employed. The home-built Kuyatt-Simpson-Type EEL spectrometer is described in detail elsewhere.[25,26] It was operated such that the kinetic energy of the electron beam incident upon the crystal was approximately 4 eV at an angle of incidence of 60° with respect to the surface normal. The spectra were measured with a resolution of 60–80 cm^{-1} (full-width at half-maximum of the elastically scattered peak), while maintaining a count rate of $1.5–3 \times 10^5$ counts/s in the elastic channel. This UHV chamber also contains a quadrupole mass spectrometer, but it was not, in general employed in the thermal desorption measurements reported here.

The techniques used for orienting, cutting, polishing, and mounting the Ru(001) crystals have been described previously.[23,26] The crystals were cleaned using periodic argon ion sputtering and routine annealing to 1000 K in 7×10^{-8} torr of O_2, followed by annealing to 1700 K in vacuo. Surface cleanliness was monitored in the two UHV chambers by Auger electron spectroscopy, EELS, and hydrogen thermal desorption.

Research purity (99.9995% min) hydrogen, CP grade (99.5%) deuterium and ethylene, and research purity (99.99% min) carbon monoxide were obtained from Matheson. The ethylene was purified further by three freeze–thaw–pump cycles. Research purity (99.99%) ethylene-d_4

(15) Michalk, G.; Moritz, W.; Pfnür, H.; Menzel, D. *Surf. Sci.* **1983**, *129*, 92.
(16) Pfnür, H.; Feulner, P.; Menzel, D. *J. Chem. Phys.* **1983**, *79*, 2400, 4613.
(17) Horsley, J. A.; Stöhr, J.; Koestner, R. J. *J. Chem. Phys.* **1985**, *83*, 3146.
(18) Koestner, R. J.; Van Hove, M. A.; Somorjai, G. A. *J. Phys. Chem.* **1983**, *87*, 203.
(19) Peebles, D. E.; Schreifels, J. A.; White, J. M. *Surf. Sci.* **1982**, *116*, 117.
(20) These results were confirmed independently in our laboratory.
(21) Williams, E. D.; Thiel, P. A.; Weinberg, W. H.; Yates, J. T., Jr. *J. Chem. Phys.* **1980**, *72*, 3496.
(22) Williams, E. D; Weinberg, W. H. *Surf. Sci.* **1979**, *82*, 93.
(23) Williams, E. D.; Weinberg, W. H. *J. Vac. Sci. Technol.* **1982**, *20*, 534.
(24) Feulner, P.; Menzel, D. *J. Vac. Sci. Technol.* **1980**, *17*, 662.
(25) Thomas, G. E.; Weinberg, W. H. *Phys. Rev. Lett.* **1978**, *41*, 1181.
(26) Thomas, G. E.; Weinberg, W. H. *Rev. Sci. Instrum.* **1979**, *50*, 497

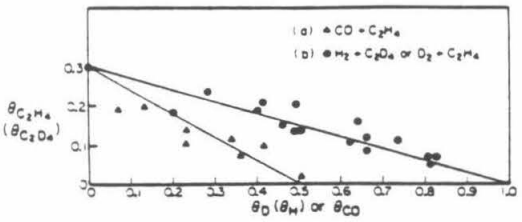

Figure 2. Inhibition of ethylene adsorption by deuterium (hydrogen) or CO precoverages: (a) fractional coverage of chemisorbed C_2H_4 as a function of CO precoverage; (b) fractional coverage of chemisorbed C_2H_4 (C_2D_4) as a function of deuterium (hydrogen) precoverage.

was purchased from Merck and Co. The purity of all gases was verified in situ by mass spectrometry in both UHV chambers.

III. Results

A. Coadsorption of Carbon Monoxide and Ethylene. Preadsorbed CO alters significantly the thermal desorption spectra of hydrogen from adsorbed ethylene on Ru(001). Figure 1a shows the hydrogen thermal desorption spectrum following a saturation exposure of 1 langmuir of C_2H_4 (1 langmuir = 10^{-6} torr-s) at 130 K, while Figure 1b–e shows a series of hydrogen thermal desorption spectra for various preexposures of carbon monoxide, followed by a constant ethylene exposure of 1 langmuir at 130 K (at which temperature no multilayer of ethylene forms). Figure 1f shows the hydrogen thermal desorption spectrum following the adsorption of 0.4 langmuir of ethylene on the clean surface. As the precoverage of CO increases, new desorption peaks of hydrogen appear at 290 and 420 K, while the 355-K peak decreases in intensity, disappearing completely at CO exposures of 1 langmuir or more. In addition, the high-temperature tail (above 480 K) shifts to lower temperature, and the total amount of hydrogen that desorbs decreases with increasing carbon monoxide coverage.

The inhibition in the chemisorption of ethylene by preadsorbed CO ($\theta_{C_2H_4}$ vs. θ_{CO}) is illustrated in Figure 2a, where $\theta_{C_2H_4}$ includes both the reversibly and irreversibly *chemisorbed* ethylene. This relationship was derived from the data of Figure 1, together with the corresponding thermal desorption spectra of molecular ethylene. In the presence of CO, approximately 20% of the chemisorbed ethylene desorbs molecularly, as is observed also on the clean surface. Displacement of CO by ethylene was not observed. However, for all CO precoverages the thermal desorption peaks of CO coadsorbed with ethylene are downshifted by approximately 20 K with respect to the desorption of equivalent coverages of CO from the otherwise clean Ru(001) surface.

The preadsorption of 0.4 langmuir ($\theta_{C_2H_4} \approx 0.13$) of ethylene, followed by 2 langmuir of carbon monoxide ($\theta_{CO} \approx 0.20$), produced hydrogen thermal desorption spectra similar to Figure 1c. Greater initial ethylene coverages blocked carbon monoxide adsorption to a larger extent, and the preadsorption of 1 langmuir of ethylene followed by any exposure of CO resulted in H_2 and C_2H_4 thermal desorption spectra that were nearly identical with those of ethylene adsorbed on the clean Ru(001) surface.

Electron energy loss spectra for various precoverages of carbon monoxide followed by an exposure of ethylene at 80 K are similar to those of ethylene adsorbed on the clean surface. As on the clean Ru(001) surface, multilayers of ethylene condense at 80 K. Annealing the crystal to 110 K desorbs this multilayer, leaving an overlayer composed of carbon monoxide and di-σ-bonded ethylene. Figure 3a shows an EEL spectrum measured after annealing a saturation coverage of ethylene adsorbed on the clean Ru(001) surface to 110 K and is indicative of di-σ-bonded ethylene. The mode assignments for this di-σ-bonded ethylene are discussed in detail elsewhere.[7] Briefly, di-σ-bonded ethylene on Ru(001) produces strong CH_2 twisting and wagging modes at 900 and 1145 cm^{-1} and a symmetric carbon–hydrogen stretching mode at 2940 cm^{-1}, which reflect the rehybridization of the carbon atoms in ethylene to nearly sp^3. Additional energy loss features at 460, 650, 775, 1040, 1450, and 3050 cm^{-1} are due respectively

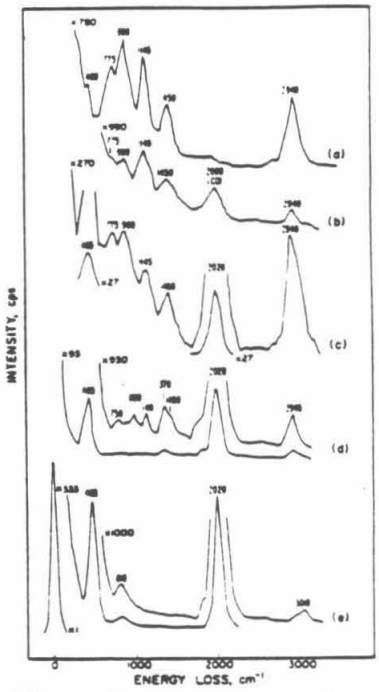

Figure 3. EEL spectra of ethylene on Ru(001): (a) 4 langmuir of C_2H_4 annealed to 120 K; (b) 1 langmuir of H_2 followed by 1 langmuir of C_2H_4 annealed to 120 K; (c) 0.6 langmuir of CO followed by 1 langmuir of C_2H_4 annealed to 120 K; (d) 0.6 langmuir of CO followed by 1 langmuir of C_2H_4 annealed to 280 K; (e) 0.6 langmuir of CO followed by 1 langmuir of C_2H_4 annealed to 400 K.

to the symmetric and asymmetric carbon–ruthenium stretching modes, the CH_2 rocking mode, the carbon–carbon stretching mode, the CH_2 scissoring mode, and the asymmetric carbon–hydrogen stretching mode of the molecularly chemisorbed ethylene. Although not all of these modes are resolved in Figure 3a, they have been assigned from other EEL spectra.

Figure 3c is an EEL spectrum measured following an exposure of 0.6 langmuir of CO ($\theta_{CO} = 0.33$) and then 1 langmuir of C_2H_4 ($\theta_{C_2H_4} = 0.08$–0.09) at 80 K with subsequent annealing to 110 K. (Figure 3b is an EEL spectrum measured following an exposure of 1 langmuir of H_2 and then 1 langmuir of C_2H_4, and will be discussed in section IIIB.) The mixed overlayer of Figure 3c consists of di-σ-bonded C_2H_4 and linearly bonded CO. The modes of both ethylene and carbon monoxide are unchanged compared to those observed when ethylene and carbon monoxide are adsorbed separately on the Ru(001) surface. The symmetric Ru—CO stretching mode and the C≡O stretching mode are observed at 465 and 2020 cm^{-1} in Figure 3c. All mode assignments of ethylene coadsorbed with carbon monoxide were confirmed by EEL spectra of CO coadsorbed with deuterated ethylene.

Annealing the mixed overlayer to between 230 and 280 K causes competing desorption and dehydrogenation of the di-σ-bonded ethylene. A subsequently measured EEL spectrum (Figure 3d) indicates the presence of ethylidyne and acetylide, the same decomposition products formed from ethylene that is adsorbed on the clean surface. The ethylidyne is characterized by the ν(CC) mode at 1140 cm^{-1}, the $\delta_s(CH_3)$ mode at 1370 cm^{-1}, the $\rho(CH_3)$ mode at 1000 cm^{-1}, and the $\nu(CH_3)$ mode at 2945 cm^{-1}.[7] Note that ethylidyne produces no losses below 1000 cm^{-1} except for ν_s(Ru-C) at 480 cm^{-1} (which is unresolved from ν(Ru–C) of CO); the loss at 750 cm^{-1} is due to the carbon–hydrogen bending mode of acetylide. In Figure 3d, the carbon–carbon stretching mode of acetylide at 1290 cm^{-1} and the carbon–hydrogen stretching

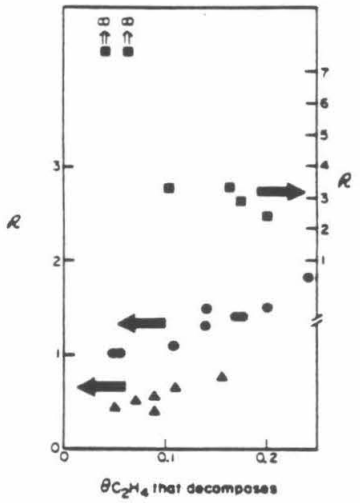

Figure 4. The ratio of ethylidyne to acetylide formed from ethylene (R) as a function of the saturation coverage of irreversibly chemisorbed ethylene for (a, ▲) a mixed CO and ethylene overlayer; (b, ●) ethylene on the clean surface; (c, ■) a hydrogen (deuterium) and C_2D_4 (C_2H_4) overlayer.

mode of acetylide at 2960 cm^{-1} are unresolved from the $\delta_s(CH_3)$ and $\nu(CH_3)$ modes of ethylidyne. This overlayer contains a small concentration of bridging CO in addition to linearly bonded CO, as indicated by the shoulder at 1840 cm^{-1} in Figure 3d.[27] This μ-CO forms near 220 K when acetylide and ethylidyne are formed, and disappears near 450 K as the CO begins to desorb. The CO thermal desorption spectrum of the overlayer corresponding to Figure 3d was virtually identical with that of a CO coverage of 0.33 adsorbed on the clean surface, except downshifted by approximately 20 K. No unusual features were observed which might be attributed to the presence of the bridging CO.

Annealing the surface above 350 K initiates decomposition of the ethylidyne, forming hydrogen adatoms, carbon adatoms, and (possibly) carbon dimers. The hydrogen from ethylidyne decomposition desorbs in either the 355 K or the 420 K thermal desorption peaks (cf. Figure 1), depending upon the CO coverage. Hydrogen thermal desorption spectra have been used to obtain the ratio (R) of ethylidyne to acetylide that is formed from ethylene coadsorbed with CO. This ratio is plotted in Figure 4a as a function of the coverage of the irreversibly chemisorbed ethylene. These data were obtained by exposing the Ru(001) surface to a variable precoverage of CO, followed by a saturation exposure of ethylene. As shown in Figure 4a,b, preadsorbed CO decreases the ratio of ethylidyne to acetylide that is formed from postadsorbed ethylene relative to the ratio observed for an equivalent coverage of ethylene on the clean surface. However, this ratio does increase with increasing ethylene coverages (lower CO precoverages), as it does for ethylene adsorbed on the clean surface. This issue will be discussed in detail in section IV.A.2.

The carbon–carbon bond of the acetylide is cleaved, forming carbon adatoms and methylidyne, when the overlayer is annealed to 400 K. An EEL spectrum of coadsorbed methylidyne and CO is shown in Figure 3e. The characteristic modes of methylidyne are a carbon–hydrogen bending mode at 810 cm^{-1} and a carbon–hydrogen stretching mode at 3010 cm^{-1}. The Ru–CH stretching mode (at 440 cm^{-1}) is obscured by the ν(Ru–CO) mode at 460 cm^{-1}. Annealing to 600 K decomposes all of the methylidyne, desorbing hydrogen and CO, and leaving only surface carbon with ν(Ru–C) at approximately 600 cm^{-1}.

B. Coadsorption of Hydrogen and Ethylene. Electron energy loss spectra of hydrogen and ethylene coadsorbed on Ru(001) are similar to those of ethylene adsorbed on the clean surface with the exception that the modes due to ethylidyne, following annealing to 280 K, are more intense relative to the modes of acetylide. This indicates that the thermal decomposition products of ethylene adsorbed on the clean and the hydrogen-precovered Ru(001) surfaces are the same under our experimental conditions. Figure 3 (a and b) compares respectively the EEL spectrum of a saturation coverage of ethylene adsorbed on the clean surface at 80 K and annealed to 110 K ($\theta_{C_2H_4} = 0.30$) with that of the Ru(001) surface exposed to 1 langmuir of H_2 ($\theta_H = 0.65$) followed by a saturation coverage of ethylene ($\theta_{C_2H_4} = 0.13$) at 80 K and subsequently annealed to 110 K. The spectrum of Figure 3b is less intense because less ethylene is adsorbed. It is apparent, however, that these spectra correspond to the same surface species, namely, di-σ-bonded ethylene. Hydrogen adatoms are also present in the overlayer corresponding to the spectrum of Figure 3b. The weak ruthenium–hydrogen modes, which occur at 780 and 1115 cm^{-1} (at this hydrogen coverage) with an intensity less than 0.04% of the elastic peak,[11] are obscured, however, by losses due to the adsorbed ethylene. A small amount of carbon monoxide is also present in the overlayer corresponding to the spectrum of Figure 3b, as indicated by the presence of the ν(C≡O) mode of CO at 2000 cm^{-1}. The weak intensity of this mode in Figure 3b (cf. Figure 3c–e) implies that the fractional coverage of CO in this overlayer is less than 0.01, and it has no influence on the chemisorption and reaction of hydrogen and ethylene.

Annealing the coadsorbed hydrogen and ethylene overlayer to higher temperatures results in EEL spectra similar to those of ethylene adsorbed on the clean Ru(001) surface. The di-σ-bonded ethylene ($\theta_{C_2H_4} \approx 0.13$) dehydrogenates to ethylidyne and acetylide between 150 and 280 K. The ratio of ethylidyne to acetylide is approximately 2.5, as judged by the areas of the hydrogen thermal desorption peaks of Figure 5b, compared to a branching ratio of 1.3 for a coverage of ethylene of 0.13 on the clean Ru(001) surface. The dependence of the ratio of ethylidyne to acetylide upon the coverage of irreversibly adsorbed ethylene for preadsorbed deuterium (hydrogen) followed by a saturation postexposure of C_2H_4 (C_2D_4) is compared to that observed for ethylene adsorbed on the clean surface in Figure 4b,c. Although there are large uncertainties in the data of Figure 4c because of the small acetylide coverages, the preadsorption of hydrogen clearly results in an increased ratio of ethylidyne to acetylide relative to the ratio observed following the dehydrogenation of an equivalent coverage of ethylene on the clean surface. Indeed, a saturation hydrogen precoverage ($\theta_H \approx 0.85$ and $\theta_{C_2H_4} \approx 0.05$) completely inhibits acetylide formation. The ethylidyne decomposes to carbon (possibly dimers) and hydrogen adatoms below 345 K. Near 400 K the carbon–carbon bond of the acetylide cleaves, forming methylidyne and surface carbon. Finally, the methylidyne decomposes, evolving hydrogen, above 480 K.

The thermal desorption spectra of hydrogen and ethylene coadsorbed on Ru(001) and ethylene adsorbed on the clean surface are somewhat different. Figure 5a illustrates the hydrogen thermal desorption spectrum after 1 langmuir of C_2H_4 is adsorbed on this surface. There is a sharp peak at 345 K, a shoulder near 420 K, and a high-temperature tail extending from 480 to 700 K. Figure 5b shows the hydrogen thermal desorption spectrum after an exposure of 1 langmuir of H_2 followed by 1 langmuir of C_2H_4 at 100 K. This spectrum exhibits a much more prominent shoulder on the high-temperature side of the (sharper) 345 K peak, and the high-temperature tail terminates between 600 and 650 K. As discussed previously,[7] and confirmed by the carbon monoxide and ethylene coadsorption experiments, the 345 K peak of Figure 5a corresponds to desorption of hydrogen limited by ethylidyne decomposition. Because of the similarity of the EEL spectra of ethylene adsorbed on the clean surface and ethylene coadsorbed with hydrogen, the high-temperature tails (above approximately 480 K) of Figure 5a,b correspond to decomposition-limited desorption of hydrogen from the same species, methylidyne.

(27) Approximately 8% based on the intensities of the CO stretching modes of linear and bridge-bonded CO, and assuming that the dipole derivatives of the CO that is bridge bonded and linearly bonded are equal.

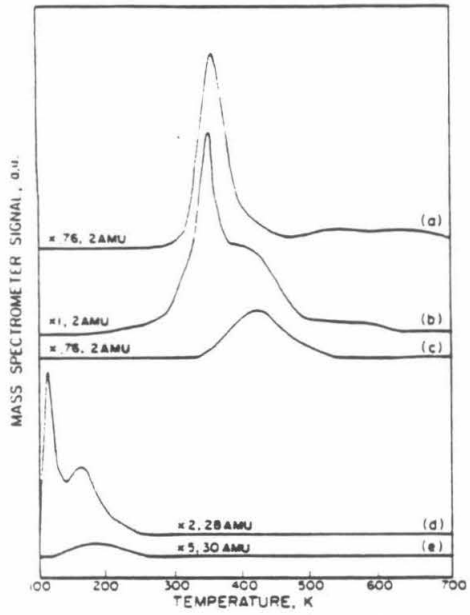

Figure 5. Thermal desorption spectra after C_2H_4 or H_2 adsorption on the clean and hydrogen precovered surfaces at 100 K: (a) H_2 thermal desorption following a 1-langmuir exposure of C_2H_4; (b) H_2 thermal desorption after 1-langmuir exposure of H_2 followed by 1 langmuir of C_2H_4; (c) H_2 thermal desorption following a 0.4-langmuir exposure of H_2; (d) C_2H_4 thermal desorption after a 1-langmuir exposure of H_2 followed by 1 langmuir of C_2H_4; (e) C_2H_4 thermal desorption after a 1-langmuir exposure of H_2 followed by 1 langmuir of C_2H_4.

The shoulder near 420 K in the hydrogen thermal desorption spectrum of coadsorbed hydrogen and ethylene (Figure 5b) is due to desorption-limited hydrogen from the Ru(001) surface. This shoulder occurs at approximately the same temperature at which a similar coverage of hydrogen desorbs from the clean surface, as may be seen in Figure 5c, and the area under the shoulder increases with increasing hydrogen precoverage. Proof that this shoulder corresponds to desorption-limited hydrogen was provided by additional thermal desorption measurements in which the hydrogen and ethylene overlayer was annealed to 800 K, and then the (uncleaned) surface was exposed to hydrogen. The subsequent hydrogen thermal desorption spectrum indicated that the shoulder (now a peak since the 345 K peak was absent) was repopulated, demonstrating that the shoulder of Figure 5b represents desorption-limited hydrogen from the surface. No other hydrogen thermal desorption peaks were observed, implying that no carbon–hydrogen bonds were formed. Complementary EEL spectra measured after annealing the carbon- and hydrogen-covered surface to various temperatures supported the presence of only C(a) and H(a): i.e., no hydrogen-containing species such as CH, CH_2, or CH_3 were observed under any conditions. This disagrees with the results of Barteau et al.[28] who reported the hydrogenation of surface carbon to methylidyne on Ru(001).

In addition to the desorption of hydrogen, annealing the mixed hydrogen and ethylene overlayer resulted in the desorption of ethylene and the formation and desorption of ethane, as shown in Figure 5d,e. Condensed ethylene desorbed in a multilayer peak at 110 K (cf. Figure 5d). Ethane and chemisorbed ethylene desorbed in broad peaks, the tails of which extend to approximately 250 K. The intermediate to ethane formation, presumably ethyl, was not sufficiently stable to be observed spectroscopically by EELS. Ethane was formed following fractional precoverages of hydrogen exceeding 0.4 and subsequent saturation exposures of ethylene. The amount of ethane that desorbed corresponds to an effective fractional surface coverage of only approximately 0.01, which is less than one-third of the amount of ethylene which desorbs molecularly. The fraction of chemisorbed ethylene which desorbs molecularly increases from 0.2 to 0.6 as the initial fractional coverage of hydrogen increases from 0 to 0.85.

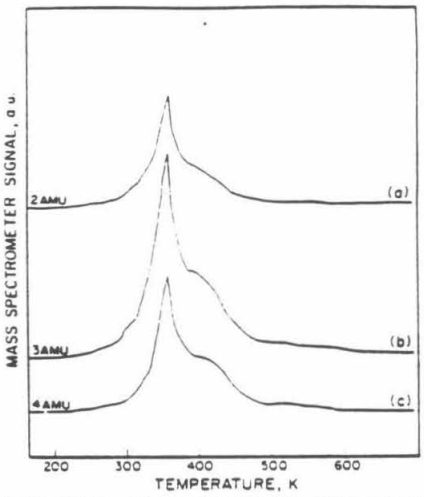

Figure 6. Thermal desorption spectra after a 1-langmuir exposure of D_2 followed by 1 langmuir of C_2H_4 at 130 K: (a) H_2 thermal desorption; (b) HD thermal desorption; (c) D_2 thermal desorption.

Thermal desorption measurements of preadsorbed deuterium and postadsorbed ethylene were carried out to examine both the extent of isotopic mixing among the adspecies and the inhibition of ethylene adsorption by deuterium. Considerable isotopic mixing occurred in the desorbed hydrogen (cf. Figure 6). These experiments also showed that within our experimental uncertainty postexposures of 1 langmuir or more of ethylene did not displace any preadsorbed deuterium. Coadsorption of deuterium (hydrogen) with molecularly chemisorbed C_2H_4 (C_2D_4) indicated that isotopic exchange between these two species was slight in that only minor amounts of any ethylene and ethane desorption products except C_2H_4 (C_2D_4) and $C_2H_4D_2$ ($C_2D_4H_2$) were observed.

The results of isotopic exchange experiments between both CCH_3 and CCH and deuterium adatoms are discussed elsewhere.[29] Briefly, electron energy loss spectra of acetylide and ethylidyne formed from C_2H_2 and coadsorbed with deuterium provide evidence for isotopic exchange between deuterium and CCH but no exchange between deuterium and ethylidyne.

Isotope exchange experiments between deuterated methylidyne and postadsorbed hydrogen [and equivalently between CH(a) and D(a)] were also carried out. Deuterated methylidyne (coadsorbed with carbon adatoms) was formed by exposing the Ru(001) surface to 4 langmuir of C_2D_4 at 100 K and annealing to 440 K such that $\theta_C \approx 0.38$ and $\theta_{CD} \approx 0.10$. The surface was then cooled to 100 K, exposed to a saturation coverage of hydrogen ($0.3 \lesssim \theta_H \lesssim 0.4$), and a thermal desorption experiment conducted. Hydrogen, HD, and D_2 were detected in desorption-limited peaks at 400 K, and in tails above 500 K due to dehydrogenation of CH and CD. No other species such as methane were observed to desorb. A comparison of the areas under the high-temperature tails of the H_2, HD, and D_2 thermal desorption spectra shows that 20 to 30% of the deuterated methylidyne underwent isotopic exchange. The observation of deuterium desorption below 400 K indicates that isotopic exchange occurs below this temperature. The occurrence

(28) Barteau, M. A.; Feulner, P.; Stengl, R.; Broughton, J. Q.; Menzel, D. *J. Catal.* **1985**, *94*, 51.

(29) Weinberg, W. H.; Parmeter, J. E.; Hills, M. M., in preparation.

of isotopic exchange between CH coadsorbed with deuterium has also been confirmed with EELS, and is reported elsewhere.[9] These EELS measurements showed no hydrogenation of methylidyne to stable methylene or methyl species.

The extent of inhibition of ethylene adsorption by preadsorbed deuterium was estimated from the H_2, HD, D_2, ethylene, and ethane thermal desorption spectra for various initial surface coverages of deuterium followed by a saturation exposure of ethylene. These data were used to construct Figure 2b, a plot of $\theta_{C_2H_4}$ vs. θ_D, where θ_D was determined from the HD, D_2, and $C_2H_4D_2$ thermal desorption spectra. Clearly, a saturation precoverage of deuterium does not completely inhibit ethylene adsorption. The inhibition of ethylene adsorption by deuterium adatoms is weaker than that by preadsorbed carbon monoxide.

IV. Discussion

A. Coadsorption of Carbon Monoxide and Ethylene. 1. Adsorption. From Figure 1 and the corresponding thermal desorption spectra of molecular ethylene, it was determined that the fraction of the di-σ-bonded ethylene which desorbed molecularly from the CO preexposed and subsequently ethylene *saturated* surface was 20% of the total fractional coverage of chemisorbed ethylene, independent of the CO coverage. This fraction is approximately the same as that observed when a saturated overlayer of ethylene is chemisorbed on the clean Ru(001) surface. This result shows that preadsorbed CO does not inhibit ethylene thermal decomposition on the surface *relative* to molecular desorption. However, preadsorbed CO does inhibit ethylene adsorption, as illustrated in Figure 2.

The approximately linear decrease in the ethylene coverage with carbon monoxide coverage suggests that CO is simply (geometrically) blocking the surface for ethylene adsorption. The reciprocal of the magnitude of the slope of the line in Figure 2a indicates that 1.7 CO admolecules poison the adsorption of one ethylene molecule. Assuming that the areas occupied by a carbon monoxide admolecule and an ethylene admolecule are inversely proportional to the saturation fractional coverages of CO (0.65) and ethylene (0.30), respectively, then 2.2 (i.e., 0.65/0.30) CO admolecules would block adsorption of one ethylene molecule. We observe that fewer CO admolecules are required to block adsorption of one ethylene molecule because ethylene has a significantly lower heat of adsorption than carbon monoxide and, unlike CO, does not form a compressible overlayer.

2. Thermal Decomposition. The results of Peebles et al.[19] and unpublished data from our laboratory indicate that the peak at 290 K in the hydrogen thermal desorption spectra for coadsorbed CO and C_2H_4 (cf. Figure 1b–e) is due to surface hydrogen that desorbs at a slightly lower temperature than does hydrogen coadsorbed with CO for the same coverages of CO and surface hydrogen. This is presumably the result of a higher effective hydrogen density due to the presence of ethylidyne and acetylide. That the peak at 290 K results from desorption-limited hydrogen was confirmed by hydrogen thermal desorption spectra of coadsorbed hydrogen and carbon monoxide on a carbon precovered surface ($\theta_C \approx 0.15$) which showed hydrogen desorption in a single peak at 290 K for fractional coverages of CO exceeding 0.35. From the observed EEL spectra both of ethylene adsorbed on the clean surface[7] and of ethylene coadsorbed with carbon monoxide, it is clear that this surface hydrogen is derived from ethylene dehydrogenation to acetylide and ethylidyne below 250 K.

The peak at 420 K in the hydrogen thermal desorption spectra of Figure 1b–e results from the decomposition of ethylidyne. Without coadsorbed CO, the ethylidyne begins to decompose near 330 K, reaching a maximum rate at 355 K. This is manifest as a rather sharp peak in the hydrogen thermal desorption spectrum at this temperature, as may be seen in Figure 1a. Preadsorbed CO not only decreases the amount of ethylidyne that is formed relative to acetylide (cf. Figure 4), but it also shifts the ethylidyne decomposition to a higher temperature. The *onset* of ethylidyne decomposition in the presence of a fractional coverage of CO of 0.4 occurs at the same temperature (approximately 380 K) at which CO begins to desorb, as shown both by thermal desorption and EELS results. This suggests that CO inhibits ethylidyne decomposition (effectively stabilizing the ethylidyne), e.g., by geometrically blocking the surface adjacent to the ethylidyne that is necessary for its decomposition. Thus as the precoverage of CO is increased, more ethylidyne is prevented from dehydrogenating prior to CO desorption. A fractional surface precoverage of CO exceeding 0.4 prevents any dehydrogenation of the ethylidyne at 355 K.

The final changes in the hydrogen thermal desorption spectra of carbon monoxide coadsorbed with ethylene on Ru(001) are a shift to lower temperature and an increased intensity (*relative* to the 355 and 420 K peaks) of the high-temperature tail above approximately 480 K, which is due to methylidyne decomposition. The former is due to the lower coverage of ethylene on the surface when CO is preadsorbed and is associated with the greater availability of vacant adsites at the temperature of methylidyne decomposition, i.e., a lower concentration of adsorbed carbon.[30] The increasing intensity of the high-temperature tail in the hydrogen thermal desorption spectra, due to methylidyne decomposition, relative to the 355 and 420 K peaks is a consequence of a reduction in ethylidyne formation relative to acetylide formation, as shown in Figure 4. Recall that methylidyne is derived only from acetylide. The enhancement of acetylide formation with increasing CO precoverage also causes the increasing relative intensity of the 290 K peak in the hydrogen thermal desorption spectra since acetylide formation produces two more hydrogen adatoms than does ethylidyne formation, and these two adatoms desorb in the 290 K peak in the presence of CO. The enhanced acetylide formation relative to ethylidyne formation in the presence of CO is obviously greater than that which would be expected due to the lower ethylene surface coverage in the presence of CO (cf. Figure 4). A reasonable explanation for this effect is that the net balance of interaction energies among hydrogen, carbon monoxide, and the intermediate(s) to ethylidyne and acetylide formation is repulsive with respect to the interaction energy which results in the absence of hydrogen. This inhibits the reaction of hydrogen with the precursor to ethylidyne formation and, therefore, favors dehydrogenation to acetylide with respect to ethylidyne formation.[31] This point of view is consistent with the repulsive interactions that occur between coadsorbed hydrogen and CO which result in phase separation of these two species.

Thus the assignment of peaks in the hydrogen thermal desorption spectra is as follows: the β_1 peak at 290 K is composed of surface hydrogen from ethylene dehydrogenation to acetylide and ethylidyne, downshifted by the presence of CO; the γ_1 peak at 355 K is composed of hydrogen from the decomposition of ethylidyne; the γ_2 peak at 420 K is composed of hydrogen from the decomposition of ethylidyne that is stabilized by coadsorbed CO; and the γ_3 peak near 530 K is composed of hydrogen from methylidyne decomposition. These assignments are consistent with the observed ratios of the peak areas. For example, in the case of Figure 1e where no peak at 355 K is observed, the stoichiometry required by the above peak assignments is $\beta_1 = (\gamma_2/3) + 3\gamma_3$. This stoichiometry has been confirmed by the thermal desorption spectrum of Figure 1e, which exhibits relative peak areas for $\beta_1:\gamma_2:\gamma_3$ of 0.55:0.3:0.15. Thus the carbon monoxide–hydrogen repulsive interactions, which cause phase separation and the lower binding energy of surface hydrogen which results in desorption at a lower temperature, allow us to confirm the stoichiometry of the decomposition products of ethylene adsorbed on the Ru(001) surface which were identified by EELS. The ratio of these peaks also confirm that only a small fraction, *if any*, of the ethylidyne decomposes to methylidyne. If we assume that ethylidyne can decompose to methylidyne, then the ratios of the peaks in these

(30) Note that the high-temperature tail in Figure 1d is similar to the tail in the hydrogen thermal desorption spectrum following the adsorption of 0.4 langmuir of C_2H_4 on the clean Ru(001) surface, shown in Figure 1f.

(31) This explanation implies that the precursor to ethylidyne formation is CCH_2. Evidence for the existence of this precursor is provided by the combined results of experiments of coadsorbed ethylene and hydrogen and coadsorbed acetylene and hydrogen. This will be discussed in detail elsewhere.[29]

hydrogen thermal desorption spectra indicate that *at most* 10% of the ethylidyne decomposes to methylidyne.

Finally, we have observed that the adsorption of ethylene also affects the bonding of preadsorbed carbon monoxide. Postadsorption of ethylene induced the formation of a small fraction of bridging carbon monoxide, which is not observed at any coverage of CO on the otherwise clean Ru(001) surface. Furthermore, the presence of carbon and methylidyne following ethylene dehydrogenation reduced the binding energy of preadsorbed carbon monoxide such that the CO desorbed at approximately 20 K below the temperature at which an equivalent fractional coverage of CO desorbs from the clean surface.

B. Coadsorption of Hydrogen and Ethylene. 1. Adsorption. Figure 2b shows that preadsorbed deuterium does not inhibit ethylene adsorption so effectively as does preadsorbed carbon monoxide. The ethylene coverage that is plotted is the fractional coverage of *chemisorbed* ethylene following multilayer desorption. Preadsorbed deuterium decreases the ethylene coverage approximately linearly, and a saturation coverage of deuterium ($\theta_D \approx 0.85$) does not completely block ethylene adsorption. The linear dependence of ethylene coverage upon deuterium precoverage suggests that the deuterium, like preadsorbed carbon monoxide, is geometrically blocking the surface with respect to the subsequent adsorption of ethylene. The results shown in Figure 2b suggest that 3.3 hydrogen adatoms poison the adsorption of one ethylene molecule. As expected, the number of hydrogen atoms required to block the adsorption of one ethylene molecule is greater than the number of carbon monoxide molecules (1.7). The extrapolated intercept of the abscissa of Figure 2b indicates a hydrogen coverage of one adatom per ruthenium unit cell is necessary to poison the surface essentially completely with respect to the subsequent adsorption of ethylene.

2. Thermal Decomposition. The preadsorption of deuterium atoms into the threefold sites on Ru(001) decreases the availability of vacant threefold sites for the products of ethylene decomposition. The ethylene decomposition products, ethylidyne and acetylide, require one and three vacant threefold sites, respectively, for hydrogen adatoms. Thus, as the deuterium precoverage is increased and fewer threefold sites are available, a larger fraction of the chemisorbed ethylene is desorbed molecularly as C_2H_4 or hydrogenated to ethane, compared to chemisorbed ethylene on the otherwise clean Ru(001) surface. The fraction of chemisorbed ethylene which desorbs molecularly as C_2H_4 increases from 0.2 to 0.6 as the fractional hydrogen precoverage increases from 0 to 0.85. The higher concentration of hydrogen (deuterium) adatoms on the surface below 250 K facilitates ethane formation, which was not observed when ethylene was adsorbed on the clean Ru(001) surface. Ethane evolution was observed only in the coverage range $0.4 \lesssim \theta_H$ (preceding a saturation exposure of ethylene), and the ethane that desorbed corresponds to an effective fractional surface coverage of approximately 0.01. We note further than ethane forms via the hydrogenation of di-σ-bonded ethylene and not ethylidyne or acetylide, which are not present on the surface at the temperature at which ethane evolution is initiated.

Thermal desorption experiments of coadsorbed deuterium and C_2H_4 or hydrogen and C_2D_4 showed that the majority ethane species were $C_2D_2H_4$ in the first case and $C_2H_2D_4$ in the latter. The predominant ethylene species that desorbed molecularly from these overlayers were C_2H_4 and C_2D_4, respectively; i.e., very little isotopic mixing with the molecularly adsorbed ethylene occurred. These results suggest that ethane formation occurs via the irreversible addition of two surface hydrogen or deuterium adatoms to ethylene.

Thermal desorption and EEL spectra of deuterium coadsorbed with CH or hydrogen coadsorbed with CD indicated that approximately 20% of the methylidyne underwent isotopic exchange. Similarly, acetylide underwent limited isotopic exchange with surface hydrogen. The mechanisms by which these exchange reactions proceed will be discussed elsewhere.[29] On the other hand, isotopic exchange between surface hydrogen and CCD_3 did not occur. This is in agreement with the results of Koel et al.[5] who identified via EELS an ethylidyne on Rh(111) at 300 K following C_2H_4 adsorption, and H_2 and C_2H_4 coadsorption. This ethylidyne underwent H–D exchange when exposed to deuterium only at high deuterium pressures (1 atm).

As discussed earlier, the 345 K peak in the hydrogen thermal desorption spectra of hydrogen and ethylene coadsorbed on Ru(001) (cf. Figure 5b) corresponds to the desorption of hydrogen that is limited by ethylidyne decomposition. The high-temperature tail, above approximately 480 K, in the spectra corresponds to the reaction-limited desorption of hydrogen from the decomposition of methylidyne which is formed by the cleavage of the carbon–carbon bond of acetylide at 400 K. The observed change in the areas of these two peaks indicates that the ratio of ethylidyne to acetylide increases with hydrogen precoverage, as shown in Figure 4. Indeed, one might expect that an increase in hydrogen or deuterium precoverage would favor ethylidyne over acetylide since the former is composed of two more hydrogen atoms.

As may be seen in Figure 5b, the shoulder at 420 K in the hydrogen thermal desorption spectra of hydrogen and ethylene adsorbed on Ru(001) is enhanced relative to that of hydrogen thermal desorption from ethylene adsorbed on the clean surface. The temperature corresponding to the maximum rate of hydrogen desorption from this shoulder is approximately 20 K lower than that at which an equivalent amount of hydrogen desorbs from the clean Ru(001) surface. However, this shoulder could be repopulated by adsorbing hydrogen on the (uncleaned) surface that results from annealing coadsorbed hydrogen and ethylene to 800 K, which desorbs the hydrogen completely. This indicates that this shoulder corresponds to desorption-limited surface hydrogen.

V. Conclusions

Both preadsorbed carbon monoxide and hydrogen (deuterium) inhibit ethylene postadsorption on the Ru(001) surface. Of the two, carbon monoxide more effectively inhibits ethylene adsorption. The EEL spectra were virtually identical for ethylene adsorbed on Ru(001), ethylene adsorbed with preadsorbed hydrogen, and ethylene adsorbed with preadsorbed carbon monoxide. In all three cases, the ethylene decomposed upon heating to ethylidyne and acetylide. The ethylidyne dehydrogenated completely to carbon and hydrogen adatoms with further heating, while the acetylide underwent carbon–carbon bond cleavage to form carbon adatoms and methylidyne. The preadsorption of CO causes surface hydrogen to desorb at a lower temperature (290 K) and ethylidyne to decompose at a higher temperature (400 K). The observed ratios of peak areas in the hydrogen thermal desorption spectra confirm the identity of the stable ethylene decomposition products, ethylidyne and acetylide, as observed via EELS.

The presence of preadsorbed CO and hydrogen alters the ratio of the ethylene decomposition products, ethylidyne and acetylide. Carbon monoxide preadsorption enhances acetylide formation relative to ethylidyne formation from postadsorbed ethylene, compared to an equivalent coverage of ethylene adsorbed on the clean surface, while hydrogen preadsorption enhances ethylidyne formation, such that a saturation preexposure of hydrogen completely suppresses acetylide formation.

The preadsorption of hydrogen initiated ethane formation and desorption (with a maximum rate at approximately 200 K). The desorption of ethylene and the formation of ethane were enhanced with increasing hydrogen precoverage, compared to the dehydrogenation products, ethylidyne and acetylide.

Acknowledgment. This work was supported by the National Science Foundation under Grant No. CHE-8516615.

Registry No. C_2H_4, 74-85-1; H_2, 1333-74-0; CO, 630-08-0; Ru, 7440-18-8.

Appendix 5

The Isolation and Characterization of Vinylidene from the Dehydrogenation of Ethylidyne on the Ru(001)-p(2x2)-O Surface

[This appendix was published as a Communication by M. M. Hills, J. E. Parmeter and W. H. Weinberg, in *The Journal of the American Chemical Society* 1987, 109, 597.]

Abstract

The first unambiguous identification of a surface vinylidene species has been observed using high resolution electron energy loss spectroscopy following the thermal decomposition at 250 K of ethylidyne that was formed from π-bonded ethylene on the Ru(001)-p(2x2)O surface. This is also the first observation of the partial dehydrogenation of adsorbed ethylidyne that does not involve carbon-carbon bond cleavage as well. The carbon atoms of the vinylidene are very nearly sp^2–hybridized, and the vinylidene is tilted with respect to the surface normal since π-electron donation from the carbon-carbon double bond to the surface is observed. Decomposition of the vinylidene to methylidyne and surface carbon occurs above 350 K with simultaneous evolution of hydrogen.

Reprinted from the Journal of the American Chemical Society, 1987, *109*, 597.

Isolation and Characterization of Vinylidene from the Dehydrogenation of Ethylidyne on the Ru(001) p(2×2)O Surface

M. M. Hills, J. E. Parmeter,† and W. H. Weinberg*

Division of Chemistry and Chemical Engineering
California Institute of Technology
Pasadena, California 91125

Received August 28, 1986

Although the structure and bonding of a variety of adsorbed species on transition-metal surfaces have been compared to those of similar ligands in homogeneous metal compounds, the chemical reactions which these two entities undergo have not been related. This connection represents the logical and necessary next step in relating the organometallic chemistry of homogeneous compounds with that of extended surfaces, i.e., the relationship between homogeneous catalysis by organometallic compounds and heterogeneous catalysis by metallic surfaces. It has been found that ethylene reacts with $Os_3(CO)_{12}$ to form a μ-vinylidene complex, $H_2Os_3(CO)_9(CCH_2)$, which can be hydrogenated to a μ-ethylidyne complex, $H_3Os_3(CO)_9(CCH_3)$.[1-3] Similarly, ethylene adsorbed on the hexagonal Ru(001),[4] Pt(111),[5] Pt(100),[6,7] Pd(111),[8] and Rh(111)[10] surfaces at room temperature forms ethylidyne, which dehydrogenates at higher surface temperatures. However, vinylidene has been neither isolated nor unambiguously identified as an intermediate in either the formation or the decomposition of adsorbed ethylidyne.[11] This paper reports the first conclusive spectroscopic identification of adsorbed vinylidene, which was observed following the annealing of adsorbed ethylidyne on the Ru(001) p(2×2)O surface.[12]

The high-resolution electron energy loss spectroscopic (EELS) measurements were carried out in an ultrahigh vacuum system that has been described in detail previously.[14] The p(2×2) oxygen overlayer on the Ru(001) surface, which is depicted in Figure 1a, corresponds to a fractional surface coverage of atomic oxygen of 0.25. The existence of this ordered overlayer was confirmed by EEL spectra which exhibit a $\nu_\perp$(Ru–O) mode at 535 cm^{-1} and a phonon mode characteristic of the ordered overlayer at 250 cm^{-1}.[15]

Exposure of the Ru(001) p(2×2)O surface to ethylene at temperatures below 240 K results in the adsorption of π-bonded molecular ethylene.[13,16] Upon annealing to 250 K, the π-bonded

---

† AT&T Bell Laboratories Predoctoral Fellow.

(1) Deeming, A. J.; Underhill, M. *J. Chem. Soc., Chem. Commun.* **1983**, 277.
(2) Deeming, A. J.; Underhill, M. *J. Chem. Soc., Dalton Trans.* **1974**, 1415.
(3) Andrews, J. R.; Kettle, S. F. A.; Powell, D. B.; Sheppard, N. *Inorg. Chem.* **1982**, *21*, 2874.
(4) Hills, M. M.; Parmeter, J. E.; Mullins, C. B.; Weinberg, W. H. *J. Am. Chem. Soc.* **1986**, *108*, 3554.
(5) Steininger, H.; Ibach, H.; Lehwald, S. *Surf. Sci.* **1982**, *117*, 685.
(6) Ibach, H. In *Proceedings of the Conference on Vibrations in Adsorbed Layers*, Jülich, 1978.
(7) The Pt(100) surface reconstructs to a slightly buckled, close-packed (5×20) superstructure.[8]
(8) Heilman, P.; Heinz, K.; Müller, K. *Surf. Sci.* **1979**, *83*, 487.
(9) Gates, J. A.; Kesmodel, L. L. *Surf. Sci.* **1983**, *124*, 68.
(10) Koel, B. E.; Bent, B. E.; Somorjai, G. A. *Surf. Sci.* **1984**, *146*, 211.
(11) Indeed, *no intermediate* has been observed in the reaction of molecularly adsorbed ethylene to ethylidyne. Likewise, no intermediate in the decomposition of adsorbed ethylidyne has been observed heretofore in which carbon–carbon bonding is preserved.
(12) The ethylidyne is a stable intermediate in the dehydrogenation of π-bonded, molecular ethylene on the Ru(001) surface on which an ordered p(2×2) overlayer of oxygen adatoms is present.[13]
(13) Hills, M. M.; Parmeter, J. E.; Weinberg, W. H., manuscript in preparation.
(14) Thomas, G. E.; Weinberg, W. H. *Rev. Sci. Instrum.* **1979**, *50*, 497.
(15) Rahman, T. S.; Anton, A. B.; Avery, N. R.; Weinberg, W. H. *Phys. Rev. Lett.* **1983**, *51*, 1979.

0002-7863/87/1509-0597$01.50/0

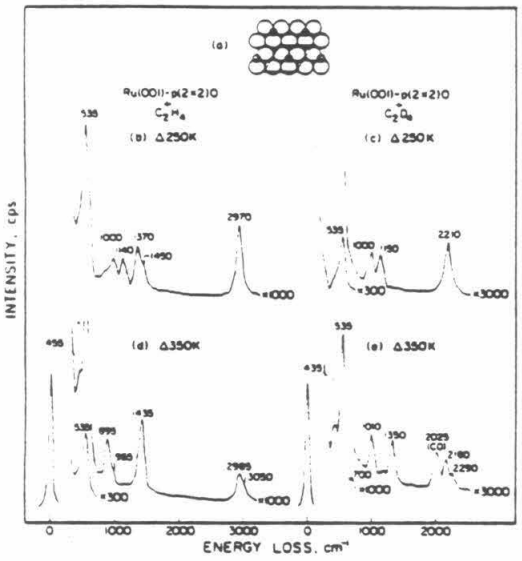

Figure 1. (a) Unit cell and basis of the p(2×2) ordered oxygen overlayer on the Ru(001) surface. The EEL spectra that result from 2-langmuir exposures of (b),(d) C_2H_4 and (c),(e) C_2D_4 on the Ru(001) p(2×2)O surface at 80 K and heated to (b),(c) 250 and (d),(e) 350 K. The intense peak at 535 cm^{-1} in all spectra is due to the $\nu_\perp$(Ru—O) mode of the p(2×2)O oxygen overlayer. The peak at 2025 cm^{-1} in spectrum (e) is due to the ν(C≡O) mode of a small amount ($\theta_{co} < 0.01$) of coadsorbed carbon monoxide.

ethylene reacts to form chemisorbed ethylidyne with the desorption of hydrogen. The ethylidyne is identified by intense ν(CC) and $\delta_s(CH_3)$ modes at 1140 and 1370 cm^{-1} (1150 and 1000 cm^{-1} for CCD_3) which are evident in the EEL spectra of Figure 1b,c.[17]

Upon heating to approximately 350 K, the ethylidyne reacts quantitatively to form vinylidene with simultaneous evolution of hydrogen. The EEL spectra of adsorbed vinylidene are shown in Figure 1d,e. The intense feature at 1435 cm^{-1} in Figure 1d is due to the overlapping ν(CC) and $\delta(CH_2)$ modes of CCH_2. The $\delta(CD_2)$ mode shifts to 1010 cm^{-1} in the deuterated spectrum (Figure 1e), permitting the observation of the ν(CC) mode of CCD_2 at 1350 cm^{-1}. The modes of the adsorbed vinylidene are assigned and compared to those of vinylidene in $H_2Os_3(CO)_9(C-CH_2)$ in Table I. The excellent agreement between the vibrational frequencies of the vinylidene ligand and the adsorbed vinylidene suggests that the bonding of the two is quite similar. An X-ray crystallographic structural determination of the triosmium cluster has shown that the CCH_2 ligand is bridge-bonded to two osmium atoms, that the carbon–carbon bond length of 1.38 Å is only slightly elongated from that of gaseous ethylene (1.34 Å), and that there is π-electron donation from the carbon–carbon double bond to the third osmium atom.[1-3] The carbon–carbon bond length of the vinylidene ligand suggests that the carbon atoms are nearly sp^2-hybridized, and due to the good agreement between the ν(CC) modes of the vinylidene ligand and the adsorbed vinylidene, the carbon atoms of the latter are also expected to be nearly sp^2-hybridized. The frequency of the ν(CC) mode of the adsorbed CCH_2 is lowered from that of CH_2CBr_2 (1593 cm^{-1})[18] and that of the μ-vinylidene ligand in $Cp_2Mn_2(CO)_4(CCH_2)$ (1542 cm^{-1})[19] due to π-electron donation from the carbon–carbon bond of the vinylidene to the ruthenium surface upon which the p(2×2) oxygen overlayer is present. This π-electron donation implies that the adsorbed vinylidene is tilted with respect to the surface normal, as is observed in $H_2Os_3(CO)_9(CCH_2)$.

Table I. Comparison of Vibrational Frequencies (in cm^{-1}) of Vinylidene on the Ru(001) p(2×2)O Surface with $Os_3H_2(CO)_9(CCH_2)$

mode	CCH_2 on Ru(001) p(2×2)O	CCD_2 on Ru(001) p(2×2)O	$Os_3H_2(CO)_9(CCH_2)$ (3)
ν(RuC)	455	435	255–311
$\tau(CH_2)$ or $\tau(CD_2)$	nr[a]	nr[a]	808
$\omega(CH_2)$ or $\omega(CD_2)$	895	700	959
$\rho(CH_2)$ or $\rho(CD_2)$	965	nr[a]	1048
$\delta(CH_2)$ or $\delta(CD_2)$	1435	1010	1328
ν(CC)	1435	1350	1467
$\nu_s(CH_2)$ or $\nu_s(CD_2)$	2985	2180	2990
$\nu_a(CH_2)$ or $\nu_a(CD_2)$	3050	2290	3052

[a] nr = not resolved.

Annealing the adsorbed vinylidene to 400 K initiates decomposition to methylidyne (identified by EELS) and surface carbon with simultaneous evolution of hydrogen, and the methylidyne decomposes above 500 K, creating additional surface carbon and evolving hydrogen.[13] Hydrogen thermal desorption spectra are also consistent with this decomposition mechanism. These spectra show that half of the total amount of hydrogen desorbs below 350 K, indicating that the species present on the surface at this temperature has a stoichiometry of C_2H_2. Another quarter of the hydrogen desorbs in a peak centered at 400 K, in accordance with the decomposition of vinylidene to methylidyne. The final quarter of the hydrogen desorbs between 500 and 700 K as the methylidyne decomposes.

In contrast to the formation of vinylidene from ethylidyne[20] and the subsequent decomposition of vinylidene to methylidyne on the Ru(001) p(2×2)O surface, ethylidyne decomposes completely near 355 K to carbon and hydrogen on the Ru(001) surface.[4,21] The fact that methylidyne is a stable intermediate in the decomposition of ethylidyne on the Ru(001) p(2×2)O surface, while it is not on the Ru(001) surface, implicates the existence of different mechanisms of the decomposition reactions on the two surfaces. On Ru(001), sp^3 hybridization and σ-bonding to the surface are favored, whereas on Ru(001) p(2×2)O sp^2 hybridization and π-donation to the surface are favored, as judged, for example, by the di-σ-bonded and π-bonded molecularly adsorbed ethylene that is observed on the respective surfaces. Hence, the π-bonded vinylidene that was isolated on the Ru(001) p(2×2)O surface is unlikely to be an (unstable) intermediate in ethylidyne decomposition on Ru(001), although a different, more nearly sp^3-hybridized vinylidene may well be involved.[22]

To summarize, adsorbed vinylidene has been isolated following the decomposition of ethylidyne on the Ru(001) p(2×2)O surface at 350 K. The bonding of the adsorbed vinylidene is analogous to that of the vinylidene ligand in $H_2Os_3(CO)_9(CCH_2)$, with very nearly sp^2-hybridized carbon atoms and tilting of the vinylidene with respect to the surface normal due to π-electron donation from the carbon–carbon double bond to the surface. Indeed, the formation of vinylidene from adsorbed ethylidyne is analogous to the reverse of the hydrogenation reaction of $H_2Os_3(CO)_9(CCH_2)$ to $H_3Os_3(CO)_9(CCH_3)$. The decomposition of ethylidyne to vinylidene on the Ru(001) p(2×2)O surface differs from the decomposition mechanism of ethylidyne on the Ru(001) surface due to electronic perturbations of the ruthenium surface by the

(16) The nature of this chemisorption bond is very different from that of the di-σ-adsorbed ethylene on the clean Ru(001) surface.[4]

(17) A detailed discussion of the assignment of all the observed vibrational modes of adsorbed ethylidyne has been presented elsewhere.[4]

(18) De Hemptinne, M. *Trans. Faraday Soc.* **1946**, *42*, 5.

(19) Folting, K.; Huffmann, J. C.; Lewis, L. N.; Coulton, K. G. *Inorg. Chem.* **1979**, *18*, 3483.

(20) The observation of ethylidyne decomposition to vinylidene, but not the reverse reaction, is a consequence of the negligible coverage of hydrogen on the surface at the temperatures at which vinylidene is stable. The recombinative desorption of hydrogen occurs below 220 K on the Ru(001) p(2×2)O surface.

(21) On the Ru(001) surface, ethylene also reacts to form acetylide (CC-H), which decomposes to methylidyne at 360 K. The methylidyne dehydrogenates between 500 and 700 K.[4]

(22) Weinberg, W. H.; Parmeter, J. E.; Hills, M. M., manuscript in preparation.

ordered oxygen overlayer. These perturbations are also manifest in the observed π-bonding of molecular ethylene at 200 K, as opposed to the di-σ-bonded molecular ethylene that is observed on the Ru(001) surface.

Acknowledgment. This work was supported by the National Science Foundation under Grant CHE-8516615.

Appendix 6

The Chemisorption and Reaction of Ethylene on Chemically Modified Ru(001) Surfaces

[This appendix was published as a paper by M. M. Hills, J. E. Parmeter and W. H. Weinberg, in *The Journal of the American Chemical Society* 1987, 109, 4224.]

Reprinted from the Journal of the American Chemical Society, 1987, *109*, 4224.

Chemisorption and Reaction of Ethylene on Chemically Modified Ru(001) Surfaces

M. M. Hills, J. E. Parmeter,† and W. H. Weinberg*

Contribution from the Division of Chemistry and Chemical Engineering, California Institute of Technology, Pasadena, California 91125. *Received December 9, 1986*

Abstract: The adsorption and reaction of ethylene on a Ru(001) surface on which ordered p(2×2) and p(1×2) overlayers of oxygen adatoms are present have been investigated using high-resolution electron energy loss spectroscopy, thermal desorption mass spectrometry, and low-energy electron diffraction. In contrast to the di-σ-bonded ethylene that is observed on clean Ru(001), ethylene chemisorbs molecularly in a π-bonded configuration at temperatures below 200 K on both the Ru(001)–p(2×2)O and Ru(001)–p(1×2)O surfaces. All of the ethylene that is chemisorbed on Ru(001)–p(1×2)O desorbs reversibly at 160 and 240 K, whereas approximately one-third of the ethylene on the Ru(001)–p(2×2)O surface desorbs molecularly at these temperatures. Upon annealing to 250 K, the irreversibly adsorbed ethylene on the Ru(001)–p(2×2)O surface dehydrogenates to ethylidyne (CCH_3), which dehydrogenates further to vinylidene (CCH_2) below 350 K. This represents the first unambiguous identification of a surface vinylidene species, as well as the first isolation of an intermediate in the decomposition of surface ethylidyne that preserves carbon–carbon bonding. The vinylidene decomposes to adsorbed carbon and methylidyne (CH) below 400 K, and the methylidyne decomposes with the evolution of hydrogen between 500 and 700 K.

I. Introduction

Recent spectroscopic investigations of the interaction of ethylene and acetylene with the Ru(001) surface have revealed both the nature of the molecularly chemisorbed species and the decomposition products of these unsaturated hydrocarbons.[1,2] Coadsorption experiments of hydrogen with ethylene, carbon monoxide with ethylene, and hydrogen with acetylene have clarified further the decomposition mechanisms.[3,4] The combined results of these studies[5] have led to the following mechanistic picture:[1-5] (1) both ethylene and acetylene chemisorb molecularly below 150 K on the Ru(001) surface, with rehybridization of the carbon atoms to nearly sp^3 occurring; (2) upon heating to between 150 and 280 K, both ethylene and acetylene form a $HCCH_2$ species, while acetylene also forms acetylide (CCH) at these temperatures; (3) the $HCCH_2$ species reacts rapidly to form acetylide and ethylidyne (CCH_3); (4) the ethylidyne decomposes to carbon adatoms and hydrogen near 350 K, while the acetylide decomposes via carbon–carbon bond cleavage near 380 K, forming methylidyne (CH) and carbon adatoms; and (5) the methylidyne dehydrogenates, evolving hydrogen above approximately 500 K.

We report here the results of a study of the interaction of ethylene with Ru(001) surfaces on which preadsorbed overlayers of dissociatively adsorbed oxygen are present. We have concentrated on the reproducible and well-characterized Ru(001)–p(2×2)O and Ru(001)–p(1×2)O surfaces, although we have also examined the effects of disordered oxygen overlayers, the fractional coverages of which varied from approximately 0.05 to 0.5. The

† AT&T Bell Laboratories Predoctoral Fellow

(1) Hills, M. M.; Parmeter, J. E.; Mullins, C. B.; Weinberg, W. H. *J. Am. Chem. Soc.* **1986**, *108*, 3554.
(2) Parmeter, J. E.; Hills, M. M.; Weinberg, W. H. *J. Am. Chem. Soc.* **1986**, *108*, 3563.
(3) Hills, M. M.; Parmeter, J. E.; Weinberg, W. H. *J. Am. Chem. Soc.* **1986**, *108*, 7215.
(4) Parmeter, J. E.; Hills, M. M.; Weinberg, W. H. *J. Am. Chem. Soc.* **1987**, *109*, 72.
(5) Weinberg, W. H.; Parmeter, J. E.; Hills, M. M. in preparation.

0002-7863/87/1509-4224$01.50/0

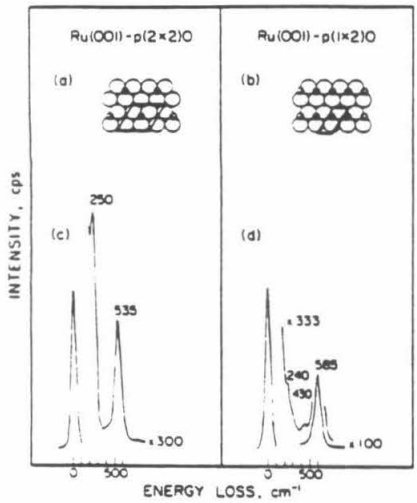

Figure 1. The structures and unit cells of the (a) p(2×2) and (b) p(1×2) ordered oxygen overlayers on the Ru(001) surface. Note that the oxygen occupies threefold hollow sites in both overlayers. Electron energy loss spectra of the (c) p(2×2) and (d) p(1×2) ordered oxygen overlayers.

p(2×2)O overlayer corresponds to a fractional surface coverage of oxygen adatoms of 0.25, while the p(1×2)O overlayer consists of three independent domains that are rotated by 120° with respect to one another and corresponds to a fractional surface coverage of oxygen adatoms of 0.5.[6,7] These two structures are shown schematically in Figure 1, parts a and b. As may be seen in Figure 1, parts c and d, electron energy loss (EEL) spectra of the p(2×2)O overlayer exhibit a ν_3(RuO) mode at 535 cm^{-1} and a surface phonon at 250 cm^{-1}.[7] Similarly, EEL spectra of the p(1×2)O overlayer exhibit a ν_1(RuO) mode at 585 cm^{-1}, a surface phonon at 240 cm^{-1}, and a ν_2(RuO) mode at 430 cm^{-1}.[7] It is these spectroscopic signatures that render reproducible the synthesis of these two well-characterized surfaces.

There are several important reasons for our interest in this system. Oxygen overlayers increase the effective "Lewis acidity" of transition metal surfaces; i.e., the propensity of the surface metal atoms to accept electrons is increased. The extent of charge transfer from the ruthenium to the oxygen adatoms of the p(2×2)O overlayer can be estimated using the observed change in the work function of +0.20 eV following the adsorption of oxygen into the p(2×2) overlayer[6] (making use of the previously determined ruthenium–oxygen bond length[7] and assuming that depolarization effects are negligible). It is found that approximately 0.03 electron is transferred from the ruthenium to each oxygen adatom of the overlayer. Similarly, it is estimated that approximately 0.04 electron is transferred from the ruthenium to each oxygen adatom of the p(1×2) overlayer, using the measured change in the work function of +0.80 eV and correcting for depolarization effects. This charge transfer increases the separation between the Fermi level of the ruthenium surface and the π^* orbital of ethylene, and this transfer could result in the adsorption of π-bonded ethylene on the oxygen precovered ruthenium surface by inhibiting back-donation into the π^* orbital. For example, the preadsorption of oxygen on Pd(100), Fe(111), Pt(111), and Ru(001)–p(1×2)O induces the formation of π-bonded molecular ethylene, as opposed to the di-σ-bonded ethylene observed on the clean surfaces.[8-11] Furthermore, the charge transfer from the ruthenium to the oxygen weakens both the metal–carbon and metal–hydrogen bonding and therefore could result in the formation of different intermediates in the ethylene decomposition reaction, possibly, although not necessarily, via the formation of oxygen-containing intermediates. Finally, the coadsorption of oxygen and ethylene permits a quantification of the extent of poisoning of molecular chemisorption of ethylene by both ordered and disordered oxygen overlayers, as well as the reduction in the extent of ethylene decomposition compared to the reduced (clean) surface.

II. Experimental Procedures

Thermal desorption mass spectrometry and low-energy electron diffraction (LEED) measurements were carried out in an ultrahigh-vacuum (UHV) apparatus that has been described in detail previously.[12] Briefly, the chamber is pumped by both a 220-L/s noble ion pump and a titanium sublimation pump, which reduce the base pressure to below 10^{-10} torr. The crystal is cooled to below 100 K with liquid nitrogen, and linear heating rates of the crystal of 5–20 K/s are achieved via resistive heating controlled by a power supply that is interfaced with an LSI-11 DEC laboratory computer. This UHV chamber contains a UTI-100C quadrupole mass spectrometer enclosed in a glass envelope for selective sampling of gases that desorb from only the well-oriented front surface of the single crystal.[13] Low-energy electron diffraction optics and a rotatable Faraday cup are available for the display of LEED patterns and the measurement of LEED beam profiles. A single-pass cylindrical mirror electron energy analyzer with an integral electron gun is available for Auger electron spectroscopy.

A second UHV chamber was used to conduct high-resolution electron energy loss spectroscopic (EELS) measurements. This chamber also has a base pressure below 10^{-10} torr using similar pumping techniques, and liquid nitrogen cooling and resistive heating of the crystal were similarly employed. The home-built Kuyatt–Simpson-type EEL spectrometer has been described in detail elsewhere.[14,15] It was operated such that the kinetic energy of the electron beam incident upon the crystal was approximately 4 eV, at an angle of incidence of 60° with respect to the surface normal. The spectra were measured with a resolution of 60–80 cm^{-1} (full-width at half-maximum of the elastically scattered peak), while maintaining a count rate of $1-3 \times 10^3$ cps in the elastic channel. This UHV chamber also contains a quadrupole mass spectrometer, but it was not, in general, employed in the thermal desorption measurements reported here.

The techniques used for orienting, cutting, polishing, and mounting the Ru(001) crystals have been described previously.[14,15] The crystals were cleaned using periodic argon ion sputtering and routine annealing to 1000 K in 7×10^{-8} torr of O_2, followed by annealing to 1700 K in vacuo. Surface cleanliness was monitored in the two UHV chambers by Auger electron spectroscopy, EELS, and hydrogen thermal desorption.

Research purity (99.98% min) oxygen ($^{16}O_2$) and CP grade (99.5%) ethylene were obtained from Matheson. The ethylene was purified further by three freeze–thaw–pump cycles. Research purity (99.98% min oxygen, 99% $^{18}O_2$) isotopically labeled oxygen was obtained from Merck and Co. The purity of all gases was verified in situ by mass spectrometry in both chambers. Gas exposures are reported in units of Langmuirs, where 1 Langmuir = 1 L = 10^{-6} torr-s. The quoted exposures have not been corrected for the relative ionization probabilities of the different gases.

III. Results

A. Molecularly Chemisorbed Ethylene on the Ru(001)–p(2×2)O and Ru(001)–p(1×2)O Surfaces. The ordered p(2×2) and p(1×2) oxygen overlayers were synthesized on the Ru(001) surface by exposing the crystal at 90 K to 0.8 and 3 L of O_2, respectively, followed by annealing to 400 K. The existence of these ordered overlayers was verified both by LEED[6] and by EELS,[7] and their structures are shown in Figure 1, together with the corresponding EEL spectra.

Exposure of the Ru(001)–p(2×2)O and Ru(001)–p(1×2)O surfaces at 80 K to 2 L or more of ethylene gives rise to a mo-

(6) Madey, T. E.; Engelhardt, H. A.; Menzel, D. *Surf. Sci.* **1975**, *48*, 304.
(7) Rahman, T. S.; Anton, A. B.; Avery, N. R.; Weinberg, W. H. *Phys. Rev. Lett.* **1983**, *51*, 1979.
(8) Stuve, E. M.; Madix, R. J.; Brundle, C. R. *Surf. Sci.* **1985**, *152/153*, 532.
(9) Seip, U.; Tsai, M.-C.; Kuppers, J.; Ertl, G. *Surf. Sci.* **1984**, *147*, 65.
(10) Steininger, H.; Ibach, H.; Lehwald, S. *Surf. Sci.* **1982**, *117*, 685.
(11) Barteau, M. A.; Broughton, J. Q.; Menzel, D. *Appl. Surf. Sci.* **1984**, *19*, 92.
(12) Williams, E. D.; Weinberg, W. H. *Surf. Sci.* **1979**, *82*, 93.
(13) Feulner, P.; Menzel, D. *J. Vac. Sci. Technol.* **1980**, *17*, 662.
(14) Thomas, G. E.; Weinberg, W. H. *J. Chem. Phys.* **1979**, *70*, 954.
(15) Thomas, G. E.; Weinberg, W. H. *Rev. Sci. Instrum.* **1979**, *50*, 497.

Table I. Comparison of Vibrational Frequencies (in cm^{-1}) of π-Bonded Ethylene on the Ru(001)–p(2×2)O and Ru(001)–p(1×2)O Surfaces at 200 K with Other Ethylene Species

mode	Ru(001)–p(2×2)O and –p(1×2)O	multilayer C_2H_4 on Ru(001)[a]	di-σ-bonded C_2H_4 on Ru(001)[a]	$C_2H_4(g)$[b]	Zeise's salt $K[PtCl_3(C_2H_4)]$[c]	C_2H_4 on Pd(100) + 0.18 ML of O[d]	C_2H_4 on Fe(111) + 1 L of O_2[e]	C_2D_4 on Pt(111) + 0.23 ML of O[f]
C_2H_4								
ν_s(CM)	440		460		403			
ν_a(CM)					490			
ρ(CH_2)		860	775	810	841			
τ(CH_2)			900					
ω(CH_2)	950	970	1145	950	975	940	985	
δ(CH_2)	1245 } g	1350/1460	1450	1342/1444	1243 } g	1510	1290 } g	
ν(CC)	1520 }	1630	1040	1623	1515 }		1565 }	
ν_s(CH_2)	3040	3000	2940	2989/3026	3013	3020	3045	
ν_a(CH_2)		3095	3050	3104	3075			
C_2D_4								
ν_s(CM)								
ν_a(CM)								
ρ(CD_2)				1009/586	597/525			
τ(CD_2)			700	728				
ω(CD_2)	695	735	900	720/780	757			
δ(CD_2)	975	1015/1125	1210	981/1078	962	985		970
ν(CC)	1350	1550	1040	1515	1353	1340		1370
ν_s(CD_2)	2220	2310	2210	2251/2200	2224	2270		2230
ν_a(CD_2)	2300		2295	2304/2345	2331			2340

[a] From ref 1. [b] From ref 7. [c] From refs 16 and 19. [d] From ref 8. [e] From ref 9. [f] From ref 10. [g] Coupled.

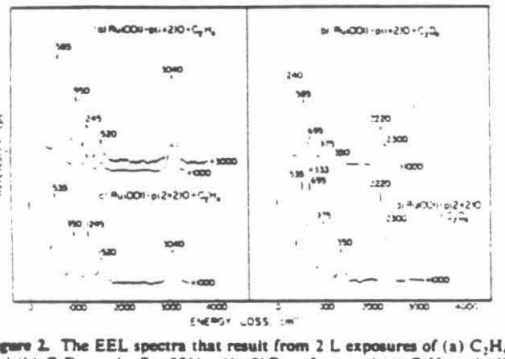

Figure 2. The EEL spectra that result from 2 L exposures of (a) C_2H_4 and (b) C_2D_4 on the Ru(001)–p(1×2)O surface, and (c) C_2H_4 and (d) C_2D_4 on the Ru(001)–p(2×2)O surface at 80 K, followed by heating to 200 K. These spectra are characteristic of π-bonded molecular ethylene on both surfaces.

lecular multilayer that is identical with that observed on the clean surface.[1] This multilayer desorbs at 115 K, leaving a chemisorbed overlayer composed of the oxygen adatoms and π-bonded molecular ethylene. Submonolayer coverages of ethylene adsorbed at 80 K are also π-bonded. Low-energy electron diffraction patterns of these overlayers of molecularly chemisorbed ethylene continue to exhibit the indistinguishable p(2×2) and p(1×2) superstructures due to the oxygen adatoms. Figure 2a,b shows EEL spectra of C_2H_4 and C_2D_4 coadsorbed with the p(1×2)O overlayer at 80 K and annealed to 200 K, while Figure 2c,d shows EEL spectra of C_2H_4 and C_2D_4 coadsorbed with the p(2×2)O overlayer at 80 K and annealed to 200 K. These spectra indicate that π-bonded molecular ethylene is formed on both surfaces. The intense ν_s(RuO) mode appears at 585 cm^{-1} in Figure 2a,b and at 535 cm^{-1} in Figure 2c,d. The ν_a(RuO) mode is not resolved from the ν_s(RuO) mode in Figure 2a,b, nor are the surface phonons resolved from the elastic peak in Figure 2a,c,d. The peaks in the spectra of Figure 2 that are due to π-bonded ethylene are assigned as follows. The intense feature at 950 cm^{-1} (695 cm^{-1} for C_2D_4) is the CH_2 (CD_2) wagging mode. The peak at 3040 cm^{-1} in Figure 2a,c is the symmetric carbon–hydrogen stretching mode from which the asymmetric stretching mode was not resolved. These modes were resolved in the EEL spectra of deuterated ethylene (cf. Figure 2b,d), with $\nu_s(CD_2)$ observed at 2220 cm^{-1} and $\nu_a(CD_2)$ at 2300 cm^{-1}. The frequencies of the carbon–hydrogen (carbon–deuterium) stretching modes as well as the CH_2 (CD_2) wagging modes are indicative of nearly sp^2-hybridized carbon atoms in the adsorbed ethylene. The modes at 1245 and 1520 cm^{-1} in the EEL spectra of chemisorbed C_2H_4 are the strongly coupled CH_2 scissoring and carbon–carbon stretching modes. The CD_2 scissoring and carbon–carbon stretching modes are essentially uncoupled in the spectra of deuterated ethylene and occur at 975 and 1350 cm^{-1}, respectively. The frequency of the ν(CC) mode in the spectra of deuterated ethylene indicates that this species is π-bonded to the surface. The strong coupling of the CH_2 scissoring and carbon–carbon stretching modes in the π-bonded C_2H_4 is in agreement with the observed coupling of these modes of C_2H_4 in Zeise's salt.[16,18,19] Although not resolved from the ruthenium–oxygen stretching mode in Figure 2a–d, the ν(Ru–C_2H_4) mode was observed at 440 cm^{-1} in EEL spectra measured 10° off-specular, in which the ν_s(RuO) mode exhibits a much lower intensity due to its largely dipolar character and strong dynamic dipole and in which the elastic peak has also decreased in intensity.

These mode assignments are compared in Table I with those of multilayer and di-σ-bonded ethylene on Ru(001), $C_2H_4(g)$, Zeise's salt, and π-bonded, molecularly chemisorbed ethylene on other group 8 transition metal surfaces.[1,8-10,16,17,19] These comparisons confirm that molecularly chemisorbed ethylene on both Ru(001)–p(2×2)O and Ru(001)–p(1×2)O is π-bonded to the surfaces and that the carbon atoms of the ethylene are very nearly sp^2-hybridized, as judged by the frequencies of the $\nu_s(CH_2)$, ν_s-(CD_2), $\nu_a(CD_2)$, and ν(CC) (of C_2D_4) modes, as well as the good agreement of all mode assignments with those of Zeise's salt, a paradigm of π-bonded ethylene. On the other hand, the carbon atoms of di-σ-bonded ethylene on the Ru(001) surface are almost completely rehybridized to sp^3, as judged by the significantly lower frequencies of the carbon–carbon and carbon–hydrogen stretching modes, and the upshifts in the CH_2 and CD_2 wagging modes.

Annealing the π-bonded ethylene on the Ru(001)–p(1×2)O surface above 240 K results in the reversible molecular desorption of all of the ethylene. This was demonstrated both by EEL spectra that were measured following the annealing of adsorbed ethylene overlayers to 240 K, which exhibited only the ν_s(RuO), ν_a(RuO), and phonon modes as in Figure 1d, and by thermal desorption spectra of these overlayers that showed only the desorption of

(16) Powell, D. B.; Scott, J. G. V.; Sheppard, N. *Spectrochim. Acta, Part A* **1972**, *28*, 327.
(17) Shimanouchi, T. *NSRDS-NBS Publ.* **1972**, *39*, 74.
(18) Powell et al. believe that there is considerable ν(CC) and $\delta(CH_2)$ character in both the 1243- and 1515-cm^{-1} bands of Zeise's salt.
(19) Hiraishi, J. *Spectrochim. Acta, Part A* **1969**, *25*, 749.

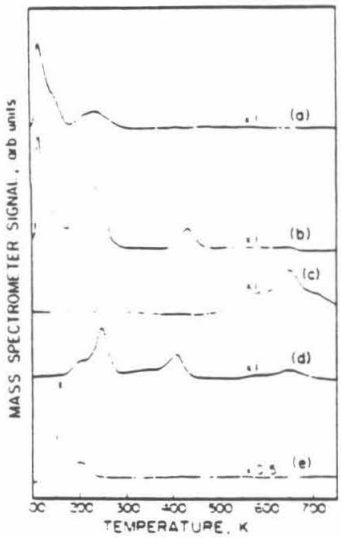

Figure 3. (a) The ethylene (mass 28) thermal desorption spectrum following a 6 L exposure of C_2H_4 on the Ru(001)–p(1×2)O surface at 90 K. (b) The ethylene and $C^{16}O$ (mass 28). (c) the $C^{18}O$ (mass 30), and (d) the hydrogen (mass 2) thermal desorption spectra following a 4 L exposure of C_2H_4 on the Ru(001)–p(2×2)^{18}O surface at 90 K. (e) The hydrogen (mass 2) thermal desorption spectrum following a 10 L exposure of H_2 on the Ru(001)–p(2×2)O surface at 90 K.

molecularly chemisorbed ethylene in a shoulder and a peak centered at 160 and 240 K, respectively, and the desorption of the molecular ethylene multilayer at 115 K (cf. Figure 3a). The fractional saturation coverage of ethylene chemisorbed on Ru(001)–p(1×2)O was estimated to be 0.10 from the ethylene thermal desorption spectra. The activation energy of desorption (equal to the heat of adsorption since the adsorption is unactivated) of ethylene desorbing in the 160 K peak is approximately 9.8 ± 1 kcal/mol, and that of ethylene desorbing in the 240 K peak is approximately 14.0 ± 1 kcal/mol, assuming preexponential factors of the desorption rate coefficients of 10^{13}–10^{14} s^{-1}.[20]

In contrast to the completely reversible adsorption of ethylene on the Ru(001)–p(1×2)O surface, only one-third of the chemisorbed ethylene on the Ru(001)–p(2×2)O surface desorbs reversibly from a saturated overlayer, the total fractional coverage of which is 0.12. As shown in Figure 3b, this reversibly adsorbed ethylene also desorbs in a peak at 240 K and a shoulder at 160 K on the multilayer peak. This thermal desorption measurement was conducted using a p(2×2)^{18}O overlayer in order to distinguish molecularly desorbed ethylene from $C^{18}O$ that is produced by the surface reaction between carbon (from the decomposition of ethylene) and oxygen (cf. Figure 3c). However, a small concentration of $C^{18}O$ due to background adsorption (fractional surface coverage between 0.01 and 0.02) is also observed to desorb, as indicated by the desorption-limited peak at approximately 450 K in Figure 3b.

Although molecularly chemisorbed ethylene on both the Ru(001)–p(2×2)O and Ru(001)–p(1×2)O surfaces desorbs in two peaks at 160 and 240 K, EEL spectra that were measured after annealing to temperatures between 115 and 240 K were identical and indicative of π-bonded ethylene. The identification of the ethylene that desorbs in the 160 K peak as a π-bonded species implies that this peak does not correspond to desorption of a second layer of ethylene.

B. Thermal Decomposition of Ethylene on the Ru(001)–p(2×2)O Surface and on Disordered Oxygen Overlayers on the

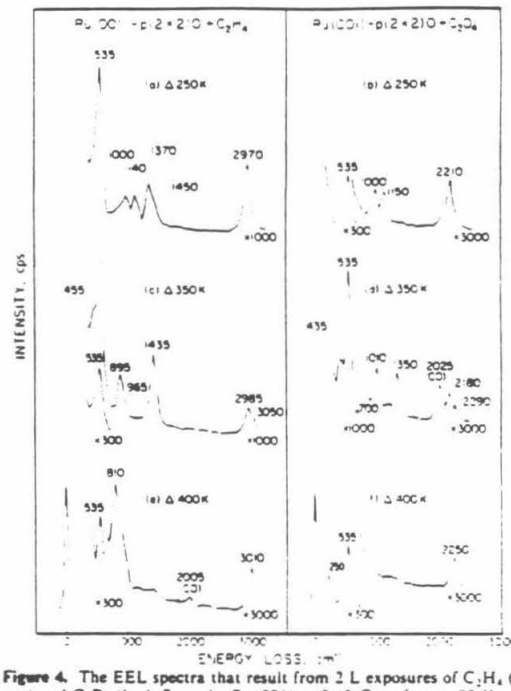

Figure 4. The EEL spectra that result from 2 L exposures of C_2H_4 (a, c, e) and C_2D_4 (b, d, f) on the Ru(001)–p(2×2)O surface at 80 K and heated to (a, b) 250 K, (c, d) 350 K, and (e, f) 400 K.

Ru(001) Surface. Electron energy loss spectra which demonstrate the effect of annealing the molecularly chemisorbed ethylene overlayer on the Ru(001)–p(2×2)O surface to higher temperatures are shown in Figure 4. Comparing the spectra of π-bonded ethylene annealed to 200 K (Figure 2c,d) to those of the same overlayers annealed to 250 K (Figure 4a,b) indicates that by 250 K the ethylene has converted completely to a new species which can be identified easily as ethylidyne. In fact, π-bonded ethylene reacts to yield ethylidyne at temperatures as low as 230 K. Ethylidyne is formed also from the decomposition of di-σ-bonded ethylene on the Ru(001) surface[1] and is characterized by carbon–carbon stretching and symmetric methyl deformation modes at 1140 and 1370 cm^{-1} for CCH_3, and at 1150 and 1000 cm^{-1} for CCD_3. The symmetric and asymmetric carbon–hydrogen stretching modes, expected at 2945 and 3045 cm^{-1} (2190 and 2280 cm^{-1} for CCD_3), were not resolved in these spectra, but appear as a single feature at 2970 cm^{-1} (2210 cm^{-1} for CCD_3). The asymmetric methyl deformation mode and the methyl rocking mode appear at 1450 and 1000 cm^{-1}, respectively, in Figure 4a, but are not resolved from the $\delta_s(CD_3)$ and $\nu_s(RuO)$ modes at 1000 and 535 cm^{-1} in Figure 4b. The $\nu(Ru{\equiv}CCH_3)$ mode of adsorbed ethylidyne, expected at 480 cm^{-1}, is not resolved from the $\nu_s(RuO)$ mode in either of the spectra of Figure 4a,b. These mode assignments of adsorbed ethylidyne have been discussed in detail elsewhere.[1]

Electron energy loss spectra that were measured following annealing this overlayer to 350 K (Figure 4c,d) demonstrate the total conversion of the ethylidyne to a new species, as judged both by the disappearance of the carbon–carbon stretching modes of CCH_3 and CCD_3 at 1140 and 1150 cm^{-1} and the CH_3 rocking mode at 1000 cm^{-1}, as well as by the appearance of new modes which are attributed to a nearly sp^2-hybridized vinylidene (CCH_2). The EEL spectrum of the deuterated vinylidene (Figure 4d) exhibits three intense peaks at 700, 1010, and 1350 cm^{-1}. The peak at 1350 cm^{-1} may be assigned unambiguously to the stretching mode of a carbon–carbon double bond since it is far

(20) Redhead, P. A. *Vacuum* **1962**, 203.

Table II. Comparison of Vibrational Frequencies (in cm^{-1}) of CCH_2 on the Ru(001)–p(2×2)O Surface with Other CCH_2 Species

mode	CCH_2 on Ru(001)–p(2×2)O	CCD_2 on Ru(001)–p(2×2)O	CCH_2 in $Os_3H_2(CO)_9(CCH_2)$[c]	CCH_2 on Pd(111)[d]	Pt(111)[e]
ν(Ru-C)	455	435	255–311	n.r.	n.r.
$\tau(CH_2)$ or (CD_2)	n.r.[a]	n.r.	808	n.r.	n.r.
$\omega(CH_2)$ or (CD_2)	895	700	959	n.r.	900
$\rho(CH_2)$ or (CD_2)	965	n.r.	1048	n.r.	n.r.
$\delta(CH_2)$ or (CD_2)	1435	1010	1467 } [b]	n.r.	1420
ν(CC)	1435	1350	1328 } [b]	1328	1100
$\nu_s(CH_2)$ or (CD_2)	2985	2180	2990	2986	2970
$\nu_a(CH_2)$ or (CD_2)	3050	2290	3052	n.r.	n.r.

[a] n.r. = not resolved. [b] Coupled. [c] From ref 22. [d] From ref 23. [e] From ref 24.

too high in frequency to correspond either to any carbon–deuterium deformation mode or to ν(CC) of a single bond. The loss features at 700 and 1010 cm^{-1} are assigned to the CD_2 wagging and scissoring modes. The other loss peaks at 435, 2180, and 2290 cm^{-1} are then assigned easily as the ν(Ru═CCD_2), $\nu_s(CD_2)$, and $\nu_a(CD_2)$ modes of the CCD_2. The ν(CO) mode of a small concentration of carbon monoxide that is due to adsorption from the background of the UHV chamber appears at 2035 cm^{-1} in Figure 4d. This CO corresponds to a fractional surface coverage of less than 0.02.[21] contributes slightly to the loss peak at 435 cm^{-1}, and has no effect upon the other adsorbates.

The EEL spectrum of the corresponding hydrogenic species (CCH_2) in Figure 4c exhibits two clearly resolved peaks at 895 and 1435 cm^{-1}. The peak at 895 cm^{-1} is due to the CH_2 wagging mode that has shifted up from 700 cm^{-1} in the deuterated spectrum. The more intense loss feature at 1435 cm^{-1} results from two overlapping peaks that correspond to the carbon–carbon stretching mode and the CH_2 scissoring mode that have shifted up from 1350 and 1010 cm^{-1}, respectively, in CCD_2. The other loss peaks at 455, 2985, and 3050 cm^{-1} are the ν(Ru═CCH_2), $\nu_s(CH_2)$, and $\nu_a(CH_2)$ modes of CCH_2. The CH_2 rocking mode is also evident at 965 cm^{-1} in Figure 4c, although the CD_2 rocking mode is not resolved from the CD_2 wagging mode in the spectrum of CCD_2 in Figure 4d.

The vibrational frequencies of this vinylidene are compared in Table II with those of vinylidene in an $Os_3H_2(CO)_9(CCH_2)$ cluster compound and to two other surface species that have been identified as CCH_2.[22-24] There is a good correspondence between the vibrational frequencies of the CCH_2 in the cluster and the vinylidene that is present on the Ru(001)–p(2×2)O surface. The CCH_2 ligand of the complex is bridge-bonded to two osmium atoms with π-electron donation from the carbon–carbon double bond to the third osmium atom, as shown schematically in Figure 5a.[22] The structure of this compound, determined by X-ray crystallography, is shown in Figure 5b.[25]

The existence of a CCH_2 species on the Ru(001)–p(2×2)O surface following ethylene adsorption at 80 K and annealing to 350 K is confirmed further by the hydrogen thermal desorption spectrum, shown in Figure 3d, from ethylene adsorbed on the Ru(001)–p(2×2)^{18}O surface. Approximately half of the hydrogen desorbs below 350 K, indicating that the surface species present at 350 K has a stoichiometry of C_2H_2. The hydrogen that desorbs in the two peaks at 210 and 250 K therefore corresponds to hydrogen that results from the dehydrogenation of π-bonded ethylene to ethylidyne and the subsequent dehydrogenation of ethylidyne to vinylidene. As may be seen by comparing the hydrogen thermal desorption spectrum of Figure 3d with that of hydrogen adsorbed on the Ru(001)–p(2×2)O surface (Figure 3e), most of the hydrogen that results from the dehydrogenation of ethylene and ethylidyne desorbs above the temperature at which chemisorbed hydrogen desorbs from the Ru(001)–p(2×2)O surface, and is therefore a reaction-limited desorption product.

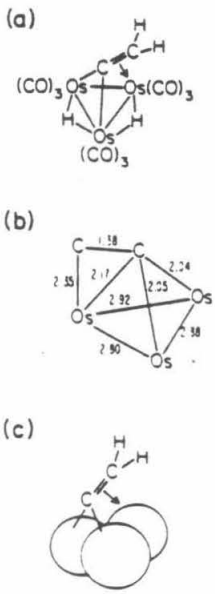

Figure 5. (a) The bonding configuration and (b) the structure of CCH_2 in $Os_3H_2(CO)_9(CCH_2)$.[25] (c) The analogous bonding configuration of CCH_2 on the Ru(001)–p(2×2)O surface.

The vinylidene could be rehydrogenated to ethylidyne, indicating that this reaction is reversible. After a saturation coverage of CCH_2 was formed, the Ru(001)–p(2×2)O surface was cooled to 80 K, exposed to 10 L of hydrogen, and annealed to 200 K. Subsequently measured EEL spectra showed the presence of ethylidyne and a small amount of unreacted vinylidene, indicating that most of the CCH_2 had been rehydrogenated. Annealing this overlayer to 350 K results in the dehydrogenation of the ethylidyne to vinylidene. In another experiment, the vinylidene was exposed to 15 L of deuterium at a surface temperature of 200–250 K. The EEL spectrum of this overlayer indicates the existence of different isotopes of ethylidyne. As expected, the species with the highest coverage is CCH_2D with a $\delta_s(CH_2D)$ mode at 1260 cm^{-1}, whereas CCH_3 is present at a lower coverage. Neither CCD_2H nor CCD_3 was detected.

As shown in Figure 3d, annealing the vinylidene overlayer on the Ru(001)–p(2×2)O surface to higher temperatures causes further hydrogen desorption in a peak at 400 K, indicating that the CCH_2 has dehydrogenated. Electron energy loss spectra of the overlayer that is formed by annealing the surface to 400 K (cf. Figure 4e,f) are consistent with this interpretation. The stable species on the surface at this temperature are carbon adatoms and methylidyne, which are formed via cleavage of the carbon–carbon bond and one carbon–hydrogen bond of vinylidene. No intermediates in the vinylidene decomposition reaction such as methylene (CH_2) or acetylide (CCH) were observed by EELS

(21) This estimate is based on the intensity of the ν(CO) mode in this spectrum compared to those of low CO coverages on the Ru(001) surface.
(22) Andrews, J. R.; Kettle, S. F. A.; Powell, D. B.; Sheppard, N. *Inorg Chem.* **1982**, *21*, 2874.
(23) Gates, J. A.; Kesmodel, L. L. *Surf. Sci.* **1983**, *124*, 68.
(24) Ibach, H.; Lehwald, S. *J. Vac. Sci. Technol.* **1978**, *15*, 407.
(25) Deeming, A. J.; Underhill, M. *J. Chem. Soc., Dalton Trans.* **1974**, 1415.

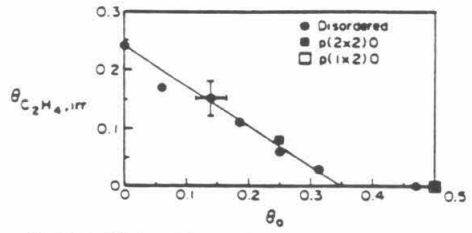

Figure 6. The inhibition of irreversible ethylene adsorption by preadsorbed oxygen adatoms.

The existence of methylidyne is indicated both by the presence of a carbon–hydrogen bending mode at 810 cm^{-1} and a carbon–hydrogen stretching mode at 3010 cm^{-1} in Figure 4e. The carbon–deuterium bending mode, expected at 615 cm^{-1} for CD, overlaps and is unresolved from the intense ν_s(RuO) mode in Figure 4f. The carbon–deuterium stretching mode, observed at 2250 cm^{-1}, is however, at the same frequency as that of methylidyne on the clean Ru(001) surface.[1,2] The ν_s(Ru≡CH) and ν_s(Ru≡CD) modes expected at 465 and 415 cm^{-1} were not resolved from the ν_s(RuO) mode in these spectra. Note, however, that the phonon mode of the p(2×2) oxygen overlayer was resolved in the spectrum of Figure 4f.

Both the hydrogen thermal desorption spectra and the EEL spectra measured following annealing this overlayer to higher temperatures show that the methylidyne dehydrogenates between 500 and 700 K. The surface carbon reacts with the oxygen adatoms (^{18}O) to form $C^{18}O$, which desorbs above 500 K, as shown in Figure 3c. This carbon monoxide desorption peak is reaction-limited, because this coverage of desorption-limited CO would appear at a much lower temperature (approximately 430 K) on this surface. Neither CO_2 nor H_2O was observed to desorb from this overlayer, indicating that the adsorbed oxygen either reacted with carbon above 500 K evolving CO or remained on the surface and desorbed only after annealing to 1700 K. Because of the absence of both spectroscopically observed intermediates and mass spectrometrically detected reaction products, neither the ethylene, ethylidyne, vinylidene, nor methylidyne reacts with the oxygen adatoms on the Ru(001)–p(2×2)O surface.

Finally, the adsorption and reaction of saturation coverages of ethylene on disordered oxygen overlayers on Ru(001) have also been investigated. The disordered oxygen overlayers were prepared by exposing the Ru(001) surface to oxygen at 80–100 K. The fractional surface coverages of oxygen were estimated by using the linear relationship between coverage and exposure, and the known coverage of 0.25 corresponding to a 0.8 L exposure of oxygen.[26] Hydrogen and ethylene thermal desorption spectra were used to evaluate the inhibition of reversible and irreversible ethylene adsorption by the preadsorbed oxygen. It was found that the fraction of ethylene that chemisorbs reversibly increases with increasing oxygen precoverage, while the amount of irreversibly adsorbed ethylene decreases approximately linearly with the oxygen precoverage. As shown in Figure 6, a fractional coverage of oxygen of approximately 0.35 inhibits ethylene decomposition completely.

IV. Discussion

A. Molecularly Chemisorbed Ethylene. It has been shown that ethylene chemisorbed on the Ru(001)–p(2×2)O and Ru(001)–p(1×2)O surfaces below 230 K is a π-bonded molecular species, for example, by comparison of the vibrational spectra to that of Zeise's salt. Calculations of the electronic structure of Zeise's anion have suggested that donation of electron density from the π orbital of ethylene to the platinum accounts for at least 75% of the total bonding of the ethylene ligand to the platinum, while back-donation from the platinum d orbitals to the ethylene π^* orbital accounts for the rest.[27] The occurrence of a small amount of back-bonding in Zeise's salt is consistent with neutron diffraction results, which show that the hydrogen atoms are bent away from the metal atom such that the carbon atoms are positioned 0.16 Å away from the plane of the four hydrogen atoms and toward the platinum atom.[28] If no back-bonding were to occur, the hydrogen and carbon atoms would remain coplanar. By analogy to Zeise's salt, the bonding of ethylene to these modified ruthenium surfaces may be described in terms of the donation of electron density from the π orbital of ethylene to the d band of the ruthenium of which the local density of *unoccupied* states has been increased by the presence of the electronegative oxygen adatoms, and the simultaneous back-donation of a small amount of electron density from the ruthenium surface to the π^* orbital of chemisorbed ethylene.

The ability of ethylene to act both as a π donor and a π^* acceptor lowers the vibrational frequency of the carbon–carbon stretching mode of chemisorbed, π-bonded C_2D_4 to 1350 cm^{-1} and of C_2D_4 in Zeise's salt to 1353 cm^{-1} from the gas-phase value of 1515 cm^{-1}. The frequency of the carbon–carbon stretching mode of π-bonded C_2H_4 cannot be compared to that of C_2H_4(g) owing to the previously discussed coupling of the $\delta(CH_2)$ and ν(CC) modes of the chemisorbed ethylene. However, the frequencies of these two modes agree with those of the ethylene ligand in Zeise's salt, suggesting that the degree of mode coupling and the bonding are similar in the two species. The bonding of ethylene to platinum in Zeise's salt increases the carbon–carbon bond length to 1.375 Å from 1.337 Å in gaseous ethylene,[28] and a similar lengthening of this bond is expected to occur in the ethylene that is π-bonded to the Ru(001)–p(1×2)O and Ru(001)–p(2×2)O surfaces.

Previous investigations[1-3] of ethylene adsorbed on clean, hydrogen precovered, and CO-precovered Ru(001) surfaces have shown that the molecularly chemisorbed ethylene is di-σ-bonded with a carbon–carbon stretching frequency of 1040 cm^{-1}. Hence, the carbon atoms of di-σ-bonded ethylene on the Ru(001) surface are essentially sp^3-hybridized, whereas those of π-bonded ethylene on the Ru(001)–p(2×2)O and Ru(001)–p(1×2)O surfaces are more nearly sp^2-hybridized. The change in the hybridization of the carbon atoms of adsorbed ethylene from sp^3 as observed on the clean surface to nearly sp^2 as observed on the oxygen precovered surfaces has also been observed for coadsorbed ethylene and oxygen on the Pd(100), Fe(111), and Pt(111) surfaces.[4-10,29] Moreover, the observed vibrational frequencies of these π-bonded ethylene species agree quite well with those of π-bonded ethylene on the Ru(001)–p(2×2)O and Ru(001)–p(1×2)O surfaces, as shown in Table I. Our results are also in agreement with those of Barteau et al.[11] for ethylene chemisorbed on the Ru(001)–p(1×2)O surface at 170 K.

Since there is no indication of any direct chemical interaction between the C_2H_4 and the oxygen adatoms, the interaction between ethylene and the Ru(001), the Ru(001)–p(2×2)O and the Ru(001)–p(1×2)O surfaces may be discussed in terms of the "Lewis acidity" of the surface. When oxygen is adsorbed, the Lewis acidity of the surface, i.e., the ability of the ruthenium atoms to accept electrons, increases. As discussed in section I, approximately 0.03 electron is transferred from the ruthenium to each oxygen adatom of the p(2×2) overlayer, and 0.04 electron is transferred to each oxygen atom of the p(1×2) overlayer. This charge transfer increases the Lewis acidity of the surface ruthenium atoms, making π-donation from ethylene to the ruthenium more favorable and π^*-back-donation from the surface less favorable, and this alters the bonding of ethylene from di-σ- to π-bonding. A similar effect has been observed when acetone is adsorbed below 200 K on the Ru(001) and the Ru(001)–p(2×2)O surfaces.[30] On Ru(001), acetone forms largely a side-on bonded

(26) The linear dependence of coverage upon exposure has been shown by Madey et al.[9] to be appropriate for fractional oxygen coverages below 0.35.

(27) Rosch, N.; Messmer, R. P.; Johnson, K. H. *J. Am. Chem. Soc.* **1974**, *96*, 3855.

(28) Love, R. A.; Koetzle, T. F.; Williams, G. J. B.; Andrews, L. C.; Bau, R. *Inorg. Chem.* **1975**, *14*, 2653.

(29) In addition, a small amount of π-bonded ethylene is present on the clean Pd(100) surface.

η^2(C,O)–$(CH_3)_2CO$ species, as well as a small amount of η^1-acetone, which is bonded through a lone pair of electrons on the oxygen atom. Addition of the p(2×2)O overlayer to the surface stabilizes the η^1-acetone with respect to the η^2-acetone, since the η^1-bonding configuration maximizes the net electron transfer from the acetone to the ruthenium. In both cases the increased Lewis acidity of the ruthenium surface increases the selectivity toward the adspecies which donate the most electron density and withdraw the least, η^1-acetone and π-bonded ethylene. Similar effects have been observed also for the coadsorption of oxygen with formaldehyde[31] and with formamide[32] on Ru(001).

On the other hand, the preadsorption of oxygen on Ru(001) does not alter the bonding of acetylene: the carbon atoms of acetylene are rehybridized to nearly sp^3 on the Ru(001), Ru(001)–p(2×2)O, and Ru(001)–p(1×2)O surfaces.[2,33] This is a consequence of the different energy levels of the unoccupied π orbitals of gaseous ethylene ($1b_{2g}$) and acetylene (π_g), which lie at −2.85 and −6.1 eV with respect to the vacuum level, respectively.[34,35] Upon adsorption, these orbital energies will downshift and broaden. Analogously, ultraviolet photoelectron spectroscopic data of Demuth and Eastman[36] show that the bonding π orbitals, π_u of acetylene and b_{1u} of ethylene, shift from −11.4 to −13.1 eV and from −10.5 eV to −11.6 eV upon adsorption of C_2H_2 and C_2H_4 on Ni(111). The Fermi level of Ru(001) lies at −5.5 eV,[37] and the Fermi levels of Ru(001)–p(2×2)O and Ru(001)–p(1×2)O lie at −5.7 and −6.3 eV with respect to the vacuum (zero) level.[6] The energy of the π_g orbital of acetylene shifts below the Fermi level of all three surfaces upon adsorption such that back-donation to the empty π_g orbital of acetylene occurs, resulting in rehybridization of the carbon atoms to sp^2. Similarly, the energy of the π^* ($1b_{2g}$) orbital of ethylene shifts sufficiently near the Fermi level of Ru(001) and broadens upon adsorption to facilitate back-donation, resulting in the formation of di-σ-bonded ethylene on the clean surface. However, the Fermi levels of the two oxygen precovered surfaces are apparently too low in energy with respect to that of the π^* orbital to allow significant back-donation. Hence, ethylene adsorbed on these two surfaces is π-bonded.

The effect of oxygen adatoms upon the postadsorption of ethylene may be compared with that of carbon, which, like oxygen, is adsorbed in threefold hollow sites on Ru(001).[7,38,39] A fractional coverage of 0.25 carbon adatom (which is equal to the coverage of oxygen adatoms in the p(2×2)O overlayer) produced by the thermal decomposition of ethylene on Ru(001) results in less charge transfer compared to the p(2×2) oxygen overlayer owing to the similar electronegativities of ruthenium (2.2) and carbon (2.55), and the greater electronegativity of oxygen (3.44). Electron energy loss spectra of ethylene adsorbed on the Ru(001) surface precovered with a fractional coverage of 0.25 carbon adatom show that this ethylene is di-σ-bonded,[40] confirming that the π-bonding of molecular ethylene induced by the p(2×2) oxygen overlayer results from an electronic perturbation of the surface.

In addition to the change in the nature of the bonding of chemisorbed ethylene on the Ru(001) surfaces modified chemically by oxygen adatoms, the total coverage of molecularly chemisorbed ethylene is also reduced. As shown by the ethylene and hydrogen thermal desorption spectra, a fractional coverage of oxygen adatoms of 0.5 reduces the saturation fractional coverage of chemisorbed ethylene to 0.10, all of which adsorbs reversibly (cf. a saturation fractional coverage of 0.30 on Ru(001) of which 0.06 desorbs reversibly). The observation that a larger fraction of π-bonded ethylene desorbs molecularly compared with di-σ-bonded ethylene is in agreement with results for ethylene adsorbed on the clean and oxygen-precovered Pd(100), Fe(111), and Pt(111) surfaces.[8-10] Indeed, all of the π-bonded ethylene adsorbed on Pd(100) is thought to desorb reversibly, independent of the oxygen precoverage.[8]

The appearance of two molecular ethylene desorption peaks above the temperature of multilayer desorption (cf. Figure 3a,b) may be related to the local structures of the p(2×2) and p(1×2) oxygen overlayers. The 240 K peak appears with greater intensity in the ethylene thermal desorption spectra of the p(2×2)O overlayer than in those of the p(1×2)O overlayer, whereas the shoulder at 160 K appears with slightly greater intensity in the spectra of the p(1×2)O overlayer. These observations suggest that the 240 K peak may correspond to ethylene chemisorbed in areas with local p(2×2)O structure, whereas the 160 K peak may correspond to ethylene chemisorbed in areas with local p(1×2)O structure. If this interpretation is correct, the coverages of ethylene corresponding to these two thermal desorption peaks are indicative of the short-range perfection in these two ordered overlayers.

The desorption of π-bonded ethylene at 240 K occurs at a slightly higher temperature than that at which di-σ-bonded ethylene desorbs molecularly.[1] The 240 K desorption temperature indicates that the strength of the ruthenium–ethylene π-bond is approximately 14 kcal/mol (perhaps slightly higher because of a small degree of rehybridization). The di-σ-bonded ethylene has a slightly lower heat of adsorption (11 kcal/mol), but a higher binding energy of approximately 80 kcal/mol. This estimate takes into account the rehybridization that occurs upon adsorption using the known carbon–carbon and carbon–hydrogen bond energies of ethylene and ethane in the gas phase.

B. Thermal Decomposition of Chemisorbed Ethylene. As mentioned above, the π-bonded, molecularly chemisorbed ethylene that is observed on the Ru(001)–p(2×2)O surface decomposes to a lesser extent than the di-σ-bonded ethylene on the clean, the hydrogen-precovered ($\theta_H = 0.25$), or the CO-precovered ($\theta_{CO} = 0.25$) ruthenium surfaces. This difference results from the much stronger modification in the electronic structures of the surface by oxygen compared with hydrogen or CO. The primary effects of preadsorbed CO and hydrogen upon ethylene adsorption and reaction are to block the adsorption of ethylene and enhance molecular desorption relative to decomposition by blocking adsorption sites of the decomposition products.[1] On the other hand, oxygen adatoms modify the chemical nature of the surface qualitatively, thereby altering the nature of the molecular bonding of ethylene (from di-σ- to π-bonding) and changing its decomposition products. For example, sp^2-hybridized vinylidene is observed as a product of the dehydrogenation of ethylene on Ru(001)–p(2×2)O, whereas it is not observed on the reduced Ru(001) surface. It appears that sp^3 hybridization and η^2-bonding are favored on Ru(001), upon which di-σ-bonded ethylene and sp^3-hybridized acetylide are formed, and that sp^2 hybridization and η^1-bonding are favored on the Ru(001)–p(2×2)O surface, upon which π-bonded ethylene and sp^2-hybridized vinylidene are formed. Ethylidyne is observed on both Ru(001) (sp^2 hybridization) and Ru(001)–p(2×2)O (η^1-bonding). The presence of coadsorbed oxygen makes sp^3 hybridization and η^2-bonding less favorable due, in part, to a weakening of the ruthenium–carbon bonds. This reduced bond strength is also manifest in less irreversible adsorption on the oxygen precovered surface: preadsorbed oxygen decreases the amount of ethylene that is adsorbed irreversibly in an approximately linear fashion.[41] Similar linear reductions in the extent of ethylene dehydrogenation by oxygen preadsorption have been observed on the Pd(100), Fe(111), and Pt(111) surfaces.[8-10]

Electron energy loss spectra of ethylene adsorbed on the Ru(001)–p(2×2)O surface show that π-bonded ethylene reacts near 230 K to form ethylidyne, all of which dehydrogenates to an

(30) Anton, A. B.; Avery, N. R.; Toby, B. H.; Weinberg, W. H. *J. Am. Chem. Soc.* **1986**, *108*, 684.
(31) Anton, A. B.; Parmeter, J. E.; Weinberg, W. H. *J. Am. Chem. Soc.* **1986**, *108*, 1823.
(32) Parmeter, J. E.; Schwalke, U.; Weinberg, W. H. *J. Am. Chem. Soc.* **1987**, *109*, 1876.
(33) Parmeter, J. E.; Weinberg, W. H., to be published.
(34) Mulliken, R. S. *J. Chem. Phys.* **1979**, *71*, 556.
(35) Dance, D. F.; Walker, I. C. *Chem. Phys. Lett.* **1973**, *18*, 601.
(36) Demuth, J. E.; Eastman, D. E. *Phys. Rev. B* **1976**, *13*, 1523.
(37) Wandelt, K.; Hulse, J.; Küppers, J. *Surf. Sci.* **1981**, *104*, 212.
(38) Chan, C.-M.; Weinberg, W. H. *J. Chem. Phys.* **1979**, *71*, 2788.
(39) Feibelman, P. J. *Surf. Sci.* **1981**, *103*, L149.
(40) Parmeter, J. E., unpublished results.

(41) The inhibition of ethylene dissociation by oxygen atoms also results in part from oxygen blocking adsorption sites of the decomposition products.

sp^2-hybridized vinylidene between 250 and 350 K with simultaneous desorption of hydrogen. It is rather likely that the π-bonded ethylene first dehydrogenates to vinylidene and that this vinylidene rehydrogenates to ethylidyne owing to the presence of surface hydrogen at temperatures below 250 K. This postulate is supported by EEL experiments, which showed that vinylidene coadsorbed with hydrogen could be rehydrogenated to ethylidyne.

In contrast to the partially irreversible adsorption of ethylene on the Ru(001)–p(2×2)O surface, π-bonded ethylene on Pd(100), precovered with 0.18 monolayer of oxygen forming a disordered overlayer, adsorbs reversibly,[42] and a variation in oxygen precoverage merely changes the ratio of di-σ-bonded to π-bonded ethylene that is formed.[8] The di-σ-bonded ethylene on Pd(100) dehydrogenates at 250 K to sp^3-hybridized $CHCH_2$ which decomposes at higher temperatures to methylidyne. As shown by EELS, the π-bonded ethylene that is chemisorbed on Pt(111) with a fractional precoverage of 0.23 oxygen adatom forms a new, previously unidentified species upon annealing to 325 K.[10] Although spectra of the corresponding deuterated species are not available to confirm our assignment, we suggest that the π-bonded ethylene coadsorbed with a fractional coverage of 0.23 oxygen adatom on Pt(111) converts to an sp^2-hybridized vinylidene. Indeed, the EEL spectrum of this vinylidene is very similar to that of vinylidene on Ru(001)–p(2×2)O. It exhibits an intense and broad loss feature at 1420 cm^{-1} probably due to the (uncoupled) $\delta(CH_2)$ and $\nu(CC)$ modes. The $\nu_s(CH_2)$ and $\nu_a(CH_2)$ modes appear at 2980 and 3080 cm^{-1}, respectively. Other modes that appear at 940, 820, and 730 cm^{-1} may be assigned to the CH_2 rocking, wagging, and twisting modes of vinylidene. On the Pt(111) surface, ethylene is di-σ-bonded and converts to ethylidyne near 300 K, and it is possible that vinylidene on the oxygen-precovered surface may also be hydrogenated to ethylidyne. Hence, the interaction of ethylene with ruthenium precovered with a p(2×2)O overlayer is similar to that observed with platinum upon which a comparable fractional coverage of oxygen is present: on both surfaces, π-bonded ethylene converts to vinylidene. Both of these surfaces are more reactive than oxygen-precovered Pd(100).

As discussed in section III.B, the identification of adsorbed vinylidene on Ru(001)–p(2×2)O is confirmed by both EEL spectra and by hydrogen thermal desorption spectra, which show that the stoichiometry of the intermediate is C_2H_2. Note that the EEL spectra of Figure 4c,d cannot be attributed to chemisorbed acetylene owing to the absence in Figure 4c of the intense carbon–hydrogen bending mode at 765 cm^{-1}, which is characteristic of acetylene chemisorbed on the Ru(001) and Ru(001)–p(2×2)O surfaces, and the observation of CH_2 and CD_2 scissoring modes at 1435 and 1010 cm^{-1} in Figure 4c,d. The presence of methylidyne at this temperature can be ruled out because of the absence of an intense CH bending mode in the EEL spectrum of Figure 4c, which would be expected at 810 cm^{-1}. The existence of CH_3 and CD_3 groups may also be excluded by examination of the EEL spectra. The vibrational frequencies of the adsorbed vinylidene agree with those of the vinylidene in the $Os_3(CO)_9(CCH_2)H_2$ complex,[22] the bonding configuration and structure of which are shown in Figure 5a,b.[25] We would expect that the vinylidene is adsorbed similarly on the ruthenium surface with the CCH_2 bridge-bonded, the carbon–carbon bond axis tilted with respect to the surface normal, elongation of the carbon–carbon bond compared with that of gaseous ethylene, and some donation of electron density from the π orbital of the CCH_2 to the d band of the ruthenium surface (cf. Figure 5c). The observed $\nu(CC)$ mode of adsorbed CCH_2 at 1435 cm^{-1} is lowered from those of $C_2H_4(g)$ at 1623 cm^{-1} and the CCH_2 ligand in $Cp_2Ru_2(CO)_2(\mu\text{-}CO)(\mu\text{-}CCH_2)$ at 1586 cm^{-1},[43] owing to the π-electron donation from the carbon–carbon bond to the metal surface that occurs in the chemisorbed vinylidene. The overlap of the $\nu(CC)$ and $\delta(CH_2)$ modes of adsorbed vinylidene at 1435 cm^{-1} indicates that these modes are not coupled significantly in this species, unlike those of π-bonded ethylene. It cannot be entirely ruled out that the $\nu(CC)$ mode appears at a slightly lower frequency than 1435 cm^{-1}, and that the $\delta(CH_2)$ mode "steals" intensity from the $\nu(CC)$ mode via mode coupling. However, the absence of any evidence for a shoulder on the low-frequency side of the peak at 1435 cm^{-1} in Figure 4c makes this unlikely.

Gates and Kesmodel[23] have suggested the presence on the Pd(111) surface of a CCH_2 adspecies as an intermediate to the formation of ethylidyne from hydrogen and acetylene. This postulated CCH_2 adspecies was coadsorbed with acetylene, hydrogen, and ethylidyne. Thus, only two of the vibrational modes were identified, $\nu(CC)$ and/or $\delta(CH_2)$ at 1437 cm^{-1} and $\nu(CH_2)$ at 2986 cm^{-1} [$\nu(CC)$ at 1372 cm^{-1} and $\nu(CD_2)$ at 2206 cm^{-1} for CCD_2]. A CCH_2 adspecies, an intermediate in the hydrogenation of acetylene to ethylidyne on Pt(111), was tentatively identified by Ibach and Lehwald[24] with mode assignments listed in Table II. The assignment of the carbon–carbon stretching mode to a loss feature at 1100 cm^{-1} suggests sp^3 hybridization of the carbon atoms of the CCH_2 on Pt(111), indicating that this species is quite different from the sp^2-hybridized CCH_2 species observed on Ru(001)–p(2×2)O and the oxygen-precovered Pt(111) surfaces. The change in hybridization of the CCH_2 species on platinum due to the presence of oxygen supports our earlier assertion that sp^3 hybridization is preferred on clean metal surfaces, whereas sp^2 hybridization is preferred in the presence of oxygen. Moreover, the observed conversion of CCH_2 to ethylidyne on palladium and platinum agrees with our observation that the conversion of ethylidyne to vinylidene is reversible on Ru(001), provided sufficient hydrogen is present.

The thermal evolution of π-bonded ethylene on Ru(001)–p(2×2)O can be summarized as follows. The ethylene reacts to form ethylidyne, possibly via a vinylidene intermediate, below 250 K. In contrast to the total dehydrogenation of ethylidyne to carbon with the simultaneous evolution of hydrogen with no stable intermediate on the Ru(001) surface, the ethylidyne on the Ru(001)–p(2×2)O surface dehydrogenates to vinylidene upon annealing to 350 K. The vinylidene decomposes to methylidyne and carbon adatoms evolving hydrogen between 350 and 450 K, possibly though an unstable acetylide intermediate. Acetylide, which was observed following the adsorption of ethylene on the Ru(001) surface, also decomposes via carbon–carbon bond cleavage to methylidyne at approximately the same temperature at which vinylidene decomposes on the Ru(001)–p(2×2)O surface. The methylidyne that is formed on Ru(001)–p(2×2)O decomposes between 500 and 700 K. Finally, the carbon reacts with oxygen adatoms to form CO, which desorbs in a reaction-limited step between 500 and 750 K.

The hydrogen thermal desorption spectra from ethylene chemisorbed on the Ru(001)–p(2×2)O surface are completely consistent with this decomposition mechanism. Hydrogen that is evolved from the ethylene and ethylidyne decomposition reactions desorbs in two peaks at 210 and 250 K. These two peaks account for half of the hydrogen desorption from the surface, consistent with the stoichiometry of the vinylidene intermediate observed on the surface at 350 K. The hydrogen thermal desorption peak at 400 K corresponds to one-quarter of the total amount of hydrogen that is desorbed and is therefore consistent with the dehydrogenation of vinylidene to methylidyne and carbon adatoms. The final quarter of the hydrogen desorbs above 500 K as the methylidyne decomposes.

Only C_2H_4, H_2 and CO were observed to desorb following the chemisorption of ethylene on the Ru(001)–p(2×2)O surface. This result is similar to the coadsorption of ethylene and oxygen on Fe(111), but unlike the coadsorption of ethylene and oxygen on Pd(100) and Pt(111), which exhibited CO_2 and H_2O desorption as well.[8-10] The absence of CO_2 and H_2O in the thermal desorption spectra from the ruthenium surface is not surprising since neither the formation of CO_2 from coadsorbed CO and oxygen[44] nor the formation of water from coadsorbed oxygen and hydrogen has

(42) As shown by EELS, the irreversibly adsorbed ethylene on the Pd(100) surface preexposed to oxygen is di-σ-bonded.[8]

(43) Evans, J.; McNulty, G. S. *J. Chem. Soc., Dalton Trans.* **1983**, 639

(44) Thomas, G. E.; Weinberg, W. H. *J. Chem. Phys.* **1979**, *70*, 454

been observed under UHV conditions on the Ru(001) surface in transient thermal desorption experiments.[45] The lower reactivity of ruthenium and iron for the oxidation of carbon monoxide and hydrogen is a consequence of the stronger metal–oxygen bonds that are formed[9,46] compared with those of platinum[47] and palladium.[48]

Finally, the chemistry of ethylene on the Ru(001)–p(2×2)O surface may be compared to the organometallic chemistry of homogeneous compounds. For example, it has been shown that ethylene reacts with $Os_3(CO)_{12}$ to form the vinyl complex, $HOs_3(CH{=}CH_2)(CO)_{10}$, which forms the vinylidene complex, $H_2Os_3(CO)_9(C{=}CH_2)$[22] upon heating. The latter can be hydrogenated to an ethylidyne complex, $H_3Os_3(CO)_9(CCH_3)$,[22,25,49] just as chemisorbed vinylidene can be rehydrogenated to ethylidyne on the Ru(001)–p(2×2)O surface. These results also suggest that the conversion of π-bonded ethylene to vinylidene on Ru(001)–p(2×2)O occurs via a vinyl intermediate.

V. Conclusions

The presence of ordered p(2×2) and p(1×2) oxygen overlayers on the Ru(001) surface gives rise to π-bonding of molecularly chemisorbed ethylene, such that the carbon atoms of the ethylene remain nearly sp^2-hybridized. This species is qualitatively different from the sp^3-hybridized, di-σ-bonded ethylene that is observed on the clean surface. Intuitively, this difference reflects the greater Lewis acidity of the Ru(001)–p(2×2)O and Ru(001)–p(1×2)O surfaces. More precisely, it is a consequence of a significant perturbation in the electronic structure of the ruthenium surface by the ordered oxygen overlayers, which increases the energy separation between the Fermi level and the π^* orbital of ethylene, making back-donation unfavorable.

As observed on the oxygen-precovered Pt(111), Pd(100), and Fe(111) surfaces, a larger fraction [one-third on Ru(001)–p(2×2)O] of π-bonded ethylene desorbs molecularly than does di-σ-bonded ethylene on the reduced surfaces. The remaining two-thirds of the saturation coverage of ethylene adsorbed on the Ru(001)–p(2×2)O surface dehydrogenates to ethylidyne probably via a vinylidene intermediate upon heating to 250 K. In contrast to the observed total decomposition of ethylidyne to carbon and hydrogen on the Ru(001) surface with no stable intermediates, the presence of oxygen induces the formation of an sp^2-hybridized vinylidene species from ethylidyne at 350 K. By analogy to the $H_2Os_3(CO)_9(CCH_2)$ cluster,[22,25,49] this chemisorbed vinylidene is almost certainly bridge-bonded to two adjacent ruthenium atoms and tilted toward a third ruthenium atom with donation of electron density from the π orbital to the d band of the ruthenium surface, as shown in Figure 5c. The chemisorbed vinylidene decomposes near 400 K to carbon adatoms and methylidyne, the latter of which dehydrogenates between 500 and 700 K. The vinylidene could be rehydrogenated to ethylidyne in the presence of hydrogen, analogous to the formation of ethylidyne from CCH_2 on reduced Pt(111) and Pd(111).[23,24] No oxygen-containing intermediates in ethylene decomposition were observed under any conditions of temperature and coverage. Oxygen adatoms reacted only with carbon adatoms, forming CO above 500 K.

Finally, the presence of oxygen favors η^1-bonding and sp^2 hybridization as shown by both the existence of π-bonded ethylene on the oxygen-precovered Pt(111), Pd(100), Fe(111), and Ru(001) surfaces,[8-11] as well as the formation of sp^2-hybridized vinylidene on these chemically modified Ru(001) and Pt(111) surfaces.[10] On the other hand, η^2-bonded, sp^3-hybridized ethylene was observed in the absence of oxygen on all four surfaces.

Acknowledgment. This work was supported by the National Science Foundation under Grant No. CHE-8516615.

(45) Hills, M. M., unpublished results.
(46) Seip, U.; Tsai, M.-C.; Christmann, K.; Küppers, J.; Ertl, G. *Surf. Sci.* **1984**, *139*, 29.
(47) Avery, N. R. *Chem. Phys. Lett.* **1983**, *96*, 371.
(48) Nyberg, C.; Tengstal, C. G. *Surf. Sci.* **1983**, *126*, 163.
(49) Deeming, A. J.; Underhill, M. *J. Chem. Soc., Chem. Commun.* **1973**, 277.

Appendix 7

Vibrational Spectra of Chemisorbed NO_2 and Condensed N_2O_4 on the Ru(001) Surface

[This appendix was published as a paper by U. Schwalke, J. E. Parmeter and W. H. Weinberg, in *The Journal of Chemical Physics* 1986, 84, 4036.]

Vibrational spectra of chemisorbed NO_2 and condensed N_2O_4 on the Ru(001) surface

U. Schwalke,[a] J. E. Parmeter,[b] and W. H. Weinberg
Division of Chemistry and Chemical Engineering, California Institute of Technology, Pasadena, California 91125

(Received 23 July 1985; accepted 14 November 1985)

Vibrational electron energy loss spectroscopy combined with thermal desorption mass spectrometry have been used to investigate the adsorption and decomposition of NO_2 on the Ru(001) surface. The results indicate that the initial NO_2 adsorption is dissociative at 80 K. The reaction products, molecularly adsorbed NO and atomically adsorbed oxygen, passivate the surface, and subsequent (submonolayer) adsorption is molecular. The molecularly adsorbed NO_2 is bound weakly (-9 kcal/mol) through the nitrogen atom with C_{2v} symmetry. With increasing exposure, the formation of N_2O_4 dimers in the condensed multilayer is observed.

I. INTRODUCTION

Nitrogen dioxide may be thought of as a free radical and, consequently, has a tendency to dimerize to N_2O_4. The NO_2 monomer has C_{2v} symmetry, and the intramolecular bonding is best described by a resonance structure in which one oxygen atom is bonded to the nitrogen atom by a double bond and the other by a single bond plus a three-electron bond.[1] The NO_2 molecule has an odd number of electrons, and the one unpaired electron appears to be localized near the nitrogen atom. Infrared spectra of NO_2 in the gas phase show three characteristic absorption bands at 1610 (the NO_2 asymmetric stretch), 1318 (the NO_2 symmetric stretch), and 750 cm^{-1} (the NO_2 bend).[2] In both the gas and liquid phases, NO_2 and N_2O_4 coexist in an equilibrium.[3] Only in the solid state does the oxide exist purely as N_2O_4. Several forms of the dimer are known, but the most stable one is the planar O_2N–NO_2 molecule.[4] In IR spectra, the most characteristic mode of N_2O_4 is an intense absorption band at approximately 1750 cm^{-1} (the NO_2 asymmetric stretch).[5]

There are currently little experimental data available concerning the interaction of NO_2 with single crystalline metal surfaces,[6–10] and, in particular, no vibrational studies have heretofore been reported. All previous results suggest that at room temperature NO_2 adsorbs only dissociatively on transition metals. On Pt(111)[7,8] and on Pt(100),[9,10] the dissociation products are NO and atomic oxygen, whereas on W(110) NO_2 dissociates completely into atomic nitrogen and oxygen.[6] The fundamental question as to whether or not NO_2 may adsorb molecularly at sufficiently low temperatures remains open. Dahlgren and Hemminger[8] found that NO_2 is adsorbed molecularly on Pt(111) at 120 K, whereas Segner *et al.*[7] reported that there is no evidence for molecularly adsorbed NO_2 even at temperatures as low as 120 K on this surface. In agreement with Dahlgren and Hemminger, evidence for molecularly adsorbed NO_2 on the reconstructed, hexagonal Pt(100) surface at 200 K has been reported subsequently.[9,10] On W(110), NO_2 adsorption at 100 K was found to be almost completely dissociative, which is expected since NO also dissociates on W(110) at 100 K.[11] However, a chemisorbed molecular NO_2 species may also be formed at higher coverages.[6] Due to the broad and overlapping features in the experimentally measured photoemission spectra, however, no more definite conclusions could be drawn. Currently, little is known concerning the multilayer state, formed by condensation under ultrahigh vacuum conditions, especially regarding the possible formation of N_2O_4 dimers. Evidence for N_2O_4 in condensed multilayers has been reported by Fuggle and Menzel,[6] but this is apparently not in agreement with previous photoemission results.[12]

The advantage of high resolution electron energy loss spectroscopy (EELS)[13] to determine the chemical identity of adsorbed species has resulted in the wide application of this technique in surface chemistry.[14] In the present study, EELS combined with thermal desorption mass spectrometry (TDMS) have been used to investigate the adsorption and decomposition of NO_2 on Ru(001) at temperatures as low as 80 K.

II. EXPERIMENTAL PROCEDURES

All EELS and TDMS measurements were carried out in an ultrahigh vacuum system which has been described in detail previously.[15] Briefly, the home-built EEL spectrometer is of the Kuyatt–Simpson type with hemispherical energy dispersing elements in both the monochromator and the analyzer. The angle of incidence of the primary electron beam was about 60° with respect to the surface normal, and an electron energy of approximately 4 eV was used. The full-width at half-maximum of the elastically scattered beam in the specular direction was less than 80 cm^{-1}, while maintaining count rates of 3×10^5 cps in the elastic channel. The TDMS measurements were performed by resistive heating of the sample and detection of the desorption products with a quadrupole mass spectrometer (UTI 100C), which was in line-of-sight of the sample. The crystal was cooled using liquid nitrogen. In order to obtain sample temperatures as low as 80 K, the partial pressure of the liquid nitrogen in the cooling reservoir was reduced by restricting the flow of liquid nitrogen. The crystal was cleaned by employing standard procedures developed in our laboratory,[16] and the resulting

[a] Feodor-Lynen Research Fellow of the Alexander von Humboldt Foundation.
[b] AT&T Bell Laboratories Predoctoral Fellow.

 0021-9606/86/074036-07$02.10

EEL spectrum of the clean surface was featureless.

Nitrogen dioxide (Matheson Gas Products, purity 99.5%) was used without further purification. In order to minimize the decomposition of NO_2 and the displacement of contaminants from the walls of the UHV chamber during the NO_2 exposure, NO_2 was introduced onto the Ru(001) surface via a directional beam doser consisting of a microcapillary array. Prior to the actual experiments, the gas dosing system was flushed several times with NO_2 in order to obtain high purity NO_2 exposures. To verify the NO_2 purity with the quadrupole mass spectrometer, it was necessary to passivate the chamber walls, since the doser was not in line-of-sight with the ionizer of the quadrupole.[17] In several cycles, the chamber was backfilled with NO_2, which was then pumped out. After this procedure, no increase in the partial pressure of any contaminant [including H_2, H_2O, CO (checked by mass 12), HNO_2, and N_2O_3] could be detected during the NO_2 backfilling, and the cracking pattern of NO_2 was similar to that reported in the literature.[18] Furthermore, no evidence of any impurities was noted in either monolayer or multilayer EEL spectra after an NO_2 exposure at 80 K.

The NO_2 exposures were determined by integrating the increase in the background pressure, as measured with an uncalibrated ionization gauge. Although the absolute accuracy in this procedure is poor, both the relative accuracy and the reproducibility are reliable.

III. RESULTS

A. Thermal desorption mass spectrometry

In Fig. 1, a set of thermal desorption spectra for molecular NO_2 desorption is shown as a function of NO_2 exposure. The adsorption temperature was 80 K, and a heating rate of 6 K/s was used in all cases. Although no molecular desorption of NO_2 is observed at exposures below approximately 1 L, suggesting initial dissociative adsorption, with increasing exposure two NO_2 desorption peaks become apparent at 140 and 130 K. The high temperature molecular peak builds in first and saturates at an exposure below 3.5 L. The peak temperature of 140 K does not shift with coverage within ± 2 K. This behavior is characteristic of first-order desorption kinetics, implying some molecular chemisorption of NO_2. Assuming a preexponential factor of the desorption rate coefficient of 10^{14} s^{-1}, an activation energy for desorption of approximately 9 kcal/mol is estimated using Redhead's analysis.[19] Other than NO_2 and its cracking fragments, and negligibly small amounts of N_2O,[20] no other desorption products were observed in the temperature range between 80 and 280 K.

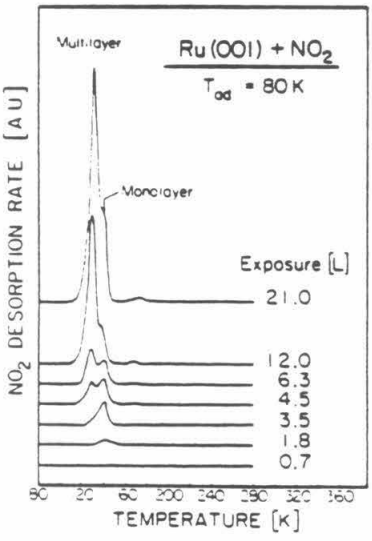

FIG. 1. Thermal desorption spectra of NO_2 as a function of exposure in units of Langmuirs, where 1 L = 10^{-6} Torr s. The NO_2 was adsorbed at 80 K, and the heating rate was 6 K/s.

The low temperature NO_2 peak at 130 K, which appears after completion of the monolayer, does not saturate with exposure, indicating the formation of a condensed multilayer. In addition, the thermal desorbing peak temperature shifts slightly upward with increasing coverage, whereas all peaks have a common leading edge. Such behavior is typical for desorption from a multilayer state[22] and can be described with zeroth-order desorption kinetics. Due to partial overlap with the monolayer peak at 140 K, the expected sharp high temperature cutoff of the multilayer peak is not resolved. Concomitant with the development of the multilayer peak, a weak desorption feature at approximately 170 K appears. Less than 5% of the total amount of desorbing NO_2 contributes to this desorption state. At present it is not clear whether this peak represents an artifact (e.g., desorption from sample supports) or is a consequence of a complex reaction in the adsorbed overlayer.

The integrated intensity of molecularly adsorbed NO_2 is plotted as a function of NO_2 exposure in Fig. 2. For an adsorption temperature of 80 K, the total amount of adsorbed NO_2 is proportional to exposure over the entire range of exposures, i.e., the probability of adsorption is the same for the monolayer as for the multilayer. This *strongly* suggests that the probability of adsorption is unity in all cases at 80 K. Support for this suggestion has been given by Segner *et al.*[7] In a molecular beam study, they determined the adsorption probability to be 0.97 for dissociative NO_2 adsorption on Pt(111) at 300 K. Another result of Fig. 2 is important to note: the solid line, which is a least-squares fit of the data points, intersects the abscissa at 1 L. This is a consequence of the fact that *no molecular NO_2 desorption occurs below this exposure*, as demonstrated in Fig. 1. Thus low coverages of NO_2 result in dissociative adsorption on Ru(001) at a temperature below the desorption temperature of molecular NO_2, namely 140 K. The EEL spectra presented in the next section verify that the initial adsorption of NO_2 on Ru(001) at 80 K is dissociative, and that the dissociation products are NO and oxygen adatoms. The desorption products of dissociatively adsorbed NO_2 are NO and N_2 near 480 K and O_2 at approximately 1500 K. Thermal desorption measurements indicate that the fractional surface coverages of NO, atomic oxygen and NO_2 in the chemisorbed monolayer are approximately 0.2, 0.2, and 0.25, i.e., the total fractional surface

in the presence of atomic oxygen, a bent configuration, which may formally be considered as NO^-,[27] is unlikely, especially since it is not observed on the reduced Ru(001) surface.[23,24] Furthermore, the observed loss at 420 cm^{-1} is far too low in frequency to be assigned to an NO bending vibration (which would be dipolar "active" in a bent configuration).

In agreement with the TDMS data, EELS indicates that the initial (exposures below approximately 1 L) adsorption of NO_2 is dissociative on Ru(001) at 80 K, due, for example, to the absence of the characteristic NO_2 bending mode near 750 cm^{-1}. With increasing NO_2 exposure, however, the intensity of loss features at 780 cm^{-1} (the NO_2 bending mode) and at 1300 cm^{-1} (the NO_2 symmetric stretching mode) becomes apparent. This is demonstrated in spectra (c) and (d) of Fig. 3. Spectrum (c) was recorded after an NO_2 exposure of 2.1 L, where molecular NO_2 desorption is clearly detectable by thermal desorption (cf. Fig. 1). In addition to the intense modes at 780 and 1300 cm^{-1}, an additional mode near 300 cm^{-1} appears in the spectrum, which is assigned to the Ru–NO_2 stretching vibration. As would be expected, these results confirm that the observed NO_2 thermal desorption peak at 140 K (cf. Fig. 1) is due to the desorption of molecularly adsorbed NO_2 rather than the recombinative desorption of $NO(a) + O(a)$. Now let us consider the frequency range above 2000 cm^{-1}. First of all, it should be noted that no modes between 2100 and 2400 cm^{-1} were detected, indicating the absence of adsorbed N_2[28] or N_2O.[29] However, concomitant with the appearance of the intense NO_2 bands, two very weak peaks at 2080 and 2600 cm^{-1} were observed. The loss at 2080 cm^{-1} is due to a combination band of the NO_2 bending and NO_2 symmetric stretching modes (rather than CO, for example, as shown later), while the loss at 2600 cm^{-1} is due to a double loss and/or an overtone of the NO_2 symmetric stretching mode.[30]

With additional NO_2 exposure, the NO_2 bending and the NO_2 symmetric stretching modes increase in intensity, and the NO stretching mode at 1880 cm^{-1} becomes broader, asymmetrically, toward lower frequencies due to the presence of a new loss peak centered at 1750 cm^{-1} [cf. Figs. 3(d) and 3(e)] that results from the NO_2 asymmetric stretching mode of N_2O_4 in the multilayer. A comparison with the thermal desorption spectra of Fig. 1 indicates that this is the exposure range where the multilayer has begun to form. The fact that the Ru–NO_2 stretching mode near 280 cm^{-1} decreases in intensity (in contrast to the other NO_2 modes) is attributed to screening effects due to the presence of the multilayer. Finally in spectrum (e) of Fig. 3, corresponding to an NO_2 exposure of 12 L, the intensity of the 1750 cm^{-1} loss is enhanced further, and a broad structure at 340 cm^{-1} has appeared. In addition, the modes at 780 and 1300 cm^{-1} are downshifted by approximately 20 cm^{-1}. Note that the combination band and the overtone/double loss band are downshifted as well, consistent with the shifts observed in the fundamental modes. This EEL spectrum of the condensed multilayer resembles the IR spectrum of N_2O_4 very closely.[5] The mode assignments of adsorbed NO_2 and N_2O_4 are summarized in Tables I and II, respectively, and will be discussed in detail in Sec. IV. In addition to the specular EELS measurements presented in Fig. 3, off-specular spectra where the energy analyzer was rotated 12° in the scattering plane toward the surface normal were recorded also. With the exception of the overtone/double loss feature near 2600 cm^{-1}, all modes showed a strong attenuation, in accordance with a long-range dipolar enhanced scattering mechanism.[13] No additional modes due to "impact" scattering were observed.

In order to illustrate the parallels between the thermal desorption results and the EELS data, a series of experiments was performed in which the surface that had been exposed to NO_2 was heated at a rate of approximately 2 K/s to the desired temperature and then allowed to cool. All spectra were recorded at 80 K so that only irreversible changes in the adsorbed overlayer were observed. A con-

TABLE II. Vibrational frequencies (cm^{-1}) of N_2O_4 in the gas phase and in the solid state (Ref. 5) compared to the EELS data of the multilayer on Ru(001). The values in parentheses correspond to combination bands of fundamental modes with lattice vibrations [Ref. 5(b)].

Mode	Infrared		EELS
	N_2O_4 gas phase	N_2O_4 solid state	multilayer on Ru(001)
NO_2 wag	430	439	440
NO_2 *a*-stretch	1748	1734	1750
		(1760)	
NO_2 rock	385	369	340
NO_2 *s*-stretch	1261	1253	1270
		(1280)	
NO_2 bend	750	738	760
		(756)	

TABLE I. Frequencies (cm^{-1}) of infrared NO_2 bands in the gas phase (Ref. 2) and in nitro complexes (Ref. 27) compared to the EELS modes of NO_2 on Ru(001) in the monolayer. The mode assignments are also given (C_{2v} symmetry).

Mode	Symmetry	Gas phase	NO_2 on Ru(001)	N-bonded nitro complexes	Bridging nitro complexes
NO_2 *s*-stretch	A_1	1318	1300	1306–1364	1171–1225
M–NO_2 stretch	A_1	---	300	290–449	---
M–O_2N stretch	A_1	---	---	---	340–370
NO_2 bend	A_1	750	780	824–854	841–866
NO_2 *a*-stretch	B_1	1610	---	1346–1488	1266–1390

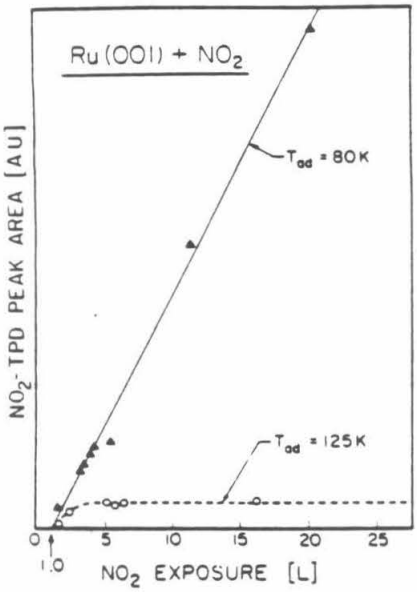

FIG. 2. Integrated intensity of molecularly desorbed NO_2 as a function of NO_2 exposure for two adsorption temperatures, 80 and 125 K.

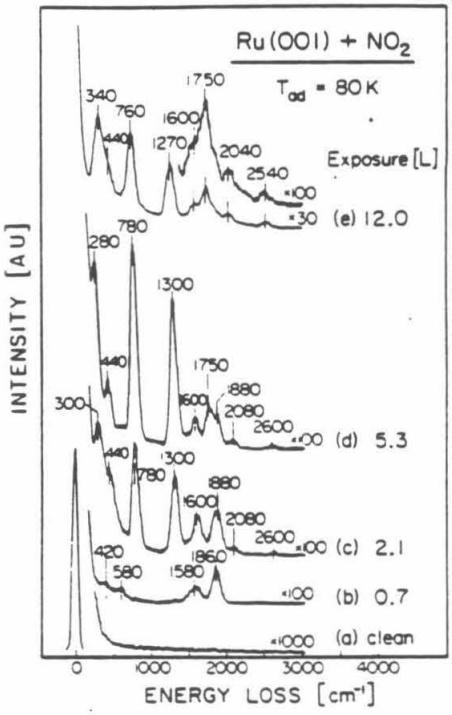

FIG. 3. Electron energy loss spectra for the clean Ru(001) surface (a) and after various exposures of the surface to NO_2 (b)–(e).

coverage is approximately 0.65. For NO_2 exposures of 1 L (or above), the total amount of NO and N_2 that desorbs at approximately 480 K is on the order of 30% to 40% of that observed after a saturation exposure of NO on the clean Ru(001) surface. This implies that the saturation fractional coverage of NO on Ru(001) is between 0.5 and 0.67.

To investigate the influence of adsorption temperature on NO_2 adsorption, experiments were carried out at elevated temperatures. During exposure, the surface temperature was held constant within $\pm$ 1 K, and, after cooling to 80 K, EEL spectra and thermal desorption spectra were measured. At an adsorption temperature of 125 K, approximately the same amount of dissociative adsorption occurs, and molecular chemisorption of NO_2 occurs also, but to a lesser extent than at 80 K. The formation of multilayers is suppressed, however. This is obvious in Fig. 2 (dashed line), where adsorption at 125 K leads to saturation at an exposure of approximately 3.0 L. Compared to adsorption at 80 K, the total amount of molecularly chemisorbed NO_2 is approximately 50% lower, indicating that at this temperature the chemisorbed NO_2 adsorption state that desorbs at 140 K is not filled completely (irreversibly).

B. Electron energy loss spectroscopy

In Fig. 3 electron energy loss spectra are shown as a function of NO_2 exposure at a surface temperature of 80 K. Obviously, the EEL spectra change significantly with increasing coverage. At low exposures, as seen in Fig. 3(b), only four losses are visible at 420, 580, 1580, and 1860 cm^{-1}.

The loss features at 1860 and 1580 cm^{-1} are associated with the nitrogen–oxygen stretching mode of linear on–top and bridge-bonded NO, respectively, which are adsorbed with their molecular axes perpendicular to the Ru(001) surface.[23] Compared to NO adsorbed on clean Ru(001), the NO stretching frequencies are blue shifted by 50 to 80 cm^{-1}, which indicates a stiffening of the intramolecular NO bond. This is not surprising since similar frequency shifts have been reported for NO adsorption on an oxygen precovered Ru(001) surface,[24] and the dissociative adsorption of an NO_2 molecule results in an NO admolecule *and* an oxygen adatom. Qualitatively, this observation can be explained by a reduction of electron backdonation into the $2\pi^*$ antibonding orbital of adsorbed NO, since the presence of the electronegative oxygen adatoms leads to an increase in the work function and a reduction in the local electron density of states at the Fermi level of the surface ruthenium atoms.[25] The loss feature at 580 cm^{-1} is a superposition of the Ru=O stretching mode (due to the presence of oxygen adatoms)[26] and the Ru–NO stretching mode of the terminally bonded linear NO. Since the metal–ligand stretching frequencies decrease with increasing coordination number,[13] the loss at 420 cm^{-1} is reasonably assigned to the Ru–NO stretching mode of the bridge-bonded NO. A bent NO species may be ruled out for two reasons. First, due to the reduced electron backdonation

densed multilayer [spectrum (a) of Fig. 4], which was obtained after an NO_2 exposure of 10 L, was first heated to 130 K. At this temperature most of the multilayer desorbs, as shown in Fig. 1. As expected the EEL spectrum [Fig. 4(b)] shows that aside from the small shoulder at 1760 cm^{-1}, most features which are due to N_2O_4 have vanished. The characteristic NO_2 bands as well as the NO stretching modes of the terminally and bridge-bonded NO at 1860 and 1600 cm^{-1}, respectively, have become clearly visible. In addition, a frequency shift of the combination band at 2080 cm^{-1} and the overtone/double loss band at 2600 cm^{-1} is observed, consistent with previous observations [Figs. 3(d) and 3(e)]. As may be seen in spectrum (c) of Fig. 4, annealing to 140 K has resulted in a strong attenuation of the fundamental vibrations of NO_2, in agreement with the observed thermal desorption of the NO_2 monolayer state at this temperature (cf. Fig. 1). The combination band at 2080 cm^{-1} and the overtone/double loss band at 2600 cm^{-1} are no longer detectable. This observation rules out the possibility that the loss feature at 2080 cm^{-1} is due to adsorbed CO, which shows a strong stretching frequency in the same range, since the CO desorption temperature is much higher (above 400 K).[16] The EEL spectrum shown in Fig. 4(d) was recorded after annealing the Ru(001) surface to 280 K. At this temperature, all adsorbed NO_2 has either desorbed or dissociated. Accordingly, in the EEL spectrum vibrational modes due only to adsorbed NO and atomic oxygen are observed. Compared to Fig. 4(c), the intensity of the NO stretching mode at 1860 cm^{-1} is enhanced, suggesting that some dissociation of the NO_2 present in Fig. 4(c) and/or conversion of bridge-bonded NO to linear on-top NO[23] has occurred between 140 and 280 K. Annealing to approximately 500 K resulted in NO dissociation as well as NO and N_2 desorption. Only the Ru=O stretching mode at approximately 580 cm^{-1} was observed by EELS. Finally, heating to 1750 K leads to complete O_2 desorption, producing a clean Ru(001) surface.

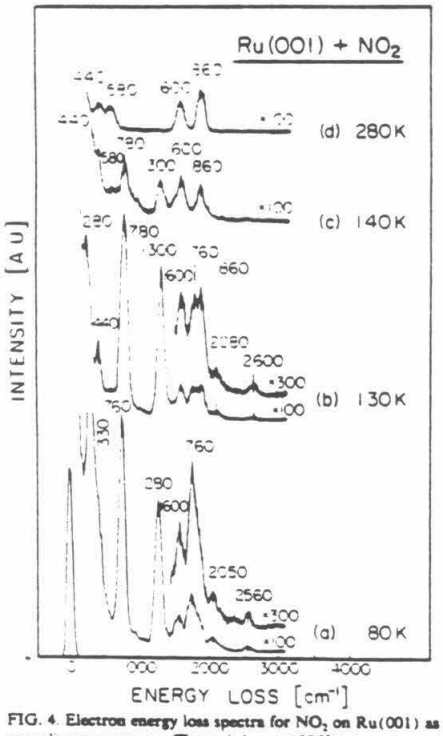

FIG. 4. Electron energy loss spectra for NO_2 on Ru(001) as a function of annealing temperature. The multilayer at 80 K (a) was heated momentarily to the temperatures indicated in (b)–(d). All spectra were recorded at 80 K.

IV. DISCUSSION

A. Adsorption in the monolayer

For the initial adsorption of NO_2 on Ru(001) at 80 K, the TDMS and EELS results have shown that NO_2 is adsorbed dissociatively. The dissociation products, adsorbed NO and atomic oxygen ($\theta_{NO} = \theta_O = 0.2$), passivate the surface, and subsequent NO_2 adsorption ($\theta_{NO_2} < 0.25$) is molecular. In the EEL spectra, chemisorbed NO_2 molecules are characterized by three vibrational losses at 300, 780, and 1300 cm^{-1} [cf. Fig. 3(c)]. Since all these modes are excited by a long-range dipolar scattering mechanism, the selection rules for dipolar scattering can be applied.[13] Accordingly, these modes must belong to the totally symmetric representation of the corresponding point group. Since exactly three losses are observed, we conclude that the adsorbate symmetry is C_{2v}.[31] If the symmetry were lower than C_{2v}, i.e., C_s or C_1, additional modes which are not allowed for C_{2v} symmetry should be observable, but this is not the case (including nonspecular scattering). For NO_2 adsorbed on Ru(001) with C_{2v} symmetry, two different bonding configurations are possible. The NO_2 molecule may bond to the surface either through the nitrogen atom (I) or in a bridged configuration (II), where the bonding occurs through the two oxygen atoms:

I II

Since the unpaired electron in the $6a_1$ orbital of NO_2 is localized at the nitrogen atom, bond formation might be expected to occur preferentially through the nitrogen atom. For example, the most stable N_2O_4 dimers contain a N–N bond.[4] Both structures (I) and (II) are well known, however, in the chemistry of nitro complexes, and IR data are available for comparison.[27] In Table I, IR data of these nitro complexes as well as those of the free NO_2 molecule are listed together with the EELS data of molecularly adsorbed NO_2 on Ru(001). The vibrations at 1300 and 780 cm^{-1} of adsorbed NO_2 have been assigned to the NO_2 symmetric stretching and NO_2 bending modes, respectively, which belong to the A_1 representation. The frequencies of these modes are close to the gas phase values indicating that adsorbed NO_2 interacts weakly with the Ru(001) surface, consistent with the low activation energy for NO_2 adsorption of approximately 9 kcal/mol. Since the NO_2 asymmetric stretching mode is of B_1 symmetry, no significant contribution near 1600 cm^{-1}

from adsorbed NO_2 would be expected in the EEL spectra. However, since the NO stretching mode of bridge-bonded nitric oxide occurs near this frequency, this expectation cannot be confirmed unambiguously. In addition to the two gas phase modes, a third A_1 mode appears near 300 cm^{-1} when the NO_2 molecule is adsorbed on the surface. If the NO_2 molecule is single bonded through the nitrogen as in structure (I), it corresponds to the Ru–NO_2 stretching mode. Alternatively, if the NO_2 molecule is bridge bonded through the two oxygen atoms as in structure (II), it would be the Ru–O_2N symmetric stretching vibration. A comparison of the EELS frequencies obtained from NO_2 adsorbed on Ru(001) with the IR bands of the nitro complexes, as well as the observation of weak chemisorption, implicate structure (I) as the correct representation of the molecular bonding of NO_2 on Ru(001).

The results reported above show clearly that NO_2 can adsorb molecularly on Ru(001) at temperatures of 125 K and below. However, the initial adsorption is dissociative, and obviously this serves to passivate the surface for molecular adsorption. The dissociation products, NO and atomic oxygen, may act in the following ways to poison the surface and stabilize the molecular adsorption: (a) blocking of reactive adsorption sites[25]; (b) indirect electronic interactions via the substrate conduction electrons[25]; and/or (c) direct electrostatic interactions, as described recently by Lang *et al.*[32] Since θ_O and θ_{NO} are each 0.2 prior to molecular adsorption of NO_2, it seems likely that a "short-range" interaction such as site blocking or a perturbation of the electronic structure of the ruthenium surface that increases the activation energy of NO_2 dissociation is responsible for this effect.

B. The NO_2/N_2O_4 multilayer

After saturation of the monolayer at 80 K, NO_2 condensation into a multilayer occurs. Correlated with the development of the multilayer, new loss features as well as frequency shifts have been observed [cf. Figs. 3(d) and 3(e)], which are due to the presence of N_2O_4 in the multilayer. This issue shall be discussed in more detail in connection with the data presented in Table II.

The planar N_2O_4 molecule (D_{2h} symmetry) has 12 normal vibrational modes, only five of which are IR active. For weak adsorption of a molecule on a surface, no symmetry breaking occurs,[13] and only the gas phase IR active modes which produce a dynamic dipole moment normal to the surface are observable by dipolar scattering in EELS. This assumption is justified in our case, since no evidence was found for any Raman active modes in the EEL spectra. (For symmetry breaking of any kind, at least the A_g modes should be observable.) Therefore, for simplicity, only the frequencies of the IR active modes of N_2O_4 are listed in Table II, together with the observed EELS vibrations from spectrum (e) of Fig. 3. It is clearly evident from Table II that the observed EEL spectrum corresponds to N_2O_4 in the condensed multilayer. When compared to the gas phase data,[5] the agreement is within 10 cm^{-1}, with the exception of the NO_2 rocking mode at 340 cm^{-1}. Since all five IR active modes are observed, one might conclude that the N_2O_4 molecules are oriented randomly in the multilayer. However, the NO_2 wagging mode at 440 cm^{-1} generates a dipole moment which is perpendicular to the plane of the molecule, whereas the dipole moments of all the other modes are in the molecular plane. The observation that the NO_2 wagging mode at 440 cm^{-1} in the EEL spectrum of the multilayer is much less intense than the other modes (in contrast to the gas phase spectrum of N_2O_4) might suggest that an orientation of the N_2O_4 molecules with the molecular plane nearly normal to the surface is favored. Our observations are merely suggestive rather than proof of this possibility, however.

The phase of N_2O_4 in the condensed multilayer has not been considered heretofore, e.g., does N_2O_4 exist in a gaseous, liquid, or crystalline state at these temperatures (80 K) under UHV conditions? The triple point of N_2O_4 is at 262 K and 140 Torr.[33] For higher temperatures (and depending on the pressure), N_2O_4 exists either as a liquid or a gas, whereas at lower temperatures only the solid or gas phase can exist. One can easily estimate from these data that for temperatures below approximately 100 K, only the solid phase of N_2O_4 can exist even under UHV conditions. Accordingly, N_2O_4 in the multilayer should form a crystalline solid, as occurs for water under similar conditions.[34] Crystalline N_2O_4 is body-centered cubic of the space group $I2/m\bar{3}(T_h)$ with six molecules per unit cell. Since the molecules are located on sites of V_h symmetry, the selection rules will be the same as for the isolated molecule.[5] Accordingly, the triply degenerate vibrations in the crystal generate five fundamental IR bands of the same intensity as the gaseous molecule. When we compare the frequencies of the EELS modes with IR *fundamentals* of solid N_2O_4, we find better agreement for the NO_2 wagging and rocking modes but worse agreement for all other modes compared to gaseous N_2O_4. However, there is one important difference between the crystalline form of N_2O_4 and the isolated gaseous molecule which must be considered: three of the five fundamental IR bands are split, each into two modes of nearly equal intensity. These additional modes arise from the coupling of the fundamentals with the lattice vibrations (18–30 cm^{-1}) in the N_2O_4 crystal,[5a,5b] or may be due to combination bands which are enhanced by Fermi resonances.[5c] For details see Refs. 5(a)–5(c), where corresponding IR spectra are shown. The additional modes are listed in Table II, according to Ref. 5(b). Taking the resolution of the EEL spectrometer of approximately 80 cm^{-1} into account, we would not be able to resolve these doublets, but rather we would obtain a convolution of both peaks. With these considerations in mind, Table II shows excellent agreement between the EELS data from the multilayer and the crystalline state IR bands of N_2O_4, in agreement with expectations based on the thermodynamic data cited above.

V. SUMMARY

Electron energy loss spectroscopy and thermal desorption mass spectrometry have been used to investigate the interaction of NO_2 with the Ru(001) surface from submonolayer to multilayer coverages. The principal findings of this work are the following:

(i) The initial adsorption of NO_2 on Ru(001) at 80 K is

dissociative (for NO_2 exposures, $\epsilon_{NO_2} \leq 1$ L). The dissociation products, adsorbed NO and atomic oxygen, passivate the surface to further decomposition. Upon heating the surface to above 300 K, the NO dissociates partially to nitrogen and oxygen adatoms. The peak temperature for desorption of both NO and N_2 is near 480 K, whereas O_2 desorbs at approximately 1500 K.

(ii) Further NO_2 exposure ($1 < \epsilon_{NO_2} < 2$ L) leads to molecularly adsorbed NO_2 in the monolayer. The NO_2 molecule is bound weakly through the nitrogen atom to the surface (~ 9 kcal/mol) with a peak temperature for desorption of 140 K. The symmetry of the NO_2 admolecule is C_{2v}.

(iii) At higher exposures ($\epsilon_{NO_2} > 2$ L), after saturation of the monolayer, condensation of multilayers occurs, and the formation of N_2O_4 dimers is observed. As expected from thermodynamic data, the dimers that exist in the multilayer resemble a "solid" more closely than a "liquid" or a "gas." The peak temperature for desorption from the multilayer is 130 K.

ACKNOWLEDGMENTS

This work was supported by the National Science Foundation under Grant No. CHE-8206487. Acknowledgment is made to the Donors of the Petroleum Research Fund, administered by the American Chemical Society, for the partial support of this research under Grant No. 15454-AC5. One of us (U. S.) gratefully acknowledges partial financial support from the Alexander von Humboldt Foundation.

[1] L. Pauling, *The Nature of the Chemical Bond* (Cornell University, Ithaca, 1980).
[2] R. V. St. Louis and B. L. Crawford, J. Chem. Phys. 42, 857 (1965).
[3] A. J. Vosper, J. Chem. Soc. A 1970, 625; M. Herman, J. C. van Craen, J. van der Auwera, and G. W. Hills, Chem. Phys. Lett. 115, 445 (1985).
[4] H. Bent, Inorg. Chem. 2, 747 (1962).
[5] (a) R. G. Snyder and I. C. Hisatsune, J. Mol. Spectrosc. 1, 139 (1957); (b) R. Wiener and E. R. Nixon, J. Chem. Phys. 26, 906 (1957); (c) B. Andrews and A. Anderson, *ibid.* 74, 1534 (1981); (d) G. M. Begun and W. H. Fletcher, J. Chem. Spectrosc. 4, 388 (1960); (e) I. C. Hisatsune, J. P. Devlin, and Y. Wada, J. Chem. Phys. 33, 714 (1960).
[6] J. C. Fuggle and D. Menzel, Surf. Sci. 79, 1 (1979).
[7] J. Segner, W. Vielhaber, and G. Ertl, Israel J. Chem. 22, 375 (1982).
[8] D. Dahlgren and J. C. Hemminger, Surf. Sci. 123, L739 (1982).
[9] U. Schwaike, H. Niehus, and G. Comsa, Surf. Sci. 152/153, 596 (1985).
[10] U. Schwaike, H. Niehus, and G. Comsa, in *Desorption Induced by Electronic Transitions*, edited by W. Brenig and D. Menzel (Springer, Berlin, 1985), p. 98.
[11] R. I. Masel, E. Umbach, J. C. Fuggle, and D. Menzel, Surf. Sci. 79, 26 (1979).
[12] C. R. Brundle, J. Vac. Sci. Technol. 13, 301 (1976).
[13] H. Ibach and D. L. Mills, *Electron Energy Loss Spectroscopy and Surface Vibrations* (Academic, New York, 1982).
[14] W. H. Weinberg, in *Experimental Methods of Surface Physics*, edited by R. L. Park and M. G. Lagally (Academic, New York, 1985), p. 23.
[15] G. E. Thomas and W. H. Weinberg, Rev. Sci. Instrum. 50, 497 (1979).
[16] G. E. Thomas and W. H. Weinberg, J. Chem. Phys. 70, 954 (1979).
[17] In a previous study (Ref. 9) where the doser opening could be moved directly in front of the ionizer of the mass spectrometer, it has been verified by the mass 46-to-mass-30 ratio that no detectable NO_2 decomposition occurs in a passivated doser line. However, if only the indirect flux is measured, this ratio decreases substantially due to NO_2 decomposition at hot ion gauge filaments, on the walls of the UHV chamber, etc.
[18] A. Cornu and R. Massot, *Compilation of Mass Spectra Data* (Heyden, London, 1975).
[19] P. A. Redhead, Vacuum 12, 203 (1962).
[20] By comparison to the chemisorption of N_2O on Ru(001) and on Ru(001) modified by the presence of oxygen adatoms (Ref. 21), this N_2O coverage is below 1% of a monolayer. Since N_2O was not observed by EELS, it may well not have been formed on the Ru(001) surface.
[21] A. B. Anton, T. E. Madey, N. R. Avery, and W. H. Weinberg (in preparation).
[22] For example, N. R. Avery, Surf. Sci. 131, 501 (1983).
[23] G. E. Thomas and W. H. Weinberg, Phys. Rev. Lett. 41, 1181 (1978).
[24] H. Conrad, R. Scala, W. Stenzel, and R. Unwin, Surf. Sci. 145, 1 (1984).
[25] P. J. Feibelman and D. R. Hamann, Phys. Rev. Lett. 52, 61 (1984), and references therein.
[26] T. S. Rahman, A. B. Anton, N. R. Avery, and W. H. Weinberg, Phys. Rev. Lett. 51, 1979 (1983).
[27] K. Nakamoto, *Infrared and Raman Spectra of Inorganic and Coordination Compounds* (Wiley, New York, 1977).
[28] A. B. Anton, N. R. Avery, B. H. Toby, and W. H. Weinberg, J. Electron Spectrosc. 29, 181 (1983). For N_2 + O coadsorbed on Ru(001), see: A. B. Anton, N. R. Avery, T. E. Madey, and W. H. Weinberg, Surf. Sci. (submitted); and A. B. Anton, PhD thesis, California Institute of Technology, 1985.
[29] T. E. Madey, A. B. Anton, N. R. Avery, and W. H. Weinberg, J. Vac. Sci. Technol. A 1, 1220 (1983). For N_2O + O coadsorbed on Ru(001), see Ref. 21.
[30] The broad width of this loss peak suggests that both an overtone and a double loss contribute. Due to the low intensity, a separation of the overtone contribution from the double scattering event is not possible. However, with increasing coverage, it is expected that the double loss becomes dominant (see Ref. 13).
[31] The fact that the loss features are consistent in frequency with the proposed bonding configuration lends considerable strength to this argument.
[32] N. D. Lang, S. Holloway, and J. K. Norskov, Surf. Sci. 150, 24 (1985).
[33] *Landolt–Bornstein, Zahlenwerte und Funktionen aus Physik, Chemie und Astronomie*, Bd. II, Teil 2(a) (Springer, Verlag, Berlin, 1960).
[34] T. E. Madey and J. T. Yates, Chem. Phys. Lett. 51, 77 (1977); P. A. Thiel, F. M. Hoffmann, and W. H. Weinberg, J. Chem. Phys. 75, 5556 (1981).

Appendix 8

The Adsorption of NO_2 on Clean Ru(001) and Ru(001) Modified Chemically by Ordered Overlayers of Oxygen Adatoms

[This appendix was published as a paper by U. Schwalke, J. E. Parmeter and W. H. Weinberg, in *Surface Science* 1986, 178, 625.]

Surface Science 178 (1986) 625–634
North-Holland, Amsterdam

THE ADSORPTION OF NO_2 ON CLEAN Ru(001) AND Ru(001) MODIFIED CHEMICALLY BY ORDERED OVERLAYERS OF OXYGEN ADATOMS

U. SCHWALKE *,☆, J.E. PARMETER ** and W.H. WEINBERG

Division of Chemistry and Chemical Engineering, California Institute of Technology, Pasadena, CA 91125, USA

Received 10 March 1986; accepted for publication 23 May 1986

High resolution electron energy loss spectroscopy and thermal desorption mass spectrometry have been used to investigate the adsorption of NO_2 on the clean Ru(001), the Ru(001)-p(2×2)-O and the Ru(001)-p(1×2)-O surfaces. On the clean surface at 80 K, the initially adsorbed NO_2 dissociates to molecularly adsorbed nitric oxide and oxygen adatoms. When the fractional surface coverage of each of these dissociation products reaches approximately 0.2, subsequent chemisorption of NO_2 is molecular. The presence of preadsorbed oxygen poisons the surface strongly with respect to dissociative adsorption and less strongly with respect to molecular adsorption of NO_2. In all cases the molecular NO_2 is chemisorbed weakly with a heat of adsorption of approximately 8–10 kcal/mol. The condensed multilayer at 80 K is composed of N_2O_4 dimers.

1. Introduction

Studies of the interaction of nitrogen dioxide with well characterized single crystalline metal surfaces have recently become the focus of considerable interest [1–6] because they are the logical extension of numerous NO and oxygen coadsorption experiments [7], in particular those where evidence for the formation of NO_2 as a stable reaction intermediate has been reported [8,9]. Additional motivation to investigate the rich surface chemistry of NO_2 has been stimulated by the recent observation of a novel heterogeneously catalyzed oxidation reaction of organic compounds by NO_2 [10].

Nitrogen dioxide is a triatomic molecule of C_{2v} symmetry. The vibrational spectrum of the free NO_2 molecule is characterized by three infrared absorption bands at 750 cm^{-1} (the NO_2 bend), 1318 cm^{-1} (the NO_2 symmetric stretch), and 1610 cm^{-1} (the NO_2 antisymmetric stretch) [11]. Since NO_2 has an unpaired electron, it can dimerize to O_2N-NO_2. The most characteristic

* Feodor-Lynen Research Fellow of the Alexander von Humboldt Foundation.
** AT&T Bell Laboratories Predoctoral Fellow.
Present address: Siemens AG, Central Research and Development, Otto-Hahn-Ring 6, D-8000 Munich 83, Fed. Rep. of Germany.

0039-6028/86/$03.50

infrared mode of the planar N_2O_4 dimer (D_{2h} symmetry) is an intense absorption band at approximately 1750 cm^{-1} (the NO_2 antisymmetric stretch) [12].

One powerful technique to measure the vibrational modes of adsorbed species on well characterized single crystalline surfaces, and hence to identify their structure and bonding, is high resolution electron energy loss spectroscopy (EELS) [13]. We have combined EELS with thermal desorption mass spectrometry (TDMS) to investigate the interaction of NO_2 with clean and oxygen modified Ru(001) surfaces at 80 K, from submonolayer to multilayer coverages.

2. Experimental procedures

All EELS and TDMS measurements were performed in an ultrahigh vacuum system which has been described in detail previously [14]. Briefly, the home-built EEL spectrometer consists of hemispherical energy dispersing elements in both the monochromator and the analyzer. The full-width at half-maximum of the elastically scattered beam varied between approximately 60 and 75 cm^{-1}, while maintaining a count rate of 3×10^5 cps. The incident beam energy was approximately 4 eV, and the angle of incidence of the electron beam was 60° with respect to the surface normal.

Nitrogen dioxide (Matheson Gas Products, 99.5% purity) was used without further purification and was introduced onto the Ru(001) surface via a directional beam doser consisting of a multicapillary array. Prior to the actual experiments, the gas dosing system was flushed several times with NO_2 to ensure high purity exposures, which was verified by in situ mass spectrometry [6]. In addition, no evidence of any impurities was noted either in monolayer or multilayer EEL spectra after NO_2 exposures at 80 K. In order to obtain the NO_2 exposures when using the beam doser, the measured increase in the integrated background pressure was corrected by a calibration factor which is determined by the geometrical arrangement of the sample and the doser. This factor has been determined experimentally in previous CO and NO adsorption experiments by comparing the exposures needed to cause the appearance of particular thermal desorption features, both after backfilling the bell jar and after using the doser.

3. Results and discussion

3.1. Chemisorption of NO_2 on clean Ru(001)

In fig. 1A, electron energy loss spectra at 80 K are shown of clean Ru(001), (a), and the Ru(001) surface exposed to NO_2, (b) and (c). After an exposure of

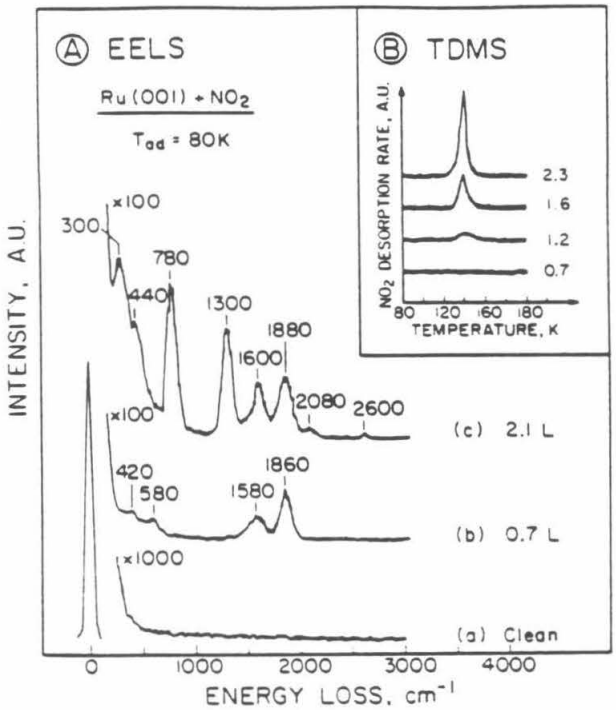

Fig. 1. (A), (a) Electron energy loss spectra of clean Ru(001) at 80 K; (b) and (c) the Ru(001) surface exposed to NO_2. All exposures are in units of langmuirs (1 L≡10^{-6} Torr s). (B) Thermal desorption spectra of NO_2 as a function of exposure. The NO_2 was adsorbed at 80 K, and the heating rate was 6 K/s.

0.7 L of NO_2, the EEL spectrum (b) of fig. 1A indicates that the initial adsorption of NO_2 is dissociative on Ru(001) at 80 K, due, for example, to the absence of the characteristic NO_2 bending vibration near 750 cm^{-1}. Only four loss peaks appear in the spectrum, which are due to adsorbed nitric oxide and atomic oxygen. The peaks at 1860 and 1580 cm^{-1} are due to the nitrogen–oxygen stretching mode of nitric oxide that is adsorbed in on-top and in bridge-bonded sites, respectively [15]. The low frequency mode at 580 cm^{-1} is a superposition of both the Ru–NO stretching mode of terminally bonded, linear NO and the Ru=O stretching mode of oxygen adatoms [15,16], whereas the low frequency mode at 420 cm^{-1} is due to the Ru–NO stretch of NO adsorbed in bridge bonded sites [7,15].

Compared to NO adsorbed on the clean Ru(001) surface [15], the nitrogen–oxygen stretching frequencies are upshifted by approximately 50 to 80 cm^{-1}. Similar shifts of these bands have been observed in the coadsorption of NO and oxygen on Ru(001) [7]. This increase in frequency results from a stiffening of the intramolecular NO bond as a consequence of reduced electron

backdonation into the $2\pi^*$ antibonding orbital of adsorbed NO, in the presence of the coadsorbed electronegative atomic oxygen. In agreement with the EELS data, no molecular desorption of NO_2 was detectable in the thermal desorption spectrum after an NO_2 exposure of 0.7 L at 80 K, as shown in fig. 1B. The only observed desorption products were NO and N_2 at approximately 480 K and O_2 near 1500 K, similar to NO adsorption and NO and O_2 coadsorption on Ru(001) [7,17].

For exposures of NO_2 of approximately 1 L or greater, molecular desorption occurs, as may be seen in fig. 1B. This molecularly chemisorbed state of NO_2 saturates at an exposure of approximately 2.3 L, and the desorption peak temperature of 140 K does not shift significantly with coverage suggesting first-order desorption kinetics. Assuming a normal pre-exponential factor of the desorption rate coefficient of 10^{14} s^{-1}, a binding energy of approximately 9 kcal/mol is consistent with these thermal desorption results [18]. The presence of weakly chemisorbed NO_2 is also evident in EEL spectrum (c) of fig. 1A, which was recorded after an exposure of 2.1 L of NO_2. In addition to the loss features due to NO and atomic oxygen, additional bands at 300 cm^{-1} (the Ru–NO_2 stretching mode), 780 cm^{-1} (the NO_2 bending mode) and 1300 cm^{-1} (the NO_2 symmetric stretching mode) are present. These results confirm that the observed desorption of molecular NO_2 at 140 K (cf. fig. 1B) is due to chemisorbed NO_2 rather than a result of the recombination of NO(a) and O(a), for example, as has been observed on a potassium modified Pt(111) surface [9]. Compared to the free molecule, the NO_2 bending and symmetric stretching modes are shifted only slightly, consistent with weak chemisorption. Since all these modes were found to be excited by a long-range dipolar scattering mechanism, they must belong to the totally symmetric representation of the corresponding point group. Since exactly three new and intense fundamental modes are observed for the molecularly chemisorbed NO_2, we conclude that the ruthenium–nitrogen molecular axis is oriented essentially perpendicular to the Ru(001) surface (C_{2v} symmetry). Bond formation is expected to occur through the nitrogen atom since the unpaired electron in the $6a_1$ orbital of NO_2 is localized at the nitrogen atom. Support for this adsorbate structure is given by the fact that the frequencies of the molecularly chemisorbed NO_2 on Ru(001) are in agreement with the infrared bands of N-bonded nitro complex compounds of C_{2v} symmetry [6].

No modes between 2100 and 2400 cm^{-1} are observed in the EEL spectra of fig. 1A indicating the absence of both adsorbed N_2 [19] and N_2O [20]. Two weak loss features at 2080 and 2600 cm^{-1} were observed, which were correlated with the presence of molecularly chemisorbed NO_2. Since the peak at 2080 cm^{-1} disappears upon heating to 150 K, it is not due, for example, to coadsorbed CO [21]. The mode at 2080 cm^{-1} is due to a combination band of the NO_2 bending and symmetric stretching modes, whereas the loss at 2600 cm^{-1} is due to a double-loss and/or an overtone of the NO_2 symmetric stretching mode [13].

For NO_2 exposures of 1 L (or above), thermal desorption measurements have shown that the total amount of NO and N_2 that desorbs at approximately 480 K is on the order of 30% to 40% of that observed after a saturation exposure of NO on the clean Ru(001) surface. From these measurements, the approximate fractional coverages of nitric oxide and atomic oxygen from NO_2 dissociation were each estimated to be 0.2 prior to the molecular chemisorption of NO_2 at 80 K. Evidently, "short-range" interactions such as site blocking [15] and/or a local perturbation of the electronic structure of the ruthenium surface [22] increase the activation barrier to NO_2 dissociation.

Since the probability of adsorption of NO_2 on Ru(001) at 80 K is essentially unity [6], the coverage of molecularly chemisorbed NO_2 could be estimated from the NO_2 exposure. The NO_2 monolayer saturates at an NO_2 exposure of approximately 2.3 L (cf. fig. 1B), which corresponds to a fractional NO_2 coverage of 0.25 (after subtracting the coverage of dissociated NO_2). Although the absolute accuracy in this estimate may be poor, the reproducibility was found to be excellent.

Previously, results concerning the interaction of NO_2 with the W(110), Pt(111) and the reconstructed hexagonal Pt(100) surfaces have been reported [1–5]. A comparison of the surface chemistry of NO_2 adsorbed on Ru(001) with those results is useful since all the surfaces are geometrically similar but the three transition metals differ greatly in their reactivity. On W(110) the adsorption of NO_2 was found to be almost completely dissociative at 100 K, leading to atomically adsorbed nitrogen and oxygen [1]. This is not unexpected, however, since NO also dissociates at 100 K on this surface [24]. In contrast, on both platinum surfaces, molecular adsorption of NO_2 has been observed at low temperatures, and the dissociation of NO_2(a) into NO(a) and O(a) becomes significant only at temperatures above 240 K [3–5]. Obviously, Ru(001) lies between these two extremes in surface reactivity: both dissociation to NO(a) and O(a) as well as molecular chemisorption of NO_2 occur at 80 K.

3.2. Chemisorption of NO_2 on oxygen modified Ru(001) surfaces

In order to investigate the influence of preadsorbed, ordered oxygen adatoms, NO_2 was adsorbed both on the Ru(001)-p(2 × 2)-O and Ru(001)-p(1 × 2)-O surfaces which correspond to initial fractional coverages of ordered atomic oxygen of 0.25 and 0.5, respectively [16]. The effect of preadsorbed oxygen on the chemisorption of NO_2 is illustrated in fig. 2. The threshold exposure of NO_2 which is necessary to observe desorption of *molecular* NO_2 decreases strongly with the oxygen precoverage, as is evident from fig. 2B. This behavior is also reflected in the EEL spectra that are shown in fig. 2A. For an initial fractional oxygen coverage of 0.25 [the p(2 × 2)-O overlayer] and an NO_2 exposure of 0.8 L, spectrum (a) of fig. 2A, the characteristic modes of

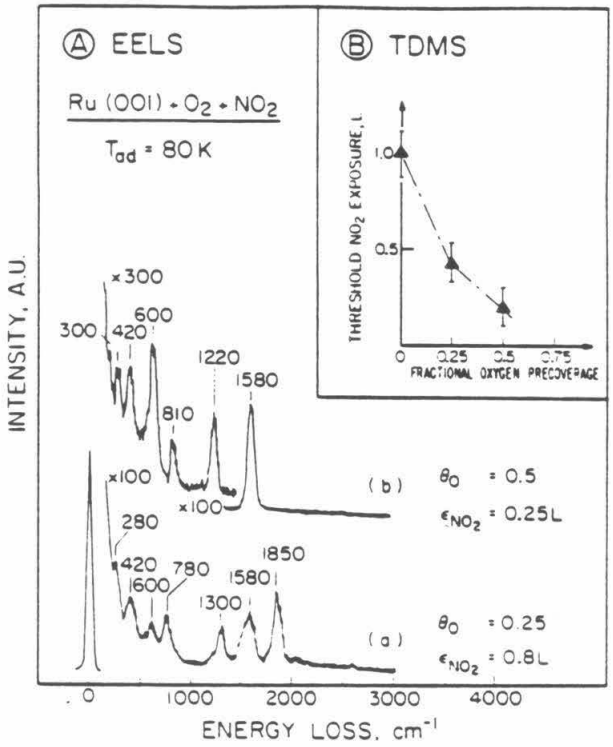

Fig. 2. (A) Electron energy loss spectra of NO_2 adsorbed on the Ru(001)-p(2 × 2)-O and the Ru(001)-p(1 × 2)-O surfaces. (a) Fractional coverage of ordered oxygen adatoms of 0.25 and NO_2 exposure of 0.8 L. (b) Fractional coverage of ordered oxygen adatoms of 0.5 and NO_2 exposure of 0.25 L. (B) Dependence of the threshold exposure of NO_2 necessary for observing the thermal desorption of molecular NO_2 on the initial fractional coverage of oxygen adatoms.

chemisorbed NO_2 at 280, 780 and 1300 cm^{-1} are present. This should be contrasted with spectrum (b) of fig. 1A, which shows no molecular chemisorption of NO_2 following a similar exposure on the clean Ru(001) surface.

However, as on clean Ru(001), the initial adsorption of NO_2 on the Ru(001)-p(2 × 2)-O surface at 80 K is dissociative, as judged by the nitrogen–oxygen and Ru–NO stretching modes of NO that is adsorbed in both bridge-bonded and on-top sites. Compared to NO_2 adsorption on clean Ru(001), there is approximately 40% as much NO_2 dissociation on the Ru(001)-p(2 × 2)-O surface, as estimated from the amounts of thermally desorbed NO and N_2. As estimated from the molecularly desorbed NO_2, the amount of molecularly chemisorbed NO_2, however, was found to be reduced only slightly compared to the clean Ru(001) surface, as shown in table 1.

The extent of NO_2 dissociation at 80 K on the Ru(001)-p(1 × 2)-O surface, corresponding to an initial fractional oxygen coverage of 0.5, is decreased

Table 1
Fractional coverages of NO_2 and its dissociation products on clean and oxygen precovered Ru(001), as estimated from thermal desorption data

	Ru(001)	Ru(001)-p(2 × 2)-O	Ru(001)-p(1 × 2)-O
θ_{NO}	0.2	0.08	0.02
θ_O	0.2	0.25 ± 0.08	0.5 ± 0.02
θ_{NO_2}	0.25	0.2	0.14
θ_{Total}	0.65	0.61	0.68

further compared to the Ru(001)-p(2 × 2)-O surface. On this surface, the extent of dissociation is approximately 10% of that observed on the clean surface (see table 1), consistent with EEL spectra where only bridge-bonded NO (the nitrogen–oxygen stretching mode at 1580 cm^{-1}) was observed. In addition, NO_2 exposures of less than 0.3 L are sufficient to observe molecularly chemisorbed NO_2. Both of these effects are shown in EEL spectrum (b) of fig. 2A. As on the clean Ru(001) surface, three intense NO_2 bands are present in the EEL spectrum, suggesting that the NO_2 molecule is adsorbed with C_{2v} symmetry on this surface also. Due to the high coverage of oxygen adatoms, however, the Lewis acidity of the Ru(001) surface is increased. This should increase the strength of the σ-bond between NO_2 and the Ru(001) surface which, in turn, could affect the intramolecular electronic structure of the NO_2. Indeed, both effects have been observed. The desorption temperature of molecular NO_2 was found to be increased by 10 K, and frequency shifts of both the NO_2 bending mode (810 cm^{-1}) and the NO_2 symmetric stretching mode (1220 cm^{-1}) are observed [cf. spectrum (b) of fig. 2A].

The frequency of the antisymmetric stretching mode of NO_2 is known to depend strongly on the electronegativities of the other ligands in inorganic compounds [25]. Accordingly, this band should shift from 1610 cm^{-1} to 1700–1800 cm^{-1} upon adsorption on the oxygen modified Ru(001) surfaces. Since no residual NO band is visible in this frequency range [cf. spectrum (b) of fig. 2A], the clear absence of the antisymmetric stretching band of NO_2 (B_1 symmetry) supports the conclusion that NO_2 is adsorbed with C_{2v} symmetry.

3.3. The NO_2/N_2O_4 multilayer

After saturation of the chemisorbed monolayer, the subsequent formation of condensed multilayers was observed at 80 K. As expected, for sufficiently large NO_2 exposures ($\gtrsim$ 5 L), no significant differences were found among the multilayer states prepared on the three different Ru(001) surfaces. Therefore, only the multilayer EEL spectrum which was obtained after exposing the clean

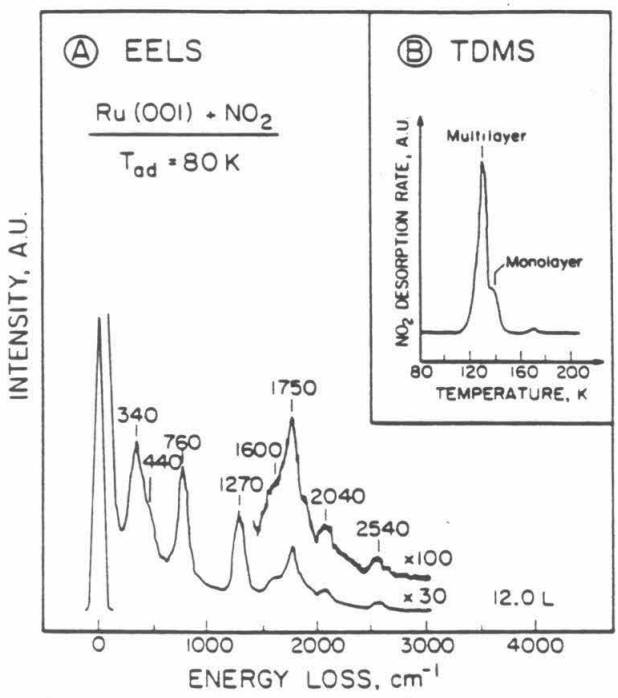

Fig. 3. (A) Electron energy loss spectrum of an N_2O_4 multilayer on Ru(001), obtained after exposing the clean surface to 12 L of NO_2. (B) The corresponding NO_2 thermal desorption spectrum.

Ru(001) surface to 12 L of NO_2 is shown in fig. 3A, together with the corresponding thermal desorption spectrum in fig. 3B. The multilayer desorption peak, which appears at 130 K after completion of the monolayer, does not saturate with NO_2 exposure, and the peak temperature shifts upward slightly with coverage [6]. In the corresponding EEL spectrum of fig. 3A, an intense new loss peak at 1750 cm^{-1} has appeared, which is due to the NO_2 antisymmetric stretching mode of the N_2O_4 dimer. In addition, a broad loss feature centered at 340 cm^{-1} (the NO_2 rocking mode of N_2O_4) is visible, and the frequencies of the NO_2 bending and symmetric stretching modes, as well as the combination band and the overtone/double-loss band, are downshifted. Except for the overtone/double-loss band, the long-range dipolar scattering mechanism was found to be operative, allowing a comparison with infrared spectra of N_2O_4. According to published thermodynamic data of N_2O_4 [23], condensed N_2O_4 at 80 K under UHV conditions should exist in a crystalline form, rather than as a "gas" or a "liquid". This expectation is borne out by comparing the EEL spectrum of the N_2O_4 multilayer of fig. 3A with IR spectra of solid, liquid and vapor phase N_2O_4 [6].

4. Conclusions

The initial adsorption of NO_2 at 80 K on the Ru(001), the Ru(001)-p(2 × 2)-O and the Ru(001)-p(1 × 2)-O surfaces is dissociative with the dissociation products being molecular NO and atomic oxygen. Subsequent to the initial dissociative adsorption, molecular chemisorption of NO_2 is also observed at 80 K. The extent of dissociative adsorption is a function of the particular surface and, not surprisingly, is greatest on the clean Ru(001) surface. For example, on this clean surface the fractional coverage of NO_2 that dissociates prior to molecular adsorption is 0.2, corresponding to a total fractional surface coverage of 0.4, i.e. $\theta_{NO} = 0.2$ and $\theta_O = 0.2$. The extent of dissociative adsorption of NO_2 decreases strongly with the fractional precoverage of the two ordered oxygen overlayers. The extent of molecularly chemisorbed NO_2 decreases less strongly such that the total coverage at saturation is approximately constant on all three surfaces (cf. table 1). The molecular NO_2 is weakly chemisorbed on each of the three surfaces, with an activation energy of desorption of approximately 9 kcal/mol. After saturation of the chemisorbed overlayer at 80 K, condensation of NO_2 occurs with the formation of N_2O_4 dimers in the multilayer.

Acknowledgements

This work was supported by the National Science Foundation under Grant No. CHE-8516615. Acknowledgement is also made to the donors of the Petroleum Research Fund, administered by the American Chemical Society, for the partial support of this research under Grant No. 15454-AC5. One of us (US) gratefully acknowledges the financial support of the Alexander von Humboldt Foundation.

References

[1] J.C. Fuggle and D. Menzel, Surface Sci. 79 (1979) 1.
[2] J. Segner, W. Vielhaber and G. Ertl, Israel J. Chem. 22 (1982) 375.
[3] D. Dahlgren and J.C. Hemminger, Surface Sci. 123 (1982) L739.
[4] U. Schwalke, H. Niehus and G. Comsa, Surface Sci. 152/153 (1985) 596.
[5] U. Schwalke, H. Niehus and G. Comsa, in: Desorption Induced by Electronic Transitions, Eds. W. Brenig and D. Menzel (Springer, Berlin, 1985) p. 98.
[6] U. Schwalke, J.E. Parmeter and W.H. Weinberg, J. Chem. Phys. 84 (1985) 4036.
[7] For example, H. Conrad, R. Scala and R. Unwin, Surface Sci. 145 (1984) 1.
[8] P.D. Schulze, D.L. Utleg and R.L. Hance, Surface Sci. 102 (1981) L9.
[9] M. Kiskinova, G. Pirug and H.P. Bonzel, Surface Sci. 140 (1984) 1.
[10] S.A. Nyarady and R.E. Sievers, J. Am. Chem. Soc. 107 (1985) 3726.
[11] R.V. St. Louis and B.L. Crawford, J. Chem. Phys. 42 (1965) 857.

[12] R. Wiener and E.R. Nixon, J. Chem. Phys. 26 (1957) 906.
[13] H. Ibach and D.L. Mills, Electron Energy Loss Spectroscopy and Surface Vibrations (Academic Press, New York, 1982);
W.H. Weinberg, in: Experimental Methods of Surface Physics, Eds. R.L. Park and M.G. Lagally (Academic Press, New York, 1985) p. 23.
[14] G.E. Thomas and W.H. Weinberg, Rev. Sci. Instr. 50 (1979) 497.
[15] G.E. Thomas and W.H. Weinberg, Phys. Rev. Letters 41 (1978) 1181.
[16] T.S. Rahman, A.B. Anton, N.R. Avery and W.H. Weinberg, Phys. Rev. Letters 51 (1983) 1979.
[17] P. Feulner, S. Kulkarni, E. Umbach and D. Menzel, Surface Sci. 99 (1980) 489.
[18] P.A. Redhead, Vacuum 12 (1962) 203.
[19] A.B. Anton, N.R. Avery, B.H. Toby and W.H. Weinberg, J. Electron Spectrosc. Related Phenomena 29 (1983) 181.
[20] T.E. Madey, A.B. Anton, N.R. Avery and W.H. Weinberg, J. Vacuum Sci. Technol. A1 (1983) 1220.
[21] G.E. Thomas and W.H. Weinberg, J. Chem. Phys. 70 (1979) 954.
[22] P.J. Feibelman and D.R. Hamann, Phys. Rev. Letters 52 (1984) 61.
[23] Landolt-Börnstein, Zahlenwerte und Funtionen aus Physik, Chemie und Astronomie, Vol. II, Part 2(a) (Springer, Berlin, 1960).
[24] R.I. Masel, E. Umbach, J.C. Fuggle and D. Menzel, Surface Sci. 79 (1979) 26.
[25] H.A. Bent, Inorg. Chem. 2 (1963) 747.